# An investigation into the timing of the Renard kimberlite cluster, Otish field, Canada

by

Ilona Maria Ranger

A thesis submitted in partial fulfillment of the requirements for the degree of

Doctor of Philosophy

Department of Earth and Atmospheric Sciences
University of Alberta

# ABSTRACT

The timing of a diamondiferous kimberlite cluster within the Archean Superior Province, the Renard cluster (Otish field, Québec), was investigated by ID-TIMS U-Pb dating of groundmass perovskite. Few Otish field kimberlites were previously dated by U-Pb perovskite (Renard 1-3 and Lac Beaver) but the Neoproterozoic dates indicated a much longer kimberlite intrusion history (~100 Myr) than is typically known for kimberlite clusters/fields. Here, a single pipe (Renard 2) is investigated in detail from ten new samples and found to record a punctuated history of intrusions from early-stage, main pipe-infilling stage, and late-stage hypabyssal kimberlites spanning over at least 20 Myr (~652-632 Ma) and possibly longer. In contrast, a new weighted average $^{206}Pb/^{238}U$ perovskite composite date of 643.8±1.0 Ma is estimated for the main Renard 2 pipe emplacement. Applying this new information to other kimberlites in the cluster (Renard 1-4, Renard 7, Renard 9, G04-296 Anomaly dyke), it was found that the U-Pb perovskite dates can record at least ~124 Myr (~663-539 Ma) of repeated hypabyssal kimberlite intrusions. In particular, the younger Otish field hypabyssal kimberlites (~539 Ma peripheral Renard 2, ~614 Ma Renard 7 and ~551 Ma Lac Beaver) overlap with the timing of the ~620-550 Ma Central Iapetus Magmatic Province LIP and alkaline-carbonatite intrusions along the margin of eastern Canada and western Greenland. The broad scale of kimberlite intrusion at ~632-629 Ma (Renard, Wemindji) across the eastern Superior Province and similar temporal and spatial connection between intrusions in Laurentia and Baltica suggest a large-scale mechanism triggered kimberlite magmas to form (e.g. combined continental extension/rifting and mantle plume(s)). In addition, a hypabyssal kimberlite from the Renard 9 pipe was found to contain grains of kassite, a rare hydrous Ca-Ti oxide ($CaTi_2O_4(OH)_2$). The first ID-TIMS U-Pb results for kassite are reported with an evaluation of several possible interpretations, including lead loss,

initial common lead isotopic composition or gain/loss of intermediate daughter products. The best estimate for the timing of kassite crystallization is taken from two multi-grain kassite fractions recording a weighted average $^{207}Pb/^{235}U$ date of 456.1±2.1 Ma (2σ).

# PREFACE

Chapter 2 has been accepted for publication as: Ranger IM, Heaman LM, Pearson DG, Muntener C, Zhuk V (2018) Punctuated, long-lived emplacement history of the Renard 2 kimberlite, Canada, revealed by new high precision U-Pb groundmass perovskite dating. Mineralogy and Petrology 112 (Suppl 2):S639-S651. Chapter 2 was presented at the 11th International Kimberlite conference in September of 2017 and a portion is reported in the 11th IKC long abstract: Ranger IM, Heaman LM, Pearson DG, Laroulandie C, Lepine I, Zhuk V (2017) Punctuated, long-lived emplacement history of kimberlites from the Renard cluster, Superior Province, Canada indicated by new high precision U-Pb groundmass perovskite dating. 11th International Kimberlite Conference Extended Abstract No. 11IKC-4493, 3 p.

Chapter 4 includes research conducted by Dr. F. Nestola at the University of Padova (Italy) for the single-crystal XRD results and Dr. A. Locock at the University of Alberta for chemical compositions by the electron microprobe.

For Chapters 2, 3 and 4, J. LeBlanc and Dr. C. Sarkar provided guidance in learning how to use the VG354 and Triton Plus thermal ionization mass spectrometers in the Radiogenic Isotope Facility and Arctic Resources Laboratory, respectively, at the University of Alberta. Dr. L. Heaman and Dr. C. Sarkar assisted with learning the HBr protocol in the U-Pb Geochronology Laboratory at the University of Alberta.

The ideas, writing, tables and figures presented in this thesis are my own work unless otherwise cited by reference in text, with the exception of feedback from Stornoway Diamond Corporation for Chapters 2-4 and Appendix A, feedback from the supervisory committee and feedback from co-authors, reviewers and Editor-in-Chief in collaboration for publication of Chapter 2.

*In memory*

*of my father,*

*Hubert*

# ACKNOWLEDGEMENTS

Many thanks to Stornoway Diamond Corporation for generously providing samples, assistance throughout sample collection and help with questions. Especially my former colleagues Colleen Laroulandie and Isabelle Lepine for working around me when they were logging under a deadline and Volodymyr Zhuk for painstakingly sawing all the Lynx and Hibou core. Thank you Robin Hopkins for his patience and staying late several times when I visited North Vancouver to collect samples. Thank you to Julie Paillard for helping with sample information and Liz Palmer for helping with sample shipments and coordinating my visits. Many thanks to Andrea De Stefano, Matt Gaudet, Ayaka, Carlos and Joey for their assistance with logging information and sample collection when I visited to sample Renard 2. I would especially like to thank all of the Stornoway crew for patiently waiting for me to write my way through this thesis.

Numerous staff at the University of Alberta kindly helped during my time at the Department of Earth and Atmospheric Sciences. Thank you to Marilyn Huff and Dave Chesterman for letting me borrow a stereomicroscope. More thank you's to Marilyn for helping fix our lab petrographic microscope and for her patience with all my questions as I was learning how to be a Teaching Assistant again. Mark Labbe and Barry Herchuk for their help with training, troubleshooting, and finding supplies for the sample preparation facilities. Barry Shaulis for help with questions around the U-Pb clean lab and sample preparation facilities. Chiranjeeb Sarkar for initially helping me learn the HBr protocol and Triton, and for help with some of my TIMS questions. James LeBlanc for his patience in gracefully answering my many questions about analyzing the U-Pb samples with the VG354 and Triton. Martin von Dollen for diligently making thin sections from the kimberlite samples. Igor Jakab who helped with camera and Digital Imaging Facility questions (the expresso machine will be ordered for you after I graduate and get a job Igor). Diane Caird for her help with all my lab chemical and safety questions, and for analyzing the XRD for a Lynx sample. Olga Levner for her helpful assistance in the Stable Isotope lab and Dr. Muehlenbachs for help understanding the data for EAS 540. Shyra Craig for helping with all sorts of my questions around the department. Nathan Gerein for his scanning electron microscope expertise and showing me how to carbon coat and run the EVO. Guibin Ma also for his recent scanning electron microscope expertise. Andrew Locock who wielded his

sharp mineralogical skills and helped narrow down what this mysterious perovskite-like mineral might be in chapter 4. Thank you to Graham Pearson and Tom Chacko for serving on the supervisory committee. Thank you also to Dr. Luth and Dr. Chakhmouradian for their helpful feedback as part of the examining committee. Many thanks to my supervisor, Larry Heaman, for financially supporting the work and his patience fielding the many questions and drafts from his student that it probably felt like he was trying to grow Chinese bamboo.

Several people gave their time to help me learn or with the work presented here. Thank you to John Armstrong for helping get the thesis started. Thank you to Tom McCandless for taking the time during visits to the U of A to talk about kimberlite geology in general. Thank you to Erin Walton for showing me how the Raman spectrometer works at MacEwan University. Many thanks to Fabrizio Nestola for graciously getting up super early to analyze kassite by XRD at the University of Padova. A big thank you to Bruce Kjarsgaard for the feedback and pep talk before my 11IKC presentation. Thank you to the committee of the 11th International Kimberlite Conference for selecting the abstract for oral presentation of the work presented in Chapter 2, and Bruce Kjarsgaard and guest editor Philip Janney for helpful reviews of the paper. Many thanks to Eugenia Sukhorukova and Edward Hung from the Association of Translators and Interpreters of Alberta for helping with Russian and Chinese translations, respectively. Thank you to the Natural Sciences and Engineering Research Council for providing funding through Discovery Grants to L.M.H. and D.G.P.

Seeing the Renard core again was a wonderful experience but in hindsight I had no idea at the start what I was getting myself into going back to university late in life and figuring out how to learn as an older student. But I made it through writing another thesis and a special thank you goes to my family and friends for being there for me during my studies. It is my hope this work will be helpful to the study of kimberlites.

# TABLE OF CONTENTS

**Appendix E: Additional geochemical and petrological data**

# LIST OF TABLES

# LIST OF FIGURES

# LIST OF SYMBOLS AND ABBREVIATIONS

| | |
|---|---|
| $^{o}$ | degree |
| $^{o}C$ | degrees Celcius |
| σ | standard deviation (sigma) |
| λ | decay constants (lambda) |
| *f* | fugacity |
| % | percent |
| ‰ | per-mille (or per-mil, parts per thousand) |
| δ | delta |
| µg | microgram |
| µl | microlitre |
| µm | micrometer |
| Å | angstroms |
| A | angular |
| AB | Aillik Bay |
| Al | aluminum |
| Am | Amazonia |
| amu | atomic mass units |
| Ar | argon |
| B | Baltica |
| Ba | barium |
| BC | Brent Crater |
| BK | Buckingham lavas |
| BM | Baie des Moutons |
| BSE | backscattered electron image |
| C | carbon |
| C | coarse (after Field and Scott Smith 1998) |
| Ca | calcium |
| CC | Callander complex |
| Ce | cerium |
| CG | Chatham-Grenville stock |
| CH | Chicoutimi |
| CIMP | Central Iapetus Magmatic Province |
| CK | coherent kimberlite |
| cm | centimetre |
| $cm^{-1}$ | wavenumber (Raman) |
| $CO_2$ | carbon dioxide |
| Cr | chromium |

| | |
|---|---|
| CRB | country rock breccia |
| CRX | country rock xenolith |
| CT | Catoctin Formation |
| *d* | interplanar spacing (XRD) |
| E | east |
| EDS | energy dispersive spectroscopy |
| EDX | Tracor Northern EDX spectrometer (Self and Buseck 1991) |
| EH | Eclipse Harbour |
| EPMA | electron probe microanalysis |
| EP-SEM | Extended Pressure mode - scanning electron microscope |
| ENE | east northeast |
| F | fine (after Field and Scott Smith 1998) |
| Fe | iron |
| FOV | field-of-view |
| Ga | billion years or giga-annums |
| GSZ | Great Slave Lake Shear zone |
| H/D | Hare Hill and Disappointment Hill |
| $H_2O$ | water |
| ha | hectare |
| HBr | hydrobromic acid |
| HCl | hydrochloric acid |
| HF | hydrofluoric acid |
| He | helium |
| HK | hypabyssal kimberlite |
| *hkl* | Miller indices (XRD) |
| HKt | transitional hypabyssal kimberlite |
| $HNO_3$ | nitric acid |
| $H_3PO_4$ | phosphoric acid |
| *I* | intensity (XRD) |
| ID-TIMS | isotope dilution – thermal ionization mass spectrometry |
| IDP | intermediate daughter product |
| Ilm | ilmenite |
| IR6 | Ice River perovskite IR6 |
| Kα | X-ray line for EPMA |
| K | potassium |
| ka | thousand years or kilo-annums |
| kas | kassite |
| kbar | kilobar |
| KI | Killinek Island |
| km | kilometre |

| | |
|---|---|
| KPK | Kimberley-type pyroclastic kimberlite |
| KPKt | transitional Kimberley-type pyroclastic kimberlite |
| kV | kilovolts |
| Lα | X-ray line for EPMA |
| Lβ | X-ray line for EPMA |
| L | lucasite-(Ce) |
| La | lanthanum |
| LA-ICP-MS | laser ablation inductively coupled plasma mass spectrometry |
| LIFH | lithium fluoride analytical crystal for EPMA |
| LIP | large igneous province |
| LM | Lac Matapedia |
| Ln | Laurentia |
| LOIB | Laurentien ocean island basalt (after Puffer 2002) |
| LREE | light rare earth element |
| LS | Lady Slipper pluton |
| m | metre |
| M | medium (after Field and Scott Smith 1998) |
| Ma | mega-annums or million years |
| mA | milliamps |
| mg | milligram |
| Mg | magnesium |
| MI | Manitou Island |
| ml | millilitre |
| mm | millimetre |
| MN | Maniitsoq |
| Mn | manganese |
| MoKα | excitation radiation (XRD) |
| MR | Mont Rigaud stock |
| MSA | Mt. St.Anselme |
| MSWD | mean square of weighted deviates |
| MVK | massive volcaniclastic kimberlite |
| Myr | million years |
| n | number |
| nA | nanoamps |
| Na | sodium |
| NAC | North Atlantic Craton |
| Nb | niobium |
| Nd | neodymium |
| nm | nanometres |
| NNE | north northeast |

| | |
|---|---|
| NNW | north northwest |
| NW | northwest |
| O | oxygen |
| P | phosphorus |
| Pb | lead |
| PDB | Pee Dee Belemnite |
| PET | pentaerythritol analytical crystal for EPMA |
| pg | picograms |
| PH | Pinney Hollow Formation |
| PPL | plane polarized light |
| ppm | parts per million |
| Pr | praseodymium |
| PR | Pound Ridge Granite Gneiss |
| R | round |
| Rb | rubidium |
| Re | rhenium |
| REE | rare earth elements |
| RG | Reading Prong dyke |
| Rn | radon |
| RP | Round Pond |
| S/H | Saglek and Hebron |
| SA | subangular |
| SC | Skinner Cove Formation |
| SE | southeast |
| SEM | secondary electron multiplier |
| SF | Sarfartoq |
| Si | silicon |
| SIMS | secondary ion mass spectrometry |
| Sm | samarium |
| Sr | strontium |
| SR | subround |
| SS | St. Simeon dykes |
| StH | St. Honoré carbonatite |
| STZ | Snowbird Tectonic zone |
| T/A | Torngat Mountains/Abloviak |
| $TaF_5$ | tantalum fluoride |
| TAP | thallium acid phthalate analytical crystal for EPMA |
| TEM | transmission electron microscopy |
| Th | thorium |
| Ti | titanium |

| | |
|---|---|
| TIMS | thermal ionization mass spectrometry |
| TK | tuffisitic kimberlite |
| TKB | tuffisitic kimberlite breccia |
| U | uranium |
| UML | ultramafic lamprophyre |
| USA | United States of America |
| V | vanadium |
| VC | very coarse (after Field and Scott Smith 1998) |
| VK | volcaniclastic kimberlite |
| VP-FESEM | Variable Pressure mode - field emission scanning electron microscope |
| VSMOW | Vienna Standard Mean Ocean Water |
| W | west |
| WDS | wavelength dispersive spectroscopy |
| wt.% | weight percent |
| Wt Avg | weighted average |
| XRD | X-ray diffraction |
| YG | Yonkers Gneiss |
| yr | year |
| $yr^{-1}$ | 1/year |
| ZAF | correction model for EPMA |

# CHAPTER 1
# INTRODUCTION

Kimberlites are rare, volatile ($H_2O$, $CO_2$) and carbonate-rich ultramafic magmas that ascend from deep (>150 km) within the mantle to form pipes, dykes or sills within Precambrian crust (Clifford 1966; Mitchell 1986; Janse 1994). Kimberlite magmas carry material (diamonds, crustal and mantle xenoliths), which is both vital to our learning about Earth's interior and economically important (Mitchell 1986). Nearly 7000 kimberlites have been found worldwide (de Wit et al. 2016) since first discovered in 1870 in South Africa (Kimberley; Lewis 1887) or possibly as early as 1837 in the USA (Syracuse, New York and Elliott County, Kentucky; Vanuxem 1842; Diller 1885, 1886; Williams 1887; Lewis 1897; Dawson 1980). Through the development of radiometric dating methods, we have learned that kimberlite magmas formed over the last ~2.8 billion years of Earth's history (e.g. Tappe et al. 2018) and not only during the Cretaceous as was initially believed (Holmes and Paneth 1936; Janse 1985). The first application of radiometric dating to kimberlites in South Africa also demonstrated that the diamonds and xenoliths (crustal and mantle) carried by kimberlite magmas can record significantly different ages from their host (e.g. Holmes and Paneth 1936; Lovering and Richards 1964; Kramers 1979). Temporal and spatial information on kimberlite intrusions and the advancement of several key theories throughout the 20$^{th}$ century, such as plate tectonics (e.g. Wilson 1963) and mantle plumes (Morgan 1971), shaped hypotheses for the geodynamic setting in which these rare magmas could be triggered to form repeatedly. These hypotheses include broad regions of kimberlite intrusions parallel to subducting oceanic lithosphere (e.g. McCandless 1999), narrow tracks of kimberlite clusters/fields generated by lithosphere moving over mantle plumes (e.g. Heaman and Kjarsgaard 2000) or scattered kimberlite intrusions in areas of intracontinental rifting (e.g. Moore et al. 2008).

An understudied kimberlite cluster in north-central Québec, the diamondiferous Renard cluster in the Otish field, is the focus of this thesis. Since its discovery in the Otish Mountains region in 2001, nine kimberlite bodies (Renard 1-10 with Renard 6 and Renard 5 combined into one body, Renard 65), two dyke systems (522±30 Ma Lynx and undated Hibou; McCandless et al. 2008) and a few kimberlite dykes (G04-296 Anomaly, North Anomaly, Southeast Anomaly) were

identified in this cluster (Godin et al. 2016). Renard 2, Renard 3 and Renard 65 form Québec's first diamond mine with commercial production since 2017. Included within the Otish field but south of the Renard cluster are two additional kimberlite occurrences; the Lac Beaver kimberlite (550.9±3.5 Ma; Girard 2001; Moorhead et al. 2003) and undated Adamantin kimberlites (Barnett and Laroulandie 2017). The Renard kimberlite pipes are modelled as South African style (Class 1) kimberlites with steep-sided diatreme to root zone pipes (Fitzgerald et al. 2009; Muntener and Scott Smith 2013; Godin et al. 2016; Muntener and Gaudet 2018; Lepine and Farrow 2018; Gaudet et al. 2018). The pipes comprise hypabyssal or coherent kimberlite to transitional to Kimberley-type pyroclastic kimberlite (formerly termed tuffisitic kimberlite) emplaced as one or more units (e.g. Skinner and Marsh 2004; Fitzgerald et al. 2009; Muntener and Scott Smith 2013; Godin et al. 2016; Muntener and Gaudet 2018). In addition, all Renard pipes include hypabyssal kimberlite dykes, irregular intrusions (cm- to tens of meters thick) or rare autoliths (e.g. Renard 9) occurring on a smaller scale (the 'c' unit described in Godin et al. 2016). Prior to this thesis only four U-Pb perovskite dates from three Renard kimberlite bodies were known and indicated that the Otish field records an unusually long span (~100 Myr) of kimberlite magmatism which partly coincides with the ~620-550 Ma rifting phase associated with the breakup of the Rodinia supercontinent (e.g. Cawood et al. 2001). The first date was determined from Renard 1 hypabyssal kimberlite material (631.6±3.5 Ma; Birkett et al. 2004). A composite emplacement date was then determined from a selection of main pipe-infilling units in Renard 2 and Renard 3 (640.5±2.8 Ma; Fitzgerald et al. 2009). Lastly, two U-Pb perovskite dates for Renard 2 (655.8±6.0 Ma) and Renard 3 (653.8±5.9 Ma) using hypabyssal kimberlite were determined by SIMS (Tappe et al. 2017). The reported U-Pb perovskite dates showed that determining the age of the Renard pipes (e.g. ~641 Ma or ~656 Ma for Renard 2; Fitzgerald et al. 2009; Tappe et al. 2017) was more complex than typically reported for kimberlites which opened questions about the kimberlite rock type used for dating and/or analytical method.

Although many advances have been made to understanding the timing of kimberlite intrusions found across North America, such a long duration recorded by the Otish field is not typical. The Renard pipes are one of Canada's known Class 1 kimberlites (pipes filled with Kimberley-type pyroclastic kimberlite; e.g. Gahcho Kué, undated Camsell Lake, Aviat, Qilalugaq) of which many were emplaced during the Neoproterozoic but comparison is difficult due to sparse or

absent sampling details (Hetman 2008; Scott Smith 2008; Scott Smith et al. 2013; see Supplementary Material 1 for Chapter 3 in Appendix C). The level of detail available from petrology studies for the internal pipe geology of the Renard kimberlites allowed for investigation of different types of kimberlite present (e.g. Kimb2a, Kimb2b and Kimb2c units in Renard 2). The choice of isotopic method to date the Renard kimberlites was constrained by the suitability of the primary groundmass minerals in the available samples. Although several isotopic techniques are used to date kimberlites (e.g. Rb-Sr phlogopite, K-Ar or Ar-Ar phlogopite, U-Th/He perovskite or U-Pb perovskite by TIMS, LA-ICP-MS or SIMS), ID-TIMS U-Pb groundmass perovskite was chosen due to the availability of perovskite and the tiny size of the crystals. For instance, perovskite crystals could range up to <~70 μm but more commonly were <40 μm and phlogopite was often altered (partially to completely) and tiny (e.g. lesser amounts of macrocryst- or phenocryst-sized phlogopite compared to groundmass-sized laths). Furthermore, several studies on North American kimberlite clusters/fields have shown ID-TIMS U-Pb perovskite to be a reliable method for dating kimberlites and characterized by smaller uncertainties which would enable the resolution of age differences within the same field (e.g. 75-45 Ma Lac de Gras, 115-92 Ma Saskatchewan-Somerset Island, 155-134 Ma Timiskaming, 157-139 Ma Chidliak, 165-152 Ma Kirkland Lake, 180-156 Ma Attawapiskat, and 225-170 Ma Churchill; Heaman 1989; Heaman and Kjarsgaard 2000; Zurevinski et al. 2008; Heaman et al. 2015; Sarkar et al. 2015a; Kjarsgaard et al. 2017).

The objectives of this thesis were to investigate the timing of the Renard kimberlites and evaluate the connection between timing of Renard kimberlite emplacement with the temporal and spatial relationship of nearby intrusions related to the breakup of the Rodinia supercontinent. The results of this investigation are presented as follows:

- Chapter 2 examines the detailed geochronology of a single kimberlite pipe (Renard 2). The timing of smaller hypabyssal kimberlite units yielded an unexpected span of at least ~20 Myr (652–632 Ma). This broad span is contrary to the belief that entire kimberlite bodies are emplaced in <1-2 Ma and challenges the practice of selecting only hypabyssal kimberlite samples to determine a representative pipe age (e.g. Allsopp et al. 1989). This chapter has been published as a journal paper in the 11$^{th}$ International Kimberlite Volume: Ranger IM,

Heaman LM, Pearson DG, Muntener C, Zhuk V (2018) Punctuated, long-lived emplacement history of the Renard 2 kimberlite, Canada, revealed by new high precision U-Pb groundmass perovskite dating. Mineralogy and Petrology 112 (Suppl 2):S639-S651. A portion of Chapter 2 was reported in the 11th IKC long abstract: Ranger IM, Heaman LM, Pearson DG, Laroulandie C, Lepine I, Zhuk V (2017) Punctuated, long-lived emplacement history of kimberlites from the Renard cluster, Superior Province, Canada indicated by new high precision U-Pb groundmass perovskite dating. 11th International Kimberlite Conference Extended Abstract No. 11IKC-4493: 3p.

- Chapter 3 applies the findings of a protracted kimberlite emplacement history recorded in a single kimberlite pipe (Renard 2) presented in Chapter 2 to evaluate the emplacement history within other pipes in the Renard cluster. This chapter demonstrates how kimberlite pipes can hold a significant amount of information in the smaller hypabyssal kimberlite intrusions that were previously overlooked. New U-Pb perovskite dates show an overlapping relationship with nearby felsic and mafic intrusions, alkaline-carbonatite intrusions and igneous provinces in both Laurentia and Baltica.

- Chapter 4 reports the first occurrence of the rare mineral kassite in a hypabyssal kimberlite sample from the Renard 9 pipe. The geochemistry and U-Pb geochronology of kassite is presented here.

- Chapter 5 summarizes the major conclusions which provide a new perspective towards determining the timing of kimberlite pipe emplacement and interpretation with the surrounding regional geology.

# CHAPTER 2

# PUNCTUATED, LONG-LIVED EMPLACEMENT HISTORY OF THE RENARD 2 KIMBERLITE, CANADA, REVEALED BY NEW HIGH PRECISION U-Pb GROUNDMAS PEROVSKITE DATING


## Abstract

Kimberlites are rare volatile-rich ultramafic magmas thought to erupt in short periods of time (<1 Ma) but there is a growing body of evidence that the emplacement history of a kimberlite can be significantly more protracted. In this study we report a detailed geochronology investigation of a single kimberlite pipe from the Renard cluster in north-central Québec. Ten new high precision ID-TIMS U-Pb groundmass perovskite dates from the main pipe-infilling kimberlites and several small hypabyssal kimberlites from the Renard 2 pipe indicate kimberlite magmatism lasted at least ~20 Myr. Two samples of the main pipe-infilling kimberlites yield identical weighted mean $^{206}Pb/^{238}U$ perovskite dates with a composite date of 643.8 ± 1.0 Ma, interpreted to be the best estimate for main pipe emplacement. In contrast, six hypabyssal kimberlite samples yielded a range of weighted mean $^{206}Pb/^{238}U$ perovskite dates between ~652-632 Ma. Multiple dates determined from these early-, syn- and late-stage small hypabyssal kimberlites in the Renard 2 pipe demonstrate this rock type (commonly used to date kimberlites) help to constrain the duration of kimberlite intrusion history within a pipe but do not necessarily reliably record the emplacement age of the main diatreme in the Renard cluster. Our results provide the first robust geochronological data on a single kimberlite that confirms the field relationships initially observed by Wagner (1914) and Clement (1982); the presence of antecedent (diatreme precursor) intrusions, contemporaneous (syn-diatreme) intrusions, and consequent (post-diatreme) cross-cutting intrusions. The results of this detailed U-Pb geochronology study indicate a single kimberlite pipe can record millions of years of magmatism, much longer than previously thought from the classical viewpoint of a rapid and short-duration emplacement history.

## Introduction

Kimberlites are rare volcanic rocks with an ultramafic composition rich in volatiles ($H_2O$, $CO_2$) first discovered in South Africa in the late 1800's and best-known for transporting diamonds from the mantle (e.g. Mitchell 1986). Originating from >150 km deep within the Earth's mantle, the mechanism triggering their generation has long been debated with hypotheses ranging from mantle plumes to subduction to rifting (e.g. McCandless 1999; Heaman and Kjarsgaard 2000; Moore et al. 2008). Kimberlite magmas are thought to ascend rapidly (seconds to months) (e.g. Canil and Fedortchouk 1999; Sparks et al. 2006; Wilson and Head 2007) and the notion of a single short-lived diatreme-filling event has long been inferred (e.g. Wagner 1914; Field and Scott Smith 1999). Thus it has become common practice in kimberlite geochronology to determine one date per intrusive body (per chronometer/mineral) and assume that this accurately constrains the entire pipe emplacement history. This assumption is certainly valid in cases where high precision geochronology on multiple samples from a single kimberlite have identical ages, as documented by the identical ID-TIMS U-Pb perovskite dates (weighted mean $^{206}Pb/^{238}U$ date of 155.8 ± 0.6 Ma) from four C14 diatreme samples in the Kirkland Lake field (Heaman and Kjarsgaard 2000). In contrast, a few detailed dating studies indicate that the ages obtained for multiple samples from the same kimberlite pipe can differ significantly. For example, a recent study of the Orion South body in the Fort à la Corne field records a protracted emplacement history of ~8 Myr (103.2 ± 2.4 to 95.5 ± 2.6 Ma, TIMS U-Pb perovskite; Kjarsgaard et al. 2017) and three independent LA-ICPMS U-Pb perovskite dates from the Finsch kimberlite vary by nearly 40 Myr (90–126 Ma; Griffin et al. 2014 and references therein).

Perovskite is typically a primary groundmass mineral crystallizing directly from kimberlite magma. Despite the fact that perovskite is a rare mineral in the crust, and there is a low probability that it could be derived from crustal contamination, there are a few examples of multiple perovskite age components in a single kimberlite sample (e.g. Elliott County kimberlite; Heaman et al. 2004). One interpretation of this age range is that some kimberlites contain xenocrystic perovskite which crystallised from a precursor kimberlite event significantly before the main eruptive body (e.g. Heaman and Kjarsgaard 2000; Heaman et al. 2004; Zurevinski et al. 2008). There are relatively few extensive high-precision dating studies of kimberlite clusters or

fields and, of those conducted in North America, most indicate that the duration of magmatism within a field can vary substantially between ~13-55 Ma (e.g. 75–45 Ma Lac de Gras, 115–92 Ma Saskatchewan-Somerset Island, 155–134 Ma Timiskaming, 157–139 Ma Chidliak, 165–152 Ma Kirkland Lake, 180–156 Ma Attawapiskat, and 225–170 Ma Churchill; Heaman and Kjarsgaard 2000; Zurevinski et al. 2008; Heaman et al. 2015; Sarkar et al. 2015a; Kjarsgaard et al. 2017). These studies form a growing body of work that indicates kimberlite magmatism within individual clusters and fields is protracted (>10 Myr).

Previous geological and geochronological studies of the Renard kimberlites (north-central Québec) have shown that within individual pipes there are multiple kimberlite phases, cross-cutting relationships, and a range of U-Pb perovskite dates (e.g. Birkett et al. 2004; Fitzgerald et al. 2009; Muntener and Scott Smith 2013; Tappe et al. 2017; Muntener and Gaudet 2018). To examine this apparent geological complexity in more detail, we present ten new high precision (±1–3 Ma 2σ) ID-TIMS U-Pb groundmass perovskite dates for the various kimberlite phases identified in the Renard 2 pipe. These results provide unprecedented insight into the emplacement history of a single kimberlite pipe.

## Geological background

## Geologic setting

The Otish kimberlite field occurs near the Otish Mountains region in north-central Québec (Figure 2.1). This kimberlite field intrudes the Archean Superior Province, specifically the Opinaca Subprovince, which is an ENE-trending belt dominated by high-grade (amphibolite- to granulite-facies) metagreywacke, mafic volcanics, migmatitic paragneiss, granite and pegmatite (Card and Poulsen 1998; Percival et al. 2012), cross-cut by a number of Proterozoic mafic dyke swarms (e.g. NW-trending 2510–2500 Ma Mistassini dyke swarm; Fahrig et al. 1986; Heaman 2004) and NNE-trending faults and lineaments of the Mistassini-Lemoyne Tectonic Zone (Moorhead et al. 2003). Several kimberlite magmas, with emplacement times spanning nearly 1 billion years, have intruded the eastern Superior Province. The kimberlites occur locally as sets of dykes (e.g. ~1100 Ma Bachelor Lake dykes in the Desmaraisville field intersected only in drill

core; Watson 1967; Alibert and Albarede 1988; Heaman et al. 2004), sets of thin (<1.2-m-thick) sills (e.g. ~629 Ma Wemindji sills; Letendre et al. 2003; Zurevinski and Mitchell 2011), and a few clusters/fields of kimberlite pipes (e.g. 180–156 Ma Attawapiskat cluster and 165–134 Ma Kirkland Lake/Timiskaming fields; Kong et al. 1999; Heaman and Kjarsgaard 2000).

A kimberlite cluster in the Otish field that has received significant attention is the diamondiferous Neoproterozoic Renard cluster (Figure 2.1). First discovered in 2001 by the Ashton Mining of Canada Inc. and SOQUEM Inc. joint venture (Foxtrot property), continued exploration in the following five years discovered nine kimberlite bodies (named Renard 1 to Renard 10 with Renard 6 and Renard 5 combined into one body (Renard 65)), two dyke systems (Lynx and Hibou) and several kimberlite dykes (G04–296, North Anomaly, Southeast Anomaly). The surface areas of the Renard kimberlites range between 0.3 and 3.1 ha and were emplaced along a ~2-km-long NNW-trending lineament (Godin et al. 2016). Within the Otish field but ~90 km south of the Renard cluster is the ~551 Ma Lac Beaver kimberlite (Girard 2001; Moorhead et al. 2003) and ~100 km to the south are the undated Adamantin kimberlites (Barnett and Laroulandie 2017).

## Renard kimberlite cluster

Birkett et al. (2004) published the first petrological work on the Renard bodies with subsequent detailed studies of the internal geology of the Renard 2 (Fitzgerald et al. 2009; Lepine and Zhuk 2017; Lepine and Farrow 2018; Muntener and Gaudet 2018), Renard 3 (Muntener and Scott Smith 2013) and Renard 65 (Gaudet et al. 2017) pipes. Recent geological descriptions of the remaining seven kimberlite bodies are summarized by Godin et al. (2016). The potential complexity in the intrusion history of the Renard pipes is highlighted in the detailed study of the Renard 3 pipe by Muntener and Scott Smith (2013), who recognize at least eight kimberlite emplacement stages based on petrology, textures and crosscutting relationships. Based on the pipe shape and internal geology, the Renard kimberlites are considered Class 1 kimberlite pipes (Fitzgerald et al. 2009; Muntener and Scott Smith 2013), comparable to those from the Kimberley area in South Africa (Skinner and Marsh 2004). Generally, most of the steep-sided diatreme (to root zone) pipes consist of one or more main pipe-infilling units ranging from HK or

CK (hypabyssal or coherent kimberlite, respectively) to transitional to KPK (Kimberley-type pyroclastic kimberlite) (e.g. Godin et al. 2016; Muntener and Gaudet 2018). The terminology used to describe the main pipe-infilling kimberlite rock types for the Renard kimberlites has evolved over the years based on literature at the time: it has been described as olivine macrocrystic material or hypabyssal and kimberlitic breccia or TKB (tuffisitic kimberlite breccia) (Birkett et al. 2004), MVK (massive volcaniclastic kimberlite) classified texturally as TKB and CK (Fitzgerald et al. 2009), VK (volcaniclastic kimberlite) classified texturally as TK (tuffisitic kimberlite) and CK classified as HK for both large and small volumes of hypabyssal kimberlite after Field and Scott Smith (1998) and Hetman et al. (2004) (Muntener and Scott Smith 2013), and MVK for TK textures and CK for large volumes of HK texture whereas the HK term was reserved for smaller volumes of this rock type (Godin et al. 2016). More recently, the term KPK was introduced (Zhuk et al. 2017; Muntener and Gaudet 2018) for TK textures following Scott Smith et al. (2013). There are two types of coherent kimberlite texturally classified as hypabyssal kimberlite occurring at Renard; those which occur as large main pipe-infilling units (referred to as CK in Godin et al. 2016) and those which are smaller, such as dykes or irregular intrusions (cm- to tens of meters thick) or as rare autoliths (noted in some pipes such as Renard 9 as <1 meter and referred to as HK in Godin et al. 2016), whose relationship to the kimberlite of which they are entrained in are not well studied. The smaller hypabyssal kimberlites are common to all the Renard pipes and identified by a geological unit code ending in the letter ‘c’ (e.g. Kimb2c for Renard 2). These small hypabyssal kimberlite units are found within the main pipe-infilling units, along the contacts between different pipe infilling units, along the pipe margin, and/or within the marginal country rock breccia, cracked country rock and/or surrounding country rock.

Renard 2 is the third largest kimberlite body in the cluster and is a steep-sided lower diatreme zone pipe comprised of two main pipe-infilling units (Kimb2a and Kimb2b; Fitzgerald et al. 2009; Godin et al. 2016; Lepine and Farrow 2018; Muntener and Gaudet 2018). Kimb2a (previously termed blue MVK) is a blue to blue-green KPK and is mineralogically classified as a phlogopite kimberlite (e.g. Fitzgerald et al. 2009; Godin et al. 2016; Muntener and Gaudet 2018). Kimb2b (previously termed brown CK) is a brown HK with textures transitional to HKt and minor KPKt (‘t’ for transitional) and is mineralogically classified as monticellite phlogopite

kimberlite (e.g. Fitzgerald et al. 2009; Godin et al. 2016; Muntener and Gaudet 2018). Dark green to black macrocrystic hypabyssal kimberlite (Kimb2c) dykes and irregular intrusions (and autoliths and xenoliths) occur throughout the pipe, marginal country rock breccia and cracked country rock and are comprised of phlogopite- or rare monticellite-dominant groundmass mineralogies (e.g. Lepine and Zhuk 2017). Many of these hypabyssal kimberlite dykes and irregular intrusions are interpreted as late-stage and emplaced after the intrusion of the main pipe-infilling units (Fitzgerald et al. 2009; Lepine and Zhuk 2017; Muntener and Gaudet 2018).

## Previous Renard geochronology

Two ID-TIMS U-Pb perovskite dates from three Renard kimberlites were reported prior to this study: a weighted mean $^{206}Pb/^{238}U$ date of 631.6 ± 3.5 Ma from Renard 1 hypabyssal material (Birkett et al. 2004) and a composite emplacement date of 640.5 ± 2.8 Ma determined from a selection of main pipe-infilling units in Renard 2 and Renard 3 (Fitzgerald et al. 2009). The details of these published U-Pb dates were not reported so we have included the individual perovskite analyses in Table 2.1 here and updated them with the same data reduction protocol as used in the current study. For the Renard 1 sample (13900) reported in Table 2.1, four perovskite fractions in total were analyzed yielding a relatively large range in $^{206}Pb/^{238}U$ dates between ~629-654 Ma. The weighted mean $^{206}Pb/^{238}U$ date for the three youngest fractions (#1, 3, 4) is 631.8 ± 2.6 Ma, very similar to the date reported by Birkett et al. (2004). These three fractions are representative of the main perovskite population consisting of dark brown, subhedral, tiny (20–40 μm) cubes and octahedrons. The oldest ~654 Ma perovskite fraction (#2) consisted of a distinct population of polycrystalline glomerocrysts, with slightly higher U content and Th/U (Table 2.1), interpreted to represent early formed perovskite cumulates, similar to those previously described from the Solane kimberlite, Lesotho (Nixon 1973).

These first perovskite age results reported for a single Renard 1 kimberlite sample (Birkett et al. 2004; details presented in Table 2.1 and Figure 2.2) illustrates the potential complexity in U-Pb dating kimberlites in the Otish field and provided the impetus to conduct a more detailed geochronology study here. In 2004, the Renard bodies were not yet defined into major geological units such as outlined by Godin et al. (2016). Therefore, the geological context of the

Renard 1 hypabyssal kimberlite sample to the main pipe-infilling units may have been unknown but Fitzgerald et al. (2009) and Patterson et al. (2009) both describe the Renard 1 material used for dating to be 'HK dykes' and 'hypabyssal dyke cutting the Renard 1 pipe', respectively.

The U-Pb results for a single perovskite fraction isolated from three different pipe-infilling units were summarized by Fitzgerald et al. (2009); two from Renard 2 and one from Renard 3. From Renard 2, the single $^{206}Pb/^{238}U$ dates of 638.0 ± 2.4 Ma (Kimb2a) and 642.6 ± 4.0 Ma (Kimb2b) (Table 2.1) are within error of the composite date reported by Fitzgerald et al. (2009). Recently, SIMS weighted mean $^{206}Pb/^{238}U$ perovskite dates were reported for Renard 2 (655.8 ± 6.0 Ma) and Renard 3 (653.8 ± 5.9 Ma) hypabyssal kimberlites (Tappe et al. 2017) and interpreted as the emplacement age for each pipe. This conclusion seems premature in the light of our new data, which highlight an unexplained age complexity in the Renard 2 pipe. Specifically, different kimberlite rock units from the same pipe have different emplacement dates of 639 ± 2 Ma and 656 ± 6 Ma (Fitzgerald et al. 2009 recalculated here; Tappe et al. 2017) or there is an unexplained discrepancy between the U-Pb ID-TIMS and SIMS perovskite dating methods, further highlighting the need for a more detailed geochronology of the Renard 2 pipe.

## Analytical methods

Renard 2 samples were collected from drill core provided by Stornoway Diamond Corporation. Thin sections were used to aid in selecting samples with groundmass perovskite. Samples were sawed and hammered into chips prior to milling in a tungsten carbide puck mill. Heavy minerals were concentrated using a Wilfley Table and magnetic minerals removed by hand magnet. Perovskite fractions were handpicked using a stereomicroscope. Where possible, crystals with visible alteration and/or mineral inclusions were avoided during grain selection. Perovskite morphology is summarized in the Results section.

The ID-TIMS U-Pb method followed the protocol for dissolution and HBr chemistry similar to Heaman et al. (2015) and detailed in Table 2.1 footnotes. The selected fractions were rinsed with Millipore ($H_2O$) and distilled acetone prior to cleaning with 2 N $HNO_3$ for ~1–2 hours at ~80 °C, followed by multiple rinses with Millipore and distilled acetone, weighed with a Mettler

UMT2 ultramicrobalance, and placed into Savillex dissolution capsules. Crystals were dissolved in a mixture of 48% HF:7 N $HNO_3$ (50:50) and a measured amount of $^{205}Pb$-$^{235}U$ tracer solution on a hotplate at ~110 °C for a minimum of 4 days. The combined purified uranium and lead aliquots were re-dissolved in a 4 µl mixture (1:99) of silicic acid and 0.05 N $H_3PO_4$ and loaded onto a single outgassed rhenium (Re) filament. Isotopic compositions of Pb and U were measured using a VG354 thermal ionization mass spectrometer operated in single Daly detector mode and a Thermo Triton Plus multi-collector thermal ionization mass spectrometer operated in multi-collector Faraday or single ion counter SEM detector mode. Details of the long-term performance of this analyser system along with reference material measurements are given in Sarkar et al. (2015b). Between 180-300 ratios of Pb and U isotopic data were collected sequentially at three (Pb) and two (U) temperature intervals: ~1170-1350 °C and ~1300-1410 °C, respectively. The U-Pb fraction information reported in Table 2.1 were calculated using YourLab (Schmitz and Schoene 2007). All U-Pb analyses were corrected for spike addition, assumed blank (5 pg Pb, 1 pg U), and initial excess/deficit of intermediate daughter element $^{230}Th$. A Th/U magma ratio of 5 was assumed for the initial kimberlite magma for this calculation following the rationale outlined in Heaman et al. (2015). The Renard 2 results indicate a model Th/U ratio for perovskite ranging between ~7-16 with two fractions as high as ~26, but adjusting the Th/U magma ratio to 1, 15 or even 30 produced only a minor correction to the $^{206}Pb/^{238}U$ date (~ < 0.1–0.3%). A correction for mass fractionation and detector bias (Faraday-SEM or -Daly) was determined using the NBS 981 and U500 standards; VG354 (Pb – 0.101%/amu ± 0.024%, U – 0.108%/amu ± 0.014%; Daly detector bias Pb – 0.239%/amu and U – 0.338%/amu) and Thermo Triton Plus (Pb – 0.090%/amu ± 0.037%, U – 0.104%/amu ± 0.043%; SEM detector bias Pb – 0.081%/ amu and U – 0.085%/amu or Pb – 0.079%/amu and U – 0.168%/amu). The Stacey and Kramers (1975) two-stage model for terrestrial lead evolution was used to estimate the isotopic composition of the initial common lead. Decay constants were taken from Jaffey et al. (1971) ($\lambda^{238}U = 1.55125 \times 10^{-10}$ yr$^{-1}$; $\lambda^{235}U = 9.84850 \times 10^{-10}$ yr$^{-1}$). Age uncertainties reported throughout the text, Table 2.1 and Figure 2.3 are reported at 2σ. Weighted mean $^{206}Pb/^{238}U$ dates and 2σ age uncertainties were calculated using Isoplot 4.15 (Ludwig 2012). Fragments of the Ice River perovskite reference material (IR6) were repeatedly analyzed to monitor accuracy. Reported TIMS weighted mean $^{206}Pb/^{238}U$ dates for this Ice River perovskite crystal using the Stacey and Kramers (1975) two-stage terrestrial model to correct for

the presence of initial common lead are 356.5 ± 1.0 Ma (2σ; MSWD = 2.1; n = 8; Heaman 2009) and 357.2 ± 0.3 Ma (2σ; MSWD = 0.66; n = 6; Burgess et al. 2012). Excluding three IR6 fragments that yielded outlier or poor results, the remaining 23 fragments weighing between ~5 and 69 µg analyzed throughout this study yielded $^{206}Pb/^{238}U$ dates between 351.7 ± 1.3 Ma (5.8 µg) to 359.1 ± 1.1 Ma (19.3 µg) and a weighted mean $^{206}Pb/^{238}U$ date of 356.7± 0.3 Ma (2σ; MSWD= 15) within uncertainty of the previously recommended value by Heaman (2009).

## Results

Ten new ID-TIMS U-Pb perovskite dates from a detailed investigation of the timing of the main pipe-infilling units and small hypabyssal kimberlites from the Renard 2 kimberlite are reported here in Table 2.1 and Figure 2.3. Perovskite crystals were dark brown to brown-black in colour with cubic to cuboctahedral habit with the exception of two types observed in the main pipe-infilling units: dark brown-black cubic (Kimb2a, 38925-3 and -4) to cubic-cuboctahedral (Kimb2b, 38927-1 and -4) and anhedral-subhedral crystals (present in both units; 38925-2 and 38927-5). Crystal habit was slightly more difficult to assess in Kimb2c samples 38906 and 38929 but generally appeared similar to other Kimb2c samples yet with more anhedral-subhedral crystals. Perovskite fractions consisted of ~90 to 410 crystals (typically ~100–200 crystals) varying in size between ~30-70 µm (majority <40 µm) and weighing ~8–28 µg. Crystals <30 µm were difficult to positively identify with a stereomicroscope and were generally avoided. An exception is fraction 38903-2 which consisted of ~20–30 µm crystals.

Two samples were investigated from the main pipe infilling units (Kimb2a, 38925; Kimb2b, 38927). A weighted mean $^{206}Pb/^{238}U$ date of 644.7 ± 1.4 Ma (MSWD = 5.1) was obtained using all three perovskite fractions analyzed from a Kimb2a sample (38925). The anhedral-subhedral perovskite in fraction 38925-2 record a single $^{206}Pb/^{238}U$ date of 647.6 ± 2.3 Ma with a slightly lower Th/U value of 14 compared with two fractions of cubic crystals and suggests these perovskite are likely xenocrystic. Excluding fraction 38925-2 yields a weighted mean $^{206}Pb/^{238}U$ date of 643.1 ± 1.7 Ma (MSWD = 0.01) for Kimb2a (38925). All three perovskite fractions from a Kimb2b sample (38927) yield a similar weighted mean $^{206}Pb/^{238}U$ date of 644.2 ± 1.3 Ma (MSWD = 0.25). Since these two dates are indistinguishable, the combined results yield a

composite weighted mean $^{206}Pb/^{238}U$ date of 643.8 ± 1.0 Ma (MSWD = 0.41; n = 5) and is interpreted as the best estimate for the timing of the Renard 2 pipe-forming event.

Weighted mean $^{206}Pb/^{238}U$ dates from eight Renard 2 hypabyssal kimberlites span at least ~20 Myr and are designated Kimb2c in Table 2.1. Three types of perovskite age patterns can be discerned; (1) those where $^{206}Pb/^{238}U$ dates for all analyzed fractions agree within analytical error and hence can be interpreted as representing reliable estimates for the emplacement age, (2) those where the dates obtained for at least two perovskite fractions agree but other fractions have dates that disagree, and (3) those where there is a significant discrepancy in the dates obtained for all fractions.

*Perovskite age pattern 1:* The oldest weighted mean $^{206}Pb/^{238}U$ dates (~652–646 Ma) were determined from five hypabyssal kimberlites; 652.2 ± 1.3 Ma (38928), 650.1 ± 1.5 Ma (38903), 650.1 ± 1.6 Ma (38916), 647.8 ± 1.3 Ma (38923), 646.3 ± 1.4 Ma (38926). Fraction 38926-1 has a younger discordant $^{206}Pb/^{238}U$ date of 555.5 ± 2.4 Ma, as compared to two fractions that produced a weighted mean $^{206}Pb/^{238}U$ date of 646.3 ± 1.4 Ma, indicating that lead-loss occurred resulting in a younger date. The youngest weighted mean $^{206}Pb/^{238}U$ date of 631.8 ± 1.4 Ma (MSWD= 0.92) was determined from one hypabyssal kimberlite sample (38901), similar to the date of 632 Ma reported by Birkett et al. (2004) for a Renard 1 hypabyssal kimberlite sample.

*Perovskite age pattern 2:* Sample 38906 records a weighted mean $^{206}Pb/^{238}U$ date of 643.9 ± 1.5 Ma from two younger fractions, nearly identical to the main pipe-infilling units Kimb2a and Kimb2b, and a single $^{206}Pb/^{238}U$ date of 650.5 ± 2.3 Ma indicating the presence of slightly older xenocrystic perovskite.

*Perovskite age pattern 3:* Multiple single $^{206}Pb/^{238}U$ dates were determined from sample 38929 (622.9 ± 2.0 Ma, 638.9 ± 1.8 Ma and 649.7 ± 2.5 Ma) from perovskites with similar U and Pb concentrations and similar Th/U values. Although the two older single fraction dates overlap reliable dates obtained for other Kimb2c samples in this study, caution is required when interpreting these data due to the lack of consistency between dates. Two possible interpretations can be considered; 1) the range of dates reflect mixing between two or more

unknown perovskite age components (preferred here), or 2) the younger ~623 Ma date is the date of the sample and the two older dates are from xenocrystic perovskite.

## Discussion

## Overview

The ID-TIMS U-Pb perovskite dating method has become a cornerstone in constraining the timing of kimberlite emplacement because perovskite is a common groundmass mineral that crystallizes directly from the magma (Heaman 1989; Heaman and Kjarsgaard 2000; Heaman et al. 2015) and relatively precise (±1–3 Ma) dates can be determined. Furthermore, most crustal rocks do not contain perovskite so, despite the fact kimberlites can entrain a significant amount of crustal (and mantle) material during transport, the probability of kimberlite magmas entraining xenocrystic perovskite is low. We have conducted a detailed U-Pb perovskite geochronology study of the Renard 2 kimberlite to investigate whether there is a protracted emplacement history, as hinted by previous U-Pb perovskite dates for the same kimberlite body that disagree by ~15 Myr (Fitzgerald et al. 2009; Tappe et al. 2017). This emplacement history is speculated in Figure 2.4 with early-, syn- and late-stage hypabyssal kimberlites in relation to eruption of the main diatreme. For all Renard 2 kimberlite samples investigated in this study, we have analyzed multiple perovskite fractions per sample to test for age complexity. To confidently identify a robust crystallization date requires excellent agreement between two or more multi-grain perovskite fractions.

## U-Pb perovskite ages from early-stage HK

Published studies from the Renard cluster have pointed out the presence of kimberlite autoliths in several Renard pipes. For example, Fitzgerald et al. (2009) observed the presence of rare hypabyssal kimberlite autoliths in the country rock breccia adjacent the Renard 2 diatreme. Muntener and Scott Smith (2013) observed that three main pipe-infilling units from Renard 3

(Kimb3b, Kimb3f and Kimb3g) contained occasional to common autoliths. Godin et al. (2016) described autoliths to be present in four of the Renard pipes (Renard 3, 4, 65 and 9).

In this study, samples of hypabyssal kimberlite (apparent thicknesses ranging from ~2 to 23 m) were randomly selected from three drill holes. The majority of these Renard 2 samples yield new U-Pb perovskite dates that are older (~652–648 Ma; 38903, 38916 collected near the pipe margin, 38923, and 38928) than the 643.8 ± 1.0 Ma main pipe infilling intrusions and these early-stage hypabyssal kimberlites are interpreted to represent xenolithic remnants from earlier intrusions (as shown in Figure 2.4a and b). Note that there is some uncertainty in classifying sample 38923 and, although we have grouped it with the Kimb2c units, it is possibly from a Kimb2b unit and additional study is needed to confirm this.

These early-stage hypabyssal kimberlites investigated in this study have dates that are slightly younger than but comparable to the less precise SIMS U-Pb date of 655.8 ± 6.0 Ma determined by Tappe et al. (2017). The $^{206}Pb/^{238}U$ date of 647.6 ± 2.3 Ma from one fraction (38925–2; Kimb2a) of dark brown-black anhedral-subhedral (likely xenocrystic) perovskite crystals and older single $^{206}Pb/^{238}U$ dates from hypabyssal kimberlite samples 38906 and 38929 all support the presence of earlier kimberlite intrusions that predate the main pipe infilling event. Field relationships of Kimb2c units, including the samples in this study, can be difficult to confidently assess from drill core. Perhaps as larger face exposures of the kimberlite become available through mine development, the full extent of single Kimb2c occurrences can be observed to assess if their morphology resembles large xenoliths.

## U-Pb perovskite ages from the Renard 2 main pipe-infilling units

The Renard 2 pipe largely consists of two main pipe-infilling KPK units denoted Kimb2a and Kimb2b (e.g. Muntener and Gaudet 2018). We have obtained independent U-Pb perovskite dates for each unit that overlap within analytical uncertainty (weighted mean $^{206}Pb/^{238}U$ date of 643.1 ± 1.7 Ma for Kimb2a and 644.2 ± 1.3 Ma for Kimb2b). Since these two dates are indistinguishable, we combined the results and obtained a composite weighted mean $^{206}Pb/^{238}U$ date of 643.8 ± 1.0 Ma (MSWD= 0.41) that we interpret as the best estimate for emplacement

time of the main Renard 2 pipe (as shown in Figure 2.4b). It supercedes the previous Renard 2 ID-TIMS U-Pb perovskite date reported by Fitzgerald et al. (2009) but is entirely consistent with their Kimb2b date of 642.6 ± 4.0 Ma based on a single perovskite fraction (fraction 2110MM-1 recalculated in Table 2.1). It is distinctly younger than the 655.8 ± 6.0 Ma SIMS U-Pb perovskite date from a hypabyssal kimberlite sample reported by Tappe et al. (2017) that they interpreted to be the age of the pipe. The 2σ analytical uncertainty of one hypabyssal kimberlite sample (38926), with a weighted mean $^{206}Pb/^{238}U$ date of 646.3± 1.4 Ma, is nearly within error of the main pipe-infilling units. One hypabyssal kimberlite sample (38906), collected near the pipe margin, yielded a weighted mean $^{206}Pb/^{238}U$ date of 643.9 ± 1.5 Ma which is simultaneous with the main pipe-forming event.

## U-Pb perovskite ages from late-stage HK

The youngest weighted mean $^{206}Pb/^{238}U$ date of 631.8 ± 1.4 Ma (MSWD= 0.92) was determined from a hypabyssal kimberlite (38901) collected between the two main pipe-infilling units. This date is clearly younger than the 643.8 ± 1.0 Ma main pipe-infilling units confirming the field observation of cross-cutting late-stage hypabyssal kimberlite (as shown in Figure 2.4c). It is interesting that the emplacement of this late-stage hypabyssal kimberlite at Renard 2 coincides with the weighted mean $^{206}Pb/^{238}U$ date of 631.6 ± 3.5 Ma for Renard 1 published by Birkett et al. (2004), raising the possibility that the main pipe emplacement at Renard 1 is older than this. A single $^{206}Pb/^{238}U$ perovskite date of 622.9±2.0 Ma from sample 38929 indicates the possible existence of even younger hypabyssal kimberlite intrusions in the Renard cluster, which has been observed within the Otish field from the Lynx dyke system and Lac Beaver kimberlite (Figure 2.2 and references therein).

## Multiple U-Pb perovskite dates from single HK samples

Multiple dates from samples 38906 and 38929, collected near and on the pipe margin respectively, demonstrate the complexity that can be recorded within a single hypabyssal kimberlite sample. This clearly indicates that caution is needed when interpreting dates from some samples within the Renard cluster where only a single date is available. This conclusion

can be extended to any kimberlite characterized by a single emplacement age determination. Indeed, microsampling isotopic studies (Malarkey et al. 2010) have highlighted the complexity in Sr isotope compositions across the spectrum of kimberlite groundmass minerals that indicate a diachroneity of crystallization times and the possibility of inherited signatures from other magmatic phases.

As far as the U-Pb perovskite approach is concerned, one perovskite fraction may not sample crystals that are representative of those crystallizing during the main emplacement event, whether it be the age of the kimberlite sample itself or of the main pipe-infilling eruption. For example, if only one fraction were completed for sample 38929 one could easily misinterpret a single perovskite date (~650, 639 or 623 Ma) as the age of kimberlite emplacement when it is possible that none of these dates are representative of the kimberlite emplacement time (or the main pipe-infilling eruption).

Few published studies of kimberlite geochronology describe multiple perovskite dates from one kimberlite sample. In most of these studies, usually differences in perovskite crystal size, morphology and/or colour are visible. For example, probable antecrystic and xenocrystic perovskite was reported from the Elliott County kimberlite in Kentucky (Heaman et al. 2004). Several morphology and colour populations occur in a single sample and eight perovskite fractions display a range in geochemistry and $^{206}Pb/^{238}U$ dates (~79– 103 Ma). The younger perovskite dates more closely document the age of main kimberlite intrusion and the older populations were interpreted to reflect contamination with earlier xenolithic kimberlite material that likely exists in the root zone of the pipe, or from deeper levels in the crust. Additional examples are given in Heaman and Kjarsgaard (2000) (145.9 ± 3.0 Ma and 153.4 ± 2.6 Ma; Buffonta), Heaman et al. (2006) (176.6 ± 3.2 Ma to 189.8 ± 3.4 Ma, JD-3; Jericho) and Zurevinski et al. (2008) (171.0±5.4 Ma and 187.5 ± 1.2 Ma, 05KD244; 183.6 ± 1.6 Ma to 223.8 ± 2.0 Ma, 04KD230; 169.2 ± 3.3 Ma to 196.5 ± 1.4 Ma, CD009; Churchill). Hypabyssal kimberlite samples in this study contained perovskite crystals that were observed by stereomicroscope to have a generally similar dark brown to brown-black colour and cubic-cuboctahedral habit with varying, yet tiny (<60 μm), size. Moreover, the U and Pb concentrations and Th/U values did not appear to range significantly between fractions. Thus,

there is no obvious physical or chemical indication that perovskite in these Renard 2 hypabyssal kimberlite samples could yield mixed age populations.

Although the new high precision composite weighted mean $^{206}Pb/^{238}U$ perovskite date of 643.8 ± 1.0 Ma obtained for the Renard 2 main pipe-infilling units demonstrates that a detailed geochronology investigation of a single pipe can reveal the main intrusion episode with improved age precision, the age results for the small volume hypabyssal kimberlites (a rock type often selected for geochronology) may not be representative of the main intrusion stage in all cases. In this study a geologically significant period of intrusion history is recorded from hypabyssal kimberlite, demonstrating that magmatism can span at least ~20 Myr within a single pipe, similar to the emplacement history for some entire kimberlite fields (e.g. Heaman et al. 2015). It is unknown at this point whether the protracted range of kimberlite magma intrusion revealed in this study for Renard 2 is a unique situation for a single kimberlite pipe or not because similar detailed geochronology studies in other pipes in other clusters/fields are lacking. However, we note that there are hints from previous studies that other kimberlite pipes could also have a protracted emplacement history (e.g. as described above for the Elliott County kimberlite; Heaman et al. 2004). The detailed U-Pb geochronology in this study offers a glimpse into the construction of the Renard 2 pipe, indicating a ~20 Myr protracted emplacement history that does not fit the classical view of rapidly formed single kimberlite pipes (e.g. Field and Scott Smith 1999; Sparks et al. 2006). Clement and Reid (1989) pointed out that many Kimberley pipes in Southern Africa consist of multiple intrusive events and certain kimberlite root zones can consist of more than twenty separate intrusions of magmatic kimberlite, as well as the presence of autoliths from earlier intrusions that were subsequently disrupted (similar observations noted by Wagner 1914; Nixon 1973; Clement 1982; Mitchell 1986). We have shown for the first time that in some cases this intrusion history is protracted and can occur over tens of millions of years.

## Conclusions

Five key observations can be made from the new Renard 2 U-Pb perovskite dates obtained in this study; (1) A high-precision composite weighted mean $^{206}Pb/^{238}U$ perovskite date of 643.8 ± 1.0 Ma from the Renard 2 main pipe-infilling units is interpreted as the current best estimate for the emplacement of the Renard 2 pipe. (2) In contrast, small hypabyssal kimberlites within the Renard 2 pipe record a protracted history that spans at least ~20 Myr (652–632 Ma). Hypabyssal kimberlite dates that are older than the main pipe-infilling units are interpreted to be kimberlite xenoliths (i.e. remnants from older hypabyssal kimberlite intrusions; e.g. Figure 2.4). Two of eight hypabyssal kimberlite samples investigated in this study have intrusion ages that coincide or nearly overlap with emplacement of the main 644 Ma Renard 2 pipe. (3) A few individual kimberlite samples contain multiple perovskite age populations (e.g. 38929) and determining precise emplacement histories from these can be challenging. (4) Although hypabyssal kimberlite material is commonly preferred for dating kimberlites because it is less contaminated with crustal material (e.g. Allsopp et al. 1989), in cases such as Renard 2 these hypabyssal kimberlites provide constraints on the duration of kimberlite magmatism in a single pipe but may not provide an accurate age for the main pipe-infilling kimberlite intrusion history. (5) Finally, our robust U-Pb dating of the Renard 2 kimberlite does not fit with the classical view for single kimberlite pipes although they are consistent with field observations from early kimberlite field studies (e.g. Wagner 1914; Clement 1982), which identified diatreme precursor (antecedent) intrusions, syn-diatreme (contemporaneous) intrusions and post-diatreme (consequent) cross-cutting intrusions. Importantly, these new dates show that the Renard 2 kimberlite magmatic system was long-lived, at least 20 Myr, and possibly as long as 30 Myr.

**Table 2.1.** ID-TIMS U-Pb groundmass perovskite results for previous study of Renard 1-3 kimberlites and this study of the Renard 2 kimberlite, Québec, Canada

| Unit | Sample | Compositional parameters | | | | | | | Isotope ratios | | | | | | Isotopic date (Ma) | | Recommended $^{206}Pb/^{238}U$ date (Ma) | | | |
|---|---|---|---|---|---|---|---|---|---|---|---|---|---|---|---|---|---|---|---|---|
| | | Weight (mg) | U (ppm) | Th/U | Pb (ppm) | $^{206}Pb^*$ (mol%) | $Pb^*/Pb_c$ | $Pb_c$ (pg) | $^{238}U/^{204}Pb$ | ± (%) | $^{206}Pb/^{204}Pb$ | ± (%) | $^{206}Pb/^{238}U$ | ± (%) | $^{206}Pb/^{238}U$ | ± (2σ) | Weighted mean | ± (2σ) | MSWD | Fractions used |
| | | (a) | (b) | (c) | (d) | (c) | (e) | (e) | (e) | (i) | (g) | (i) | (g) | (f) | (g) | (h) | (g) | | | | |
| *Previous Study* | | | | | | | | | | | | | | | | | | | | |
| Renard 1 | 13900-1 | 0.113 | 80 | 30 | 71.2 | 82.3 | 11 | 692 | 809.6 | 0.7 | 100.72 | 0.55 | 0.10248 | 0.50 | 629.0 | 3.0 | 631.8 | 2.6 | 6.9 | 1, 3, 4 |
| Renard 1 | 13900-2 | 0.081 | 96 | 34 | 113.8 | 85.1 | 17 | 516 | 950.3 | 1.4 | 119.30 | 1.29 | 0.10682 | 0.52 | 654.3 | 3.2 | | | | |
| Renard 1 | 13900-3 | 0.156 | 55 | 25 | 48.7 | 82.8 | 11 | 651 | 819.5 | 1.2 | 103.28 | 0.97 | 0.10437 | 0.84 | 640.0 | 5.1 | | | | |
| Renard 1 | 13900-4 | 0.134 | 77 | 24 | 66.7 | 83.3 | 11 | 754 | 856.3 | 3.2 | 106.26 | 0.64 | 0.10337 | 3.17 | 634.1 | 19.2 | | | | |
| Kimb2a | 2007MM-1 | 0.046 | 94 | 22 | 71.7 | 89.7 | 17 | 179 | 1526.9 | 1.7 | 176.61 | 1.53 | 0.10403 | 0.39 | 638.0 | 2.4 | | | | |
| Kimb2b | 2110MM-1 | 0.076 | 117 | 31 | 120.2 | 89.4 | 23 | 391 | 1434.0 | 2.7 | 168.11 | 2.68 | 0.10481 | 0.66 | 642.6 | 4.0 | | | | |
| Kimb3d/g | 3010MM-1 | 0.070 | 124 | 20 | 88.9 | 88.5 | 14 | 419 | 1302.4 | 2.4 | 154.81 | 2.07 | 0.10523 | 1.25 | 645.0 | 7.7 | | | | |
| *This Study* | | | | | | | | | | | | | | | | | | | | |
| *Renard 2 main pipe-infilling units* | | | | | | | | | | | | | | | | | | | | |
| Kimb2a | 38925-2 | 0.022 | 101 | 14 | 55.7 | 87.3 | 9 | 119 | 1196.5 | 4.4 | 144.15 | 3.80 | 0.10568 | 0.37 | 647.6 | 2.3 | 643.1 | 1.7 | 0.01 | 3, 4 |
| Kimb2a | 38925-3 | 0.025 | 89 | 26 | 79.3 | 87.7 | 16 | 113 | 1260.6 | 4.7 | 149.99 | 4.10 | 0.10488 | 0.39 | 643.0 | 2.4 | | | | |
| Kimb2a | 38925-4 | 0.026 | 101 | 26 | 91.2 | 87.9 | 17 | 134 | 1270.7 | 3.9 | 151.09 | 3.39 | 0.10492 | 0.39 | 643.2 | 2.4 | | | | |
| Kimb2b | 38927-1 | 0.026 | 153 | 14 | 83.7 | 89.9 | 12 | 163 | 1543.1 | 3.2 | 179.80 | 2.89 | 0.10503 | 0.39 | 643.8 | 2.4 | 644.2 | 1.3 | 0.25 | 1, 4, 5 |
| Kimb2b | 38927-4 | 0.025 | 156 | 12 | 73.7 | 90.2 | 11 | 154 | 1594.4 | 3.4 | 185.19 | 3.01 | 0.10504 | 0.37 | 643.9 | 2.3 | | | | |
| Kimb2b | 38927-5 | 0.019 | 151 | 10 | 64.1 | 89.9 | 9 | 120 | 1556.5 | 4.3 | 181.43 | 3.87 | 0.10520 | 0.35 | 644.8 | 2.1 | | | | |
| *Renard 2 hypabyssal kimberlite (HK)* | | | | | | | | | | | | | | | | | | | | |
| Kimb2c | 38901-1 | 0.008 | 120 | 13 | 61.2 | 86.2 | 8 | 55 | 1181.2 | 10.0 | 139.18 | 8.68 | 0.10282 | 0.46 | 630.9 | 2.7 | 631.8 | 1.4 | 0.92 | 1-3 |
| Kimb2c | 38901-2 | 0.010 | 85 | 13 | 43.1 | 87.8 | 9 | 42 | 1408.1 | 13.5 | 163.03 | 12.03 | 0.10318 | 0.38 | 633.0 | 2.3 | | | | |
| Kimb2c | 38901-3 | 0.028 | 99 | 11 | 45.1 | 89.4 | 10 | 119 | 1511.4 | 4.4 | 173.22 | 3.90 | 0.10287 | 0.38 | 631.2 | 2.3 | | | | |
| Kimb2c | 38903-1 | 0.015 | 115 | 13 | 60.8 | 89.4 | 11 | 78 | 1500.1 | 6.8 | 176.56 | 6.14 | 0.10589 | 0.36 | 648.8 | 2.2 | 650.1 | 1.5 | 1.5 | 1-3 |
| Kimb2c | 38903-2 | 0.017 | 110 | 9 | 47.7 | 86.6 | 7 | 105 | 1130.5 | 5.0 | 137.69 | 4.39 | 0.10615 | 0.41 | 650.4 | 2.5 | | | | |
| Kimb2c | 38903-3 | 0.024 | 110 | 11 | 51.1 | 89.7 | 10 | 113 | 1511.7 | 5.2 | 178.63 | 4.82 | 0.10646 | 0.50 | 652.2 | 3.1 | | | | |
| Kimb2c | 38906-1 | 0.013 | 97 | 15 | 55.1 | 89.8 | 13 | 51 | 1653.8 | 10.9 | 191.06 | 9.84 | 0.10480 | 0.37 | 642.5 | 2.2 | 643.9 | 1.5 | 2.0 | 1, 4 |
| Kimb2c | 38906-2 | 0.017 | 105 | 12 | 52.1 | 88.9 | 10 | 83 | 1417.9 | 6.4 | 168.25 | 5.72 | 0.10618 | 0.37 | 650.5 | 2.3 | | | | |
| Kimb2c | 38906-4 | 0.015 | 83 | 12 | 39.3 | 90.7 | 12 | 47 | 1836.0 | 11.9 | 210.96 | 10.89 | 0.10525 | 0.34 | 645.1 | 2.1 | | | | |

**Table 2.1.** Continued.

| Unit | Sample | Compositional parameters | | | | | | | Isotope ratios | | | | | | Isotopic date (Ma) | | Recommended $^{206}Pb/^{238}U$ date (Ma) | | | |
|---|---|---|---|---|---|---|---|---|---|---|---|---|---|---|---|---|---|---|---|---|
| | | Weight (mg) | U (ppm) | Th/U | Pb (ppm) | $^{206}Pb^*$ (mol %) | $Pb^*/Pb_c$ | $Pb_c$ (pg) | $^{238}U/^{204}Pb$ | ± (%) | $^{206}Pb/^{204}Pb$ | ± (%) | $^{206}Pb/^{238}U$ | ± (%) | $^{206}Pb/^{238}U$ | ± (2σ) | Weighted mean | ± (2σ) | MSWD | Fractions used |
| | | (a) | (b) | (c) | (d) | (c) | (e) | (e) | (e) | (i) | (g) | (i) | (g) | (f) | (g) | (h) | (g) | | | | |
| Kimb2c | 38916-1 | 0.019 | 87 | 16 | 53.3 | 90.0 | 14 | 69 | 1614.0 | 7.7 | 189.43 | 6.99 | 0.10638 | 0.33 | 651.7 | 2.1 | 650.1 | 1.6 | 5.6 | 1, 3 |
| Kimb2c | 38916-3 | 0.022 | 75 | 13 | 39.1 | 90.8 | 13 | 61 | 1793.9 | 9.0 | 207.40 | 8.20 | 0.10574 | 0.39 | 647.9 | 2.4 | | | | |
| Kimb2c | 38923-1 [J] | 0.020 | 115 | 15 | 65.7 | 90.5 | 14 | 87 | 1697.8 | 6.1 | 197.20 | 5.51 | 0.10570 | 0.26 | 647.7 | 1.6 | 647.8 | 1.3 | 0.02 | 1, 3 |
| Kimb2c | 38923-3 [J] | 0.025 | 138 | 13 | 71.5 | 90.9 | 13 | 126 | 1745.6 | 4.3 | 202.29 | 3.93 | 0.10573 | 0.36 | 647.9 | 2.2 | | | | |
| Kimb2c | 38926-1 | 0.027 | 121 | 11 | 49.4 | 84.6 | 6 | 189 | 1115.5 | 2.7 | 118.24 | 2.32 | 0.08999 | 0.45 | 555.5 | 2.4 | | | | |
| Kimb2c | 38926-2 | 0.025 | 76 | 10 | 32.5 | 90.8 | 10 | 71 | 1788.1 | 7.6 | 205.96 | 6.89 | 0.10528 | 0.33 | 645.3 | 2.0 | 646.3 | 1.4 | 2.1 | 2, 3 |
| Kimb2c | 38926-3 | 0.022 | 114 | 10 | 49.8 | 90.8 | 11 | 94 | 1754.1 | 5.6 | 203.00 | 5.08 | 0.10564 | 0.33 | 647.4 | 2.0 | | | | |
| Kimb2c | 38928-1 | 0.012 | 104 | 8 | 40.1 | 89.6 | 8 | 53 | 1575.2 | 10.3 | 185.68 | 9.29 | 0.10665 | 0.27 | 653.3 | 1.6 | 652.2 | 1.3 | 4.1 | 1, 4 |
| Kimb2c | 38928-4 | 0.019 | 106 | 7 | 36.9 | 90.1 | 7 | 85 | 1602.3 | 6.2 | 187.81 | 5.62 | 0.10618 | 0.34 | 650.6 | 2.1 | | | | |
| Kimb2c | 38929-1 | 0.010 | 81 | 13 | 42.0 | 90.8 | 13 | 29 | 1979.9 | 20.5 | 227.68 | 18.88 | 0.10604 | 0.40 | 649.7 | 2.5 | | | | |
| Kimb2c | 38929-2 | 0.010 | 85 | 14 | 45.5 | 90.4 | 13 | 31 | 1914.6 | 19.0 | 217.24 | 17.40 | 0.10419 | 0.30 | 638.9 | 1.8 | | | | |
| Kimb2c | 38929-3 | 0.018 | 94 | 14 | 47.4 | 91.0 | 13 | 57 | 1940.1 | 9.5 | 214.60 | 8.67 | 0.10145 | 0.34 | 622.9 | 2.0 | | | | |

(a) *Previous study:* U-Pb perovskite results summarized in Birkett et al. (2004) for Renard 1 and in Fitzgerald et al. (2009) for Renard 2 and 3. *This study:* multi-grain fractions of groundmass perovskite, typically ~100-200 crystals

(b) Each fraction weighed using a Mettler UMT2 ultramicrobalance

(c) Concentrations determined by isotope dilution (±1-2% 2 sigma)

(d) Model Th/U ratio calculated from radiogenic $^{208}Pb/^{206}Pb$ ratio and $^{206}Pb/^{238}U$ date

(e) Pb* and $Pb_c$ represent radiogenic and common Pb, respectively; mol % $^{206}Pb^*$ with respect to radiogenic, blank and initial common Pb

(f) Corrected for fractionation, spike, common Pb, and blank (5 pg Pb; 1 pg U). Blank IC: $^{206}Pb/^{204}Pb = 18.24±2.0\%$; $^{207}Pb/^{204}Pb = 15.64±2.0\%$; $^{208}Pb/^{204}Pb = 37.50±2.0\%$ (uncertainties 1-sigma). Excess over blank was assigned to initial common Pb

(g) Errors are 2-sigma, propagated using the algorithms of Schmitz and Schoene (2007)

(h) Calculations are based on the decay constants of Jaffey et al. (1971). $^{206}Pb/^{238}U$ dates corrected for initial disequilibrium in $^{230}Th/^{238}U$ using Th/U [magma] = 5

(i) Corrected for fractionation, spike, and blank Pb only

[J] See Discussion (sample 38923)

Stacey and Kramers (1975) used to estimate initial common lead isotopic composition

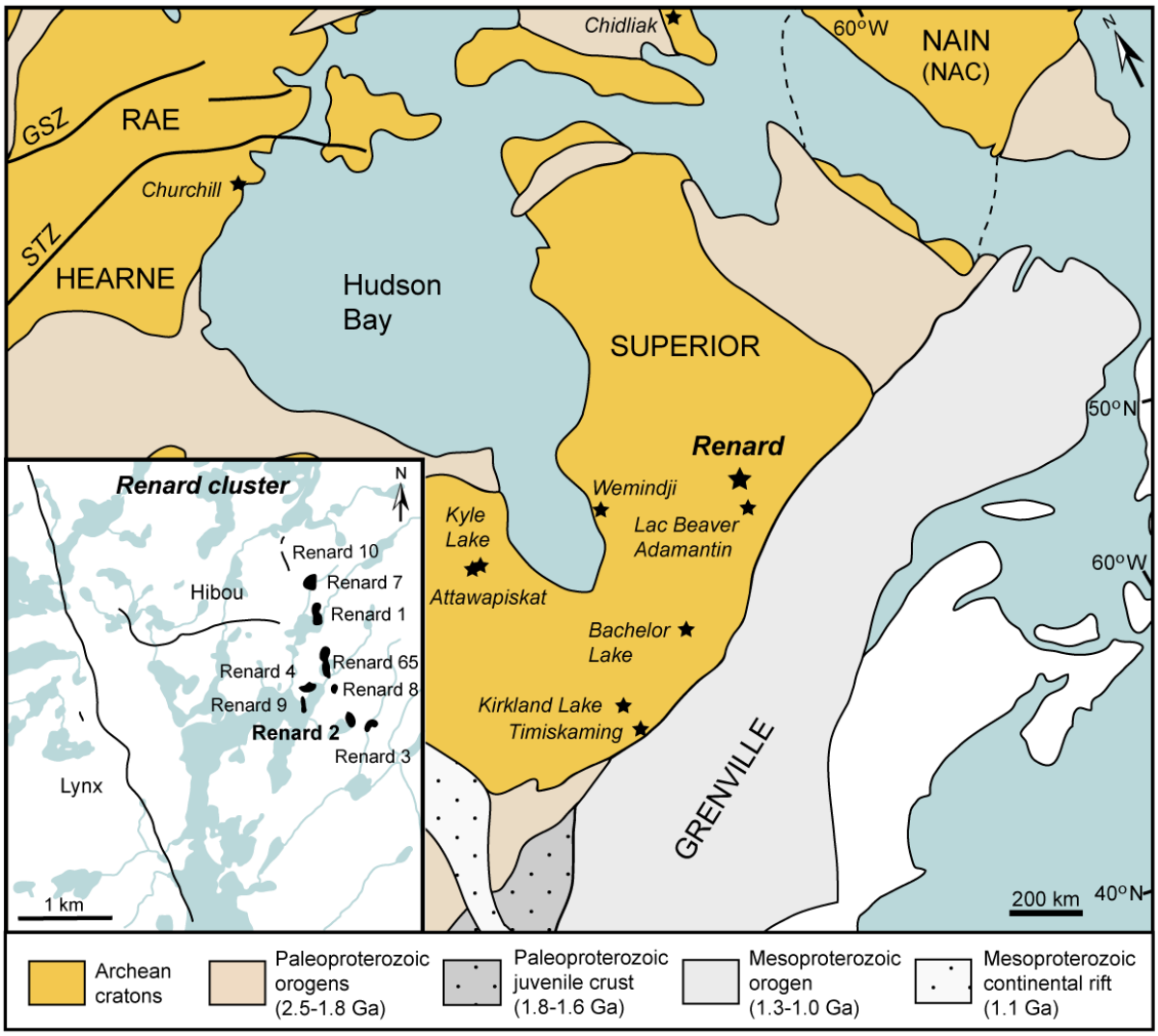


**Fig. 2.1** Simplified regional geology of eastern Canada and Greenland (pre-drift position) modified from Hoffman (1989), Card and Poulsen (1998), Zurevinski et al. (2008), Heaman et al. (2015), Godin et al. (2016) and Barnett and Laroulandie (2017). Inset shows the location of the Renard kimberlite cluster within the Otish field in the Superior Province (Québec). Approximated latitude/longitude and north arrow from Hoffman (1989). GSZ, Great Slave Lake Shear zone; STZ, Snowbird Tectonic zone; NAC, North Atlantic Craton

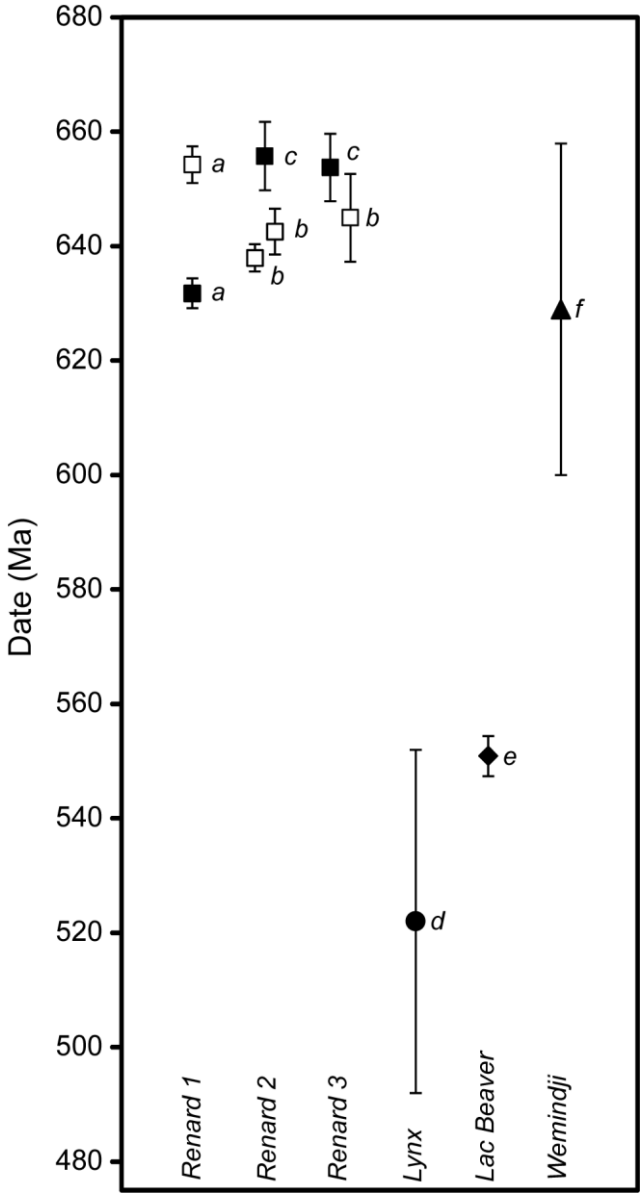


**Fig. 2.2** Summary of previously published U-Pb dates from Renard and nearby kimberlites in Québec. Weighted mean and single fraction $^{206}Pb/^{238}U$ perovskite dates denoted with closed and open squares, respectively for Renards 1–3 (a) Birkett et al. (2004), (b) Fitzgerald et al. (2009) with recalculated dates presented in Table 2.1, and (c) Tappe et al. (2017); U-Pb groundmass ilmenite isochron date (closed circle) for the Lynx dyke system (d) McCandless et al. (2008); U-Pb perovskite date (closed diamond) for the Lac Beaver hypabyssal kimberlite pipe (e) Moorhead et al. (2003); Rb-Sr phlogopite isochron date (closed triangle) for the Wemindji sills (f) Letendre et al. (2003).

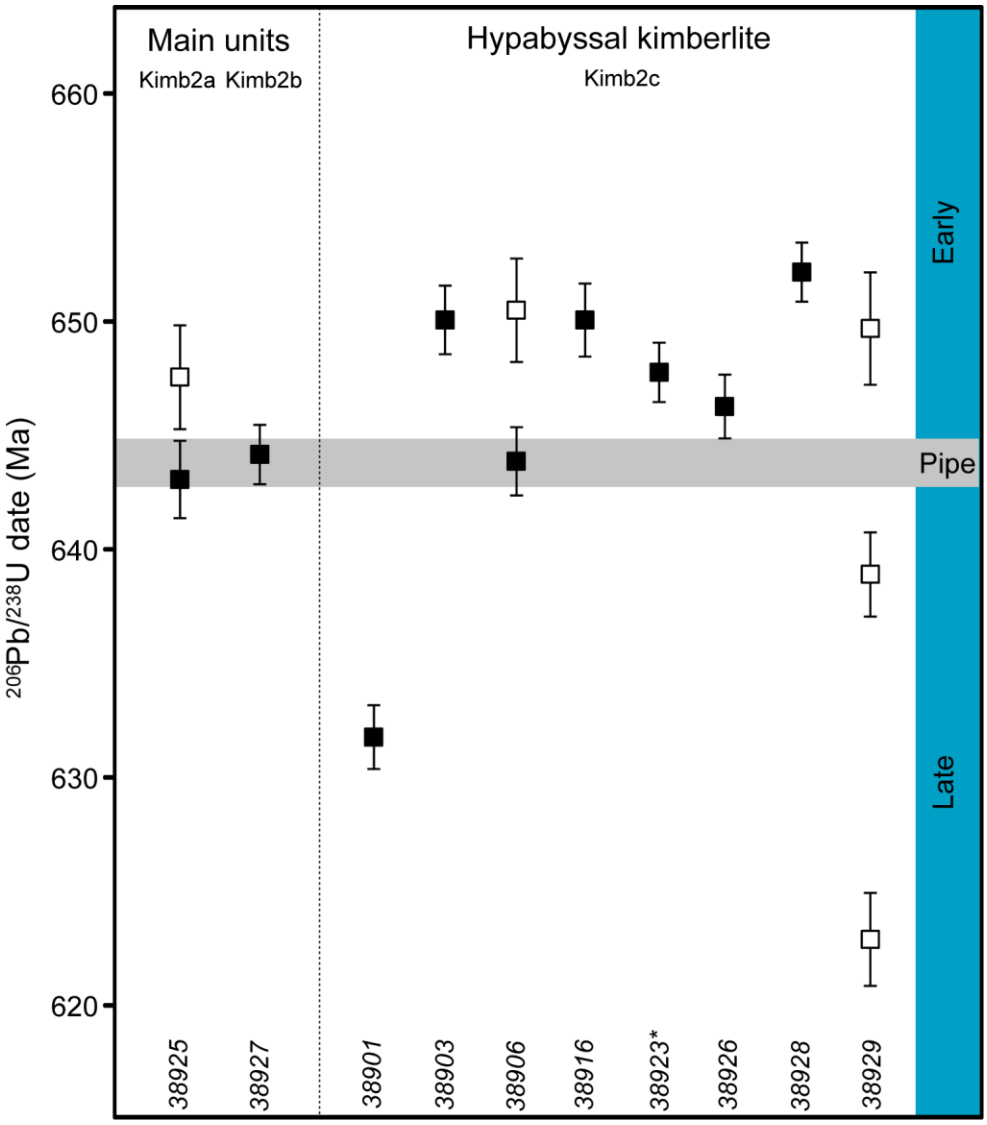


**Fig. 2.3** Summary of new ID-TIMS $^{206}Pb/^{238}U$ perovskite dates from Renard 2 (Québec) obtained in this study separated into main pipe infilling (Kimb2a and Kimb2b) and hypabyssal kimberlite (Kimb2c) units. Weighted mean and single fraction $^{206}Pb/^{238}U$ dates are denoted with closed and open squares, respectively. Gray bar represents the best estimate for timing of emplacement of the Renard 2 main pipe-infilling units. Sample 38923 denoted with an asterisk (*) to indicate it is possibly not a hypabyssal kimberlite (Kimb2c) (see Discussion).

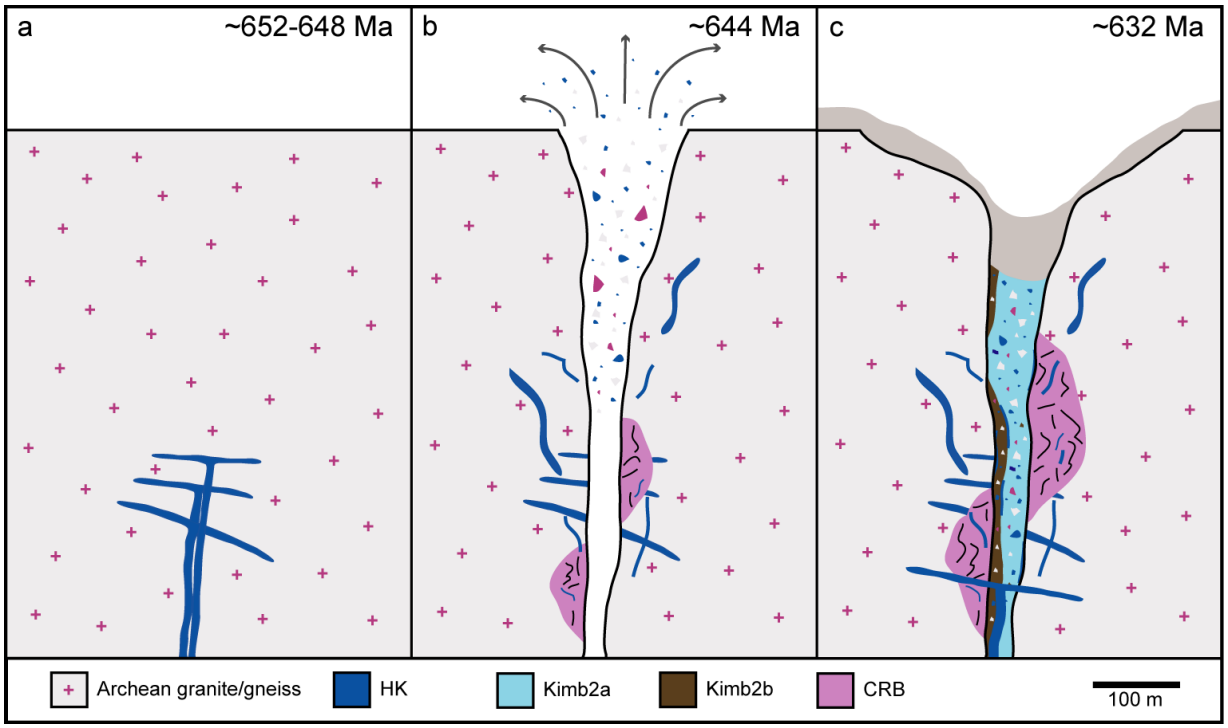


**Fig. 2.4** Simplified sketch hypothesizing the intrusion history of Renard 2 (modified after Fitzgerald et al. 2009). (a) Intrusion of early-stage hypabyssal kimberlites at ~652 Ma and ~648 Ma. Older hypabyssal kimberlite intrusions shown here as sheets. (b) Eruption of the Renard 2 main pipe-infilling units at ~644 Ma, that includes entrainment of syn-diatreme hypabyssal kimberlite and possible hypabyssal kimberlite xenoliths from earlier intrusions. (c) Intrusion of late-stage hypabyssal kimberlites at ~632 Ma and possibly younger. CRB, country rock breccia; Kimb2a and Kimb2b, main pipe-infilling units; HK, hypabyssal kimberlite (e.g. Kimb2c).

# CHAPTER 3

# A NEW PERSPECTIVE ON THE KIMBERLITE-LIP-RODINIA SUPERCONTINENT CONNECTION FROM HIGH PRECISION U-Pb GROUNDMASS PEROVSKITE DATING OF THE NEOPROTEROZOIC RENARD CLUSTER, CANADA


## Abstract

New high-precision U-Pb groundmass perovskite dates from hypabyssal kimberlite and several main pipe units collected from the Neoproterozoic Renard cluster (Otish field, Québec) reveal for the first time a protracted kimberlite intrusion history, both within a kimberlite cluster and within a single kimberlite pipe. Samples of hypabyssal kimberlite within six Renard pipes (Renard 1-4, 7 and 9) and the G04-296 Anomaly dyke revealed a broad range of punctuated magmatism over at least ~124 Myr (~663-539 Ma) across the kimberlite cluster. This is contrary to the conventional interpretation that entire kimberlite bodies are emplaced within <1 Ma. In contrast, several main pipe units from four pipes (Renard 1-4) suggest a narrower ~8 Myr (~646-638 Ma) range of eruption for the main kimberlite body, but a younger (~625 Ma) date for the main pipe-infilling magmatism from Renard 9 suggests that not all pipes within the cluster erupted at the same time. These new U-Pb dates provide more robust constraints on the temporal and spatial connection to the nearby Central Iapetus Magmatic Province and the breakup of the Rodinia supercontinent. Notably, a temporal connection is observed between the youngest (~615-539 Ma) kimberlite magmatism in the Otish field and the second rifting phase related to the opening of the Iapetus Ocean. The older >615 Ma Renard kimberlites are more difficult to explain but the broad area of kimberlite magmatism (Otish, Wemindji) in the eastern Superior Province suggests a large-scale mechanism related to large igneous province formation, perhaps by combined continental extension/rifting and impingement of one or more mantle plumes. A similar temporal and spatial connection also occurs between the opening of the Iapetus Ocean and the emplacement of kimberlites and other alkaline intrusions in Baltica. Key to this study is that single hypabyssal kimberlite samples within the Renard pipes record a much broader range in U-Pb dates than previously known and implies kimberlite magmas likely repeatedly intruded

into the Archean crust of the Superior Province in response to Rodinia's protracted breakup history.

## Introduction

As Earth's deepest ultramafic magma, kimberlite (and the xenoliths it carried) originated from great depths (>150 km) and offer rare glimpses of material from the deep Earth. These rare diamond-bearing rocks occur worldwide and mainly formed in the last half of Earth's history, usually intruding into the thick crust of Archean cratons as dykes, sills or pipes in clusters/fields (Clifford 1966; Mitchell 1986; Ernst 2014; Tappe et al. 2018). We rely on the snapshot of geologic information collected from limited outcrops, drill core and mining faces from large eroded pipes or small dykes to learn more about kimberlite magmas (e.g. Brown and Valentine 2013; Ault et al. 2015). Hence our knowledge of kimberlite has evolved from its original names hardebank, blue ground and yellow ground (e.g. Lewis 1887; Wagner 1914), then 'basaltic' and 'micaceous' kimberlite (Wagner 1914), and now referred to as Group 1 and Group 2 kimberlite (or orangeite for Group 2; Smith 1983; Mitchell 1995). What initially triggers kimberlite magmas to form deep in the mantle is hypothesized to range from large-scale tectonic processes such as intracontinental rifting (e.g. Phipps 1988; Moore et al. 2008) or subduction of oceanic lithosphere (e.g. McCandless 1999; Currie and Beaumont 2011) to mantle plumes (e.g. Crough et al. 1980; Heaman and Kjarsgaard 2000). A key line of evidence comes from the temporal and spatial patterns of kimberlites emplaced across the crust. For example, the Great Meteor hotspot track in eastern North America left a distinct 2000 km-long NW-SE younging age progression across eastern North America recorded in four kimberlite fields (Heaman and Kjarsgaard 2000).

Shared between these hypotheses is the assumption that a single kimberlite feeder rapidly ascends from the mantle to intrude into the crust as a single dyke/sill/pipe (or entire cluster). This notion has shaped our perspective of kimberlite emplacement for more than one hundred years (e.g. Voit 1907; Wagner 1914; Williams 1932; Dawson 1967, 1980; Clement 1982). Early- and late-stage kimberlite intrusions adjacent the pipe are usually assumed to originate from a single kimberlite feeder emplaced within the limits of isotopic dating techniques [<1-2 Ma; e.g. Smith et al. (1985) regarding MacIntyre and Dawson (1976) results for New Elands;

Mitchell 1986]. Hence current pipe formation models envision a single kimberlite feeder explosively fragmenting in the crust (either at surface or at depth due to groundwater or volatiles) incorporating these fragments (e.g. autoliths) of a parent feeder magma which wanes to emplace late-stage dykes (e.g. Field and Scott Smith 1999; Lorenz et al. 1999; Skinner and Marsh 2004; Cas et al. 2006, 2008a; Sparks et al. 2006; Wilson and Head 2007; Skinner 2008). Kimberlite is known to sometimes occur as regional dyke swarms (e.g. Mitchell 1986, page 38-40 for summary) yet few researchers consider the possibility dykes near the pipes could have intruded during different events (e.g. Voit 1907; Williams 1932; MacIntyre and Dawson 1976; Dawson 1980; Clement 1982; Lorenz and Kurszlaukis 2007). Relying on knowledge gained thus far about kimberlite pipe emplacement mechanisms, it follows that any piece of kimberlite within the pipe sampled for geochronology should provide a representative date for the emplacement time of the entire body, assuming suitable minerals for isotopic dating are present (e.g. Allsopp et al. 1989). In the last decade high precision geochronology has shown that many individual fields/clusters tend to record a ~10-55 Myr duration to their magmatism, such as in North America (e.g. 75-45 Ma Lac de Gras, 115-92 Ma Saskatchewan-Somerset Island, 155-134 Ma Timiskaming, 157-139 Ma Chidliak, 165-152 Ma Kirkland Lake, 180-156 Ma Attawapiskat, and 225-170 Ma Churchill; Heaman and Kjarsgaard 2000; Creaser et al. 2004; Zurevinski et al. 2008; Heaman et al. 2015; Sarkar et al. 2015a; Kjarsgaard et al. 2017). Recently there have been some detailed geochronology studies that challenge the conventional view of rapid single-event kimberlite emplacement histories. Examples of protracted kimberlite pipe emplacement include the Orion South kimberlite in Saskatchewan (~8 Myr duration; Kjarsgaard et al. 2017) and the Renard 2 kimberlite in Québec (>20 Myr duration for hypabyssal kimberlite emplacement; Ranger et al. 2018).

This >20 Myr span of kimberlite intrusion history occurs within a single pipe, the Renard 2 pipe (Renard cluster, Otish field), in the Archean Superior Province. The Otish field is unusual because it records a long (>100 Myr, ~656-551 Ma from U-Pb perovskite geochronology) duration of Neoproterozoic kimberlite magmatism (Moorhead et al. 2003; Tappe et al. 2017). This kimberlite field lies distal to a broad region of alkaline-carbonatite intrusions and large igneous province magmatism recording two phases (760-700 Ma and 620-550 Ma) of continental extension and rifting related to the opening of the Iapetus Ocean during the breakup of the

supercontinent Rodinia (e.g. Aleinikoff et al. 1995; Cawood et al. 2001). The carbonatites were originally included by Doig (1970) into the North Atlantic Alkaline Rock Province extending along a rift system from eastern North America to Greenland to Scandinavia. Later Heaman et al. (2003, 2004) recognized two periods of kimberlite and related magmatism (~632-629 Ma Renard and Wemindji, ~584-550 Ma Abloviak and Lac Beaver) across eastern North America and Greenland, referring to the eastern North American intrusions as the Eocambrian/Cambrian Labrador Sea Province. How these kimberlite and related magmas were connected to Rodinia's breakup was unknown with the information available at that time but a connection to upwelling mantle and rifting was postulated by Heaman et al. (2003, 2004). Recently, Tappe et al. (2017) interpreted the ~656-629 Ma Renard and Wemindji kimberlites to have been emplaced by a 'tectonically controlled' mechanism due to the absence of temporal and spatial relationships with Neoproterozoic LIPs. Our understanding of the temporal and spatial relationships between kimberlite intrusions and the movement of plates during supercontinent breakup/assembly has grown to include links with periodicity in timing, lithosphere thickness, plume center locations, alkaline and carbonatite intrusions, rifts and the large volumes of basalts in LIPs (e.g. Milanovskiy and Mal'kov 1980; Larsen and Rex 1992; Bailey 1993; Gibson et al. 1995; Heaman et al. 2003; Bailey and Woolley 2005; Kumar et al. 2007; Vaughan and Storey 2007; Moore et al. 2008; Jelsma et al. 2009; Chalapathi Rao and Lehmann 2011; Ernst 2014; Kargin 2014; Tappe et al. 2014). Ernst (2014) and Chalapathi Rao and Lehmann (2011) note several examples which include kimberlites that intruded several hundreds of km's distal to the LIP and inferred plume center, such as the ~65 Ma Deccan LIP, alkaline and carbonatite intrusions and 65-62 Ma Group 2 Mainpur kimberlites in the Bastar craton. Near the Otish field, the 1115-1085 Ma Keweenawan LIP and associated ~1.1 Ga Midcontinent rift system coincide with the Abitibi dyke swarm (~1141 Ma), ultramafic lamprophyres (~1144 Ma) and carbonatites (~1100 Ma, ~1160 Ma ) in the Lake Superior region near Wawa and distal ~1172-1076 Ma kimberlites (Kyle Lake, Bachelor Lake) near James Bay (e.g. Queen et al. 1996; Heaman et al. 2004 and references therein; Ernst 2014 and references therein; Wu et al. 2017). With more high precision geochronology, the connection between the duration of kimberlite magmatism, alkaline-carbonatite intrusions, LIPs and supercontinent breakup/assembly can be deduced.

This study presents new high precision ID-TIMS U-Pb groundmass perovskite dates from six Renard pipes and a nearby dyke (G04-296 Anomaly) in the Renard kimberlite cluster (Otish field, Québec). Prior to this study, five U-Pb perovskite dates indicated a >100 Myr span of kimberlite magmatism in the Otish field (~656-551 Ma; Moorhead et al. 2003; Birkett et al. 2004; Fitzgerald et al. 2009; Tappe et al. 2017). Furthermore, recent U-Pb perovskite dates from multiple kimberlite units within the Renard 2 pipe revealed a more complex intrusion history in a single pipe than previously recognized (Ranger et al. 2018). These findings are combined with the results of the present study to investigate in detail the relationship between this protracted period of Neoproterozoic kimberlite magmatism and the breakup of Rodinia.

## Regional geology

The Renard cluster is part of the Otish kimberlite field in north-central Québec (Figure 3.1). It is located within the ENE-trending Opinaca Subprovince of the Archean Superior Province, and is flanked by Proterozoic orogens (New Quebec and Ungava) and the Grenville Province (Hoffman 1989; Card and Poulsen 1998; Percival et al. 2012). The Opinaca Subprovince is dominated by amphibolite- to granulite-facies metagreywacke, mafic volcanics, migmatitic paragneiss, granite and pegmatite (Card and Poulsen 1998; Percival et al. 2012). A few Neoarchean U-Pb zircon dates (2666-2636 Ma) were reported for felsic crust in the Opinanca Subprovince, just east of the Otish field (Morfin et al. 2013). The NW-trending 2515-2500 Ma Mistassini dyke swarm (Fahrig et al. 1986; Heaman 2004; Hamilton 2009) occurs within the Otish Mountains region, along with NNE-trending faults and lineaments of the Mistassini-Lemoyne Tectonic Zone (Moorhead et al. 2003).

Numerous Mesoproterozoic to Mesozoic kimberlites intruded the Superior Province (Figure 3.1), including the ~1100 Ma Bachelor Lake dykes (Watson 1967; Alibert and Albarede 1988), ~1123-1076 Ma Kyle Lake kimberlites (Heaman et al. 2004), ~629 Ma Wemindji sills (Letendre et al. 2003), ~253-220 Ma Pagwachuan cluster (Delgaty et al. 2017), ~180-156 Ma Attawapiskat cluster (Heaman and Kjarsgaard 2000 and references therein) and ~165-134 Ma Kirkland Lake/Timiskaming fields (Heaman and Kjarsgaard 2000; Heaman et al. 2004). Between 2001-2006, nine Class 1 kimberlite bodies (named Renard 1 to 10 with Renard 6 and Renard 5

combined into one body, Renard 65), two dyke systems (Lynx, Hibou) and several kimberlite dykes (G04-296 Anomaly, North Anomaly, Southeast Anomaly) were discovered on the Foxtrot property (Godin et al. 2016). The Renard pipes follow a ~2-km-long NNW-trending lineament parallel to the Lynx dyke system, a ~4.2 km-long series of east-dipping en echelon hypabyssal kimberlite dykes ~2 km to the west. The Hibou dyke occurs as a ~1.9 km-long north-dipping, E-W trending dyke system (McCandless et al. 2008; Godin et al. 2016). A U-Pb groundmass ilmenite date of 522±30 Ma was reported for a sample of Lynx kimberlite (McCandless et al. 2008). Within the Otish field approximately 90-100 km south of the Renard cluster are the undated Adamantin kimberlites (Barnett and Laroulandie 2017) and the 550.9±3.5 Ma (U-Pb perovskite date) Lac Beaver kimberlite dyke swarm and pipe (Girard 2001; Moorhead et al. 2003).

The petrology of several Renard bodies is summarized in the early work of Birkett et al. (2004) followed by later work on Renard 2 (Fitzgerald et al. 2009; Lepine and Zhuk 2017; Lepine and Farrow 2018; Muntener and Gaudet 2018), Renard 3 (Muntener and Scott Smith 2013), Renard 4 (Gofton 2007) and Renard 65 (Gaudet 2016; Gaudet et al. 2018) with remaining kimberlites outlined in Godin et al. (2016). The Renard kimberlites are modeled as steep-sided diatreme to root zone Class 1 (South African style) pipes. The pipes comprise of generally more than one main pipe-infilling unit, which vary from hypabyssal (HK) (or coherent, CK) to Kimberley-type pyroclastic kimberlite (KPK, formerly termed tuffisitic kimberlite). An exception is the more elongate dyke-like Renard 10 intrusion. The pipes are partially surrounded by country rock breccia, cracked country rock or country rock unaffected by kimberlite. The internal geology of the Renard pipes is assigned major geological unit codes for different kimberlite phases identified by different petrological characteristics (e.g. Kimb2a and Kimb2b for Renard 2; Godin et al. 2016). The code F indicates further petrological work is needed on this sample (e.g. FKimb3h). Smaller hypabyssal kimberlites (e.g. dykes/sheets, irregular intrusions) are observed in all pipes and denoted with the letter ‘c’ (e.g. Kimb7c).

## Analytical methods

Drill core and outcrop samples were provided by Stornoway Diamond Corporation. Detailed description of sample preparation methods are reported by Ranger et al. (2018). Perovskite fractions selected for U-Pb geochronology consisted of ~70-390 crystals (typically ~100-200 crystals) weighing ~6-70 µg and ranging between ~20-70 µm in diameter (most ~30-60 µm). Perovskite crystals <30 µm were difficult to positively identify and avoided in the majority of multi-grain fractions. Grains showing visible alteration and/or mineral inclusions were avoided during grain selection. The ID-TIMS U-Pb method followed the protocol similar to Heaman et al. (2015). U and Pb isotopic compositions were measured using a VG354 thermal ionization mass spectrometer operated in single Daly detector mode and a Thermo Triton Plus multi-collector thermal ionization mass spectrometer operated in multi-collector Faraday or single ion counter SEM detector mode (Sarkar et al. 2015b). Individual analyses consisted of ~100-400 isotopic ratios (typically ~180-300). Pb and U isotopic data were collected sequentially at 2-3 staggered temperature intervals between ~1120-1420$^{o}$C (typically ~1200-1350$^{o}$C). Table 3.1 reports U-Pb results calculated using YourLab (Schmitz and Schoene 2007). The isotopic composition of the initial common lead incorporated by perovskite during crystallization was estimated using the Stacey and Kramers (1975) two-stage model for terrestrial lead evolution. Decay constants are those reported by Jaffey et al. (1971) ($\lambda^{238}U=1.55125 \times 10^{-10}$ yr$^{-1}$; $\lambda^{235}U=9.84850 \times 10^{-10}$ yr$^{-1}$). Age uncertainties are reported as 2σ. Isoplot 4.15 was used to calculate weighted average $^{206}Pb/^{238}U$ dates and 2σ age uncertainties (Ludwig 2012). The Ice River perovskite (IR6) was measured repeatedly throughout this study to monitor accuracy of the U-Pb dates. TIMS weighted average $^{206}Pb/^{238}U$ dates reported for this Ice River perovskite crystal (IR6) are 356.5±1.0 Ma (2σ; MSWD =2.1; n=8; Heaman 2009) and 357.2±0.3 Ma (2σ; MSWD=0.66; n=6; Burgess et al. 2012) using the Stacey and Kramers (1975) two-stage terrestrial model. A summary of U-Pb results for 25 IR6 fragments (excluding four outlier/poor results) weighing between ~5-69 µg yielded $^{206}Pb/^{238}U$ dates between 351.7±1.3 Ma (5.8 µg) to 359.1±1.1 Ma (19.3 µg) with a weighted average $^{206}Pb/^{238}U$ date of 356.6±0.2 Ma (2σ; MSWD=15), within uncertainty of the value recommended by Heaman (2009).

## U-Pb perovskite results

New ID-TIMS U-Pb perovskite dates for 19 samples collected from six Renard kimberlites (Renard 1-4, 7 and 9) and the G04-296 Anomaly are reported in Table 3.1 and Figures 3.2 and 3.3. Analytical uncertainty for individual fractions varies between 1-3 Ma (2σ). The dominant (and more easily visible) crystal habit in concentrate was selected for most samples. Some anhedral-subhedral crystals occur in several main pipe-infilling units but were not examined in detail here (except 31543-2). Several samples of the main pipe-infilling units (e.g. Kimberley-type pyroclastic kimberlite breccias) yielded sparse, tiny or no perovskite in thin section (e.g. Kimb3b). Th/U ratios for all perovskite analyzed in this study record a limited range of 6-19, which is much narrower than the 2.8-116 range reported by Tappe et al. (2017) for Renard 2 and 3 pipes only. An evaluation of the interpretation for the new Renard U-Pb perovskite dates is presented in Supplementary Material 3 in Appendix C.

**Renard 1:** Dark brown-black octahedral crystals (~88-243 crystals, ~30-50 μm) from one main pipe-infilling unit (Kimb1d; 37375B) yielded a weighted average $^{206}Pb/^{238}U$ date of 646.0±1.6 Ma (2σ; n=2; MSWD=2.0) which provides the best estimate for the timing of the Renard 1 pipe emplacement. Dark brown-black cubic-cuboctahedral crystals from two hypabyssal kimberlites (Kimb1c-body; 37317B, ~243 crystals, ~30-60 μm; 37322B, ~96 crystals, ~30-50 μm) yielded broadly similar $^{206}Pb/^{238}U$ dates of 643.1±2.5 Ma and 640.4±2.8 Ma, respectively.

**Renard 2:** Details of the previously published Renard 2/3 composite date reported in Birkett et al. (2004) and new data for ten Renard 2 samples are reported in Ranger et al. (2018). One additional hypabyssal kimberlite sample (Kimb2c; 38919) collected from ~4 m outside the pipe margin (~657 m apparent downhole depth) is reported here. Two fractions of patchy dark to light brown cubic to cuboctahedral crystals (~151-191 crystals, ~20-60 μm) were analyzed. Fraction 38919-2 is discordant relative to nearly concordant fraction 38919-1. Fraction 38919-1 yielded a $^{206}Pb/^{238}U$ date of 539.1±2.0 Ma, which is the best estimate for the timing of hypabyssal kimberlite emplacement at this sample locality and the youngest U-Pb perovskite date obtained for Renard kimberlites in this study.

**Renard 3:** The Renard 3 pipe consists of six main pipe-infilling units from two feeder zones and is characterized by the most complex internal geology in the Renard cluster (Muntener and Scott Smith 2013). Five main pipe-infilling units amenable to U-Pb perovskite dating were investigated to constrain the duration of kimberlite pipe-infilling. Kimb3f (31543) contained dark brown-black cubic crystals (31543-1) which unfortunately did not yield a result. A fraction of dark brown-black anhedral-subhedral perovskite crystals from sample Kimb3f (31543-2; ~169 crystals, ~30-70 μm) yielded a single $^{206}Pb/^{238}U$ date of 643.6±2.8 Ma. Three fractions of dark brown-black mainly cubic-cuboctahedral crystals in Kimb3d (31559, ~92-378 crystals, ~30-50 μm) yielded a weighted average $^{206}Pb/^{238}U$ date of 642.6±1.2 Ma (2σ; n=3; MSWD=5.5) whereas the two younger identical fractions (31559-2 and 31559-3) yielded a weighted average $^{206}Pb/^{238}U$ date of 641.3±1.4 Ma (2σ; n=2; MSWD=0.027). The two weighted average dates are within analytical error, but the latter date records identical dates and lower MSWD. The third fraction (31559-1) yielded a slightly older $^{206}Pb/^{238}U$ date of 645.4±2.0 Ma and slightly lower U and Pb abundances (Table 3.1). Two fractions of mainly dark brown-black cubic to cuboctahedral crystals in Kimb3g (31556, ~95-100 crystals, ~30-70 μm) yielded a weighted average $^{206}Pb/^{238}U$ date of 640.5±1.1 Ma (2σ; n=2; MSWD=8.7). Two fractions of dark brown-black cubic to cuboctahedral crystals in FKimb3h (31555, ~95-100 crystals, ~30-60 μm) yielded a weighted average $^{206}Pb/^{238}U$ date of 644.9±1.1 Ma (2σ; n=2; MSWD=0.5). Kimb3i (31548) contained dark brown-black mixed cubic-cuboctahedral and octahedral crystals of similar size/colour and difficult to discern from each other at this scale. Two fractions of dark brown-black mixed cubic-cuboctahedral-octahedral crystals (~90-100 crystals, ~30-60 μm) yielded single $^{206}Pb/^{238}U$ dates of 641.0±2.8 Ma and 647.1±2.2 Ma. A hypabyssal kimberlite sample (Kimb3c; 31552B) was examined and three fractions of dark brown cubic to cuboctahedral crystals (~98-326 crystals, ~30-60 μm) yielded a weighted average $^{206}Pb/^{238}U$ date of 633.2±1.4 Ma (2σ; n=3; MSWD=0.12), which is distinctly younger than the main pipe-infilling units.

**Renard 4:** Two fractions of dark brown to brown-black cubic to cuboctahedral perovskite crystals (~87-354 crystals, ~30-50 μm) from one Renard 4 main pipe-infilling unit (Kimb4b; 39289) yielded different $^{206}Pb/^{238}U$ dates of 645.7±2.1 Ma (39289-2) and 638.0±2.7 Ma (39289-4). The two fractions are outside of analytical error; therefore, the younger single fraction date of 638.0±2.7 Ma is interpreted as the best estimate for timing of Renard 4 pipe emplacement.

Two hypabyssal kimberlites (Kimb4c; 39282B, 39283B) similarly yielded a range of perovskite dates; two fractions of reddish brown cubic to cuboctahedral crystals (~95-204 crystals, ~30-60 μm) from 39282B yielded distinct $^{206}Pb/^{238}U$ dates of 647.7±1.9 Ma and 663.0±2.2 Ma. Three fractions of dark brown-black cubic to cuboctahedral crystals (~70-358 crystals, ~30-60 μm) from 39283B yielded a weighted average $^{206}Pb/^{238}U$ date of 648.2±1.2 Ma (2σ; n=3; MSWD=7.2) whereas the two younger fractions (39283B-1 and 39283B-2) yielded a weighted average $^{206}Pb/^{238}U$ date of 646.8±1.5 Ma (2σ; n=2; MSWD=1.08). The two weighted average dates are within analytical error but the latter date is associated with a lower MSWD value. The third fraction yielded a slightly older $^{206}Pb/^{238}U$ date of 651.7±2.3 Ma.

**Renard 7:** Three hypabyssal kimberlite samples (Kimb7c; 35789B, 35790B, 35791) were examined. Dark brown mainly octahedral crystals in 35791 (~95-96 crystals, ~30-60 μm) and 35789B (~98-100 crystals, ~30-50 μm) yielded weighted average $^{206}Pb/^{238}U$ dates of 647.9±2.6 Ma (2σ; n=2; MSWD=2.6) and 614.3±2.6 Ma (2σ; n=2; MSWD=4.1), respectively. One fraction of dark brown-black cubic to cuboctahedral crystals with whitish coating (~93 crystals, ~30-50 μm) in 35790B yielded a $^{206}Pb/^{238}U$ date of 646.2±3.3 Ma.

**Renard 9:** One main pipe-infilling unit from Renard 9 (Kimb9b; 31468) yielded perovskite with whitish coating, which made crystal habit difficult to assess. Two fractions of brown cubic to cuboctahedral crystals with whitish coating (~163-204 crystals, ~30-60 μm) were analyzed. Fraction 31468-1 produced the most concordant $^{206}Pb/^{238}U$ date of 625.0±2.2 Ma, which is interpreted as the best estimate for timing of the Renard 9 pipe emplacement and is the youngest pipe dated in this study. A hypabyssal kimberlite (Kimb9c; 31497) yielded an older weighted average $^{206}Pb/^{238}U$ date of 640.7±1.4 Ma (2σ; n=3; MSWD=3.3) from dark brown cubic to cuboctahedral crystals (~100-391 crystals, ~30-40 μm).

**G04-296 Anomaly:** A hypabyssal kimberlite (31577-2) yielded a $^{206}Pb/^{238}U$ date of 632.8±2.4 Ma from patchy brown fragments (including cubic to cuboctahedral fragments; ~245 crystals, ~20-40 μm).

## Discussion

## Emplacement of Renard kimberlites

The new ID-TIMS U-Pb perovskite dates for the Renard cluster (this study; Ranger et al. 2018; Figure 3.3; Table 3.1) reveal that hypabyssal kimberlites in the Otish field, both small intrusions and large main pipe-infills, intruded at punctuated intervals over a minimum duration of ~124 Myr (~663-539 Ma), the longest known record of magmatism within a single kimberlite cluster. Previously only three Renard kimberlite bodies (Renards 1-3) were dated by U-Pb perovskite geochronology. Birkett et al. (2004) applied ID-TIMS U-Pb geochronology to perovskite from Renard 1 hypabyssal material to determine a date of 631.6±3.5 Ma, which was updated in Ranger et al. (2018) to 631.8±2.6 Ma. Subsequently an ID-TIMS U-Pb perovskite composite emplacement date of 640.5±2.8 Ma was obtained from a selection of three main pipe-infilling units in Renard 2 and Renard 3 (Fitzgerald et al. 2009), which was updated in Ranger et al. (2018) to 639±2 Ma for Renard 2. Two SIMS U-Pb perovskite dates for hypabyssal kimberlite from Renard 2 (655.8±6.0 Ma) and Renard 3 (653.8±5.9 Ma) were reported by Tappe et al. (2017). Recently, Ranger et al. (2018) reported ID-TIMS U-Pb perovskite dates from Renard 2 for the main pipe-infilling units (643.8±1.0 Ma; Kimb2a and Kimb2b) and early-stage, main pipe-infilling stage, and late-stage hypabyssal kimberlite samples which recorded at least a ~20 Myr span (~652-632 Ma and possibly younger).

U-Pb dating of at least one main pipe-infilling unit from four Renard pipes (Renard 1-4) suggests a narrow ~8 Myr eruption history between ~646-638 Ma. New weighted average $^{206}Pb/^{238}U$ dates for Renard 1 (646.0±1.6 Ma), Renard 2 (643.8±1.0 Ma) and Renard 3 (640.5±1.1 Ma to 644.9±1.1 Ma) confirm that the main pipe-infilling stage is in fact >10 Myr older or younger than the previously reported hypabyssal kimberlite dates (631.6±3.5 Ma for Renard 1, Birkett et al. 2004; 655.8±6.0 Ma for Renard 2 and 653.8±5.9 Ma for Renard 3, Tappe et al. 2017). A detailed examination of three out of six Renard 3 main pipe-infilling units uncovered a relatively short duration of ~4 Myr (~645-641 Ma) for this stage of pipe development (akin to Orion South, Kjarsgaard et al. 2017). In detail, the Kimb3d and Kimb3g weighted average ~641 Ma dates support a combined Kimb3dg unit. Single dates from Kimb3i and possibly Kimb3d may record

a more complex history likely incorporating older xenocrystic or inherited perovskite (as seen in some hypabyssal kimberlites). Although it appears that the main pipe-infilling stage of most Renard kimberlites is constrained to a relatively narrow time window, the Renard 9 main pipe-infilling unit Kimb9b records a $^{206}Pb/^{238}U$ date of 625.0±2.2 Ma which indicates that some of the main pipe intrusion may have occurred later but similar in timing with the ~633-632 Ma hypabyssal kimberlite intrusions.

In contrast to the main pipe-infilling units, the new U-Pb dates from smaller hypabyssal kimberlites ('c' unit samples; e.g. dykes/sheets, irregular intrusions) show a pattern of early-stage, main pipe-infilling stage, and late-stage hypabyssal kimberlite intrusion spanning at least ~20 Myr between ~652-632 Ma, as initially reported in Ranger et al. (2018), persists in several pipes within the cluster. Dates from the hypabyssal kimberlites older than the main pipe-infilling units support the prior observation of autoliths in Renard 4 and Renard 9 (Godin et al. 2016). The oldest date recorded from Renard 4 ($^{206}Pb/^{238}U$ date of 663.0±2.2 Ma) suggests that mixing of older and younger kimberlite material in this hypabyssal kimberlite sample (39282B) likely occurred similar to Renard 2 (e.g. 38929). An older kimberlite body of this age has not yet been discovered but older hypabyssal kimberlite dates occur repeatedly in at least four pipes (Renard 1-4; Figure 3.3). If these older dates reflect the presence of xenocrystic perovskite in some samples, then a prediction is that older kimberlites do exist in the Otish field. Tappe et al. (2017) used single hypabyssal kimberlite samples from Renard 2 and Renard 3 and assumed the pipes formed at the same time (~655 Ma) before intrusion of the 632 Ma Renard 1 body due to an absence of documented data from previous Renard dating studies and the close proximity of the two pipes at the south end of the cluster. Similarly, Birkett et al. (2004) used a single hypabyssal kimberlite sample to date the Renard 1 pipe. This study and that of Ranger et al. (2018) reveal multiple kimberlite dates from single pipes in the range of ~655 Ma and ~632 Ma do occur if only hypabyssal kimberlite samples are selected for dating. It is clear that selecting only one hypabyssal kimberlite sample from a single Renard pipe can be misleading and miss the protracted >20 Myr emplacement history. Tappe et al. (2017) conceded that this ~20 Myr difference between Renard 1 and Renards 2 and 3 is similar to the duration recorded across some kimberlite fields, but did not believe there was enough geological evidence to justify the difference in age. This study confirms that a distinct ~633-632 Ma late-stage intrusive event is

recorded in at least three pipes (Renard 1-3) and a single $^{206}Pb/^{238}U$ date from the G04-296 Anomaly. Significantly older kimberlite xenoliths or younger kimberlite intrusions compared to the main pipe-infilling stages of kimberlite magmatism are contrary to the long-held belief that entire kimberlite bodies are emplaced in <1-2 Ma (e.g. Wagner 1914; Mitchell 1986; Field and Scott Smith 1999). In addition, two younger dates from Renard 7 (weighted average $^{206}Pb/^{238}U$ date of 614.3±2.6 Ma) and Renard 2 ($^{206}Pb/^{238}U$ date of 539.1±2.0 Ma for the sample that is peripheral to the pipe) documented in this study extend the range of kimberlite magmatism at Renard. These new observations demonstrate that even younger hypabyssal kimberlite could be accidently sampled from within a Renard pipe. The possibility of mixing between older and younger kimberlite material was not considered by Tappe et al. (2017). Instead these authors challenged the validity of the 522 Ma U-Pb ilmenite date for the Lynx dyke system (McCandless et al. 2008) and assumed that the dyke systems formed at broadly the same time as the pipes between 655-630 Ma (and not >100 Myr later) in line with existing published U-Pb perovskite emplacement ages (Birkett et al. 2004; Fitzgerald et al. 2009). In contrast, the present study clearly shows a protracted period of hypabyssal kimberlite activity in the Renard cluster (currently recognized in the Renard 2 and 7 pipes) similar to elsewhere in Québec, such as the 551 Ma Lac Beaver kimberlite (Moorhead et al. 2003). Furthermore, the Renard pipes are aligned along a NNW-trending lineament similar to the Lynx dyke system, consistent with the possibility of repeated kimberlite magma intrusion following structural weaknesses in the crust. Key to the present study is the idea that relying upon single hypabyssal kimberlite samples in the Otish field for geochronology could accidently produce misleading emplacement dates for the main pipe-infilling stage of pipe construction given the possibility of selecting samples that may be at least ~100 Myr younger or more than ~10 Myr older than the main pipe-infilling material.

## Relationship to the breakup of eastern Rodinia

The new and published ID-TIMS U-Pb perovskite dates confirm a lengthy predominantly Neoproterozoic history of kimberlite intrusion within the Otish field, which can be divided into two main periods (~>663-615 Ma and ~551-539 Ma; Moorhead et al. 2003; Birkett et al. 2004; Fitzgerald et al. 2009; Tappe et al. 2017; Ranger et al. 2018; this study). Importantly, this refined Renard kimberlite emplacement history (summarized in Figures 3.3 and 3.5)

demonstrates that the majority of Renard kimberlite magmatism does not coincide with the voluminous mafic magmatism related to the two phases of rift-related intrusion recorded along Laurentia's southeastern margin as the Iapetus opened (760-700 Ma and 620-550 Ma; e.g. Aleinikoff et al. 1995; Cawood et al. 2001). Notably, there is a coeval relationship between the younger <615 Ma Renard hypabyssal kimberlites and magmatism related to the second phase within the Grenville Province, Appalachian Mountains, and both sides of the Labrador coast (summarized in Supplementary Material 1 in Appendix C, which includes a selection of more recent age information excluding older publications, such as K-Ar dates, where possible).

Dated dyke swarms and intrusions associated with the ~620-550 Ma Central Iapetus Magmatic Province LIP (Ernst and Buchan 1997, 2001; Ernst and Bell 2010) along Laurentia's southeastern margin were divided into four pulses (615 Ma, 590 Ma, 560 Ma and 550 Ma). Firstly (Pulse 1), the opening of the Iapetus ocean is thought to be marked by the intrusion of the 615 Ma Long Range dykes in Labrador and Newfoundland (615±2 Ma, Kamo et al. 1989; 614+6/-4 Ma, Kamo and Gower 1994). In the present study, we demonstrate for the first time contemporaneous basaltic and kimberlitic magmatism between the Long Range dykes located approximately 900 km east of the 614 Ma hypabyssal kimberlite in the Renard 7 pipe. This was followed by Pulse 2, represented by the 590 Ma Grenville dyke swarm along the Ottawa graben (590+2/-1 Ma, Kamo et al. 1995; ~>579-577 Ma, Halls et al. 2015). Pulse 3 at ~560 Ma includes both the 80-km-wide Sept Iles layered intrusion along the St. Lawrence rift system, which coincides with crustal doming near Sept Iles (565±4 Ma; Higgins and van Breemen 1998), and the Catoctin Formation with felsic feeder dykes in the Appalachian Blue Ridge Mountains (564±9 Ma and 572±5 Ma dykes, Aleinikoff et al. 1995; 562±5 Ma, Southworth and Aleinikoff 2007; 571-563 Ma tuffs, Southworth et al. 2009b). The last pulse (4) at ~550 Ma is marked by the Tibbit Hill Formation near the Sutton Mountains triple junction (554+4/-2 Ma, Kumarapeli et al. 1989; Kumarapeli 1993), the Skinner Cove Formation (550.5+3/-2 Ma, McCausland et al. 1997; 550±5 Ma and 556± 5 Ma, Hodych et al. 2004) and the Mt. St-Anselme basalts (550±7 Ma, Hodych and Cox 2007). The last pulse was observed by Puffer (2002) to coincide with a change in composition from continental flood basalts to resemble ocean island basalts, termed plume-derived LOIB (or Laurentian OIB). In addition, numerous rift-related felsic and mafic intrusions associated with the CIMP LIP occur from Newfoundland to the Appalachians and

coincide with this ~65 Myr period of igneous activity (see Supplementary Material 1 in Appendix C for details). A new $^{206}Pb/^{238}U$ date of 539.1±2.0 Ma from a hypabyssal kimberlite peripheral to the Renard 2 pipe, along with the previously determined age of the Lac Beaver kimberlite (551 Ma; Moorhead et al. 2003), are similar in timing with this last pulse of CIMP-related magmatism before the final opening of the Iapetus. The younger (<615 Ma) kimberlites also temporally correlate with 606-550 Ma alkaline (ultramafic lamprophyre)-carbonatite dykes (or transitional aillikite to kimberlite in the Sarfartoq region; Secher et al. 2009; Tappe et al. 2012) in Labrador and Greenland (Torngat Mountains, Labrador coast, Aillik Bay, Sarfartoq, possibly Umanak; Larsen and Rex 1992; Tappe et al. 2004, 2006, 2007, 2008, 2011, 2012; Secher et al. 2009), the 585-550 Ma alkaline-carbonatite complexes with dykes along the St. Lawrence rift system (Callander, Brent, Manitou Island, possibly Iron Island and Burritt Island, St. Honoré, Chicoutimi or Arvida, Baie des Moutons; Kumarapeli and Saull 1966; Gittins et al. 1967; Doig and Barton 1968; Doig 1970; Kumarapeli 1977, 1985) including the slightly younger 532 Ma Mt. Rigaud and Chatham-Grenville syenite-granite stocks in the Ottawa graben (McCausland et al. 2007), and in Scandinavia which was initially recognized by Doig (1970).

A temporal and spatial relationship between the Renard kimberlites and the CIMP LIP becomes clearer when examined with this new U-Pb data (Figures 3.4 and 3.5). It is apparent that kimberlite and related rocks intruded over a broad area into the thicker lithosphere of the Superior Province (~663-539 Ma Otish, 629 Ma Wemindji) and North Atlantic Craton (~559 Ma Maniitsoq, ~587-557 Ma Sarfartoq). The CIMP LIP and associated rift-related magmatism intruded the thinner lithosphere of the Appalachians and Grenville Province. The alkaline-carbonatite complexes/dykes are associated with the St Lawrence rift system and Labrador Sea coasts. A distal spatial relationship between Neoproterozoic magmatism in western Greenland and eastern North America with the timing of rifting related to the final stages of Iapetus opening has been previously speculated (e.g. Doig 1970; Larsen and Rex 1992; Secher et al. 2009). Spatial relationships between alkaline-carbonatite intrusions and rifting (e.g. Kumarapeli and Saull 1966; Doig 1970; Gittins 1988; Burke et al. 2003, 2008; Rukhlov and Bell 2010), kimberlites (e.g. Larsen and Rex 1992; Donnelly et al. 2011) and LIPs (e.g. Chalaphathi Rao and Lehman 2011; Ernst 2014) have been observed in other cratons. A large-scale mechanism, such as a mantle plume, could be a plausible trigger for CIMP-related magmatism across eastern

North America and western Greenland, and the distal younger ~587-539 Ma kimberlite and related rocks (Maniitsoq, Sarfartoq, Lac Beaver, Renard 2) in the Superior Province and North Atlantic Craton.

The older kimberlites (~663-625 Ma Renard and Wemindji), emplaced at least ~10-15 Myr prior to the documented onset of rifting, are more difficult to explain due to the lack of other well-dated coeval intrusions in eastern North America and Greenland. The 629 Ma Wemindji sills and ~633-632 Ma Renard hypabyssal kimberlites are ~400 km apart, which further supports that a large-scale feature influenced formation of kimberlite magmas over a broad area of crust prior to 615 Ma. Recent isotopic dating along Laurentia's margin suggests there is potential for finding additional information in this age range. For example, a U-Pb zircon date of 624±2 Ma for one Rand Hill dyke (Adirondack dykes; Hodych and Bennett 2009) is at least ~36 Myr older than previously reported (~578-528 Ma, K-Ar, Geraghty et al. 1979; ~588-542 Ma, K-Ar, Isachsen et al. 1988). Dates for the earlier rifting phase were recently expanded from 760-700 Ma to ~765-680 Ma preserved in two Appalachian Mountain massifs (Shenandoah, French Broad; e.g. Fokin 2003; Tollo et al. 2004; McClellan and Gazel 2014 and references therein). The Shenandoah massif (which includes the Catoctin Formation) contains possible younger U-Pb zircon dates from felsic plutons (666±10 Ma Stewartsville, 653±19 Ma Mobley Mountain; Fokin 2003). Older publications with K-Ar dates were not examined in detail here (e.g. Onslow dike, Doig and Barton 1968; Brent crater alkaline dykes, Kumarapeli 1977).

## Relationship to Baltica and Amazonia

A shared 620-550 Ma rifting history between Laurentia and Amazonia has not yet been recognized (e.g. see discussion in Ernst and Bell 2010) but a ~626-542 Ma shared history with Baltica appears to correlate with the second phase of rifting (Figure 3.6). Neoproterozoic dyke swarms similar in timing to the 615 Ma Long Range dykes and 590 Ma Grenville dyke swarm occur along the rifted Baltoscandian margin (e.g. Andréasson 1994; Andréasson et al. 1998), such as the Egersund basaltic dyke swarm in southwest Norway (616±3 Ma, Bingen et al. 1998; 600±10 Ma, Walderhaug et al. 2007) and along the Scandinavian Caledonides (Sarek, Kebnekaise, Corrovare Nappe, Hamningberg; Zwaan and Van Roermund 1990; Svenningsen

1996, 2001; Roberts and Walker 1997; Paulsson and Andreasson 2002; Baird et al. 2014; Kirsch and Svenningsen 2016). The Ottfjället dolerite dyke swarm may also be related but is dated by K-Ar (665±10 Ma; Claesson and Roddick 1983). Baltica has several ~590-542 Ma carbonatite-alkaline complexes, including the well-known Alnö in northeast Sweden, the nearby Avike Bay carbonatite complex, and Fen in southern Norway (Kresten et al. 1977; Dahlgren 1994; Meert et al. 1998, 2007; Rukhlov and Bell 2010) also similar in timing to some alkaline-carbonatite complexes/dykes and the 590 Ma Grenville intrusion (noted by Ernst and Bell 2010) in Laurentia. Two Neoproterozoic igneous provinces in Baltica parallel in timing with the CIMP in eastern Laurentia (e.g. Shumlyanskyy et al. 2007, 2016; Larsen et al. 2018); the ~580-560 Ma Seiland Igneous Province with coeval alkaline-carbonatite intrusions (Roberts et al. 2006, 2010) and the ~590-550 Ma Volyn large igneous province and nearby Sławatycze Formation tuffs (Compston et al. 1995), which may contain older material (Bakun-Czubarow et al. 2008; Shumlyanskyy et al. 2016). Hypabyssal and volcaniclastic kimberlites of the ~626-589 Ma Kaavi-Kuopio Group I kimberlite province (O'Brien et al. 2003) and the ~759-747 Ma Kuusamo kimberlite province (O'Brien and Bradley 2008; Phillips et al. 2017) within the Archean Karelian craton in Finland also suggest a similar temporal and spatial relationship to the breakup of Rodinia (O'Brien and Tyni 1999; Kargin 2014; O'Brien 2015).

The temporal and spatial relationship between Neoproterozoic kimberlites in Laurentia (and perhaps Baltica) and basaltic magmatism in the CIMP, Seiland and Volyn point towards an LIP-related trigger to magma formation. LIPs are commonly interpreted as products of mantle plumes linked to the breakup of supercontinents (e.g. Courtillot et al. 1999; Dalziel et al. 2000; Eldholm and Coffin 2000; Ernst and Buchan 2001; Heaman 2008). Mantle plume-related processes have been proposed to explain Neoproterozoic kimberlite magmatism in Labrador and Greenland (e.g. Nelson 1989; Larsen and Rex 1992; Digonnet et al. 2000; Tachibana et al. 2006), and mafic magmatism along Laurentia's southeastern margin (e.g. Kumarapeli 1993; Higgins and van Breemen 1998; Puffer 2002), and the Baltoscandian margin (e.g. Torsvik et al. 1996). Several plume centers in Laurentia have been proposed, including near the Sept Iles intrusion (Higgins and van Breemen 1998), near the Sutton Mountains and Tibbit Hill Formation (e.g. Kumarapeli 1993; Puffer 2002; Hodych and Cox 2007; Ernst and Bell 2010), between the Long Range and Grenville dykes (Ernst and Buchan 1997) or possibly at the triple point between

Laurentia-Baltica-Amazonia (Ernst and Bell 2010). But if an upwelling mantle plume triggered the CIMP LIP, then the location of a possible Neoproterozoic hotspot track (with a similar magmatic expression as the much younger Great Meteor hotspot track; Heaman and Kjarsgaard 2000) during the main period of Renard magmatism (~656-632 Ma) is not known. Puffer (2002) suggested that the absence of a hotspot track at ~550 Ma was due to the position of the plume relative to Laurentia and Gondwana's movement. In other words, if following Li et al.'s (2008) model, the continental crust of Laurentia may have drifted southwards towards the plume until ~550 Ma, but then after ~550 Ma changed direction to drift northwards towards the equator away from the plume. Puffer's (2002) suggestion could be extended towards the positions of Laurentia, Baltica and Amazonia prior to 550 Ma. There is much debate regarding models reconstructing Rodinia, the rate of plate motion, and results of paleomagnetism studies (e.g. McCausland et al. 2007, 2011; Mitchell et al. 2011; Merdith et al. 2017; Appendix C Supplementary Material 2), but the Rodinia configuration presented by Li et al. (2008) is most commonly accepted and used for discussion here. The 600 Ma high- and low-latitude Rodinia reconstructions presented by Li et al. (2008), and summarized in Figure 3.7, show that between 720-600 Ma Laurentia may have drifted rapidly southwards to high-latitudes or remained nearly stationary at low-latitudes. With either option, a hotspot track prior to 600 Ma is unlikely (e.g. a high-latitude Laurentia would not have crossed over a plume center). If a plume head arrived at ~600 Ma (Ernst and Buchan 1997), during the main 600-550 Ma phase of plume-related activity, a high-latitude Laurentia may have drifted slightly whereas a low-latitude Laurentia would have drifted significantly towards higher latitudes. The absence of a hotspot track between 600-550 Ma would favor the high-latitude option.

Prior to 615 Ma, if Amazonia and Baltica had remained adjacent to Laurentia then perhaps these cratons could have passed over a developing or already present plume center (following the high-latitude option) and recorded older (perhaps not yet discovered) Neoproterozoic magmatism. Long-lived (100-150 Myr) mantle plumes are predicted to double in size to ~2000-3000 km diameter during their ascent to flatten at the base of the lithosphere (e.g. Griffiths and Campbell 1990; Condie 2001). Using a Sutton Mountains plume center this diameter could include younger ~615-539 Ma Otish kimberlites (Figure 3.6). Perhaps the older >625 Ma Renard kimberlites represent a distal intracontinental response to the thick Superior lithospheric mantle

and the edge of a long-lived plume? One possible interpretation is that this Neoproterozoic kimberlite magmatism is formed by a combination of continental extension/rifting and mantle plume(s) over Rodinia's protracted breakup history. This hypothesis could explain more than 100 Myr of repeated kimberlite intrusion in the Otish field, as Laurentia may have drifted southwards towards a 600 Ma plume center. Although the triggering mechanism for the ~663-625 Ma Superior Province kimberlites is not clear, there are widespread repeatable events at ~650 Ma (hypabyssal kimberlite in Renard pipes 1-4), ~630 Ma (Renard, Wemindji, Kaavi-Kuopio), and coeval <615 Ma dates between Laurentia and Baltica which support the presence of older kimberlite emplaced during a similar long-lived event. Although some magmatism may have been derived by lithospheric thinning from continental extension and rifting (e.g. Tappe et al. 2004, 2006, 2008, 2012; Secher et al. 2009), the results of this study and Ranger et al. (2018) support a temporal relationship between the Renard cluster and the CIMP LIP.

## Conclusions

New high precision ID-TIMS U-Pb groundmass perovskite dates determined from six Renard pipes (Renard 1-4, 7, 9) and the G04-296 Anomaly dyke obtained in this study identify the first example of a protracted kimberlite intrusion history within a single cluster and pipe recorded from small hypabyssal kimberlites. The salient conclusions of this study are:

1) The Otish field kimberlites have a more complex intrusion history than previously known. Single hypabyssal kimberlite samples from Renard may not be representative of the main pipe-infilling eruption, which is contrary to the assumption that entire kimberlite bodies are emplaced within <1 Ma. Some hypabyssal kimberlites recorded >10 Myr of emplacement history (e.g. ~35 Myr at Renard 7 and >100 Myr at Renard 2).
2) Unlike hypabyssal kimberlite samples, the main pipe-infilling units of four Renard pipes (Renard 1-4) gave new U-Pb dates that indicate a relatively short (~8 Myr) pipe emplacement event.
3) The majority of Renard kimberlites (and Wemindji sills) were emplaced into the eastern Superior Province prior to 615 Ma (~656-625 Ma), i.e. between the Franklin and CIMP LIP events. Younger hypabyssal kimberlites (Renard 2, Renard 7, Lac Beaver) overlap with the

CIMP LIP and associated rift-related intrusions along the Laurentian margin and St. Lawrence rift system. A mechanism of continental extension/rifting and mantle plume(s) is speculated based on the plate reconstruction model of Li et al. (2008). These new findings support a prolonged connection between multiple kimberlite intrusions, large igneous provinces and supercontinent breakup.

4) A $^{206}Pb/^{238}U$ date of 663.0±2.2 Ma from Renard 4 is interpreted as indicating the presence of xenocrystic perovskite in this sample. If correct, this suggests that even older kimberlites could have intruded into this part of the Superior Province.

**Table 3.1.** ID-TIMS U-Pb groundmass perovskite results for kimberlites of the Otish field, Québec, Canada.

| Unit | Sample | Compositional parameters | | | | | | | Isotope ratios | | | | | | Isotopic date (Ma) | | Recommended $^{206}Pb/^{238}U$ date (Ma) | | | |
|---|---|---|---|---|---|---|---|---|---|---|---|---|---|---|---|---|---|---|---|---|
| | | Weight (mg) | U (ppm) | Th/U | Pb (ppm) | $^{206}Pb^*$ (mol %) | $Pb^*/Pb_c$ | $Pb_c$ (pg) | $^{238}U/^{204}Pb$ | ± (%) | $^{206}Pb/^{204}Pb$ | ± (%) | $^{206}Pb/^{238}U$ | ± (%) | $^{206}Pb/^{238}U$ | ± (2σ) | Weighted Average | ± (2σ) | MSWD | Fractions Used |
| | (a) | (b) | (c) | (d) | (c) | (e) | (e) | (e) | (i) | (g) | (i) | (g) | (f) | (g) | (h) | (g) | | | | |
| *Renard 1* | | | | | | | | | | | | | | | | | | | | |
| Kimb1d | 37375B-1 | 0.008 | 123 | 10 | 53.5 | 85.9% | 6 | 62 | 1111.0 | 8.7 | 134.59 | 7.53 | 0.10522 | 0.37 | 644.9 | 2.3 | 646.0 | 1.6 | 2.0 | 1, 2 |
| Kimb1d | 37375B-2 | 0.019 | 143 | 9 | 59.3 | 88.7% | 8 | 130 | 1369.7 | 4.0 | 162.33 | 3.52 | 0.10560 | 0.37 | 647.1 | 2.3 | | | | |
| Kimb1c-body | 37317B-3 | 0.030 | 76 | 19 | 53.1 | 86.9% | 12 | 127 | 1159.2 | 4.1 | 139.34 | 3.57 | 0.10491 | 0.41 | 643.1 | 2.5 | | | | |
| Kimb1c-body | 37322B-1 | 0.009 | 102 | 13 | 56.3 | 81.3% | 6 | 76 | 787.9 | 7.0 | 99.99 | 5.69 | 0.10444 | 0.45 | 640.4 | 2.8 | | | | |
| *Renard 2* | | | | | | | | | | | | | | | | | | | | |
| Kimb2c | 38919-1 | 0.011 | 99 | 11 | 37.9 | 88.2% | 8 | 43 | 1738.9 | 13.0 | 169.55 | 11.57 | 0.08722 | 0.38 | 539.1 | 2.0 | | | | |
| Kimb2c | 38919-2 | 0.016 | 77 | 12 | 29.1 | 88.3% | 9 | 47 | 1858.4 | 11.9 | 169.89 | 10.58 | 0.08176 | 0.47 | 506.6 | 2.3 | | | | |
| *Renard 3* | | | | | | | | | | | | | | | | | | | | |
| Kimb3f | 31543-2 | 0.026 | 102 | 14 | 56.8 | 86.6% | 9 | 150 | 1127.4 | 3.6 | 136.09 | 3.15 | 0.10500 | 0.46 | 643.6 | 2.8 | | | | |
| Kimb3i | 31548-1 | 0.019 | 89 | 7 | 32.0 | 88.1% | 6 | 82 | 1336.6 | 6.5 | 157.44 | 5.72 | 0.10455 | 0.45 | 641.0 | 2.8 | | | | |
| Kimb3i | 31548-2 | 0.014 | 135 | 7 | 48.1 | 88.5% | 6 | 88 | 1373.0 | 6.0 | 162.66 | 5.34 | 0.10559 | 0.35 | 647.1 | 2.2 | | | | |
| FKimb3h | 31555-1 | 0.015 | 128 | 10 | 55.0 | 89.6% | 9 | 83 | 1541.0 | 6.4 | 179.94 | 5.72 | 0.10528 | 0.26 | 645.3 | 1.6 | 644.9 | 1.1 | 0.5 | 1, 2 |
| FKimb3h | 31555-2 | 0.016 | 155 | 11 | 69.7 | 89.3% | 9 | 112 | 1467.5 | 4.7 | 172.00 | 4.17 | 0.10514 | 0.26 | 644.5 | 1.6 | | | | |
| Kimb3g | 31556-1 | 0.026 | 145 | 15 | 80.8 | 90.7% | 14 | 139 | 1715.5 | 3.7 | 197.39 | 3.39 | 0.10472 | 0.25 | 642.0 | 1.5 | 640.5 | 1.1 | 8.7 | 1, 2 |
| Kimb3g | 31556-2 | 0.018 | 136 | 14 | 72.5 | 90.5% | 13 | 94 | 1701.4 | 5.6 | 194.94 | 5.09 | 0.10415 | 0.28 | 638.7 | 1.7 | | | | |
| Kimb3d | 31559-1 | 0.011 | 101 | 9 | 39.6 | 88.5% | 7 | 53 | 1434.7 | 10.3 | 168.76 | 9.17 | 0.10529 | 0.33 | 645.4 | 2.0 | | | | |
| Kimb3d | 31559-2 | 0.016 | 138 | 11 | 63.9 | 88.8% | 9 | 102 | 1406.5 | 5.1 | 164.80 | 4.56 | 0.10457 | 0.29 | 641.2 | 1.8 | 641.3 | 1.4 | 0.027 | 2, 3 |
| Kimb3d | 31559-3 | 0.046 | 134 | 10 | 55.9 | 89.1% | 8 | 279 | 1407.7 | 1.9 | 164.98 | 1.73 | 0.10462 | 0.39 | 641.4 | 2.4 | | | | |
| Kimb3c | 31552B-1 | 0.008 | 98 | 10 | 66.9 | 54.7% | 1 | 247 | 211.5 | 2.1 | 39.54 | 1.12 | 0.10324 | 1.36 | 633.4 | 8.2 | 633.2 | 1.4 | 0.12 | 1-3 |
| Kimb3c | 31552B-2 | 0.011 | 89 | 13 | 45.9 | 89.9% | 12 | 41 | 1742.7 | 13.7 | 197.51 | 12.44 | 0.10315 | 0.32 | 632.9 | 1.9 | | | | |
| Kimb3c | 31552B-3 | 0.041 | 91 | 13 | 45.4 | 90.1% | 11 | 148 | 1607.7 | 3.5 | 183.77 | 3.12 | 0.10327 | 0.33 | 633.6 | 2.0 | | | | |
| *Renard 4* | | | | | | | | | | | | | | | | | | | | |
| Kimb4b | 39289-2 | 0.010 | 131 | 13 | 68.5 | 87.9% | 9 | 69 | 1318.9 | 7.7 | 156.66 | 6.83 | 0.10536 | 0.35 | 645.7 | 2.1 | | | | |
| Kimb4b | 39289-4 | 0.034 | 115 | 12 | 56.6 | 88.2% | 9 | 189 | 1300.2 | 2.7 | 152.99 | 2.40 | 0.10404 | 0.44 | 638.0 | 2.7 | | | | |
| Kimb4c | 39282B-2 | 0.012 | 116 | 11 | 53.5 | 90.6% | 11 | 52 | 1775.5 | 10.5 | 205.38 | 9.55 | 0.10570 | 0.31 | 647.7 | 1.9 | | | | |
| Kimb4c | 39282B-3 | 0.017 | 121 | 7 | 43.0 | 91.1% | 9 | 77 | 1777.4 | 6.8 | 210.18 | 6.25 | 0.10832 | 0.35 | 663.0 | 2.2 | | | | |

**Table 3.1.** Continued.

| Unit | Sample | Compositional parameters | | | | | | | Isotope ratios | | | | | | Isotopic date (Ma) | | Recommended $^{206}Pb/^{238}U$ date (Ma) | | | |
|---|---|---|---|---|---|---|---|---|---|---|---|---|---|---|---|---|---|---|---|---|
| | | Weight (mg) | U (ppm) | Th/U | Pb (ppm) | $^{206}Pb^*$ (mol %) | $Pb^*/Pb_c$ | $Pb_c$ (pg) | $^{238}U/^{204}Pb$ | ± (%) | $^{206}Pb/^{204}Pb$ | ± (%) | $^{206}Pb/^{238}U$ | ± (%) | $^{206}Pb/^{238}U$ | ± (2σ) | Weighted Average | ± (2σ) | MSWD | Fractions Used |
| | (a) | (b) | (c) | (d) | (c) | (e) | (e) | (e) | (i) | (g) | (i) | (g) | (f) | (g) | (h) | (g) | | | | |
| Kimb4c | 39283B-1 | 0.018 | 51 | 18 | 33.6 | 89.2% | 14 | 41 | 1586.8 | 13.8 | 185.00 | 12.48 | 0.10540 | 0.34 | 646.0 | 2.1 | 646.8 | 1.5 | 1.08 | 1, 2 |
| Kimb4c | 39283B-2 | 0.015 | 93 | 15 | 54.3 | 89.9% | 13 | 58 | 1639.2 | 9.4 | 190.94 | 8.47 | 0.10566 | 0.32 | 647.5 | 2.0 | | | | |
| Kimb4c | 39283B-3 | 0.070 | 54 | 16 | 32.9 | 90.5% | 15 | 147 | 1647.2 | 3.6 | 192.97 | 3.26 | 0.10639 | 0.37 | 651.7 | 2.3 | | | | |
| *Renard 7* | | | | | | | | | | | | | | | | | | | | |
| Kimb7c | 35789B-2 | 0.012 | 79 | 14 | 43.4 | 81.6% | 6 | 77 | 834.8 | 7.0 | 101.67 | 5.80 | 0.10054 | 0.70 | 617.5 | 4.1 | 614.3 | 2.6 | 4.1 | 2, 4 |
| Kimb7c | 35789B-4 | 0.009 | 82 | 14 | 46.5 | 78.5% | 5 | 67 | 701.4 | 8.1 | 87.63 | 6.39 | 0.09962 | 0.56 | 612.2 | 3.3 | | | | |
| Kimb7c | 35790B-1 | 0.015 | 67 | 16 | 42.1 | 85.6% | 9 | 61 | 1089.9 | 9.0 | 132.63 | 7.73 | 0.10544 | 0.54 | 646.2 | 3.3 | | | | |
| Kimb7c | 35791-1 | 0.016 | 93 | 9 | 43.0 | 76.9% | 3 | 161 | 577.7 | 3.2 | 78.59 | 2.46 | 0.10543 | 0.55 | 646.2 | 3.4 | 647.9 | 2.6 | 2.6 | 1, 2 |
| Kimb7c | 35791-2 | 0.010 | 131 | 8 | 58.5 | 77.5% | 3 | 146 | 594.1 | 3.5 | 80.74 | 2.73 | 0.10615 | 0.64 | 650.4 | 4.0 | | | | |
| *Renard 9* | | | | | | | | | | | | | | | | | | | | |
| Kimb9b | 31468-1 | 0.027 | 101 | 11 | 46.6 | 88.2% | 9 | 129 | 1359.0 | 4.1 | 156.09 | 3.59 | 0.10181 | 0.37 | 625.0 | 2.2 | | | | |
| Kimb9b | 31468-2 | 0.017 | 111 | 10 | 43.7 | 88.8% | 8 | 80 | 1564.7 | 6.6 | 168.58 | 5.89 | 0.09637 | 0.37 | 593.1 | 2.1 | | | | |
| Kimb9c-1 | 31497-1 | 0.009 | 95 | 10 | 42.2 | 87.4% | 7 | 44 | 1323.0 | 12.6 | 156.01 | 11.18 | 0.10454 | 0.40 | 641.0 | 2.4 | 640.7 | 1.4 | 3.3 | 1-3 |
| Kimb9c-1 | 31497-2 | 0.009 | 109 | 11 | 49.0 | 90.5% | 11 | 39 | 1839.8 | 14.4 | 210.36 | 13.17 | 0.10471 | 0.34 | 641.9 | 2.1 | | | | |
| Kimb9c-1 | 31497-3 | 0.029 | 110 | 10 | 50.7 | 83.7% | 5 | 224 | 894.8 | 2.3 | 110.65 | 1.93 | 0.10387 | 0.53 | 637.1 | 3.2 | | | | |
| *G04-296 Anomaly* | | | | | | | | | | | | | | | | | | | | |
| | 31577-2 | 0.006 | 123 | 6 | 38.0 | 88.3% | 6 | 33 | 1533.7 | 17.5 | 175.89 | 15.72 | 0.10315 | 0.40 | 632.8 | 2.4 | | | | |

(a) Multi-grain fractions of groundmass perovskite, typically ~100-200 crystals.

(b) Each fraction weighed using a Mettler UMT2 ultramicrobalance.

(c) Concentrations determined by isotope dilution (±1-2% 2 sigma).

(d) Model Th/U ratio calculated from radiogenic $^{208}Pb/^{206}Pb$ ratio and $^{206}Pb/^{238}U$ age.

(e) Pb* and $Pb_c$ represent radiogenic and common Pb, respectively; mol % $^{206}Pb^*$ with respect to radiogenic, blank and initial common Pb.

(f) Corrected for fractionation, spike, common Pb, and blank (5 pg Pb; 1 pg U). Blank IC: $^{206}Pb/^{204}Pb = 18.24\pm2.0\%$; $^{207}Pb/^{204}Pb = 15.64\pm2.0\%$; $^{208}Pb/^{204}Pb = 37.50\pm2.0\%$ (uncertainties 1-sigma). Excess over blank was assigned to initial common Pb.

(g) Errors are 2-sigma, propagated using the algorithms of Schmitz and Schoene (2007).

(h) Calculations are based on the decay constants of Jaffey et al. (1971). $^{206}Pb/^{238}U$ ages corrected for initial disequilibrium in $^{230}Th/^{238}U$ using Th/U [magma] = 5.

(i) Corrected for fractionation, spike, and blank Pb only.

Stacey and Kramers (1975) used to estimate initial common lead isotopic composition

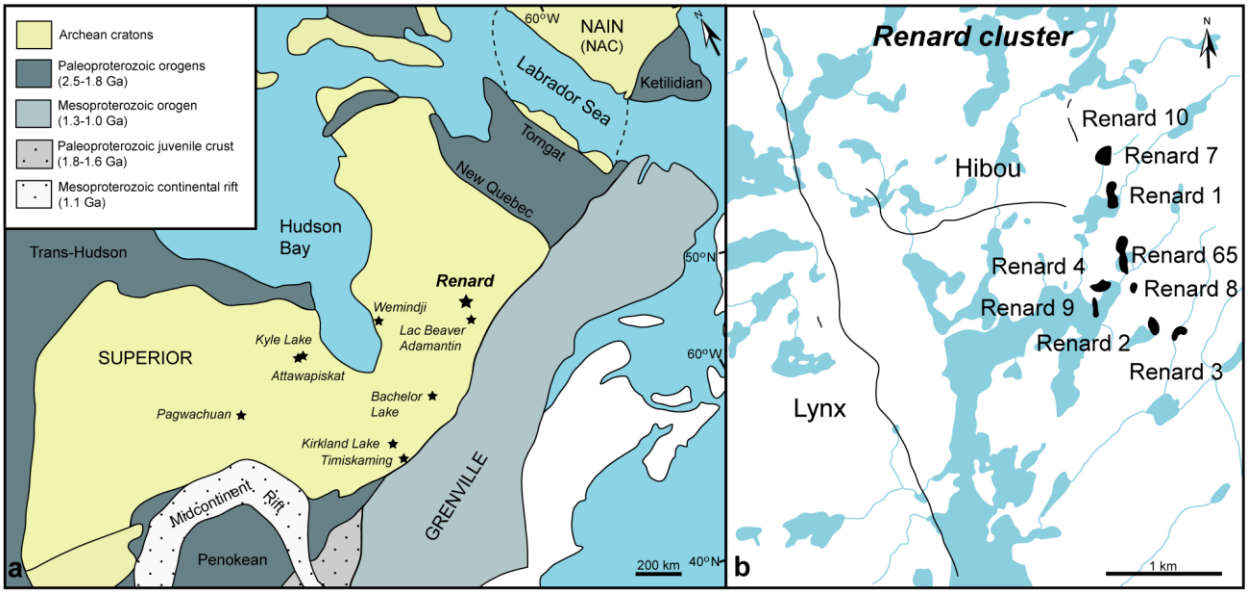


**Fig. 3.1**. (a) Locations of Superior Province kimberlites within the simplified regional geology of eastern Canada and the pre-drift position of Greenland (modified from Hoffman 1989; Card and Poulsen 1998; Godin et al. 2016; Barnett and Laroulandie 2017; Delgaty et al. 2017). Latitude/longitude and north arrow are approximated from Hoffman (1989). NAC = North Atlantic Craton. (b) Sketch of the Renard kimberlite cluster (Otish field, Québec) with locations of Renards 1-10 and the surface outlines interpreted for the Lynx and Hibou dyke systems (modified after Godin et al. 2016). The G04-296 Anomaly dyke is located ~9 km SW of the Renard cluster.

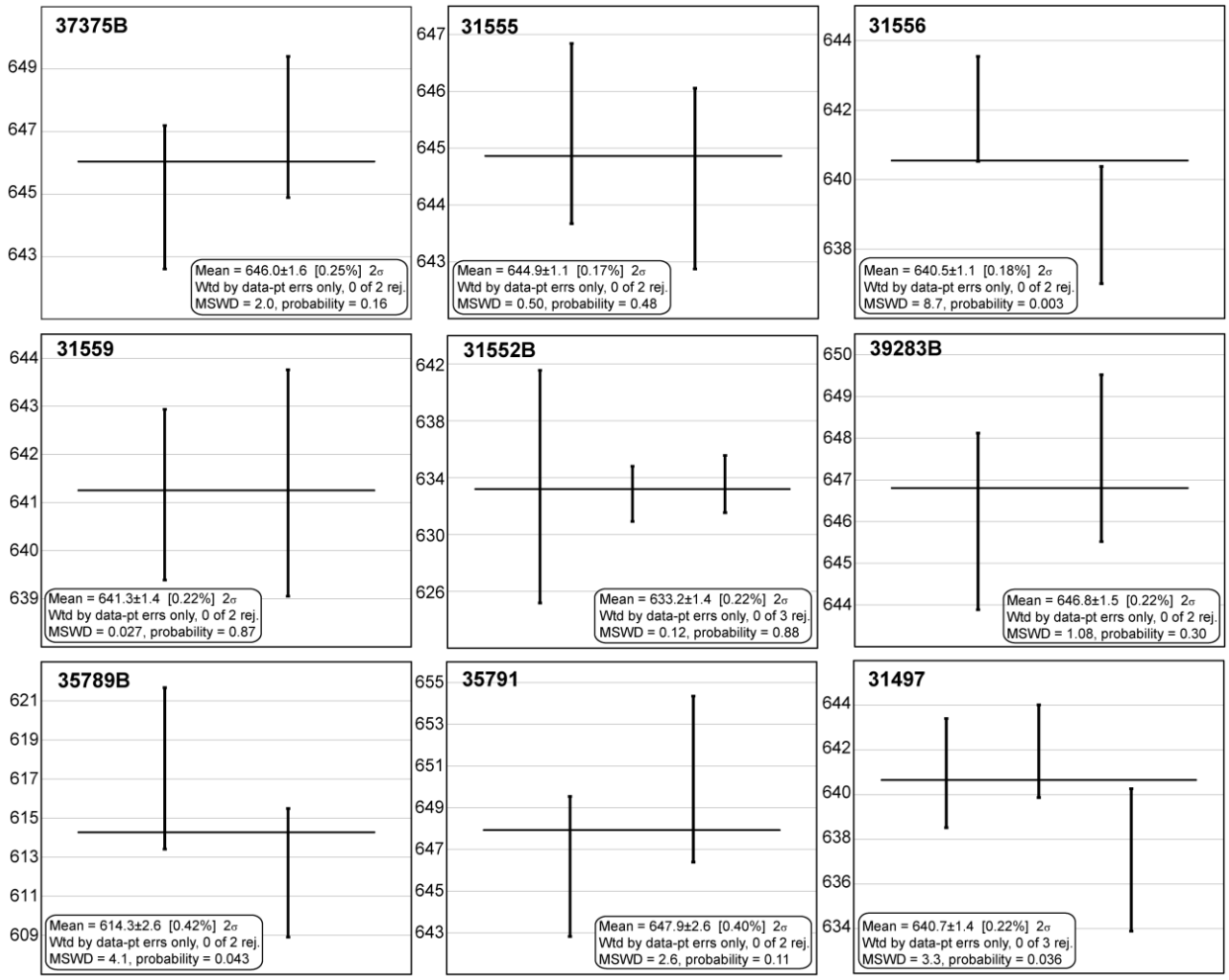


**Fig. 3.2.** Weighted average $^{206}Pb/^{238}U$ dates of multi-grain groundmass perovskite fractions from Renard 1 (37375B), Renard 3 (31555, 31556, 31559, 31552B), Renard 4 (39283B), Renard 7 (35789B, 35791), and Renard 9 (31497). Dates in Ma.

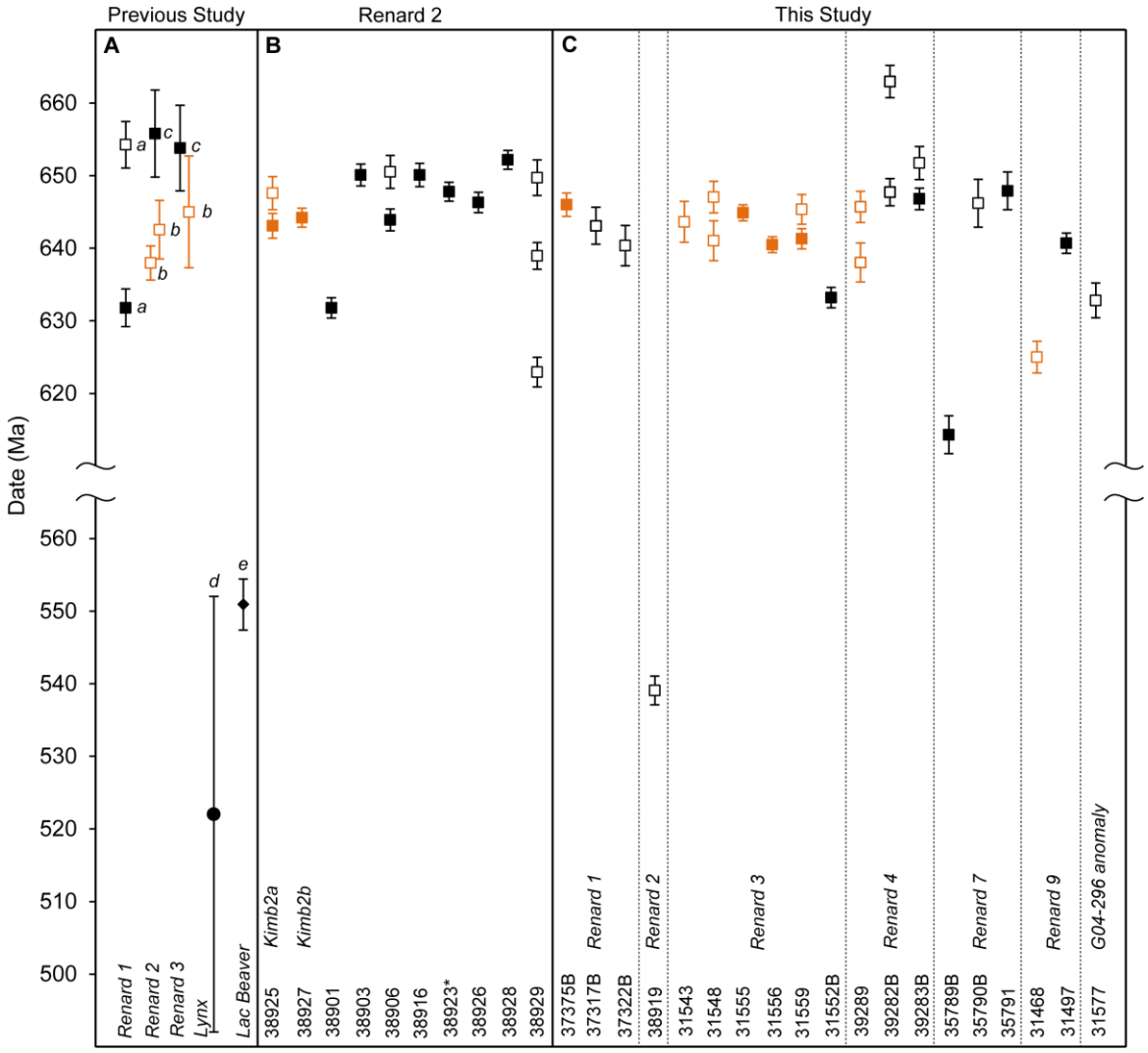


**Fig. 3.3.** Summary of dates from the Otish field (Québec). Symbols for the main pipe-infilling units in orange and smaller hypabyssal kimberlite samples in black. *Panel A*: previously published weighted average (closed) and single (open) $^{206}Pb/^{238}U$ perovskite dates for Renard 1-3 [a - Birkett et al. (2004), b - Fitzgerald et al. (2009) with recalculated dates presented in Ranger et al. (2018), and c - Tappe et al. (2017)], (d) U-Pb groundmass ilmenite isochron date for the Lynx dyke system (McCandless et al. 2008), and (e) U-Pb perovskite date for the Lac Beaver hypabyssal kimberlite pipe (Moorhead et al. 2003). *Panel B*: ID-TIMS weighted average (closed) and single (open) $^{206}Pb/^{238}U$ perovskite dates from the Renard 2 main pipe-infilling units (Kimb2a and Kimb2b) and hypabyssal kimberlites (Kimb2c) from Ranger et al. (2018) [sample 38923 denoted with an asterisk (*) to indicate it is possibly not a Kimb2c]. *Panel C*: new ID-TIMS weighted average (closed) and single (open) $^{206}Pb/^{238}U$ perovskite dates from the main pipe-infilling units and hypabyssal kimberlites from Renard 1-4, 7, 9 and G04-296 Anomaly.

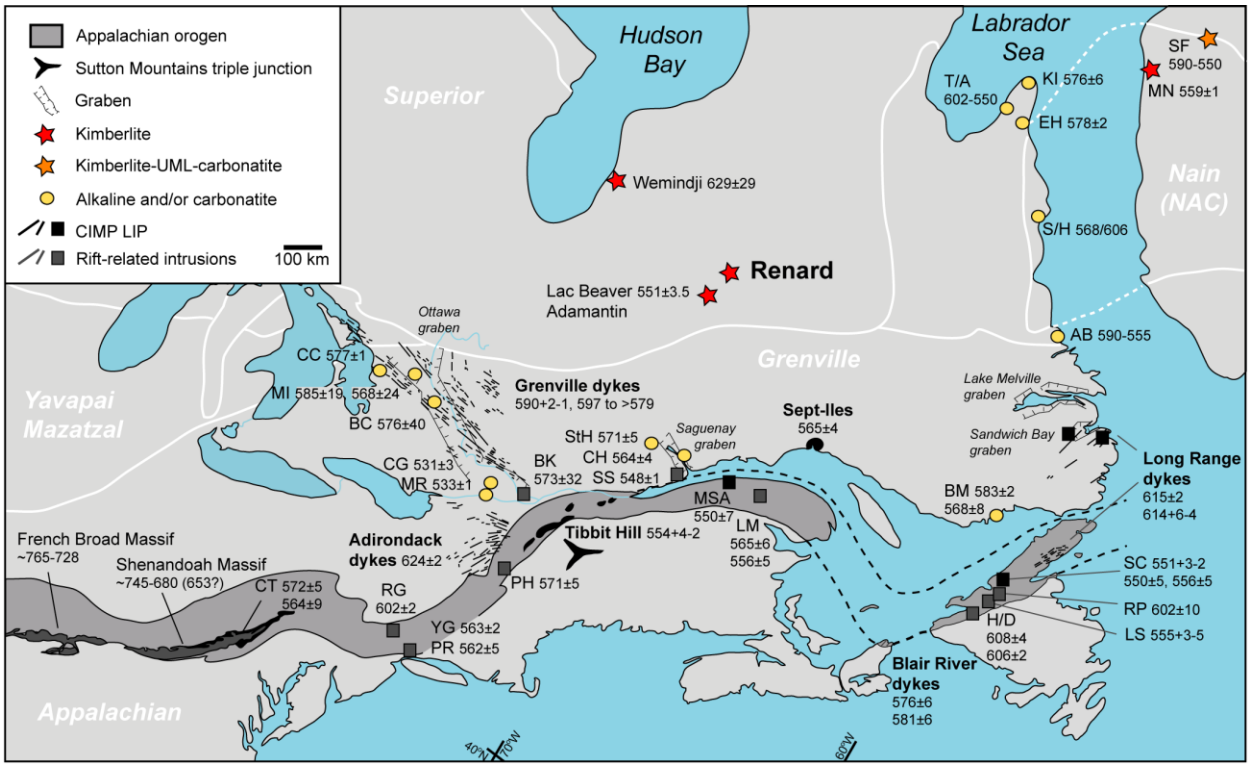


**Fig. 3.4**. Simplified regional geology map of eastern North America and western Greenland with approximate locations of Neoproterozoic CIMP LIP and rift-related intrusions, alkaline-carbonatite complexes and dykes, kimberlites and proposed location of the Sutton Mountains triple junction (modified from Doig and Barton 1968; Shafiqullah et al. 1968; Kumarapeli 1977; Card and Poulsen 1998; Cawood et al. 2001; Puffer 2002; Tollo et al. 2004; Hodych and Cox 2007; Godin et al. 2016; Barnett and Laroulandie 2017; Google Maps 2018 for Great Lakes; Supplementary Material 1 in Appendix C). Dates in Ma. Aillik Bay-AB, Baie des Moutons-BM, Brent crater-BC, Buckingham lavas-BK, Callander complex-CC, Catoctin Formation-CT, Chatham-Grenville stock-CG, Chicoutimi-CH, Eclipse Harbour-EH, Hare Hill and Disappointment Hill-H/D, Killinek Island-KI, Lac Matapedia-LM, Lady Slipper pluton-LS, Maniitsoq-MN, Mont Rigaud stock-MR, Mt. St. Anselme-MSA, Pinney Hollow Formation-PH, Pound Ridge Granite Gneiss-PR, Reading Prong dyke-RG, Round Pond-RP, Saglek and Hebron-S/H, Sarfartoq-SF, Skinner Cove Formation-SC, St. Honoré carbonatite-StH, St. Simeon dykes-SS, Torngat Mountains/Abloviak-T/A, Yonkers Gneiss-YG.

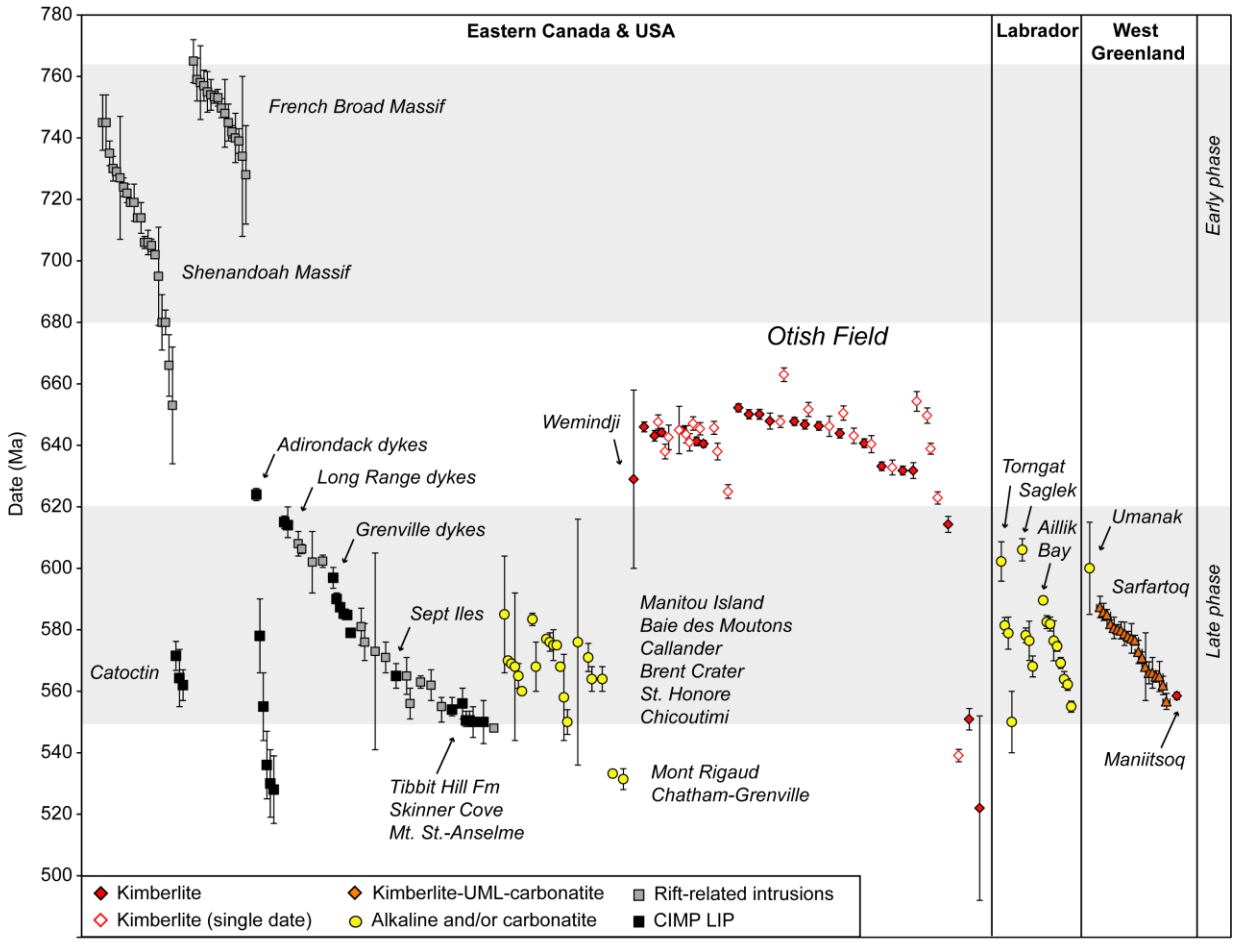


**Fig. 3.5.** Summary of published dates for igneous rocks emplaced between ~765-520 Ma in eastern North America and western Greenland. Timing of the two phases of rifting (765-680 Ma and 620-550 Ma) denoted in light grey (e.g. Cawood et al. 2001; McClellan and Gazel et al. 2014). See Supplementary Material 1 in Appendix C for details and references.

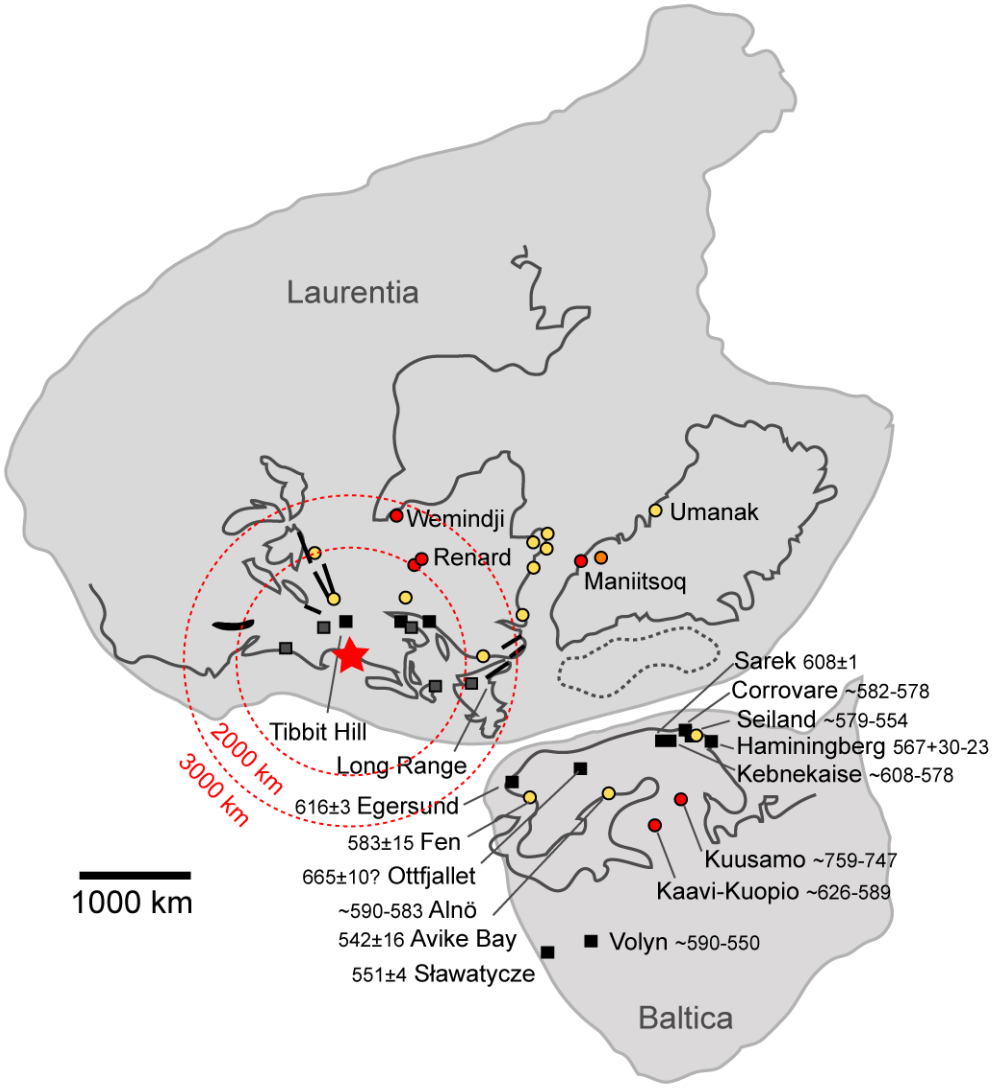


**Fig. 3.6.** Sketch of Laurentia and Baltica with approximate locations of major Neoproterozoic intrusions (black and grey squares), alkaline-carbonatite complexes and dykes (yellow circles), and kimberlites (red circles) (modified after Li et al. 2008; Ernst and Bell 2010). Dates in Ma. See Supplementary Material 1 in Appendix C for details.

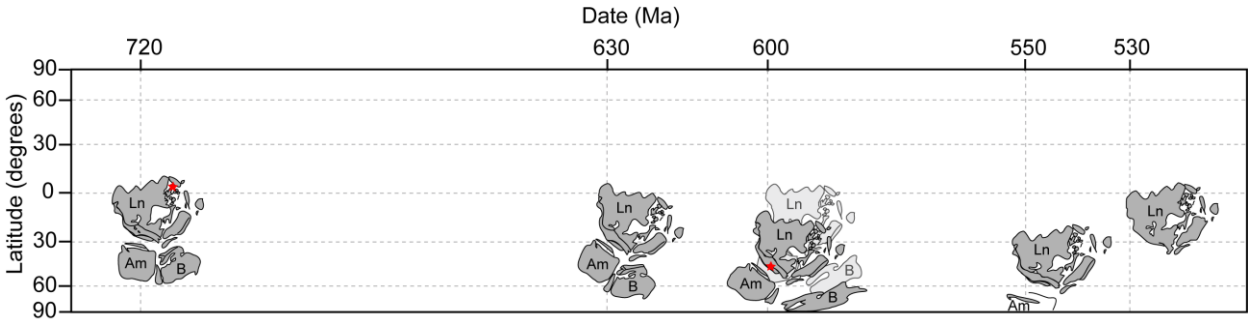


**Fig. 3.7.** Simplified sketch of the positions of Laurentia (Ln), Baltica (B) and Amazonia (Am) between 720 Ma to 530 Ma using the high-latitude (dark grey) and low-latitude (light grey at 600 Ma) options modified after Li et al. (2008). Locations of inferred plume centers (red stars) for the Franklin LIP at 720 Ma and CIMP LIP at 600 Ma after Ernst and Bleeker (2010).

# CHAPTER 4
# FIRST IDENTIFICATION AND U-Pb DATING OF KASSITE $CaTi_2O_4(OH)_2$ FROM A RENARD 9 HYPABYSSAL KIMBERLITE, QUÉBEC, CANADA


## Abstract

We report the second known occurrence of the rare hydrous Ca-Ti oxide kassite ($CaTi_2O_4(OH)_2$) replacing perovskite in kimberlite. Kassite was identified in a hypabyssal kimberlite sample from the Renard 9 pipe (Otish field, Québec). The grains were investigated using a variety of techniques (electron microprobe, Raman, X-ray diffraction and scanning electron microscope) but were positively identified using Raman and X-ray diffraction. Detailed analysis showed the grains can contain minor amounts of lucasite-(Ce), $TiO_2$ (anatase), calcite, and Mn-rich ilmenite.

The first ID-TIMS U-Pb date for kassite is presented. The U-Pb results for two multi-grain kassite fractions are slightly discordant yet the $^{206}Pb/^{238}U$ and $^{207}Pb/^{235}U$ dates are remarkably similar with weighted average dates of 447.5±1.2 Ma and 456.1±2.1 Ma, respectively. We interpret the best estimate for the timing of kassite crystallization to be constrained by the weighted average $^{207}Pb/^{235}U$ date of 456.1±2.1 Ma (2σ) in this hypabyssal kimberlite.


## Introduction

Grains of kassite (a rare hydrous Ca-Ti oxide; $CaTi_2O_4(OH)_2$) containing minor amounts of lucasite-(Ce), $LREETi_2O_5(OH)$ (where LREE = light rare-earth elements dominated by Ce), were identified for the first time in a hypabyssal kimberlite sample from the Renard 9 pipe (Otish field, Québec). There are few reports of naturally occurring kassite, its polymorph cafetite $Ca[Ti_2O_5](H_2O)$, or the isostructural LREE-rich equivalent to kassite named lucasite-(Ce). The reported occurrences of these minerals are summarized in Table 4.1. Occurrences of kassite in kimberlite are extremely rare; only one well-documented example has been reported from the Iron Mountain kimberlite in the State Line field in Wyoming (Mitchell and Chakhmouradian 1998; Chakhmouradian and Mitchell 2000; Martins et al. 2014). The present study reports

electron microprobe, Raman spectra and X-ray diffraction results that confirm the identity of kassite and also the first ID-TIMS U-Pb date for kassite in the Renard 9 hypabyssal kimberlite.

## Mineralogical background

Since Kukharenko et al.'s (1959) first report of cafetite and an unnamed mineral later identified as kassite (Kukharenko et al. 1965), these rare minerals have been reported from over a dozen localities worldwide (USA, Canada, Greenland, Russia, South Africa, China, Europe, eastern Pacific ocean; Table 4.1). Both minerals were originally found in 1938 in miarolitic cavities in ore pegmatites from the type locality in the Afrikanda complex (Kola Peninsula, Russia) and can occur naturally in a variety of rock types or as synthetic kassite (Rudashevskiy et al. 1977; Self and Buseck 1991; Huang et al. 2010). Petrographically, kassite resembles perovskite, titanite or $TiO_2$ polymorphs (Martins et al. 2013), making this mineral difficult to identify by standard optical microscopy. When reviewing the literature for kassite and cafetite, care must be taken due to inconsistent reports which reflect how easily these minerals can be confused (e.g. Evans et al. 1986; Anthony et al. 1997; Yakovenchuk et al. 1999, 2005). Kukharenko et al. (1959) initially assigned cafetite the chemical formula of $(Ca, Mg)(Fe, Al)_2Ti_4O_{12}\cdot 4H_2O$ due to the presence of Fe, Mg, and Al in their chemical analyses and then in 1965 kassite was assigned the chemical formula of $CaTi_2O_4(OH)_2$. A revision was followed after Milton (1985) and Evans et al. (1986), who thought the original kassite and cafetite X-ray data of Kukharenko et al. (1959, 1965) had been accidently mixed up, based on their study of material from Magnet Cove (Arkansas). Despite similarities between the XRD patterns, unit cell parameters and density of the Magnet Cove sample and Kukharenko et al.'s original report for cafetite, the mineral database entries for cafetite and kassite were subsequently switched to follow the Magnet Cove 'kassite' reported by Evans et al. (1986). However, Self and Buseck (1991) found their TEM results for kassite from Josephine Creek (Oregon) to have unit-cell parameters close to those reported by Kukharenko et al. (1965) for kassite (except for the halved b parameter) and concluded that the two minerals were not mixed up in the original report. These authors proposed that Fe should not be used to distinguish kassite from cafetite. Samples described as kassite by Milton (1985), Evans et al. (1986) and Smith (1989) may in fact be cafetite; see discussion in Self and Buseck (1991) and Pekov et al. (2004). Krivovichev et al. (2003) revised

the chemical formula of cafetite to $Ca[Ti_2O_5](H_2O)$ and determined that Kukharenko et al.'s (1959) original formula containing Fe was likely the result of magnetite or titanomagnetite mixed with their sample (initially described as iron hydroxides by Pekov 1998). Grey et al. (2003) studied chromian kassite from the Saranovskoye chromite deposit in Russia and revised its ideal chemical formula as $Ca[Ti_2O_4(OH)_2]$ and its symmetry as monoclinic (space group $P2_1/a$). It was not until the research of Self and Buseck (1991), Men'shikov et al. (1995, an unpublished study cited in Pekov 1998), Grey et al. (2003) and Krivovichev et al. (2003) that kassite and cafetite were determined to be dimorphs and not chemically distinct minerals, as originally described by Kukharenko et al. (1965). Although several studies have reported the presence of kassite (Table 4.1), only a few include supporting XRD or Raman results to assist in identification, such as Martins et al. (2014) which provides additional data to the study of Chakhmouradian and Mitchell (2000) and Mitchell and Chakhmouradian (1998).

Lucasite-(Ce) ($CeTi_2(O,OH)_6$) was first reported by Nickel et al. (1987) from an olivine lamproite tuff concentrate from the AK1 diatreme at the Argyle diamond mine (Western Australia). Subsequent reports are sparse but lucasite-(Ce) has been noted to occur with kassite from the USA (Mitchell and Chakhmouradian 1998; Chakhmouradian and Mitchell 2000). Nickel et al. (1987) determined a monoclinic symmetry (space group *I*2/*a)* for lucasite-(Ce), which was later suggested to be similar in structure to kassite (Self and Buseck 1991; Grey et al. 2003; Krivovichev et al. 2003). The chemical formula for lucasite-(Ce) is also reported as $Ce[Ti_2O_5(OH)]$ or $LREETi_2O_5(OH)$ (Mitchell and Chakhmouradian 1998; Chakhmouradian and Mitchell 2000; Grey et al. 2003).

Representative images, chemical compositions, and XRD patterns from the literature are summarized in Supplementary Materials 1, 2 and 3 in Appendix D, respectively.

## Geologic setting

The Renard 9 kimberlite was discovered in 2003 and is one of nine Class 1 kimberlite bodies within the diamondiferous Renard cluster (Otish field, Québec) in the Archean Superior Province (Figure 4.1; Godin et al. 2016). Kimberlites within the Otish field include two dyke systems

(undated Hibou and 522±30 Ma Lynx; McCandless et al. 2008), several kimberlite dykes (G04-296 Anomaly, North Anomaly, Southeast Anomaly), the undated Adamantin kimberlites (Barnett and Laroulandie 2017) and the 550.9±3.5 Ma Lac Beaver kimberlite dyke swarm and pipe (Moorhead et al. 2003). The Renard 9 pipe is elongate in shape, 0.7 ha in surface area and dips to the east (Godin et al. 2016). Renard 9 is located directly south of the Renard 4 pipe and is entirely covered by Lac Lagopede. The pipe is considered to contain lower diatreme to root zone phases and comprises two main pipe-infilling units (Kimb9a and Kimb9b; Godin et al. 2016). Godin et al. (2016) describes Renard 9 as follows: Kimb9a is a massive volcaniclastic kimberlite (MVK) of pale green to grey-green Kimberley-type pyroclastic kimberlite (KPK, formerly termed TK or tuffisitic kimberlite; Scott Smith et al. 2013) filling the majority of the pipe. Kimb9b is a brown coherent (CK) or hypabyssal (HK) kimberlite with rare variable transitional textures of hypabyssal kimberlite to tuffisitic kimberlite, is classified as a perovskite monticellite phlogopite kimberlite and occurs as a minor infill (2% of the current modelled pipe). From east to west, the texture of Kimb9b becomes similar to KPK. As well the amount of country rock xenolith dilution in Kimb9a increases so much so that the contact relationship along the west and south sides of the pipe margin appear gradational with the country rock breccia. Smaller hypabyssal kimberlite units termed Kimb9c are present throughout the Renard 9 pipe and surrounding country rock breccia and cracked country rock. These units occur as dykes, irregular intrusions or autoliths (usually <1 m thick in drill core). The dykes are classified as phlogopite monticellite kimberlite and have a high magnetic response. The irregular intrusions are classified as phlogopite spinel monticellite kimberlite and are non-magnetic and carbonate-rich. Autoliths may be present and thought to be undiluted Kimb9a prior to forming kimberlite breccia (Godin et al. 2016). New U-Pb perovskite dates for Renard 9 include a $^{206}Pb/^{238}U$ date of 625.0±2.2 Ma for one main pipe-infilling unit (Kimb9b) and a weighted average $^{206}Pb/^{238}U$ date of 640.7±1.4 Ma from a hypabyssal kimberlite (Kimb9c; 31497) (Ranger 2019 this work).

## Analytical methods

A sample of hypabyssal kimberlite drill core (Kimb9c-1; 31462) from the Renard 9 pipe, provided by Stornoway Diamond Corporation, was found to contain kassite which has not yet been identified in other kimberlite samples in previous work (Ranger et al. 2018; Ranger 2019).

Backscattered electron images and spectra used to assist in identifying mineral phases were collected with a Zeiss Sigma 300 VP-FESEM or a Zeiss EVO LS15 EP-SEM, operating with 15 kV or 20 kV accelerating voltage and both equipped with Bruker energy dispersive X-ray spectroscopy systems.

Major/minor element compositions were measured in thin section with the JEOL 8900R electron microprobe operating with an accelerating voltage of 20 kV, beam current of 20 nA and beam width of 0 (<1) μm. Quantitative wave-length dispersive (WDS) analysis was completed with counting times on peak and background of 30 and 15 seconds, respectively. Elements were standardized using the following standards, analytical crystals and X-ray spectral lines with the ZAF correction: rutile for Ti, $Cr_2O_3$-CB1 for Cr and V-metal for V (Kα, PET); $PrPO_4$ for Pr (Lβ, PET); albite-VA for Na and diopside for Mg (Kα, TAP); plagioclase for Ca, sanidine-MAD for K and apatite-ON for P (Kα, PETH); diopside for Si and FrankSmith-CB1 for Al (Kα, TAPJ); ilmenite for Fe and spessartineSK for Mn (Kα, LIFH); $CePO_4$ for Ce and $LaPO_4$ for La (Lα, LIFH); $NdPO_4$ for Nd and $SmPO_4$ for Sm (Lβ, LIFH). Analyses were monitored with the DUR rutile and CB1 $TiO_2$ standards. Rare earth elements (REE) were standardized following Pyle et al. (2002).

A Bruker SENTERRA spectrometer with an Ar+ laser source (532 nm) housed at MacEwan University was used to collect Raman spectra from thin section. Two spectra and background were collected over a 10 second integration time with a spot size of ~1 μm (100x magnification) over a spectral range of 45-1545 $cm^{-1}$ using a laser power of 10 mW and resolution of ~3-4 $cm^{-1}$. Raman spectra were processed with the OPUS 6.5 spectroscopy software and plotted with Spekwin32 (Menges 2015).

The XRD data were collected on a polycrystalline grain using a Rigaku-Oxford Diffraction Supernova single-crystal X-ray diffractometer installed at the Department of Geosciences at the University of Padova. The diffractometer is equipped with an X-ray micro-source (MoKα wavelength, operating conditions of 50 kV and 0.8 mA). The beam size was 120 μm and the sample-to-detector distance was 68 mm. The detector was a Pilatus 200K (Dectris). The X-ray

diffractogram was obtained by a 0-360° phi rotation in powder diffraction transmission mode. The grains show a variable grain size, with an average size ranging between 40 and 60 µm.

Sample preparation and the ID-TIMS U-Pb method were the same as outlined in Ranger et al. (2018) with HBr chemistry protocols similar to Heaman et al. (2015). Multi-grain fractions weighing ~6-21 µg and ranging between ~30-60 µm in grain size were handpicked for U-Pb dating using a binocular stereomicroscope. Grains <30 µm were avoided during grain selection but tiny black mineral inclusions were prevalent and unavoidable. Isotopic compositions of U and Pb were measured using a VG354 thermal ionization mass spectrometer (single Daly detector mode; fraction 31462C-1) and a Thermo Triton Plus multi-collector thermal ionization mass spectrometer (single ion counter SEM detector mode; fractions 31462C-2 and -3) (Sarkar et al. 2015b). Approximately 180-240 ratios of Pb and U isotopic data were collected sequentially from three (Pb) and two (U) staggered temperature intervals between ~1215-1390°C. The U-Pb results are reported in Table 4.2 with 2σ uncertainties and dates calculated using YourLab (Schmitz and Schoene 2007). The Stacey and Kramers (1975) two-stage model for terrestrial lead evolution was used to estimate the isotopic composition of the initial common lead. Decay constants of $^{238}U=1.55125 \times 10^{-10}$ yr$^{-1}$ and $^{235}U=9.84850 \times 10^{-10}$ yr$^{-1}$ were taken from Jaffey et al. (1971). Wetherill concordia, weighted average $^{206}Pb/^{238}U$ dates and 2σ uncertainties were calculated using Isoplot 4.15 (Ludwig 2012). Seven Ice River perovskite (IR6) fragments were measured to monitor accuracy throughout this study. The IR6 fragments weighed between ~5-61 µg and yielded $^{206}Pb/^{238}U$ dates between 351.8±2.2 Ma (5.1 µg) and 359.0±0.7 Ma (60.9 µg) with a weighted average $^{206}Pb/^{238}U$ date of 357.6±0.5 Ma (2σ; MSWD=11), within analytical uncertainty of the recommended weighted average $^{206}Pb/^{238}U$ date of 356.5±1.0 Ma reported by Heaman (2009).

## Results

**Petrography:** Minor amounts of tiny brown kassite appear randomly disseminated throughout the thin section of this macrocrystal opaque-rich carbonate hypabyssal kimberlite. The kimberlite consists of olivine pseudomorphed by serpentine (±opaques, carbonate) with few necklace-textured opaques set in a fine-grained uniform groundmass of phlogopite (altered),

opaques, and carbonate, with minor serpentine, olivine and apatite. Opaque minerals range from euhedral to anhedral, sometimes with irregular rims. Few atoll spinels are present.

Brown kassite grains range from anhedral to euhedral with high relief. Most grains are <~0.05 mm (few <~0.1 mm) and anisotropic but their interference colour is masked by the mineral colour. Larger grains may show slight undulatory extinction. The kassite grains resemble perovskite, apart from a slight grainy texture when viewed in plane-polarized light (e.g. Figure 4.2) which arises from the presence of platy crystals observed in BSE images. Relict cores are not obvious but some grains contain black inclusions or appear intergrown with opaques. Overgrowths or alteration rims are not obvious with petrographic microscope.

**Major/minor element composition:** Preliminary EDS of kassite from the heavy mineral concentrate revealed less Ca compared with Ti, as well as the presence of Mn and Fe, which are uncharacteristic for perovskite. This spectrum resembles the EDX spectrum for kassite presented by Self and Buseck (1991) (Figures 1-8 in Supplementary Material 6 in Appendix D). Further BSE imaging and quantitative analysis by EPMA in thin section revealed subhedral to anhedral grains ~30-100 μm in size, comprising platy and/or radiating kassite crystals along with lesser amounts of lucasite-(Ce), a $TiO_2$ polymorph, and ilmenite. A selection of BSE images is presented in Figure 4.3 and show that kassite grains appear chemically heterogenous. Details of the EPMA analyses and BSE images are presented in Supplementary Material 4 in Appendix D.

Table 4.3 summarizes representative chemical compositions of kassite averaged from 7 grains (n=11) from internal areas within the grains: $TiO_2$ (~59 wt.%), CaO (~12 wt.%, ) and MnO (~7 wt.%), with minor amounts of FeO (~3 wt.%), $Ce_2O_3$ (~3 wt.%), $La_2O_3$ (~1 wt.%), and $Nd_2O_3$ (~1 wt.%), totaling an average of 86.97 wt.%. Representative compositions of kassite along the grain rim appear similar (n=11 from 8 grains): $TiO_2$ (~60 wt.%), CaO (~14 wt.%, ) and MnO (~7 wt.%), with minor amounts of FeO (~3 wt.%), $Ce_2O_3$ (~2 wt.%), $La_2O_3$ (~1 wt.%), and $Nd_2O_3$ (<1 wt.%), totaling an average of 86.76 wt.%

Irregular bright (i.e. characterized by high average atomic number) areas occur both internally and along the rim but are represented by several different phases (kassite, lucasite-(Ce), and

ilmenite). Some of these bright areas have major-element compositions resembling that of kassite (n=6 from 3 grains), but show slightly higher LREE contents: $TiO_2$ (~58 wt.%), CaO (~10 wt.%), MnO (~8 wt.%), with minor amounts of $Ce_2O_3$ (~5 wt.%), $La_2O_3$ (~3 wt.%), FeO (~3 wt.%), and $Nd_2O_3$ (~1 wt.%). These differences suggest that some brighter areas may be a mixture of kassite and lucasite-(Ce). Examples of these kassite compositions include the blocky-shaped areas within Figure 4.3b (lower right) and tiny bright areas in Figure 4.3d (lower left and top right) and Figure 4.3f (upper right). Minor amounts of a phase resembling lucasite-(Ce) in composition were found along the grain rim or possibly as a tiny inclusion in Figure 4.3e, and possibly along the rim in Figure 4.3c. The composition from one grain is: $TiO_2$ (~57 wt.%), $Ce_2O_3$ (~16 wt.%), $La_2O_3$ (~10 wt.%), CaO (~3 wt.%), $Nd_2O_3$ (~4 wt.%), with minor amounts of MnO, FeO, and $Pr_2O_3$ (<1 wt.% each), totaling 93.43 wt.%. Mn-rich ilmenite (MnO ~8 wt.%) occurs along the rim of the large grain in Figure 4.3d.

A $TiO_2$ phase appears present along some rims. The composition from one analysis of anatase is: $TiO_2$ (~93 wt.%), and minor CaO (~2 wt.%) and FeO (~1 wt.%). BSE images indicate few dark gray areas similar to these analyses are present in other grains and usually near the rim.

Relict perovskite was not analyzed during the EPMA session but further EDS reconnaissance by scanning electron microscope of the large grain in Figure 4.3d found spectra resembling perovskite (Figure 16 in Supplementary Material 6 in Appendix D). The size, shape and texture of kassite within the groundmass and the morphology of individual grains from the heavy mineral concentrate suggests that perovskite was the precursor mineral for kassite pseudomorphs (see Supplementary Material 6 in Appendix D).

**Raman spectra:** The only well characterized example of Raman spectra for kassite is reported by Martins et al. (2014). Proyer et al. (2014) present a Raman spectrum of kassite or cafetite from marble, with major peaks at 283, 332, 372, 396, 469, 547, 604, 677 and 707 $cm^{-1}$ but note that their data do not match well with the available published spectra. There are no published Raman spectra available for lucasite-(Ce). The acquired Raman spectra are summarized in Figure 4.4 and Supplementary Material 5 (Appendix D). Several of the Raman spectra show roughly similar peaks (e.g. ~687, ~460, ~354, ~245, ~154, ± ~116 $cm^{-1}$; Figure 4.4b) of varying

intensity and shape (cf. Figures 4.4b and 4.4c), which are similar to the kassite spectra reported by Martins et al. (2014). Several grains exhibit a strong ~145 $cm^{-1}$ peak, similar to Martins et al.'s (2014) anatase, in the spectra resembling kassite (e.g. spot 5 in Figure 4.4b and spot 3 in Figure 4.4c). In addition, a single strong ~145 $cm^{-1}$ peak for anatase is recorded in a few grains (e.g. Figure 4.4c). Minor calcite appears present at ~1086 $cm^{-1}$ (e.g. spot 5 in Figure 4.4b).

**X-ray diffraction:** Figure 4.5 presents a representative diffractogram for a kassite grain with d-spacings labelled on each diffraction peak in Å (angstroms). Five peaks (3.05, 2.49, 2.09, 1.92, and 1.87 Å) record a calcite impurity (maximum 10% of grain) which was observed in all the grains but it is uncertain if calcite is within the grain matrix or on the grain surface. Major peaks at 4.70, 3.24, 2.58, 2.26, 2.02, 1.73, 1.59 and 1.49 Å appear similar to the strong X-ray diffraction lines reported for kassite by Martins et al. (2014): 4.81, ~3.29, 2.601, 2.308, 2.284, 2.050, 2.034, 1.778, 1.764, ~1.60, and ~1.50 Å. Similar data were reported by Zajzon et al. (2013) and to some extent, Kukharenko et al. (1965) (summarized in Supplementary Material 3 in Appendix D).

**ID-TIMS U-Pb Geochronology:** Orange grains of kassite are common in the heavy mineral concentrate. Three fractions were tested: an initial test of ~50 orange cubic to cuboctahedral grains and fragments (~30-50 μm, some with black inclusions; 31462C-1) and two additional fractions consisting of ~250 orange cubic to cuboctahedral grains and fragments (Figure 4.6; ~30-60 μm, some with black inclusions; 31462C-2 and 31462C-3). The three kassite fractions have uranium and lead concentrations that range 90-158 ppm and 26-34 ppm, respectively, and Th/U values between 7-10; geochemical features that are similar to perovskite (Table 4.2). The proportion of radiogenic $^{206}Pb$ to total Pb is high (93-96%), which is slightly higher than the proportion found in Renard perovskite (Ranger et al. 2018; Ranger 2019 this work). Figure 4.7 presents the U-Pb results on a Wetherill concordia diagram. Fraction 1 is reversely discordant with a slightly older $^{206}Pb/^{238}U$ date of 473.0±3.3 Ma. The other two fractions yield overlapping and slightly discordant (~10-12% discordance) $^{206}Pb/^{238}U$ dates of 448.1±1.3 Ma and 445.9±2.3 Ma (2σ), $^{207}Pb/^{235}U$ dates of 456.4±2.4 Ma and 455.3±4.4 Ma (2σ), and $^{207}Pb/^{206}Pb$ dates of 498±12 Ma and 503±22 Ma (2σ), respectively.

# Discussion

## Comparison with published examples

During U-Pb dating of groundmass perovskite in kimberlite samples from Renard 9, the grains analyzed from one hypabyssal kimberlite (Kimb9c; 31462C) collected from along the pipe margin yielded U-Pb dates unlike those obtained for other Renard kimberlites. Further investigation revealed the mineral to be dominantly comprised of kassite and not perovskite as originally assumed. Perovskite ($CaTiO_3$) is known to occur in silica-undersaturated alkaline rocks and commonly as a primary magmatic mineral in hypabyssal kimberlites as single crystals (usually <0.5 mm, typically ~20-50 μm) disseminated throughout the groundmass (e.g. Mitchell 1986, 1996; Chakhmouradian and Mitchell 2000). Perovskite is considered unstable in $CO_2$-rich fluids during the late stages of kimberlite formation and is known to become altered and/or replaced by reaction rims or pseudomorphs usually composed of $TiO_2$ phases such as anatase (e.g. Boctor and Meyer 1979; Mitchell 1986, 2002; Mitchell and Chakhmouradian 1998; Chakhmouradian and Mitchell 2000). The rare mineral kassite has also been documented as an alteration product of perovskite in kimberlites, with the best studied example from a serpentine-calcite kimberlite from Iron Mountain, State Line field in Wyoming (Mitchell and Chakhmouradian 1998; Chakhmouradian and Mitchell 2000; Martins et al. 2014). Few other occurrences of kassite in kimberlite-related studies have been reported and unfortunately provide minimal supporting information for its identification. These occurrences include: (a) kassite, Fe-oxide and titanite mantling ilmenite within a clinopyroxenitic mantle xenolith (Chino Valley, Arizona; Baziotis et al. 2013a, b); (b) an "unknown" Ca-titanate inclusion in amphibole from a mica-amphibolite rich nodule (Wesselton kimberlite, South Africa; Dawson and Smith 1977); (c) kassite as part of a thin reaction rim assemblage containing Ti-Fe oxides, titanite, and perovskite, and developed after ilmenite megacrysts (Monastery kimberlite, South Africa; Kamenetsky et al. 2014); (d) kassite replacing perovskite in ultramafic dikes (Greenland; Mitchell et al. 1999).

In the Iron Mountain kimberlite example, Mitchell and Chakhmouradian (1998) were able to ascertain the crystallization order of perovskite alteration in multiphase pseudomorphs after Nb-REE-poor perovskite. Kassite was interpreted by these authors as an early replacement phase of

perovskite, which was then followed by anatase, minor titanite, calcite, then Mn-rich ilmenite and, lastly, a LREE-Ti oxide of composition resembling lucasite-(Ce), which was later confirmed by Chakhmouradian and Mitchell (2000). The LREE-Ti oxide occurs within fractures as tiny prismatic crystals (10 μm length, 4 μm width) associated with ilmenite and thought to form from LREE released from the perovskite (Mitchell and Chakhmouradian 1998; Figure 3n in Chakhmouradian and Mitchell 2000). Anatase was optically identified in thin section in their study. Ilmenite occurs either as thin discontinuous rims between kassite and anatase or along fractures, which Mitchell and Chakhmouradian (1998) interpreted as belonging to a single stage of ilmenite crystallization. In Mitchell and Chakhmouradian's (1998) study, kassite was interpreted as an intermediate phase formed during deuteric alteration of perovskite to anatase following the reactions:

$CaTiO_3$ (perovskite) + $CO_2$ (g) => $TiO_2$ (anatase) + $CaCO_3$ (calcite) (after Nesbitt et al. 1981) (1)

$2CaTiO_3$ (perovskite) + $CO_2$ + $H_2O$ => $CaTi_2O_4(OH)_2$ (kassite) + $CaCO_3$ (calcite) (2)

$CaTi_2O_4(OH)_2$ (kassite) + $CO_2$ => $2TiO_2$ (anatase) + $CaCO_3$ (calcite) + $H_2O$ (3)

Note $H_2O$ is needed in reaction (2) for kassite to form. Martins et al. (2014) thermodynamically modelled the stability fields of perovskite, kassite and anatase, and found that kassite forms within a limited field (a 'kassite wedge') corresponding to uniquely high $f(H_2O)$ conditions. High temperatures (e.g. 400$^oC$) appear to limit formation of kassite and calcite. Chakhmouradian and Mitchell (2000) also determined that T <350$^oC$ and P <2 kbar were needed for reaction (1) to take place in kimberlite. In this case, calcite was deposited near perovskite so the $TiO_2$ rim appeared 'spongy' or 'cavernous' or as a relict perovskite core surrounded by calcite (±serpentine) then rimmed by $TiO_2$ similar to the appearance of atoll spinels. Tiny calcite inclusions in anatase were observed by Mitchell and Chakhmouradian (1998). Similar to the Iron Mountain example, calcite appears to be absent from the cores of the kassite grains examined in the present work. The size, shape and disseminated nature of kassite pseudomorphs indicate that they developed after groundmass perovskite. EDS results suggest minor possible relict perovskite may be present in the grain in Figure 4.3d. Titanite appears to be absent.

Modal zoning observed in the Iron Mountain pseudomorphs (Mitchell and Chakhmouradian 1998; Chakhmouradian and Mitchell 2000) appears absent in the Renard 9 sample. The texture of kassite in this study most resembles the BSE images of >60 μm-size platy-textured grains identified by Martins et al. (2014) in the Iron Mountain material (their Figure 1a-c; Supplementary Material 1 in Appendix D). Chemically the Renard 9 kassite most closely resembles kassite from the Monastery kimberlite (Kamenetsky et al. 2014), or Iron Mountain kimberlite and Prairie Lake Complex (Mitchell and Chakhmouradian 1998; Martins et al. 2014). Kassite in this study contains higher MnO (~7 wt.%) than the previously reported examples, but much less than "Mn-kassite" (~24-26 wt.%; Galuskin et al. 2004; Zajzon et al. 2013). The composition of kassite in the Renard 9 sample has slightly lower Ca and Ti contents relative to the ideal chemical composition reported by Grey et al. (2003): CaO 23.98, $TiO_2$ 68.32, $H_2O$ 7.70, total 100.00 wt.%.

Unlike the late stage lucasite-(Ce) confined to fractures in kassite from the Iron Mountain kimberlite, possible lucasite-(Ce) in this study appears randomly dispersed throughout few kassite pseudomorphs. Only two published lucasite-(Ce) compositions are available for comparison (Nickel et al. 1987; Mitchell and Chakhmouradian 1998) but resemble lucasite-(Ce) in this study. The chemical compositions can sometimes be difficult to categorize as kassite or lucasite-(Ce) within the small bright (high average atomic number) areas due to compositional variation in Ca, Mn, and LREE contents. This suggests the existence of a solid solution between kassite and lucasite-(Ce) (Nickel et al. 1987; Self and Buseck 1991), as proposed by Mitchell and Chakhmouradian (1998).

Minor amounts of Mn-rich ilmenite along the rim of the grain in Figure 4.3d indicate an increase in $Mn^{2+}$ and $Fe^{2+}$ activities near the end of alteration comparable to that seen in the Iron Mountain kimberlite (Wyoming) and Sebljavr carbonatite (Russia) (Mitchell and Chakhmouradian 1998). Martins et al. (2014) also noted kassite replacement by ilmenite along the rim and fractures of a grain from the Iron Mountain kimberlite, based on BSE images.

## Evaluation of U-Pb kassite data

Two of the kassite fractions (31462C-2 and -3) yield slightly discordant but very similar $^{207}Pb/^{235}U$ and $^{206}Pb/^{238}U$ dates. In order to evaluate the potential for kassite to record geologically meaningful U-Pb dates, we review several possibilities. It is worth noting that the U-Pb kassite results presented here have features in common with the U-Pb systematics of mantle baddeleyite reported for the Île Bizard alnöite, Québec (see discussion in Heaman and LeCheminant 2000).

***1) The U-Pb results are geologically meaningless***. An independent age estimate for this hypabyssal kimberlite sample is unavailable but the U-Pb kassite dates could lead one to suggest the margin of eastern Laurentia experienced at least one Ordovician event. At this time there are no known Ordovician kimberlite intrusion dates or regional disturbances in this part of the Superior Province.

***2) The U-Pb results record an episodic event resulting in Pb loss***. If the daughter element had been removed by Pb-loss during an event that post-dates Renard 9 kimberlite emplacement then the $^{206}Pb/^{238}U$ and $^{207}Pb/^{235}U$ dates would be younger than the $^{207}Pb/^{206}Pb$ dates and appear discordant. A similar result is possible if the parent element (U) had been added. Here the $^{206}Pb/^{238}U$ and $^{207}Pb/^{235}U$ dates are very similar and the $^{207}Pb/^{206}Pb$ dates are older. If this hypabyssal kimberlite intruded during the main phase of Renard kimberlite magmatism and the observed kassite discordance is explained by Pb loss then the findings can be accounted for by partial Pb loss. Figure 4.8a shows an example using the most concordant fraction from the main pipe infill Kimb9b (31468-1) with an upper intercept of ~636 Ma and a lower intercept of ~340 Ma. If the partial Pb loss was recent, then perhaps the weighted average of the $^{207}Pb/^{206}Pb$ dates (499±10 Ma) could estimate the timing of perovskite alteration to kassite (Figure 4.8b). Although this would be a compelling explanation for the discordant dates, these estimated dates could also be considered suspect as it is unlikely two multi-grain fractions would both record nearly the same amount of discordance by this process. In addition, there are no known Devonian/Carboniferous disturbances in this part of the Superior Province that could explain Pb loss in these grains at this time.

***3) The U-Pb results reflect the initial common lead isotopic composition acquired during grain formation.*** The initial common lead isotopic composition may be unlike estimates from the two-stage model of Stacey and Kramers (1975) used for other Renard 9 samples ($^{206}Pb/^{204}Pb$ ≈18.00 and $^{207}Pb/^{204}Pb$ ≈15.59 for fractions #2 and #3). An independent estimate of this common lead isotopic composition using a co-crystallized unradiogenic groundmass mineral was not possible in this study (Ranger 2019). There are no known North American Ordovician kimberlite intrusions at this time to compare with this sample and few Neoproterozoic kimberlites of similar age to the Otish field in North America. Lead isotopic compositions are available for younger kimberlites in the State Line field (Alibert and Albarede 1988) but not the ~600 Ma Georges Creek and 615 Ma Chicken Park kimberlites or the nearby ~572±49 Ma Green Mountain diatreme in Colorado (Carlson and Marsh 1989; Lester et al. 2001; Heaman et al. 2003). Published examples of initial lead isotopic compositions are sparse. An example from Heaman (1989), who studied perovskite from the 158 Ma Kirkland Lake kimberlite in the Superior Province, reports an initial lead isotopic composition of $^{206}Pb/^{204}Pb$ ≈18.67 and $^{207}Pb/^{204}Pb$ ≈15.53. Figure 4.8c shows the minor shift of the 31462C results away from concordia when using an initial lead isotopic composition approximately comparable to the Kirkland Lake kimberlite reported in Heaman (1989). The minor change shows a much different initial common lead isotopic composition may be needed to shift results towards concordia. Although a possibility, it unfortunately cannot be assessed at this time.

***4) The U-Pb results record gain/loss of intermediate daughter products***. The branched decay of $^{238}U$ and $^{235}U$ to the stable daughter products of $^{206}Pb$ and $^{207}Pb$ produces 18 and 15 intermediate daughter products, respectively. The majority of these IDPs are short-lived with half-lives of less than 22 years except for $^{234}U$ (~246 ka), $^{230}Th$ (~75 ka) and $^{226}Ra$ (~1.62 ka) in the $^{238}U$-$^{206}Pb$ chain and $^{231}Pa$ (~34 ka) in the $^{235}U$-$^{207}Pb$ chain (Schoene 2014). Secular equilibrium between parent and intermediate daughters is assumed (i.e. decay under a closed system) unless decay has been disturbed. The possible loss or gain of intermediate daughter products in an amount other than secular equilibrium, either initially as the mineral crystallized or at a later time, has been discussed in other studies (e.g. Mattinson 1973; Schärer 1984; Heaman and LeCheminant 2000).

Examining IDPs with the longest half-lives, a loss of $^{234}U$ and $^{230}Th$ from the $^{238}U$-$^{206}Pb$ chain or a gain of $^{231}Pa$ in the $^{235}U$-$^{207}Pb$ chain could produce younger $^{206}Pb/^{238}U$ or older $^{207}Pb/^{235}U$ dates, respectively (Figure 4.8d). Schoene (2014) notes that at high temperature, fractionation of $^{234}U$ from $^{238}U$ is assumed to be minor. Mattinson (1973) points out that secular equilibrium will remain between $^{234}U$ and $^{238}U$. A calculation by Parrish (1990), using Schärer's (1984) equations, for a corrected $^{206}Pb/^{238}U$ found the correction was limited to -0.108 Ma for deficit initial $^{230}Th$. Little is known about $^{231}Pa$ disequilibrium (Schoene 2014) but excess $^{231}Pa$ in zircon has been reported by Anczkiewicz et al. (2001). Anczkiewicz et al. (2001) observed a wide range of $^{207}Pb/^{235}U$ dates between fractions to correspond to a nearly uniform $^{206}Pb/^{238}U$ date. Such correspondence is not observed here in the present work.

Mattinson (1973), Schärer (1984), and Heaman and LeCheminant (2000) discussed the possibility of diffusional loss of the noble gas Rn. Schoene (2014) noted that a loss of $^{222}Rn$ would have little effect on the calculated date due to its short half-life (3.8 days). Heaman and LeCheminant (2000) discussed diffusion of IDPs at high temperature to explain the discordant mantle baddeleyite data in their Île Bizard sample. They specifically focused on Rn because as a gas this IDP can diffuse quickly. Radon occurs in both the $^{238}U$ ($^{222}Rn$ and $^{218}Rn$) and $^{235}U$ ($^{219}Rn$) decay chains. $^{222}Rn$ has a longer half-life than $^{219}Rn$ (3.9 seconds) therefore loss of $^{222}Rn$ would have a greater impact on the $^{238}U$ decay chain producing less radiogenic daughter product $^{206}Pb$ and younger $^{206}Pb/^{238}U$ dates. If kassite experienced loss of an intermediate daughter product within the $^{238}U$ decay chain, such as $^{222}Rn$, then the slightly younger weighted average $^{206}Pb/^{238}U$ date of 447.5±1.2 Ma (2σ) would provide a better estimate for the timing of diffusion closure (e.g. end of radon loss) of the kassite grains. The slightly older weighted average $^{207}Pb/^{235}U$ date of 456.1±2.1 Ma (2σ) would best estimate the time of kassite crystallization. Similar to scenario #2, the $^{207}Pb/^{206}Pb$ dates would be older but the dates between $^{206}Pb/^{238}U$ and $^{207}Pb/^{235}U$ would less likely be uniform due to less $^{206}Pb$ produced. The study by Heaman and LeCheminant (2000) included an independent estimate of timing for their sample using perovskite to help rationalize which date was most suitable. An independent age estimate is so far not possible here but the loss of intermediate daughter product(s), such as radon, could be the

best explanation at this time for the observed discordance in these two kassite fractions from this particular hypabyssal kimberlite.

Our current knowledge of the behaviour of kassite in kimberlites is developing, when compared with other more commonly found minerals (e.g. Mitchell and Chakhmouradian 1998; Chakhmouradian and Mitchell 2000; Martins et al. 2014). Martins et al. (2014) make a compelling point that the perovskite composition, and the dissolved constituents and ratio of $H_2O/CO_2$ in the fluid would also influence the type of alteration minerals that form. These variables are unknown for the Renard kimberlites and strong consideration should also be given to scenario #1. But the similarity of the $^{206}Pb/^{238}U$ and $^{207}Pb/^{235}U$ results to the Île Bizard U-Pb baddeleyite study by Heaman and LeCheminant (2000) suggests intermediate daughter product loss (scenario #4) may serve as the best interpretation until new evidence is presented.

## Conclusions

1) A hypabyssal kimberlite sample (Kimb9c; 31462) from the Renard 9 pipe contains the rare mineral kassite which likely pseudomorphed groundmass perovskite.
2) In addition to kassite grains, the pseudomorphs contain compositions resembling minor lucasite-(Ce), anatase, calcite, and Mn-rich ilmenite.
3) Two multi-grain fractions of kassite produced similar weighted average $^{207}Pb/^{235}U$ and $^{206}Pb/^{238}U$ dates of ~456 Ma and ~448 Ma, respectively. Due to the limited published information for kassite, further investigation is needed to fully understand the significance of this mineral and U-Pb date. Several possibilities are considered.
4) Kassite was not found during U-Pb perovskite dating of other Renard pipes. There are a few samples (e.g. see Appendix A) which may contain a groundmass mineral other than perovskite but its grain size and habit make identification challenging. Raman and XRD appear to be the most suitable methods to identify kassite. EPMA results cannot differentiate between kassite and cafetite.

**Table 4.1.** Summary of localities reporting naturally occurring kassite, cafetite and/or lucasite-(Ce).

| Country | Locality | Kassite | Cafetite | Lucasite-(Ce) | Chemical composition | XRD | Raman | Image | Size | Colour | Habit | Rock Type | Reference |
|---|---|---|---|---|---|---|---|---|---|---|---|---|---|
| Russia | Afrikanda massif, Kola peninsula | #1 | YES | --- | YES | YES | --- | YES | cafetite; 1-15 mm (c axis) and 0.01-0.3 mm (a axis) | pale yellow, (diamond luster) (indeterminate mineral); ocher-yellow to colourless (cafetite) | crusts, plate/leaf crystals in aggregates/rosettes, pseudomorphs (indeterminate mineral); fibrous (moss-shaped) aggregates, radial needle intergrowths, rare prismatic crystals, pseudomorphs (cafetite) | miarolitic cavities in ore pegmatite | Kukharenko et al. (1959) |
| Russia | Afrikanda massif, Kola peninsula | YES | YES | --- | YES | YES | --- | YES | 1-15mm (c axis), 0.01-0.3mm (a axis) (cafetite); 1mm (kassite) | ocher-yellow (cafetite); shades of yellow, (diamond (adamantine) luster) (kassite) | in miarolic voids; as growths, pseudomorphs, moss-shaped aggregates, rare radial needles, single needles (cafetite); pseudomorphs, replacement, crusts, lamellar or leaf crystals forming aggregates or rosettes, growths (kassite) | miarolitic cavities in ore pegmatite | Kukharenko et al. (1965) |
| Russia | Afrikanda, Kola peninsula | YES | YES | --- | YES; #2 | --- | --- | --- | --- | --- | --- | holotype specimens (Mineralogical Museum of St. Petersburg University) | Pekov (1998) cites Men'shikov et al. (1995) |
| Russia | Afrikanda massif, Kola peninsula | --- | YES | --- | YES | YES | --- | --- | --- | --- | --- | holotype specimen (13420) (from AA Kukharenko) | Krivovichev et al. (2003) |
| Russia | Khibiny alkaline massif, Kola Peninsula | --- | YES | --- | --- | YES; #3 | --- | --- | --- | --- | --- | --- | Pekov (1998) |
| Russia | Kukisvumchorr and Rasvumchorr mountains, Khibiny, Kola peninsula | --- | YES | --- | YES | --- | --- | YES; #4 | --- | orange, yellowish | spherolites with thin <1mm diameter plates | #4; natrolite veins | Krivovichev et al. (2003) |
| Russia | #5 | --- | YES; #5 | --- | YES; #5 | --- | --- | YES | --- | --- | --- | --- | Yakovenchuk et al. (1999) |
| Russia | Mt. Kukisvumchorr (Kirov Mine) | --- | YES | --- | YES | --- | --- | --- | up to 1 mm | orange | spherulites (thin lamellae) | natrolite veins in rischorrite | Yakovenchuk et al. (2005) |

**Table 4.1.** Continued.

| Country | Locality | Kassite | Cafetite | Lucasite-(Ce) | Chemical composition | XRD | Raman | Image | Size | Colour | Habit | Rock Type | Reference |
|---|---|---|---|---|---|---|---|---|---|---|---|---|---|
| Russia | Mt. Rasvumchorr | --- | YES | --- | YES | YES | --- | YES | up to 0.8 mm | ochre-brown | spherulites | in voids in natrolite in rischorrite | Yakovenchuk et al. (2005) |
| Russia | Kovdor deposit | --- | YES | --- | --- | --- | --- | YES | --- | --- | --- | --- | Moiseev and Chukanov (2006) |
| Russia | Kovdor alkaline-ultrabasic massifs, Kola peninsula | --- | YES | --- | --- | --- | --- | --- | --- | light brown | --- | peralkaline pegmatite | Chukanov et al. (2004) |
| Russia | Wiluy deposit, Yakutia | YES; #6 | --- | --- | YES | --- | --- | YES | <7-8 μm | --- | hexagonal crosssection, discus-like, pinacoidal, prismatic, rhombohedral, twins, split crystals (e.g. aggregate) | serpentinite | Galuskin et al. (2004) |
| Russia | Wiluy deposit, Republic of Sakha-Yakutia | YES; #6 | --- | --- | --- | --- | --- | --- | --- | --- | --- | aposkarn serpentinite | Galuskina et al. (2007) |
| Russia | Saranovskoye chromite deposit, Urals | YES; #7 & #8 | --- | --- | YES; #9 | --- | --- | --- | --- | --- | --- | --- | Popova et al. (1998) |
| Russia | Saranovskoye chromite deposit, Urals | YES; #7 | --- | --- | YES (chromian kassite) | YES; Single-crystal | --- | --- | single crystal flakes 0.01-0.02 mm thick; general size unknown | bright green (transparent, diamantine luster) | tabular/platy or rosette-like aggregates | in fractures in chromite body | Grey et al. (2003) |
| Russia | Saranovskoye chromite deposit, Urals | YES | --- | --- | YES; #10 | YES | --- | --- | <6 mm diameter | bright green (transparent, diamond luster) | hexagonal tabular, lamellar crystals; split; rosette-like intergrowths | from mineralized crack in chromite ore | Pekov et al. (2004) |
| Russia | --- | #8 | --- | --- | --- | --- | --- | --- | --- | --- | --- | --- | Ivanov (2016) |
| USA | Diamond Jo quarry, Magnet Cove, Arkansas | #11 | #11 | --- | --- | #11 | --- | --- | --- | --- | --- | #11; quartz syenite | Milton (1985) |
| USA | Diamond Jo quarry, Magnet Cove, Arkansas | #11 | #11 | --- | --- | #11 | --- | #11 | <0.5 mm (rosettes), <0.1 mm (spherules) | brownish-pink (rosettes) or yellow (spherules) | platy rosettes or spherules | miarolitic cavities in nepheline syenite | Evans et al. (1986) |
| USA | Diamond Jo quarry, Magnet Cove, Arkansas | #11 | #11 | --- | --- | --- | --- | #11 | <1 mm | pinkish to brown (rosettes) or yellow/white/ tan (spheres), clear-translucent | rosettes or spheres | miarolitic cavities in syenite | Smith (1989) |

**Table 4.1.** Continued.

| Country | Locality | Kassite | Cafetite | Lucasite-(Ce) | Chemical composition | XRD | Raman | Image | Size | Colour | Habit | Rock Type | Reference |
|---|---|---|---|---|---|---|---|---|---|---|---|---|---|
| USA | Chino Valley, Arizona | YES | --- | --- | --- | --- | --- | YES | --- | --- | --- | clinopyroxenite (mantle xenolith) | Baziotis et al. (2013a) |
| USA | Chino Valley, Arizona | YES | --- | --- | --- | --- | --- | --- | --- | --- | --- | clinopyroxenite (mantle xenolith) | Baziotis et al. (2013b) |
| USA | Josephine Creek, Oregon | YES | --- | --- | SEM | YES | --- | --- | μm size | --- | grains | 1 cm spheriod "unusual" specimen | Self and Buseck (1991) |
| USA | Iron Mountain, Wyoming | YES | --- | YES | YES | --- | --- | YES | tens to 170 μm diameter perovskite | sand-yellow or brownish, translucent | possible twinned crystals; roundish perovskite | serpentine-calcite kimberlite | Mitchell and Chakhmouradian (1998) |
| USA | Iron Mountain, Wyoming | YES | --- | YES | --- | --- | --- | YES | --- | --- | --- | kimberlite | Chakhmouradian and Mitchell (2000) |
| USA | Iron Mountain, Wyoming | YES | --- | --- | YES (not reported) | --- | YES; #13 | --- | 100 μm to 1 mm | --- | --- | serpentine-calcite kimberlite | Martins et al. (2013) |
| USA | Iron Mountain, Wyoming | YES (CTO) | --- | --- | YES | YES | YES (map) | YES | --- | --- | --- | kimberlite | Martins et al. (2014) |
| Canada | Prairie Lake complex, Ontario | YES | --- | --- | --- | YES | YES; #13 | --- | 100 μm to 1 mm | --- | --- | silicocarbonatite | Martins et al. (2013) |
| Canada | Prairie Lake complex, Ontario | YES (CTO) | --- | --- | YES | YES | YES | YES | --- | --- | --- | carbonatite | Martins et al. (2014) |
| Greenland | Sarfartoq, Sismiut, Maniitsoq | YES | --- | --- | --- | --- | --- | --- | --- | --- | --- | ultramafic dikes | Mitchell et al. (1999) |
| Hungary | Perkupa evaporate mine | YES; #6 | --- | --- | YES | YES | --- | YES | < few hundred μm | white or light yellow | polyphase aggregates in pyrophanite | serpentinite | Zajzon et al. (2013) |
| Greece | Kimi Complex | #14 | #14 | --- | SEM | --- | YES | YES | --- | --- | --- | marble | Proyer et al. (2014) |
| South Africa | Monastery kimberlite | YES | --- | --- | YES | --- | --- | YES | <1 mm (e.g. <50 μm) | --- | --- | ilmenite megacrysts | Kamenetsky et al. (2014) |
| South Africa | Wesselton kimberlite | #15 | --- | --- | #15 | --- | --- | --- | 20 μm | --- | inclusion in amphibolite | nodule (mica, amphibolite) | Dawson and Smith (1977) |
| Australia | Argyle AK1 diatreme, Kimberley region | --- | --- | YES | YES | YES | --- | YES | 0.5-1 mm diameter | brown to gray (translucent, resinous luster) | subhedral fragments, aggregates | olivine lamproite tuff (concentrate) | Nickel et al. (1987) |
| China | Zhaoanzhuang-type iron-ore deposit, Wuyang (Henan Province), China | YES; #16 | --- | --- | --- | YES | --- | YES; #17 | 0.01-0.02 mm | honey-yellow (greasy luster) | hexagonal cross-section, in geodes, aggregates | ultrabasic-alkaline complex | Yu et al. (1982) |

**Table 4.1.** Continued.

| Country | Locality | Kassite | Cafetite | Lucasite-(Ce) | Chemical composition | XRD | Raman | Image | Size | Colour | Habit | Rock Type | Reference |
|---|---|---|---|---|---|---|---|---|---|---|---|---|---|
| Eastern Pacific Ocean | Ocean Drilling Program Hole 504B | YES | --- | --- | --- | --- | --- | YES | e.g. submicrometer; 30-100 nm wide lamellae (trellis) | --- | e.g. trellis texture | oceanic basalts | Shau et al. (2000) |

**Note:**

#1 - kassite not yet named

#2 - Pekov (1998) cite a revisional study was completed by Yu. P. Men'shikov, I.V. Pekov, I.M. Kulikova and N.V. Chukanov in 1995 on the Afrikanda cafetite and kassite holotype specimens from Mineralogical Museum of St. Petersburg University (data not reported in Pekov 1998)

#3 - X-ray pattern resembling cafetite found by Yu. P. Men'shikov (data not reported in Pekov 1998)

#4 - see Yakovenchuk et al. (1999)

#5 - Yakovenchuk et al. (1999) in Russian. See Yakovenchuk et al. (2005). Incorrect formula for cafetite.

#6 - kassite and Mn-kassite; Galuskin et al. (2004) report Ti-Mn-phase ($MnTi_2O_4(OH)_2xH_2O$(?) (tentatively termed Mn-kassite) and Galuskina et al. (2007) cite a possible new manganese kassite ($MnTi_2O_4(OH)_2$)

#7 - chromian kassite (2 wt% $Cr_2O_3$)

#8 - reference not available through Interlibrary loans

#9 - chemical composition for Popova et al. (1998) listed in Grey et al. (2003)

#10 - chemical composition similar to Grey et al. (2003)

#11 - Milton (1985) discusses possible X-ray data mix up in Kukharenko et al. (1959) and reports their findings as kassite but X-ray data similar to Kukharenko et al.'s cafetite. Similarly Evans et al. (1986) further this discussion and their kassite X-ray data matches cafetite of Kukharenko et al. (1965); Smith (1989) cites Evans et al. (1986)

#12 - unclear if accessory minerals occur with "kassite"

#13 - unclear which sample

#14 - Proyer et al. (2014) tentatively identifed the hydrous Ca-Ti oxide in their study as kassite/cafetite but were unable to determine which polymorph

#15 - unknown Ca-titanate not identified by Dawson and Smith (1977) but a kassite-like composition listed in Table 4 (specimen 5; sample 1082) suggested by Self and Buseck (1991) and Mitchell and Chakhmouradian (1998)

#16 - see introduction of Self and Buseck (1991) for comments regarding kassite identification by Yu et al. (1982). Described negative uniaxial optic sign.

#17 - mineral difficult to see in image

**Table 4.2.** ID-TIMS U-Pb kassite data for hypabyssal kimberlite (31462) in the Renard 9 kimberlite, Québec, Canada.

| Unit | Sample | Compositional parameters | | | | | | | Isotope ratios | | | | | | | | | Isotopic date (Ma) | | | | | |
|---|---|---|---|---|---|---|---|---|---|---|---|---|---|---|---|---|---|---|---|---|---|---|---|
| | | Weight | U | Th | Pb | $^{206}$Pb* | Pb* | $Pb_c$ | $^{238}$U | ± | $^{206}$Pb | ± | $^{207}$Pb | ± | $^{206}$Pb | ± | corr. | $^{207}$Pb | ± | $^{207}$Pb | ± | $^{206}$Pb | ± |
| | | (mg) | (ppm) | U | (ppm) | (mol%) | $Pb_c$ | (pg) | $^{204}$Pb | (%) | $^{204}$Pb | (%) | $^{235}$U | (%) | $^{238}$U | (%) | coef. | $^{206}$Pb | (2σ) | $^{235}$U | (2σ) | $^{238}$U | (2σ) |
| | (a) | (b) | (c) | (d) | (c) | (e) | (e) | (e) | (i) | (g) | (i) | (g) | (f) | (g) | (f) | (g) | | (h) | (g) | (h) | (g) | (h) | (g) |
| Kimb9c-1 | 31462C-1 | 0.006 | 90 | 10 | 25.7 | 93.2% | 13.88 | 9 | 6916.2 | 111.6 | 544.57 | 107.86 | 0.53082 | 3.78 | 0.07613 | 0.72 | 0.47 | 221.4 | 81.0 | 432.4 | 13.3 | 473.0 | 3.3 |
| Kimb9c-1 | 31462C-2 | 0.021 | 122 | 9 | 30.3 | 96.0% | 22.66 | 27 | 7310.4 | 22.7 | 544.30 | 21.96 | 0.56744 | 0.66 | 0.07198 | 0.31 | 0.61 | 498.3 | 11.8 | 456.4 | 2.4 | 448.1 | 1.3 |
| Kimb9c-1 | 31462C-3 | 0.011 | 158 | 7 | 33.5 | 94.7% | 14.23 | 24 | 5661.3 | 25.8 | 423.50 | 24.72 | 0.56587 | 1.19 | 0.07162 | 0.53 | 0.56 | 503.2 | 22.0 | 455.3 | 4.4 | 445.9 | 2.3 |

(a) Multi-grain fractions of kassite crystals.

(b) Each fraction weighed using a Mettler UMT2 ultramicrobalance.

(c) Concentrations determined by isotope dilution (±1-2% 2 sigma).

(d) Model Th/U ratio calculated from radiogenic $^{208}$Pb/$^{206}$Pb ratio and $^{206}$Pb/$^{238}$U age.

(e) Pb* and $Pb_c$ represent radiogenic and common Pb, respectively; mol % $^{206}$Pb* with respect to radiogenic, blank and initial common Pb.

(f) Corrected for fractionation, spike, common Pb, and blank (5 pg Pb; 1 pg U). Blank IC: $^{206}$Pb/$^{204}$Pb = 18.24±2.0%; $^{207}$Pb/$^{204}$Pb = 15.64±2.0%; $^{208}$Pb/$^{204}$Pb = 37.50±2.0% (uncertainties 1-sigma). Excess over blank was assigned to initial common Pb.

(g) Errors are 2-sigma, propagated using the algorithms of Schmitz and Schoene (2007).

(h) Calculations are based on the decay constants of Jaffey et al. (1971). $^{206}$Pb/$^{238}$U ages corrected for initial disequilibrium in $^{230}$Th/$^{238}$U using Th/U [magma] = 5.

(i) Corrected for fractionation, spike, and blank Pb only.

Stacey and Kramers (1975) used to estimate initial common lead isotopic composition

**Table 4.3.** Summary of representative or average electron microprobe chemical compositions of kassite, lucasite-(Ce), anatase, and ilmenite.

| | Kassite | | | Lucasite-(Ce) | Anatase | Ilmenite |
|---|---|---|---|---|---|---|
| | internal | rim | bright | | | |
| | n=11 from 7 grains | n=11 from 8 grains | n=6 from 3 grains | n=1 from 1 grain | n=1 from 1 grain | n=1 from 1 grain |
| $SiO_2$ | 0.67 | 0.18 | 0.23 | 0.542 | 0.091 | 2.068 |
| $Al_2O_3$ | nd | nd | nd | nd | nd | nd |
| $TiO_2$ | 58.58 | 59.74 | 57.96 | 56.965 | 92.536 | 50.028 |
| FeO | 3.30 | 2.78 | 2.57 | 0.958 | 1.091 | 31.610 |
| MgO | 0.15 | 0.16 | 0.08 | nd | nd | 0.980 |
| MnO | 7.44 | 7.03 | 7.65 | 0.231 | 0.424 | 7.872 |
| CaO | 11.66 | 13.88 | 10.09 | 3.250 | 1.778 | 0.419 |
| $Na_2O$ | nd | nd | nd | nd | nd | nd |
| $K_2O$ | nd | nd | nd | 0.020 | nd | 0.030 |
| $P_2O_5$ | nd | nd | nd | nd | nd | nd |
| $V_2O_3$ | nd | nd | nd | nd | nd | nd |
| $Cr_2O_3$ | nd | nd | nd | 0.293 | nd | nd |
| $La_2O_3$ | 1.45 | 0.80 | 2.94 | 10.232 | 0.019 | nd |
| $Ce_2O_3$ | 2.91 | 1.75 | 5.10 | 16.139 | 0.287 | 0.004 |
| $Pr_2O_3$ | 0.02 | 0.02 | 0.16 | 0.795 | nd | nd |
| $Nd_2O_3$ | 0.79 | 0.42 | 1.22 | 4.005 | nd | nd |
| $Sm_2O_3$ | nd | nd | nd | nd | nd | nd |
| *Total* | *86.97* | *86.76* | *87.99* | *93.430* | 96.226 | *93.012* |
| *calculated on:* | | | | | | |
| | *6 oxygens* | | | | *2 oxygens* | *3 oxygens* |
| Si | 0.029 | 0.008 | 0.010 | 0.027 | 0.001 | 0.054 |
| Al | nd | nd | nd | nd | nd | nd |
| Ti | 1.931 | 1.949 | 1.940 | 2.168 | 0.975 | 0.987 |
| Fe | 0.121 | 0.101 | 0.096 | 0.041 | 0.013 | 0.693 |
| Mg | 0.010 | 0.011 | 0.005 | nd | nd | 0.038 |
| Mn | 0.276 | 0.266 | 0.288 | 0.010 | 0.005 | 0.175 |
| Ca | 0.547 | 0.636 | 0.481 | 0.176 | 0.027 | 0.012 |
| Na | nd | nd | nd | nd | nd | nd |
| K | 0.003 | nd | nd | 0.001 | nd | 0.001 |
| P | nd | nd | nd | nd | nd | nd |
| V | nd | nd | nd | nd | nd | nd |
| Cr | nd | nd | nd | 0.012 | nd | nd |
| La | 0.023 | 0.013 | 0.048 | 0.191 | nd | nd |
| Ce | 0.047 | 0.028 | 0.083 | 0.299 | 0.002 | nd |
| Pr | 0.001 | 0.001 | 0.003 | 0.015 | nd | nd |
| Nd | 0.012 | 0.007 | 0.023 | 0.072 | nd | nd |
| Sm | nd | nd | nd | nd | nd | nd |

nd = not detected

Limit of determination removed (6σ; Potts 1992).

Zero (0) values included in average.

Bright = high average atomic number areas in BSE images.

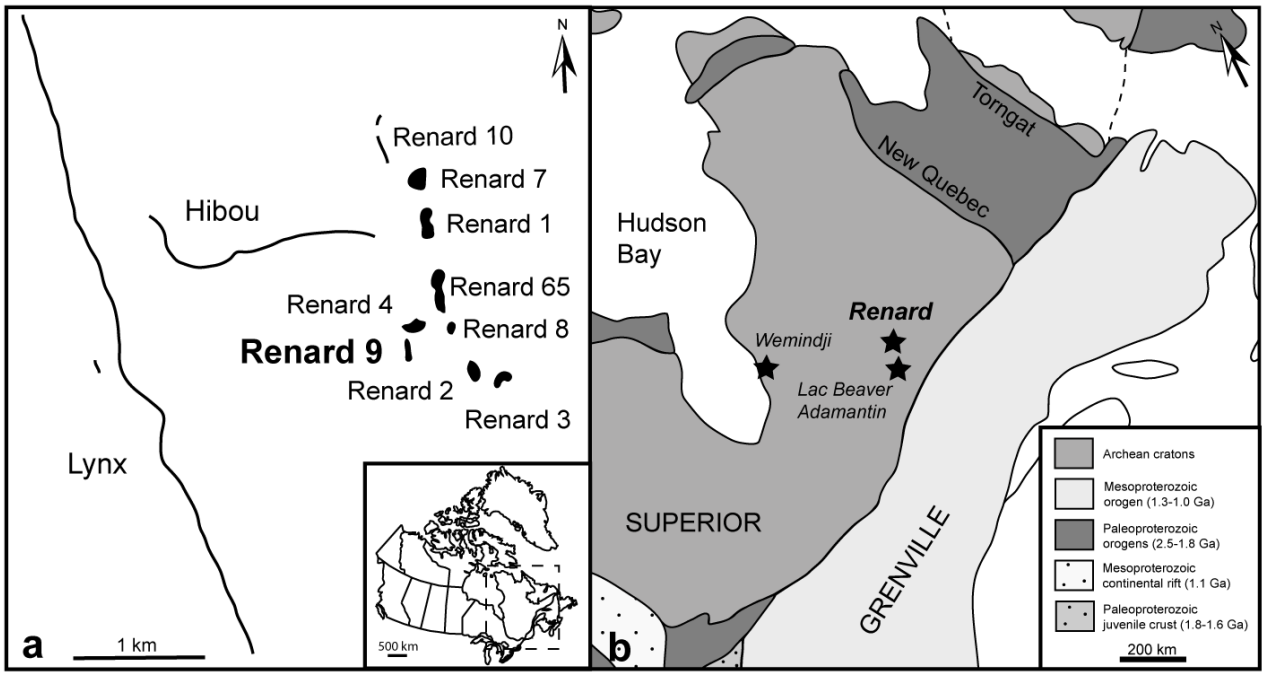


**Fig. 4.1** Simplified geology of (a) the Renard cluster located within the Otish field of north-central Québec (Superior Province) and (b) the regional geology of eastern Canada (modified from Card and Poulsen 1998; Hoffman 1989; Godin et al. 2016; Barnett and Laroulandie 2017). GSZ - Great Slave Lake Shear zone; STZ - Snowbird Tectonic zone.

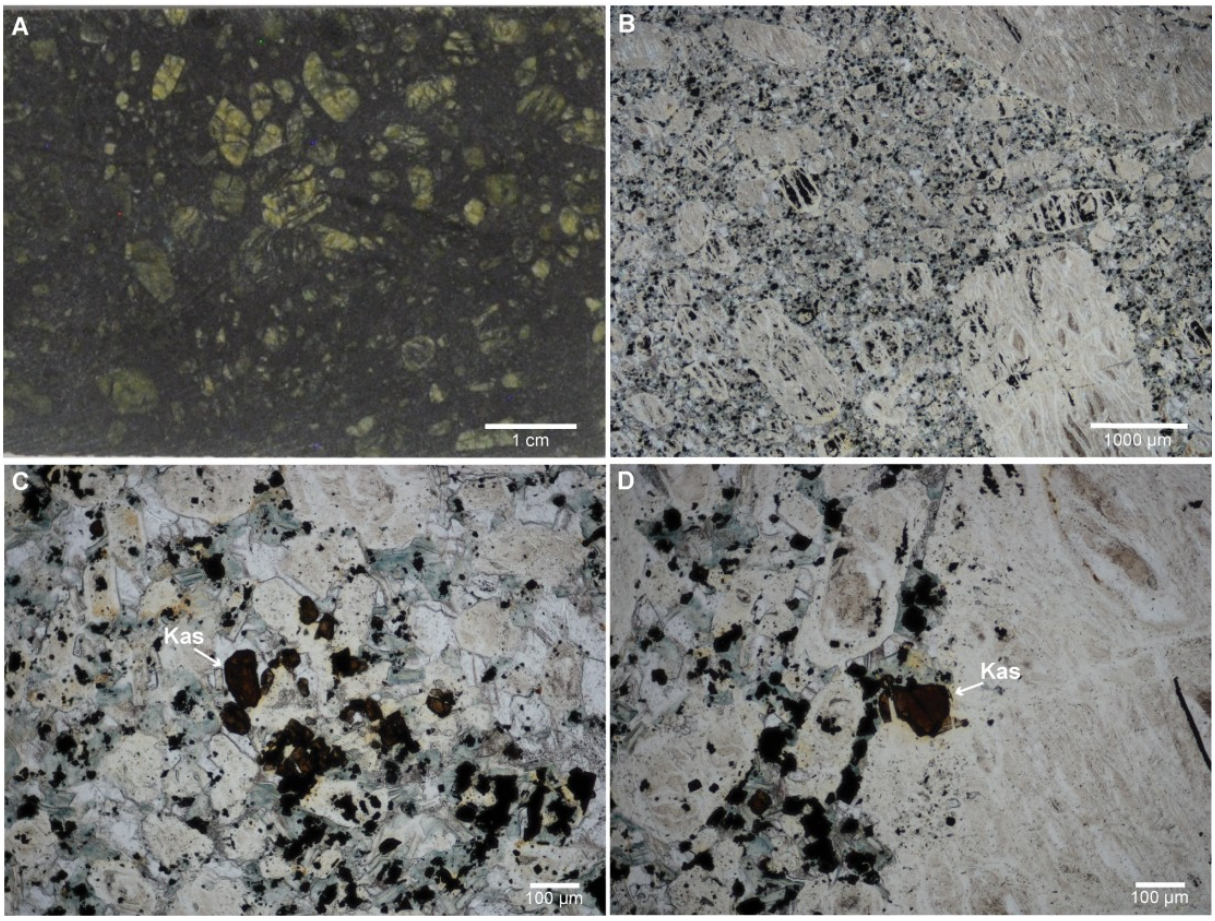


**Fig. 4.2** Wet core photo of sample 31462 in (a) showing light green serpentinized olivine macrocrysts in a fine-grained dark crystalline groundmass, and photomicrographs of b) serpentinized olivine macrocrysts in a uniform groundmass (PPL), and (c-d) large kassite grains corresponding to Figure 4.3 (images D and E, respectively) labelled as Kas=kassite and with condenser lens up in both PPL photomicrographs for additional light.

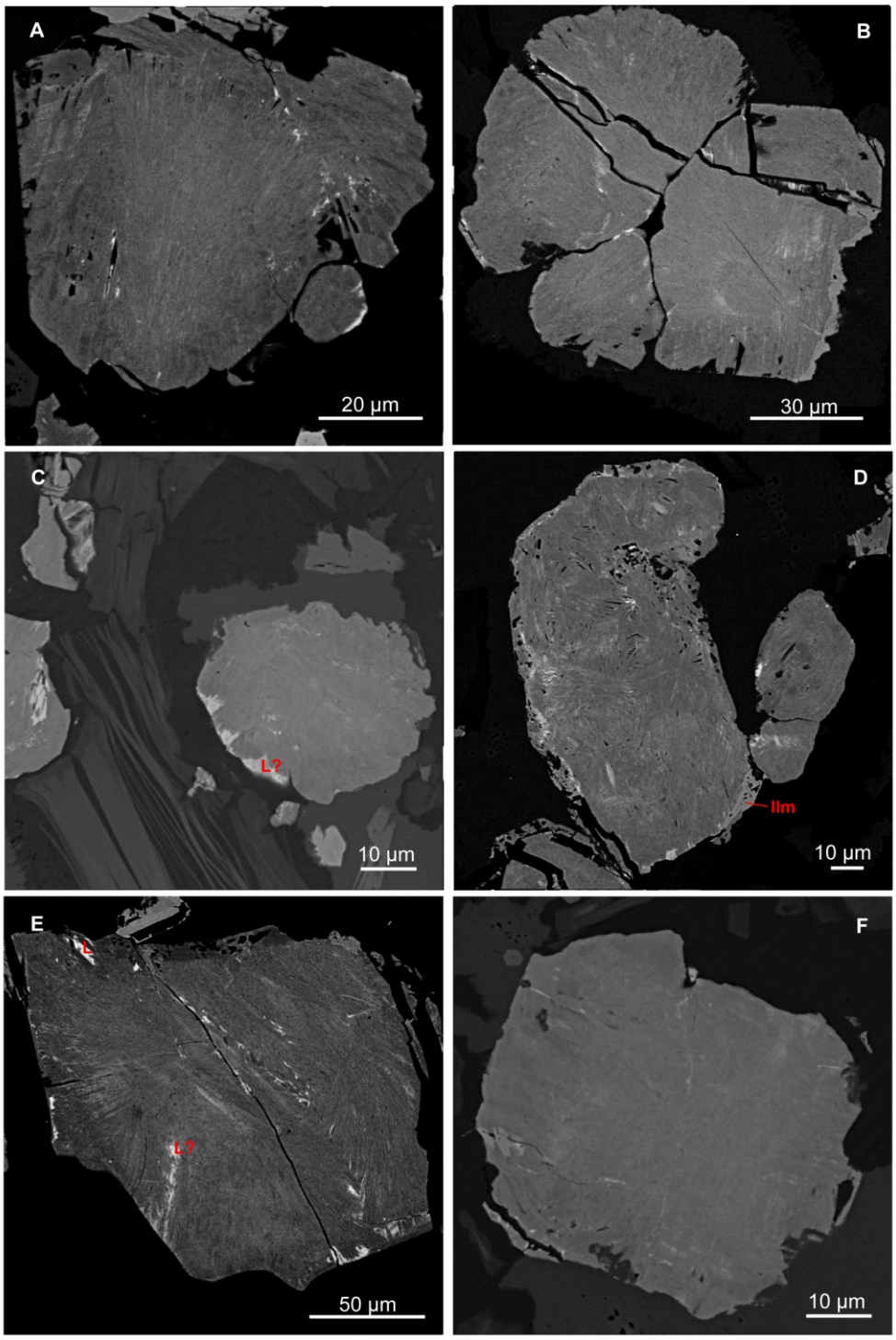


**Fig. 4.3** BSE images from the scanning electron microscope of representative kassite grains in thin section 31462. Images C and E contain compositions resembling lucasite-(Ce) (labelled L in red). Image D contains a composition resembling Mn-rich ilmenite (labelled Ilm in red, lower right rim).

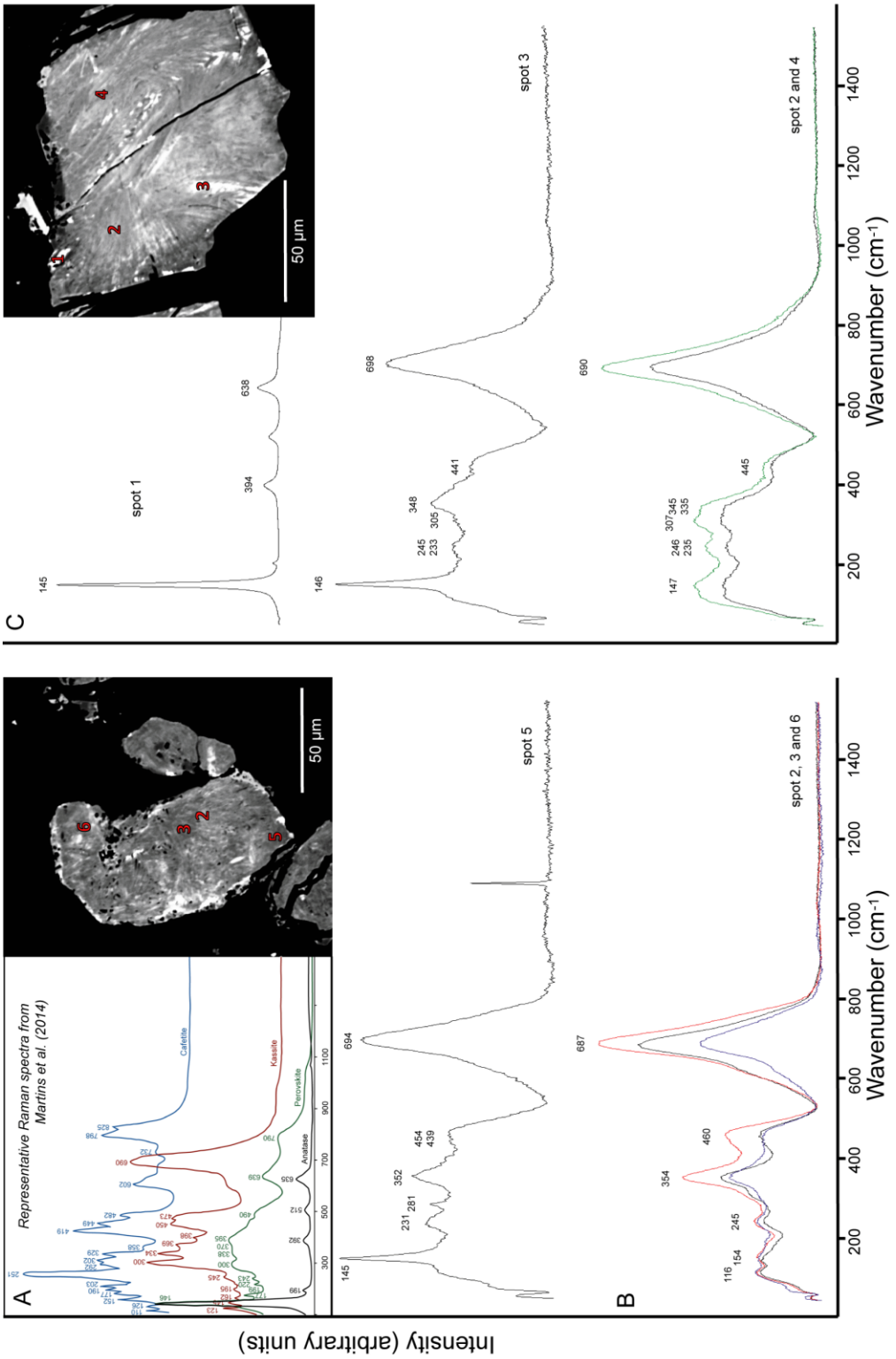


**Fig. 4.4** Representative Raman spectra of; (a) typical anatase, perovskite, kassite and cafetite from Martins et al. (2014), and (b-c) large grains in Figure 4.3d and 4.3e, respectively.

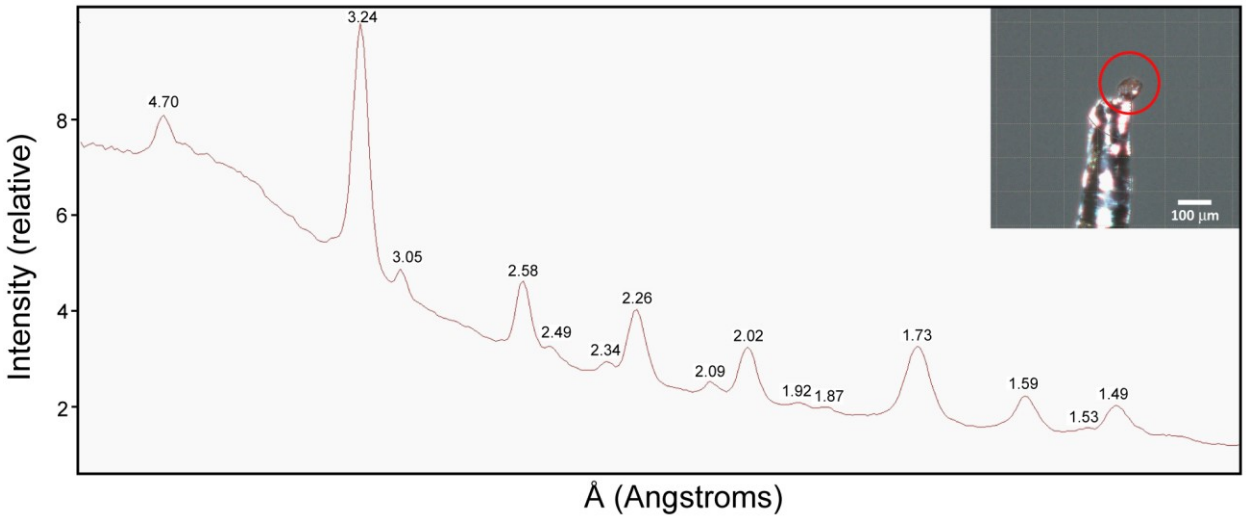


**Fig. 4.5** Representative XRD pattern of kassite.

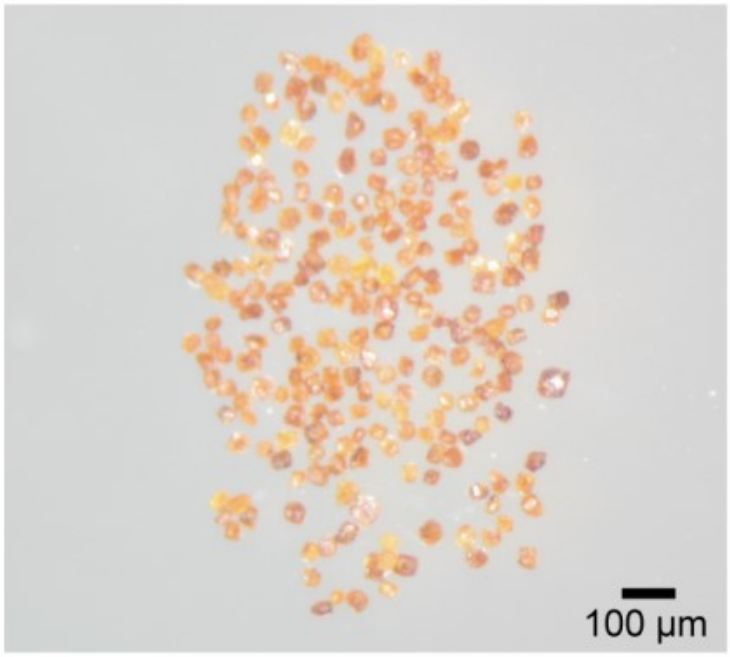


**Fig. 4.6** Photomicrograph of multi-grain fraction 31462C-2 for ID-TIMS U-Pb isotopic dating.

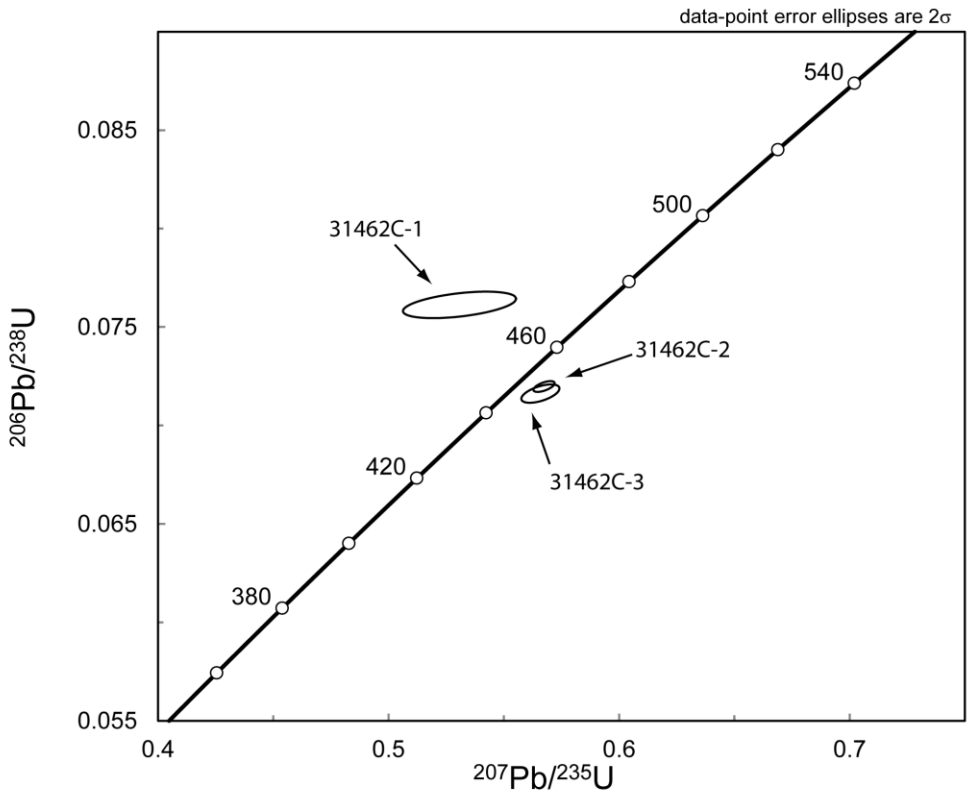


**Fig. 4.7** U-Pb concordia diagram of ID-TIMS U-Pb kassite fractions (31462C-1 to -3).

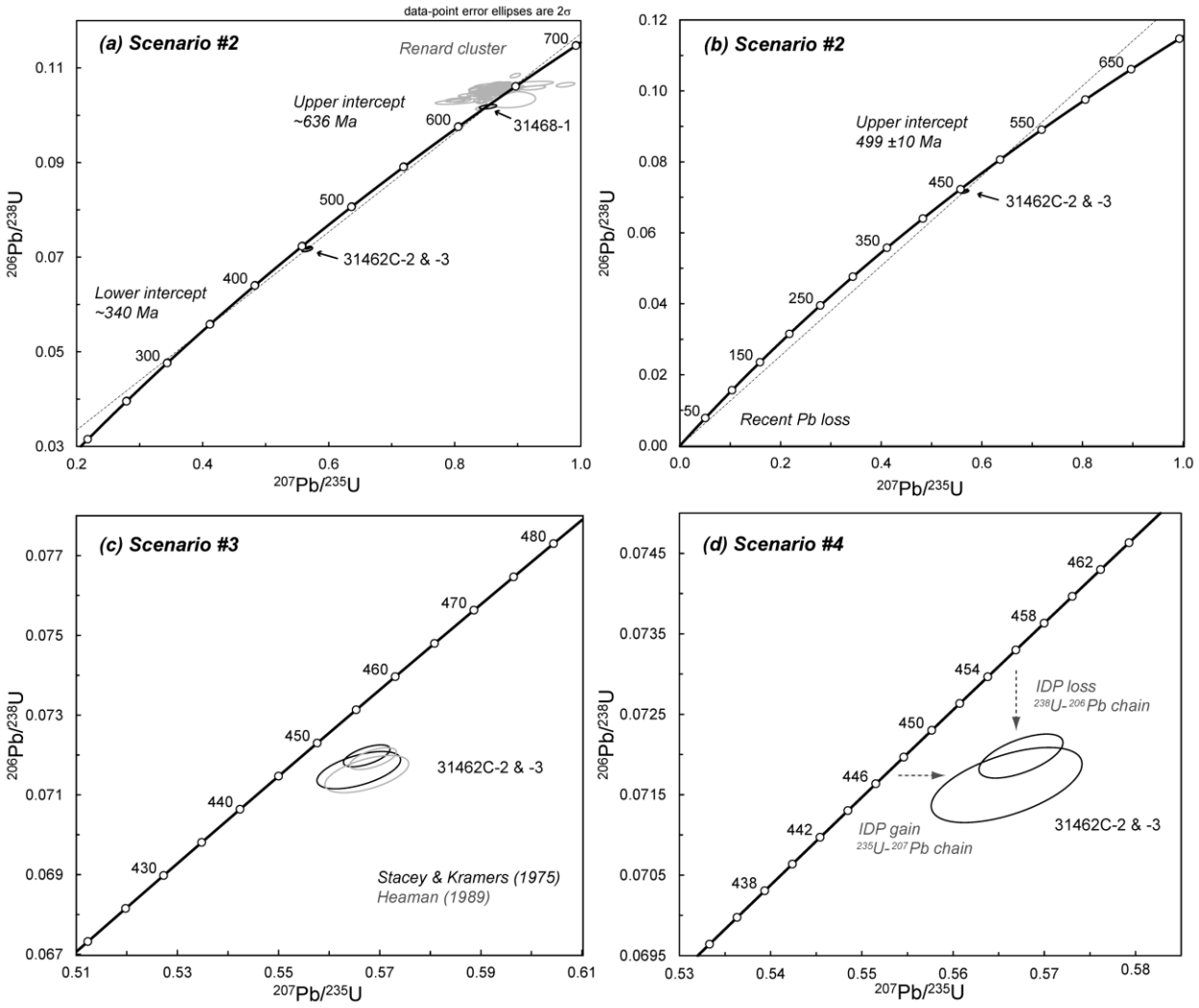


**Fig. 4.8** U-Pb concordia diagrams outlining possibilities described for scenarios #2, #3 and #4: (a) Pb loss since the main phase of Renard kimberlite magmatism (light gray), (b) recent Pb loss, (c) different initial common Pb isotopic composition than Stacey and Kramers (1975) using an example reported for the Kirkland Lake kimberlite (Heaman 1989) with an approximated initial lead isotopic composition, and (d) sketch of the effects of intermediate daughter product (IDP) loss or gain from the $^{238}$U-$^{206}$Pb and $^{235}$U-$^{207}$Pb decay chains, respectively (modified after Schoene 2014). Dashed lines show direction of loss/gain only and not a calculated amount.

# CHAPTER 5
# CONCLUSIONS

The Archean Superior Province has been intruded by kimberlite magmas several times from the Mesoproterozoic to Mesozoic (e.g. Heaman and Kjarsgaard 2000; Letendre et al. 2003; Heaman et al. 2004; Zurevinski and Mitchell 2011). One of the more poorly understood of these kimberlite fields/clusters is the diamondiferous Neoproterozoic Renard kimberlite cluster within the Otish field in north-central Québec. This cluster comprises nine kimberlite bodies (Renards 1-10), two dyke systems (~522 Ma Lynx and undated Hibou; McCandless et al. 2008) and several kimberlite dykes (G04-296 Anomaly, North Anomaly, Southeast Anomaly) discovered in the Otish Mountains region since 2001 (Godin et al. 2016). South of the Renard cluster and part of the Otish field are the ~551 Ma Lac Beaver (Girard 2001; Moorhead et al. 2003) and undated Adamantin kimberlites (Barnett and Laroulandie 2017). Most of the Renard bodies are steep-sided diatreme (to root zone) pipes modelled as Class 1 (South African style) kimberlites consisting of one or more main pipe-infilling units ranging from hypabyssal or coherent kimberlite to transitional to Kimberley-type pyroclastic kimberlite (e.g. Skinner and Marsh 2004; Fitzgerald et al. 2009; Muntener and Scott Smith 2013; Godin et al. 2016; Muntener and Gaudet 2018). Two types of coherent kimberlite, texturally classified as hypabyssal kimberlite, are common in all Renard pipes either as large-scale main pipe-infilling units (coherent kimberlite) or small-scale hypabyssal kimberlite dykes, irregular intrusions (cm- to tens of meters thick) or rare autoliths (e.g. Renard 9) which are difficult to characterize in drill core (Godin et al. 2016). Prior to this thesis, only five U-Pb perovskite dates from the Otish field were published (~656-632 Ma and ~551 Ma; Moorhead et al. 2003; Birkett et al. 2004; Fitzgerald et al. 2009; Tappe et al. 2017) and revealed an unexplained age complexity for the Renard 2 pipe and a remarkably long duration (~100 Myr) of kimberlite magmatism.

Chapter 2 presents new ID-TIMS U-Pb perovskite dates from ten samples from a single kimberlite pipe, Renard 2. A new high-precision composite weighted average $^{206}Pb/^{238}U$ perovskite date of 643.8±1.0 Ma was determined for the two main pipe-infilling units and is interpreted as the best estimate for timing of the main pipe-forming event. In contrast, six samples of smaller hypabyssal kimberlites within the pipe record a longer intrusion history

spanning at least ~20 Myr (~652-632 Ma). Only two hypabyssal kimberlite samples recorded dates coinciding with or nearly overlapping the emplacement age of the main pipe. Dates older than ~644 Ma suggest the presence of early-stage hypabyssal kimberlite intrusions (e.g. now xenoliths) in the same region. Dates younger than ~644 Ma indicate late-stage hypabyssal kimberlite intrusions can occur >10 Myr after the main pipe eruption. Importantly, some hypabyssal kimberlites are characterized by multiple perovskite dates which indicate that caution is needed when interpreting single dates from the Renard cluster. These new U-Pb results for early-stage, main pipe-infilling stage, and late-stage hypabyssal kimberlites are unlike the classical view of kimberlite emplacement within <1-2 Ma but confirm the early field studies of Wagner (1914) and Clement (1982) from South African kimberlite pipes.

Chapter 3 expands on the detailed U-Pb geochronology study of the Renard 2 pipe presented in Chapter 2 to several other kimberlites in the Renard cluster (Renard 1-3, 7, 9 and the G04-296 Anomaly dyke). This chapter highlights and further confirms the protracted kimberlite intrusion history (~100 Myr) for the Renard cluster. Samples of hypabyssal kimberlite record a large range of dates within individual pipes (e.g. ~35 Myr span in Renard 7) or peripheral to a pipe (e.g. >100 Myr span for Renard 2). In contrast, the new and published dates for Renard 1-4 record a narrow (~8 Myr span; ~646-638 Ma) range for the main pipe-forming event. A younger date of ~625 Ma obtained for Renard 9 suggests that not all pipes were emplaced within this narrow time frame. The younger dates from Renard 2, Renard 7 and the Lac Beaver hypabyssal kimberlite overlap with the breakup of Rodinia, specifically, the second phase of continental rifting recorded in the ~620-550 Ma Central Iapetus Magmatic Province and associated rift-related intrusions along the Laurentian margin and St. Lawrence rift system (e.g. Cawood et al. 2001). Many Renard kimberlites and the Wemindji kimberlite sills ~400 km to the west intruded the Archean Superior Province crust prior to 615 Ma (~656-629 Ma) between the Franklin and CIMP LIP events (~720-620 Ma; see Supplementary Material 1 summarized in Appendix C). Following Li et al.'s (2008) plate reconstruction model, it is speculated that continental extension and rifting may have been followed by the impingement of one or more mantle plume(s) which provided the heat necessary to repeatedly trigger Neoproterozoic kimberlite magmatism over Rodinia's protracted breakup history forming the Iapetus Ocean. This chapter shows that key age information was hidden in the kimberlite pipes that would have been missed with classical

sampling and suggests that the history of supercontinent breakup can be recorded in both LIPs and multiple kimberlite intrusions.

Chapter 4 presents new geochemical and age information for the rare hydrous Ca-Ti oxide kassite, $CaTi_2O_4(OH)_2$. Orange polycrystalline aggregates of this mineral with a habit and textural characteristics resembling those of perovskite were found in a hypabyssal kimberlite sample from the Renard 9 pipe. After an initial reconnaissance with the electron microprobe, Raman and XRD results confirmed the grains to be kassite. Kassite in this sample is associated with minor amounts of lucasite-(Ce), anatase, calcite, Mn-rich ilmenite, and possible perovskite. The first ID-TIMS U-Pb dates for kassite from two multi-grain fractions gave slightly discordant results with very similar $^{206}Pb/^{238}U$ and $^{207}Pb/^{235}U$ dates. Possible causes for this discordance were evaluated, such as lead loss, initial lead isotopic composition, and loss of intermediate daughter products. Although an unambiguous interpretation is not possible due to the absence of an independent age estimate for this sample, the pattern of discordance in the U-Pb dates bears a strong resemblance to the data of Heaman and LeCheminant (2000) for mantle baddeleyite in the Île Bizard alnöite (Québec). Specifically, loss of radon gas, one of the intermediate daughter products of both the $^{238}U$ and $^{235}U$ decay chains, from the kassite grains would result in spuriously young ages. This process would have a larger impact on $^{206}Pb/^{238}U$ dates than on $^{207}Pb/^{235}U$ dates. If this interpretation is correct, the weighted average $^{207}Pb/^{235}U$ date of 456.1±2.1 Ma is the best minimum estimate for the timing of kassite crystallization.

Based on the research conducted in this thesis, it has been shown that the Otish field kimberlites have a much more complex intrusion history than previously known, which is dominantly recorded by the previously overlooked smaller hypabyssal kimberlite units. It is not yet known if this complex history is unique to the Renard kimberlite cluster. The new U-Pb perovskite results presented here offer a new perspective to the study of single kimberlite pipes, their connection with LIPs and with the breakup and assembly of supercontinents.

## Future research

The outcome of this research poses new questions about the Renard kimberlite cluster. Several recent published papers describe the internal geology of the Renard 2, Renard 3 and Renard 65 pipes (Fitzgerald et al. 2009; Muntener and Scott Smith 2013; Gaudet et al. 2018; Lepine and Farrow 2018; Muntener and Gaudet 2018) but there is still much more to be learned from the Otish field. Suggestions for future research include:

1) Attempt to determine the initial lead isotopic composition of Renard kimberlite magmas to further assess the $^{206}Pb/^{238}U$ dates, if suitable unradiogenic minerals can be found (e.g. coarser-grained fresh phlogopite, titanomagnetite, ulvöspinel-magnetite; e.g. Stamm et al. 2018).

2) Given the results from chapters 2 and 3, additional mineralogical, geochemical and age study of the smaller hypabyssal kimberlites ('c' unit samples; e.g. Lepine and Zhuk 2017) and their relationship to the main pipe-infills within the pipes. Further study could help address difficulties noted with kimberlite terminology (e.g. Cas et al. 2008a, b).

3) Further explore the timing of hypabyssal kimberlite intrusions peripheral to the Renard pipes and throughout the Otish field, including the dyke-like Renard 10 body. Given the difficulty in finding perovskite in the Lynx and Hibou dyke systems, and the presence of secondary minerals (e.g. oxide veining), an age dating study combined with detailed petrography may assist with future isotopic dating.

4) Further mineralogical and geochemical investigation of kassite and lucasite-(Ce) in Renard 9. The detailed internal geology of the Renard 9 pipe has not yet been published but future petrological studies may help assess the significance of these rare minerals. An independent emplacement age estimate for a Renard 9 sample containing kassite (e.g. U-Pb perovskite or Rb-Sr phlogopite) would be helpful to better understand the kassite U-Pb systematics. In addition, the U-Pb systematics of kassite from other kimberlites could be compared to investigate the conditions of kassite formation and whether it crystallizes late in kimberlite magma evolution or forms from alteration of pre-existing minerals. For example, the Iron Mountain kimberlite in the State Line field was previously determined by Heaman et al. (2003) to record a weighted average $^{206}Pb/^{238}U$ date of 408.4±2.6 Ma from perovskite.

5) Other isotopic data completed on Otish field kimberlites in this study include a few Sr, O and C isotopic compositions. The Sr, Nd, Pb, and Hf isotope compositions of kimberlite

magmas have been used to distinguish their mantle origins (e.g. Smith 1983, Heaman 1989, Nowell et al. 2004). In this study the perovskite Sr isotopic compositions were measured from the Renard 3 pipe (~641 Ma 31556-1; $^{87}Sr/^{86}Sr_m$ = 0.703815±0.000011) and a Renard 7 hypabyssal kimberlite (~641 Ma 35791-1; $^{87}Sr/^{86}Sr_m$ = 0.702867±0.000006). These results indicate that perovskite in some Renard kimberlites have variable Sr isotopic compositions that for the most part are significantly less radiogenic than previously reported Renard kimberlite whole-rock Sr isotopic compositions (Tappe et al. 2017). In the Tappe et al. (2017) study ten whole-rock hypabyssal kimberlite samples were analyzed ($^{87}Sr/^{86}Sr_m$ = 0.704744, n=1, from Renard 2; $^{87}Sr/^{86}Sr_m$ = 0.705767-0.708276, n=4, from Renard 3; $^{87}Sr/^{86}Sr_m$ = 0.704170-0.713599, n=4, from Lynx dykes; $^{87}Sr/^{86}Sr_m$ = 0.706682, n=1, from Hibou dyke). Their whole-rock Sr isotopic results (most $^{87}Sr/^{86}Sr_i$ = 0.70241-0.70442 calculated using a date of 655 Ma) were interpreted to reflect an asthenospheric (convecting upper mantle) source for kimberlite magmatism due to the low initial Sr in their samples compared to worldwide kimberlite likely reflecting the absence of mantle phlogopite. The whole-rock carbonate $\delta^{18}O$ and $\delta^{13}C$ measured in this present study across a section of Lynx hypabyssal kimberlite (sample 31594; Table 1 and Figures 22-23 in Appendix E) show greater variability in $\delta^{18}O$ (10.0 to 17.3‰ for calcite, relative to VSMOW) compared to $\delta^{13}C$ (-5.6 to -4.1‰ for calcite, relative to PDB). $\delta^{18}O$ within the kimberlite intrusion is less variable (14.2 to 15.7‰) compared to the lower contact (17.3‰, 31594G-1, dark grey area; 10.0‰, 31594G-2, light grey area). Yet all these $\delta^{18}O$ values fall outside range of published mantle oxygen isotope compositions contrary to $\delta^{13}C$ (e.g. mantle ranges of $\delta^{18}O$ ~6 to 9‰ and $\delta^{13}C$ ~ -2 to -8‰; Giuliani et al. 2014). Tappe et al. (2017) also determined O and C isotopic compositions from the same hypabyssal kimberlite samples used in their study to determine Sr, and found a similar range of $\delta^{18}O$ (10.1 to 19.7‰) and $\delta^{13}C$ (−5.6 to −4.2‰, not including one outlier at -8.64‰ in Renard 3). Some researchers have pointed out that high $\delta^{18}O$ in kimberlite falling outside mantle range could reflect the interaction with deuteric, low temperature meteoric and/or hydrothermal fluids (e.g. $\delta^{18}O$ >9‰ in Figure 7 of Giuliani et al. 2014). In addition, the retention of the original oxygen isotopic composition could be related to the size of the intrusion (e.g. small dyke/veins versus large plutons noted for carbonatites by Deines 1989) or emplacement level (Deines and Gold 1973). The Lynx dyke sampled here has a narrow apparent thickness (1.4 m) with a relatively shallow downhole (apparent) depth of ~53 m consistent with the modelled near surface (within ~95 m) average

thickness (1.8 m) described for the Lynx dyke system (Godin et al. 2016). It would not be unrealistic for groundmass carbonate in this sample to be less resistant to alteration by fluids since the Neoproterozoic Renard cluster kimberlites intruded the Superior Province. Furthermore, thin sections for 31594 indicate tiny carbonate veinlets crosscut or rim grains and tiny (~0.1-3 mm) possible altered country rock xenoliths may be present, which could impact O and Sr results determined by whole-rock kimberlite.

Additional future work could include a study of the internal geochemical and isotopic characteristics of perovskite from the Otish field. Malarkey et al. (2010) tested several minerals (xenocryst and phenocryst olivine, apatite, perovskite, phlogopite and calcite) and whole-rock kimberlite samples from the Jos kimberlite (Somerset Island, Canada) and found that the largest variation in isotopic Sr was observed in perovskite, apatite and calcite. For example, Malarkey et al. (2010) reported a range of $^{87}Sr/^{86}Sr_i$ values in perovskite from the Jos kimberlite (0.704855-0.705269) and suggested that perovskite crystallized while the magma was assimilating crust. But they did not consider if the perovskite (or other minerals) could be recording inheritance within a single crystal or if hydrothermal/meteoric fluids contributed to the elevated Sr isotopic ratios (e.g. such as in calcite described by Giuliani et al. 2017). Although limited by the perovskite grain size in many Renard samples, future work using a combination of imaging, chemical analysis of zoned crystals, and spot Sr-O isotopic analyses at the spatial resolution of perovskite zoning may give some insight if Sr results from the Renard hypabyssal kimberlites could reflect zoned inheritance, crustal contamination and/or some combination of both.

6) In addition, Malarkey et al. (2010) noted significant differences between the Rb-Sr phlogopite and U-Pb perovskite dates for the Jos kimberlite. Therefore the possibility of crustal contamination/alteration or inheritance should be taken into consideration in future dating studies if mica-based geochronometers are tried.

7) It is presently unknown if punctuated intrusion histories similar to that observed from hypabyssal kimberlites in some Renard pipes could occur in other kimberlite fields. For example, very little detailed age information is published for Neoproterozoic kimberlites in Finland or North America (Supplementary Material 1 in Appendix C). Detailed age studies may help assess if similar intrusion histories occur within and/or peripheral to other kimberlite bodies.

# REFERENCES


Agashev AM, Pokhilenko NP, Takazawa E, McDonald JA, Vavilov MA, Watanabe T, Sobolev NV (2008) Primary melting sequence of a deep (>250 km) lithospheric mantle as recorded in the geochemistry of kimberlite-carbonatite assemblages, Snap Lake dyke system, Canada. Chem Geol 255:317-328

Aleinikoff JN, Zartman RE, Walter M, Rankin DW, Lyttle PT, Burton WC (1995) U-Pb ages of metarhyolites of the Catoctin and Mount Rogers formations, central and southern Appalachians: evidence for two pulses of Iapetan rifting. Am J Sci 295:428-454

Alibert C, Albarede F (1988) Relationships between mineralogical, chemical, and isotopic properties of some North American kimberlites. J Geophys Res 93:7643-7671

Allsopp HL, Bristow JW, Smith CB, Brown R, Gleadow AJW, Kramers JD, Garvie OG (1989) A summary of radiometric dating methods applicable to kimberlites and related rocks. In: Ross J, Jaques AL, Ferguson J, Green DH, O'Reilly SY, Danchin RV, Janse AJA (eds) Kimberlites and related rocks. Proceedings of the Fourth International Kimberlite conference, Special Publication - Geological Society of Australia, vol 1, no 14, pp 343-357

Anczkiewicz R, Oberli F, Burg JP, Villa IM, Günther D, Meier M (2001) Timing of normal faulting along the Indus Suture in Pakistan Himalaya and a case of major $^{231}Pa/^{235}U$ initial disequilibrium in zircon. Earth Planet Sc Lett 191:101-114

Andreasson PG (1994) The Baltoscandian Margin in Neoproterozoic-early Palaeozoic times. Some constraints on terrance derivation and accretion in the Arctic Scandinavian Caledonides. Tectonophysics 231:1-32

Andréasson P-G, Svenningsen OM, Albrecht L (1998) Dawn of Phanerozoic orogeny in the North Atlantic tract; Evidence from the Seve-Kalak Superterrane, Scandinavian Caledonides. Gff 120(2):159-172

Anthony JW, Bideaux RA, Bladh KW, Nichols MC (1997) Handbook of Mineralogy, Halides, Hydroxides, Oxides, Volume III Mineralogical Society of America: http://wwwhandbookofmineralogyorg/indexhtml

Armstrong JP, Stubley MP, Chang FY (2008) Geology and exploration history of the Aviat kimberlite cluster, Northern Rae Craton, Melville Peninsula, Nunavut, Canada. 9th International Kimberlite Conference Extended Abstract 9IKC-A-00266, 3 p

Ault AK, Flowers RM, Bowring SA (2015) Synchroneity of cratonic burial phases and gaps in the kimberlite record: episodic magmatism or preservational bias? Earth Planet Sc Lett 410:97–104

Bailey DK (1993) Petrogenetic implications of the timing of alkaline, carbonatite, and kimberlite igneous activity in Africa. S Afr J Geol 96(3):67-74

Bailey DK, Woolley AR (2005) Repeated, synchronous magmatism within Africa: Timing, magnetic reversals, and global tectonics. In: Foulger GR, Natland JH, Presnall DC, Anderson DL (eds) Plates, plumes, and paradigms. Geological Society of America Special Paper 388:365–377

Baird GB, Figg SA, Chamberlain KR (2013) Geochemistry and intrusive age of the Kebne dyke complex in the Kebnekaise Massif, northern Swedish Caledonides; comparison of the tholeiitic continental-oceanic transition rocks in the Seve-Kalak Superterrane. Abstracts with Programs - Geological Society of America 45 (7):761

Baird GB, Figg SA, Chamberlain KR (2014) Intrusive age and geochemistry of the Kebne Dyke Complex in the Seve Nappe Complex, Kebnekaise Massif, arctic Sweden Caledonides. GFF 136(4):556-570

Bakun-Czubarow N, Bialowolska A, Fedoryshyn Y, Pecskay Z (2008) Ediacaran Volhynian flood basalts in western margin of East European Craton; large continental igneous province. International Geological Congress, Abstracts = Congres Geologique International, Resumes, January 01, 2008, Vol. 33, Abstract 1352619

Barnett RL, Laroulandie C (2017) Barium and titanium enrichment of zoned phlogopite xenocrysts and phenocrysts in the Adamantin kimberlites, Québec, Canada. 11th International Kimberlite Conference Extended Abstract No. 11IKC-004587, 3 p

Baziotis I, Asimow PD, Koroneos A, Poli G, Ntaflos T (2013a) Multi-stage history of compound mantle xenoliths from western USA: implications for metasomatic processes in the deep mantle. Bulletin of the Geological Society of Greece, vol XLVII, Proceedings of the 13th International Congress, Chania, Sept 2013, 10 p

Baziotis I, Asimov PD, Ntaflos T, Koroneos A, Poli G (2013b) High- to low- pressure features of compound xenoliths: implications from Fe-Ti-Ca metasomatism and glass formation. Goldschmidt 2013 conference abstracts:673

Bingen B, Demaiffe D, van Breemen O (1998) The 616 Ma old Egersund basaltic dike swarm, SW Norway, and Late Neoproterozoic opening of the Iapetus ocean. J Geol 106:565-574

Birkett TC, McCandless TE, Hood CT (2004) Petrology of the Renard igneous bodies: host rocks for diamond in the northern Otish Mountains region, Quebec. Lithos 76:475-490

Boctor NZ, Meyer HOA (1979) Oxide and sulfide minerals in kimberlite from Green Mountain, Colorado. In: Boyd FR, Meyer HOA (eds) Kimberlites, diatremes, and diamonds; their geology, petrology, and geochemistry. Proceedings of the International Kimberlite Conference, 1979, Issue 2, Vol. 1:217-228

Brem AG, Davis DW, McNicoll VJ, Lin S, van Staal CR (2005) Geochronological studies in the Long Range Mountains of southwestern Newfoundland. Geological Association of Canada, Abstract Volume 30:18

Brown RJ, Valentine GA (2013) Physical characteristics of kimberlite and basaltic intraplate volcanism and implications of a biased kimberlite record. Geological Society of America Bulletin 125(7-8):1224-1238

Burke K, Ashwal LD, Webb SJ (2003) New way to map old sutures using deformed alkaline rocks and carbonatites. Geology 31(5):391-394

Burke K, Khan SD, Mart RW (2008) Grenville Province and Monteregian carbonatite and nepheline syenite distribution related to rifting, collision, and plume passage. Geology 36(12):983-986

Burgess SD, Bowring SA, Heaman LM (2012) High-precision U-Pb geochronology of Ice River perovskite: a possible interlaboratory and intertechnique EARTHTIME standard. American Geophysical Union 2012 Fall Meeting, San Francisco, California (December 3-7), Abstract V23A-2787

Canil D, Fedortchouk Y (1999) Garnet dissolution and the emplacement of kimberlites. Earth Planet Sc Lett 167:227-237

Card KD, Poulsen KH (1998) Geology and mineral deposits of the Superior province of the Canadian Shield (Chapter 2). In: Lucas S, St-Onge MR (co-ord) Geology of the Precambrian Superior and Grenville Provinces and Precambrian Fossils in North America. Geological Survey of Canada, Geology of Canada, no 7, pp 13-204

Carlson JA, Marsh SW (1989) Discovery of the George Creek kimberlite dikes, Colorado. In: Ross J, Jaques AL, Ferguson J, Green DH, O'Reilly SY, Danchin RV, Janse AJA (eds)

Proceedings of the Fourth International Kimberlite Conference, Kimberlites and related rocks vol. 2, GSA Special Publication No. 14:1169-1178

Cas RAF, Hayman PC, Pittari A, Porritt LA (2006) The problems with existing volcanological models and related terminology for kimberlite pipes. 2006 Kimberlite Emplacement Workshop, Saskatoon, 5 p

Cas RAF, Hayman PC, Pittari A, Porritt L (2008a) Some major problems with existing models and terminology associated with kimberlite pipes from a volcanological perspective, and some suggestions. J Volcanol Geotherm Res 174:209-225

Cas R, Porritt L, Pittari A, Hayman P (2008b) A new approach to kimberlite facies terminology using a revised general approach to the nomenclature of all volcanic rocks and deposits: Descriptive to genetic. J Volcanol Geotherm Res 174(1-3):226-240

Cawood PA, McCausland PJA, Dunning GR (2001) Opening Iapetus: Constraints from the Laurentian margin in Newfoundland. GSA Bulletin 113(4):443-453

Cawood PA, van Gool JAM, Dunning GR (1996) Geological development of eastern Humber and western Dunnage zones: Corner Brook - Glover Island region, Newfoundland. Can J Earth Sci 33:182-198

Chakhmouradian AR, Mitchell RH (2000) Occurrence, alteration patterns and compositional variation of perovskite in kimberlites. Can Mineral 38:975-994

Chalapathi Rao NV, Lehmann B (2011) Kimberlites, flood basalts and mantle plumes: New insights from the Deccan Large Igneous Province. Earth Sci Rev 107(3-4):315-324

Chukanov NV, Moiseev MM, Pekov IV, Lazebnik KA, Rastsvetaeva RK, Zayakina NV, Ferraris D, Ivaldi G (2004) Nabalamprofillit Ba(Na, Ba)($Na_3Ti[Ti_2O_2Si_4O_{14}](OH,F)_2$; novyy sloistyy titanosilikat gruppy lamprofillita iz shchelochno-ul'traosnovnykh massivov Inagli i Kovdor, Rossiya [Nabalamprophyllite Ba(Na, Ba)($Na_3Ti[Ti_2O_2Si_4O_{14}](OH,F)_2$ - a new layer titanosilicate of the lamprophyllite group from Inagli and Kovdor alkaline-ultrabasic massifs, Russia]. Zapiski Vserossiyskogo Mineralogicheskogo Obshchestva = Proceedings of the Russian Mineralogical Society, 2004, 133(1):59-72

Claesson S (1976) The age of the Ottfjallet dolerites of Sarv Nappe, Swedish Caledonides. Geol Foren Stockh Forh 98:370-374

Claesson S, Roddick JC (1983) $^{40}Ar/^{39}Ar$ data on the age and metamorphism of the Ottfjallet dolerites, Sarv Nappe, Swedish Caledonides. Lithos 16:61-73

Clarke LB, Le Bas MJ, Spiro B (1994) Rare earth, trace element and stable isotope fractionation of carbonatites at Kruidontein, Transvaal, S Africa. In: Meyer HOA, Leonardos OH (eds) Kimberlites, Related Rocks and Mantle Xenoliths, Companhia de Pesquisa de Recursos Minerais, Rio de Janeiro (Proceedings of the Fifth International Kimberlite Conference), pp 236-251

Clement CR (1982) A comparative geological study of some major kimberlite pipes in the Northern Cape and Orange Free State. Doctoral thesis (2 volumes), University of Cape Town

Clement CR, Reid AM (1989) The origin of kimberlite pipes: an interpretation based on synthesis of geological features displayed by southern African occurrences. In: Ross J, Jaques AL, Ferguson J, Green DH, O'Reilly SY, Danchin RV, Janse AJA (eds) Kimberlites and related rocks. Proceedings of the Fourth International Kimberlite conference, Special Publication - Geological Society of Australia, vol 1, no 14, pp 632-646

Clifford TN (1966) Tectono-metallogenic units and metallogenic provinces of Africa. Earth Planet Sc Lett 1:421-434

Compston W, Sambridge MS, Reinfrank RF, Moczydlowska M, Vidal G, Claesson S (1995) Numerical ages of volcanic rocks and the earliest faunal zone within the Late Precambrian of east Poland. Journal of the Geological Society, London 152:599-611

Condie KC (2001) Mantle plumes and their record in Earth history. Cambridge University Press, 306 p

Condie K, Pisarevsky SA, Korenaga J, Gardoll S (2015) Is the rate of supercontinent assembly changing with time? Precambr Res 259:278-289

Courtillot V, Jaupart C, Manighetti I, Tapponnier P, Besse J (1999) On causal links between flood basalts and continental breakup. Earth Planet Sc Lett 166:177-195

Creaser RA, Grütter H, Carlson J, Crawford B (2004) Macrocrystal phlogopite Rb–Sr dates for the Ekati property kimberlites, Slave Province, Canada: evidence for multiple intrusive episodes in the Paleocene and Eocene. Lithos 76(1-4):399-414

Crough ST, Morgan WJ, Hargraves RB (1980) Kimberlites: their relation to mantle hotspots. Earth Planet Sc Lett 50:260-274

Currie KL (1976) The Alkaline Rocks of Canada; Geological Survey of Canada Bulletin 239, 228 p

Currie CA, Beaumont C (2011) Are diamond-bearing Cretaceous kimberlites related to low-angle subduction beneath western North America? Earth Planet Sc Lett 303(1-2):59-70

Currie KL, van Breemen O, Hunt PA, van Berkel JT (1992) Age of high-grade gneisses south of Grand Lake, Newfoundland. Atlantic Geology 28:153-161

Dahlgren S (1994) Late Proterozoic and Carboniferous ultramafic magmatism of carbonatitic affinity in southern Norway. Lithos 31:141-154

Dalziel IWD, Lawver LA, Murphy JB (2000) Plumes, orogenesis, and supercontinental fragmentation. Earth Planet Sc Lett 178:1-11

Dawson JB (1967) A review of the geology of kimberlite. In: Wyllie PJ (ed) Kimberlites (Chapter 8), Ultramafic and Related Rocks, John Wiley & Sons, Inc:241-251

Dawson JB (1980) Kimberlites and their xenoliths, Springer-Verlag, New York, 252 p

Dawson JM, Smith Jv (1977) The MARID (mica-amphibole-rutile- ilmenite-diopside) suite of xenoliths in kimberlite. Geochim Cosmochim Acta 41:309-323

de Wit M, Bhebhe Z, Davidson J, Haggerty SE, Hundt P, Jacob J, Lynn M, Marshall TR, Skinner C, Smithson K, Stiefenhofer J, Robert M, Revitt A, Spaggiari R, Ward J (2016) Overview of Diamond Resources in Africa. Episodes 39(2):199-237

Deines P (1989) Stable isotope variations in carbonatites. In: Bell K (ed) Carbonatites: Genesis and Evolution. Unwin Hyman, London, pp 301-359

Deines P (2002) The carbon isotope geochemistry of mantle xenoliths. Earth Sci Rev 58:247-278

Deines P, Gold DP (1973) The isotopic composition of carbonatite and kimberlite carbonates and their bearing on the isotopic composition of deep-seated carbon. Geochim Cosmochim Acta 37:1709-1733

Delgaty J, Fulop A, Seller M, Hartley M, Zayonce L, Januszczak N, Kurszlaukis S (2017) Ontario's newest kimberlite cluster - the Pagwachuan cluster. 11th International Kimberlite Conference Extended Abstract No 11IKC-4517:4p

Denyszyn SW, Davis DW, Halls HC (2009a) Paleomagnetism and U-Pb geochronology of the Clarence Head dykes, Arctic Canada: orthogonal emplacement of mafic dykes in a large igneous province. Can J Earth Sci 46:155-167

Denyszyn SW, Halls HC, Davis DW, Evans DAD (2009b) Paleomagnetism and U-Pb geochronology of Franklin dykes in High Arctic Canada and Greenland: a revised age and paleomagnetic pole constraining block rotations in the Nares Strait region. Can J Earth Sci 46:689-705

Digonnet S, Goulet N, Bourne JH, Stevenson R (1996) Genesis and comparison of kimberlitic dykes from the Ungava Bay area, northern Quebec, and from west Greenland. In Wardle RJ and Hall J (compilers). Eastern Canadian Shield Onshore-Offshore Transect (ECSOOT), Transect Meeting (March 14-15, 1996), The Univeristy of British Columbia, LITHOPROBE Secretariat, Report No. 57:38-43

Digonnet S, Goulet N, Bourne J, Stevenson R, Archibald D (2000) Petrology of the Abloviak Aillikite dykes, New Quebec: evidence for a Cambrian diamondiferous alkaline province in northeastern North America. Can J Earth Sci 37:517-533

Diller JS (1885) Dikes of peridotite cutting the carboniferous rocks of Kentucky. Science January 23, 1885:65

Diller JS (1886) Notes on the peridotite of Elliott County, Kentucky. Amer J Sci 32:121-125

Doig R (1970) An alkaline rock province linking Europe and North America. Can J Earth Sci 7:22-28

Doig R, Barton Jr. JM (1968) Ages of carbonatites and other alkaline rocks in Quebec. Can J Earth Sci 5:1401-1407

Donnelly CL, Griffin WL, O'Reilly SY, Pearson NJ, Shee SR (2011) The kimberlites and related rocks of the Kuruman Kimberlite Province, Kaapvaal Craton, South Africa. Contrib Mineral Petrol 161:351-371

Eldholm O, Coffin MF (2000) Large igneous provinces and plate tectonics. In: Richards MA, Gordon RG, van der Hilst RD (eds) The history and dynamics of global plate motions, Geophysical Monograph 121:309-326

Elming S-Å, Kravchenko SN, Layer P, Rusakov OM, Glevasskaya AM, Mikhailova NP, Bachtadse V (2007) Paleomagnetism and 40Ar/39Ar age determinations of the Ediacaran traps from the southwestern margin of the East European Craton, Ukraine: relevance to the Rodinia break-up. Journal of the Geological Society 164:969–982

Ernst RE (2014) Large Igneous Provinces. Cambridge University Press, 653 p

Ernst RE, Bell K (2010) Large igneous provinces (LIPs) and carbonatites. Mineral Petrol 98(1-4):55-76

Ernst R, Bleeker W (2010) Large igneous provinces (LIPs), giant dyke swarms, and mantle plumes: significance for breakup events within Canada and adjacent regions from 2.5 Ga to the Present. Can J Earth Sci 47:695-739

Ernst RE, Buchan KL (1997) Giant radiating dyke swarms: their use in identifying Pre-Mesozoic Large Igneous Provinces and mantle plumes. In: Mahoney JJ, Coffin MF (eds) Large Igneous Provinces, Continental, Oceanic and Planetary Flood Volcanism. American Geophysical Union, Geophysical Monograph 100:294-333

Ernst RE, Buchan KL (2001) Large mafic magmatic events through time and links to mantle-plume heads. in Ernst RE, Buchan KL (eds) Mantle Plumes: Their Identification Through Time: Boulder, Colorado, Geological Society of America Special Paper 352:483-575

Essex RM (1992) Age and Petrogenesis of the Striped Rock Granite Pluton: Blue Ridge Province, Southwestern Virginia. Masters thesis, Virginia Polytechnic Institute and State University, Blacksburg, Virginia, 98 p

Evans Jr. HT, Dwornik EJ, Milton C (1986) Kassite from the Diamond Jo quarry, Magnet Cove, Hot Spring County, Arkansas: The problem of cafetite and kassite. Am Mineral 71:1045-1048

Fahrig WF, Christie KW, Chown EH, Janes D, Machado N (1986) The tectonic significance of some basic dyke swarms in the Canadian Superior Province with special reference to the geochemistry and paleomagnetism of the Mistassini swarm, Quebec, Canada. Can J Earth Sci 23:238-253

Ferguson J, Currie KL (1972) The Geology and Petrology of the Alkaline Carbonatite at Callander Bay, Ontario Geological Survey of Canada Bulletin 217, 103 p

Fetter AH, Goldberg SA (1995) Age and geochemical characteristics of bimodal magmatismin theNeoproterozoic GrandfatherMountain rift basin. J Geol 103:313–326

Field M, Scott Smith BH (1998) Textural and genetic classification schemes for kimberlites: a new perspective. Seventh International Kimberlite Conference Extended Abstract, pp 214-216

Field M, Scott Smith BH (1999) Contrasting geology and near-surface emplacement of kimberlite pipes in Southern Africa and Canada. In: Gurney JJ, Gurney JL, Pascoe MD,

Richardson SH (eds) Proceedings of the VIIth International Kimberlite Conference, vol 1, pp 214-237

Fitzgerald CE, Hetman CM, Lepine I, Skelton DS, McCandless TE (2009) The internal geology and emplacement history of the Renard 2 kimberlite, Superior Province, Quebec, Canada. Lithos 112:513-528

Fokin MA (2003) Space-Time analysis of magmatism: the igneous record for an Early Cryogenian plume track in central Appalachian Orogen. MSC thesis, Viginia Polytechnic Institute and State University, 67 p

Frei D, Hutchison MT, Gerdes A, Heaman LM (2008) Common-lead corrected U-Pb age dating of perovskite by laser ablation - magnetic sectorfield ICP-MS. 9th International Kimberlite Conference Extended Abstract No. 9IKC-A-00216, 3 p

Galuskin E, Galuskina I, Dzieranowski P (2004) New natural phase $MnTi_2O_4(OH)_2$ $H_2O$ with uncertain structure – indicator of sea floor metasomatism. Polskie Towarzystwo Mineralogiczne – Prace Specjalne (Mineralogical Society of Poland – Special Papers) 24:157–160

Galuskina I, Galuskin E, Wlodyka R, Dzierzanowski P, Wrzalik R (2007) Atoll garnets in "Achtarandite" serpentinites: morphology, composition and mode of origin. Mineralogia Polonica 38(2):139-149

Gartzos EG (1977) The geology and petrology of the Iron and Manitou Islands alkaline carbonatite complexes at Nipissing Lake, Ontario. MSc thesis, McMaster University, 138 p

Gaudet MA (2016) The Renard 65 kimberlites: emplacement-related processes in Kimberley-type pyroclastic kimberlites. MSc thesis, University of British Columbia, 155 p

Gaudet M, Kopylova M, Muntener C, Zhuk V, Nathwani C (2018) Geology of the Renard 65 kimberlite pipe, Québec, Canada. Mineral Petrol 112(S2):433-445

Gaudet M, Kopylova M, Zhuk V (2017) The principal role of silicic crustal xenolith assimilation in the formation of Kimberley-type pyroclastic kimberlites – a petrographic study of the Renard 65 kimberlite pipe, Canada. 11th International Kimberlite Conference Extended Abstract No. 11IKC-004565, 3 p

Geraghty EP, Isachsen YW, Wright SF (1979) Dikes of Rand Hill, Northeast Adirondacks, as paleostrain indicators. Office of Nuclear Regulatory Research, IS Nuclear Regulatory

Commission, Boston College, University of the State of New York, Final Report, NUREG-CR-0889, 13 p

Gibson SA, Thompson RN, Leonardos OH, Dickin AP, Mitchell JG (1995) The Late Cretaceous impact of the Trindade mantle plume: evidence from large-volume, mafic, potassic magmatism in SE Brazil. J Petrol 36(1):189-229

Giuliani A, Phillips D, Kamenetsky VS, Fiorentini ML, Farquhar J, Kendrick MA (2014) Stable isotope (C, O, S) compositions of volatile-rich minerals in kimberlites: A review. Chem Geol 374-375:61-83

Giuliani A, Soltys A, Phillips D, Kamenetsky VS, Maas R, Goemann K, Woodhead JD, Drysdale RN, Griffin WL (2017) The final stages of kimberlite petrogenesis: Petrography, mineral chemistry, melt inclusions and Sr-C-O isotope geochemistry of the Bultfontein kimberlite (Kimberley, South Africa). Chem Geol 455:342-356

Girard R (2001) Caracterisation de l'intrusion kimberlitique du lac Beaver, Monts Otish - Petrographie et mineralogie. Ressources naturelles Geologie Quebec, MB 2001-08, 23 pp

Gittins J (1988) The origin of carbonatites. Nature 335:295-296

Gittins J, MacIntyre RM, York D (1967) The ages of carbonatite complexes in eastern Canada. Can J Earth Sci 4:651-655

Godin P, Hopkins R, Bedell P (2016) Updated Renard Diamond Project Mine Plan and Mineral Reserve Estimate, Quebec, Canada, NI 43-101 Technical Report, March 30, 2016, 278 pp

Gofton EL (2007) The Renard 4 kimberlite: implications for ascent of kimberlites in the shallow crust. MSc thesis, University of British Columbia, 127 p

Goldberg SA, Butler JR, Fullagar PD (1986) The Bakersville dike swarm: geochronology and petrogenesis of Late Proterozoic basaltic magmatism in the southern Appalachian Blue Ridge. Am J Sci286:403–430

Grey IE, Mumme WG, Pekov IV, Pushcharovsky DY (2003) The crystal structure of chromian kassite from the Saranovskoye Deposit, Northern Urals, Russia. Am Mineral 88(8-9):1331-1335

Griffiths RW, Campbell IH (1990) Stirring and structure in mantle starting plumes. Earth Planet Sc Lett 99:66-78

Griffin WL, Batumike JM, Greau Y, Pearson NJ, Shee SR, O'Reilly SY (2014) Emplacement ages and sources of kimberlites and related rocks in southern Africa: U–Pb ages and Sr–Nd isotopes of groundmass perovskite. Contrib Mineral Petr 168:1032

Gurnis M, Torsvik TH (1994) Rapid drift of large continents during the late Precambrian and Palaeozoic:Palaeomagnetic constraints and dynamic models. Geology 22:1023-1026

Halls HC, Lovette A, Hamilton M, Söderlund U (2015) A paleomagnetic and U–Pb geochronology study of the western end of the Grenville dyke swarm: Rapid changes in paleomagnetic field direction at ca. 585Ma related to polarity reversals? Precambr Res 257:137-166

Hamilton MA (2009) U-Pb isotopic dating of a diabase dyke of the Mistassini swarm, Quebec. Rapport déposé au Ministère des Ressources Naturelles et de la Faune, 493 Québec, MB200917, 13 p

Harris GA, Pearson DG, Liu J, Hardman MF, Snyder DB, Kelsch D (2018) Mantle composition, age and geotherm beneath the Darby kimberlite field, west central Rae Craton. Mineral Petrol 112 (Suppl1):S57-S70

Harlan SS, Heaman L, LeCheminant AN, Premo WR (2003) Gunbarrel mafic magmatic event: a key 780Ma time marker for Rodinia plate reconstructions. Geology 31:1053–1056

Heaman LM (1989) The nature of the subcontinental mantle from Sr-Nd-Pb isotopic studies on kimberlitic perovskite. Earth Planet Sc Lett 92:323-334

Heaman LM (2004) 2.5-2.4 Ga global magmatism: remnants of supercontinents or products of superplumes? Geological Society of America Abstracts with Programs, Annual Meeting, Denver, Colorado, November 7-10, 2004, 36(5):255

Heaman LM (2008) Precambrian large igneous provinces: an overview of geochronology, origins and impact on Earth evolution. J Geol Soc India 72:15-34

Heaman LM (2009) The application of U–Pb geochronology to mafic, ultramafic and alkaline rocks: An evaluation of three mineral standards. Chem Geol 261:43-52

Heaman LM, Creaser RA, Cookenboo HO, Chacko T (2006) Multi-Stage Modification of the Northern Slave Mantle Lithosphere: Evidence from Zircon- and Diamond-Bearing Eclogite Xenoliths Entrained in Jericho Kimberlite, Canada. J Petrol 47:821-858

Heaman LM, Kjarsgaard BA (2000) Timing of eastern North American kimberlite magmatism: continental extension of the Great Meteor hotspot track? Earth Planet Sc Lett 178:253-268

Heaman L, Kjarsgaard BA, Creaser RA (2003) The timing of kimberlite magmatism in North America: implications for global kimberlite genesis and diamond exploration. Lithos 71(2-4):153-184

Heaman LM, Kjarsgaard BA, Creaser RA (2004) The temporal evolution of North American kimberlites. Lithos 76:377-397

Heaman LM, LeCheminant AN (2000) Anomalous U-Pb systematics in mantle-derived baddeleyite xenocrysts from Ile Bizard: evidence for high temperature radon diffusion? Chem Geol 172:77-93

Heaman LM, LeCheminant AN, Rainbird RH (1992) Nature and timing of Franklin igneous events Canada; implications for a late Proterozoic mantle plume and the break-up of Laurentia. Earth Planet Sci Lett 109:117–131

Heaman LM, Pell J, Grütter HS, Creaser RA (2015) U–Pb geochronology and Sr/Nd isotope compositions of groundmass perovskite from the newly discovered Jurassic Chidliak kimberlite field, Baffin Island, Canada. Earth Planet Sc Lett 415:183-199

Hetman CM (2008) Tuffisitic kimberlite (TK): A Canadian perspective on a distinctive textural variety of kimberlite. J Volcanol Geoth Res 174:57-67

Hetman CM, Scott Smith BH, Paul JL, Winter FW (2004) Geology of the Gahcho Kué kimberlite pipes, NWT, Canada: root to diatreme magmatic transition zones. In: Mitchell RH, Grutter HS, Heaman LM, Scott-Smith BH, Stachel T (eds) Proceedings of the 8th International Kimberlite Conference, C. Roger Clement Volume 1, Lithos 76:51–74

Higgins MD, van Breemen O (1998) The age of the Sept Iles Layered Mafic Intrusion, Canada: implications for the Late Neoproterozoic/Cambrian history of southeastern Canada. J Geol 106(4):421-432

Hodych J, Bennett V (2009) U-Pb zircon dating and paleomagnetism of Proterozoic mafic dykes in the Adirondacks at Rand Hill, NY. Eos, Transactions, American Geophysical Union, 2009, Vol. 90, Issue 22, Jt. Assem. Suppl.:JA143

Hodych JP, Cox RA (2007) Ediacaran U–Pb zircon dates for the Lac Matapédia and Mt. St.-Anselme basalts of the Quebec Appalachians: support for a long-lived mantle plume during the rifting phase of Iapetus opening. Can J Earth Sci 44(4):565-581

Hodych JP, Cox RA, Košler J (2004) An equatorial Laurentia at 550 Ma confirmed by Grenvillian inherited zircons dated by LAM ICP-MS in the Skinner Cove volcanics of western Newfoundland: implications for inertial interchange true polar wander. Precambr Res 129(1-2):93-113

Hoffman PF (1989) Precambrian geology and tectonic history of North America. In: Bally AW, Palmer AR (eds) The Geology of North America - An overview. Vol A. Geological Society of America, Boulder, Colorado, pp 447-512

Holm-Denoma CS, Southworth S, Merschat AJ (2012) Detrital zircon geochronology of Neoproterozoic-Cambrian strata of the Appalachian Blue Ridge; Mt. Rogers, VA area. Abstracts with Programs - Geological Society of America, November, 2012, 44(7):172

Holm-Denoma CS, Southworth CS, Merschat AJ, McClellan E (2015) The detrital record of Neoproterozoic to Cambrian rocks from the southern Appalachian Blue Ridge; protracted rifting, rapid unroofing, and stabilization of the margin. Abstracts with Programs - Geological Society of America, 2015, 47(7):859

Holmes A, Paneth FA (1936) Helium-ratios of rocks and minerals from the diamond pipes of South Africa. Proceedings of the Royal Society of London, Series A: Mathematical and Physical Sciences 154(882):385-413

Huang Y-J, Tsai M-C, Chiu H-T, Sheu H-S, Lee C-Y (2010) Artificial Synthesis of Platelet-Like Kassite and Its Transformation to $CaTiO_3$. Crystal Growth & Design 10(3):1221-1225

Hunt L, Stachel T, McCandless TE, Armstrong J, Muehlenbachs K (2012) Diamonds and their mineral inclusions from the Renard kimberlites in Quebec. Lithos 142-143:267-284

Hutchison MT, Heaman LM (2008) Chemical and physical characteristics of diamond crystals from Garnet Lake Sarfartoq, West Greenland: an association with carbonatitic magmatism. Can Mineral 46:1063-1078

Isachsen YW, Kelly WM, Sinton C, Coish RA, Heizler MT (1988) Dikes of the northeast Adirondack region - introduction to their distribution, orientation, mineralogy, chronology, magnetism, chemistry, and mystery. In: Isachsen YW (ed) Field trip guidebook, New York State Geological Association, Albany, NY:215-243

Ivanov OK (2016) Mineralogy of Saranovsk chromite deposit of the Urals; Mineralogical almanac 21 (2) (Mineralogiya Saranovskogo khromitovogo mestorozhdeniya Urala: Mineralogicheskiy al'manakh, tom 21, vyp. 2), 128 p

Jaffey AH, Flynn KF, Glendenin LE, Bentley WC, Essling AM (1971) Precision Measurement of Half-Lives and Specific Activities of $^{235}U$ and $^{238}U$. Physical Review C 4:1889-1906

Janse AJA (1985) Kimberlites; where and when. In: Glover JE (ed) Publs Geol Dep & Univ Extension, University of Western Australia 8, pp 19-61

Janse AJA (1994) Is Clifford's rule still valid? Affirmative examples from around the world. In: Meyer HOA, Leonardos OH (eds) Diamonds: characterization, genesis and exploration, Volume 2. Proceedings of the Fifth International Kimberlite Conference, CPRM - Special Publication 1/B Jan/94, pp 215-235

Jelsma H, Barnett W, Richards S, Lister G (2009) Tectonic setting of kimberlites. Lithos 112:155-165

Kamenetsky VS, Belousova EA, Giuliani A, Kamenetsky MB, Goemann K, Griffin WL (2014) Chemical abrasion of zircon and ilmenite megacrysts in the Monastery kimberlite: implications for the composition of kimberlite melts. Chem Geol 383:76-85

Kamo SL, Gower CF (1994) Note: U-Pb baddeleyite dating clarifies age of characteristic paleomagnetic remanence of Long Range dykes, southeastern Labrador. Atlantic Geology 30:259-262

Kamo SL, Gower CF, Krogh TE (1989) Birthdate for the Iapetus Ocean? A precise U-Pb zircon and baddeleyite age for the Long Range dikes, southeast Labrador. Geology 17:602-605

Kamo SL, Heaman LM, Lumbers SB (1989) Age for a Lamprophyre Dike, Callander Bay, Ontario: Use of Ti-bearing Minerals as a Potential Geochronometer. Geological Association of Canada Program with Abstracts 14:A41

Kamo SL, Krogh TE, Kumarapeli PS (1995) Age of the Grenville dyke swarm, Ontario-Quebec: implications for the timing of Iapetan rifting. Can J Earth Sci 32:273-280

Kargin AV (2014) Geochemistry of mantle metasomatism related to formation of kimberlites in the northern East European Platform. Geology of Ore Deposits 56(6):409-430

Keller J, Hoefs J (1995) Stable isotope characteristics of recent natrocarbonatites from Oldoinyo Lengai. In: Bell K, Keller J (eds) Carbonatite volcanism: Oldoinyo Lengai and Petrogenesis of Natrocarbonatites. Springer-Verlag, pp 113-123

Kienlen B, Blackmore E, Curry N, Gill G, Kolebaba M, Lyon R, Ozyer C, Pratt Z, Vanderspeigel R (2008) The Amaruk project in Canada's new Pelly Bay Diamond District. 9th International Kimberlite Conference Extended Abstract 9IKC-A-00334, 3 p

Kinny PD, Griffin BJ, Heaman LM, Brakhfogel FF, Spetsius ZV (1997) SHRIMP U-Pb ages of perovskite from Yakutian kimberlites. Russian Geology and Geophysics 38(1):97-105

Kirsch M, Svenningsen O (2016) Root zone of a continental rift: the Neoproterozoic Kebnekaise Intrusive Complex, northern Swedish Caledonides. GFF 138(1):31-53

Kirwan PJ, Daly JS, Menuge JF (1989) A minimum age for the deposition of the Dalradian Supergroup sediments in Ireland: Terra Abs. supp. Terra Nova 1:16

Kjarsgaard BA, Heaman LM, Sarkar C, Pearson DG (2017) The North America mid-Cretaceous kimberlite corridor: wet, edge-driven decompression melting of an OIB-type deep mantle source. Geochem Geophy Geosy 18:2727-2747

Kramers JD (1979) Lead, uranium, strontium, potassium and rubidium in inclusion-bearing diamonds and mantle-derived xenoliths from Southern Africa. Earth Planet Sc Lett 42:58-70

Kresten P, Printzlau I, Rex D, Vartiainen H, Woolley A (1977) New ages of carbonatitic and alkaline ultramafic rocks from Sweden and Finland. Geologiska Föreningen i Stockholm Förhandlingar 99(1):62-65

Kong JM, Boucher DR, Scott Smith BH (1999) Exploration and geology of the Attawapiskat kimberlites, James Bay Lowland, Northern Ontario, Canada. In: Gurney JJ, Gurney JL, Pascoe MD, Richardson SH (eds) Proceedings of the VIIth International Kimberlite Conference, vol 1, pp 452-467

Krivovichev SV, Yakovenchuk VN, Burns PC, Pakhomovsky YA, Menshikov YP (2003) Cafetite, $Ca[Ti_2O_5](H_2O)$: Crystal structure and revision of chemical formula. Am Mineral 88:424-429

Kukharenko AA, Kondratyeva VV, Kovyatsina VM (1959) Cafetite, a new hydrous titanate of calcium and iron. Zapiski Vsesoyuznogo Mineralogicheskogo Obshchestva 88:444-453 (in Russian)

Kukharenko AA, Orlova MP, Bulakh AG, Bagdasarov EA, Rimskaya-Korsakova OM, Nefedov YI, llyinskiy GA, Sergeyev AC, Abakumova NB (1965) The Caledonian Complex of

Ultrabasic Alkaline Rocks and Carbonatites of the Kola Peninsula and Northern Karelia. Nedra Press, Moscow, 772 p (in Russian)

Kumar A, Heaman LM, Manikyamba C (2007) Mesoproterozoic kimberlites in south India: A possible link to ~1.1Ga global magmatism. Precambr Res 154(3-4):192-204

Kumarapeli PS (1977) The St. Lawrence Paleo-rift system: a comparative study. In: Ramberg IB, Neumann E-R (eds) Tectonics and Geophysics of Continental Rifts:367-384

Kumarapeli PS (1985) Vestiges of Iapetan rifting in the craton west of the North Appalachians. Geoscience Canada 12(2):54-59

Kumarapeli PS (1993) A plume-generated segment of the rifted margin of Laurentia, Southern Canadian Appalachians, seen through a completed Wilson Cycle. Tectonophysics 219:47-55

Kumarapeli PS, Dunning GR, Pinston H, Shaver J (1989) Geochemistry and U-Pb zircon age of comenditic metafelsites of the Tibbit Hill Formation, Quebec Appalachians. Can J Earth Sci 26:1374-1383

Kumarapeli PS, Saull VA (1966) The St. Lawrence Valley System: a North American equivalent of the East African Rift Valley System. Can J Earth Sci 3:639-658

Kupsch B, Armstrong JP (2013) Exploration and geology of the Qilalugaq kimberlites, Rae Isthmus, Nunavut, Canada. In: Pearson DG et al (eds) Proceedings of the 10th International Kimberlite Conference, vol. 2, Special Issue of the Journal of the Geological Society of India:67-78

Lafleur J, Hogarth DD (1981) Cambro-Proterozoic volcanism near Buckingham, Quebec. Can J Earth Sci 18:1817-1823

Larsen O, Moller J (1968a) K/Ar age determinations from western Greenland. I. Reconnaissance programme. Rapport, Grønlands Geologiske Undersøgelse, 15:82-86

Larsen O, Moller J (1968b) Potassium-argon age studies in West Greenland. Can J Earth Sci 5:683-691

Larsen RB, Grant T, Sørensen BE, Tegner C, McEnroe S, Pastore Z, Fichler C, Nikolaisen E, Grannes KR, Church N, ter Maat GW, Michels A (2018) Portrait of a giant deep-seated magmatic conduit system: The Seiland Igneous Province. Lithos 296-299:600-622

Larsen LM, Rex DC (1992) A review of the 2500 Ma span of alkaline-ultramafic, potassic and carbonatitic magmatism in West Greenland. Lithos 28:367-402

LeCheminant AN, Heaman LM (1994) 779 Ma mafic magmatism in the northwestern Canadian Shield and northern Cordillera: a new regional time-marker. Eighth International Conference on Geochronology and Isotope Geology. U.S. Geological Survey Circular, vol. 1107:197

Lepine I, Farrow DJ (2018) 3D geological modelling of the Renard 2 kimberlite pipe, Québec, Canada: from exploration to extraction. Mineral Petrol 112, Supplement 2:411-419

Lepine I, Zhuk V (2017) The Renard 2 coherent kimberlitic units, Québec Canada – spatial distribution and economic implications. 11th International Kimberlite Conference Extended Abstract No. 11IKC-004547, 3 p

Lester AP, Larson EE, Farmer GL, Stern CR, Funk JA (2001) Neoproterozoic kimberlite emplacement in the Front Range, Colorado. Rocky Mountain Geology 36(1):1-12

Letendre J, L'Heureux M, Nowicki T, Creaser R (2003) The Wemindji kimberlites: exploration and geology. 8th International Kimberlite Conference Long Abstract FLA-0311, 4 p

Lewis HC (1887) IV.—On a Diamantiferous Peridotite and the Genesis of the Diamond. Geol Mag 4:22-24

Lewis HC (1897) Papers and notes on the genesis and matrix of the diamond (edited by TG Bonney). Longmans, Green, and Co, New York, 73 p

Li Q-L, Li X-H, Liu Y, Wu F-Y, Yang J-H, Mitchell RH (2010) Precise U–Pb and Th–Pb age determination of kimberlitic perovskites by secondary ion mass spectrometry. Chem Geol 269(3-4):396-405

Li ZX, Bogdanova SV, Collins AS, Davidson A, De Waele B, Ernst RE, Fitzsimons ICW, Fuck RA, Gladkochub DP, Jacobs J, Karlstrom KE, Lu S, Natapov LM, Pease V, Pisarevsky SA, Thrane K, Vernikovsky V (2008) Assembly, configuration, and break-up history of Rodinia: A synthesis. Precambr Res 160(1-2):179-210

Lorenz V, Kurszlaukis S (2007) Root zone processes in the phreatomagmatic pipe emplacement model and consequences for the evolution of maar–diatreme volcanoes. J Volcanol Geoth Res 159(1-3):4-32

Lorenz V, Zimanowski B, Buttner R, Kurszlaukis S (1999) Formation of kimberlite diatremes by explosive interaction of kimberlite magma with groundwater: field and experimental aspects. In: Gurney JJ, Gurney JL, Pascoe MD & Richardson SH (eds) Proceedings of the VIIth International Kimberlite Conference:522-528

Lovering JF, Richards JR (1964) Potassium-argon age study of possible lower-crust and upper-mantle inclusions in deep-seated intrusions. J Geophys Res 69(22):4895-4901

Lowden JA, Stockwell CH, Tipper HW, Wanless RK (1963) Age Determinations and Geological Studies. Geological Survey of Canada Paper 62-17, 140 p

Ludwig KR (2012) User's Manual for Isoplot 3.75. Berkeley Geochronology Center Special Publication no 5 (revised January 30, 2012), 75 pp

Macdonald FA, Schmitz MD, Crowley JL, Roots CF, Jones DS, Maloof AC, Strauss JV, Cohen PA, Johnston DT, Schrag DP (2010) Calibrating the Cryogenian. Science 327 (5970):1241-1243

Macintyre RM, Dawson JB (1976) Age and significance of some South African kimberlites. Fourth European Colloquium of Geochronology, Cosmochronology and Isotope Geology, Amsterdam, April 5-10, 1976, Volume of Abstracts:66

Malarkey J, Pearson DG, Kjarsgaard BA, Davidson JP, Nowell GM, Ottley CJ, Stammer J (2010) From source to crust: Tracing magmatic evolution in a kimberlite and a melilitite using microsample geochemistry. Earth Planet Sc Lett 299:80-90

Malka E, Stevenson RK, David J (2000) Sm-Nd geochemistry and U-Pb geochronology of the Mont Rigaud Stock, Quebec, Canada: a late magmatic event associated with the formation of the Iapetus rift. The Journal of Geology 108:569-583

Martins T, Chakhmouradian AR, Medici L (2013) Kassite from the Prairie Lake (Ontario) and Iron Mountain (Wyoming) and its relation to perrovskite alteration. GAC-MAC-SEG Joint Annual Meeting Abstracts, Ottawa:133

Martins T, Chakhmouradian AR, Medici L (2014) Perovskite alteration in kimberlites and carbonatites: the role of kassite, $CaTi_2O_4(OH)_2$. Physics and Chemistry of Minerals 41(6):473-484

Masun KM, Doyle BJ, Ball S, Walker S (2004) The geology and mineralogy of the Anuri kimberlite, Nunavut, Canada. Lithos 76:75-97

Mattey D, Lowry D, Macpherson C (1994) Oxygen isotope composition of mantle peridotite. Earth Planet Sc Lett 128:231-241

Mattinson JM (1973) Anomalous isotopic composition of lead in young zircons. Carnegie Institution of Washington Year Book 72:613-616

McCandless TE (1999) Kimberlites: mantle expressions of deep-seated subduction. In: Gurney JJ, Gurney JL, Pascoe MD, Richardson SH (eds) Proceedings of the VIIth International Kimberlite Conference, vol 2, pp 545-549

McCandless TE, Schulze D, Bellis A, Taylor LA, Liu Y, van Rythoven AD (2008) Morphology and chemistry of diamonds from the Lynx kimberlite dyke complex, northern Otish Mountains, Quebec. 9th International Kimberlite Conference Extended Abstract No. 9IKC-A-00369, 3 p

McCausland PJA, Hankard F, Van der Voo R, Hall CM (2011) Ediacaran paleogeography of Laurentia: Paleomagnetism and 40Ar–39Ar geochronology of the 583Ma Baie des Moutons syenite, Quebec. Precambr Res 187(1-2):58-78

McCausland PJA, Hodych JP (1998) Paleomagnetism of the 550Ma Skinner Cove volcanics of western Newfoundland and the opening of the Iapetus Ocean. Earth Planet Sc Lett 163:15–29

McCausland PJA, Hodych JP, Dunning GR (1997) Evidence from western Newfoundland for the final breakup of Rodinia? U-Pb age and paleolatitude of the Skinner Cove volcanics. Abstract Volume, GAC/MAC Annual Meeting, May 19-21, 1997:A99

McCausland PJ, Pisarevsky S, Jourdan F, Higgins M (2009) Laurentia at 571 Ma: preliminary paleomagnetism and Ar-Ar age of the Ediacaran St Honore alkali intrusion, Quebec. Geological Association of Canada, 2009 Joint Assembly, Abstract GA12A-01

McCausland PJA, Van der Voo R, Hall CM (2007) Circum-Iapetus paleogeography of the Precambrian–Cambrian transition with a new paleomagnetic constraint from Laurentia. Precambr Res 156(3-4):125-152

McClellan E, Gazel E (2014) The Cryogenian intra-continental rifting of Rodinia: Evidence from the Laurentian margin in eastern North America. Lithos 206-207:321-337

Meert JG (2014) Ediacaran-Early Ordovician paleomagnetism of Baltica: a review. Gondwana Research 25:159-169

Meert JG, Torsvik TH, Eide EA, Dahlgren S (1998) Tectonic Significance of the Fen Province, S. Norway: Constraints from Geochronology and Paleomagnetism. J Geol 106:553-564

Meert JG, Van der Voo R, Powell CM, Li ZX, McElhinny MW, Chen Z, Symons DTA (1993) A Plate-Tectonic Speed Limit? Nature 363:216–217

Meert JG, Walderhaug HJ, Torsvik TH, Hendriks BWH (2007) Age and paleomagnetic signature of the Alno carbonatite complex (NE Sweden): additional controversy for the Neoproterozoic paleoposition of Baltica. Precambr Res 154:159-174

Menges F (2015) Spekwin32 - optical spectroscopy software, Version 1.72.0. http://www.effemm2.de/spekwin/

Merdith AS, Collins AS, Williams SE, Pisarevsky S, Foden JD, Archibald DB, Blades ML, Alessio BL, Armistead S, Plavsa D, Clark C, Muller RD (2017) A full-plate global reconstruction of the Neoproterozoic. Gondwana Research 50:84-134

Milanovskiy YY, Mal'kov BA (1980) Epochs of kimberlite volcanism and global compressive and expansionary cycles of the Earth. Doklady Akad Nauk SSSR 252:62-65

Miller BV, Barr SM (2004) Metamorphosed gabbroic dikes related top opening of Iapetus Ocean at the St. Lawrence promontory: Blair River Inlier, Nova Scotia, Canada. J Geol 112:277-288

Miller CF, Hatcher RD, Ayers JC, Coath CD, Harrison TM (2000) Age and zircon inheritance of eastern Blue Ridge plutons, southwestern North Carolina and northeastern Georgia, with implications for magma history and evolution of the southern Appalachian orogen. Am J Sci 300:142-172

Milton C (1985) Kassite $CaTi_2O_4(OH)_2$ from Magnet Cove, Arkansas. Geological Society of America, Northeastern Section, 20th Annual Meeting, March 13-16, 1985, Lancaster, Pennsylvania, Abstracts with Programs:168

Milton JE, Hickey KA, Gleeson SA, Friedman RM (2017) New U/Pb constraints on the age of the Little Dal Basalts and Gunbarrel-related volcanism in Rodinia. Precambr Res 296:168-180

Mitchell RH (1986) Kimberlites: mineralogy, geochemistry, and petrology. Plenum Press, New York, 442 p

Mitchell RH (1995) Kimberlites, orangeites, and related rocks. Springer Science+Business Media, New York, 410 p

Mitchell RH (1996) Perovskites: a revised classification scheme for an important rare earth element host in alkaline rocks, Chapter three. In: Jones AP, Wall F, Williams CT (1996) Rare Earth Minerals: Chemistry, origin and ore deposits:41-76

Mitchell RH (1997) Kimberlites, orangeites, lamproites, melilitites, and minettes: a petrographic atlas. Almaz Press Inc., Thunder Bay, 243 p

Mitchell RH (2002) Perovskites. Modern and ancient. Almaz Press Inc., Thunder Bay, 318 p

Mitchell RH, Chakhmouradian AR (1998) Instability of perovskite in a $CO_2$-rich environment: examples from carbonatite and kimberlite. Can Mineral 36(4):939-952

Mitchell RH, Scott Smith BH, Larsen LM (1999) Mineralogy of ultramafic dikes from the Sarfartoq, Sismiut and Maniitsoq areas, west Greenland. 7th International Kimberlite Conference, Cape Town: 574-583

Mitchell RN, Evans DAD, Kilian TM (2010) Rapid Early Cambrian rotation of Gondwana. Geology 38(8):755–758

Mitchell RN, Kilian TM, Raub TD, Evans DAD, Bleeker W, Maloof AC (2011) Sutton hotspot: resolving Edicaran-Cambrian tectonics and true polar wander for Laurentia. Am J Sci 311:651-663

Moiseev MM, Chukanov NV (2006) Mineralogy of alkaline pegmatites and hydrothermalites of the Kovdor phlogopite deposit. Novye Dannye Mineral 41:56–70 (in Russian)

Moore A, Blenkinsop T, Cotterill F (2008) Controls on post-Gondwana alkaline volcanism in Southern Africa. Earth Planet Sc Lett 268:151-164

Moorhead J, Beaumier M, Girard R, Heaman L (2003) Distribution, structural controls and ages of kimberlite fields in the Superior province of Quebec. 8th International Kimberlite Conference Long Abstract FLA-0275, 5 p

Morfin S, Sawyer EW, Bandyayera D (2013) Large volumes of anatectic melt retained in granulite facies migmatites: An injection complex in northern Quebec. Lithos 168-169:200-218

Morgan WJ (1971) Convection plumes in the lower mantle. Nature 230:42-43

Muntener C, Gaudet M (2018) Geology of the Renard 2 pipe to 1000 m depth, Renard Mine, Québec, Canada: insights into Kimberley-type pyroclastic kimberlite emplacement. Mineral Petrol 112, Supplement 2:421-432

Muntener C, Scott Smith BH (2013) Economic Geology of Renard 3, Québec, Canada: A Diamondiferous, Multi-Phase Pipe Infilled with Hypabyssal and Tuffisitic Kimberlite. In: Pearson DG et al (eds) Proceedings of 10th International Kimberlite Conference, J Geol Soc India special issue 2:241-256

Nelson DR (1989) Isotopic characteristics and petrogenesis of the lamproites and kimberlites of central west Greenland. Lithos 22:265-274

Nesbitt HW, Bancroft GM, Fyfe WS, Karkhanis SN, Nishijima A (1981) Thermodynamic stability and kinetics of perovskite dissolution. Nature 289:358-362

Nickel EH, Grey IE, Madsen IC (1987) Lucasite-(Ce), $CeTi_2(O,OH)_6$, a new mineral from Western Australia: Its description and structure. Am Mineral 72:1006-1010

Nixon PH (1973) The geology of Mothae, Solane, Thaba Putsoa and Blow 13. In: Nixon PH (ed) Lesotho kimberlites, Lesotho National Development Corporation, pp 39-47

Nowell GM, Pearson DG, Bell DR, Carlson RW, Smith CB, Kempton PD, Noble SR (2004) Hf isotope systematics of kimberlites and their megacrysts: New consraints on their source regions. J Petrol 45(8):1583-1612

O'Brien H (2015) Chapter 4.4 - Kimberlite-Hosted Diamonds in Finland. In: Maier WD, Lahtinen R, O'Briend H (eds) Mineral Deposits of Finland. Elsevier, New York:345-375

O'Brien HE, Bradley J (2008) New kimberlite discoveries in Kuusamo, northern Finland. 9th International Kimberlite Conference Extended Abstract No 9IKC-A-00346, 3 p

O'Brien H, Lehtonen M, Spencer R, Birnie A (2003) Lithospheric mantle in eastern Finland: a 250 km 3D transect. 8th International Kimberlite Conference Long Abstract FLA-0261, 5 p

O'Brien HF, Peltonen P, Vartiainen H (2005) Kimberlites, carbonatites, and alkaline rocks. In: Lehtinen M, Nurmi PA, Ramo OT (eds) Precambrian Geology of Finland, Key to the Evolution of the Fennoscandian Shield (Chapter 14). Elsevier B.V., Amsterdam:605-644

O'Brien HE, Tyni M (1999) Mineralogy and geochemistry of kimberlties and related rocks from Finland. In: Gurney JJ, Gurney JL, Pascoe MD, Richardson SH (eds) Proceedings of the VIIth International Kimberlite Conference, The P.H. Nixon volume 2:625-636

Ownby SE, Miller CF, Berquist PJ, Carrigan CW, Wooden JL, Fullagar PD (2004) U–Pb geochronology and geochemistry of a portion of the Mars Hill terrane, North Carolina–Tennessee: constraints on origin, history, and tectonic assembly. In: Tollo RP, Corriveau L, McLelland J, Bartholomew MJ (eds) Proterozoic Tectonic Evolution of the Grenville Orogen in North America. Geological Society of America Memoir 197:609–632

Parrish RR (1990) U-Pb dating of monazite and its application to geological problems. Can J Earth Sci 27:1431-1450

Patterson M, Francis D, McCandless T (2009) Kimberlites: Magmas or mixtures? Lithos 112:191-200

Paulsson O, Andréasson P-G (2002) Attempted break-up of Rodinia at 850 Ma: geochronological evidence from the Seve-Kalak Superterrance, Scandinavian Caledonides. Journal of the Geological Society, London 159:751-761

Pedersen RB, Dunning GR, Robins B (1989) U-Pb ages of nepheline syenite pegmatites from the Seiland magmatic province, N Norway. In: Gayer RA (ed) The Caledonide geology of Scandinavia. Graham & Trotman, London:3-8

Pehrsson SJ, Buchan KL (1999) Borden dykes of Baffin Island, Northwest Territories: a Franklin U–Pb baddeleyite age and a paleomagnetic reinterpretation. Can J Earth Sci 36(1):65–73

Pekov IV (1998) Minerals First Discovered on the Territory of the Former Soviet Union, 369 p

Pekov IV, Schneider J, Pushcharovsky DY (2004) On the X-ray powder diffractogram of kassite and its relationship with cafetite (O poroshkovoy rentgenogramme kassita i yego sootnosheniyakh s kafetitom). Zapiski Vserossiyskogo Mineralogicheskogo Obshchestva = Proceedings of the Russian Mineralogical Society 133(3):51-55 (in Russian)

Peltonen P, Irmeli M (2001) An ion microprobe U-Th-Pb study of zircon xenocrysts from the Lachtojoki kimberlite pipe, Eastern Finland. Bulletin of the Geological Survey of Finland 73:47-58

Percival JA, Skulski T, Sanborn-Barrie M, Stott GM, Leclair AD, Corkery MT, Boily M (2012) Geology and tectonic evolution of the Superior Province, Canada (Chapter 6). In: Percival JA, Cook FA, Clowes RM (eds) Tectonic Styles in Canada: The LITHOPROBE Perspective. Geological Association of Canada, Special Paper 49, pp 321–378

Phillips D, Zhong D, Matchan EL, Maas R, Farr H, O'Brien H, Giuliani A (2017) A comparison of geochronology methods applied to kimberlites and related rocks from the Karelian craton, Finland. 11th International Kimberlite Conference Extended Abstract No. 11IKC-4480, 3 p

Phipps SP (1988) Deep rifts as sources for alkaline intraplate magmatism in eastern North America. Nature 334:27-31

Pisarevsky S, Murphy B, Hamilton M, Soederlund U, Hodych J (2013) U-Pb geochronology and paleomagnetism of the Neoproterozoic St Simeon dolerite dykes, Quebec: an eastern

Laurentian perspective of Ediacaran Rodinia breakup. Geophysical Research Abstracts, January 1, 2013, vol 15, Abstract EGU 2013-3693

Popova VI, Popov VA, Kanonerov AA (1998) Chromium-bearing kassite, $CaTi_2O_4(OH)_2$, from the Saranovskoye deposit—a first finding on the Urals. Miass 2:75–77

Potts PJ (1992) A handbook of silicate rock analysis. Blackie Academic & Professional, New York, 622 p

Proyer A, Baziotis I, Mposkos E, Rhede D (2014) Ti- and Zr-minerals in calcite-dolomite marbles from the ultrahigh-pressure Kimi Complex, Rhodope mountains, Greece: implications for the P-T evolution based on reaction textures, petrogenetic grids, and geothermobarometry. Am Mineral 99:1429-1448

Puffer JH (2002) A late Neoproterozoic eastern Laurentian superplume: location, size, chemical composition, and environmental impact. Am J Sci 302:1-27

Pyle JM, Spear FS, Wark DA (2002) Electron Microprobe Analysis of REE in Apatite, Monazite and Xenotime: Protocols and Pitfalls. Reviews in Mineralogy and Geochemistry 48(1):337-362

Queen M, Heaman LM, Hanes JA, Archibald DA, Farrar E (1996) $^{40}Ar/^{39}Ar$ phlogopite and U-Pb perovskite dating of lamprophyre dykes from the eastern Lake Superior region: evidence for a 1.14 Ga magmatic precursor to Midcontinent Rift volcanism. Can J Earth Sci 33:958-965

Ranger IM (2019) An investigation into the timing of the Renard kimberlite cluster, Otish field, Canada. PhD thesis, University of Alberta, in progress

Ranger IM, Heaman LM, Pearson DG, Muntener C, Zhuk V (2018) Punctuated, long-lived emplacement history of the Renard 2 kimberlite, Canada, revealed by new high precision U-Pb groundmass perovskite dating. Mineral Petrol 112 (Suppl2):S639-S651

Robert B, Besse J, Blein O, Greff-Lefftz M, Baudin T, Lopes F, Meslouh S, Belbadaoui M (2017) Constraints on the Ediacaran inertial interchange true polar wander hypothesis: a new paleomagnetic study in Morocco (West African Craton). Precambr Res 295:90-116

Roberts D, Walker N (1997) U-Pb zircon age of a dolerite dyke from near Hamningberg, Varanger Peninsula, North Norway, and its regional significance. Norges geologiske undetsokelse Bulletin 432:95-102

Roberts RJ, Corfu F, Torsvik TH, Ashwal LD, Ramsay DM (2006) Short-lived mafic magmatism at 560–570 Ma in the Norwegian caledonites: U–Pb zircon ages from the Seiland Igneous Province. Geological Magazine 143:887–903

Roberts RJ, Corfu F, Torsvik TH, Hetherington CJ, Ashwal LD (2010) Age of alkaline rocks in the Seiland Igneous Province, Northern Norway. Journal of the Geological Society 167(1):71-81

Roberts RJ, Corfu F, Torsvik TH, Ramsay DM, Ashwal LD (2004) Redefining the magmatic evolution of the Kalak Nappe Complex. Session 10: Gunnar Kautsky Memorial Symposium: The North Atlantic Caledonides, GFF 126:84

Rosenbaum J, Sheppard SMF (1986) An isotopic study of siderites, dolomites and ankerites at high temperatures. Geochim Cosmochim Acta 50:1147-1150

Rudashevskiy LS, Firfarova IB, Tsekhovol'skaya DI (1977) Sinteticheskiy analog i utochneniye svoystv kassita i gidrokassita. Zapiski Vsesoyuznogo Mineralogicheskogo Obshchestva 1977(1):114-120 (in Russian)

Rukhlov AS, Bell K (2010) Geochronology of carbonatites from the Canadian and Baltic Shields, and the Canadian Cordillera: clues to mantle evolution. Miner Petrol 98(1-4):11-54

Sarkar C, Heaman LM, Pearson DG (2015a) Duration and periodicity of kimberlite volcanic activity in the Lac de Gras kimberlite field, Canada and some recommendations for kimberlite geochronology. Lithos 218-219:155-166

Sarkar C, Kjarsgaard BA, Pearson DG, Heaman LM, Locock AJ, Armstrong JP (2018) Geochronology, classification and mantle source characteristics of kimberlites and related rocks from the Rae Craton, Melville Peninsula, Nunavut, Canada. Mineral Petrol 112 (Suppl2):S653-S672

Sarkar C, Pearson DG, Heaman LM, Woodland SJ (2015b) Precise Pb isotope ratio determination of picogram-size samples: A comparison between multiple Faraday collectors equipped with $10^{12}$ Ω amplifiers and multiple ion counters. Chem Geol 395:27-40

Schärer U (1984) The effect of initial 230Th disequilibrium on young U-Pb ages: the Makalu case, Himalaya. Earth Planet Sc Lett 67:191-204

Schmitz MD, Schoene B (2007) Derivation of isotope ratios, errors, and error correlations for U-Pb geochronology using $^{205}Pb$-$^{235}U$-($^{233}U$)-spiked isotope dilution thermal ionization mass spectrometric data. Geochem Geophy Geosy 8 (8). doi:10.1029/2006GC001492

Schoene B (2014) 4.10: U-Th-Pb Geochronology. Treatise on Geochemistry (Second Edition), Volume 4:341-378

Scott Smith BH (2008) Canadian kimberlites: Geological characteristics relevant to emplacement. J Volcanol Geoth Res 174:9-19

Scott Smith Petrology Inc. (2006) Kimberlite Basics 1 course notes.

Scott Smith BH, Nowicki TE, Russel JK, Webb KJ, Mitchell RH, Hetman CM, Harder M, Skinner EMW, Robey JvA (2013) Kimberlite terminology and classification. In: Pearson DG et al. (eds) Proceedings of 10th International Kimberlite Conference, J Geol Soc India special issue 2:1-17

Secher K, Heaman LM, Nielsen, TFD, Jensen SM, Schjoth F, Creaser RA (2009) Timing of kimberlite, carbonatite, and ultramafic lamprophyre emplacement in the alkaline province located 64$^{o}$-67$^{o}$ in southern West Greenland. Lithos 112S:400-406

Self PG, Buseck PR (1991) Structure model for kassite, $CaTi_2O_4(OH)_2$. Am Mineral 76(1-2):283-287

Shafiqullah M, Tupper WM, Cole TJS (1968) K-Ar ages on rocks from the crater at Brent, Ontario. Earth Planet Sc Lett 5:148-152

Shau Y-H, Torii M, Horng C-S, Peacor DR (2000) Subsolidus evolution and alteration of titanomagnetite in ocean ridge basalts from Deep Sea Drilling Project/Ocean Drilling Program Hole 504B, Leg 83: implications for the timing of magnetization. Journal of Geophysical Reseach 105 (B10):23635-23649

Shumlyanskyy L, Andréasson PG (2004) New geochemical and geochronological data from the Volyn Flood Basalt in Ukraine and correlation with large igneous events in Baltoscandia. GFF 126:85–86

Shumlyanskyy LV, Andreasson PG, Buchan KL, Ernst RE (2007) The Volynian flood basalt province and coeval (Ediacaran) magmatism in Baltoscandia and Laurentia. Mineral Journ (Ukraine) 29:47-55

Shumlyanskyy L, Nosova AA (2008) Age of lithospheric source of Vendian trappes of Volyn. Reports of the National Academy of Sciences of Ukraine 1:115-118 (In Russian with English abstract)

Shumlyanskyy L, Nosova A, Billström K, Söderlund U, Andréasson P-G, Kuzmenkova O (2016) The U–Pb zircon and baddeleyite ages of the Neoproterozoic Volyn Large Igneous Province: implication for the age of the magmatism and the nature of a crustal contaminant. GFF 138(1):17-30

Skinner EMW (2008) The emplacement of class 1 kimberlites. J Volcanol Geoth Res 174(1-3):40-48

Skinner EMW, Marsh JS (2004) Distinct kimberlite pipe classes with contrasting eruption processes. Lithos 76:183-200

Smith Jr AE (1989) Minerals from the miarolitic cavities at the Diamond Jo Quarry, Magnet Cove, Hot Spring County, Arkansas. Rocks and Minerals 64(4):300-307

Smith CB (1983) Pb, Sr and Nd isotopic evidence for sources of southern African Cretaceous kimberlites. Nature 304:51-54

Smith RC II (2003) Late Neoproterozoic felsite (602.3 +/-2 Ma) and associated metadiabase dikes in the Reading Prong, Pennsylvania, and rifting of Laurentia. Northeastern Geology and Environmental Sciences 25(3):175-185

Smith CB, Allsopp HL, Kramers JD, Hutchinson G, Roddick JC (1985) Emplacement ages of Jurassic-Cretaceous South African kimberlites by the Rb-Sr method on phlogopite and whole-rock samples. Transactions of the Geological Society of South Africa 88:249-266

Southworth S, Aleinikoff JN (2007) Time versus tectonic significance; the disconformity at the base of the Chilhowee Group and the Neoproterozoic-Cambrian boundary. Abstracts with Programs - Geological Society of America, March 2007 39(2):9

Southworth S, Aleinikoff JN, Bailey CM, Burton WC, Crider EA, Hackley PC, Smoot JP, Tollo RP (2009a) Geologic map of the Shenandoah National Park region, Virginia: U.S. Geological Survey Open-File Report 2009-1153, 96 p

Southworth S, Satkoski AM, Samson SC, Aleinikoff JN (2011) The great Paleozoic unconformity; provenance of Neoproterozoic-Cambrian rocks of the Appalachians using detrital zircons. Abstracts with Programs - Geological Society of America, October, 2011,43(5):205

Southworth S, Tollo RP, Aleinikoff JN, Bailey C, Burton WC, Crider E, Hackley PC, Kunk MJ, Mundil R, Naeser CN, Naeser N, Smoot J (2009b) New geologic map and geochronology of the Shenandoah National Park region, Virginia. Geological Society of America, Abstracts with Programs, Annual Meeting, Portland, Oregon, October 18-21, 2009 41(7):365

Southworth S, Tollo RP, Aleinikoff JN, Bailey C, Burton WC, Crider E, Hackley PC, Kunk MJ, Mundil R, Naesser CN, Naeser N, Smoot J (2010) Geologic map and geochronology of the Shenandoah National Park region, Virginia. Geological Society of America Abstracts with Programs 42(1):91

Sparks RSJ, Baker L, Brown RJ, Field M, Schumacher J, Stripp G, Walters A (2006) Dynamical constraints on kimberlite volcanism. J Volcanol Geoth Res 155:18-48

Stacey JS, Kramers JD (1975) Approximation of terrestrial lead isotope evolution by a two-stage model. Earth Planet Sc Lett 26:207-221

Stamm N, Schmidt MW, Szymanowski D, von Quadt A, Mohapi T, Fourie A (2018) Primary petrology, mineralogy and age of the Letseng-la-Terae kimberlite (Lesotho, Southern Africa) and parental magmas of Group-I kimberlites. Contrib Mineral Petrol 173:76

Su Q, Goldberg SA, Fullager PD (1994) Precise U–Pb ages of Neoproterozoic plutons in the southern Appalachian Blue Ridge and their implications for the initial rifting of Laurentia. Precambr Res 68:81–95

Svenningsen OM (1994) The Baltica-Iapetus passive margin dyke complex in the Sarektjåkkå Nappe, northern Swedish Caledonides. Geological Journal 29:323–354

Svenningsen OM (1996) Passive margins—past and (almost) present: GFF:A41-A42

Svenningsen OM (2001) Onset of seafloor spreading in the Iapetus Ocean at 608 Ma: precise age of the Sarek Dyke Swarm, northern Swedish Caledonides. Precambr Res 110:241-254

Symons DTA, Chiasson AD (1991) Paleomagnetism of the Callander Complex and the Cambrian apparent polar wander path for North America. Can J Earth Sci 28:355-363

Tachibana Y, Kaneoka I, Gaffney A, Upton B (2006) Ocean-island basalt–like source of kimberlite magmas from West Greenland revealed by high $^{3}He/^{4}He$ ratios. Geology 34(4):273-276

Tappe S, Brand NB, Stracke A, van Acken D, Liu C-Z, , Strauss H, Wu F-Y, Luguet A, Mitchell RH (2017) Plates or plumes in the origin of kimberlites: U/Pb perovskite and Sr-Nd-Hf-Os-C-O isotope constraints from the Superior craton (Canada). Chem Geol 455:57-83

Tappe S, Foley S, Jenner G, Heaman L, Kjarsgaard B, Romer R, Stracke A, Joyce N, Hoefs J (2006) Genesis of ultramafic lamprophyres and carbonatites at Aillik Bay, Labrador: a consequence of incipient lithospheric thinning beneath the North Atlantic craton. J Petrol 47:1261–1315

Tappe S, Foley SF, Kjarsgaard BA, Romer RL, Heaman LM, Stracke A, Jenner GA (2008) Between carbonatite and lamproite – Diamondiferous Torngat ultramafic lamprophyres formed by carbonate-fluxed melting of cratonic MARID-type metasomes. Geochim Cosmochim Acta 72:3258-3286

Tappe S, Foley SF, Stracke A, Romer RL, Kjarsgaard BA, Heaman LM, Joyce N (2007) Craton reactivation on the Labrador Sea margins: $^{40}Ar/^{39}Ar$ age and Sr–Nd–Hf–Pb isotope constraints from alkaline and carbonatite intrusives. Earth Planet Sc Lett 256(3-4):433-454

Tappe S, Jenner GA, Foley SF, Heaman L, Besserer D, Kjarsgaard BA, Ryan B (2004) Torngat ultramafic lamprophyres and their relation to the North Atlantic Alkaline Province. Lithos 76(1-4):491-518

Tappe S, Kjarsgaard BA, Kurszlaukis S, Nowell GM, Phillips D (2014) Petrology and Nd-Hf Isotope Geochemistry of the Neoproterozoic Amon Kimberlite Sills, Baffin Island (Canada): Evidence for Deep Mantle Magmatic Activity Linked to Supercontinent Cycles. J Petrol 55(10):2003-2042

Tappe S, Pearson DG, Nowell G, Nielsen T, Milstead P, Muehlenbachs K (2011) A fresh isotopic look at Greenland kimberlites: Cratonic mantle lithospheric imprint on deep source signal. Earth Planet Sc Lett 305:235-248

Tappe S, Simonetti A (2012) Combined U–Pb geochronology and Sr–Nd isotope analysis of the Ice River perovskite standard, with implications for kimberlite and alkaline rock petrogenesis. Chem Geol 304-305:10-17

Tappe S, Smart K, Torsvik T, Massuyeau M, de Wit M (2018) Geodynamics of kimberlites on a cooling Earth: Clues to plate tectonic evolution and deep volatile cycles. Earth Planet Sc Lett 484:1-14

Tappe S, Steenfelt A, Nielsen T (2012) Asthenospheric source of Neoproterozoic and Mesozoic kimberlites from the North Atlantic craton, West Greenland: new high-precision U-Pb and Sr-Nd isotope data on perovskite. Chem Geol 320-321:113-127

Taylor HP, Frechen J, Degens ET (1967) Oxygen and carbon isotope studies of carbonatites from the Laacher See District, West Germany and the Alno District, Sweden. Geochim Cosmochim Acta, 31:407-430

Terry RD, Chilingar GV (1955) Summary of "Concerning some additional aids in studying sedimentary formations" by M.S. Shvetsov. Journal of Sedimentary Petrology 25(3):229-234

Tollo RP, Aleinikoff JN (1996) Petrology and U–Pb geochronology of the Robertson River Igneous Suite, Blue Ridge province, Virginia — evidence for multistage magmatism associated with an early episode of Laurentian rifting. Am J Sci 296:1045-1090

Tollo RP, Aleinikoff JN, Bartholomew MJ, Rankin DW (2004) Neoproterozoic A-type granitoids of the central and southern Appalachians: intraplate magmatism associated with episodic rifting of the Rodinian supercontinent. Precambr Res 128(1-2):3-38

Tollo RP, Aleinikoff JN, Mundil R, Southworth S, Cosca MA, Rankin DW, Rubin A, Kentner A, Parendo C, Ray M (2012) Igneous activity, metamorphism, and deformation in the Mount Rogers area of SW Virginia and NW North Carolina: A geologic record of Precambrian tectonic evolution of the southern Blue Ridge Province. In: Eppes MC, Bartholomew J (eds) From the Blue Ridge to the Coastal Plain: Field Excursions in the Southeastern United States. Geological Society of America Field Guide 29:1–66

Torsvik TH, Smethurst MA, Meert JG, Van der Voo R, McKerrow WS, Brasier MD, Sturt BA, Walderhaug HJ (1996) Continental break-up and collision in the Neoproterozoic and Palaeozoic - A tale of Baltica and Laurentia. Earth Sci Rev40:229-258

Tyni M (1997) Diamond prospecting in Finland - a review. In: Papunen H (ed) Mineral Deposits: research and exploration, where do they meet? Balkema, Rotterdam:789-791

Vanuxem L (1842) Geology of New York Part III comprising the survey of the Third Geological District. Albany, W. & A. White & J. Visscher, 307 p

Vaughan APM, Storey BC (2007) A new supercontinent self-destruct mechanism: evidence from the Late Triassic - Early Jurassic. Journal of the Geological Society, London 164:383-392

Voit FW (1907) Kimberlite dykes and pipes. Transactions of the Geological Society of South Africa 10(1):69-74

Wagner PA (1914) The diamond fields of Southern Africa. The Transvaal Leader, Johannesburg, 355 p

Walderhaug HJ, Torsvik TH, Halvorsen E (2007) The Egersund dykes (SW Norway): a robust Early Ediacaran (Vendian) palaeomagnetic pole from Baltica. Geophys J Int 168(3):935-948

Walsh GJ, Aleinikoff JN (1999) U-Pb zircon age of metafelsite from the Pinney Hollow Formation: implications for the development of the Vermont Appalachians. Am J Sci 299: 157-170

Watson KD (1967) Kimberlites of eastern North America. In: Wyllie PJ (ed) Ultramafic and Related Rocks. John Wiley & Sons, Inc, pp 312-323

Williams AF (1932) The genesis of the diamond, vol. 1. Ernest Benn Limited, London, 352 p

Williams GH (1887) On the serpentine of Syracuse, N.Y. Science IX(214):232-233

Williams H, Gillispie RT, Van Breemen O (1985) A late Precambrian rift-related igneous suite in western Newfoundland. Can J Earth Sci 22:1727-1735

Wilson JT (1963) Evidence from islands on the spreading of ocean floors. Nature 197:536-538

Wilson L, Head III JW (2007) An integrated model of kimberlite ascent and eruption. Nature 447:53-57

Wilson MR, Kjarsgaard BA, Taylor B (2007) Stable isotope composition of magmatic and deuteric carbonate phases in hypabyssal kimberlite, Lac de Gras field, Northwest Territories, Canada. Chem Geol 242:435-454

Woolley AR, Bergman SC, Edgar AD, Le Bas MJ, Mitchell RH, Rock NMS, Scott Smith BH (1996) Classification of lamprophyres, lamproites, kimberlites, and the kalsilitic, melilitic, and leucitic rocks. Can Mineral 34:175-186

Wu F-Y, Mitchell RH, Li Q-L, Zhang C, Yang Y-H (2017) Emplacement age and isotopic composition of the Prairie Lake carbonatite complex, Northwestern Ontario, Canada. Geol Mag 154(2):217-236

Wu F-Y, Yang Y-H, Mitchell RH, Li Q-L, Yang J-H, Zhang Y-B (2010) In situ U–Pb age determination and Nd isotopic analysis of perovskites from kimberlites in southern Africa and Somerset Island, Canada. Lithos 115(1-4):205-222

Yakovenchuk VN, Ivanyuk GY, Pakhomovsky YA, Menshikov YP (1999) Minerals of the Khibiny massif. Zemlya, Moscow:326p (in Russian)

Yakovenchuk VN, Ivanyuk GY, Pakhomovsky YA, Men'shikov YP (2005) Khibiny. Laplania Minerals, Apatity, 2005:111-112

Yang Y-H, Wu F-Y, Wilde SA, Liu X-M, Zhang Y-B, Xie L-W, Yang J-H (2009) In situ perovskite Sr–Nd isotopic constraints on the petrogenesis of the Ordovician Mengyin kimberlites in the North China Craton. Chem Geol 264(1-4):24-42

Yu S, Li S, Uu IC, Atuang L, Li Z (1982) A preliminary study on the mineralogy of the Zraoanzhuang-type iron ore deposit Wuyang, Henan Province, China. Zrongguo Dizhi Kexueyuan Yichan Dizhi Kuangchan Yanjuiso Sokan 5:1-22 (in Chinese)

Zajzon N, Váczi T, Fehér B, Takács Á, Szakáll S, Weiszburg TG (2013) Pyrophanite pseudomorphs after perovskite in Perkupa serpentinites (Hungary): a microtextural study and geological implications. Physics and Chemistry of Minerals 40(8):611-623

Zurevinski SE, Heaman LM, Creaser RA (2011) The origin of Triassic/Jurassic kimberlite magmatism, Canada: Two mantle sources revealed from the Sr-Nd isotopic composition of groundmass perovskite. Geochem Geophy Geosy 12, Q09005 doi:10.1029/2011gc003659

Zurevinski SE, Heaman LM, Creaser RA, Strand P (2008) The Churchill kimberlite field, Nunavut, Canada: petrography, mineral chemistry, and geochronology. Can J Earth Sci 45:1039-1059

Zurevinski SE, Mitchell RH (2011) Highly evolved hypabyssal kimberlite sills from Wemindji, Quebec, Canada: insights into the process of flow differentiation in kimberlite magmas. Contrib Mineral Petr 161:765-776

Zhuk V, Lepine I, Laroulandie C (2017) Continuity of Kimberley-type pyroclastic kimberlite phases within Renard 2 over 1,000 m depth – insights to the geological and emplacement model, Superior craton, Canada. 11th International Kimberlite Conference Extended Abstract No. 11IKC-004540, 3 p

Zwaan BK, Van Roermund HLM (1990) A rift-related mafic dyke swarm in the Corrovarre Nappe of the Caledonian Middle Allochthon Troms, North Norway, and its tectonometamorphic evolution. Nor Geol Unders Bull 419:25-44

# APPENDIX A
# SAMPLE DESCRIPTIONS

## Notes to thin section and hand sample descriptions

Table 1 summarizes modal mineralogy visually estimated from one thin section from one sample examined by petrographic microscope. Description and naming of samples followed Mitchell (1995, 1997), Woolley et al. (1996), Field and Scott Smith (1998), Scott Smith (2006) and Scott Smith et al. (2013). Rock names may slightly differ from the detailed work of Fitzgerald et al. (2009), Muntener and Scott Smith (2013) and Godin et al. (2016). Additional examination by scanning electron microscope and EPMA is needed for several fine-grained minerals. Percentages were visually estimated for hand samples following Terry and Chilingar (1955). Shape of country rock xenoliths (CRX) described as angular (A), subangular (SA), subround (SR) or round (R). Olivine macrocryst size (F, M, C, VC) taken from Field and Scott Smith (1998) for hand samples. Revised olivine macrocryst size of >1 mm taken from Scott Smith et al. (2013) for thin sections.

Note it is uncertain if samples 31556, 35789, 37317, 38916, 38923, 38926, and 39289 contain fully altered groundmass monticellite. The texture of this fine-grained groundmass mineral resembles monticellite but the mineral is fully altered therefore the interpretation is subjective and labelled as (monticellite?) in the rock name. These samples are marked by ( $^{D2}$ ) in the monticellite column in Table 1 (footnote d). Fresh monticellite was identified in one sample (37375).

Samples with the rock name '? kimberlite' are described in the Table 1 footnote. A visual estimate % of the minerals in thin section was not determined due to the variability across the thin section and hand sample. A brief description of the mineralogy of the lapilli and inter-clast matrix is as follows:

38925: One type of lapilli was observed. The groundmass was difficult to see but generally appears to contain phlogopite, perovskite, opaques, serpentine, ±microlitic clinopyroxene, carbonate, tiny altered olivine (?), biotite xenocrysts (?). The inter-clast matrix appears to

dominantly contain a brown fine-grained mineral, a high relief blocky/elongate/fibrous secondary mineral [pyroxene, microlitic clinopyroxene (?)], serpentine and few opaques.

31543: Two types of lapilli were observed. Lapilli 1 contained likely orange phlogopite, perovskite, opaques, serpentine, ±carbonate, tiny altered olivine (?). Lapilli 2 was less abundant (one found) and contained colourless phlogopite, opaques with distinct texture, carbonate, and serpentine. The inter-clast matrix appears to dominantly contain a brown fine-grained mineral, a high relief blocky/anhedral/granular/elongate/fibrous secondary mineral [pyroxene, microlitic clinopyroxene (?)], phlogopite, few perovskite, few opaques, ± tiny altered olivine (?), carbonate, serpentine.

31468: Two types of lapilli were observed. Lapilli 1 contained orange phlogopite, perovskite, opaques, tiny monticellite (?), tiny altered olivine (?), ±serpentine, carbonate. Lapilli 2 contained colourless phlogopite, perovskite, opaques, carbonate, ±tiny altered olivine (?). The inter-clast matrix appears to dominantly contain a brown fine-grained mineral, a high relief blocky/anhedral/granular/elongate secondary mineral [pyroxene, microlitic clinopyroxene (?)], phlogopite, few opaques, carbonate, and serpentine.

**Table 1.** Summary of modal mineralogy (visually estimated %) of Renard and G04-296 Anomaly kimberlite samples.

| Sample ID | Unit Code | Rock Type | Texture | Olivine texture | Olivine Alteration | Macrocryst (vol %) | | Phenocryst / microphenocryst (vol %) | |
|---|---|---|---|---|---|---|---|---|---|
| | | | | | | olivine | phlogopite | olivine | phlogopite |
| (a) | | | | | | (b) | | (c ) | |
| ***Renard 1*** | | | | | | | | | |
| 37317 | Kimb1c-body | hypabyssal | uniform | macrocrystic | altered +/- fresh relicts | 10-15 | --- | 15-20 | 5-10 |
| 37322 | Kimb1c-body | hypabyssal | uniform | macrocrystic | altered +/- fresh relicts | 15-20 | <2 | 15-20 | 10-15 |
| 37375 | Kimb1d | hypabyssal | uniform | macrocrystic | altered +/- fresh relicts | 15-20 | <3 | 7-15? | 10-15 |
| ***Renard 2*** | | | | | | | | | |
| 38901 | Kimb2c | hypabyssal | uniform, minor segregations | macrocrystic | altered | 15-20 | <1 | 15-20 | 7-15 |
| 38903 | Kimb2c | hypabyssal | uniform | macrocrystic | altered +/- fresh relicts | 25-30 | <1 | 15-20 | 10-15 |
| 38906 | Kimb2c | hypabyssal | uniform | aphanitic | altered | 5 | --- | 20-30 | 7-10 |
| 38916 | Kimb2c | hypabyssal | uniform, minor segregations | macrocrystic | altered | 20-25 | <1 | 15-20 | 5-7 |
| 38919 | Kimb2c | hypabyssal | uniform, minor segregations | macrocrystic | altered | 25-30 [B] | --- | 15-20 | <1 |
| 38923 | Kimb2c | hypabyssal | uniform, minor segregations | macrocrystic | fresh to altered (variable) | 15-20 | --- | 10-15 | --- |
| 38925 | Kimb2a | TK (KPK) | magmaclastic (lapilli present) | sparsely macrocrystic | altered | <2-10 | --- | <5? | <1 |
| 38926 | Kimb2c | hypabyssal | uniform | macrocrystic | altered +/- fresh relicts | 15-25 [B] | 10-15 | 15-20 | 7-10 |
| 38927 | Kimb2b | hypabyssal/coherent to minor transitional HK | magmatic, patchy alteration (lacks lapilli) | macrocrystic | altered +/- fresh relicts | 10-25 | --- | 7-15 | <1 |
| 38928 | Kimb2c | hypabyssal | uniform | macrocrystic | altered +/- fresh relicts | 20-30 | 5-7 | 10-15 | 5-7 |
| 38929 | Kimb2c | hypabyssal | uniform | macrocrystic | altered | 15-20 | --- | 10-15 | 5-10 |
| ***Renard 3*** | | | | | | | | | |
| 31543 | Kimb3f | transitional HK | magmaclastic (lapilli present) | sparsely macrocrystic | altered | <5-15 | --- | <10? | <1 |
| 31548 | Kimb3i | hypabyssal/coherent | magmatic, patchy alteration (lacks lapilli) | macrocrystic | altered +/- fresh relicts | 20-25 [B] | --- | 10-20 | 3-5? |
| 31552 | Kimb3c | hypabyssal | uniform, minor segregations | macrocrystic | altered | 20-30 | --- | 15-20 | <1 |
| 31555 | FKimb3h | hypabyssal/coherent | magmatic (lacks lapilli) | macrocrystic | fresh to altered (variable) | 20-25 | <1 | 10-15 | 15-20 |
| 31556 | Kimb3g | hypabyssal/coherent to transitional HK | magmatic, patchy alteration (incipient lapilli?) | macrocrystic | altered | 10-25 | --- | 10-15 | --- |
| 31559 | Kimb3d | hypabyssal/coherent | magmatic, patchy alteration (lacks lapilli) | macrocrystic | altered +/- fresh relicts | 15-30 | --- | 10-15 | --- |
| ***Renard 4*** | | | | | | | | | |
| 39282 | Kimb4c | hypabyssal | uniform | macrocrystic | altered | 20-25 | --- | 15-20 | 10-15 |
| 39283 | Kimb4c | hypabyssal | uniform, segregationary | macrocrystic | altered +/- fresh relicts | 20-25 [B] | --- | 15-20 | <1 |
| 39289 | Kimb4b | hypabyssal/coherent | magmatic (lacks lapilli) | macrocrystic | fresh to altered (variable) | 13-23 [B] | --- | 10-15 | <1 |
| ***Renard 7*** | | | | | | | | | |
| 35789 | Kimb7c | hypabyssal | uniform | macrocrystic | altered | 20-25 [B] | <1 | 10-15? | <5 |
| 35790 | Kimb7c | hypabyssal | uniform, minor segregations | macrocrystic | altered | 15-25 | --- | 15-25 | <5-7 |
| 35791 | Kimb7c | hypabyssal | uniform | macrocrystic | altered | 20-25 [B] | <1 | 10-20? | 10-15 |
| ***Renard 9*** | | | | | | | | | |
| *31462** | *Kimb9c-1* | *hypabyssal* | *uniform* | *macrocrystic* | *altered* | *37* | --- | *19* | --- |
| 31468 | Kimb9b | transitional HK | magmaclastic (lapilli present) | sparsely macrocrystic to | altered | 5-20 | --- | <10? | --- |
| 31497 | Kimb9c-1 | hypabyssal | uniform | macrocrystic | altered | 15-25 | --- | 15-20 | 10-15 |
| ***G04-296 Anomaly*** | | | | | | | | | |
| 31577 | --- | hypabyssal | uniform, minor segregations | aphanitic | fresh +/- altered | 5-10 | --- | 25-30 | <1-2 |

**Table 1.** Continued.

| Sample ID | Unit Code | Groundmass (vol %) | | | | | | | | Xenoliths (vol %) | | | Alteration/Unknowns (vol %) | |
|---|---|---|---|---|---|---|---|---|---|---|---|---|---|---|
| | | olivine? | monticellite | phlogopite | opaques | perovskite | apatite | carbonate | serpentine | crustal | mantle | opaques | chlorite? | unknowns |
| (a) | | (d) | (d) | (e) | (f) | (f) | | | | (g) | | (h ) | (i) | |
| ***Renard 1*** | | | | | | | | | | | | | | |
| 37317 | Kimb1c-body | --- | 10-15? [D2] | <5? | 5-7 | <3 | <1 | 10-20 | <5? | --- | --- | --- | <1? | --- |
| 37322 | Kimb1c-body | <2 | --- | <3-5 | 5-7 | 5-7 [F] | ? | 20-25 | 7-10 | --- | --- | <1 [H] | <3 | --- |
| 37375 | Kimb1d | <3? | 10-20 [D1] | <5? | 3-5 | <3? [F] | --- | 5-15? | <1? | --- | --- | --- | <1? | --- |
| ***Renard 2*** | | | | | | | | | | | | | | |
| 38901 | Kimb2c | 7-10 | --- | 5-10 | 7-10 | <5 | <1 | 20-25 | <5 | 5 | --- | <2 [H] | <1 | <1 |
| 38903 | Kimb2c | 5-10 | --- | <5 | 7-10 | 5-7 | <1 | 20-25 | <2 | <2 | --- | <1 [H] | <1 | <1 |
| 38906 | Kimb2c | 7-10 | --- | <5? | 7-10 | 5-7 | --- | 20-25 | <1 | --- | --- | <1 | <1 | --- |
| 38916 | Kimb2c | | 5-10 [D2] | <5? | 5-7 | <3-5 | <1 | 15-20 | <2? | --- | --- | <2 [H] | <1 | --- |
| 38919 | Kimb2c | 5-10? | --- | <5? | 5-7 | <1? | <1 | 15-20 | <3? | <2 | --- | <1 [H] | present | --- |
| 38923 | Kimb2c | 5-15 [D2] | 5-15? [D2] | 20-30 [E2] | 5-7 | 5-7 | <1? | 20-30 | <1? | 5-10 | ? | <2 [H] | <1 | --- |
| 38925 | Kimb2a | (k) see description of lapilli and inter-clast matrix below | | | | | | | | 10-50 [Gl] | --- | --- | present | --- |
| 38926 | Kimb2c | --- | 7-10 [D2] | 5-7 | 5-7 | 3-5 | <1 | 20-25 | <5? | <1 | ? | <2 | --- | 3-5 |
| 38927 | Kimb2b | 5-7 | --- | 20-30 [E1] | <3 | 5-7 | ? | 5-7? | <1 | 10-30 [Gl] | ? | <2 [H] | present | --- |
| 38928 | Kimb2c | 5-10? | --- | 5-7 | 5-7 | 3-5 | <1 | 20-25 | <5? | <1 | --- | <2 [H] | <1 | --- |
| 38929 | Kimb2c | <5 | --- | 2-5 | 7-10 | <3-5 | <2 | 20-25 | <1 | ? | ? | <1 | <1 | <1 |
| ***Renard 3*** | | | | | | | | | | | | | | |
| 31543 | Kimb3f | (k) see description of lapilli and inter-clast matrix below | | | | | | | | 10-40? [G2] | --- | --- | --- | --- |
| 31548 | Kimb3i | 5-7? | --- | 15-20? [E1] | 5-7? | 3-5? | <2-3 | <3-5? | 15-20? | 3-7? | ? | --- | present? | <2 |
| 31552 | Kimb3c | <5? | --- | <3 | 5-7 | <2 | <1? | 20-30 | <1 | <2 | --- | <1 | <1 | --- |
| 31555 | FKimb3h | 5-7? | --- | 5-7 | 7-10 | 3-5 | <1 | 15-20? | 10-15? | <3 | --- | <2 [H] | present | --- |
| 31556 | Kimb3g | <5 [D2] | 15-25? [D2] | 10-20? [E1] | <3 | <3 | <1 | <5? | <5-10? | 10-40? [G1] | ? | <1 | present | --- |
| 31559 | Kimb3d | 5-15 | --- | 20-25 [E1] | 5-7 | 5-7 | ? | <2? | <2? | 15-30? [G1] | ? | <1 | present | --- |
| ***Renard 4*** | | | | | | | | | | | | | | |
| 39282 | Kimb4c | <5-7? | --- | 5-7 | 5-7 | <3 | <2 | 15-20 | 7-10 | <2-3 | --- | <1 | present | --- |
| 39283 | Kimb4c | <7 | --- | <5 | 7-10 | <3-5 | <1 | 25-30 | <2-3? | --- | --- | <1 [H] | present | --- |
| 39289 | Kimb4b | --- | 10-20? [D2] | 15-20 | 5-7 | 5-7 | <1? | 7-15? | 7-15? | <5 | --- | <2 [H] | present? | --- |
| ***Renard 7*** | | | | | | | | | | | | | | |
| 35789 | Kimb7c | --- | 10-15? [D2] | <3 | 5-7 | <5 | <1? | 15-25 | <2? | --- | --- | --- | <2? | --- |
| 35790 | Kimb7c | 5-7? | --- | <5 | <5 | <2 | <1 | 5-15 | 5-15 | --- | ? | --- | <1 | --- |
| 35791 | Kimb7c | 5-10? | --- | 5-7 | <5-7 | <2 | <2 | 10-15? | 15-20? | --- | <1 | <1 | present | --- |
| ***Renard 9*** | | | | | | | | | | | | | | |
| *31462** | *Kimb9c-1* | *3* | --- | *8* | *10* | *1(kassite)* | *2* | *15* | --- | *4* | --- | --- | *present* | --- |
| 31468 | Kimb9b | (k) see description of lapilli and inter-clast matrix below | | | | | | | | 10-40? [G2] | --- | <1 | present | --- |
| 31497 | Kimb9c-1 | <5? | --- | <5 | 5-7 | <5 | <1 | 15-20 | 7-10? | <3-5 | --- | <1 | --- | --- |
| ***G04-296 Anomaly*** | | | | | | | | | | | | | | |
| 31577 | --- | <5 | --- | <1-2 | 10-15 | <2? | <1-2 | 25-30 | <1-2 | --- | <1? | <1 | --- | --- |

**Table 1.** Continued.

| Sample ID | Unit Code | Veining (vol %) | | Rock name |
|---|---|---|---|---|
| | | vol % | minerals | |
| (a) | | | | (j) |
| ***Renard 1*** | | | | |
| 37317 | Kimb1c-body | <1? | carb | (monticellite?)-carbonate kimberlite |
| 37322 | Kimb1c-body | --- | --- | carbonate kimberlite |
| 37375 | Kimb1d | --- | --- | monticellite kimberlite |
| ***Renard 2*** | | | | |
| 38901 | Kimb2c | <1-2 | opaques, carb | carbonate kimberlite |
| 38903 | Kimb2c | --- | --- | carbonate kimberlite |
| 38906 | Kimb2c | --- | --- | carbonate kimberlite |
| 38916 | Kimb2c | --- | --- | carbonate kimberlite |
| 38919 | Kimb2c | <2 | carb | carbonate kimberlite |
| 38923 | Kimb2c | --- | --- | phlogopite-carbonate kimberlite |
| 38925 | Kimb2a | --- | --- | ? kimberlite |
| 38926 | Kimb2c | --- | --- | carbonate kimberlite |
| 38927 | Kimb2b | <2 | carb, serp, talc? | phlogopite kimberlite |
| 38928 | Kimb2c | --- | --- | carbonate kimberlite |
| 38929 | Kimb2c | --- | --- | carbonate kimberlite |
| ***Renard 3*** | | | | |
| 31543 | Kimb3f | <1 | serp, talc? | ? kimberlite |
| 31548 | Kimb3i | <2 | serp, carb | serpentine-phlogopite kimberlite |
| 31552 | Kimb3c | <1 | carb, opaques, serp | carbonate kimberlite |
| 31555 | FKimb3h | <1 | carb | serpentine-carbonate kimberlite |
| 31556 | Kimb3g | --- | --- | phlogopite-(monticellite?) kimberlite |
| 31559 | Kimb3d | <3 | carb, serp | phlogopite kimberlite |
| ***Renard 4*** | | | | |
| 39282 | Kimb4c | --- | --- | carbonate kimberlite |
| 39283 | Kimb4c | <1 | carb, serp | carbonate kimberlite |
| 39289 | Kimb4b | <2 | carb, serp | (monticellite?)-phlogopite kimberlite |
| ***Renard 7*** | | | | |
| 35789 | Kimb7c | <3? | carb, serp | (monticellite?)-carbonate kimberlite |
| 35790 | Kimb7c | <1 | opaques | phlogopite-opaques-carbonate-serpentine kimberlite |
| 35791 | Kimb7c | <2 | carb, serp | carbonate-serpentine kimberlite |
| ***Renard 9*** | | | | |
| *31462** | *Kimb9c-1* | --- | --- | *opaques-carbonate kimberlite* |
| 31468 | Kimb9b | --- | --- | ? kimberlite |
| 31497 | Kimb9c-1 | <2 | carb | carbonate kimberlite |
| ***G04-296 Anomaly*** | | | | |
| 31577 | --- | <1 | opaques, carb | carbonate kimberlite |

**Table 1.** Continued.

(a) The modal mineralogy is a visually estimated volume % except for thin section 31462 (labelled with *) measured by point counting. In addition to the vol. % in this table, 31462 visually contains trace amounts of phenocrystal phlogopite, phenocryst-size opaques (including possible rutile) and groundmass serpentine.

(b) Macrocyst size taken as >1 mm (after Scott Smith et al. 2013). Visual estimate % for olivine macrocrysts includes few megacrysts in thin section (labelled as [B]).

(c) Phenocryst/microphenocryst visual estimate % determined by size (>0.1 mm but <1mm) and may contain anhedral/rounded olivine similar to macrocrysts, along with euhedral to subhedral phenocrysts.

(d) Difficult to discern in some samples if groundmass contains fully altered monticellite, tiny olivine or another mineral. [D1] Sample 37375 contains fresh monticellite. [D2] Samples containing fully altered grains with groundmass texture resembling abundant monticellite (37317, 38926, 39289, 35789), or contains grains which are very difficult to determine if the mineral is olivine, monticellite or another mineral (38916), or contains grains resembling both altered olivine and a tiny granular mineral (possibly monticellite?; 31556, 38923).

(e) [E1] Sample appears to contain two types of groundmass phlogopite (both pleochroic orange but as tiny lathes or as an anhedral fine-grained mineral). 31548 may contain a mix of anhedral phlogopite and serpentine. [E2] Difficult to distinguish primary from secondary phlogopite in sample 38923.

(f) Some estimates may contain overlap between perovskite and opaques. [F] Sample 37322 appears to contain two types of grains resembling perovskite; dark brown, high relief, anhedral to euhedral (cubic to cuboctahedral) crystals and light brown, low relief, anhedral (round) crystals which are generally smaller (e.g. many <30 µm). 37375 may also contain two types similar to 37322 but in trace amounts.

(g) Sample 38925 contains a CRX with orthopyroxene, feldspar and biotite. [G1] Crustal xenolith estimate includes masses of, or replacement by, a fine-grained high relief mineral (anhedral to elongate, can be microlitic (needle-like or fibrous) texture (i.e. microlitic clinopyroxene) but sometimes coarser; possibly pyroxene?) and CRX appear more diverse and complexly altered. [G2] Lesser amounts of high relief mineral described in ([G1]) and also contains macrocryst-size grains resembling highly altered pyroxene (including CRX containing similar pyroxene, biotite and altered minerals).

(h ) Phenocryst and/or macrocryst-sized (>0.1 mm) opaques present (including possible rutile in some samples). [H] Groundmass-size (<0.1 mm) rutile may be present (<1%). Unknown if opaques or rutile are crustal or mantle derived.

(i) Present = chlorite estimation included within mineral visual estimate % (secondary) and not obvious as a separate mineral.

(j) Rock name determined by groundmass minerals >2/3 modal % of the major groundmass mineral (e.g. Scott Smith 2006).

(k) Description of lapilli and inter-clast matrix:

38925: One type of lapilli with a groundmass that is difficult to see but appears to contain phlogopite, perovskite, opaques, serpentine, ± microlitic clinopyroxene, carbonate, tiny altered olivine (?), biotite xenocrysts (?). The inter-clast matrix appears to dominantly contain a brown fine-grained mineral, a high relief blocky/elongate/fibrous secondary mineral (pyroxene, microlitic clinopyroxene?), serpentine and few opaques.

31543: Two types of lapilli. Lapilli 1 contains likely orange phlogopite, perovskite, opaques, serpentine, ±carbonate, tiny altered olivine (?). Lapilli 2 (one found) contains colourless phlogopite, opaques of distinct texture, carbonate, and serpentine. The inter-clast matrix appears to dominantly contain a brown fine-grained mineral, a high relief blocky/anhedral/granular/elongate/fibrous secondary mineral (pyroxene, microlitic clinopyroxene?), phlogopite, few perovskite, few opaques ±tiny altered olivine (?), carbonate, serpentine.

31468: Two types of lapilli. Lapilli 1 contains orange phlogopite, perovskite, opaques, tiny monticellite (?), tiny altered olivine (?) ±serpentine, carbonate. Lapilli 2 contains colourless phlogopite, perovskite, opaques, carbonate ±tiny altered olivine (?). The inter-clast matrix appears to dominantly contain a brown fine-grained mineral, a high relief blocky/anhedral/granular/elongate secondary mineral (pyroxene, microlitic clinopyroxene?), phlogopite, few opaques, carbonate, and serpentine.

| | |
|---|---|
| SAMPLE ID: | 37317 |
| BODY: | Renard 1 |
| DOWNHOLE (APPARENT) DEPTH: | 315.64 m |
| UNIT CODE: | Kimb1c-body |
| ROCK NAME: | (monticellite?)-carbonate kimberlite |

HAND SAMPLE DESCRIPTION: Dark yellow/greenish-grey macrocrystic hypabyssal kimberlite. Olivine macrocrysts are yellowish green-brown or white/yellowish green (hard to see) likely fully altered but some larger macrocrysts contain translucent areas (fresh relicts or alteration mineral?) [F-C (VC)] with some flow alignment. Fine-grained uniform crystalline groundmass of carbonate and likely serpentine (groundmass reacts with HCl). Groundmass includes tiny white to yellowish-white elongate grains (reacts with HCl). Country rock xenoliths not obvious. Several olivine macrocrysts with inclusions (white mineral, kelyphite, dark metallic grey mineral, black mineral).

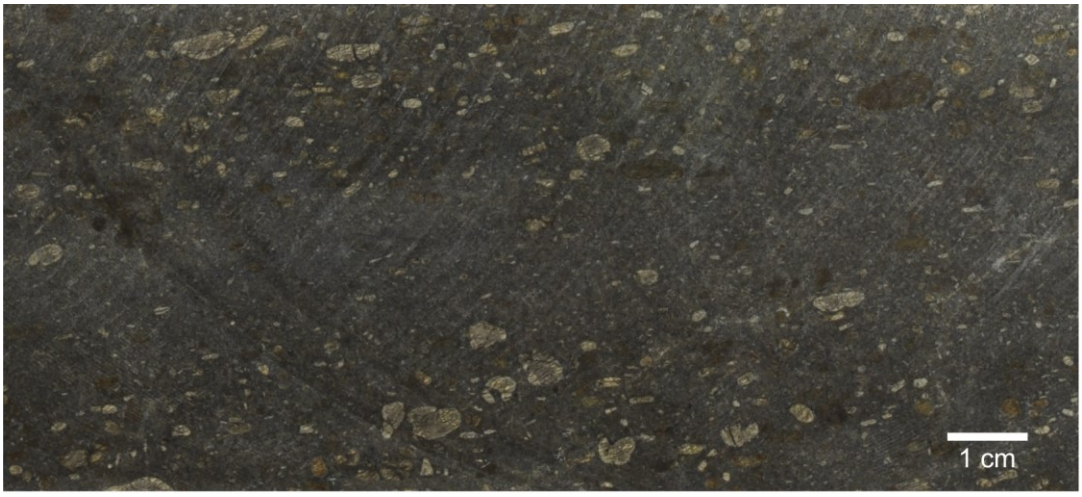

Photo (wet) of drill core sample 37317.

Photomicrograph of thin section for sample 37317 (PPL).

| | |
|---|---|
| SAMPLE ID: | 37322 |
| BODY: | Renard 1 |
| DOWNHOLE (APPARENT) DEPTH: | 339.45 m |
| UNIT CODE: | Kimb1c-body |
| ROCK NAME: | carbonate kimberlite |

HAND SAMPLE DESCRIPTION: Dark greyish-green macrocrystic hypabyssal kimberlite. Olivine macrocrysts are medium brown or white/yellowish-green with medium brown rims ± black specks (smaller macrocrysts hard to see), fully to possibly partially altered (some larger macrocrysts contain translucent areas which may be fresh relicts?) [F-C (VC)]. Fine-grained uniform crystalline groundmass of carbonate and likely serpentine (groundmass reacts with HCl). Phlogopite macrocrysts possible but hard to see. Country rock xenoliths not obvious. Observed few olivine macrocrysts with inclusions (dark brown mineral, chrome diopside, kelyphite).

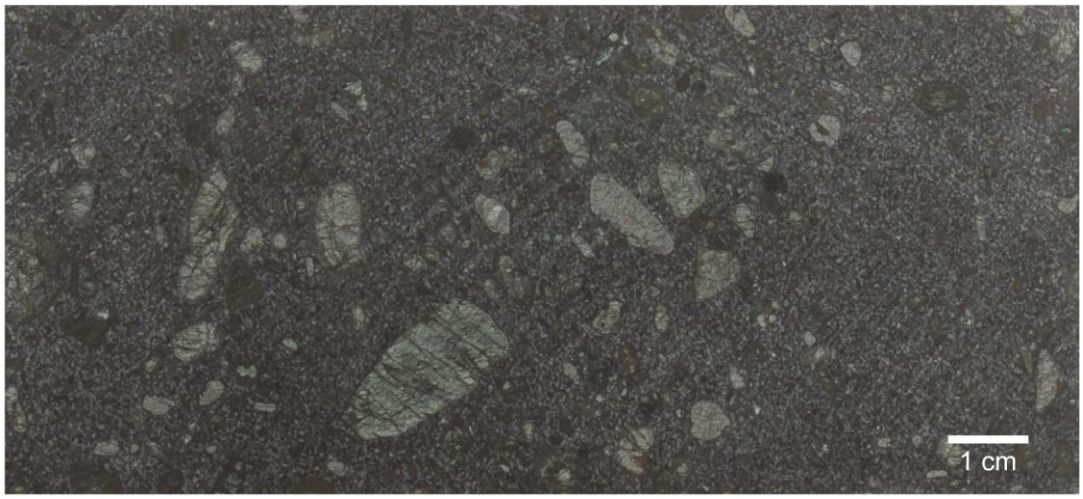

Photo (wet) of drill core sample 37322.

Photomicrograph of thin section for sample 37322 (PPL; carbon coated).

| | |
|---|---|
| SAMPLE ID: | 37375 |
| BODY: | Renard 1 |
| DOWNHOLE (APPARENT) DEPTH: | 71.64 m |
| UNIT CODE: | Kimb1d |
| ROCK NAME: | monticellite kimberlite |

HAND SAMPLE DESCRIPTION: Dark grey to black macrocrystic hypabyssal kimberlite. Olivine macrocrysts are light to medium yellowish-brown or clear/translucent areas (smaller macrocrysts are hard to see), fully to partially altered to likely serpentine. Many macrocrysts have altered rims/fractures with fresh relict cores or areas of fresh relicts [F-C (VC)] and some oblong macrocrysts appear flow aligned. Fine-grained uniform>segregationary crystalline groundmass of carbonate and serpentine (groundmass reacts with HCl). Irregular greenish-white segregations react strongly to HCl. Country rock xenoliths (<~1%) are whitish-green ± medium green or greenish white rims, <~3 mm (SA-SR) and fully altered. Some light green areas are diffuse and difficult to see if initially were country rock xenoliths or segregations. Trace chrome diopside xenocrysts and few olivine macrocrysts with inclusions (chromite, white mineral) observed.

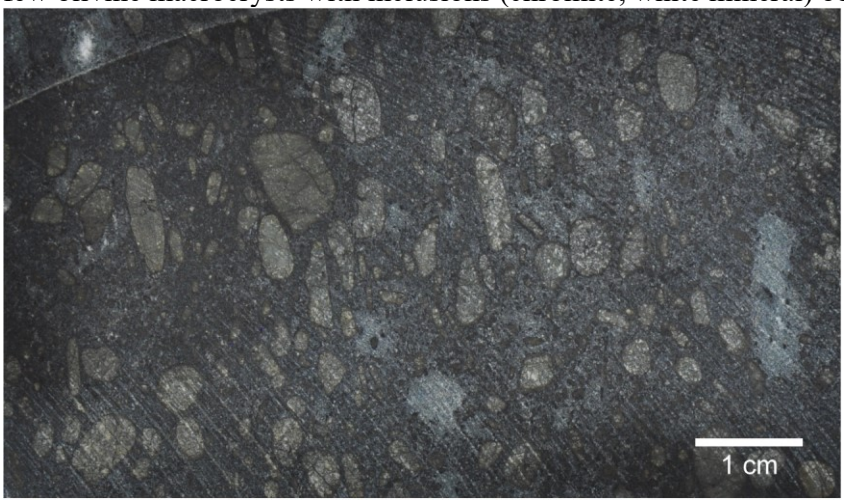

Photo (wet) of drill core sample 37375.

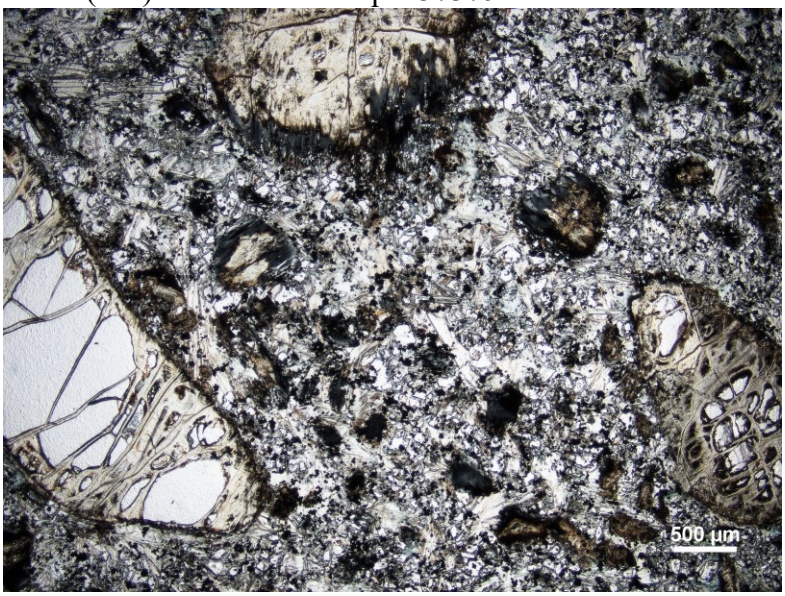

Photomicrograph of thin section for sample 37375 (PPL).

| | |
|---|---|
| SAMPLE ID: | 38901 |
| BODY: | Renard 2 |
| DOWNHOLE (APPARENT) DEPTH: | 412.06 m |
| UNIT CODE: | Kimb2c |
| ROCK NAME: | carbonate kimberlite |

HAND SAMPLE DESCRIPTION: Dark grey-black macrocrystic hypabyssal kimberlite. Olivine macrocrysts are dark yellowish brown-green (hard to see) likely altered to serpentine ± carbonate (F-C). Fine-grained uniform carbonate-rich crystalline groundmass (groundmass reacts with HCl). Country rock xenoliths (<5%) are white with black specks (likely mica), up to ~1.5 cm (SA-SR) and fully to partially altered. Observed two kelyphytized garnet xenocrysts (one adjacent an olivine macrocryst).

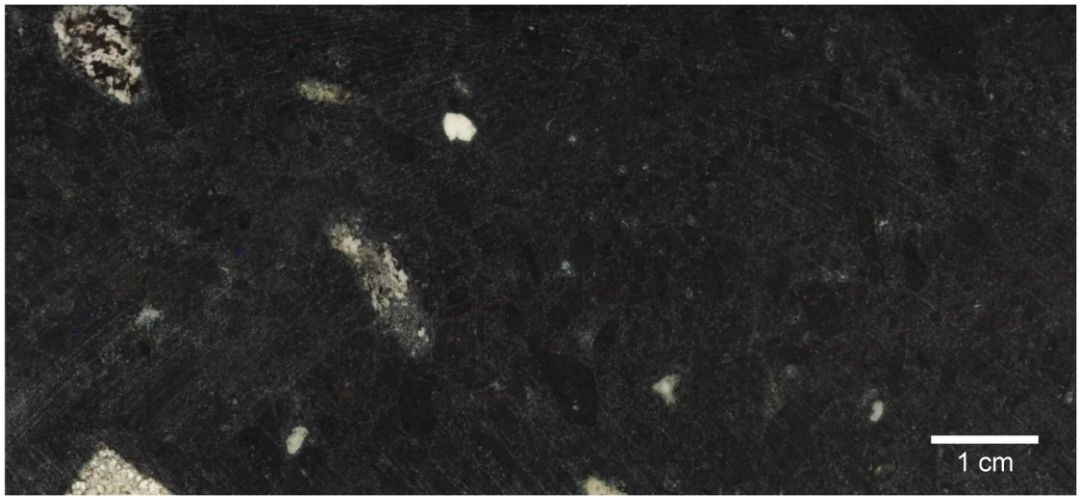

Photo (wet) of drill core sample 38901.

Photomicrograph of thin section for sample 38901 (PPL).

| | |
|---|---|
| SAMPLE ID: | 38903 |
| BODY: | Renard 2 |
| DOWNHOLE (APPARENT) DEPTH: | 492.86 m |
| UNIT CODE: | Kimb2c |
| ROCK NAME: | carbonate kimberlite |

HAND SAMPLE DESCRIPTION: Dark greenish-grey black macrocrystic hypabyssal kimberlite. Olivine macrocrysts are light-medium green to dark brownish-green (hard to see) fresh to fully altered to likely serpentine [F-C (VC)]. Fine-grained uniform carbonate-rich crystalline groundmass (groundmass strongly reacts with HCl). Country rock xenoliths (<~2%) are black, dark green or white, up to ~1.5 cm (A-SR) and likely fully altered.

Photo (wet) of drill core sample 38903.

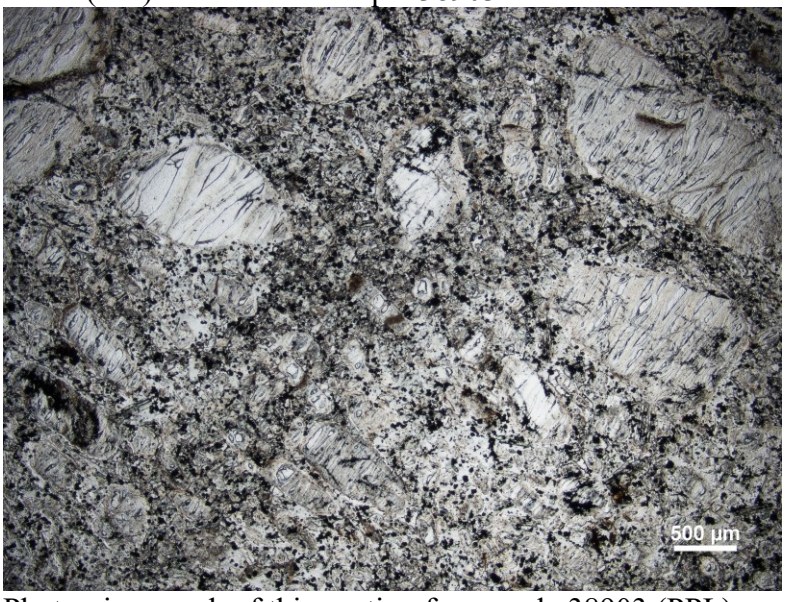

Photomicrograph of thin section for sample 38903 (PPL).

| | |
|---|---|
| SAMPLE ID: | 38906 |
| BODY: | Renard 2 |
| DOWNHOLE (APPARENT) DEPTH: | 685.98 m |
| UNIT CODE: | Kimb2c |
| ROCK NAME: | carbonate kimberlite |

HAND SAMPLE DESCRIPTION: Dark grey-black aphanitic (sparsely macrocrystic) hypabyssal kimberlite. Olivine macrocrysts are minor and along one edge of core, dark brown or brown-green ± light green areas and fractures filled with metallic gray mineral (hard to see) and fully altered [F (M-C)]. Fine-grained uniform carbonate-rich crystalline groundmass (groundmass reacts with HCl). Some areas of groundmass have slightly patchy appearance with more small white segregations in macrocrystic area. Country rock xenoliths (<1%) are white, up to ~ 8mm (A) and fully altered. Few white veinlets (reacts with HCl).

Photo (wet) of drill core sample 38906.

Photomicrograph of thin section for sample 38906 (PPL).

| | |
|---|---|
| SAMPLE ID: | 38916 |
| BODY: | Renard 2 |
| DOWNHOLE (APPARENT) DEPTH: | 606.17 m |
| UNIT CODE: | Kimb2c |
| ROCK NAME: | carbonate kimberlite |

HAND SAMPLE DESCRIPTION: Dark grey-black macrocrystic hypabyssal kimberlite. Olivine macrocrysts are greyish-black or dark brownish-green ± patchy light-green areas or some light-green (hard to see) and fully altered [F-C (VC)]. Fine-grained uniform carbonate-rich crystalline groundmass (groundmass reacts with HCl). Country rock xenoliths (<5%) are patchy white/green and possibly black, up to ~1.5 cm (SR-SA) and fully to partially altered. Observed two olivine macrocrysts with inclusions (chromite, kelyphite). Minor white veinlets (reacts with HCl).

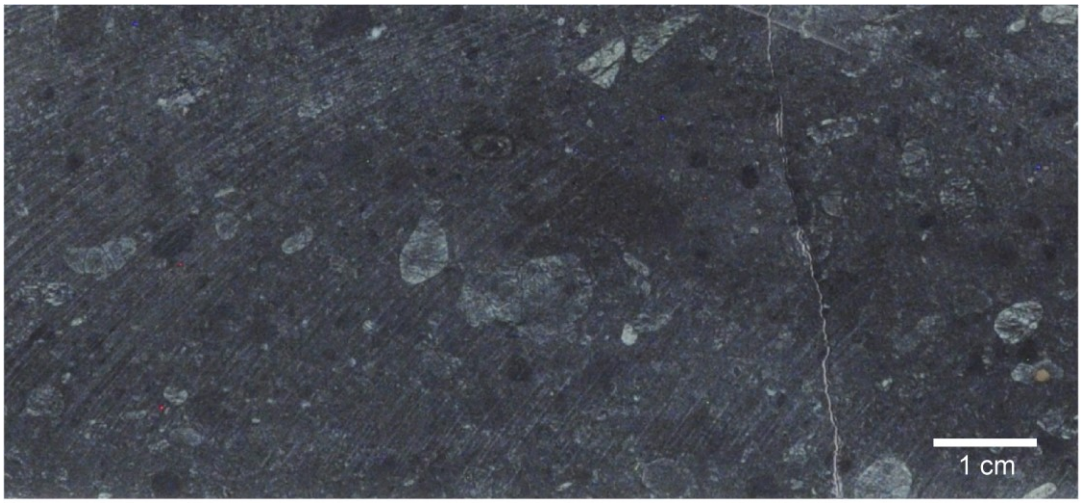

Photo (wet) of drill core sample 38916.

Photomicrograph of thin section for sample 38916 (PPL).

| | |
|---|---|
| SAMPLE ID: | 38919 |
| BODY: | Renard 2 |
| DOWNHOLE (APPARENT) DEPTH: | 657.32 m |
| UNIT CODE: | Kimb2c |
| ROCK NAME: | carbonate kimberlite |

HAND SAMPLE DESCRIPTION: Dark greenish grey-black macrocrystic hypabyssal kimberlite. Olivine macrocrysts are greenish-brown ± white patches (hard to see) and likely fully altered to serpentine ± carbonate [F-C (VC)]. Fine-grained uniform carbonate-rich crystalline groundmass (groundmass reacts with HCl) with minor segregations (white and yellowish-green minerals; carbonate and serpentine?). One side of the core has more abundant white interstitial areas and small segregations. Country rock xenoliths (<~5%) are white, greenish-white, dark green or black, up to ~1.3 cm (A-SR) and fully altered. Observed an olivine macrocryst with kelyphytic garnet inclusion. Few veinlets filled with white carbonate ± dark grey metallic mineral. Trace yellow metallic sulfides.

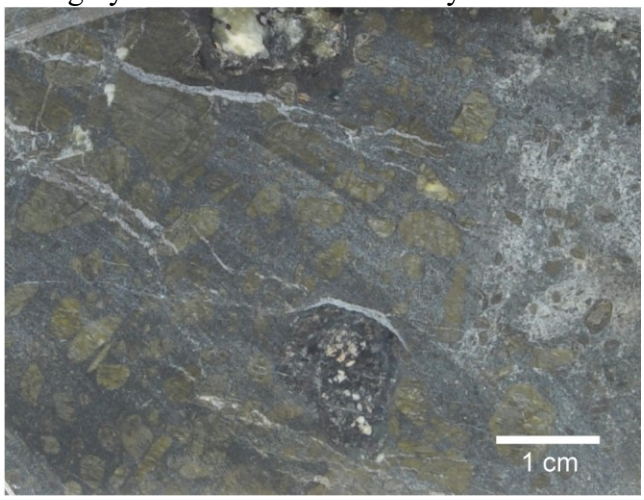

Photo (wet) of drill core sample 38919.

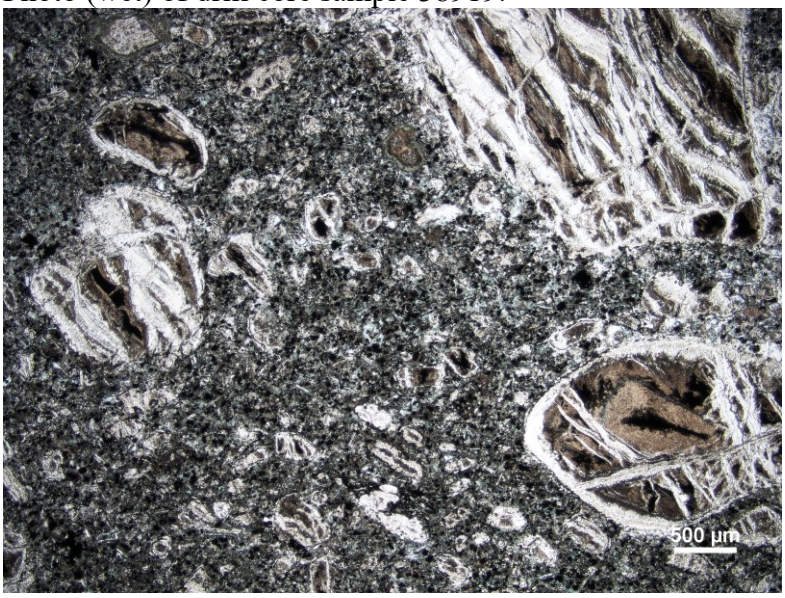

Photomicrograph of thin section for sample 38919 (PPL).

| | |
|---|---|
| SAMPLE ID: | 38923 |
| BODY: | Renard 2 |
| DOWNHOLE (APPARENT) DEPTH: | 286.71 m |
| UNIT CODE: | Kimb2c |
| ROCK NAME: | phlogopite-carbonate kimberlite |

HAND SAMPLE DESCRIPTION: Brownish-black macrocrystic hypabyssal kimberlite. Olivine macrocrysts are dark brownish-green to dark brown to light green (hard to see), partially to fully altered and contain translucent fresh relict olivine (F-VC). Fine-grained uniform carbonate-rich groundmass (groundmass reacts with HCl). Patchy areas in groundmass likely due to more abundant altered country rock xenoliths. Country rock xenoliths (~10-15%) are black, dark green, whitish-green or white, up to ~1.5 cm (A-SR) and fully altered. Few thin white carbonate veinlets (reacts with HCl).

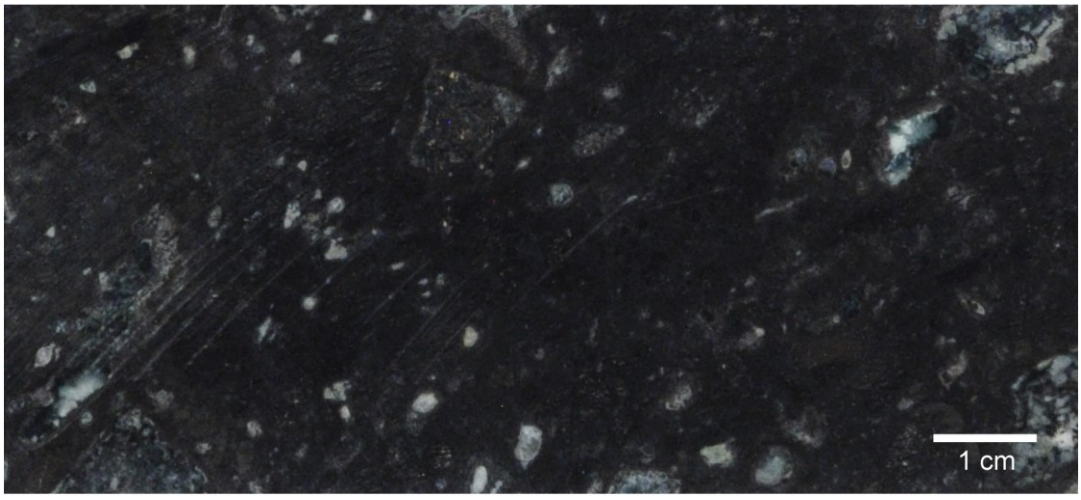

Photo (wet) of drill core sample 38923.

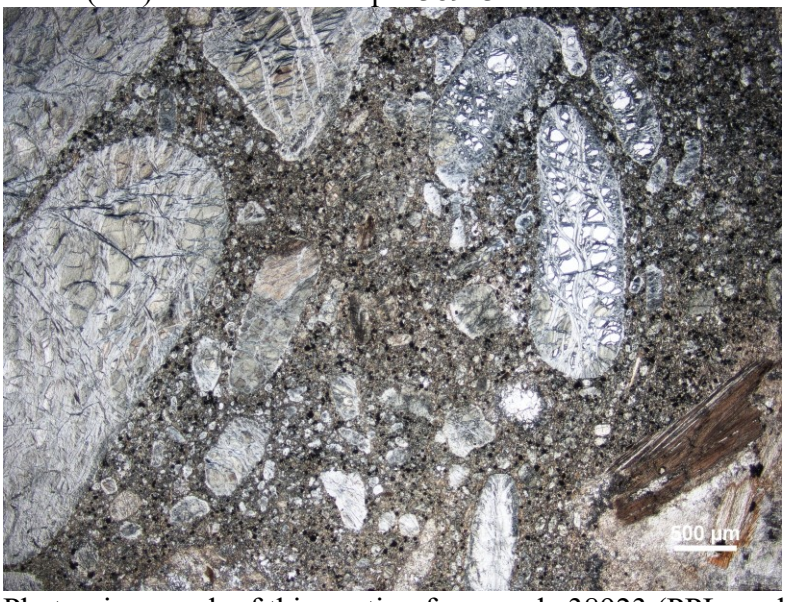

Photomicrograph of thin section for sample 38923 (PPL; carbon coated).

| | |
|---|---|
| SAMPLE ID: | 38925 |
| BODY: | Renard 2 |
| DOWNHOLE (APPARENT) DEPTH: | 344.90 m |
| UNIT CODE: | Kimb2a |
| ROCK NAME: | ? kimberlite |

HAND SAMPLE DESCRIPTION: Greenish blue tuffisitic kimberlite (TK or KPK) with massive, magmaclastic texture. Cored (olivine, CRX) and uncored lapilli range from full to partial selvages, including several large (~1-3.5cm) CRX-cored lapilli. Olivine macrocrysts are fully altered dark greenish brown ± white (F-C) with many plucked out of core. Inter-clast matrix greenish-blue in colour and fine-grained with common radiating fibrous mineral, matrix-supported, loosely packed and poorly sorted. Country rock xenoliths (~50-60%) range from large xenocrysts of white ± brown mica with patchy yellowish-green or green alteration or mostly brown mica with greenish alteration (partially altered) and small xenocrysts of fresh white to fully altered yellowish-green or yellowish-beige, up to ~4 cm (A-SR). Dark brown biotite xenocrysts present. Observed one altered (mostly plucked out) olivine macrocryst with chrome diopside inclusion.

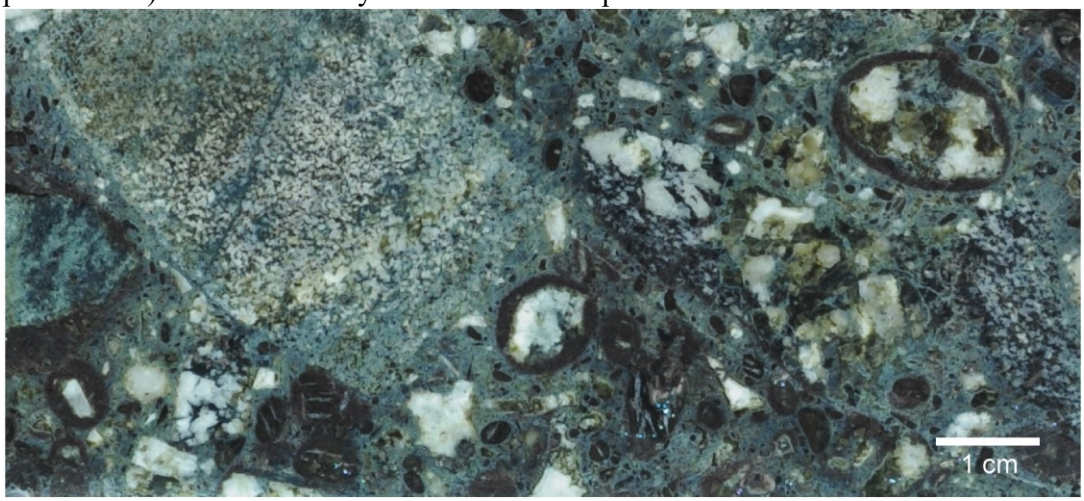

Photo (wet) of drill core sample 38925.

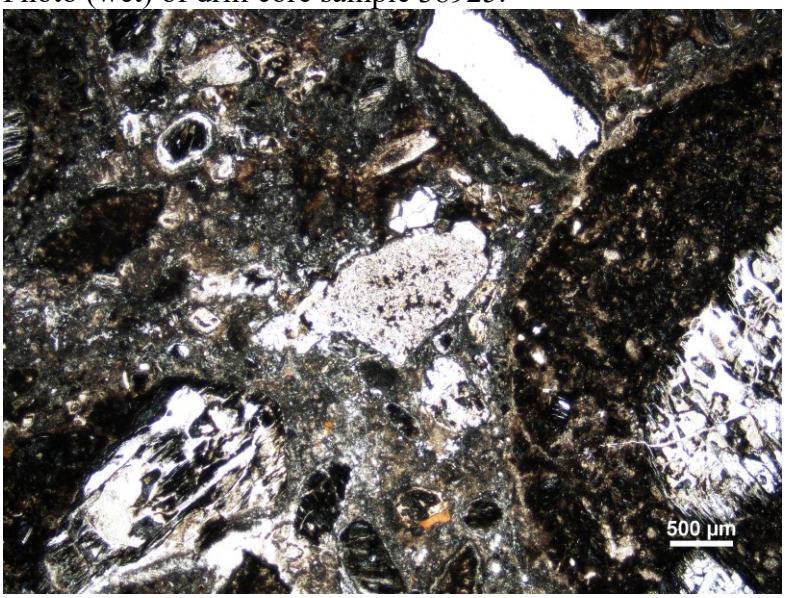

Photomicrograph of thin section for sample 38925 (PPL).

| | |
|---|---|
| SAMPLE ID: | 38926 |
| BODY: | Renard 2 |
| DOWNHOLE (APPARENT) DEPTH: | 387.44 m |
| UNIT CODE: | Kimb2c |
| ROCK NAME: | carbonate kimberlite |

HAND SAMPLE DESCRIPTION: Dark greenish-black macrocrystic hypabyssal kimberlite. Olivine macrocrysts are medium brownish-green to light yellowish-green, fully to partially altered with translucent fresh relict olivine (F-VC). Fine-grained uniform crystalline groundmass of carbonate and possible serpentine (some of groundmass reacts with HCl). Tiny (~1 mm) phlogopite macrocrysts appear abundant and more visible on cut slabbed surface. Country rock xenoliths (<1%) are white to light green, up to >2 cm (A-SR), and fully altered. One possible tiny garnet xenocryst observed.

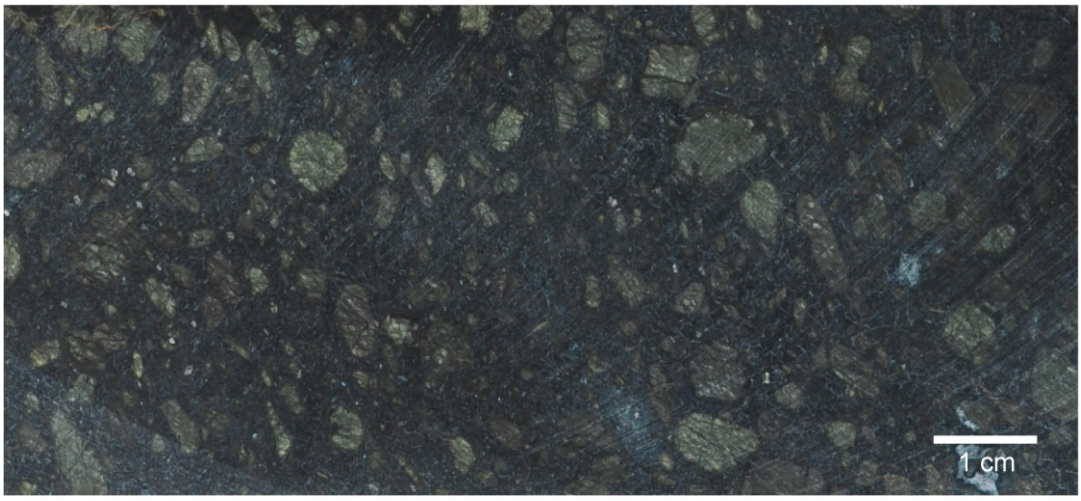

Photo (wet) of drill core sample 38926.

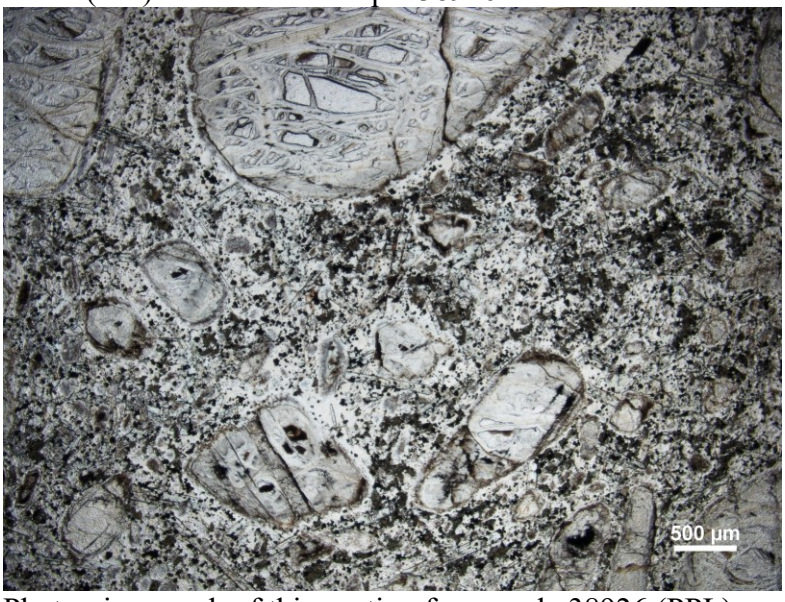

Photomicrograph of thin section for sample 38926 (PPL).

| | |
|---|---|
| SAMPLE ID: | 38927 |
| BODY: | Renard 2 |
| DOWNHOLE (APPARENT) DEPTH: | 443.86 m |
| UNIT CODE: | Kimb2b |
| ROCK NAME: | phlogopite kimberlite |

HAND SAMPLE DESCRIPTION: Dark brown macrocrystic hypabyssal kimberlite to minor transitional HK [HK(t)]. Olivine macrocrysts are black and/or translucent colourless-pale green (fresh) to dark greenish-brown (partially to fully altered) (hard to see) [F-C (VC)]. Crystalline groundmass appears fine-grained and uniform (groundmass reacts strongly with HCl) with minor irregular areas of patchy light brown alteration. Country rock xenoliths (~15%) range from white ± dark brown (e.g. mica) ± patchy medium-dark green alteration (partially altered) and creamy white ± green cores (sometimes reacts with HCl) or patchy dark green smaller xenocrysts (fully altered), up to ~4.5 cm (A-SR). Adjacent kimberlite appears patchy light brown surrounding some CRX. Dark brown biotite xenocrysts observed. Observed one dark orange pyrope with kelyphite, one altered olivine macrocryst with possible white pyroxene inclusion and one xenolith (?) of altered olivine, white pyroxene and chrome diopside.

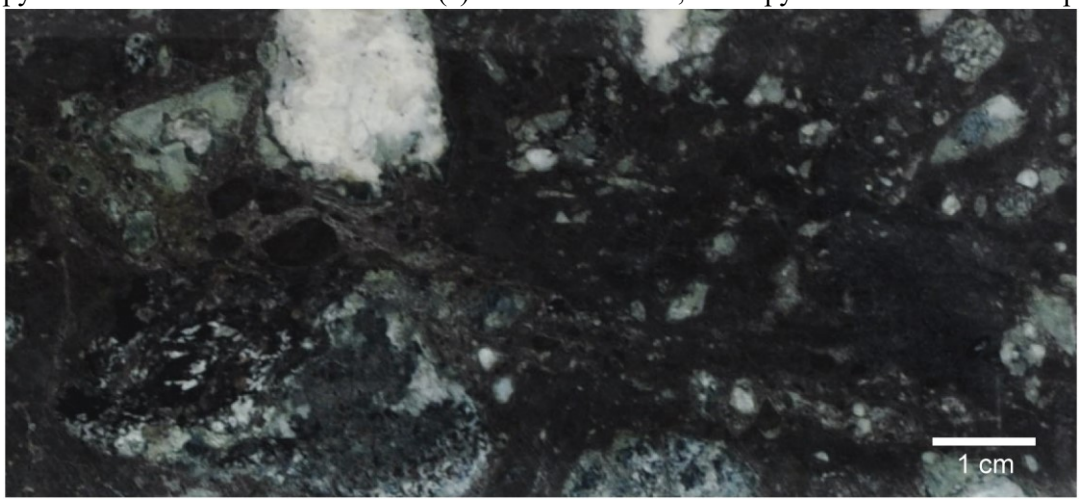


Photo (wet) of drill core sample 38927.

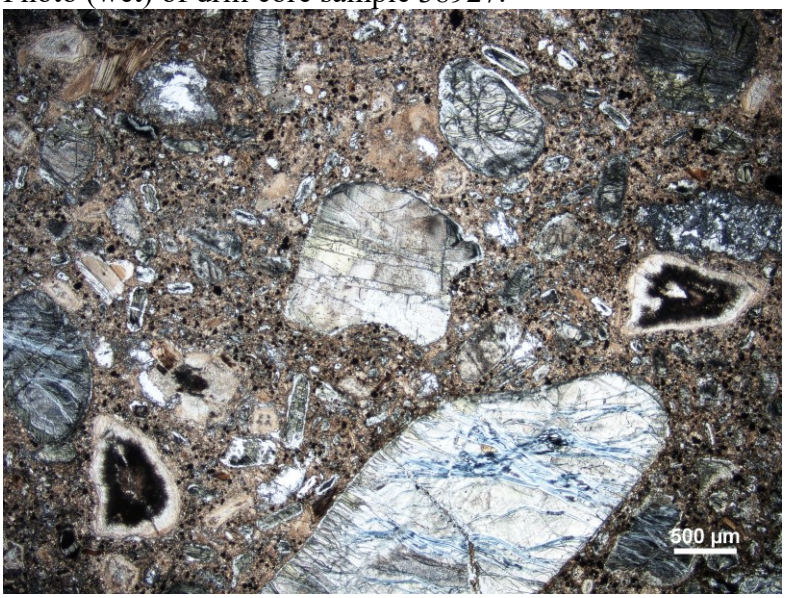


Photomicrograph of thin section for sample 38927 (PPL).

| | |
|---|---|
| SAMPLE ID: | 38928 |
| BODY: | Renard 2 |
| DOWNHOLE (APPARENT) DEPTH: | 459.65 m |
| UNIT CODE: | Kimb2c |
| ROCK NAME: | carbonate kimberlite |

HAND SAMPLE DESCRIPTION: Dark grey macrocrystic hypabyssal kimberlite. Olivine macrocrysts are light to medium green likely fully altered to serpentine ± black rims/fractures (F-VC) and somewhat flow aligned. Fine-grained uniform carbonate-rich crystalline groundmass (groundmass reacts with HCl). Country rock xenoliths (<1%) are black to dark brownish-green or white and dark green, <3 mm in size (A-SA) and fully altered. Few whitish brown veinlets (reacts with HCl).

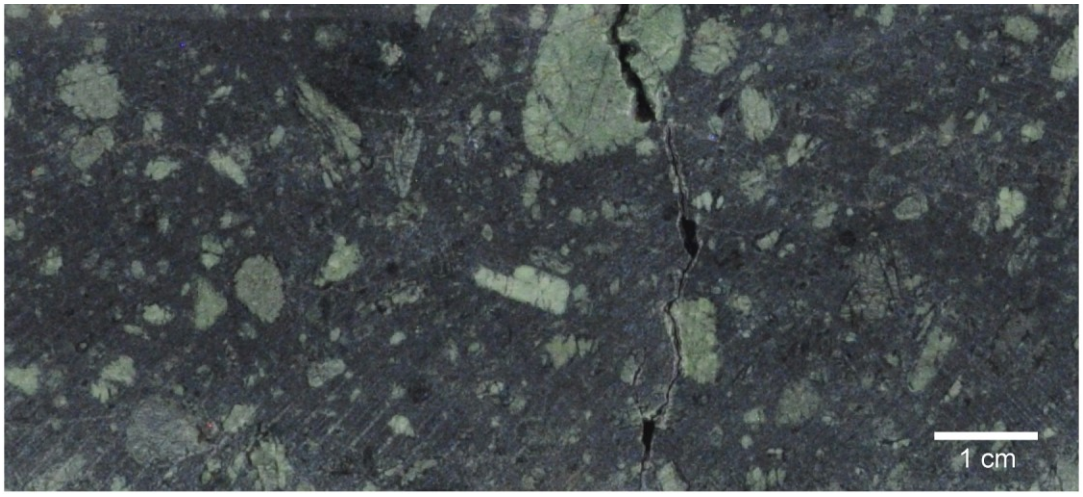

Photo (wet) of drill core sample 38928.

Photomicrograph of thin section for sample 38928 (PPL).

| | |
|---|---|
| SAMPLE ID: | 38929 |
| BODY: | Renard 2 |
| DOWNHOLE (APPARENT) DEPTH: | 498.16 m |
| UNIT CODE: | Kimb2c |
| ROCK NAME: | carbonate kimberlite |

HAND SAMPLE DESCRIPTION: Dark grey-black macrocrystic hypabyssal kimberlite. Olivine macrocrysts are dark brownish-black ± white patches (hard to see) and fully altered (F-VC). Fine-grained uniform carbonate-rich crystalline groundmass (groundmass reacts with HCl). Country rock xenoliths (<1%) are white and dark green, <1.1 cm, oblong (A) and fully altered. A few thin white carbonate veinlets (reacts with HCl).

Photo (wet) of drill core sample 38929.

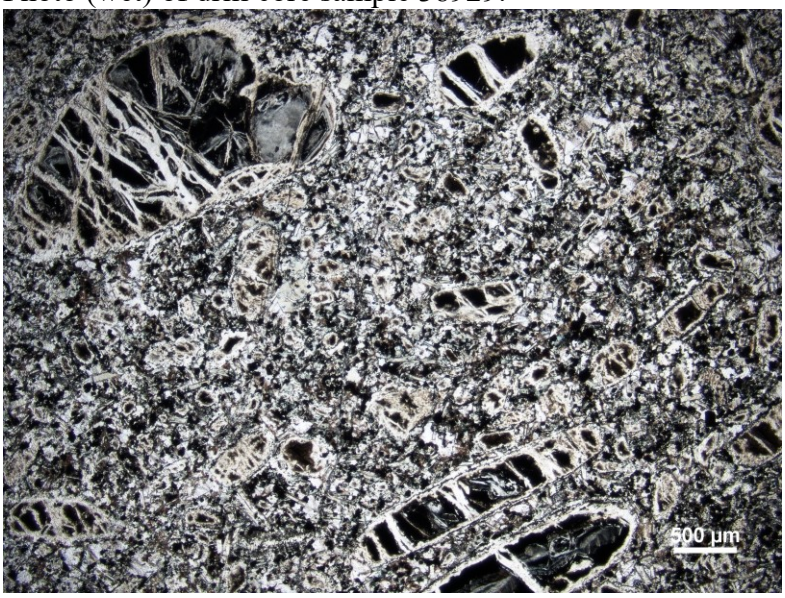

Photomicrograph of thin section for sample 38929 (PPL).

| | |
|---|---|
| SAMPLE ID: | 31543 |
| BODY: | Renard 3 |
| DOWNHOLE (APPARENT) DEPTH: | 19.63 m |
| UNIT CODE: | Kimb3f |
| ROCK NAME: | ? kimberlite |

HAND SAMPLE DESCRIPTION: Medium brown transitional hypabyssal kimberlite (HKt) with magmaclastic texture. Cored (olivine, CRX) and uncored lapilli range from full to partial selvages or with diffuse margins (uncored lapilli). Olivine macrocrysts are fully altered dark greenish brown (hard to see) [F-C (VC)] with a very large (~18 mm) partially altered megacryst with fresh relict core. Combination of uniform crystalline groundmass (slightly more abundant) and patchy light brown to pale greenish-blue areas of alteration. Groundmass/matrix reacts weakly to no reaction with HCl. Country rock xenoliths (~25-40%) ranges from pale green alteration rims or patchy green (partially altered) and smaller xenocrysts of pale greenish-white or dark yellowish green with creamy white rims or zoned white cores-dark yellowish green-creamy white rims (sometimes reacts with HCl) (fully altered), up to ~4.5 cm (A-SR). Dark brown biotite xenocrysts present. Adjacent kimberlite irregularly altered pale greenish-blue surrounding some CRX. Observed trace chromite, white or pale green pyroxene, and one altered olivine macrocryst with chrome diopside inclusion.

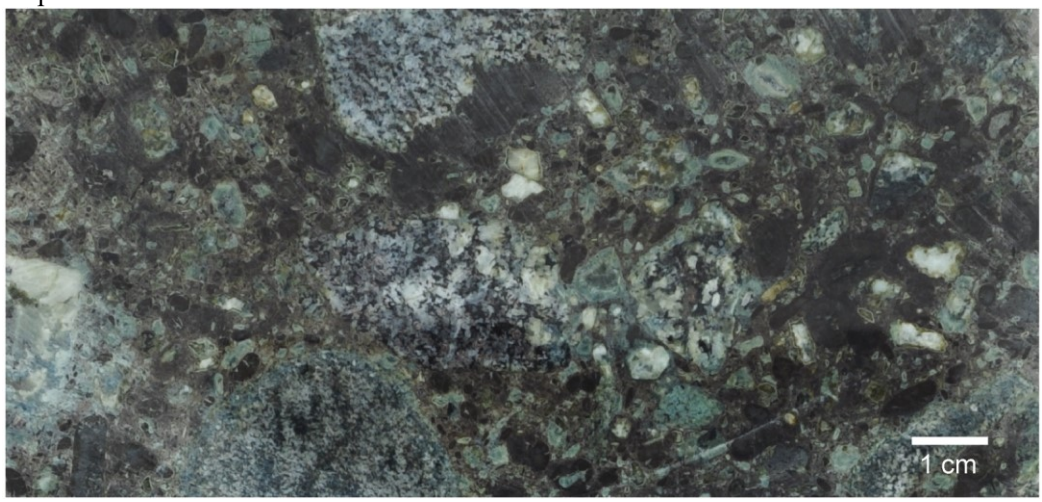


Photo (wet) of drill core sample 31543.

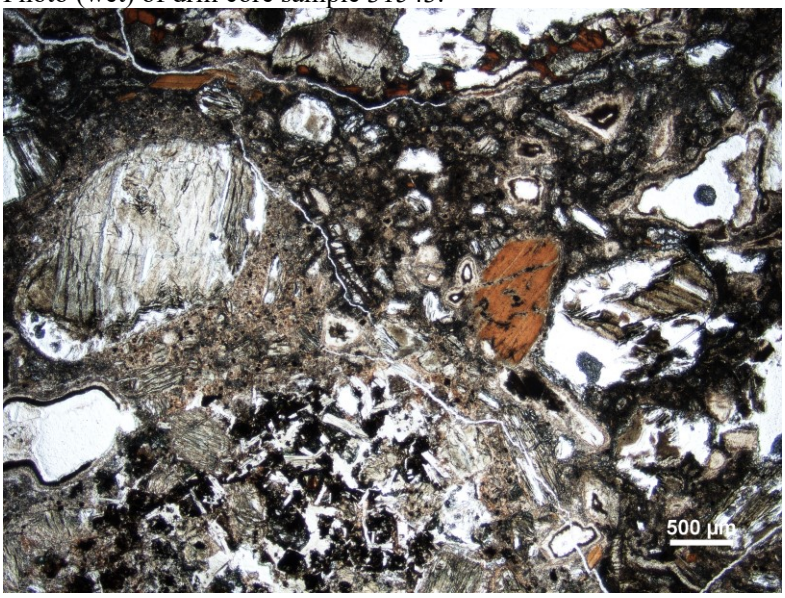


Photomicrograph of thin section for sample 31543 (PPL).

| | |
|---|---|
| SAMPLE ID: | 31548 |
| BODY: | Renard 3 |
| DOWNHOLE (APPARENT) DEPTH: | 103.00 m |
| UNIT CODE: | Kimb3i |
| ROCK NAME: | serpentine-phlogopite kimberlite |

HAND SAMPLE DESCRIPTION: Dark greenish-black macrocrystic hypabyssal kimberlite. Olivine macrocrysts are translucent colourless (fresh) to yellow-green brown (partially to fully altered) (hard to see) [F-C (VC)]. Crystalline groundmass is uniform with possible minor serpentine segregations and minor patchy areas of alteration (groundmass reacts to HCl). Country rock xenoliths (<5%) are present ranging from white, dark green or a combination of both (fully altered) or patchy white and dark green with mica (partially altered), up to ~7.5 cm (A-SR). Adjacent kimberlite appears patchy light brown surrounding some CRX with diffuse altered margins. Observed one fresh olivine macrocryst with purple garnet inclusion and one large (~11 cm) dunite (olivine) xenolith. A few thin white irregular veinlets (reacts with HCl).

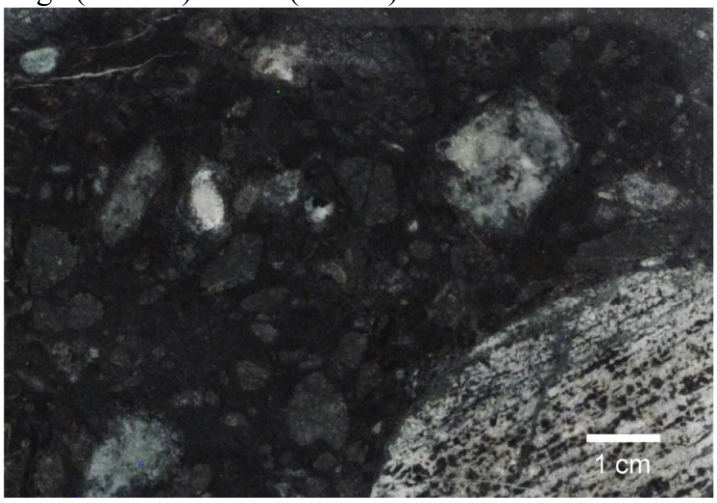

Photo (wet) of drill core sample 31548.

Photomicrograph of thin section for sample 31548 (PPL).

| | |
|---|---|
| SAMPLE ID: | 31552 |
| BODY: | Renard 3 |
| DOWNHOLE (APPARENT) DEPTH: | 33.55 m |
| UNIT CODE: | Kimb3c |
| ROCK NAME: | carbonate kimberlite |

HAND SAMPLE DESCRIPTION: Dark grey-black macrocrystic hypabyssal kimberlite. Olivine macrocrysts are medium yellowish green ± minor white areas (hard to see) and fully altered to likely serpentine [F-C (VC)]. Fine-grained uniform carbonate-rich crystalline groundmass with minor white segregations (groundmass reacts strongly with HCl). Difficult to see but serpentine may be present in groundmass. Country rock xenoliths (<~5%) are white, brown and light to dark green, up to ~1.3 cm (SA-SR) and fully to partially altered. Trace kelyphite xenocrysts, an olivine macrocryst with kelyphitic garnet inclusion and a few garnets with kelyphite inclusions (?) observed. Many thin white veinlets (reacts with HCl) and some very fine veinlets filled with white and dark metallic minerals. Possible very fine-grained yellowish sulfides.

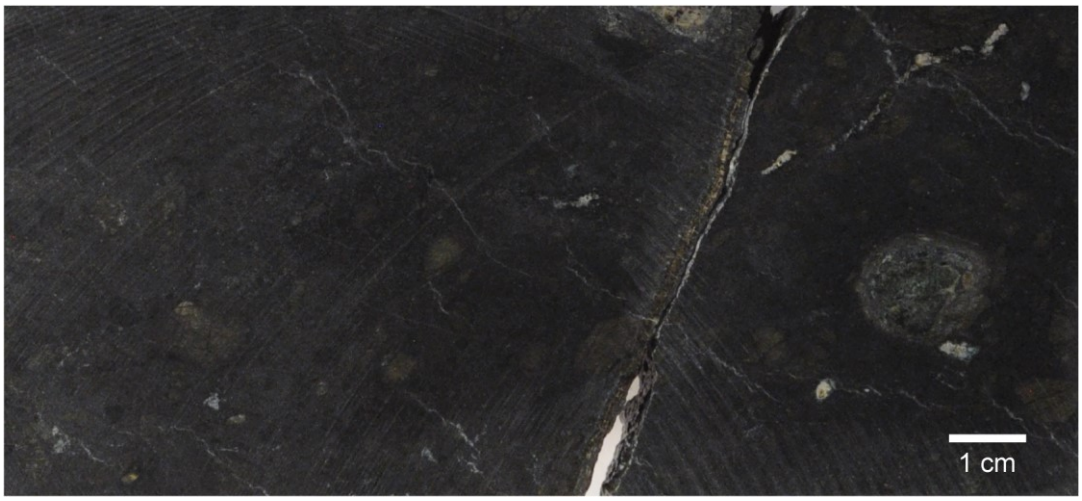

Photo (wet) of drill core sample 31552.

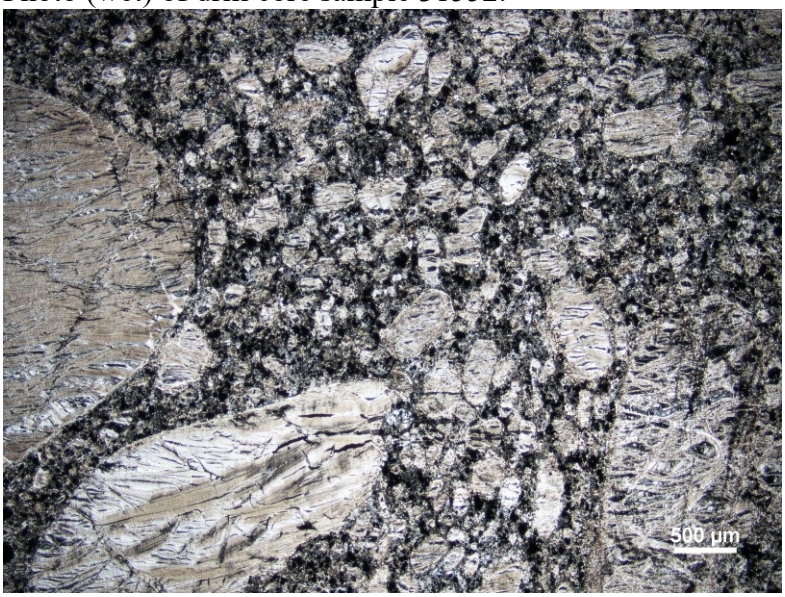

Photomicrograph of thin section for sample 31552 (PPL).

| | |
|---|---|
| SAMPLE ID: | 31555 |
| BODY: | Renard 3 |
| DOWNHOLE (APPARENT) DEPTH: | 95.68 m |
| UNIT CODE: | FKimb3h |
| ROCK NAME: | serpentine-carbonate kimberlite |

HAND SAMPLE DESCRIPTION: Dark grey-black macrocrystic hypabyssal kimberlite. Olivine macrocrysts are translucent pale green (fresh) to yellowish-green ± fresh relicts (partially to fully altered) (hard to see) [F-C (VC)]. Crystalline groundmass is uniform and carbonate-rich with minor serpentine segregations (groundmass reacts strongly to HCl). Country rock xenoliths (<5%) range from creamy white ± dark green rims or patchy areas (fully altered) to patchy white or white/yellowish brown with brown mica (partially altered), up to ~5 cm (A-SR). White alteration reacts strongly with HCl. Difficult to see alteration with adjacent kimberlite but a large xenolith has a few mm's thick alteration halo of fully serpentinized brown olivine macrocrysts. Observed two kelyphitic garnets (including an ~18 mm kelyphitic pink garnet), and two olivine macrocrysts with kelyphite as inclusion or attached material. Few thin white irregular veinlets (reacts with HCl).

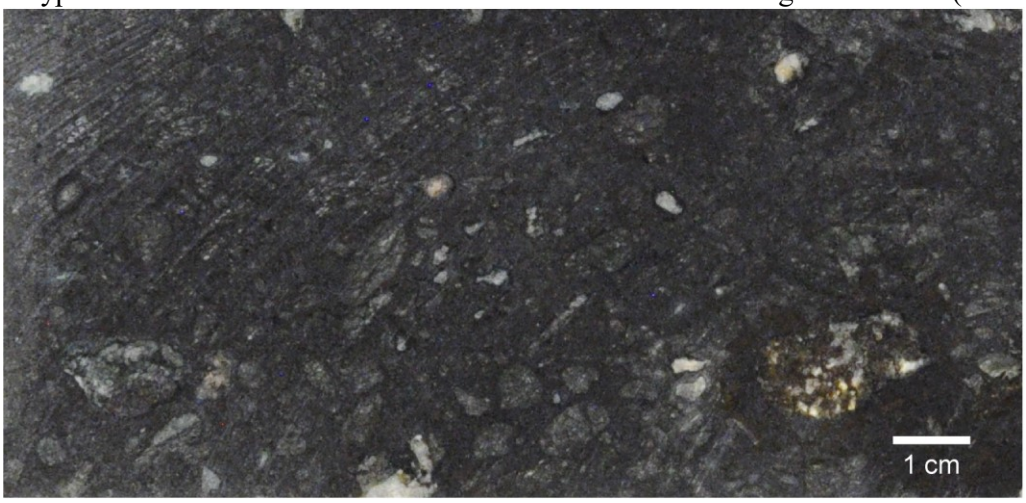

Photo (wet) of drill core sample 31555.

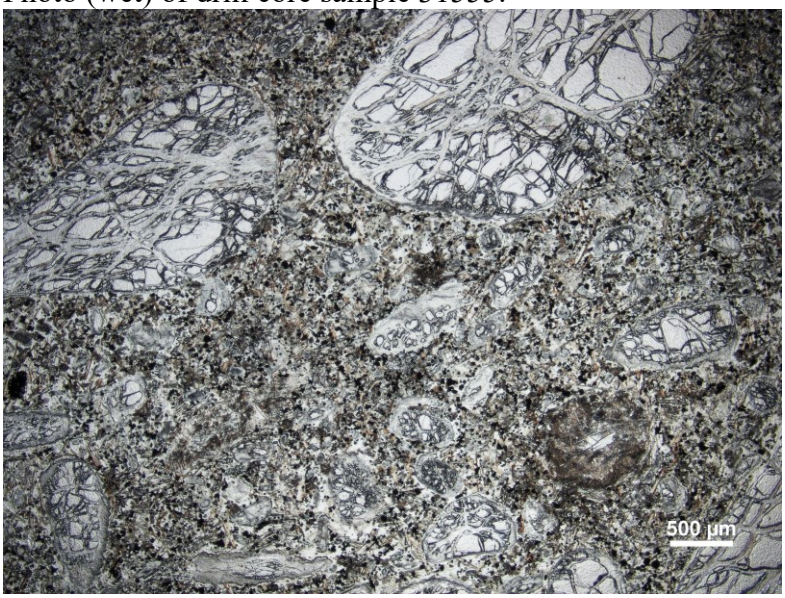

Photomicrograph of thin section for sample 31555 (PPL).

SAMPLE ID: 31556
BODY: Renard 3
DOWNHOLE (APPARENT) DEPTH: 118.39 m
UNIT CODE: Kimb3g
ROCK NAME: phlogopite-(monticellite?) kimberlite

HAND SAMPLE DESCRIPTION: Medium brown macrocrystic hypabyssal kimberlite to transitional HK [HK(t)]. Olivine macrocrysts are dark green/yellow brown (fully altered) with trace translucent colourless to pale green (partially altered) olivine possible (hard to see) (F-C). Crystalline groundmass is dominantly fine-grained and uniform with minor carbonate (groundmass weakly reacts to no reaction with HCl) with lesser patchy light brown areas of alteration. Country rock xenoliths (~30-50%) range from white ± dark brown (e.g. mica) with patchy medium-dark green alteration (partially altered) and creamy white ± green or green ± creamy white small xenocrysts (fully altered), up to ~8 cm (A-SR). Altered white CRX sometimes reacts with HCl. Dark brown biotite xenocrysts observed. Adjacent kimberlite can sometimes appear patchy light brown and is more noticeable surrounding smaller fully altered CRX. Few possible incipient cored lapilli but hard to see. Trace chromite and a few olivine macrocrysts with inclusions (pale green mineral, chrome diopside, chromite).

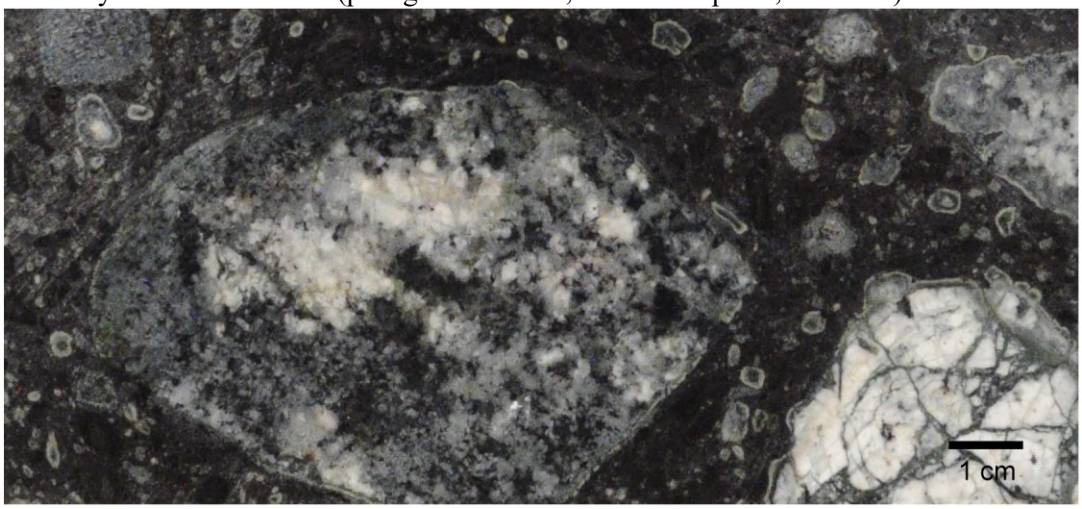

Photo (wet) of drill core sample 31556.

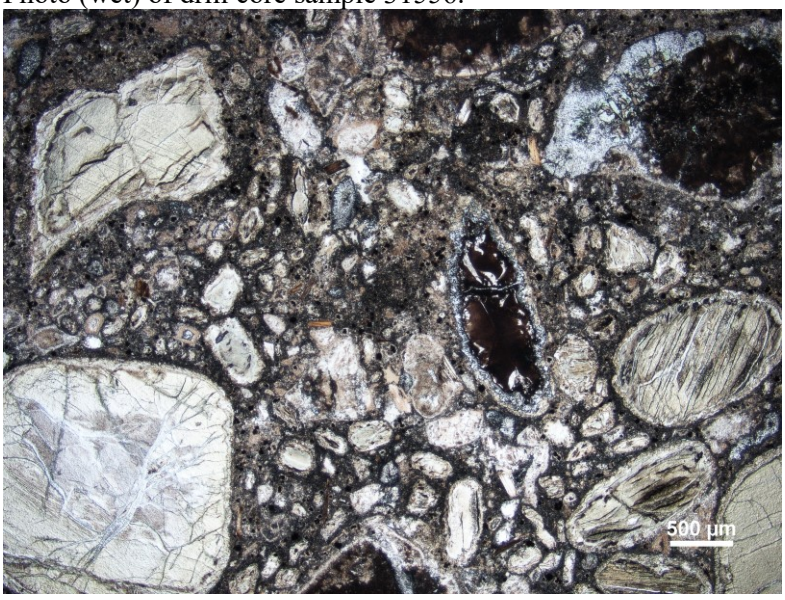

Photomicrograph of thin section for sample 31556 (PPL).

| | |
|---|---|
| SAMPLE ID: | 31559 |
| BODY: | Renard 3 |
| DOWNHOLE (APPARENT) DEPTH: | 124.68 m |
| UNIT CODE: | Kimb3d |
| ROCK NAME: | phlogopite kimberlite |

HAND SAMPLE DESCRIPTION: Dark brown-black macrocrystic hypabyssal kimberlite. Olivine macrocrysts are translucent colourless to pale green (fresh) to yellow-green brown (partially to fully altered) (hard to see) [F-C (VC)]. Crystalline groundmass is fine-grained and uniform (white interstitial carbonate appears present but groundmass reacts weakly with HCl) with minor patchy areas of alteration. Country rock xenoliths (~10-15%) range from creamy white, dark green, or combinations of white with dark green patches ± mica or dark green cores with creamy pale green rim, up to ~7 cm (A-SR). Altered white CRX sometimes reacts with HCl. Fully to partially altered and alteration can appear patchy light brown in surrounding kimberlite. Observed possible kelyphite garnet, few pale yellow pyroxene (?) and a ~4 cm olivine-rich (dunite) xenolith (or olivine megacryst). Few thin white irregular veinlets (barely reacts with HCl?).

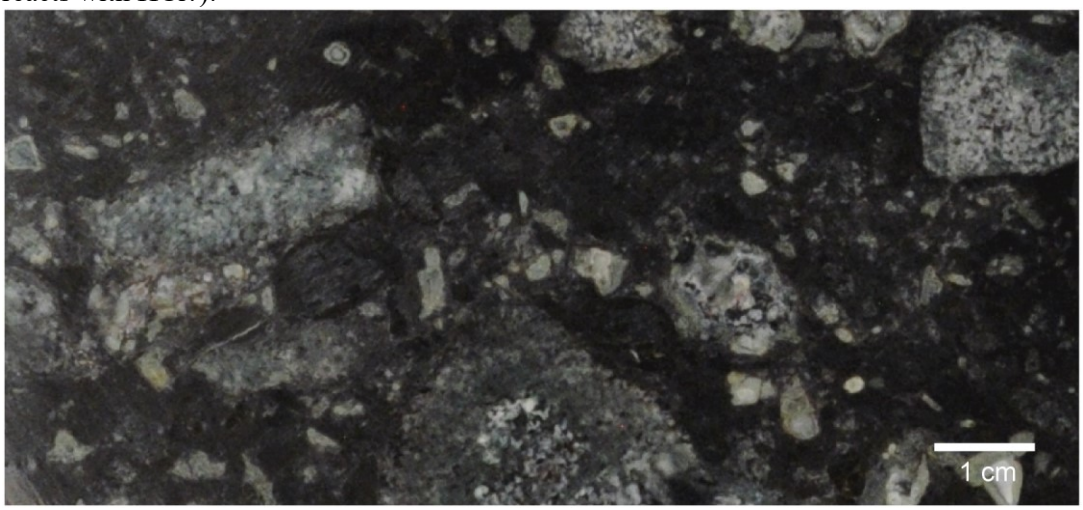

Photo (wet) of drill core sample 31559.

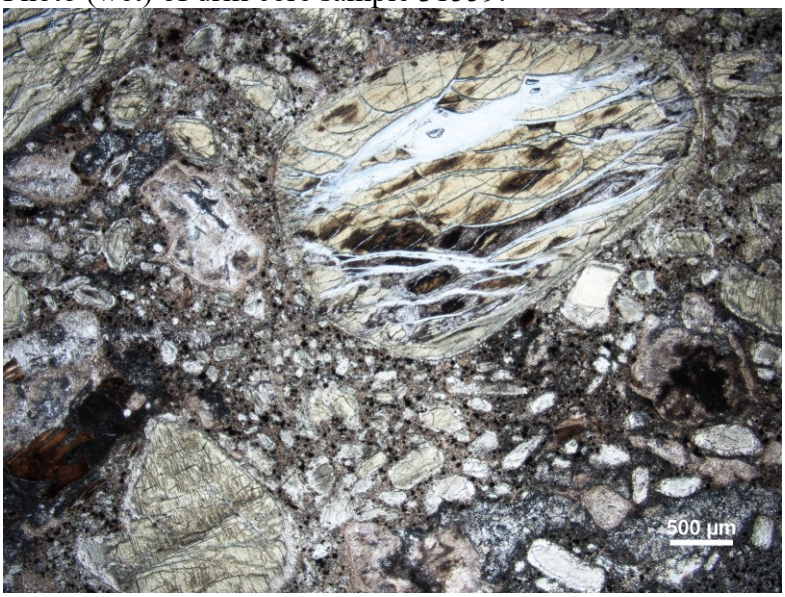

Photomicrograph of thin section for sample 31559 (PPL).

| | |
|---|---|
| SAMPLE ID: | 39282 |
| BODY: | Renard 4 |
| DOWNHOLE (APPARENT) DEPTH: | 194.52 m |
| UNIT CODE: | Kimb4c |
| ROCK NAME: | carbonate kimberlite |

HAND SAMPLE DESCRIPTION: Dark grey-black macrocrystic hypabyssal kimberlite. Olivine macrocrysts are dark yellowish-green ± bright red or light green areas (hard to see) and fully altered, except a few large macrocrysts have clear/translucent areas in their cores which may be fresh relict olivine (?) [F-C (VC)]. Fine-grained uniform carbonate-rich crystalline groundmass (groundmass reacts strongly with HCl). Difficult to see but possible groundmass serpentine may be present. Country rock xenoliths (<~5%) are patchy dark green and white or patchy white ± red alteration, up to ~4 cm (A-SR) and fully to partially altered. Observed an olivine macrocryst with kelyphite, kelyphitic garnet with inclusions (possible pyroxene, altered olivine?), trace kelyphite and kelyphitic garnet xenocrysts and trace chromite xenocrysts. Patchy reddish alteration throughout core.

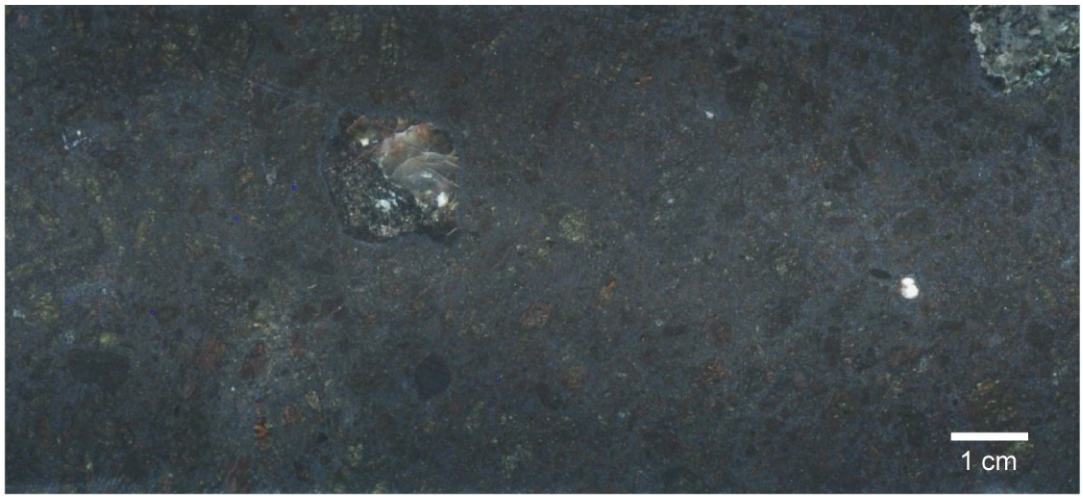

Photo (wet) of drill core sample 39282.

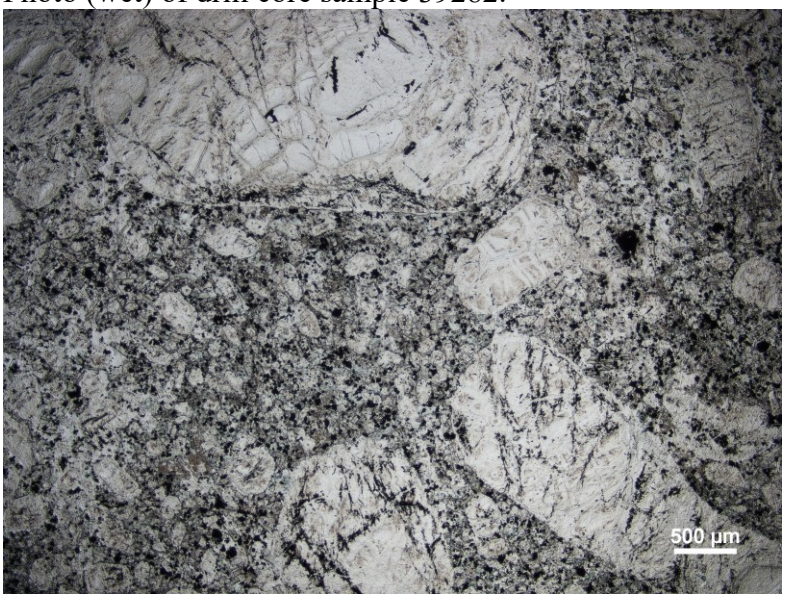

Photomicrograph of thin section for sample 39282 (PPL).

| | |
|---|---|
| SAMPLE ID: | 39283 |
| BODY: | Renard 4 |
| DOWNHOLE (APPARENT) DEPTH: | 298.65 m |
| UNIT CODE: | Kimb4c |
| ROCK NAME: | carbonate kimberlite |

HAND SAMPLE DESCRIPTION: Dark grey-black macrocrystic hypabyssal kimberlite. Olivine macrocrysts are clear/translucent fresh with brownish rims/fractures of alteration (hard to see) [F-C (VC)]. Fine-grained uniform carbonate-rich crystalline groundmass (groundmass reacts strongly with HCl). Difficult to see but possible groundmass serpentine may be present. Country rock xenoliths (<~5%) are patchy white and medium to dark green (with brown mica), up to ~2.5 cm (A-SA) and fully to partially altered. Observed few olivine macrocrysts with inclusions (dark nonmetallic mineral (?), garnet) and trace kelyphitic garnet xenocrysts. Core is not magmaclastic but there are a few areas where the fine-grained groundmass appears to concentrate into round areas surrounded by slightly coarser areas (uncertain texture?). A few white ± green veins (some react to HCl and some do not).

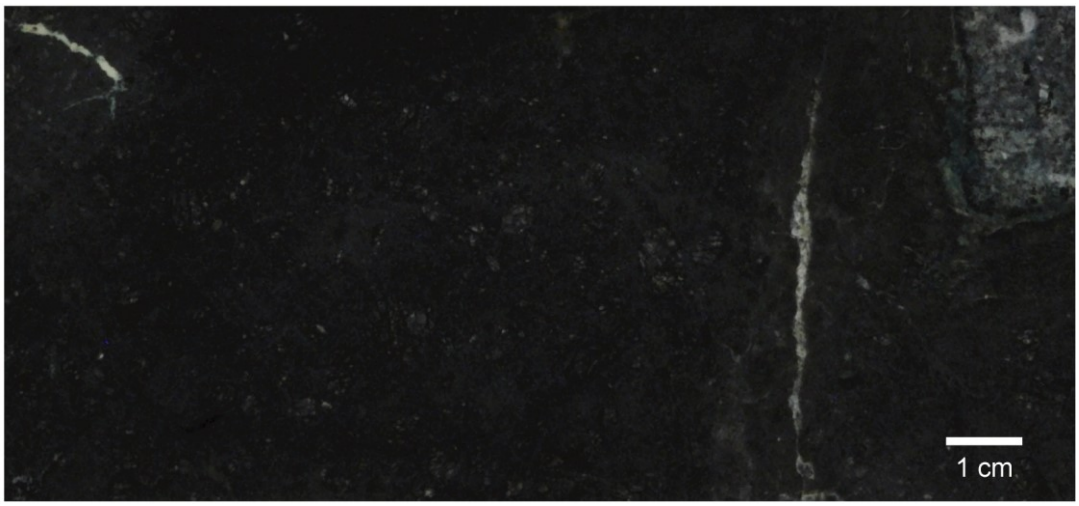

Photo (wet) of drill core sample 39283.

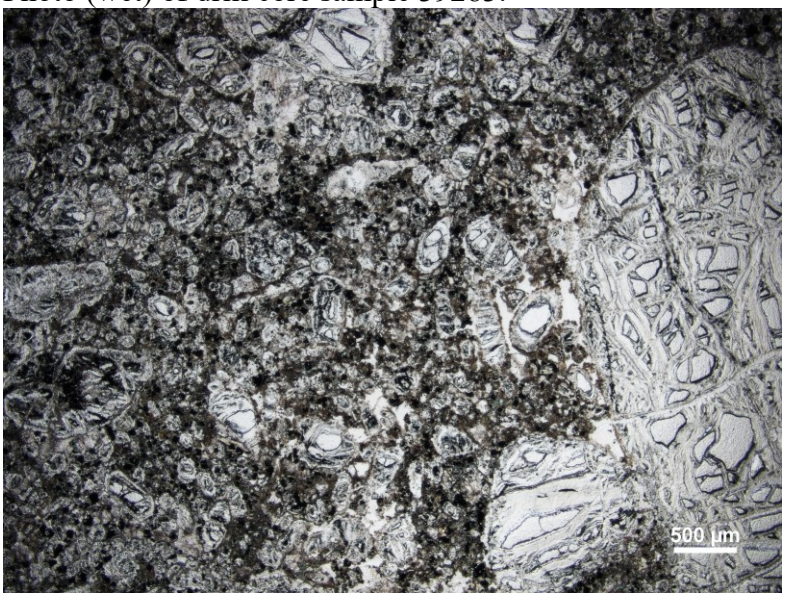

Photomicrograph of thin section for sample 39283 (PPL).

| | |
|---|---|
| SAMPLE ID: | 39289 |
| BODY: | Renard 4 |
| DOWNHOLE (APPARENT) DEPTH: | 244.29 m |
| UNIT CODE: | Kimb4b |
| ROCK NAME: | (monticellite?)-phlogopite kimberlite |

HAND SAMPLE DESCRIPTION: Dark grey-black macrocrystic hypabyssal kimberlite. Olivine macrocrysts are translucent pale green (fresh) to yellow/greenish-brown (partially to fully altered) (hard to see) [F-C (VC)]. One fresh olivine megacryst up to ~3 cm long with minor alteration rim. Crystalline groundmass is fine-grained, uniform and carbonate-rich (groundmass reacts strongly with HCl). Country rock xenoliths (<10%) are present with many yellow-white in colour with patchy yellow-green to dark green alteration or white alteration (some white CRX reacts with HCl but some white areas do not) ± relict biotite, up to ~3.5 cm (A-SR) and fully to partially altered. Alteration appears diffuse into surrounding kimberlite creating a light brown groundmass. Three kelyphytic garnets observed. Few thin irregular white veinlets (reacts with HCl).

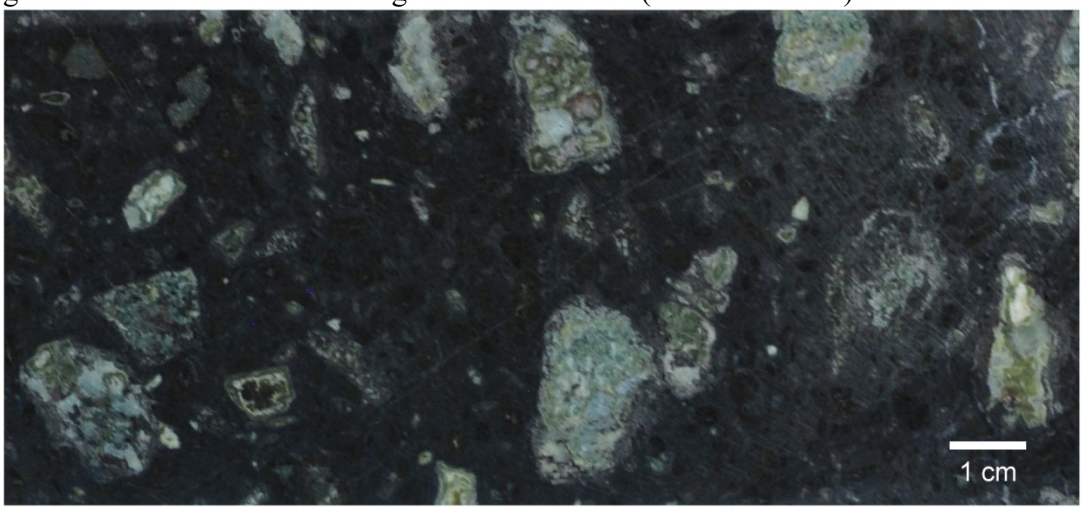


Photo (wet) of drill core sample 39289.

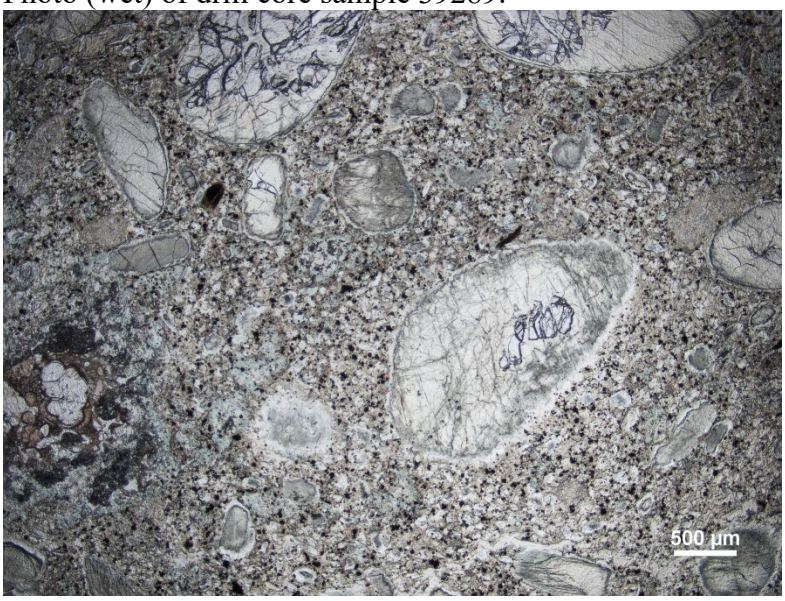


Photomicrograph of thin section for sample 39289 (PPL).

| | |
|---|---|
| SAMPLE ID: | 35789 |
| BODY: | Renard 7 |
| DOWNHOLE (APPARENT) DEPTH: | 45.09 m |
| UNIT CODE: | Kimb7c |
| ROCK NAME: | (monticellite?)-carbonate kimberlite |

HAND SAMPLE DESCRIPTION: Dark greenish-black macrocrystic hypabyssal kimberlite. Olivine macrocrysts are dark greenish-black ± light greenish rims or light-medium green ± black areas/fracture/cores and white areas (hard to see) or medium brown coloration to macrocrysts along one end of the core. Olivine macrocrysts appear fully altered to likely serpentine ± black mineral [F-C (VC)]. Fine-grained uniform crystalline groundmass of carbonate and possible serpentine (groundmass reacts strongly with HCl). Groundmass contains minor white segregations and more carbonate-rich uniform areas. Country rock xenoliths not obvious. Observed an olivine macrocryst with kelyphite and trace chromite xenocrysts. Small, short white carbonate (reacts with HCl) parallel veins along one side of core. It is possible some of the 'segregations' on the cut slabbed face may reflect this style of veining.

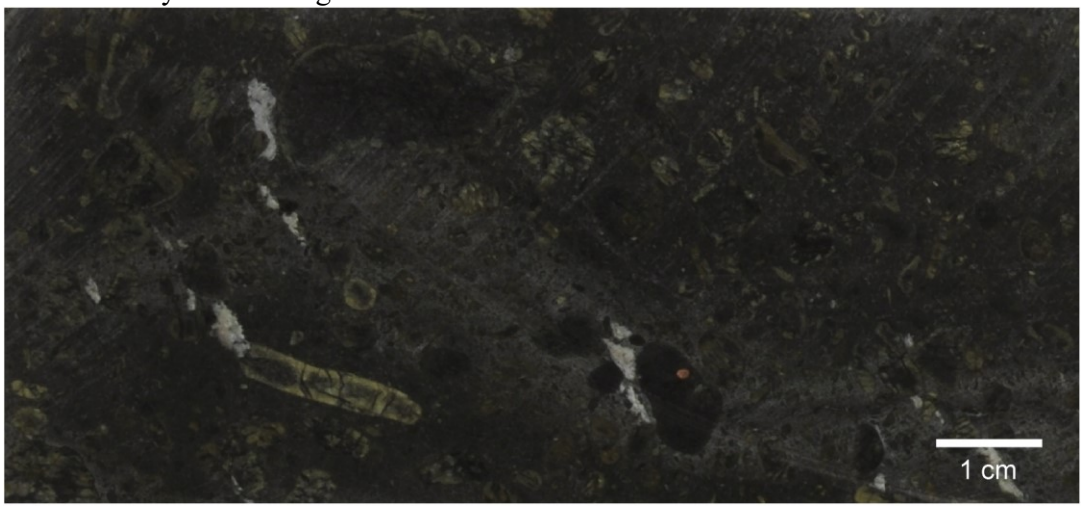

Photo (wet) of drill core sample 35789.

Photomicrograph of thin section for sample 35789 (PPL; carbon coated).

| | |
|---|---|
| SAMPLE ID: | 35790 |
| BODY: | Renard 7 |
| DOWNHOLE (APPARENT) DEPTH: | 108.44 m |
| UNIT CODE: | Kimb7c |
| ROCK NAME: | phlogopite-opaques-carbonate-serpentine kimberlite |

HAND SAMPLE DESCRIPTION: Medium greyish-green macrocrystic hypabyssal kimberlite. Olivine macrocrysts are light whitish-green, dark green or patchy black with light to medium green ± creamy white rims (smaller macrocrysts hard to see) and fully altered but this alteration varies (± patchy black cores and/or fractures, ± creamy white (does not appear to react with HCl) or brown rims, cores of whitish-green, dark green, white or whitish grey) [F-C (VC)]. Fine-grained uniform carbonate = (approximate) serpentine crystalline groundmass (groundmass reacts weakly with HCl). Country rock xenoliths difficult to identify if present. Observed a few olivine macrocrysts with inclusions (black mineral, possibly kelyphite) and trace chromite xenocrysts. A few olivine macrocrysts appear to contain inclusions filled with likely groundmass (holes?). Several thin white and green veinlets (partially reacts with HCl).

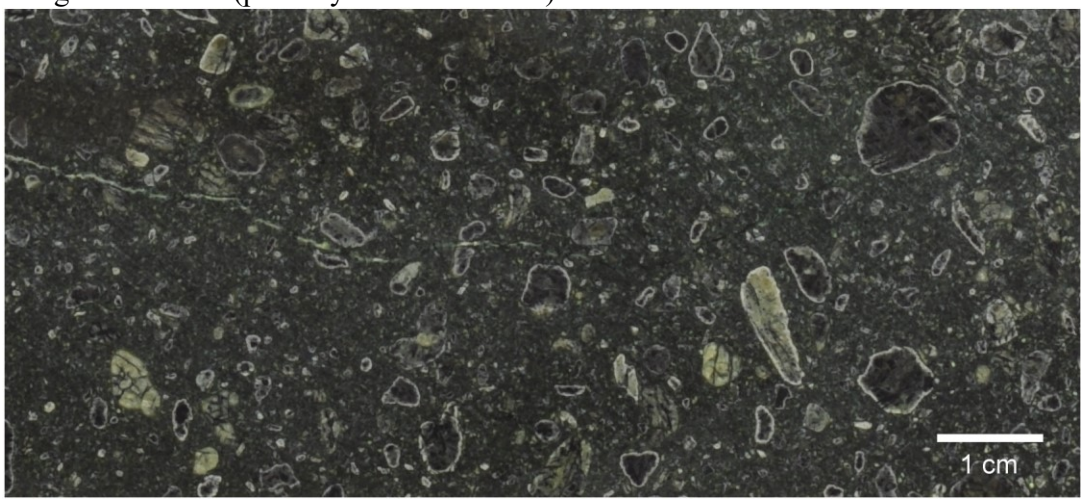

Photo (wet) of drill core sample 35790.

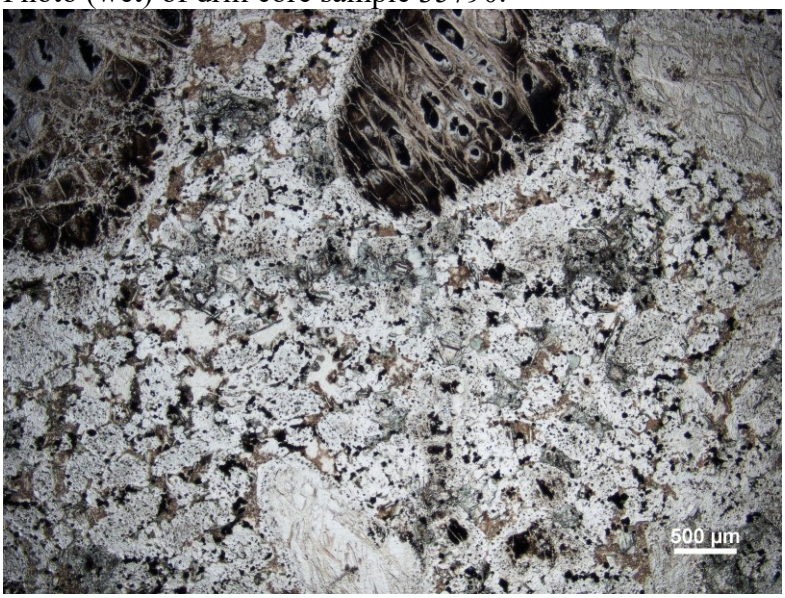

Photomicrograph of thin section for sample 35790 (PPL).

| | |
|---|---|
| SAMPLE ID: | 35791 |
| BODY: | Renard 7 |
| DOWNHOLE (APPARENT) DEPTH: | 87.95 m |
| UNIT CODE: | Kimb7c |
| ROCK NAME: | carbonate-serpentine kimberlite |

HAND SAMPLE DESCRIPTION: Dark grey-black macrocrystic hypabyssal kimberlite. Olivine macrocrysts are dark greenish brown ± minor white areas and fully altered to likely serpentine ± carbonate [F-C (VC)]. Fine-grained uniform carbonate-rich crystalline groundmass (groundmass reacts strongly with HCl). Country rock xenoliths are not obvious. Observed one olivine macrocryst with kelyphite inclusion. Thin white veinlets crosscutting a thicker white/dark green/brown vein (both react with HCl). Core appears slightly lighter in colour on side with thicker vein.

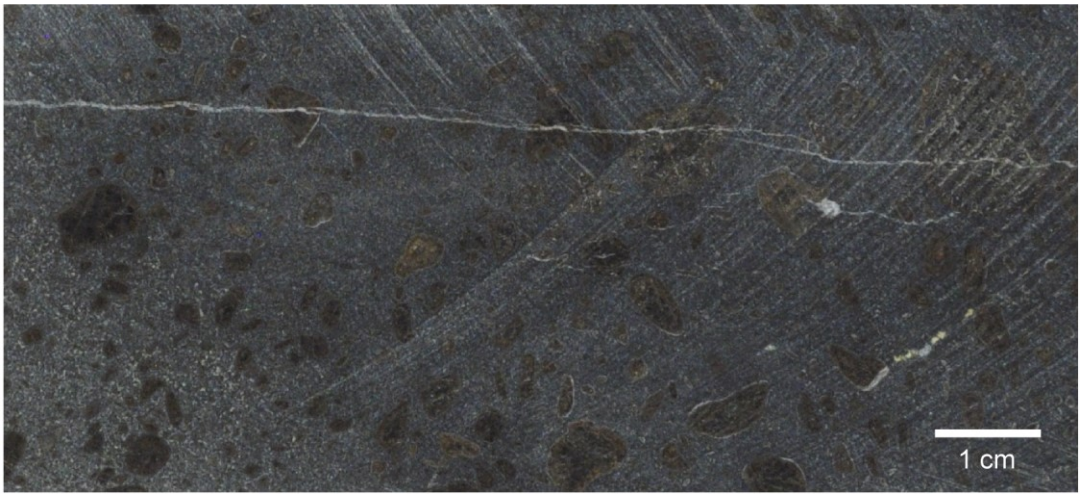

Photo (wet) of drill core sample 35791.

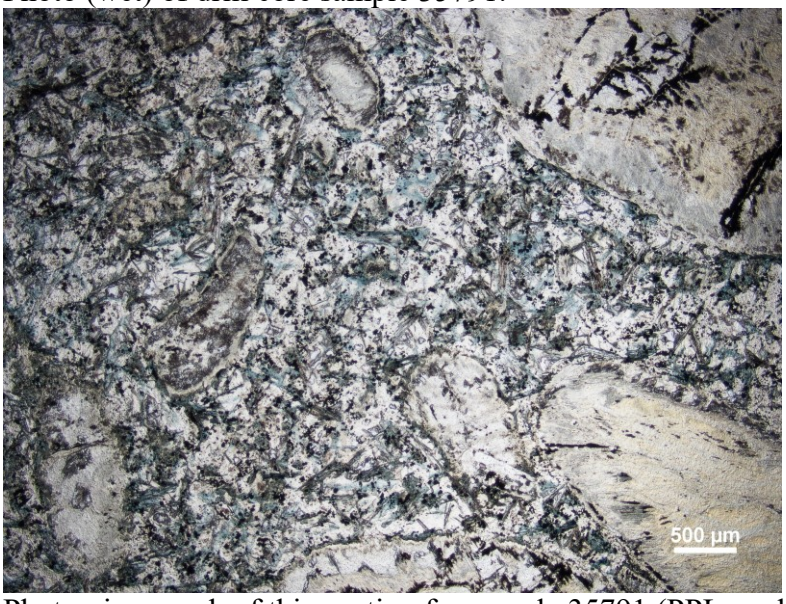

Photomicrograph of thin section for sample 35791 (PPL; carbon coated).

| | |
|---|---|
| SAMPLE ID: | 31462 |
| BODY: | Renard 9 |
| DOWNHOLE (APPARENT) DEPTH: | 22.16 m |
| UNIT CODE: | Kimb9c |
| ROCK NAME: | opaques-carbonate kimberlite |

HAND SAMPLE DESCRIPTION: Dark greenish-gray macrocrystic hypabyssal kimberlite. Olivine macrocrysts are light-medium green ± black cores and fully altered to likely serpentine (F-VC) and some oblong macrocrysts indicate slight flow alignment. Fine-grained uniform carbonate-rich crystalline groundmass with tiny white segregations (groundmass reacts with HCl). Tiny orange to creamy beige specks visible in groundmass. Country rock xenoliths (<2%) are patchy white or pink with black and/or dark green alteration, up to ~2.5 cm (R-A) and partially to fully altered. Observed a few olivine macrocrysts with tiny inclusions and trace kelyphitic garnet xenocrysts. Patchy brown coloration along one end of core.

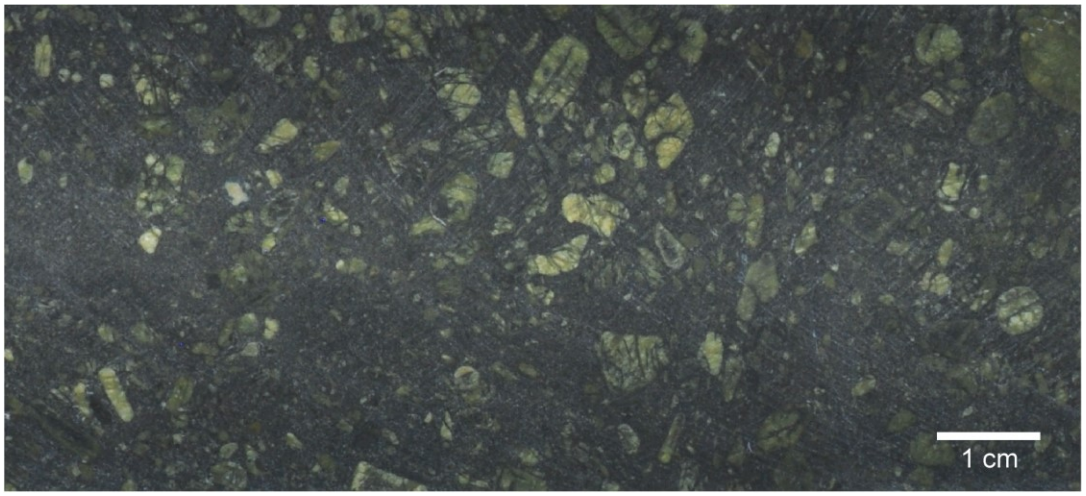

Photo (wet) of drill core sample 31462.

Photomicrograph of thin section for sample 31462 (PPL; carbon coated).

| | |
|---|---|
| SAMPLE ID: | 31468 |
| BODY: | Renard 9 |
| DOWNHOLE (APPARENT) DEPTH: | 70.08 m |
| UNIT CODE: | Kimb9b |
| ROCK NAME: | ? kimberlite |

HAND SAMPLE DESCRIPTION: Dark brown transitional hypabyssal kimberlite (HKt) with magmaclastic texture. Cored (olivine, CRX) and uncored lapilli range from distinct round to partial selvages to diffuse margins. Olivine macrocrysts are fully altered greenish-brown (hard to see) [F-C (VC)]. Combination of uniform crystalline groundmass (more abundant) and patchy light brown areas of alteration. Groundmass/matrix reacts strongly with HCl. Country rock xenoliths (~15%) range from variable white, pale pink, black with patchy medium-dark green alteration (e.g. partially altered) and smaller xenocrysts of creamy white ± green cores (sometimes reacts to HCl) or patchy dark green (fully altered), up to ~5 cm (A-SR). Dark brown biotite xenocrysts present. Adjacent kimberlite often looks patchy and altered (transitional) where CRX are not included within cored lapilli but this is not consistent as some CRX have unaltered adjacent crystalline groundmass. Observed one altered olivine macrocryst with two kelyphytic garnet inclusions within cored lapilli.

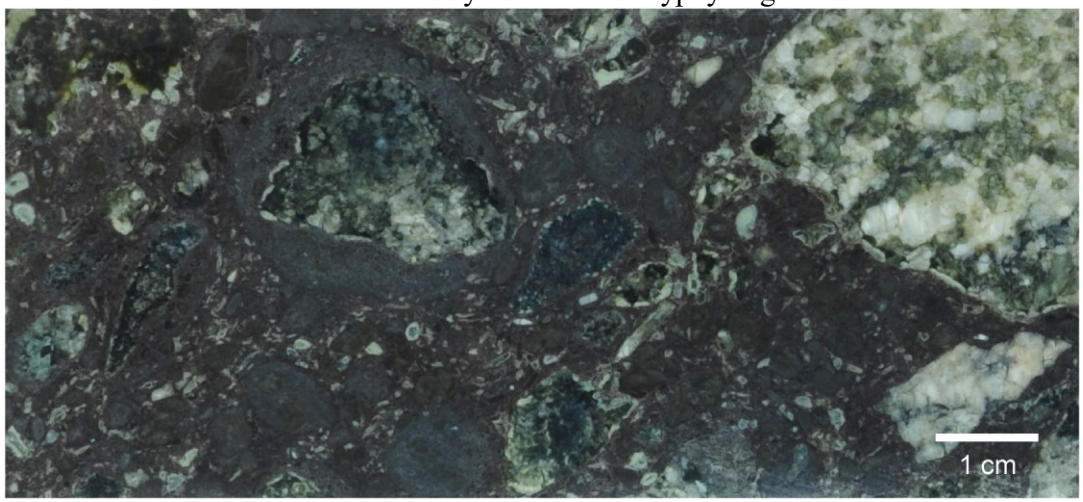


Photo (wet) of drill core sample 31468.

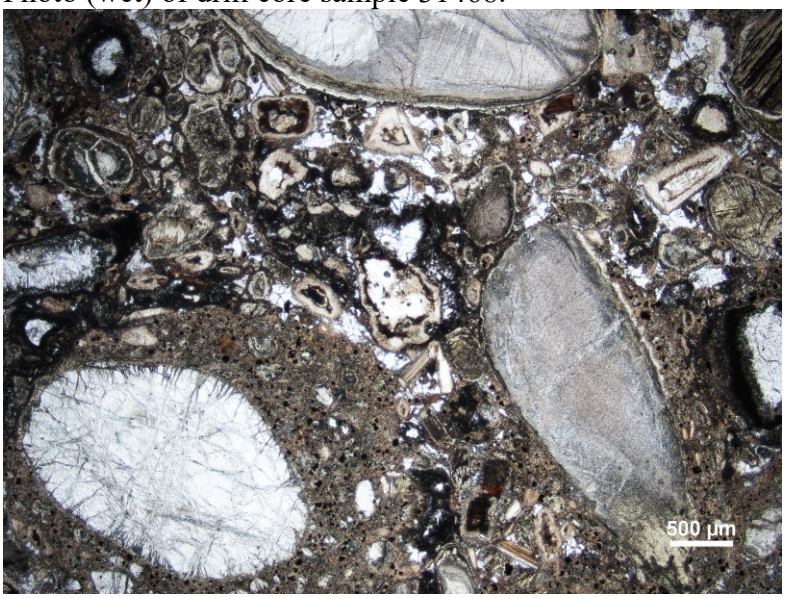


Photomicrograph of thin section for sample 31468 (PPL).

| | |
|---|---|
| SAMPLE ID: | 31497 |
| BODY: | Renard 9 |
| DOWNHOLE (APPARENT) DEPTH: | 153.02 m |
| UNIT CODE: | Kimb9c-1 |
| ROCK NAME: | carbonate kimberlite |

HAND SAMPLE DESCRIPTION: Dark grey-black macrocrystic hypabyssal kimberlite. Olivine macrocrysts are dark greenish brown ± clear/translucent areas in core (hard to see) and fully to partially altered to likely serpentine with fresh relict olivine [F-C (VC)]. Fine-grained uniform carbonate-rich crystalline groundmass (groundmass reacts with HCl) with possible serpentine. Country rock xenoliths (~5-10%) are white, greenish-white, or patchy white/brown (mica), up to ~5 cm (SA-SR) and fully to partially altered. Patchy brown alteration to the olivine macrocrysts throughout this sample, likely from alteration halos surrounding the country rock xenoliths. Trace white mineral, kelyphite and chromite xenocrysts observed. Thin white (reacts with HCl) ± dark green veinlets.

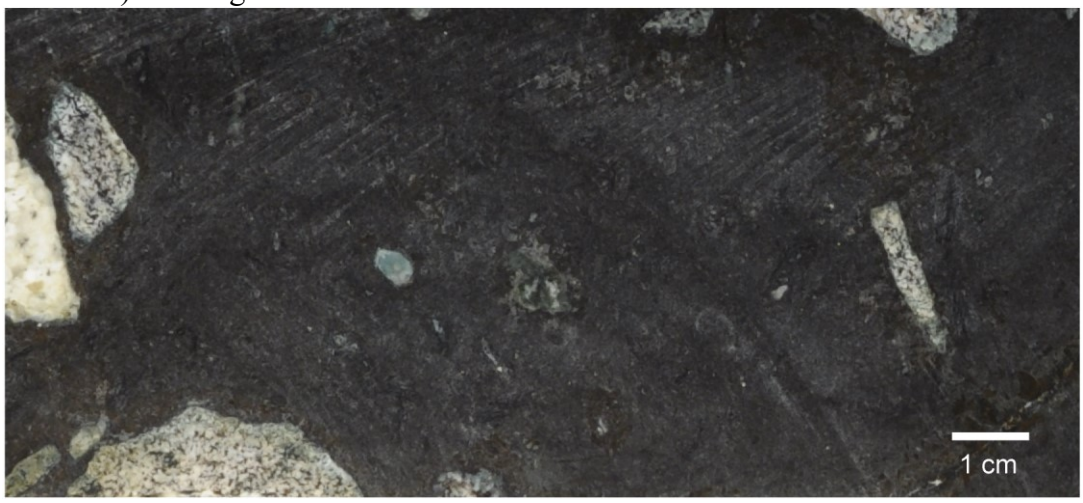

Photo (wet) of drill core sample 31497.

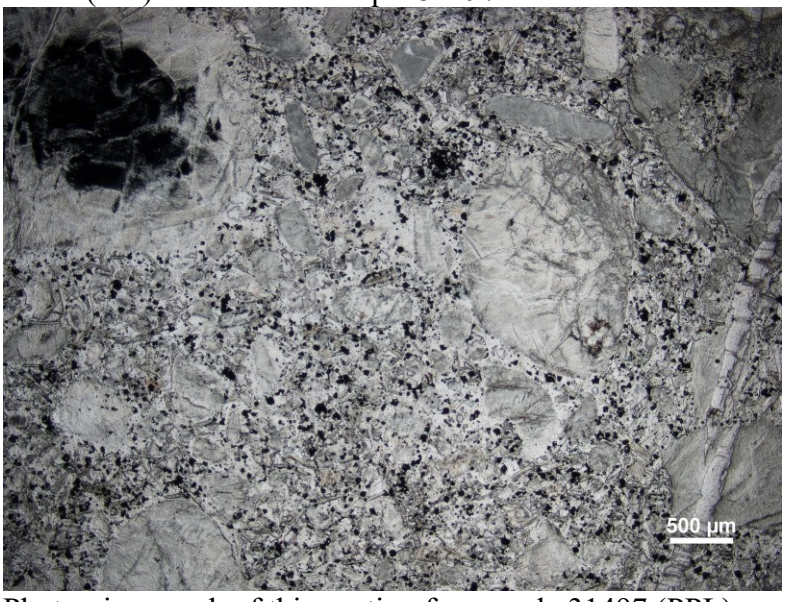

Photomicrograph of thin section for sample 31497 (PPL).

| | |
|---|---|
| SAMPLE ID: | 31577 |
| BODY: | G04-296 Anomaly |
| DOWNHOLE (APPARENT) DEPTH: | not applicable |
| UNIT CODE: | not applicable |
| ROCK NAME: | carbonate kimberlite |

HAND SAMPLE DESCRIPTION: Dark grey-black macrocrystic hypabyssal kimberlite. Olivine macrocrysts are black with few translucent areas and fully altered with possible fresh relicts but difficult to see in hand sample [F-C (VC)] and some macrocrysts appear flow aligned. Fine-grained uniform > segregationary carbonate-rich crystalline groundmass (groundmass reacts with HCl). Country rock xenoliths not obvious. One olivine macrocryst with garnet observed. Altered brown crust around outside of sample.

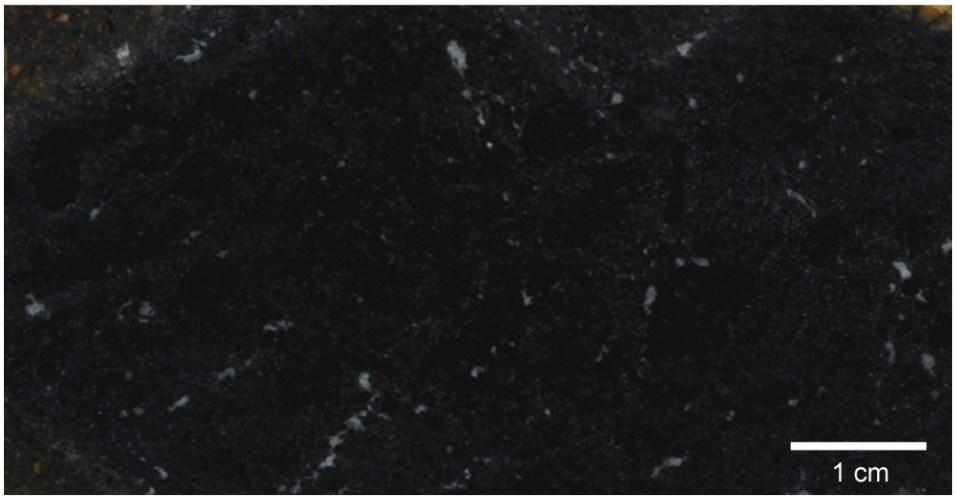

Photo (wet) of sample 31577.

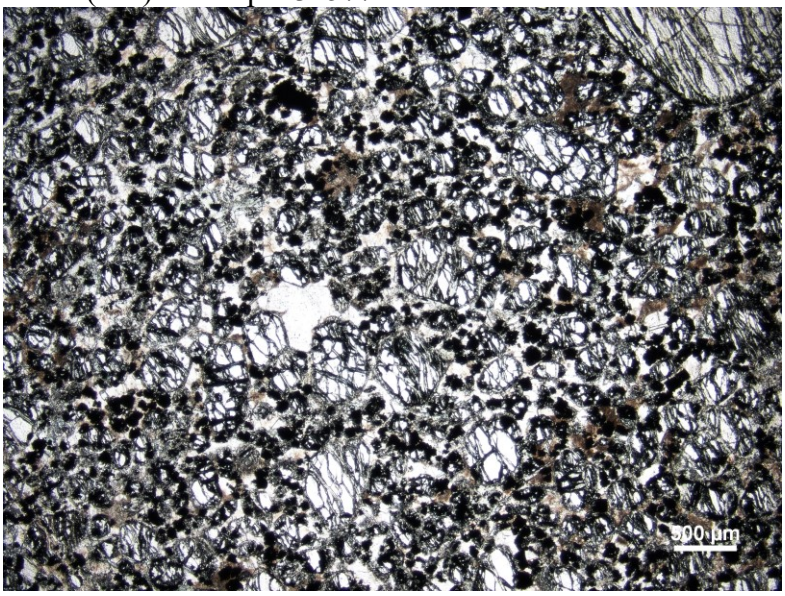

Photomicrograph of thin section for sample 31577 (PPL; carbon coated).

# APPENDIX B

# ID-TIMS U-Pb RESULTS FOR ICE RIVER PEROVSKITE (IR6) STANDARD

**Table 1.** ID-TIMS U-Pb results for Ice River perovskite (IR6) standard.

| Sample | Compositional parameters | | | | | | | Isotope ratios | | | | | | Isotopic date (Ma) | |
|---|---|---|---|---|---|---|---|---|---|---|---|---|---|---|---|
| | Weight | U | Th | Pb | $^{206}Pb^*$ | Pb* | $Pb_c$ | $\frac{^{238}U}{^{204}Pb}$ | ± | $\frac{^{206}Pb}{^{204}Pb}$ | ± | $\frac{^{206}Pb}{^{238}U}$ | ± | $\frac{^{206}Pb}{^{238}U}$ | ± |
| | (mg) | (ppm) | U | (ppm) | (mol %) | $Pb_c$ | (pg) | | (%) | | (%) | | (%) | | (2σ) |
| (a) | (b) | (c) | (d) | (c) | (e) | (e) | (e) | (i) | (g) | (i) | (g) | (f) | (g) | (h) | (g) |
| Ice River-4 | 0.069 | 106 | 24 | 46.8 | 92.1% | 25 | 124 | 3847.9 | 4.2 | 238.52 | 3.92 | 0.05721 | 0.31 | 358.6 | 1.1 |
| Ice River-5 | 0.061 | 104 | 24 | 45.9 | 91.6% | 23 | 114 | 3635.6 | 4.7 | 226.05 | 4.31 | 0.05712 | 0.33 | 358.1 | 1.1 |
| Ice River-8 | 0.046 | 101 | 22 | 42.2 | 91.5% | 22 | 85 | 3635.0 | 6.5 | 224.74 | 5.92 | 0.05678 | 1.17 | 356.0 | 4.0 |
| Ice River-9 | 0.061 | 136 | 2 | 13.5 | 92.5% | 5 | 133 | 4069.0 | 3.9 | 251.10 | 3.66 | 0.05726 | 0.19 | 359.0 | 0.7 |
| Ice River-10 | 0.048 | 137 | 7 | 24.1 | 92.6% | 10 | 103 | 4198.0 | 5.2 | 258.62 | 4.81 | 0.05728 | 0.27 | 359.0 | 1.0 |
| Ice River-11 | 0.046 | 93 | 23 | 39.3 | 91.5% | 22 | 79 | 3636.8 | 6.8 | 226.16 | 6.26 | 0.05714 | 0.31 | 358.2 | 1.1 |
| Ice River-12 | 0.009 | 129 | 21 | 48.8 | 90.1% | 17 | 24 | 3690.5 | 27.0 | 226.86 | 24.79 | 0.05650 | 0.29 | 354.3 | 1.0 |
| Ice River-13 | 0.006 | 124 | 24 | 52.7 | 89.2% | 17 | 17 | 3820.0 | 42.5 | 232.56 | 39.16 | 0.05607 | 0.37 | 351.7 | 1.3 |
| Ice River-14 | 0.013 | 104 | 25 | 45.9 | 90.0% | 19 | 28 | 3503.8 | 21.5 | 216.63 | 19.66 | 0.05659 | 0.33 | 354.8 | 1.1 |
| Ice River-15 | 0.010 | 85 | 24 | 36.4 | 90.1% | 19 | 18 | 4074.0 | 39.4 | 248.92 | 36.52 | 0.05658 | 0.36 | 354.8 | 1.2 |
| Ice River-38 | 0.023 | 102 | 24 | 42.4 | 89.3% | 17 | 54 | 2956.3 | 10.4 | 184.83 | 9.34 | 0.05632 | 0.72 | 353.2 | 2.5 |
| Ice River-39 | 0.020 | 103 | 23 | 43.1 | 90.9% | 20 | 41 | 3603.5 | 13.9 | 224.65 | 12.80 | 0.05725 | 0.37 | 358.9 | 1.3 |
| Ice River-40 | 0.026 | 127 | 11 | 30.3 | 92.5% | 14 | 54 | 4289.7 | 10.3 | 263.70 | 9.62 | 0.05722 | 0.41 | 358.7 | 1.4 |
| Ice River-41 | 0.022 | 102 | 24 | 44.6 | 91.9% | 24 | 39 | 4119.1 | 14.6 | 253.12 | 13.58 | 0.05698 | 0.36 | 357.2 | 1.3 |
| Ice River-43 | 0.019 | 118 | 13 | 31.8 | 93.1% | 18 | 32 | 5155.5 | 18.9 | 309.44 | 17.79 | 0.05647 | 0.34 | 354.1 | 1.2 |
| Ice River-44 | 0.023 | 125 | 12 | 30.6 | 93.0% | 16 | 41 | 4870.9 | 13.8 | 294.82 | 12.97 | 0.05678 | 0.30 | 356.0 | 1.1 |
| Ice River-45 | 0.018 | 124 | 11 | 30.5 | 92.3% | 14 | 38 | 4423.5 | 15.5 | 270.07 | 14.41 | 0.05693 | 0.32 | 356.9 | 1.1 |
| Ice River-46 | 0.019 | 133 | 10 | 28.5 | 93.1% | 14 | 37 | 4968.7 | 15.5 | 302.84 | 14.58 | 0.05728 | 0.31 | 359.1 | 1.1 |
| Ice River-47 | 0.008 | 104 | 25 | 46.4 | 90.9% | 22 | 16 | 4695.0 | 46.2 | 282.47 | 43.23 | 0.05623 | 0.37 | 352.7 | 1.3 |
| Ice River-48 | 0.020 | 99 | 24 | 44.2 | 88.9% | 17 | 48 | 2853.5 | 11.8 | 180.31 | 10.62 | 0.05677 | 0.36 | 355.9 | 1.3 |
| Ice River-49 | 0.013 | 134 | 2 | 12.4 | 92.0% | 4 | 30 | 4426.9 | 20.4 | 269.43 | 19.04 | 0.05677 | 0.34 | 356.0 | 1.2 |
| Ice River-50 | 0.007 | 112 | 10 | 25.3 | 86.8% | 7 | 22 | 2756.6 | 30.4 | 173.68 | 27.23 | 0.05640 | 0.42 | 353.7 | 1.5 |
| Ice River-51 | 0.019 | 105 | 21 | 41.2 | 90.9% | 19 | 39 | 3626.9 | 14.8 | 225.21 | 13.61 | 0.05704 | 0.41 | 357.6 | 1.4 |
| Ice River-52 | 0.022 | 116 | 15 | 34.1 | 92.3% | 17 | 42 | 4372.0 | 13.7 | 265.79 | 12.78 | 0.05661 | 0.35 | 355.0 | 1.2 |
| Ice River-53 | 0.005 | 85 | 27 | 39.3 | 89.9% | 20 | 9 | 6224.7 | 114.9 | 367.75 | 109.21 | 0.05609 | 0.63 | 351.8 | 2.2 |
| Ice River-54 | 0.030 | 123 | 11 | 29.6 | 93.5% | 17 | 51 | 5133.3 | 11.5 | 309.88 | 10.91 | 0.05681 | 0.41 | 356.2 | 1.4 |

(a) Single grain fractions of IR6 perovskite

(b) Each fraction weighed using a Mettler UMT2 ultramicrobalance

(c) Concentrations determined by isotope dilution (±1-2% 2 sigma)

(d) Model Th/U ratio calculated from radiogenic $^{208}Pb/^{206}Pb$ ratio and $^{206}Pb/^{238}U$ date

(e) Pb* and Pbc represent radiogenic and common Pb, respectively; mol % $^{206}Pb^*$ with respect to radiogenic, blank and initial common Pb

(f) Corrected for fractionation, spike, common Pb, and blank (5 pg Pb; 1 pg U). Blank IC: $^{206}Pb/^{204}Pb = 18.24±2.0\%$; $^{207}Pb/^{204}Pb = 15.64±2.0\%$; $^{208}Pb/^{204}Pb = 37.50±2.0\%$ (uncertainties 1-sigma). Excess over blank was assigned to initial common Pb

(g) Errors are 2-sigma, propagated using the algorithms of Schmitz and Schoene (2007)

(h) Calculations are based on the decay constants of Jaffey et al. (1971). $^{206}Pb/^{238}U$ dates corrected for initial disequilibrium in $^{230}Th/^{238}U$ using Th/U

(i) Corrected for fractionation, spike, and blank Pb only

Stacey and Kramers (1975) used to estimate initial common lead isotopic composition

# APPENDIX C

## SUPPLEMENTARY MATERIAL FOR CHAPTER 3

## Supplementary Material 1: Summary of ca. 780-530 Ma dates

**Table 1.** Summary of ca. 780-530 Ma dates from Canada, USA and west Greenland.

| Label | Occurrence | Rock Type | Date (Ma) | ± (Ma) | Method | Sampling Details | Reference |
|---|---|---|---|---|---|---|---|
| | ***West Greenland*** | | | | | | |
| SF | Sarfartoq | kimberlite dyke | 585.8 | 2.8 | U-Pb perovskite (concordia age) | 265849 | Tappe et al. (2012) |
| SF | Sarfartoq | kimberlite dyke | 566.0 | 3.6 | U-Pb perovskite (concordia age) | 444201 | Tappe et al. (2012) |
| SF | Sarfartoq | kimberlite dyke | 580.2 | 1.5 | U-Pb perovskite (wt avg concordia age) | 444206 | Tappe et al. (2012) |
| SF | Sarfartoq | kimberlite dyke | 570.9 | 1.9 | U-Pb perovskite (wt avg concordia age) | 444269 | Tappe et al. (2012) |
| SF | Sarfartoq | kimberlite dyke | 587.4 | 3.5 | U-Pb perovskite (concordia age) | 464611 | Tappe et al. (2012) |
| SF | Sarfartoq | kimberlite dyke | 584.9 | 1.7 | U-Pb perovskite (wt avg concordia age) | 464633 | Tappe et al. (2012) |
| SF | Sarfartoq | kimberlite dyke | 564.8 | 1.8 | U-Pb perovskite (wt avg concordia age) | 464645 | Tappe et al. (2012) |
| SF | Sarfartoq | kimberlite dyke | 561.9 | 3.0 | U-Pb perovskite (concordia age) | 472519 | Tappe et al. (2012) |
| SF | Sarfartoq | kimberlite dyke | 576.6 | 1.6 | U-Pb perovskite (wt avg concordia age) | 472522 | Tappe et al. (2012) |
| SF | Sarfartoq | kimberlite dyke | 577.9 | 1.6 | U-Pb perovskite (wt avg concordia age) | 477423 | Tappe et al. (2012) |
| SF | Sarfartoq | kimberlite dyke | 556.7 | 2.6 | U-Pb perovskite (wt avg concordia age) | 483815 | Tappe et al. (2012) |
| SF | Sarfartoq | kimberlite dyke | 579.8 | 2.8 | U-Pb perovskite (concordia age) | 491803 | Tappe et al. (2012) |
| SF | Sarfartoq | kimberlite dyke | 581.9 | 1.3 | U-Pb perovskite (wt avg concordia age) | 491807 | Tappe et al. (2012) |
| SF | Sarfartoq | kimberlite dyke | 580.6 | 3.5 | U-Pb perovskite (wt avg concordia age) | 491912 | Tappe et al. (2012) |
| SF | Sarfartoq | aillikite dyke | 577.2 | 4.8 | 206Pb/238U perovskite (1 fraction) | 444281 | Tappe et al. (2011) |
| SF | Sarfartoq | aillikite sheet | 578.7 | 3.8 | Rb-Sr phlogopite | 266511 | Tappe et al. (2011) |
| SF | Sarfartoq | carbonatite sheet | 572.8 | 3.8 | Rb-Sr phlogopite | 483828 | Tappe et al. (2011) |
| SF | Sarfartoq | carbonatite | 564.8 | 4.9 | Rb-Sr phlogopite | 483828 | Secher et al. (2009) |
| | Sarfartoq | carbonatite breccia | 572 | 11 | Rb-Sr phlogopite | 266511 | Secher et al. (2009) |
| | Sarfartoq | carbonatite | 560 | 13 | Rb-Sr phlogopite | 444227 | Secher et al. (2009) |
| SF | Sarfartoq (Garnet Lake) | kimberlite | 568 | 11 | 207Pb/206Pb perovskite (wt avg) | 05DS07-155b | Hutchison and Heaman (2008) |
| SF | Sarfartoq (Garnet Lake) | kimberlite | 566 | 5 | U-Pb perovskite (concordia) | | Frei et al. (2008) |

**Table 1.** Continued.

| Label | Occurrence | Rock Type | Date (Ma) | ± (Ma) | Method | Sampling Details | Reference |
|---|---|---|---|---|---|---|---|
| MN | Maniitsoq (Majuagaa) | kimberlite dyke | 558.5 | 1.2 | 206Pb/238U perovskite (wt avg) | 491720 | Tappe et al. (2011) |
| | Maniitsoq (~20km NW Majuagaa) | kimberlite dyke | 556.5 | 3.6 | Rb-Sr phlogopite | sample 483862 | Tappe et al. (2011) |
| | Maniitsoq (Majuagaa) | kimberlite dyke | 565.9 | 2.0 | U-Pb perovskite (1 fraction) | sample 491718 | Secher et al. (2009) |
| | Maniitsoq (Majuagaa) | kimberlite dyke | 561.8 | 1.2 | U-Pb perovskite (wt avg) | sample 491720 | Secher et al. (2009) |
| | Maniitsoq (Majuagaa) | kimberlite dyke | 555 | 15 | Rb-Sr phlogopite | sample 483862 | Secher et al. (2009) |
| | Umanak district (Qingussaq) | biotite lamprophyre dyke | 600 | 15 | K/Ar | GGU 24496 | Larsen and Moller (1968a) |
| | Umanak | lamprophyre-carbonatite intrusions | 600 | 15 | K/Ar | | Larsen and Moller (1968b) |
| | ***Torngat Mountains/Abloviak & Labrador Sea*** | | | | | | |
| T/A | Torngat Mountains | mela-aillikite dyke | 578.9 | 5.2 | 206Pb/238U perovskite (1 fraction) | Q15 | Tappe et al. (2008) |
| T/A | Torngat Mountains | aillikite dyke | 602.2 | 6.4 | 206Pb/238U perovskite (1 fraction) | Q24 | Tappe et al. (2008) |
| T/A | Torngat Mountains | aillikite dyke | 581.4 | 2.6 | 206Pb/238U perovskite (wt avg) | Q39 | Tappe et al. (2004, 2008) |
| | Torngat Mountains | aillikite dyke | 584 | 3.6 | 206Pb/238U perovskite (1 fraction) | Q39 | Tappe et al. (2004) |
| T/A | Abloviak | aillikite dyke | 550 | 10 | 40Ar/39Ar phlogopite | 3 samples | Digonnet et al. (2000) |
| | Torngat/Abloviak | kimberlitic dykes | 546 | 12 | Ar-Ar phlogopite | | Digonnet et al. (1996) |
| KI | Saglek (Killinek Island) | mela-aillikite dyke | 576.4 | 6.4 | 206Pb/238U perovskite (1 fraction) | ST266 | Tappe et al. (2008) |
| EH | Saglek (Eclipse Harbour) | mela-aillikite dyke | 578.2 | 2.4 | 206Pb/238U perovskite (1 fraction) | ST267 | Tappe et al. (2008) |
| S/H | Saglek (Saglek) | mela-aillikite dyke | 568.1 | 3.4 | 206Pb/238U perovskite (1 fraction) | ST264 | Tappe et al. (2008) |
| S/H | Saglek (Hebron) | mela-aillikite dyke | 606.0 | 3.6 | 206Pb/238U perovskite (1 fraction) | ST263 | Tappe et al. (2008) |
| AB | Aillik Bay | damtjernite dyke | 555.0 | 1.8 | 206Pb/238U perovskite (1 fraction) | ST211A (Main Turnavik Island) | Tappe et al. (2006) |
| AB | Aillik Bay | aillikite dyke | 562.2 | 1.9 | 206Pb/238U perovskite (wt avg) | ST123 | Tappe et al. (2006) |
| AB | Aillik Bay | damtjernite dyke | 563.9 | 2.5 | 206Pb/238U perovskite (1 fraction) | ST256 (Makkovik Bay east shore) | Tappe et al. (2006) |
| AB | Aillik Bay | mela-aillikite dyke | 569.2 | 1.8 | 206Pb/238U perovskite (1 fraction) | ST114A | Tappe et al. (2006) |
| AB | Aillik Bay | damtjernite dyke | 574.6 | 1.6 | 206Pb/238U perovskite (1 fraction) | ST174 (Pigeon Island) | Tappe et al. (2006) |
| AB | Aillik Bay | aillikite dyke | 576.4 | 6.5 | 206Pb/238U perovskite (wt avg) | ST228 | Tappe et al. (2006) |
| AB | Aillik Bay | damtjernite dyke | 581.9 | 2.3 | 206Pb/238U perovskite (wt avg) | ST140A (Aillik Bay east shore) | Tappe et al. (2006) |

**Table 1.** Continued.

| Label | Occurrence | Rock Type | Date (Ma) | ± (Ma) | Method | Sampling Details | Reference |
|---|---|---|---|---|---|---|---|
| AB | Aillik Bay | damtjernite dyke | 582.5 | 2.1 | 206Pb/238U perovskite (wt avg) | ST188A (Red Island) | Tappe et al. (2006) |
| AB | Aillik Bay | aillkite dyke | 589.6 | 1.3 | 206Pb/238U perovskite (wt avg) | ST220II | Tappe et al. (2006) |
| | ***Eastern Canada & USA*** | | | | | | |
| | Wemindji | macrocryst-dominated | 629 | 29 | Rb-Sr phlogopite | | Letendre et al. (2003) |
| | Lac Beaver | from hypabyssal pipe | 550.9 | 3.5 | U-Pb perovskite | | Moorhead et al. (2003) |
| | Amon sills | kimberlite | 673 | 11 | U-Pb rutile | | Tappe et al. (2014) |
| | **CIMP LIP and rift-related intrusions** | | | | | | |
| | Long Range dykes | olivine gabbro | 614 | +6-4 | U-Pb zircon and baddeleyite | southeast Labrador | Kamo and Gower (1994) |
| | Long Range dykes | mafic | 615 | 2 | U-Pb zircon and baddeleyite | southeast Labrador | Kamo et al. (1989) |
| | Grenville dyke swarm | diabase | 584.8 | 0.6 | 206Pb/238U baddeleyite (wt avg) | Augusta Lake (GD2) | Halls et al. (2015) |
| | Grenville dyke swarm | diabase | 585.2 | 0.8 | 206Pb/238U baddeleyite (wt avg) | Sand Bay (GD-29) | Halls et al. (2015) |
| | Grenville dyke swarm | diabase | 587.3 | 0.7 | 206Pb/238U baddeleyite (wt avg) | Key River (GD15) | Halls et al. (2015) |
| | Grenville dyke swarm | diabase | >579 | | U-Pb baddeleyite | Mattawa | Halls et al. (2015) |
| | Grenville dyke swarm | diabase | 596.9 | 3.4 | U-Pb baddeleyite | French River | Halls et al. (2015) |
| | Grenville dyke swarm | diabase | 590 | +2-1 | U-Pb baddeleyite and zircon | composite from three dykes | Kamo et al. (1995) |
| | Adirondack dykes (Rand Hill dikes) | diabase, olivine diabase | 588-542 | | K/Ar | see page 217 for more reference/details (diabase and olivine diabase) | Isachsen et al. (1988) |
| | Rand Hill dikes (Northeast Adirondacks) | pitted olivine diabase | 528 | 11 | K/Ar whole rock | RH-23-77 | Geraghty et al. (1979) |
| | Rand Hill dikes (Northeast Adirondacks) | pitted olivine diabase | 530 | 11 | K/Ar whole rock | RH-22-77 | Geraghty et al. (1979) |
| | Rand Hill dikes (Northeast Adirondacks) | pitted olivine diabase | 555 | 11 | K/Ar whole rock | RH-16-77 | Geraghty et al. (1979) |
| | Rand Hill dikes (Northeast Adirondacks) | pitted olivine diabase | 578 | 12 | K/Ar whole rock | RH-20-77 | Geraghty et al. (1979) |
| | Rand Hill dikes (Northeast Adirondacks) | diabase (basalt or andesite) | 536 | 11 | K/Ar whole rock | RH-24-77 | Geraghty et al. (1979) |
| | Adirondack dykes (Rand Hill dikes) | alkalic dyke | 624 | 2 | U-Pb zircon | | Hodych and Bennett (2009) |
| SC | Skinner Cove Formation | ankaramite | 550 | 5 | 206Pb/238U zircon (wt mean) | Newfoundland | Hodych et al. (2004) |
| SC | Skinner Cove Formation | trachyte | 556 | 5 | 206Pb/238U zircon (wt mean) | Newfoundland | Hodych et al. (2004) |
| SC | Skinner Cove Formation | ankaramite flow | 550.5 | +3-2 | U-Pb zircon | Humber Arm allochthon (W Newfoundland) | Cawood et al. (2001) |
| SC | Skinner Cove Formation | ankaramite flow | 550.5 | +3-2 | U-Pb zircon | Humber Arm allochthon (W Newfoundland) | McCausland et al. (1997) |
| | Sept Iles Layered Mafic Intrusion | gabbro | 565 | 4 | U-Pb zircon | Quebec | Higgins and van Breemen (1998) |
| MSA | Mt. St.-Anselme volcanics | basalt flow | 550 | 7 | 206Pb/238U zircon (wt mean) | | Hodych and Cox (2007) |
| LM | Lac Matapedia volcanics | basalt flow | 565 | 6 | 206Pb/238U zircon (wt mean) | | Hodych and Cox (2007) |
| LM | Lac Matapedia volcanics | basalt flow | 556 | 5 | 206Pb/238U zircon (wt mean) | | Hodych and Cox (2007) |

**Table 1.** Continued.

| Label | Occurrence | Rock Type | Date (Ma) | ± (Ma) | Method | Sampling Details | Reference |
|---|---|---|---|---|---|---|---|
| | Tibbit Hill Formation | metafelsites | 554 | +4-2 | U-Pb zircon | Waterloo area (Quebec) (W-O6) | Kumarapeli et al. (1989) |
| CT | Shenandoah Massif (Catoctin Formation) | metarhyolite | 562 | 5 | U-Pb zircon | Pennsylvania | Southworth and Aleinikoff (2007) |
| CT | Shenandoah Massif (Catoctin Formation) | metarhyolite | 564 | 9 | U-Pb zircon | Pennsylvania (SM-10-89 (sample 1)) | Aleinikoff et al. (1995) |
| CT | Shenandoah Massif (Hypabyssal felsic dike (Catoctin)) | felsic dike | 572 | 5 | U-Pb zircon | Virginia (BR-38-90 (sample 3)) | Aleinikoff et al. (1995) |
| CT | Shenandoah Massif (Catoctin Formation) | felsic tuffs | 571-563 | | U-Pb zircon | | Southworth et al. (2009b) |
| CT | Catoctin Formation | felsic tuffs | 571-563 | | U-Pb zircon | | Southworth et al. (2010) |
| RP | Round Pond granite | granite | 602 | 10 | U-Pb zircon | Newfoundland | Williams et al. (1985) |
| LS | Lady Slipper pluton | tonalitic gneiss | 555 | +3-5 | U-Pb zircon (lower intercept) | Humber Arm allochthon (W Newfoundland) | Cawood et al. (1996) |
| H/D | Hare Hill | leucogranite | 608 | 4 | U-Pb zircon | Newfoundland | Currie et al. (1992) |
| H/D | Disappointment Hill Complex | tonalite pluton | 606.3 | 1.5 | U-Pb zircon | internal Humber Zone (Newfoundland) | Brem et al. (2005) |
| | Blair River inlier | metagabbroic dike 1 | 581 | 6 | U-Pb zircon | northern Cape Breton Island (Nova Scotia) (SMB98-7) | Miller and Barr (2004) |
| | Blair River inlier | metagabbroic dike 2 | 576 | 6 | U-Pb zircon | northern Cape Breton Island (Nova Scotia) (SMB98-8) | Miller and Barr (2004) |
| SS | St Simeon mafic dolerite dykes (Quebec) | dolerite | 548 | 1 | U-Pb baddeleyite | | Pisarevsky et al. (2013) |
| BK | Buckingham Lavas | aphanitic trachyandesite | 573 | 32 | K-Ar whole rock | see Table 3 | Lafleur and Hogarth (1981) |
| PH | Pinney Hollow Formation | metafelsite | 571 | 5 | U-Pb zircon | Central Vermont | Walsh and Aleinikoff (1999) |
| YG | Yonkers Gneiss | gneissic granitoid | 563 | 2 | U-Pb zircon | southeast New York (YG91-2) | Tollo et al. (2004) |
| PR | Pound Ridge Granite Gneiss | granitoid | 562 | 5 | U-Pb zircon | southeast New York (PR90-1) | Tollo et al. (2004) |
| RG | Reading Prong dyke | felsite | 602.3 | 2 | U-Pb zircon | Pennsylvania | Smith (2003) |
| | Shenandoah Massif (Dillons Mill Pluton) | granite | 695 | 16 | 206Pb/238U zircon (avg) | MF-02-3 | Fokin (2003) |
| | Shenandoah Massif (White Oak Creek Pluton) | biotite granite | 745 | 9 | 206Pb/238U zircon (avg) | QCY-863 | Fokin (2003) |
| | Shenandoah Massif (Stewartsville Pluton) | biotite granite | 666 | 10 | 206Pb/238U zircon (avg) | MF-02-1, sville-1 | Fokin (2003) |
| | Shenandoah Massif (Suck Mountain Pluton) | granite | 727 | 20 | 206Pb/238U zircon (avg) | SM-5-95, SM-16-95 | Fokin (2003) |
| | Shenandoah Massif (Mobley Mountain Pluton) | biotite granite | 653 | 19 | 206Pb/238U zircon (avg) | CL-12-95 | Fokin (2003) |
| | Shenandoah Massif (Rockfish River Pluton) | granodiorite | 680 | 9 | 206Pb/238U zircon (avg) | JR-75-19 | Fokin (2003) |
| | Shenandoah Massif (Robertson River (Amissville Pluton)) | granite | 745 | 9 | 206Pb/238U zircon (avg) | R-4-95 | Fokin (2003) |
| | Shenandoah Massif (Robertson River (Quartz trachyte)) | Quartz trachyte | 714 | 5 | SHRIMP | Sample 4 | Southworth et al. (2009a) |
| | Shenandoah Massif (Robertson River (Quartz trachyte)) | Quartz trachyte | 719 | 6 | SHRIMP | Sample 5 | Southworth et al. (2009a) |
| | Shenandoah Massif (Robertson River (volcanics)) | | 719-714 | | unclear | | Southworth et al. (2009b) |
| | Shenandoah Massif (Robertson River Igneous Suite) | volcanic | 719-714 | | U-Pb zircon | | Southworth et al. (2010) |

**Table 1.** Continued.

| Label | Occurrence | Rock Type | Date (Ma) | ± (Ma) | Method | Sampling Details | Reference |
|---|---|---|---|---|---|---|---|
| | Shenandoah Massif (Robertson River (Rivanna)) | granite | 735 | 4 | U-Pb zircon | RR90-102 | Tollo and Aleinikoff (1996) |
| | Shenandoah Massif (Robertson River (Hitt Mountain)) | alkali feldspar syenite | 706 | 2 | U-Pb zircon | RR90-98 | Tollo and Aleinikoff (1996) |
| | Shenandoah Massif (Robertson River (White Oak)) | alkali feldspar granite | 724 | 3 | U-Pb zircon | RR90-53 | Tollo and Aleinikoff (1996) |
| | Shenandoah Massif (Robertson River (Arrington Mountain)) | alkali feldspar granite | 730 | 4 | U-Pb zircon | RR90-63 | Tollo and Aleinikoff (1996) |
| | Shenandoah Massif (Robertson River (Battle Mountain)) | alkali feldspar granite | 705 | 2 | U-Pb zircon | RRDH-5 | Tollo and Aleinikoff (1996) |
| | Shenandoah Massif (Robertson River (Battle Mountain)) | felsite | ~702 | | U-Pb zircon | RR 85-22 | Tollo and Aleinikoff (1996) |
| | Shenandoah Massif (Robertson River (Laurel Mills)) | granite | 729 | 1 | U-Pb zircon | RR 85-24 | Tollo and Aleinikoff (1996) |
| | Shenandoah Massif (Robertson River (Cobbler Mountain)) | alkali feldspar quartz syenite | 722 | 3 | U-Pb zircon | RRSA-74 | Tollo and Aleinikoff (1996) |
| | Shenandoah Massif (Suck Mountain) | biotite granite | 680 | 4 | 207Pb/206Pb zircon (wt avg, SHRIMP) | SM92-28 | Tollo et al. (2004) |
| | Shenandoah Massif (Polly Wright Cove) | biotite granite | 706 | 4 | U-Pb zircon | PWC-5 | Tollo et al. (2004) |
| | French Broad Massif (Bakersville dike swarm) | Metadiabase | 734 | 26 | Rb–Sr whole rock | | Goldberg et al. (1986) |
| | French Broad Massif (Bakersville dike swarm) | metagabbro dikes | 759 | 7 | not reported | | Aleinikoff (unpub data 2012) cited in Tollo et al. (2012) |
| | French Broad Massif (Bakersville dike swarm) | metagabbro dikes | 757 | 5 | not reported | | Aleinikoff (unpub data 2012) cited in Tollo et al. (2012) |
| | French Broad Massif (Mount Rogers Formation; Wilburn member) | | 749.7 | 3.1 | U-Pb zircon CA-TIMS | WS-04-78 | Tollo et al. (2012) |
| | French Broad Massif (Mount Rogers Formation; Whitetop member) | | 753.3 | 2.0 | U-Pb zircon CA-TIMS | MR-06-39 | Tollo et al. (2012) |
| | French Broad Massif (Mount Rogers Formation; Buzzard Rock member) | | 755.0 | 6.6 | U-Pb zircon CA-TIMS | MR-06-37 | Tollo et al. (2012) |
| | French Broad Massif (Mount Rogers Formation; Fees member) | | 753.1 | 2.7 | U-Pb zircon CA-TIMS | MWC-05-37 | Tollo et al. (2012) |
| | French Broad Massif (Mount Rogers Formation) | metarhyolite (Whitetop Rhyolite Member) | 758 | 12 | U-Pb zircon | 2 samples, WS2-83-50, WS4-83-75; Whitetop Rhyolite Member | Aleinikoff et al. (1995) |
| | French Broad Massif (Striped Rock Granite Pluton) | granite | 748 | 11 | U-Pb zircon | RE-90-7 | Essex (1992) |
| | French Broad Massif (Brown Mountain metagranite) | metagranite | 765 | 7 | U-Pb zircon | | Fetter and Goldberg (1995) |

**Table 1.** Continued.

| Label | Occurrence | Rock Type | Date (Ma) | ± (Ma) | Method | Sampling Details | Reference |
|---|---|---|---|---|---|---|---|
| | French Broad Massif (Grandfather Mountain Formation) | metarhyolite | 742 | 2 | U-Pb zircon | | Fetter and Goldberg (1995) |
| | French Broad Massif (Meadlock Mountain) | orthogneiss | 728 | 16 | 206Pb/238U zircon (wt mean) | CAR 1501 | Ownby et al. (2004) |
| | French Broad Massif (Beech Pluton) | metagranite | 745 | 6 | U-Pb zircon | BG3 | Su et al. (1994) |
| | French Broad Massif (Crossnore Pluton) | metagranite | 754 | 5 | U-Pb zircon (lower intercept) | C1, maximum age | Su et al. (1994) |
| | French Broad Massif (Lansing Pluton) | metagranite | 739 | 4 | U-Pb zircon | L5 | Su et al. (1994) |
| | French Broad Massif (Warrensville Pluton) | metagranite | 740 | 8 | U-Pb zircon | W4 | Su et al. (1994) |
| | Pink Beds pluton (Blue Ridge) | | 670 | 80 | 207Pb/206Pb zircon | A13; detrital zircon core (Pb loss) | Miller et al. (2000) |
| | Pink Beds pluton (Blue Ridge) | | 720 | 40 | 206Pb/238U zircon | A13; detrital zircon core (~true age) | Miller et al. (2000) |
| | Chilhowee group (Blue Ridge) | | 760 peak | | U-Pb zircon SHRIMP | detrital zircon | Holm-Denoma et al. (2012) |
| | Chilhowee group (Blue Ridge) | | 780-770, 764-756, 755-748 populations | | U-Pb zircon | detrital zircon | Holm-Denoma et al. (2015) |
| | Blue Ridge | | 788±26 to 540±22 | | U-Pb zircon | detrital zircon | Southworth et al. (2011) |
| | **Alkaline and/or carbonatite intrusions** | | | | | | |
| BM | Baie des Moutons syenite complex | red syenite, red feldspar dyke, green syenite | 583.4 | 2 | 40Ar-39Ar hornblende | 3 samples (MB20, MB36, MB44) | McCausland et al. (2011) |
| BM | Mutton Bay carbonatites and syenite | carbonatite dyke, syenite pluton | 568 | 8 | K-Ar | along coast near Labrador | Doig and Barton (1968) |
| StH | St Honoré carbonatite | carbonatite intrusion | 571 | 4.6 | Ar-Ar phlogopite | Quebec | McCausland et al. (2009) |
| StH | St Honoré carbonatite complex | | 564 | 4 | K/Ar | | Kumarapeli (1977) |
| CH | Chicoutimi carbonatites (Arvida) | | 564 | 4 | K-Ar | near St Lawrence river | Doig and Barton (1968) |
| | Burritt Island | | NA | | NA | | Currie (1976) |
| | Iron Island | | NA | | NA | | Currie (1976) |
| | Iron Island complex | | NA | | NA | | Gartzos (1977) |
| MI | Manitou Island | | 565 | 4 | K/Ar | Ontario | Kumarapeli (1977) |
| MI | Manitou Island | fenite zone | 569 | | K-Ar biotite | Ontario | Currie (1976) |
| MI | Manitou Island (Newman Island) | | 570 | | K-Ar biotite | Newmans Island (Ontario) | Gittins et al. (1967) |
| MI | Manitou Island (Newman Island) | carbonatite | 560 | | K-Ar biotite | Newman Island, Ontario (GSC 61-160) | Lowden et al. (1963) |
| MI | Manitou Island | apatite-magnetite-biotite-pyroxene sovite and pyroxene-biotite-apatite silicocarbonatite | 585 | 19 | U-Pb zircon | C-6, NI-PYR | Rukhov and Bell (2010) |
| MI | Manitou Island | apatite-magnetite-biotite-pyroxene sovite and pyroxene-biotite-apatite silicocarbonatite | 568 | 24 | Pb-Pb isochron zircon | C-6, NI-PYR, R-4DYKE | Rukhov and Bell (2010) |
| BC | Brent Crater (nearby alkaline dykes) | | 558-676 | | K/Ar | | Kumarapeli (1977) |
| BC | Brent crater | alnoite (vein, sill, fragment?) | 576 | 40 | K/Ar | Ontario (sample 3) | Shafiqullah et al. (1968) |
| CC | Callander complex | nepheline syenite | 577 | 1 | U-Pb zircon | | Kamo et al (1995) (cited as unpublished data) |
| CC | Callander alkaline complex | | 575 | 5 | U-Pb zircon | Ontario | Symons and Chiasson (1991) |

**Table 1.** Continued.

| Label | Occurrence | Rock Type | Date (Ma) | ± (Ma) | Method | Sampling Details | Reference |
|---|---|---|---|---|---|---|---|
| CC | Callander Bay | lamprophyre | 550 | 4 | Pb-Pb isochron (sphene, anatase, brookite, apatite, rutile) | | Kamo et al. (1989) |
| CC | Callander Bay | lamprophyre | 576 | 3 | Pb-Pb isochron (sphene, anatase, brookite, apatite, rutile) | | Symons and Chiasson (1991) |
| CC | Callander Bay | lamprophyre | 568 | | K-Ar biotite | Ontario | Currie (1976) |
| CC | Callander Bay | nepheline syenite | 575 | | K-Ar biotite | | Currie (1976) |
| CC | Callander Bay complex | two lamprophyre dykes | 558 | 14 | K-Ar | | Ferguson and Currie (1972) |
| CG | Chatham-Grenville stock | granite and syenite | 531.4 | 3.4 | 40Ar-39Ar hornblende | Quebec (sides MR10, CG31, CG14) | McCausland et al. (2007) |
| MR | Mont Rigaud | hornblende syenite | 533.2 | 1.1 | 40Ar-39Ar hornblende | Quebec (site 10) | McCausland et al. (2007) |
| MR | Mont Rigaud stock | syenite | 556 | +15-12 | U-Pb zircon | Quebec (MR94-2) | Malka et al. (2000) |
| MR | Mont Rigaud stock | granite | 564 | +10-8 | U-Pb zircon | Quebec (MR94-17) | Malka et al. (2000) |
| | ***Western Canada & USA*** | | | | | | |
| | Chicken Park | kimberlite type not reported | 614.5 | 2.1 | 206Pb/238U perovskite (wt avg) | | Heaman et al. (2003) |
| | Chicken Park dike | unclear (possibly hypabyssal kimberlite) | 640-620 | | 40Ar/39Ar phlogopite | fine-grained matrix phlogopite | Lester et al. (2001) |
| | Chicken Park dike | kimberlite type not reported | ~700 | | Rb-Sr whole rock | six-point isochron | McCallum (pers comm 1996) cited in Lester et al. (2001) |
| | George Creek | kimberlite dykes | ~600 | | Rb-Sr | weathered surficial samples | Carlson and Marsh (1989) |
| | Green Mountain diatreme | kimberlite type not reported | 800-500 | | 40Ar/39Ar | phlogopite megacrysts from kimberlite, granodiorite xenolith mineral separates (biotite, hornblende) | Lester et al. (2001) |
| | Green Mountain diatreme | kimberlite type not reported | 572 | 49 | Sm-Nd isochron (clinopyroxene and pyrope garnet megacrysts; whole rock) | includes whole rock data from Alibert and Albarade (1988) | Lester et al. (2001) |
| | Gahcho Kué cluster (AK5034, Kennady Lake cluster) | kimberlite type not reported | 542.2 | 2.6 | Rb-Sr phlogopite | | Heaman et al. (2003) |
| | Gahcho Kué cluster (Tuzo, Tesla, Hearne) | kimberlite type not reported | 542 | 6 | Ar-Ar phlogopite | | Hetman et al. (2004) |
| | Gahcho Kué cluster (Tuzo, Tesla, Hearne) | kimberlite type not reported | 531 | 6 | Ar-Ar phlogopite | | Hetman et al. (2004) |
| | Gahcho Kué cluster (Tuzo, Tesla, Hearne) | kimberlite type not reported | 534 | 11 | Ar-Ar phlogopite | | Hetman et al. (2004) |
| | Snap Lake | kimberlite dyke | 522.9 | 6.9 | Rb-Sr phlogopite | | Hetman et al. (2004) |
| | Snap Lake | kimberlite dyke | 537 | 11 | Rb-Sr phlogopite | SL6 | Agashev et al. (2008) |
| | Pelly Bay Diamond District | kimberlite type not reported | ~540 | | Rb-Sr phlogopite | | Kienlen et al. (2008) |
| | Aviat | kimberlite type not reported | ~560-500 | | not reported | | Armstrong et al. (2008) |
| | Aviat | hypabyssal kimberlite | 532.6 | 3.8 | 206Pb/238U perovskite (single fraction) | AV1 | Sarkar et al. (2018) |
| | Aviat | hypabyssal kimberlite | 537.7 | 4.2 | 206Pb/238U perovskite (single fraction) | AV4 | Sarkar et al. (2018) |

**Table 1.** Continued.

| Label | Occurrence | Rock Type | Date (Ma) | ± (Ma) | Method | Sampling Details | Reference |
|---|---|---|---|---|---|---|---|
| | Qilalugaq field | kimberlite type not reported | 546 | | not reported | | Kupsch and Armstrong (2013) |
| | Qilaugaq | kimberlite type not reported | 545.5 | 3.8 | 206Pb/238U perovskite (single fraction) | A61 (Q1-4 pipe) | Sarkar et al. (2018) |
| | Qilaugaq | kimberlite type not reported | 536.3 | 3.4 | 206Pb/238U perovskite (single fraction) | A88 (Q1-4 pipe) | Sarkar et al. (2018) |
| | Qilaugaq | kimberlite type not reported | 530.6 | 5.8 | 206Pb/238U perovskite (single fraction) | A94 | Sarkar et al. (2018) |
| | Darby | kimberlite type not reported | 542.2 | 2.6 | Rb-Sr phlogopite | drill core | Harris et al. (2018) |
| | Anuri | volcaniclastic kimberlite | 613 | 6 | Rb-Sr phlogopite | single phlogopite macrocryst | Masun et al. (2004) |
| | Gunbarrel magmatic event | 8 mafic sheets | 780.3 | 1.4 | U-Pb baddeleyite (composite concordia) | | Harlan et al. (2003) |
| | NW Canadian Shield, Tsezotene Formation (Mackenzie Mountains), Tuchodi Formation (Muskwa Range) | gabbro, gabbro sill, diabase dyke | 779 | 2 | U-Pb baddeleyite | 4 samples | LeCheminant and Heaman (1994) |
| | Little Dal Basalts | diabase | 778.4 | 1.8 | 207Pb/206Pb zircon (weighted mean CA-ID-TIMS) | JM0132 | Milton et al. (2017) |
| | Little Dal Basalts | diabase | 775.1 | 0.54 | 206Pb/238U zircon (weighted mean CA-ID-TIMS) | JM0132 | Milton et al. (2017) |
| | Franklin igneous event | gabbro sills, diabase dykes | 723 | +4-2 | U-Pb baddeleyite (composite concordia) | 6 samples | Heaman et al. (1992) |
| | Victoria Island (Lower Sill) | gabbro sills | 718 | 2 | U-Pb baddeleyite & zircon (concordia) | | Heaman et al. (1992) |
| | Clarence Head dykes (Clarence Head) | diabase | 716 | 1 | 206Pb/238U baddeleyite (wt avg) | CL-2 | Denyszyn et al. (2009a) |
| | Clarence Head dykes (Craig Harbour) | diabase | 713 | 2 | 206Pb/238U baddeleyite (wt avg) | CH-1 | Denyszyn et al. (2009a) |
| | Clarence Head dykes (Cape Faraday) | diabase | 713 | 3 | 206Pb/238U baddeleyite (wt avg) | CF-1 | Denyszyn et al. (2009a) |
| | Ellesmere Island (Cadogan Glacier dyke) | diabase | 721 | 2 | 206Pb/238U baddeleyite (avg) | | Denyszyn et al. (2009b) |
| | Greenland (Qaanaaq dyke) | diabase | 721 | 4 | 206Pb/238U baddeleyite (avg) | | Denyszyn et al. (2009b) |
| | Devon Island (Belcher Glacier dyke) | diabase | 726 | 24 | 207Pb/206Pb baddeleyite (avg) | | Denyszyn et al. (2009b) |
| | Greenland (Granville Fjord sill (Thule sill)) | diabase | 712 | 2 | 206Pb/238U baddeleyite (avg) | | Denyszyn et al. (2009b) |
| | Victoria Island | diabase sill | 716.33 | 0.54 | 206Pb/238U baddeleyite (wt mean) | S8 | Macdonald et al. (2010) |
| | Baffin Island (Borden dykes) | diabase | 720 | 8 | 206Pb/238U baddeleyite | FA-790810, fraction C, minimum age | Pehrsson and Buchan (1999) |
| | Baffin Island (Borden dykes) | diabase | 716 | +4-5 | 206Pb/238U baddeleyite (wt avg) | FA-790609, minimum age | Pehrsson and Buchan (1999) |

**Table 1.** Continued.

| Label | Occurrence | Rock Type | Date (Ma) | ± (Ma) | Method | Sampling Details | Reference |
|---|---|---|---|---|---|---|---|
| | ***Rockall and North Scotland*** | | | | | | |
| | Mam sill | | 625 | 47 | Sm-Nd isochron (plagioclase, augite, whole rock) | | Kirwan et al. (1989) |
| | ***Scandinavia*** | | | | | | |
| | **Igneous Provinces** | | | | | | |
| | Volyn (Ratne basalt) | high-Ti basalt | 573 | 14 | 206Pb/238U zircon (wt avg) | | Shumlyanskyy et al. (2016) |
| | Volyn (Ivanchi) | basalt | 561 | 14 | Ar-Ar whole rock (plateau) | Site 1 Upper basalt, U118.00 | Elming et al. (2007) |
| | Volyn (Rafalovka) | basalt | 580 | 9 | Ar-Ar whole rock (plateau) | Site 2, U99.97 | Elming et al. (2007) |
| | Volyn (Basaltovoe) | basalt | 593 | 5 | Ar-Ar whole rock (plateau) | Site 4, U144.96 | Elming et al. (2007) |
| | Volyn (Basaltovoe) | basalt | 582 | 7 | Ar-Ar whole rock (plateau) | Site 4, U145.96 | Elming et al. (2007) |
| | Volyn | rhyolitic dacite | 571 | 13 | 206Pb/238U zircon (wt avg) | date in abstract and Fig 4 (3 analyses) | Shumlyanskyy et al. (2016) |
| | Volyn | rhyolitic dacite | 567 | 11 | 206Pb/238U zircon (wt avg) | date in text (4 of 5 grains) | Shumlyanskyy et al. (2016) |
| | Volyn | olivine dolerite | 626 | 17 | 206Pb/238U baddeleyite (wt avg) | same sample as ca 567 Ma date | Shumlyanskyy et al. (2016) |
| | Volyn | olivine dolerite | 567 | 61 | 207Pb/206Pb baddeleyite (wt avg) | same sample as ca 626 Ma date | Shumlyanskyy et al. (2016) |
| | Volhynian Series basalts | basalt | 590-560 | | K/Ar and Ar/Ar whole rock | | Bakun-Czubarow et al. (2008) |
| | Volhynian (Cryogean dolerites) | | 640 and 750 | | K/Ar whole rock | | Bakun-Czubarow et al. (2008) |
| | Volyn region | basalt | 549 | 29 | 207Pb/206Pb zircon | | Shumlyansky and Nosova (2008) |
| | Volyn | | 576 | 14 | U-Pb zircon NORD-SIM | 4 zircon crystals (concordant) | Shumlyanskyy and Andreasson (2004) |
| | Volyn | | 514 | 8 | U-Pb zircon NORD-SIM | 4 zircon crystals (nearly concordant) | Shumlyanskyy and Andreasson (2004) |
| | Slawatycze Formation tuffs (Kaplonsy drill core) | | 551 | 4 | U-Pb zircon | PL-92-77 | Compston et al. (1995) |
| | Slawatycze Formation tuffs (Kaplonsy drill core) | | 588 | 8 | U-Pb zircon | PL-92-77 | Compston et al. (1995) |
| | Slawatycze Formation tuffs (Kaplonsy drill core) | | 635 | 10 | U-Pb zircon | PL-92-77 | Compston et al. (1995) |
| | Seiland Igneous Province (Soroy) | | 577 | 21 | U-Pb zircon | | Roberts et al. (2004) |
| | Seiland Igneous Province (Soroy) | | 567 | 4 | U-Pb zircon | | Roberts et al. (2004) |
| | Seiland Igneous Province (Soroy) | | 554 | 6 | U-Pb zircon | | Roberts et al. (2004) |
| | Seiland Igneous Province (Oksfjord) | | 566 | 1 | U-Pb zircon | | Roberts et al. (2004) |
| | Seiland Igneous Province (Oksfjord) | | 564 | 2 | U-Pb zircon | | Roberts et al. (2004) |
| | Seiland Igneous Province (Oksfjord) | | 559 | 7 | U-Pb zircon | | Roberts et al. (2004) |
| | Seiland Igneous Province (Hasvik Gabbro, Soroy) | | 562 | 6 | U-Pb zircon | | Roberts et al. (2006) |
| | Seiland Igneous Province (Storelv Gabbro) | | 569 | 5 | U-Pb zircon | | Roberts et al. (2006) |
| | Seiland Igneous Province (diorite, Breivikbotn Gabbro) | diorite | 571 | 4 | U-Pb zircon | | Roberts et al. (2006) |

**Table 1.** Continued.

| Label | Occurrence | Rock Type | Date (Ma) | ± (Ma) | Method | Sampling Details | Reference |
|---|---|---|---|---|---|---|---|
| | Seiland Igneous Province (Oksfjord) | gabbro | 565 | 9 | U-Pb zircon | | Roberts et al. (2006) |
| | Seiland Igneous Province (Oksfjord) | monzonite | 566 | 4 | U-Pb zircon | | Roberts et al. (2006) |
| | Seiland Igneous Province (Oksfjord) | monzodiorite | 565 | 5 | U-Pb zircon | | Roberts et al. (2006) |
| | Seiland Igneous Province (Oksfjord) | norite | 570 | 9 | U-Pb zircon | | Roberts et al. (2006) |
| | Seiland Igneous Province (Oksfjord) | orthopyroxenite | 566 | 1 | U-Pb zircon | | Roberts et al. (2006) |
| | Seiland Igneous Province (Breivikbotn Syenite Complex) | syenite gneiss | 570 | 2 | U-Pb zircon (estimated) | RJR-03-116 | Roberts et al. (2010) |
| | Seiland Igneous Province (Breivikbotn Syenite Complex) | syenite gneiss | 579 | 14 | U-Pb zircon (estimated) | RJR-04-245 | Roberts et al. (2010) |
| | Seiland Igneous Province | nepheline syenite pegmatites | 531 | 2 | U-Pb zircon | | Pedersen et al. (1989) |
| | Seiland Igneous Province (Stjernoy (Lillebukt Alkaline Complex)) | nepheline syenite pegmatites | 523 | 2 | U-Pb zircon | | Pedersen et al. (1989) |
| | **Intrusions** | | | | | | |
| | Egersund dykes (Norway) | basalt | 616 | 3 | 207Pb/206Pb baddeleyite | | Bingen et al. (1998) |
| | Egersund dykes (Norway) | | 600 | 10 | 40Ar/39Ar biotite | | Walderhaug et al. (2007) |
| | Ottfjället dolerite dyke swarm (Sweden) | dolerite | 665 | 10 | K-Ar whole rock | mean of 660, 662 and 672 Ma dates citing Claesson (1976) | Claesson and Roddick (1983) |
| | Ottfjall Dolerite (Sarek Mountains) | | 715 | 10 | K-Ar whole rock | 74237 | Claesson (1976) |
| | Ottfjall Dolerite (Sarek Mountains) | | 735 | 260 | Rb-Sr whole-rock | | Claesson (1976) |
| | Sarek Dyke Swarm (Seve Nappe Complex, Sweden) | diabase | 573 | 74 | Sm-Nd mineral-whole rock isochron | 903-1C, 843 and 851 | Svenningsen (1994) |
| | Sarek Dyke Swarm (Seve Nappe Complex, Sweden) | | 608 | 1 | U-Pb zircon | | Svenningsen (1996) |
| | Sarek Dyke Swarm (Sweden) | dioritic pods in dykes | 607.9 | 0.7 | 207Pb/206Pb zircon | | Svenningsen (2001) |
| | Sarek Dyke Swarm (Sweden) | dioritic pods in dykes | 609.1 | +30-2.1 | U-Pb zircon (upper intercept) | | Svenningsen (2001) |
| | Sarek Dyke Swarm (Sweden) | dioritic pods in dykes | 608 | 1 | U-Pb zircon | | Svenningsen (2001) |
| | Vistas Granite (Seve Nappe Complex, Kebnekaise Mts) | granite | 605 | 42 | U-Pb zircon | rim analyses | Paulsson & Andréasson (2002) |
| | Kebne Dyke Complex (Sweden) | metagabbro, metagranitoid | 608-596 | | 206Pb/238U zircon | | Baird et al. (2014) |
| | Kebne Dyke Complex (Sweden) | metagabbro, metagranitoid | 604 | 2 | U-Pb zircon CA-TIMS | preliminary | Baird et al. (2013) |
| | Kebne Dyke Complex (Kebnekaise Intrusive Complex) | gabbronorite | 578 | 9 | U-Pb zircon | K941 | Kirsch and Svenningsen (2016) |
| | Corrovare Nappe dyke swarm (Kalak Nappe Complex) | mafic dyke | 582 | 30 | Sm-Nd isochron (whole rock, clinopyroxene, plagioclase) | 9828, 9967 | Zwaan and Van Roermund (1990) |
| | Corrovare Nappe dyke swarm (Kalak Nappe Complex) | mafic dyke | 578 | 64 | Rb-Sr (whole rock, clinopyroxene, plagioclase) | 9828, 9967 | Zwaan and Van Roermund (1990) |
| | Hamningberg dyke | dolerite | 567.1 | +30-23 | U-Pb zircon | | Roberts and Walker (1997) |

**Table 1.** Continued.

| Label | Occurrence | Rock Type | Date (Ma) | ± (Ma) | Method | Sampling Details | Reference |
|---|---|---|---|---|---|---|---|
| | **Carbonatite complex** | | | | | | |
| | Alno carbonatite complex | alnoite dike, sovite dike, sovite | 584 | 7 | Ar-Ar biotite, K-feldspar (mean) | Alno1, Alno2 and A6 | Meert et al. (2007) |
| | Alno carbonatite complex | | 589.7 | 4.4 | U-Pb baddeleyite | P2-036 | Rukhlov and Bell (2010) |
| | Alno carbonatite complex | | 582.8 | 5.7 | U-Pb apatite | P2-037 | Rukhlov and Bell (2010) |
| | Fen carbonatite complex | damtjernite and phonolite | 583 | 15 | Ar-Ar mica (mean) | DS7,PS2 | Meert et al. (1998) |
| | Fen carbonatite complex (satellite dykes) | damtjernite | 578 | 24 | Rb-Sr mica | | Dahlgren (1994) |
| | Avike Bay carbonatite complex | alnoite dyke | 542 | 16 | K-Ar phlogopite | | Kresten et al. (1977) |
| | Seiland Igneous Province (Breivikbotn Carbonatite Complex) | malignite to silicocarbonatite | 574 | 5 | U-Pb zircon | RJR-02-34D and 34E | Roberts et al. (2010) |
| | Seiland Igneous Province (Breivikbotn Carbonatite Complex) | malignite to silicocarbonatite | 568-558 | | 206Pb/238U titanite | | Roberts et al. (2010) |
| | **Kimberlite** | | | | | | |
| | Kuusamo (Finland) | (Group I hypabyssal kimberlite) kimberlite type dated unclear | 759 | 15 | 206Pb/238U perovskite (wt mean) | KP (Kalettomanpuro) | O'Brien and Bradley (2008) |
| | Kuusamo (Finland) | (Group I hypabyssal kimberlite) kimberlite type dated unclear | 756.8 | 2.1 | 206Pb/238U perovskite (wt mean) | KV (Kattaisenvaara) | O'Brien and Bradley (2008) |
| | Kaavi-Kuopio (Finland) | kimberlite type not reported | 626-589 | | U-Pb perovskite (ion probe) | | O'Brien et al. (2003) |
| | Kaavi-Kuopio (Finland) | kimberlite type not reported | 600 | | not reported | | O'Brien et al. (2005) |
| | Eastern Finland Kimberlite Province | magmatic | 590 | | K-Ar | pipe No. 2 | Tyni (1997), O'Brien and Tyni (1999) |
| | Eastern Finland Kimberlite Province | magmatic | 430 | | K-Ar | pipe No. 1 | Tyni (1997), O'Brien and Tyni (1999) |
| | Finnish kimberlite | kimberlite type not reported | 600 | | not reported | | H O'Brien (pers comm 2000) cited in Peltonen and Irmeli (2001) |
| | Kuusamo (Finland) | (Group 1) kimberlite type not reported | 747 | 4 | Rb-Sr phlogopite | KP01-04 (Kalettomanpuro) and KV001-61.4m (Kattaisenvara) | Phillips et al. (2017) |
| | Kuusamo (Finland) | (Group 1) kimberlite type not reported | 747.8 | 1.0 | 40Ar/39Ar kinoshitalite | KP01-04 (Kalettomanpuro) | Phillips et al. (2017) |

# Supplementary Material 2: Compilation of plate velocity determinations

**Table 1.** Compilation of plate velocity determinations for Laurentia between 700-500 Ma.

| Time (Ma) | Velocity (cm/yr) | Velocity (degree/Ma) | Velocity (plate speed/5) | Note | Reference |
|---|---|---|---|---|---|
| ***Estimates between 700-620 Ma*** | | | | | |
| 700-600 | | | ~8 | Figure 3 | Condie et al. (2015) |
| 660-650 | ~5 | | | Laurentia; Figure 14 | Torsvik et al. (1996) |
| 650-640 | ~6 | | | Laurentia; Figure 14 | Torsvik et al. (1996) |
| 640-630 | ~7 | | | Laurentia; Figure 14 | Torsvik et al. (1996) |
| 630-620 | ~8 | | | Laurentia; Figure 14 | Torsvik et al. (1996) |
| ***Estimates between 620-500 Ma*** | | | | | |
| 620-610 | ~11 | | | Laurentia; Figure 14 | Torsvik et al. (1996) |
| 615-590 | 38 | | | different model than Li et al (2008) | McCausland et al. (2007) |
| 615-575 | | 2-4 (mean=3) | | WAC/LAU/BAL: event I; APW | Robert et al. (2017) |
| 610-600 | ~12 | | | Laurentia | Gurnis and Torsvik (1994) |
| 610-600 | ~11 | | | Laurentia; Figure 14 | Torsvik et al. (1996) |
| 608-550 | | 1.4 | | | Meert (2014) |
| 600-590 | ~8 | | | Laurentia | Gurnis and Torsvik (1994) |
| 600-590 | ~4 | | | Laurentia; Figure 14 | Torsvik et al. (1996) |
| 600-500 | | | ~5 | Figure 3 | Condie et al. (2015) |
| 590-580 | ~1 | | | Laurentia | Gurnis and Torsvik (1994) |
| 590-580 | ~8 | | | Laurentia; Figure 14 | Torsvik et al. (1996) |
| ~580-560 | 40 | | | APW | McCausland et al. (2011) |
| 580-570 | ~12 | | | Laurentia | Gurnis and Torsvik (1994) |
| 580-570 | ~16 | | | Laurentia; Figure 14 | Torsvik et al. (1996) |
| 580-550 | 16 | | | Laurentia; minimum | Meert et al. (1993) |
| post-580 | >40 | | | | McCausland et al. (2011) |
| 575-565 | | 3-18.5 (mean=10) | | WAC/LAU/BAL: event II; APW | Robert et al. (2017) |
| 575-565 | | 6 | | WAC/LAU/BAL: event II; TPW | Robert et al. (2017) |
| 575-565 | >60? | | | different model than Li et al (2008) | McCausland et al. (2007) |
| 575-565 | 29 | | | different model than Li et al (2008) | McCausland et al. (2007) |
| 570-560 | ~17 | | | Laurentia | Gurnis and Torsvik (1994) |
| 570-560 | ~21 | | | Laurentia; Figure 14 | Torsvik et al. (1996) |
| 570-550 | ~34 | | | | McCausland and Hodych (1998) |
| 560-550 | ~16 | | | Laurentia | Gurnis and Torsvik (1994) |
| 560-550 | ~19 | | | Laurentia; Figure 14 | Torsvik et al. (1996) |
| 550-540 | ~9 | | | Laurentia | Gurnis and Torsvik (1994) |
| 550-540 | ~11 | | | Laurentia; Figure 14 | Torsvik et al. (1996) |
| 550-500 | | 1.94 | | | Meert (2014) |
| Early Cambrian | 16(+12-8) | | | | Mitchell et al. (2010) |

*plate speed=degree/100Myr*

## Supplementary Material 3: Evaluation of Renard U-Pb perovskite dates

Perovskite typically contains significant amounts of common lead; therefore, the $^{206}Pb/^{238}U$ date provides the best estimate for timing of perovskite crystallization as the more abundant $^{206}Pb$ is less susceptible to variable amounts of initial common lead incorporated in perovskite during crystallization (Heaman 1989; Kinny et al. 1997; Heaman and Kjarsgaard 2000). Furthermore, the amount of measured $^{207}Pb$ is much smaller than $^{206}Pb$ which makes relying on $^{207}Pb/^{235}U$ and $^{207}Pb/^{206}Pb$ dates not ideal as the initial common lead will have a greater effect on the analytical error (e.g. Li et al. 2010). U-Pb perovskite results can be evaluated by the individual or weighted average $^{206}Pb/^{238}U$ date , or by linear regression from U-Pb isochron, Wetherill or Tera-Wasserburg concordia plots if multiple analyses record a range of U/Pb compositions (e.g. Heaman and Kjarsgaard 2000; Wu et al. 2010). The majority of Renard samples contain ~80-90% radiogenic lead (mol% $^{206}Pb^*$) but analyses can be as low as ~54% indicating a higher amount of common lead (Table 3.1 in Chapter 3; Ranger et al. 2018). In addition, most samples record minor variation in $^{238}U/^{204}Pb$ where two or more analyses are reported (except 31552B and 31497), making linear regression less suitable. Many Renard analyses are offset above concordia, possibly due to the initial common lead content of the kimberlite magma when perovskite crystallized differing from the Stacey and Kramers (1975) two-stage model composition (Figure 1). An independent estimate of the initial common lead using an unradiogenic mineral (e.g. phlogopite, titanomagnetite, monticellite) was not feasible due to tiny grain size, alteration and/or scarcity of representative minerals in the available samples (which also precluded dating by some isotopic methods, such as Rb-Sr phlogopite). Figure 2 provides an example of three perovskite analyses from sample 31552B (Kimb3c, Renard 3) which records a wide range of $^{238}U/^{204}Pb$ (212-1743). The weighted average $^{206}Pb/^{238}U$ date (633.2±1.4 Ma, MSWD=0.12) compares well with linear regression by $^{238}U$-$^{206}Pb$ isochron (633.3±1.4 Ma, MSWD=0.31), by Wetherill concordia (633.7±2.4 Ma, MSWD=0.023) and by Tera-Wasserburg concordia (636±1.3 Ma, MSWD=2.7). The new U-Pb perovskite dates reported in Chapters 2 and 3 as single $^{206}Pb/^{238}U$ dates or weighted average $^{206}Pb/^{238}U$ dates are interpreted as the best estimate for the timing of Renard kimberlite emplacement.

When a large range in $^{206}Pb/^{238}U$ dates are reported, only a few samples with two or more analyses (38919 and 38926 from Renard 2, 31468 from Renard 9; Figure 3) suggest at least one analysis is discordant due to Pb loss. Both 38919 and 31468 record similar upper intercept dates (549±25 Ma and 630±28 Ma, respectively) to the most concordant fraction $^{206}Pb/^{238}U$ date (539.1±2.0 Ma and 625.0±2.2 Ma, respectively). The weighted average $^{206}Pb/^{238}U$ date of 646.3±1.4 Ma for 38926 was determined from two analyses offset above concordia. A linear regression through all three analyses records an upper intercept date (603±15 Ma) which is not comparable to the weighted average date but 38926-1 appears discordant. Figure 4 plots samples which possibly may contain discordance (38929 from Renard 2, 39289 from Renard 4).

The $^{206}Pb/^{238}U$ perovskite dates record complex perovskite crystallization which could indicate mixing between older and younger kimberlite or inheritance within single samples. As described in Ranger et al. (2018), three perovskite age patterns emerged from the new data; (1) all $^{206}Pb/^{238}U$ dates agree within analytical error for the sample and a weighted average estimates the emplacement age, (2) at least two $^{206}Pb/^{238}U$ dates agree within analytical error but remaining dates for the same sample do not agree, and (3) all $^{206}Pb/^{238}U$ dates for the same sample do not agree within analytical error. $^{206}Pb/^{238}U$ dates outside of analytical error (either younger or older) may be an indication of mixing/inheritance if lead loss is not indicated.

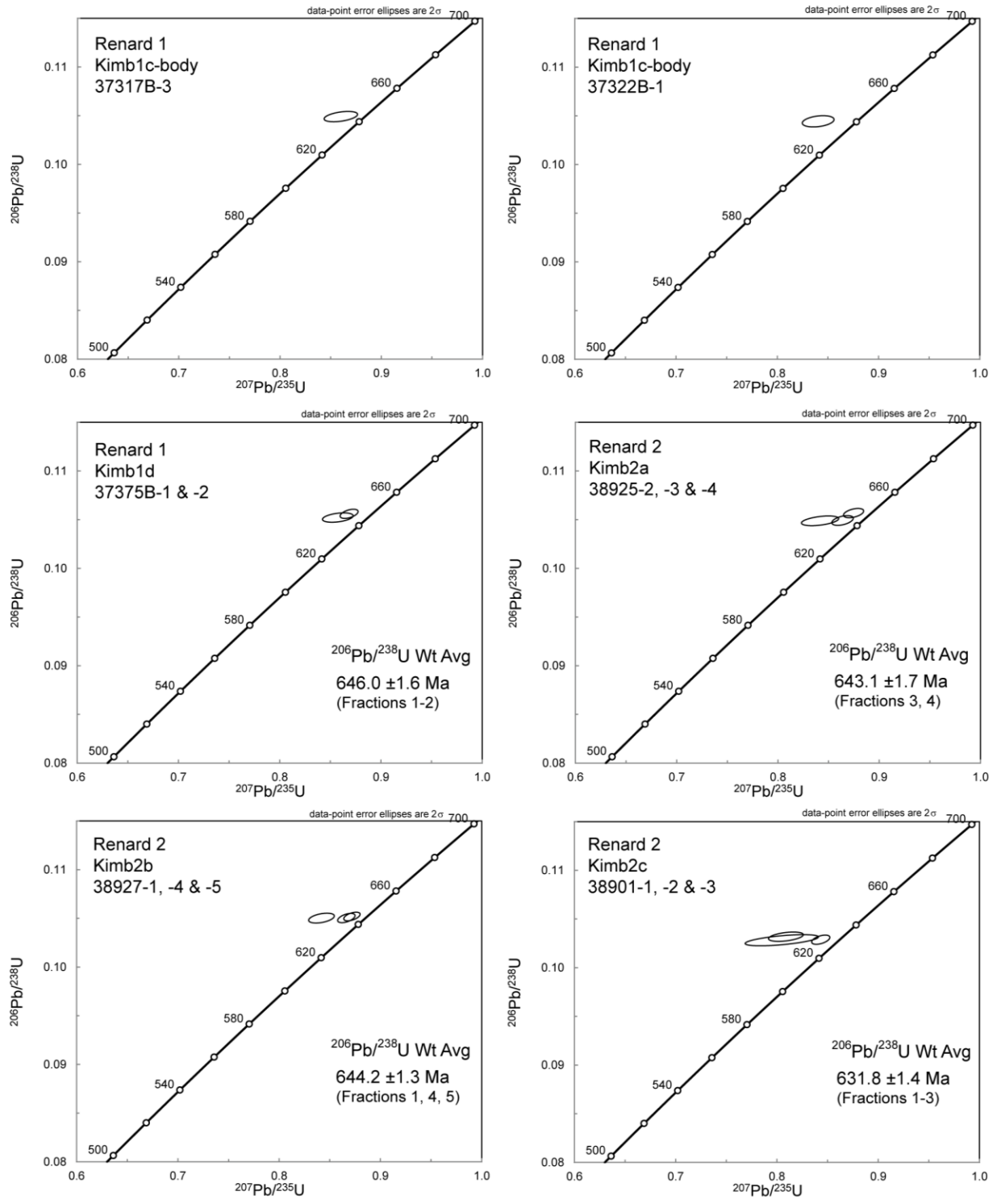


**Fig. 1.** Wetherill concordia diagrams from this study and Ranger et al. (2018).

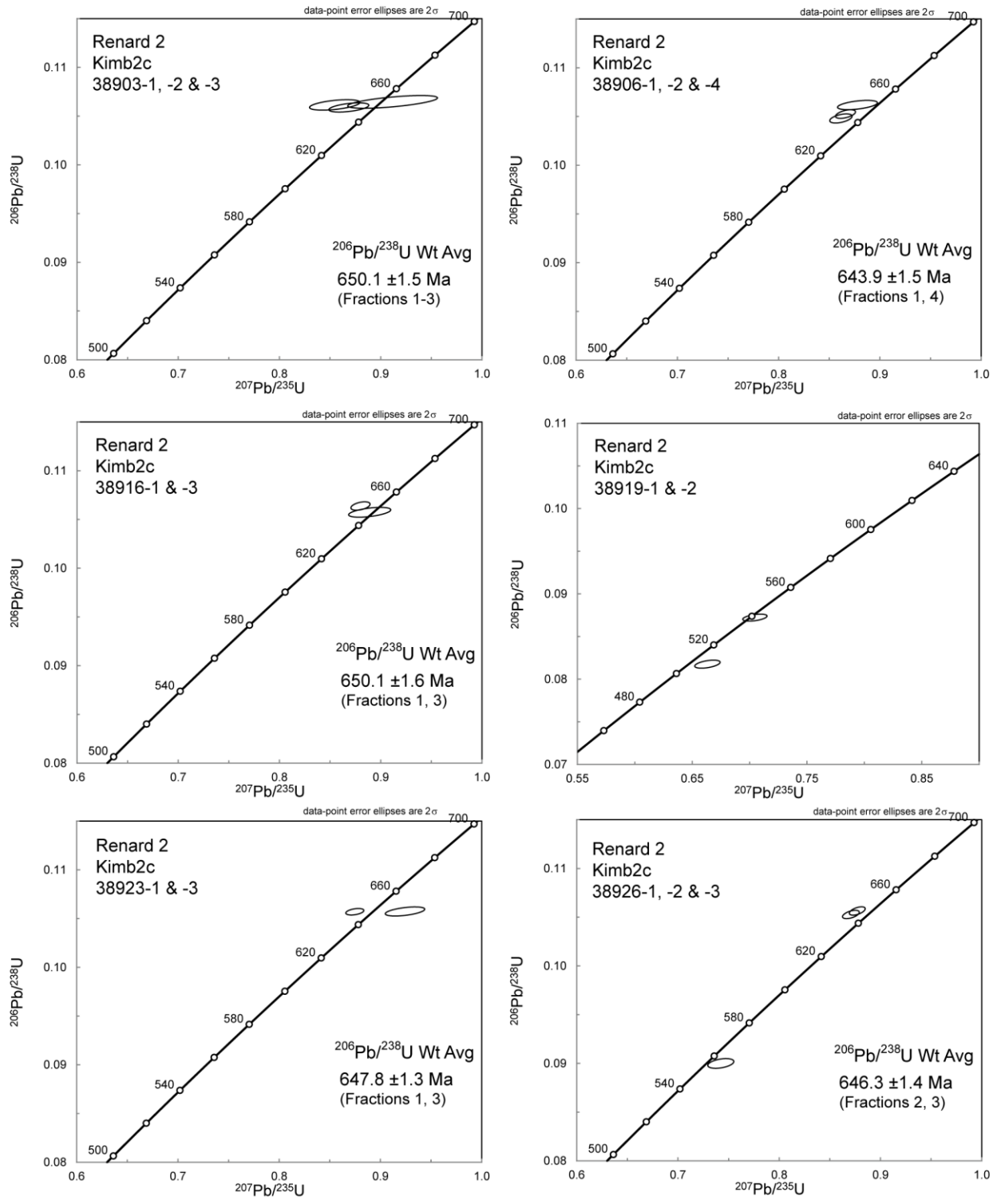


**Fig. 1.** Continued.

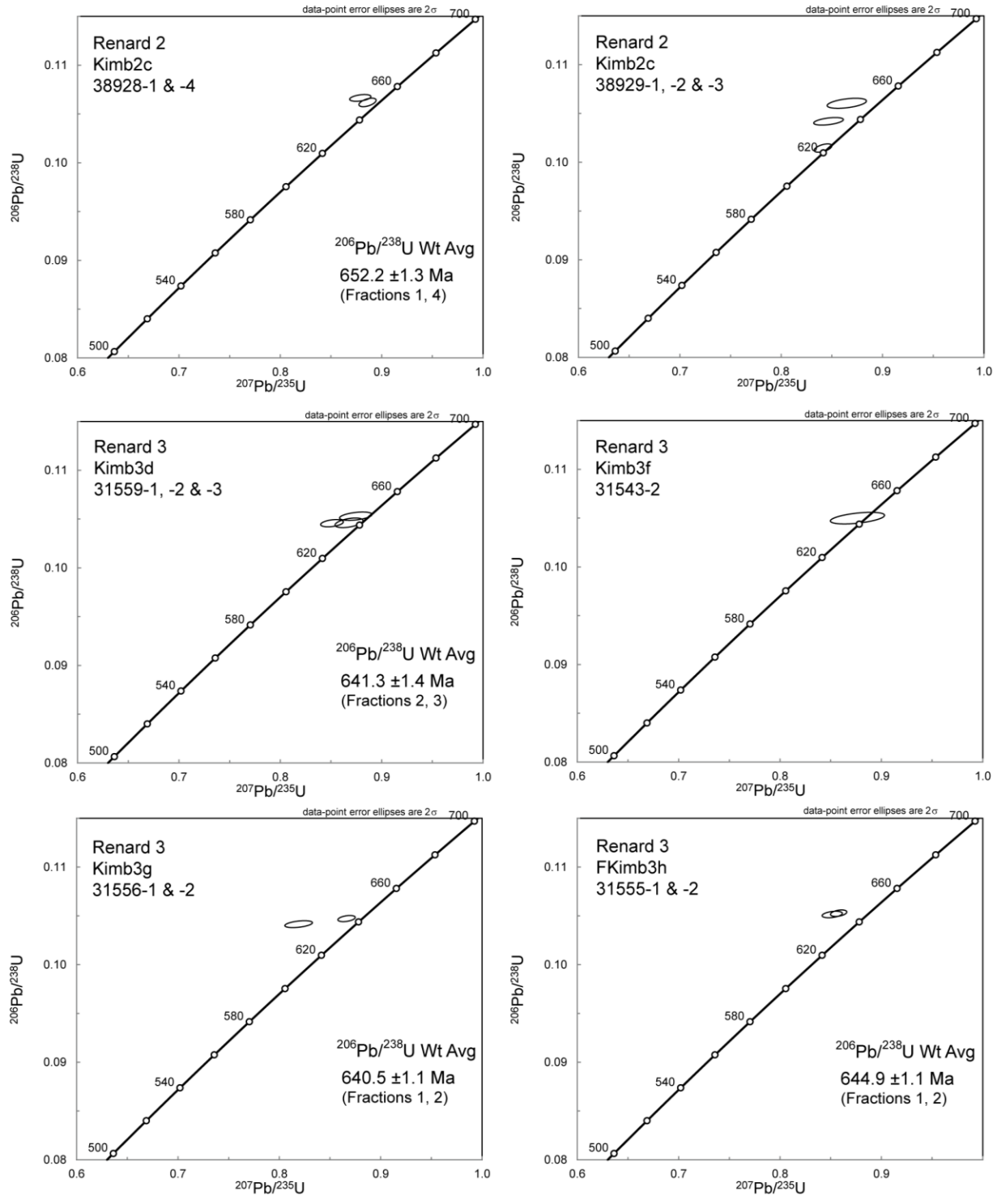


**Fig. 1.** Continued.

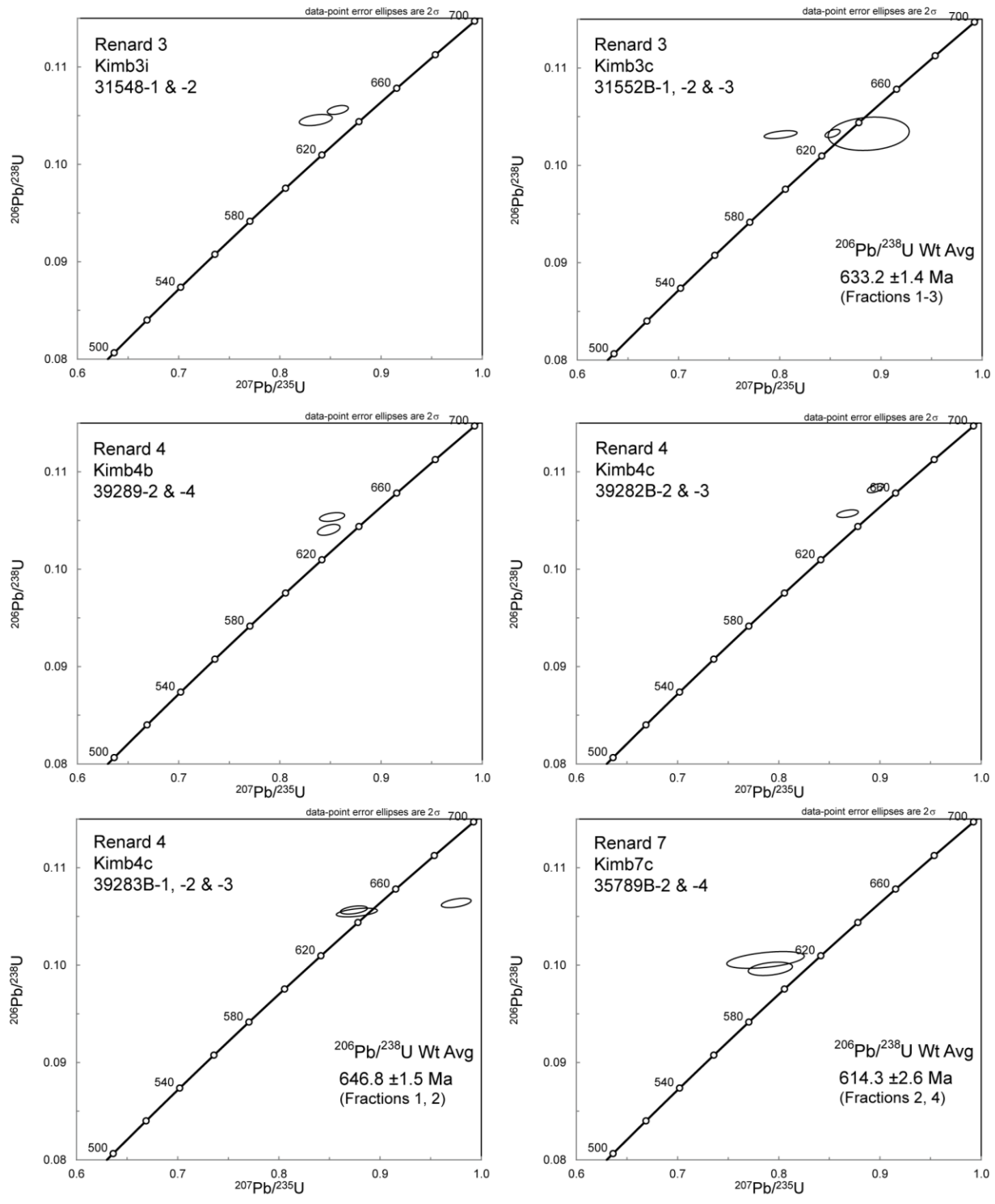


**Fig. 1.** Continued.

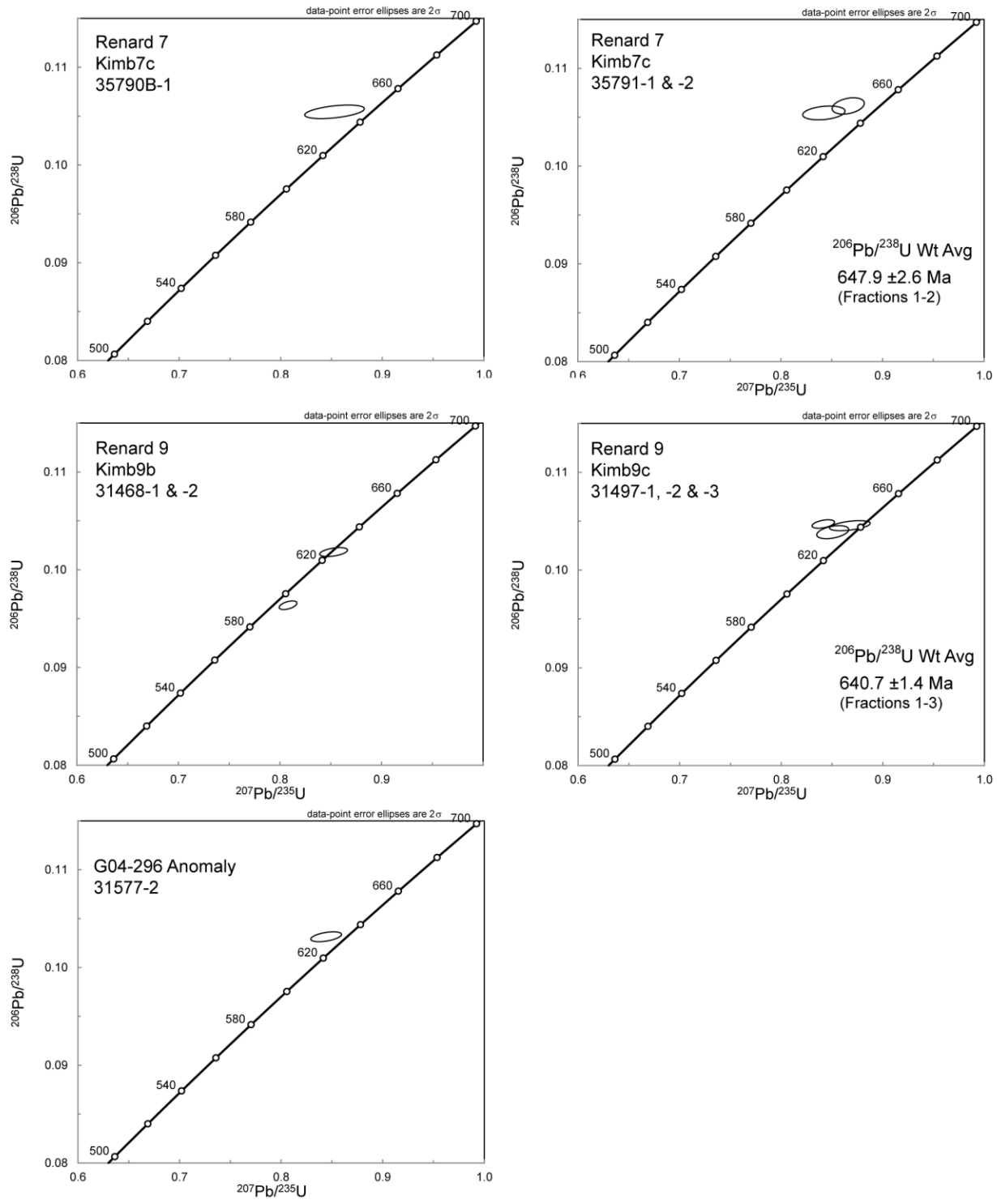


**Fig. 1.** Continued.

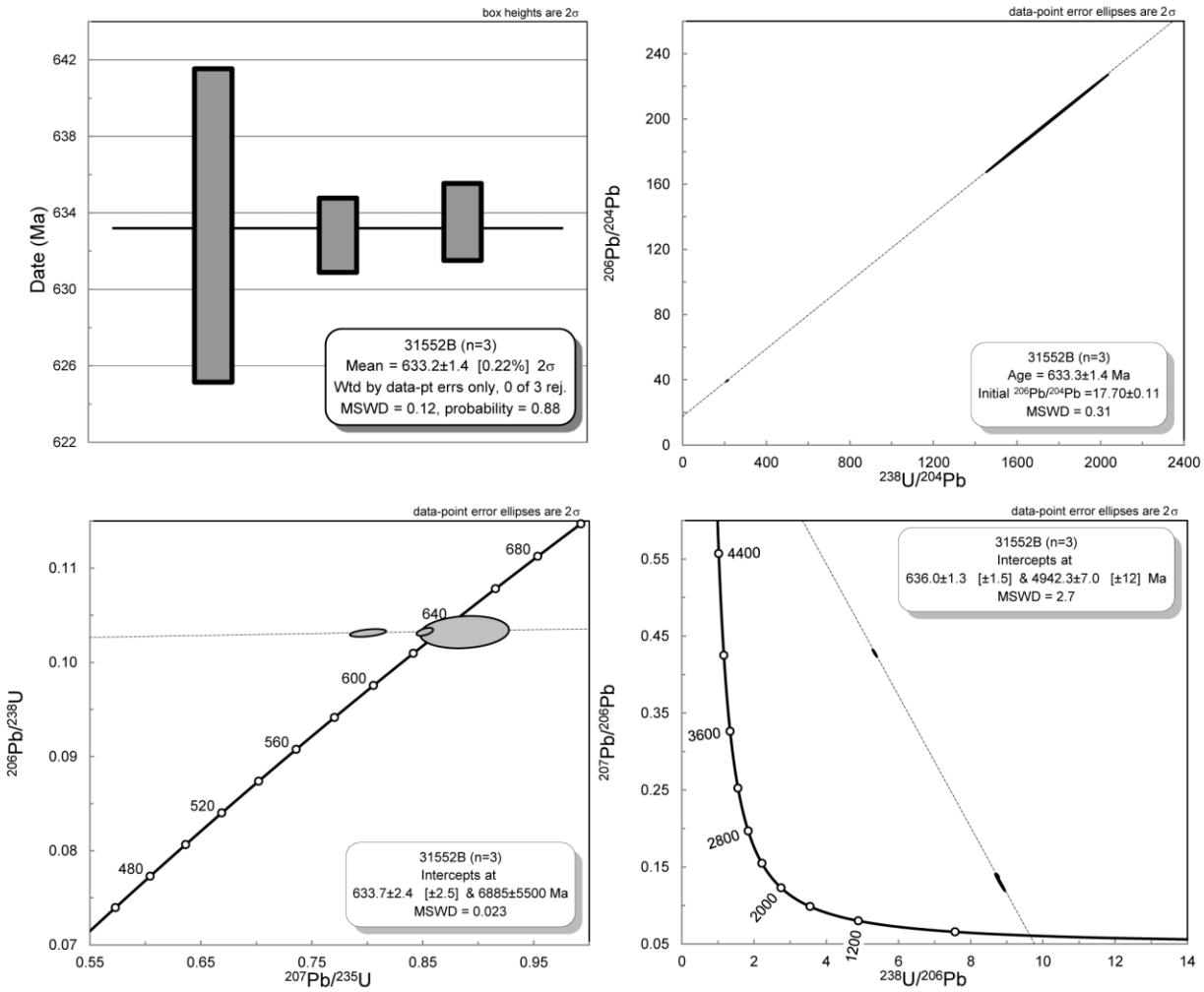


**Fig. 2.** Weighted average $^{206}Pb/^{238}U$, $^{238}U$-$^{206}Pb$ isochron, Wetherill and Terra-Wasserburg concordia diagrams for sample 31552B.

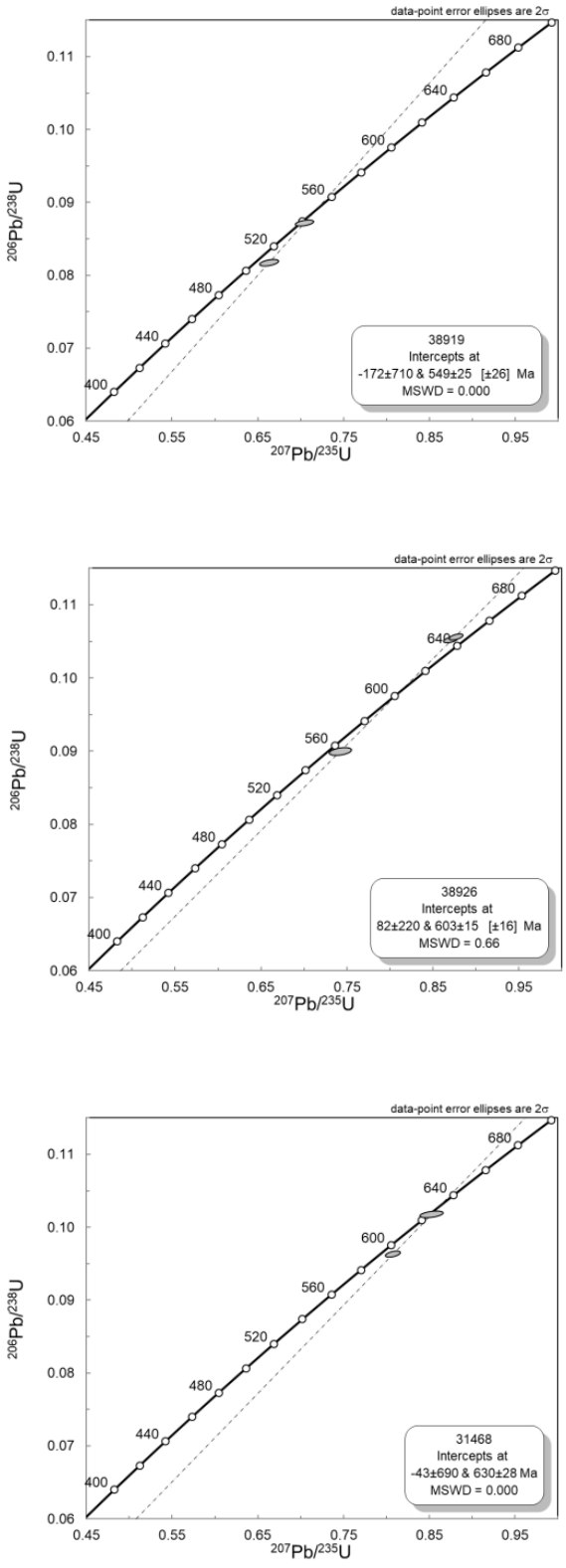


**Fig. 3.** Wetherill concordia diagrams for samples 38919, 38926 and 31468.

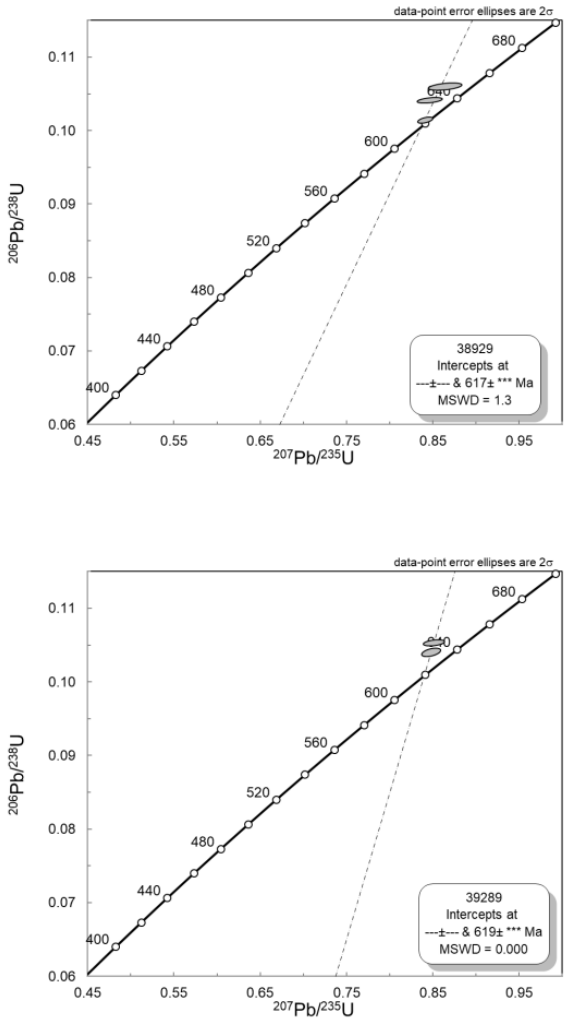


**Fig. 4.** Wetherill concordia diagrams for samples 38929 and 39289.

# APPENDIX D

# SUPPLEMENTARY MATERIAL FOR CHAPTER 4

## Supplementary Material 1: Published images of kassite, cafetite and/or lucasite-(Ce)

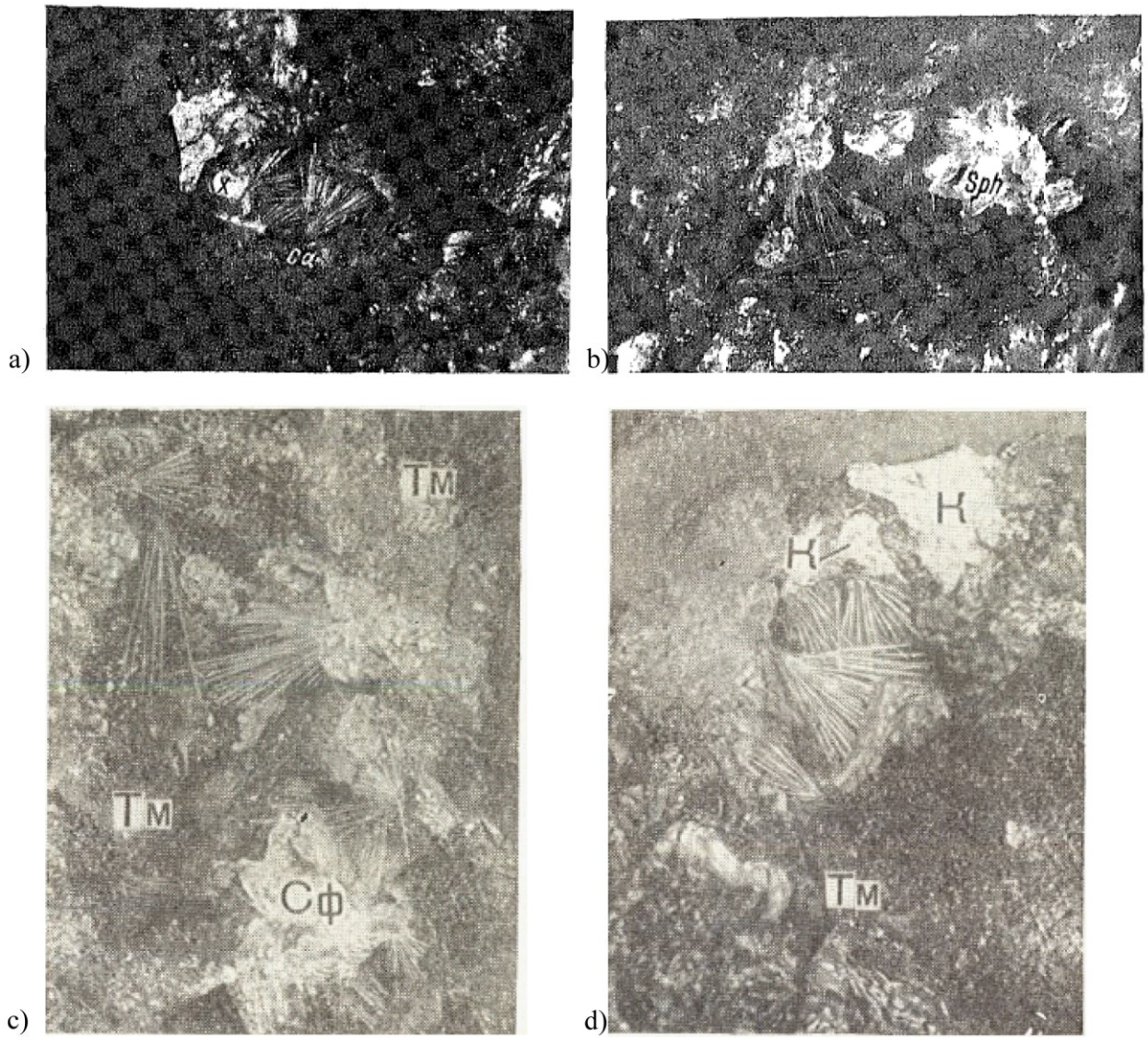


**Fig. 1.** Published images of kassite, cafetite and/or lucasite-(Ce). Note scale as shown in original reference (sometimes not presented). (a) Kukharenko et al. (1959): cafetite (Ca) needles on unnamed (x) mineral. (b) Kukharenko et al. (1959): cafetite needles on titanite (Sph). (c) Kukharenko et al. (1965): cafetite needles in miarolic voids with titanomagnetite (Тм) and sphene (Сф). Scale x3. (d) Kukharenko et al. (1965): kassite aggregates (K) with cafetite needles and titanomagnetite (Тм). Scale x3.

e)

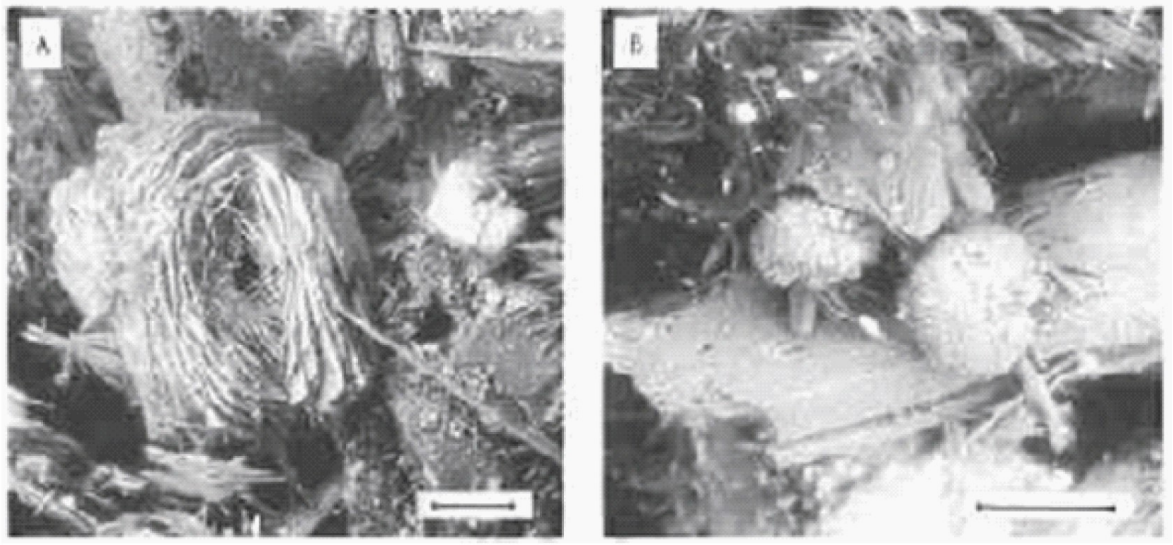


f)

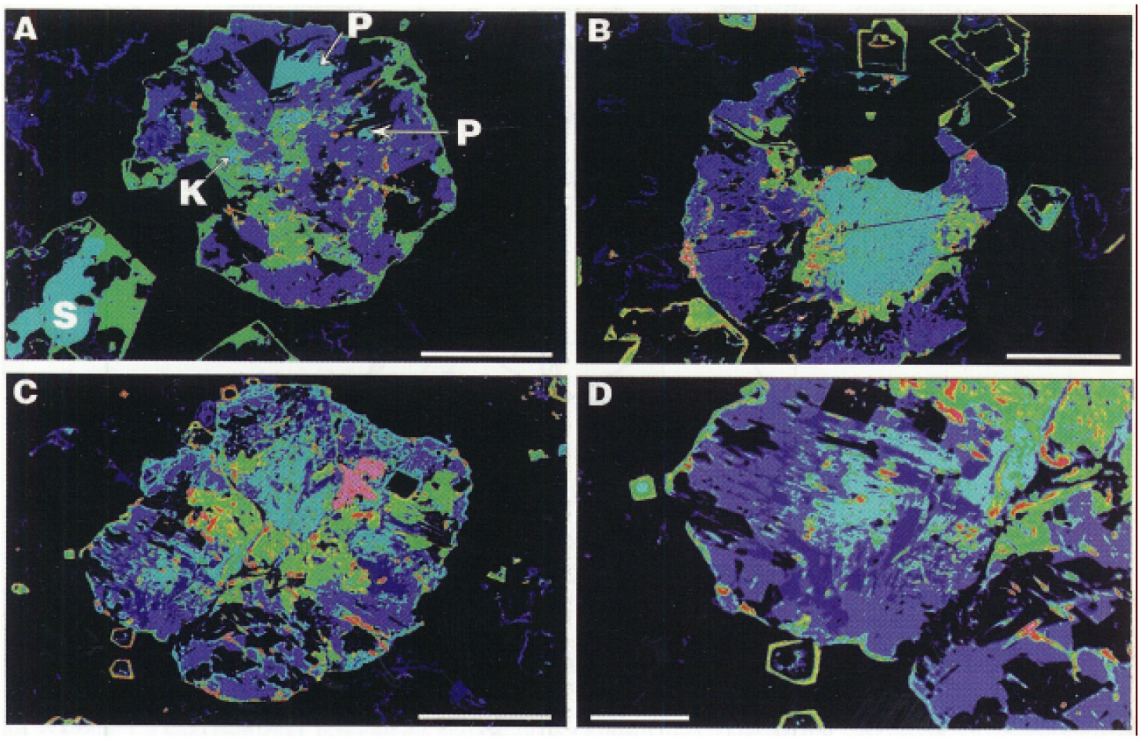


**Fig.1.** Continued. (e) Evans et al. (1986): Diamond Jo quarry (Magnet Cove, Arkansas) likely cafetite. (f) Mitchell and Chakhmouradian (1998): BSE images of perovskite pseudomorphs (Iron Mountain, Wyoming; P, perovskite; kassite (K), bluish green; anatase and titanite, blue; ilmenite, green and yellowish green; lucasite-(Ce), red; barite, purple; calcite and groundmass minerals, black; scale 50 μm for A-C, 20 μm for D).

g)

h)

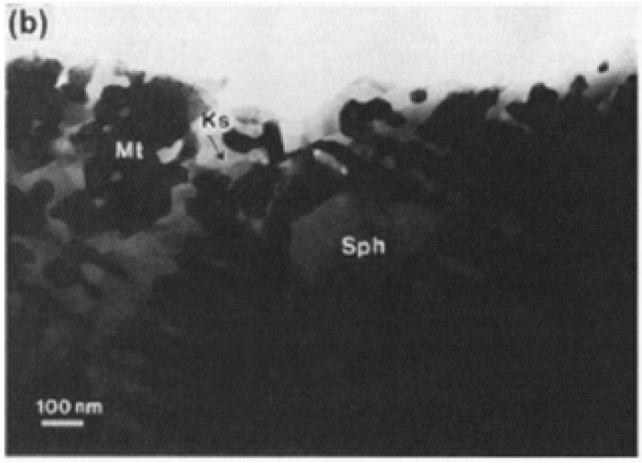


i)

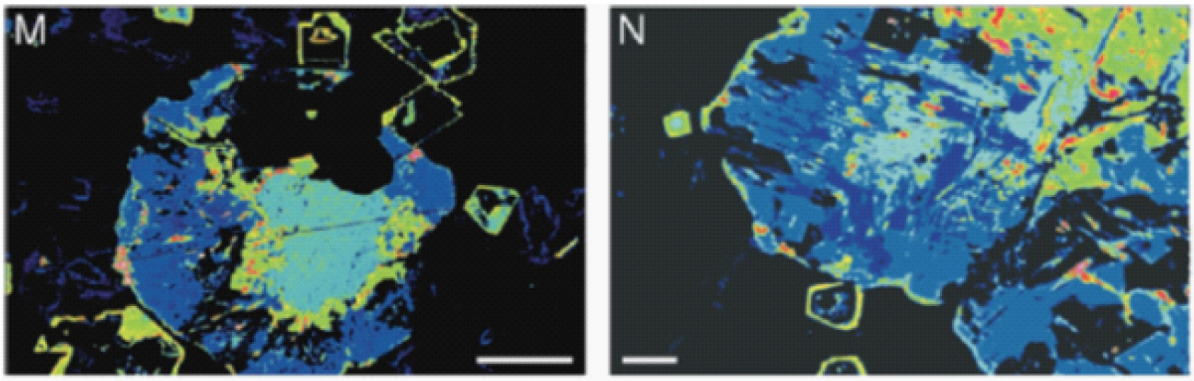


**Fig. 1.** Continued. (g) Yakovenchuk et al. (1999): cafetite. (h) Shau et al. (2000): TEM image of kassite (Ks), titanite (Sph) and magnetite (Mt). (i) Chakhmouradian and Mitchell (2000): False color images of perovskite pseudomorphs (Iron Mountain, Wyoming) from Mitchell and Chakhmouradian (1998) (kassite, pale blue; anatase, blue; Mn-rich ilmenite, green; titanite, dark blue; lucasite-(Ce), red).

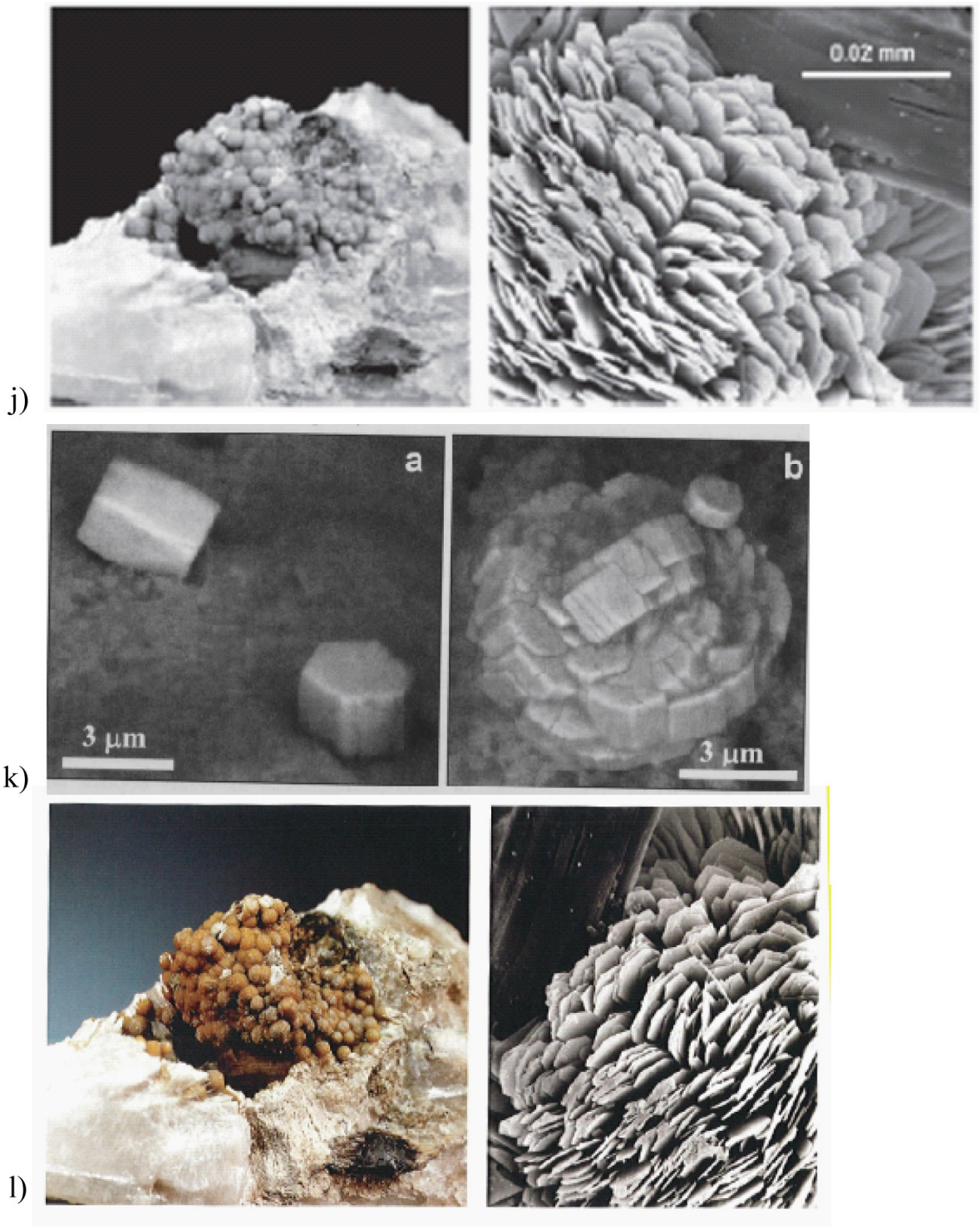


**Fig.1.** Continued. (j) Krivovichev et al. (2003): cafetite spherolites ~8x8x8mm$^3$ (left) and cafetite SEM BSE image (right). (k) Galuskin et al. (2004): BSE images of prismatic (a) and split aggregate (b) of "Mn-kassite." (l) Yakovenchuk et al. (2005): spherulites of cafetite from Mt. Rasvumchoor in (left) natrolite vein void (no. 20; FOV 1.7 x 1.6 cm) and (right) magnified image (FOV 80 x 70 μm).

m)

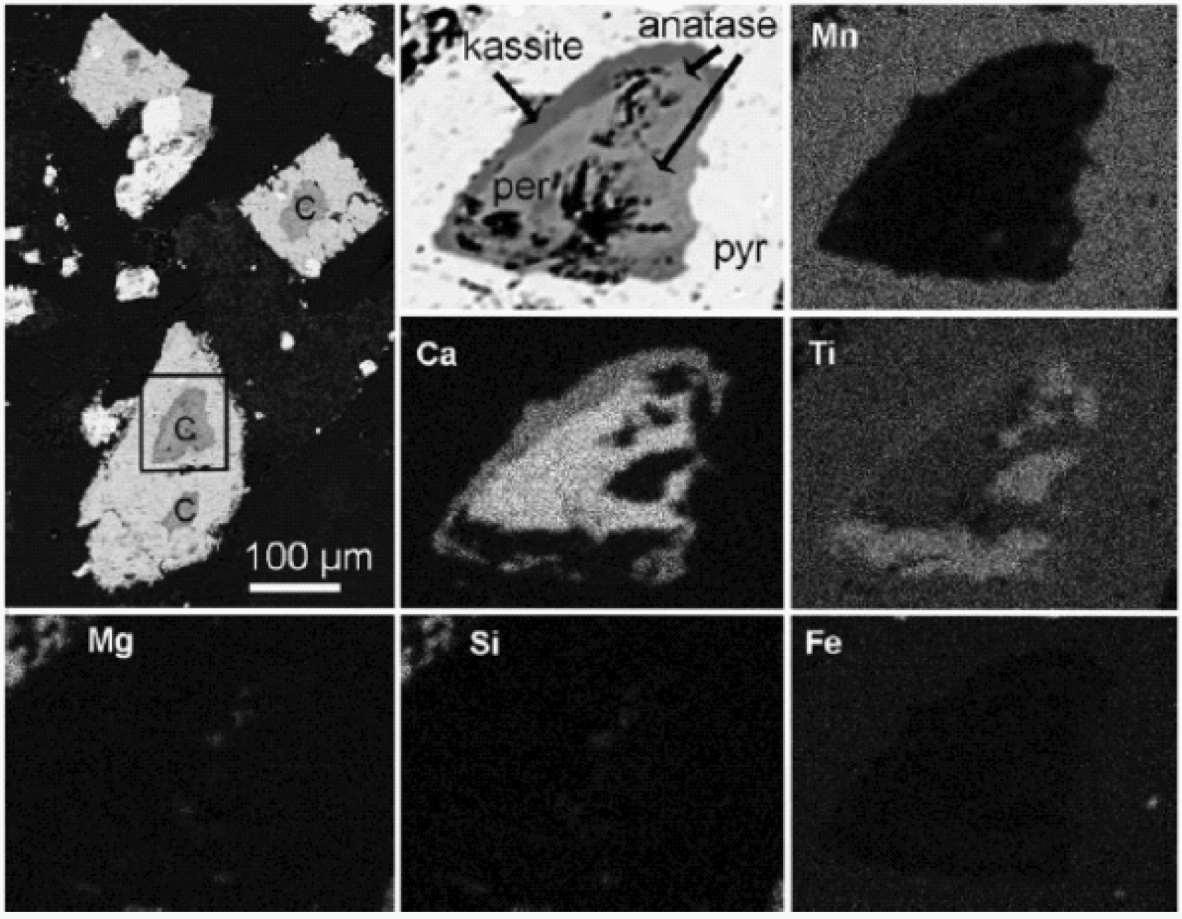


n)

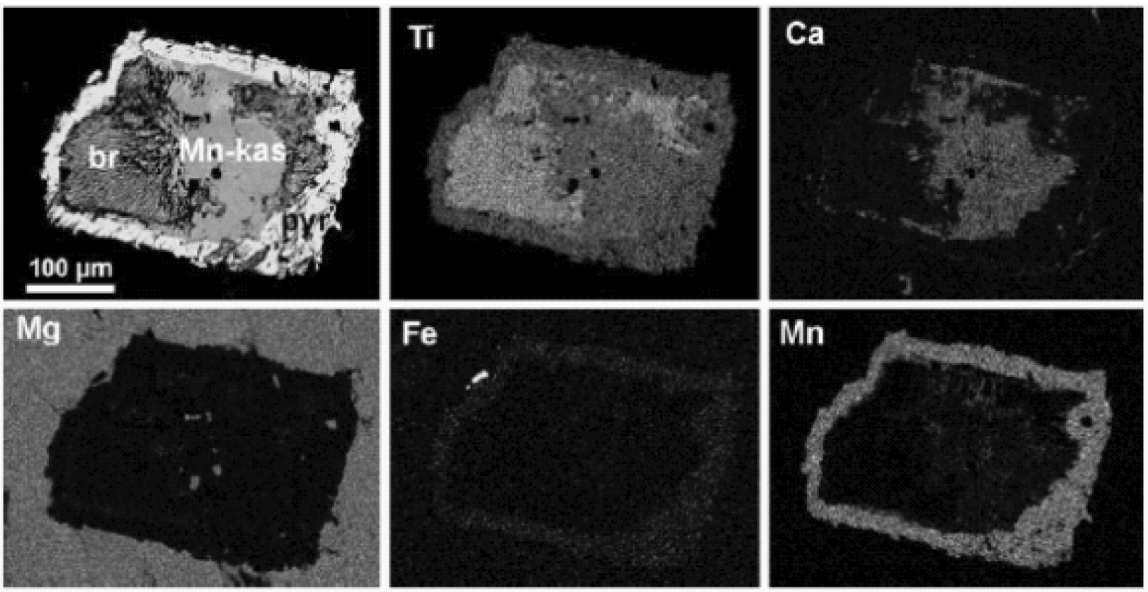


**Fig. 1.** Continued. (m) Zajzon et al. (2013): BSE images and element maps of perovskite core, kassite, anatase and pyrophanite (pyr). (n) Zajzon et al. (2013): BSE images and element maps of pyrophanite (pyr), Mn-bearing kassite (Mn-kas) and brookite (br).

o)

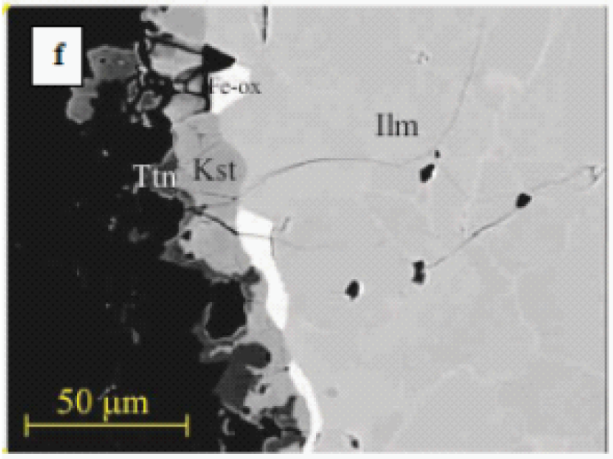


p)

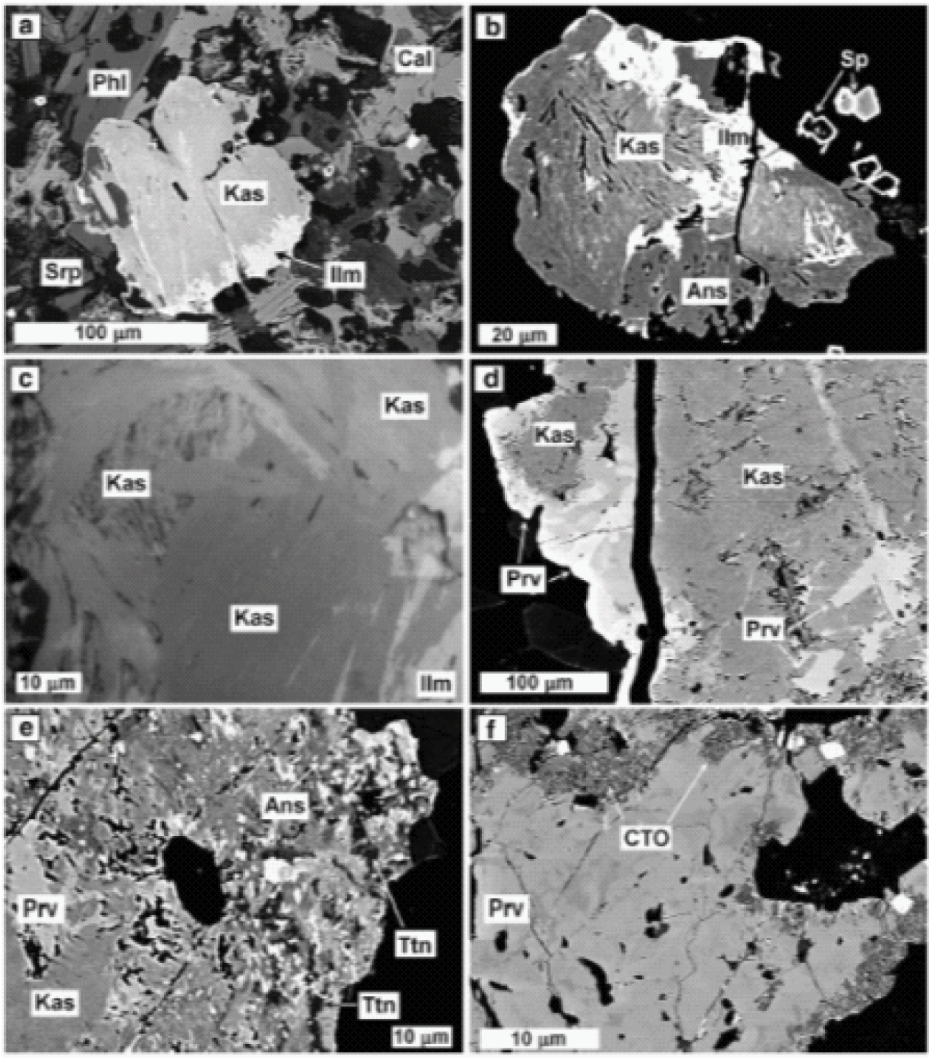


**Fig. 1.** Continued. (o) Baziotis et al. (2013a): BSE image of ilmenite (Ilm), kassite (Kst), Fe-oxide (Fe-Ox) and titanite. (p) Martins et al. (2014): BSE images and photomicrographs of pseudomorphs after perovskite from Iron Mountain (Wyoming) (Kas, kassite; Ilm, ilmenite; Ans, anatase; Prv, perovskite; Ttn, titanite).

q)

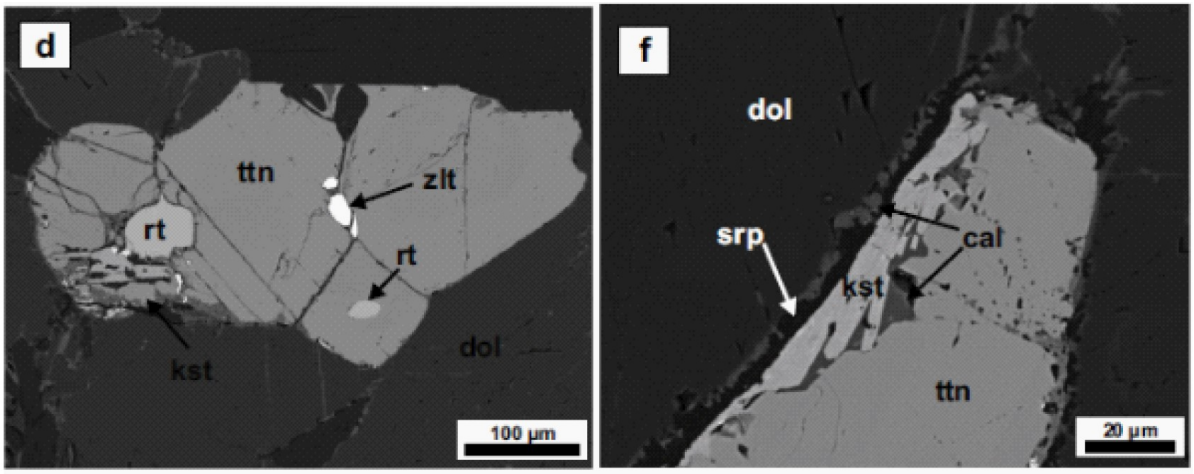


r)

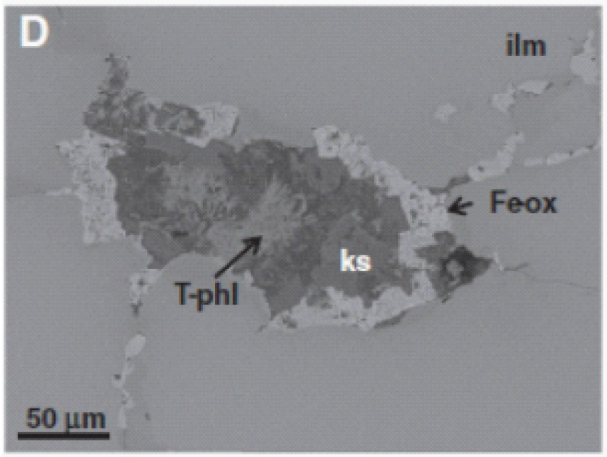


s)

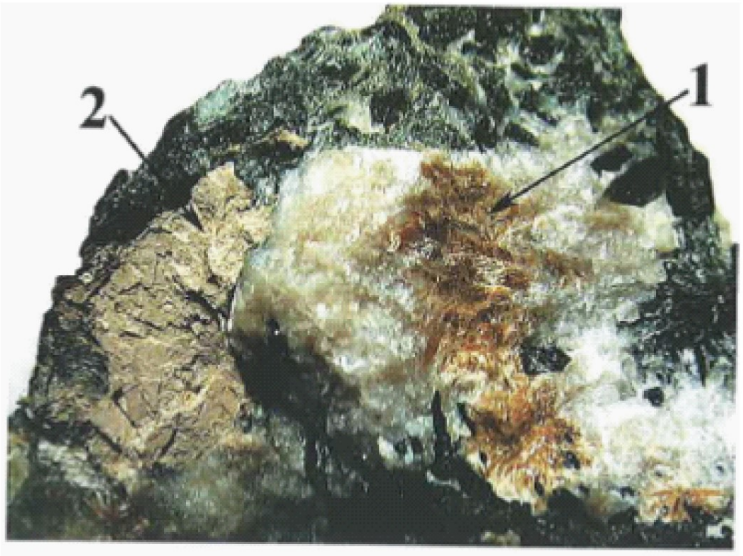


**Fig. 1.** Continued. (q) Proyer et al. (2014): BSE images of titanite with kassite (kst). (r) Kamenetsky et al. (2014): BSE images of alteration in ilmenite (ilm, ilmenite; Fe-ox, Fe-oxides; ks, kassite). (s) Moiseev and Chukanov (2006): cafetite (arrow #1).

# Supplementary Material 2: Published representative compositions

**Table 1.** Published representative compositions of kassite, cafetite and lucasite-(Ce) by EMPA or scanning electron microscope.

| | **Kukharenko et al. (1965)** | **Dawson and Smith (1977)** | **Mitchell and Chakhmouradian (1998)** | | **Popova et al. (1998) taken from Grey et al. (2003)** | **Grey et al. (2003)** | **Pekov et al. (2004)** |
|---|---|---|---|---|---|---|---|
| | Afrikanda massif, Kola peninsula | Wesselton, South Africa | Iron Mountain, Wyoming | | Saranovskoye, Northern Urals | Saranovskoye, Northern Urals | Saranovskoye, Urals |
| Wt % | **Kassite** | **Ca-titanate** | **Kassite 3** | **Kassite 4** | **Kassite** | **Chromian kassite** | **Kassite** |
| $SiO_2$ | 0.55 | 0.3 | nd | nd | 0.16 | | |
| $Al_2O_3$ | 0.98 | 0 | 0.35 | nd | 0.80 | 0.5 | 0.50 |
| $TiO_2$ | 65.59 | 64.0 | 62.72 | 60.31 | 60.34 | 64.18 | 64.18 |
| FeO | | 0.7 | nd | nd | 0.01 | | |
| $Fe_2O_3$ | 1.92 | -- | 0.99 | 1.93 | | 0.37 | 0.37 |
| MgO | none | 0.6 | 0.15 | nd | 0.57 | 0.52 | 0.52 |
| MnO | | 0 | nd | 0.52 | | 0.08 | 0.08 |
| $MnO_2$ | | | | | | | |
| CaO | 23.03 | 23.7 | 20.96 | 19.46 | 20.85 | 22.94 | 22.94 |
| $Na_2O$ | 0.11 | 0 | nd | nd | 0.09 | | |
| $K_2O$ | 0.04 | 0 | | | | | |
| $V_2O_3$ | | | | | | 0.25 | 0.25 |
| $Cr_2O_3$ | | 0 | | | 2.34 | 2.24 | 2.24 |
| NiO | | 0 | | | | | |
| SrO | 0.05 | | nd | nd | | | |
| $ZrO_2$ | | | | | | | |
| $Nb_2O_5$ | | | 1.02 | 1.15 | | | |
| BaO | | | | | | | |
| $La_2O_3$ | | | nd | 1.49 | | | |
| $Ce_2O_3$ | | | 2.46 | 3.48 | | | |
| $Pr_2O_3$ | | | nd | nd | | | |
| $Nd_2O_3$ | | | 1.23 | 1.43 | | | |
| $Sm_2O_3$ | | | | | | | |
| $HfO_2$ | | | | | | | |
| $Ta_2O_5$ | | | nd | nd | | | |
| $ThO_2$ | | | nd | nd | | | |
| O-F | 0.04 | | | | | | |
| -O=F | | | | | | | |
| Cl | | | | | 0.21 | | |
| $-O=Cl_2$ | | | | | 0.05 | | |
| $H_2O$ | | | | | | | |
| $H_2O+$ | 8.04 | | | | | | |
| $H_2O-$ | traces | | | | | | |
| $H_2O$ (-100) | | | | | | | |
| $H_2O$ (+100) | | | | | | | |
| $H_2O$ (-110) | | | | | | | |
| $H_2O$ (+110) | | | | | | | |
| *Total* | *100.35* | *89.6* | *89.88* | *89.77* | *85.32* | *91.08* | *91.08* |
| | $O=F_2$ (0.02) for Total=100.33 | Table 4, #5<br>Sample 1082<br>Mean 3 analyses | Analyses 3 and 4 of Table 2 | | | Average 8 analyses | |

**Table 1.** Continued.

| | Galuskin et al. (2004) | | | | Zajzon et al. (2013) | | | |
|---|---|---|---|---|---|---|---|---|
| | Wiluy deposit, Yakutia | | | | Perkupa evaporate mine, Hungary | | | |
| Wt % | **Kassite** | **Kassite** | **"Mn-kassite"** | **"Mn-kassite"** | **Kassite 1** | **Kassite 2** | **Kasite 3** | **"Mn-kassite"** |
| $SiO_2$ | 0.28 | 0.18 | 0.5 | 0.43 | | | | |
| $Al_2O_3$ | nd | nd | 0.58 | 0.11 | | | | |
| $TiO_2$ | 63.33 | 64.25 | 55.54 | 56.51 | 66.89 | 68.01 | 68.73 | 59.78 |
| FeO | | | | | 0.65 | 0.39 | 0.65 | 1.35 |
| $Fe_2O_3$ | 1.37 | 1.26 | 3.72 | 4.23 | | | | |
| MgO | nd | nd | 0.35 | 0.48 | | | | |
| MnO | 1.08 | 0.61 | 24.13 | 24.82 | 0.67 | 0.53 | 0.74 | 26.16 |
| $MnO_2$ | | | 1.96 | 3.4 | | | | |
| CaO | 21.74 | 22.14 | nd | 0.17 | 22.97 | 22.81 | 21.58 | 1.15 |
| $Na_2O$ | nd | nd | nd | nd | | | | |
| $K_2O$ | | | | | | | | |
| $V_2O_3$ | | | | | | | | |
| $Cr_2O_3$ | 0.08 | 0.05 | nd | nd | | | | |
| NiO | | | | | | | | |
| SrO | | | | | | | | |
| $ZrO_2$ | 0.34 | 0.24 | 0.1 | 0.07 | | | | |
| $Nb_2O_5$ | | | | | | | | |
| BaO | | | | | | | | |
| $La_2O_3$ | | | | | | | | |
| $Ce_2O_3$ | 0.4 | 0.39 | nm | nm | | | | |
| $Pr_2O_3$ | | | | | | | | |
| $Nd_2O_3$ | | | | | | | | |
| $Sm_2O_3$ | | | | | | | | |
| $HfO_2$ | 0.06 | 0.65 | nd | nd | | | | |
| $Ta_2O_5$ | | | | | | | | |
| $ThO_2$ | | | | | | | | |
| O-F | 0.05 | 0.45 | nm | nm | | | | |
| -O=F | 0.02 | 0.19 | | | | | | |
| Cl | | | | | | | | |
| -O=$Cl_2$ | | | | | | | | |
| $H_2O$ | 10.91 | 10.6 | 13.68 | 10.46 | 7.57 | 7.64 | 7.65 | 11.08 |
| $H_2O$+ | | | | | | | | |
| $H_2O$- | | | | | | | | |
| $H_2O$ (-100) | | | | | | | | |
| $H_2O$ (+100) | | | | | | | | |
| $H_2O$ (-110) | | | | | | | | |
| $H_2O$ (+110) | | | | | | | | |
| *Total* | *99.6* | *100.63* | *100.57* | *100.68 (NOTE 1)* | *98.75* | *99.37* | *99.35* | *100* |
| | $Ce_2O_3$: $Ce_2O_3$+$La_2O_3$+$Y_2O_3$ | | | | Mn-kassite composition by EDX; total includes MgO (1.01 wt%) and Cl (0.47 wt%) (see paper) | | | |
| | FeO and $H_2O$: calculated on charge balance | | | | | | | |
| | Note (1): calculated (O=40.63 wt%) and measured (O=40.21 wt%) (see paper) | | | | $H_2O$ in wt% assuming two (OH)- (see paper) | | | |

**Table 1.** Continued.

| | Proyer et al. (2014) | Kamenetsky et al. (2014) | Martins et al. (2014) | | | | | |
|---|---|---|---|---|---|---|---|---|
| | Kimi Complex, Greece | Monastery kimberlite, South Africa | Iron Mountain, Wyoming | | | Prairie Lake complex, Ontario | | |
| Wt % | **Kassite** | **Kassite** | **CTO 1** | **CTO 2** | **CTO 3** | **CTO 4** | **CTO 5** | **CTO 6** |
| $SiO_2$ | 0.43 | 3.46 | 0.09 | 0.19 | 1.04 | 0.03 | 0.1 | 0.17 |
| $Al_2O_3$ | nd | 0.05 | 0.28 | 0.24 | 0.22 | 0.03 | 0.07 | 0.08 |
| $TiO_2$ | 66.12 | 57.92 | 63.96 | 63.4 | 62.5 | 62.25 | 63.88 | 63.55 |
| FeO | nd | 1.9 | | | | | | |
| $Fe_2O_3$ | | | 1.54 | 1.65 | 0.83 | 1.14 | 1.15 | 0.91 |
| MgO | 0.54 | 2.85 | 0.04 | nd | nd | 0.05 | 0.08 | 0.08 |
| MnO | nd | 0.03 | 0.11 | 0.13 | 0.11 | 3.64 | 0.57 | 0.55 |
| $MnO_2$ | | | | | | | | |
| CaO | 22.67 | 17.4 | 20.57 | 20.35 | 20.45 | 18.17 | 21.65 | 20.78 |
| $Na_2O$ | nd | 1.21 | | | | | | |
| $K_2O$ | nd | 0.21 | nd | nd | 0.16 | nd | nd | nd |
| $V_2O_3$ | | | na | na | na | na | na | na |
| $Cr_2O_3$ | nd | <0.07 | na | na | na | na | na | na |
| NiO | | | | | | | | |
| SrO | | 0.66 | 0.12 | 0.1 | 0.1 | nd | nd | nd |
| $ZrO_2$ | | 0.48 | 0.07 | 0.05 | 0.04 | 0.04 | 0.11 | nd |
| $Nb_2O_5$ | | 3.72 | 0.55 | 0.5 | 0.51 | 0.92 | 1.31 | 0.98 |
| BaO | | 0.07 | 0.26 | 0.19 | 0.31 | 0.2 | 0.2 | 0.19 |
| $La_2O_3$ | | | 0.48 | 0.52 | 0.32 | 0.9 | 0.78 | 1.09 |
| $Ce_2O_3$ | | | 1.81 | 1.88 | 2.03 | 1.63 | 1.05 | 1.96 |
| $Pr_2O_3$ | | | 0.24 | 0.05 | 0.22 | nd | nd | nd |
| $Nd_2O_3$ | | | 0.97 | 1.15 | 1.09 | 0.66 | 0.3 | 0.77 |
| $Sm_2O_3$ | | | 0.29 | 0.08 | 0.19 | 0.19 | 0.18 | 0.13 |
| $HfO_2$ | | <0.07 | | | | | | |
| $Ta_2O_5$ | | | 0.2 | 0.23 | nd | 0.13 | nd | nd |
| $ThO_2$ | | | 0.23 | 0.29 | 0.31 | 0.16 | nd | 0.23 |
| O- | -0.12 | | | | | | | |
| F | 0.29 | | | | | | | |
| -O=F | | | | | | | | |
| Cl | | | | | | | | |
| $-O=Cl_2$ | | | | | | | | |
| $H_2O$ | | 7.71 | | | | | | |
| $H_2O+$ | | | | | | | | |
| $H_2O-$ | | | | | | | | |
| $H_2O$ (-100) | | | | | | | | |
| $H_2O$ (+100) | | | | | | | | |
| $H_2O$ (-110) | | | | | | | | |
| $H_2O$ (+110) | | | | | | | | |
| *Total* | *89.93* | *97.67* | *91.81* | *91* | *90.43* | *90.14* | *91.43* | *91.47* |
| | SEM analysis | $H_2O$ by stoichiometry | See Martins et al (2014) for calculated $H_2O$ | | | | | |
| | | | Total here is Martins et al. (2014) Subtotal (WDS) | | | | | |
| | 5K6a2 | | CTO = Ca-Ti oxide | | | | | |

**Table 1.** Continued.

| | **Kukharenko et al. (1959)** | **Kukharenko et al. (1965)** | **Krivovichev et al. (2003)** | | |
|---|---|---|---|---|---|
| | Afrikanda massif, Kola peninsula | Afrikanda massif, Kola peninsula | Afrikanda massif, Kola peninsula | Mt. Kukisvumchorr, Khibiny | Mt. Rasvumchorr, Khibiny |
| Wt % | **Cafetite** | **Cafetite** | **Cafetite** | **Cafetite** | **Cafetite** |
| $SiO_2$ | 1.00 | 1.00 | | 0.13 | 0.41 |
| $Al_2O_3$ | 2.02 | 2.02 | | 0.05 | 0.41 |
| $TiO_2$ | 54.11 | 54.11 | 67.78 | 64.83 | 66.23 |
| FeO | 0.49 | 0.49 | 0.27 | 0.97 | 0.66 |
| $Fe_2O_3$ | 22.00 | 22.00 | | | |
| MgO | 1.44 | 1.44 | | | |
| MnO | 0.20 | 0.20 | | 0.06 | 0.06 |
| $MnO_2$ | | | | | |
| CaO | 6.23 | 6.23 | 20.8 | 19.17 | 20.21 |
| $Na_2O$ | 0.28 | 0.28 | 0.64 | 1.63 | 0.8 |
| $K_2O$ | 0.4 | 0.40 | | 0.18 | 0.17 |
| $V_2O_3$ | | | | | |
| $Cr_2O_3$ | | | | | |
| NiO | | | | | |
| SrO | | | | --- | 0.12 |
| $ZrO_2$ | | | | | |
| $Nb_2O_5$ | | | 0.15 | 2.14 | 2.35 |
| BaO | | | | | |
| $La_2O_3$ | | | | | |
| $Ce_2O_3$ | | | | | |
| $Pr_2O_3$ | | | | | |
| $Nd_2O_3$ | | | | | |
| $Sm_2O_3$ | | | | | |
| $HfO_2$ | | | | | |
| $Ta_2O_5$ | | | | | |
| $ThO_2$ | | | | | |
| O-F | | | | | |
| -O=F | | | | | |
| Cl | | | | | |
| $-O=Cl_2$ | | | | | |
| $H_2O$ | | | | | |
| $H_2O+$ | | | | | |
| $H_2O-$ | | | | | |
| $H_2O$ (-100) | | 3.46 | | | |
| $H_2O$ (+100) | | 8.83 | | | |
| $H_2O$ (-110) | 3.46 | | | | |
| $H_2O$ (+110) | 8.83 | | | | |
| *Total* | *100.46* | *100.46* | *89.64* | *89.18* | *91.42* |
| | Table 3 | | Sample 13420 | Averaged values, see Krivovichev et al. (2003) for range in compositions | |
| | (Ca, Mg) (Fe, Al)$_2$Ti$_4$O$_{12}$·4H$_2$O | | Subtotal from see Krivovichev et al. (2003); see paper for estimated $H_2O$ | | |

**Table 1.** Continued.

| | Yakovenchuk et al. (2005) | | | Nickel et al. (1987) | Mitchell and Chakhmouradian (1998) |
|---|---|---|---|---|---|
| | Ideal composition (#3) | Mt. Kukisvumchorr (#1) | Mt. Rasvumchorr (#2) | Argyle AK1 diatreme, Australia | Iron Mountain, Wyoming |
| Wt % | **Cafetite** | **Cafetite** | **Cafetite** | **Lucasite** | **LREE-Ti oxide** |
| $SiO_2$ | | 0.20 | --- | 0.25 | 0.86 |
| $Al_2O_3$ | | 0.02 | 0.22 | 0.04 | nd |
| $TiO_2$ | 68.32 | 65.21 | 63.53 | 47.93 | 53.04 |
| FeO | | 1.02 | 0.83 | | nd |
| $Fe_2O_3$ | | | | | 0.59 |
| MgO | | | | 0.03 | nd |
| MnO | | 0.07 | 0.05 | | nd |
| $MnO_2$ | | | | | |
| CaO | 23.98 | 20.13 | 22.46 | 0.62 | 5.79 |
| $Na_2O$ | | 1.40 | 0.47 | | nd |
| $K_2O$ | | 0.16 | 0.06 | | |
| $V_2O_3$ | | | | | |
| $Cr_2O_3$ | | | | | |
| NiO | | | | | |
| SrO | | | | | nd |
| $ZrO_2$ | | | | | |
| $Nb_2O_5$ | | 2.15 | 3.08 | | 1.95 |
| BaO | | | | | |
| $La_2O_3$ | | | | 13.12 | 12.66 |
| $Ce_2O_3$ | | | | 24.99 | 16.53 |
| $Pr_2O_3$ | | | | 5.5 | 1.6 |
| $Nd_2O_3$ | | | | 5.9 | 4.71 |
| $Sm_2O_3$ | | | | | |
| $HfO_2$ | | | | | |
| $Ta_2O_5$ | | | | | nd |
| $ThO_2$ | | | | | 0.78 |
| O- | | | | | |
| F | | | | | |
| -O=F | | | | | |
| Cl | | | | | |
| -O=$Cl_2$ | | | | | |
| $H_2O$ | 7.70 | | | | |
| $H_2O$+ | | | | | |
| $H_2O$- | | | | | |
| $H_2O$ (-100) | | | | | |
| $H_2O$ (+100) | | | | | |
| $H_2O$ (-110) | | | | | |
| $H_2O$ (+110) | | | | | |
| *Total* | *100.00* | *90.36* | *90.70* | *98.38* | *98.51* |
| | | | | Average 8 analyses | Table 2 #11 |

# Supplementary Material 3: Published XRD

**Table 1.** Published XRD data for kassite, cafetite and lucasite-(Ce).

| **Kukharenko et al. (1959)** Kola Peninsula | | | | | |
|---|---|---|---|---|---|
| | **Cafetite** | | | **Indeterminate mineral** | |
| **# of lines** | ***I*** | **dα/*n*** | **dβ/*n*** | ***I*** | **dα/*n*** |
| 1 | 3 | (8.68) | 7.86 | 2p | 7.7 |
| 2 | 10 | 7.84 | (7.11) | 3p | 7.2 |
| 3 | 2 | 3.74 | 3.39 | 3 | 5.2 |
| 4 | 2 | (3.58) | 3.24 | 1 | 4.98 |
| 5 | 8 | 3.26 | (2.96) | 5 | 4.77 |
| 6 | 1 | 3.08 | 2.79 | 1 | 4.53 |
| 7 | 1 | 2.99 | 2.71 | 1 | 4.17 |
| 8 | 1 | (2.84) | 2.57 | 1 | 3.84 |
| 9 | 3 | 2.78 | 2.52 | 4 | (3.63) |
| 10 | 4 | 2.62 | 2.37 | 10 | 3.30 |
| 11 | 8 | 2.557 | (2.318) | 1 | 2.90 |
| 12 | 3 | 2.403 | 2.178 | 2 | 2.63 |
| 13 | 2 | (2.333) | 2.115 | 1 | (2.52) |
| 14 | 1 | 2.288 | 2.074 | 1 | 2.41 |
| 15 | 4 | 2.104 | (1.907) | 2 | 2.31 |
| 16 | 7 | 1.910 | 1.731 | 4 | 2.29 |
| 17 | 2 | (1.869) | 1.694 | 3p | 2.05 |
| 18 | 2 | 1.801 | 1.633 | 1 | 1.971 |
| 19 | 4 | 1.696 | 1.537 | 3 | 1.945 |
| 20 | 1 | 1.646 | 1.492 | 1 | 1.782 |
| 21 | 1 | 1.598 | 1.449 | 10 | 1.761 |
| 22 | 4 | 1.570 | 1.423 | 1 | 1.679 |
| 23 | 2 | 1.532 | 1.389 | 1 | 1.652 |
| 24 | 3p | 1.417 | 1.285 | 1 | 1.631 |
| 25 | 2 | 1.389 | 1.259 | 2 | 1.607 |
| 26 | --- | --- | --- | 3 | 1.516 |
| 27 | --- | --- | --- | 4 | 1.501 |
| 28 | --- | --- | --- | 1 | 1.442 |
| 29 | --- | --- | --- | 2-3 | 1.359 |
| 30 | --- | --- | --- | 1 | 1.304 |
| 31 | --- | --- | --- | 2 | 1.220 |
| 32 | --- | --- | --- | 2 | 1.196 |
| 33 | --- | --- | --- | 2 | 1.162 |
| 34 | --- | --- | --- | 1 | 1.149 |
| 35 | --- | --- | --- | 1 | 1.139 |
| 36 | --- | --- | --- | 1 | 1.092 |
| 37 | --- | --- | --- | 2 | 1.085 |

Table 2, units not reported

| **Kukharenko et al. (1965)** Kola Peninsula | | | |
|---|---|---|---|
| **Cafetite** | | **Kassite** | |
| ***I*** | **dα/*n*** | ***I*** | **dα/*n*** |
| 10 | 7.84 | 2p* | 7.7 |
| 2 | 3.74 | 3p | 7.2 |
| 8 | 3.26 | 3 | 5.2 |
| 1 | 3.08 | 1 | 4.98 |
| 1 | 2.99 | 5 | 4.77 |
| 3 | 2.78 | 1 | 4.53 |
| 4 | 2.62 | 1 | 4.17 |
| 8 | 2.557 | 1 | 3.84 |
| 3 | 2.403 | 4 | (3.63) |
| 1 | 2.888 | 10 | 3.30 |
| 4 | 2.104 | 1 | 2.90 |
| 4 | 2.104 | 2 | 2.63 |
| 7 | 1.910 | 1 | (2.52) |
| 2 | 1.801 | 1 | 2.41 |
| 4 | 1.696 | 2 | 2.31 |
| 1 | 1.646 | 4 | 2.29 |
| 1 | 1.598 | 3p | 2.05 |
| 4 | 1.570 | 1 | 1.971 |
| 2 | 1.532 | 3 | 1.945 |
| 3p | 1.417 | 1 | 1.785 |
| 2 | 1.389 | 10 | 1.761 |
| | | 1 | 1.679 |
| | | 1 | 1.652 |
| | | 1 | 1.631 |
| | | 2 | 1.607 |
| | | 3 | 1.516 |
| | | 4 | 1.501 |
| | | 1 | 1.442 |
| | | 2-3 | 1.359 |
| | | 1 | 1.304 |
| | | 2 | 1.220 |
| | | 2 | 1.196 |
| | | 2 | 1.162 |
| | | 1 | 1.149 |
| | | 1 | 1.139 |
| | | 1 | 1.092 |
| | | 2 | 1.085 |

p not defined in Table 76 for cafetite
p defined in Table 78 for kassite as *p-blurred lines

**Table 1.** Continued.

| Kukharenko et al. (1965) (from Evans et al. 1986) Kola Peninsula | | | | Yu et al. (1982) Wuyang, China | | Evans et al. (1986) Magnet Cove, Arkansas | |
|---|---|---|---|---|---|---|---|
| "Cafetite" | | "Kassite" | | Kassite | | Kassite (likely cafetite) | |
| d (obs) (Å) | I (rel) | d (obs) (Å) | I (rel) | d | I | d (obs) (Å) | I (rel) |
| 7.86 | 10 | 7.7 | 2 | 4.80 | 4 | 7.85 | 10 |
| | | 7.2 | 3 | 3.62 | 4 | 4.49 | 1 |
| | | 5.2 | 3 | 3.36 | 10 | 4.22 | 0.5 |
| | | 4.99 | 1 | 2.29 | 5 | 3.94 | 1 |
| 3.75 | 2 | 4.78 | 5 | 1.77 | 8 | 3.70 | 2 |
| | | 4.54 | 1 | 1.51 | 4 | 3.59 | 3 |
| 3.27 | 8 | 4.18 | 1 | | | 3.26 | 7 |
| | | 3.85 | 1 | | | 3.18 | 1 |
| 3.09 | 1 | 3.64 | 4 | | | 3.10 | 1 |
| 3.00 | 1 | 3.31 | 10 | | | 2.99 | 4 |
| | | 2.90 | 1 | | | 2.91 | 2 |
| 2.79 | 3 | 2.63 | 2 | | | 2.79 | 3 |
| 2.63 | 4 | 2.52 | 1 | | | | |
| 2.562 | 8 | 2.41 | 1 | | | 2.565 | 7 |
| | | 2.31 | 2 | | | 2.510 | 0.5 |
| 2.408 | 3 | 2.29 | 4 | | | 2.410 | 1 |
| 2.388 | 1 | 2.05 | 3 | | | 2.385 | 2 |
| | | 1.975 | 1 | | | 2.332 | 3 |
| | | 1.949 | 3 | | | 2.291 | 2 |
| | | 1.789 | 1 | | | 2.234 | 1 |
| 2.108 | 4 | 1.765 | 10 | | | 2.109 | 3 |
| | | 1.682 | 1 | | | 2.038 | 0.5 |
| | | 1.655 | 1 | | | 1.910 | 8 |
| | | 1.634 | 1 | | | 1.898 | 6 |
| | | 1.610 | 2 | | | 1.849 | 3 |
| 1.801 | 2 | 1.519 | 3 | | | 1.804 | 2 |
| | | 1.504 | 4 | | | 1.772 | 0.5 |
| | | 1.445 | 1 | | | 1.718 | 1 |
| 1.696 | 1 | 1.307 | 1 | | | 1.697 | 1 |
| | | 1.223 | 2 | | | 1.599 | 0.5 |
| 1.573 | 4 | 1.198 | 2 | | | 1.577 | 1 |
| | | 1.164 | 2 | | | 1.555 | 2 |
| 1.535 | 2 | 1.151 | 1 | | | 1.532 | 3 |
| | | 1.141 | 1 | | | 1.473 | 1 |
| 1.420 | 3 | 1.094 | 1 | | | 1.416 | 1 |
| 1.389 | 1 | 1.087 | 2 | | | | |
| kX units converted to Å (see paper) | | | | Chart 22<br><br>Unit reported as D in paper | | | |

**Table 1.** Continued.

| **Nickel et al. (1987)** Argyle AK1, Western Australia | | | |
|---|---|---|---|
| **Lucasite-(Ce)** | | | |
| $I_{est}$ | $d_{meas}$ (Å) | $d_{calc}$ (Å) | hkl |
| 3 | 6.49 | 6.514 | 011 |
| 3 | 4.449 | 4.450 | 110 |
| 10 | 3.376 | 3.378 | $\bar{1}12$ |
| 6 | 3.257 | 3.257 | 022 |
| 8 | 3.203 | 3.201 | 112 |
| | | 3.200 | $\bar{1}21$ |
| 1 | 3.122 | 3.121 | 121 |
| 1 | 3.048 | 3.046 | 013 |
| 7 | 2.584 | 2.584 | 200 |
| 4 | 2.541 | 2.542 | 130 |
| 5 | 2.225 | 2.226 | 202 |
| | | 2.225 | 220 |
| 2 | 2.066 | 2.067 | $\bar{2}22$ |
| 4 | 2.029 | 2.030 | $\bar{2}13$ |
| 1 | 1.915 | 1.916 | 213 |
| | | 1.915 | $\bar{2}31$ |
| 1 | 1.882 | 1.882 | 231 |
| 6 | 1.8306 | 1.8306 | $\bar{2}04$ |
| 2 | 1.7320 | 1.7325 | 134 |
| | | 1.7321 | $\bar{1}43$ |
| 1 | 1.7270 | 1.724 | 051 |
| | | 1.720 | 204 |
| 2 | 1.5964 | 1.5965 | $\bar{3}21$ |
| 1 | 1.4839 | 1.4834 | 330 |

| **Krivovichev et al. (2003) (from Martins et al. 2014)** Kola Peninsula | | | | |
|---|---|---|---|---|
| **Cafetite** | | | | |
| *h* | *k* | *l* | $d_{calc}$ | *I* |
| 0 | 0 | 2 | 7.879 | 100 |
| 0 | 2 | 0 | 6.043 | 5 |
| 0 | 1 | 4 | 3.746 | 6 |
| -1 | 1 | 3 | 3.693 | 5 |
| 1 | 2 | 1 | 3.596 | 9 |
| -1 | 2 | 2 | 3.589 | 6 |
| 1 | 2 | 2 | 3.274 | 32 |
| -1 | 2 | 3 | 3.264 | 22 |
| -1 | 1 | 4 | 3.201 | 5 |
| -1 | 3 | 2 | 2.99 | 16 |
| 1 | 2 | 3 | 2.919 | 4 |
| -1 | 2 | 4 | 2.91 | 5 |
| -1 | 3 | 3 | 2.794 | 8 |
| 0 | 0 | 6 | 2.626 | 4 |
| 1 | 3 | 3 | 2.568 | 18 |
| -1 | 3 | 4 | 2.562 | 9 |
| 0 | 5 | 1 | 2.389 | 5 |
| 1 | 3 | 4 | 2.333 | 9 |
| -1 | 4 | 4 | 2.234 | 4 |
| -1 | 3 | 6 | 2.108 | 5 |
| -1 | 3 | 7 | 1.912 | 5 |
| -2 | 4 | 1 | 1.912 | 15 |
| 2 | 4 | 0 | 1.898 | 5 |
| -2 | 4 | 2 | 1.897 | 7 |
| 2 | 2 | 4 | 1.853 | 4 |
| 0 | 4 | 7 | 1.805 | 4 |
| 0 | 6 | 5 | 1.697 | 9 |
| 3 | 1 | 2 | 1.535 | 4 |

| **Pekov et al. (2004)** Saranovskoye chromite deposit, Urals | | |
|---|---|---|
| **Kassite** | | |
| $I_{(see\ note)}$ | $d_{(see\ note)}$, Å | *hkl* |
| 26 | 4.763 | 002 |
| 6 | 4.540 | 110 |
| 2 | 4.490 | 020 |
| 1 | 4.203 | 012 |
| 1 | 4.110 | $11\bar{1}$ |
| 1 | 4.086 | 111 |
| 1 | 4.061 | 021 |
| 100 | 3.300 | $11\bar{2}$, 112 |
| 97 | 3.273 | 022 |
| 1 | 2.857 | 031 |
| 1 | 2.784 | $12\bar{2}$ |
| 16 | 2.633 | 200 |
| 23 | 2.603 | 130 |
| 1 | 2.385 | 004 |
| 19 | 2.316 | $20\bar{2}$ |
| 37 | 2.282 | 132 |
| 1 | 2.209 | 221 |
| 1 | 2.185 | 041, 033 |
| 1 | 2.120 | $11\bar{4}$ |
| 16 | 2.059 | $22\bar{2}$ |
| 16 | 2.046 | 222 |
| 4 | 2.032 | 042 |
| 1 | 1.987 | $21\bar{3}$ |
| 1 | 1.961 | $12\bar{4}$ |
| 1 | 1.952 | 124 |
| 1 | 1.939 | $23\bar{1}$, 231 |
| 1 | 1.867 | 015 |
| 1 | 1.855 | $22\bar{3}$ |
| 1 | 1.836 | 043 |
| 18 | 1.776 | $20\bar{4}$ |
| 41 | 1.762 | $13\bar{4}$, 204 |
| 19 | 1.756 | 134 |
| 1 | 1.702 | 150 |
| 1 | 1.685 | $24\bar{1}$ |
| 1 | 1.653 | $22\bar{4}$ |
| 11 | 1.627 | $31\bar{2}$ |
| 16 | 1.603 | 242, $15\bar{2}$, 152 |
| 1 | 1.566 | 016, 053 |
| 24 | 1.516 | 330 |
| 15 | 1.499 | 026, 116, 060 |
| 1 | 1.466 | 251 |
| 2 | 1.448 | $33\bar{2}$ |
| 1 | 1.442 | 332 |
| 1 | 1.429 | 062 |
| 1 | 1.3838 | 154 |
| 5 | 1.3605 | $13\bar{6}$ |
| 2 | 1.3188 | 400 |
| 3 | 1.3082 | $22\bar{6}$ |

Data from Appendix 1 of Martins et al. (2014); I≥4 listed

Column 2
Subscript to *I* and *d* may be change or measurement

**Table 1.** Continued.

| **Yakovenchuk et al. (2005)** Mt. Rasvumchorr | | **Zajzon et al. (2013)** Perkupa serpentinite, Hungary | | | |
|---|---|---|---|---|---|
| **Cafetite** | | **Kassite** | | | |
| | | **No.** | **d (A)** | **Int (%)** | ***hkl*** |
| 7.90 | 100 | 1 | 4.7784 | 26 | 002 |
| 2.631 | 8 | 2 | 4.552 | 9.4 | 110 |
| 3.946 | 5 | 3 | | | |
| 1.578 | 5 | 4 | | | |
| 3.754 | 4 | 5 | | | |
| 2.573 | 4 | 6 | | | |
| | | 7 | 3.3066 | 82 | -112 |
| | | 8 | 3.2852 | 86 | 112 |
| | | | 3.2777 | 100 | 022 |
| | | 9 | | | |
| | | 10 | | | |
| | | 11 | | | |
| | | 12 | 2.6374 | 23 | 200 |
| | | 13 | 2.6097 | 38 | 130 |
| | | 14 | | | |
| | | 15 | | | |
| | | 16 | | | |
| | | 17 | | | |
| | | 18 | 2.3164 | 26 | -202 |
| | | 19 | 2.2868 | 52 | 132 |
| | | 20 | | | |
| | | 21 | | | |
| | | | 2.0300 | 17 | -222 |
| | | 22 | 2.0497 | 18 | 222 |
| | | | 2.0390 | 12 | 042 |
| | | 23 | | | |
| | | 24 | | | |
| | | 25 | | | |
| | | 26 | 1.7772 | 24 | -204 |
| | | | 1.7655 | 29 | -134 |
| | | 27 | 1.7641 | 15 | 204 |
| | | | 1.759 | 46 | 134 |
| | | 28 | | | |
| | | 29 | | | |
| | | 30 | 1.6269 | 13 | -312 |
| | | 31 | 1.6047 | 12 | 152 |
| | | 32 | 1.5173 | 25 | 330 |
| | | 33 | 1.5015 | 11 | 060 |
| | | 34 | | | |
| Units not given | | calculated using Grey et al. (2003) (see paper) | | | |

**Table 1.** Continued.

| Martins et al. (2014) Prairie Lake carbonatite | | | | | | Martins et al. (2014) | | | | | |
|---|---|---|---|---|---|---|---|---|---|---|---|
| **Kassite** | | | | | | **Kassite (condensed)** | | | | | |
| ***h*** | ***k*** | ***l*** | ***d* (obs)** | ***d* (calc)** | ***I*** | ***h*** | ***k*** | ***l*** | $d_{obs}$ | $d_{calc}$ | ***I*** |
| 0 | 0 | 2 | 4.81 | 4.77 | 16 | 0 | 0 | 2 | 4.81 | 4.77 | 16 |
| 1 | 1 | 0 | 4.53 | 4.56 | 1 | 1 | 1 | -2 | 3.3 | 3.31 | 63 |
| 0 | 2 | 0 | 4.5 | 4.5 | 1 | 1 | 1 | 2 | 3.29 | 3.29 | 86 |
| 0 | 1 | 2 | 4.19 | 4.22 | 1 | 0 | 2 | 2 | 3.28 | 3.27 | 100 |
| 1 | 1 | $\bar{1}$ | 4.12 | 4.12 | 2 | 2 | 0 | 0 | 2.644 | 2.642 | 4 |
| 0 | 2 | 1 | 4.07 | 4.07 | 1 | 1 | 3 | 0 | 2.601 | 2.607 | 24 |
| 1 | 1 | $\bar{2}$ | 3.3 | 3.31 | 63 | 2 | 0 | -2 | 2.32 | 2.319 | 8 |
| 1 | 1 | 2 | 3.29 | 3.29 | 86 | 2 | 0 | 2 | 2.308 | 2.305 | 14 |
| 0 | 2 | 2 | 3.28 | 3.27 | 100 | 1 | 3 | -2 | 2.294 | 2.291 | 1 |
| 0 | 3 | 1 | 2.857 | 2.859 | 2 | 1 | 3 | 2 | 2.284 | 2.284 | 45 |
| 2 | 0 | 0 | 2.644 | 2.642 | 4 | 0 | 4 | 0 | 2.243 | 2.248 | 5 |
| 1 | 3 | 0 | 2.601 | 2.607 | 24 | 0 | 4 | 1 | 2.188 | 2.188 | 4 |
| 0 | 2 | 3 | 2.597 | 2.598 | 1 | 2 | 2 | -2 | 2.060 | 2.061 | 8 |
| 0 | 0 | 4 | 2.387 | 2.387 | 3 | 2 | 2 | 2 | 2.050 | 2.051 | 17 |
| 1 | 2 | $\bar{3}$ | 2.342 | 2.337 | 1 | 0 | 4 | 2 | 2.034 | 2.033 | 15 |
| 2 | 0 | $\bar{2}$ | 2.32 | 2.319 | 8 | 2 | 0 | -4 | 1.778 | 1.778 | 14 |
| 2 | 0 | 2 | 2.308 | 2.305 | 14 | 1 | 3 | -4 | 1.764 | 1.764 | 61 |
| 1 | 3 | $\bar{2}$ | 2.294 | 2.291 | 1 | 3 | 1 | 2 | 1.621 | 1.622 | 5 |
| 1 | 3 | 2 | 2.284 | 2.284 | 45 | 2 | 4 | -2 | 1.616 | 1.614 | 4 |
| 0 | 4 | 0 | 2.243 | 2.248 | 5 | 2 | 4 | 2 | 1.609 | 1.609 | 7 |
| 0 | 4 | 1 | 2.188 | 2.188 | 4 | 1 | 5 | -2 | 1.604 | 1.604 | 10 |
| 2 | 2 | $\bar{2}$ | 2.06 | 2.061 | 8 | 1 | 5 | 2 | 1.600 | 1.602 | 13 |
| 2 | 2 | 2 | 2.050 | 2.051 | 17 | 3 | 3 | 0 | 1.516 | 1.519 | 9 |
| 0 | 4 | 2 | 2.034 | 2.033 | 15 | 1 | 1 | -6 | 1.504 | 1.505 | 11 |
| 1 | 4 | $\bar{1}$ | 2.021 | 2.023 | 1 | 0 | 6 | 0 | 1.499 | 1.498 | 9 |
| 2 | 0 | $\bar{4}$ | 1.778 | 1.778 | 14 | | | | | | |
| 0 | 5 | 1 | 1.767 | 1.767 | 1 | | | | | | |
| 1 | 3 | $\bar{4}$ | 1.764 | 1.764 | 61 | | | | | | |
| 1 | 4 | 3 | 1.731 | 1.732 | 3 | | | | | | |
| 2 | 4 | $\bar{1}$ | 1.685 | 1.686 | 2 | | | | | | |
| 1 | 5 | $\bar{1}$ | 1.676 | 1.676 | 2 | | | | | | |
| 2 | 2 | $\bar{4}$ | 1.653 | 1.653 | 1 | | | | | | |
| 2 | 2 | 4 | 1.642 | 1.643 | 3 | | | | | | |
| 3 | 1 | $\bar{2}$ | 1.631 | 1.629 | 2 | | | | | | |
| 3 | 1 | 2 | 1.621 | 1.622 | 5 | | | | | | |
| 2 | 4 | $\bar{2}$ | 1.616 | 1.614 | 4 | | | | | | |
| 2 | 4 | 2 | 1.609 | 1.609 | 7 | | | | | | |
| 1 | 5 | $\bar{2}$ | 1.604 | 1.604 | 10 | | | | | | |
| 1 | 5 | 2 | 1.600 | 1.602 | 13 | | | | | | |
| 0 | 5 | 3 | 1.568 | 1.565 | 1 | | | | | | |
| 3 | 3 | 0 | 1.516 | 1.519 | 9 | | | | | | |
| 1 | 1 | $\bar{6}$ | 1.504 | 1.505 | 11 | | | | | | |
| 0 | 6 | 0 | 1.499 | 1.498 | 9 | | | | | | |

**Table 1.** Continued.

| **Martins et al. (2014)** continued… | | | | | | **Martins et al. (2014)** continued… | | | | | |
|---|---|---|---|---|---|---|---|---|---|---|---|
| **Kassite** | | | | | | **Kassite (condensed)** | | | | | |
| ***h*** | ***k*** | ***l*** | ***d* (obs)** | ***d* (calc)** | ***I*** | ***h*** | ***k*** | ***l*** | $d_{obs}$ | $d_{calc}$ | ***I*** |
| 3 | 3 | $\bar{2}$ | 1.45 | 1.45 | 1 | | | | | | |
| 3 | 3 | 2 | 1.444 | 1.445 | 3 | | | | | | |
| 0 | 6 | 2 | 1.428 | 1.43 | 2 | | | | | | |
| 1 | 6 | 1 | 1.426 | 1.425 | 1 | | | | | | |
| 1 | 3 | $\bar{6}$ | 1.36 | 1.36 | 7 | | | | | | |
| 2 | 0 | 6 | 1.359 | 1.359 | 5 | | | | | | |
| 2 | 2 | $\bar{6}$ | 1.307 | 1.308 | 4 | | | | | | |
| 2 | 6 | 0 | 1.303 | 1.303 | 5 | | | | | | |
| 2 | 2 | 6 | 1.301 | 1.301 | 4 | | | | | | |
| 3 | 3 | 4 | 1.278 | 1.278 | 3 | | | | | | |
| 0 | 6 | 4 | 1.269 | 1.269 | 4 | | | | | | |
| 2 | 6 | $\bar{2}$ | 1.259 | 1.259 | 3 | | | | | | |
| 1 | 7 | $\bar{1}$ | 1.237 | 1.238 | 3 | | | | | | |
| 4 | 2 | $\bar{2}$ | 1.227 | 1.227 | 1 | | | | | | |
| 4 | 2 | 2 | 1.223 | 1.223 | 2 | | | | | | |
| 3 | 5 | $\bar{2}$ | 1.219 | 1.218 | 4 | | | | | | |
| 3 | 5 | 2 | 1.216 | 1.215 | 5 | | | | | | |
| 1 | 7 | $\bar{2}$ | 1.208 | 1.208 | 1 | | | | | | |
| 3 | 1 | $\bar{6}$ | 1.176 | 1.175 | 3 | | | | | | |
| 2 | 4 | $\bar{6}$ | 1.168 | 1.168 | 3 | | | | | | |
| 3 | 1 | 6 | 1.166 | 1.167 | 3 | | | | | | |
| 1 | 5 | $\bar{6}$ | 1.164 | 1.164 | 4 | | | | | | |
| 2 | 4 | 6 | 1.164 | 1.163 | 1 | | | | | | |
| 1 | 5 | 6 | 1.161 | 1.161 | 2 | | | | | | |
| 4 | 0 | $\bar{4}$ | 1.159 | 1.16 | 1 | | | | | | |
| 4 | 0 | 4 | 1.153 | 1.152 | 16 | | | | | | |
| 2 | 6 | $\bar{4}$ | 1.146 | 1.146 | 1 | | | | | | |
| 2 | 6 | 4 | 1.142 | 1.142 | 3 | | | | | | |
| 4 | 4 | $\bar{2}$ | 1.11 | 1.11 | 2 | | | | | | |
| 4 | 4 | 2 | 1.106 | 1.106 | 1 | | | | | | |
| 0 | 8 | 2 | 1.094 | 1.094 | 1 | | | | | | |
| Micro-XRD | | | | | | Data from Appendix 1 of Martins et al. (2014); I≥4 listed | | | | | |

**Table 1.** EPMA data (weight %).

| $SiO_2$ | $Al_2O_3$ | $TiO_2$ | $V_2O_3$ | $Cr_2O_3$ | MnO | FeO | MgO | CaO | $La_2O_3$ | $Ce_2O_3$ | $Pr_2O_3$ | $Nd_2O_3$ | $Sm_2O_3$ | $Na_2O$ | $K_2O$ | $P_2O_5$ | Total | Comment |
|---|---|---|---|---|---|---|---|---|---|---|---|---|---|---|---|---|---|---|
| 0.28 | 0.01 | 58.17 | 0.00 | 0.00 | 7.72 | 2.62 | 0.11 | 10.49 | 2.52 | 4.61 | 0.00 | 0.00 | 0.00 | 0.00 | 0.00 | 0.00 | 86.52 | 31462_Circle2_grain1_1 |
| 0.44 | 0.02 | 57.07 | 0.00 | 0.00 | 7.90 | 3.51 | 0.12 | 8.88 | 2.56 | 5.50 | 0.48 | 1.70 | 0.00 | 0.00 | 0.00 | 0.00 | 88.17 | 31462_Circle2_grain1_2 |
| 0.13 | 0.01 | 58.39 | 0.00 | 0.00 | 6.72 | 2.25 | 0.10 | 11.46 | 2.61 | 5.05 | 0.58 | 1.54 | 0.07 | 0.02 | 0.00 | 0.00 | 88.93 | 31462_Circle2_grain1_3 |
| 1.86 | 0.02 | 57.36 | 0.00 | 0.00 | 8.81 | 5.20 | 0.25 | 8.68 | 1.48 | 3.14 | 0.09 | 0.87 | 0.00 | 0.02 | 0.00 | 0.02 | 87.80 | 31462_Circle2_grain1_4 |
| 0.18 | 0.01 | 60.62 | 0.00 | 0.00 | 5.31 | 2.31 | 0.16 | 15.42 | 1.05 | 2.28 | 0.21 | 0.80 | 0.04 | 0.00 | 0.01 | 0.02 | 88.40 | 31462_Circle2_grain1_5 |
| 0.95 | 0.03 | 61.13 | 0.00 | 0.00 | 4.40 | 3.15 | 0.13 | 11.73 | 1.89 | 4.65 | 0.36 | 1.35 | 0.06 | 0.01 | 0.00 | 0.00 | 89.85 | 31462_Circle2_grain2_1 |
| 1.02 | 0.03 | 59.41 | 0.00 | 0.00 | 5.01 | 2.82 | 0.17 | 14.29 | 1.29 | 2.78 | 0.31 | 0.85 | 0.05 | 0.00 | 0.00 | 0.02 | 88.04 | 31462_Circle2_grain2_2 |
| 0.05 | 0.01 | 60.77 | 0.00 | 0.00 | 4.24 | 1.45 | 0.12 | 16.94 | 1.02 | 2.18 | 0.10 | 0.61 | 0.01 | 0.04 | 0.00 | 0.02 | 87.58 | 31462_Circle2_grain2_3 |
| 0.55 | 0.01 | 55.08 | 0.00 | 0.01 | 3.31 | 1.87 | 0.49 | 10.97 | 4.72 | 8.59 | 1.01 | 2.70 | 0.19 | 0.00 | 0.01 | 0.01 | 89.54 | 31462_Circle2_grain3_1 |
| 0.50 | 0.00 | 59.85 | 0.00 | 0.00 | 3.92 | 2.12 | 0.18 | 15.45 | 1.33 | 2.86 | 0.08 | 0.88 | 0.06 | 0.00 | 0.00 | 0.00 | 87.24 | 31462_Circle2_grain3_2 |
| 0.10 | 0.02 | 60.01 | 0.00 | 0.00 | 6.42 | 2.78 | 0.17 | 14.68 | 0.70 | 1.48 | 0.01 | 0.54 | 0.04 | 0.00 | 0.01 | 0.00 | 86.96 | 31462_Circle2_grain3_3 |
| 0.04 | 0.01 | 57.80 | 0.09 | 0.00 | 1.18 | 26.02 | 15.65 | 0.15 | 0.00 | 0.02 | 0.00 | 0.04 | 0.08 | 0.08 | 0.00 | 0.01 | 101.17 | 31462_Circle1_grain1_1 |
| 0.38 | 0.30 | 40.65 | 0.05 | 0.00 | 5.94 | 45.69 | 2.44 | 0.18 | 0.05 | 0.10 | 0.00 | 0.03 | 0.00 | 0.02 | 0.00 | 0.02 | 95.84 | 31462_Circle1_grain1_2 |
| 3.10 | 0.29 | 65.55 | 0.00 | 0.00 | 1.84 | 16.60 | 2.34 | 3.00 | 0.15 | 0.37 | 0.11 | 0.12 | 0.00 | 0.03 | 0.01 | 0.00 | 93.50 | 31462_Circle1_grain1_3 |
| 0.25 | 0.01 | 48.34 | 0.00 | 0.61 | 0.29 | 2.27 | 0.09 | 1.42 | 12.56 | 24.27 | 1.93 | 4.64 | 0.01 | 0.00 | 0.00 | 0.00 | 96.67 | 31462_Circle1_grain1_4 |
| 0.22 | 0.03 | 89.79 | 0.03 | 0.00 | 0.16 | 4.23 | 0.22 | 0.87 | 0.05 | 0.15 | 0.00 | 0.08 | 0.06 | 0.03 | 0.02 | 0.01 | 95.97 | 31462_Circle1_grain1_5 |
| 0.18 | 0.01 | 93.18 | 0.08 | 0.00 | 0.08 | 1.38 | 0.03 | 0.67 | 0.00 | 0.18 | 0.12 | 0.08 | 0.00 | 0.02 | 0.02 | 0.00 | 96.04 | 31462_Circle1_grain1b_1 |
| 2.35 | 0.01 | 57.42 | 0.00 | 0.00 | 3.18 | 3.68 | 0.23 | 14.71 | 1.23 | 2.87 | 0.07 | 0.77 | 0.00 | 0.00 | 0.01 | 0.03 | 86.57 | 31462_Circle1_grain1b_2 |
| 0.16 | 0.01 | 59.70 | 0.00 | 0.00 | 6.06 | 2.69 | 0.13 | 13.26 | 1.53 | 3.21 | 0.36 | 1.11 | 0.11 | 0.00 | 0.00 | 0.00 | 88.35 | 31462_Circle1_grain2_1 |
| 0.12 | 0.02 | 60.39 | 0.00 | 0.00 | 4.99 | 2.69 | 0.23 | 15.95 | 0.70 | 1.61 | 0.32 | 0.47 | 0.04 | 0.01 | 0.01 | 0.00 | 87.56 | 31462_Circle1_grain2_2 |
| 0.19 | 0.01 | 57.63 | 0.00 | 0.02 | 7.63 | 2.31 | 0.11 | 8.91 | 5.03 | 6.55 | 0.45 | 1.66 | 0.06 | 0.02 | 0.00 | 0.00 | 90.56 | 31462_Circle3_grain1_1 |
| 0.12 | 0.02 | 58.86 | 0.00 | 0.00 | 10.17 | 3.11 | 0.16 | 9.18 | 2.60 | 3.57 | 0.40 | 0.90 | 0.02 | 0.00 | 0.07 | 0.01 | 89.20 | 31462_Circle3_grain1_2 |
| 0.17 | 0.01 | 59.94 | 0.00 | 0.00 | 10.35 | 3.54 | 0.27 | 10.93 | 0.92 | 1.67 | 0.20 | 0.55 | 0.00 | 0.00 | 0.00 | 0.02 | 88.57 | 31462_Circle3_grain1_3 |
| 2.09 | 0.01 | 50.08 | 0.00 | 0.00 | 7.91 | 31.64 | 1.01 | 0.44 | 0.01 | 0.08 | 0.03 | 0.00 | 0.00 | 0.01 | 0.05 | 0.02 | 93.39 | 31462_Circle3_grain1_4 |
| 0.08 | 0.00 | 59.47 | 0.00 | 0.00 | 11.06 | 3.55 | 0.20 | 9.96 | 1.07 | 2.07 | 0.37 | 0.47 | 0.07 | 0.00 | 0.00 | 0.00 | 88.39 | 31462_Circle3_grain1_5 |
| 0.18 | 0.02 | 57.96 | 0.00 | 0.00 | 8.67 | 2.15 | 0.05 | 9.19 | 3.46 | 5.50 | 0.45 | 1.87 | 0.12 | 0.00 | 0.01 | 0.00 | 89.64 | 31462_Circle3_grain1_6 |
| 0.30 | 0.01 | 61.05 | 0.00 | 0.00 | 5.97 | 2.85 | 0.21 | 15.59 | 0.52 | 1.23 | 0.13 | 0.29 | 0.09 | 0.00 | 0.01 | 0.00 | 88.25 | 31462_Circle3_grain2a_1 |
| 0.06 | 0.00 | 60.65 | 0.00 | 0.00 | 4.27 | 1.30 | 0.09 | 15.57 | 2.15 | 3.63 | 0.37 | 1.06 | 0.09 | 0.00 | 0.00 | 0.00 | 89.24 | 31462_Circle3_grain2a_2 |
| 0.16 | 0.02 | 61.19 | 0.00 | 0.00 | 5.78 | 2.50 | 0.17 | 15.54 | 0.67 | 1.47 | 0.00 | 0.54 | 0.05 | 0.01 | 0.00 | 0.00 | 88.09 | 31462_Circle3_grain2a_3 |
| 2.12 | 0.03 | 83.74 | 0.00 | 0.00 | 1.01 | 1.77 | 0.56 | 2.73 | 0.24 | 0.64 | 0.09 | 0.17 | 0.02 | 0.01 | 0.01 | 0.02 | 93.15 | 31462_Circle3_grain2a_4 |
| 0.57 | 0.03 | 57.03 | 0.00 | 0.38 | 0.28 | 1.00 | 0.02 | 3.27 | 10.33 | 16.24 | 1.18 | 4.16 | 0.13 | 0.00 | 0.04 | 0.01 | 94.65 | Line 1 c4_g1 |
| 0.60 | 0.00 | 58.36 | 0.00 | 0.00 | 6.56 | 2.90 | 0.17 | 12.49 | 1.59 | 3.17 | 0.35 | 0.95 | 0.00 | 0.01 | 0.00 | 0.01 | 87.17 | Line 2 c4_g1 |
| 0.88 | 0.00 | 57.53 | 0.00 | 0.00 | 7.06 | 3.14 | 0.15 | 11.74 | 1.66 | 3.13 | 0.18 | 0.94 | 0.07 | 0.02 | 0.00 | 0.01 | 86.51 | Line 3 c4_g1 |
| 1.28 | 0.00 | 54.68 | 0.00 | 0.11 | 2.27 | 1.40 | 0.06 | 7.83 | 6.18 | 11.44 | 1.03 | 3.33 | 0.19 | 0.00 | 0.01 | 0.01 | 89.80 | Line 4 c4_g1 |
| 1.25 | 0.00 | 57.45 | 0.00 | 0.00 | 6.22 | 3.47 | 0.17 | 11.88 | 1.76 | 3.29 | 0.24 | 0.93 | 0.05 | 0.00 | 0.00 | 0.00 | 86.70 | Line 5 c4_g1 |
| 1.00 | 0.02 | 58.25 | 0.00 | 0.00 | 6.01 | 3.09 | 0.17 | 13.46 | 1.09 | 2.27 | 0.38 | 0.60 | 0.01 | 0.04 | 0.00 | 0.01 | 86.41 | Line 6 c4_g1 |
| 0.14 | 0.02 | 60.07 | 0.00 | 0.00 | 5.88 | 2.32 | 0.20 | 14.74 | 0.99 | 1.98 | 0.00 | 0.57 | 0.06 | 0.00 | 0.00 | 0.00 | 86.97 | 31462_c4_g1_7 |
| 0.11 | 0.00 | 59.13 | 0.00 | 0.00 | 9.19 | 3.36 | 0.18 | 10.57 | 1.34 | 2.87 | 0.27 | 0.91 | 0.09 | 0.00 | 0.00 | 0.00 | 88.03 | 31462_c4_g2_1 |
| 0.16 | 0.01 | 59.58 | 0.00 | 0.00 | 8.22 | 3.09 | 0.23 | 13.88 | 0.69 | 1.43 | 0.00 | 0.35 | 0.00 | 0.00 | 0.01 | 0.00 | 87.68 | 31462_c4_g2_2 |

**Table 1.** Continued.

| $SiO_2$ | $Al_2O_3$ | $TiO_2$ | $V_2O_3$ | $Cr_2O_3$ | MnO | FeO | MgO | CaO | $La_2O_3$ | $Ce_2O_3$ | $Pr_2O_3$ | $Nd_2O_3$ | $Sm_2O_3$ | $Na_2O$ | $K_2O$ | $P_2O_5$ | Total | Comment |
|---|---|---|---|---|---|---|---|---|---|---|---|---|---|---|---|---|---|---|
| 2.82 | 0.03 | 56.17 | 0.00 | 0.00 | 5.55 | 5.42 | 0.23 | 11.79 | 1.24 | 3.10 | 0.20 | 0.82 | 0.05 | 0.01 | 0.00 | 0.02 | 87.46 | 31462_c6_g1_1 |
| 0.11 | 0.00 | 60.83 | 0.00 | 0.00 | 4.49 | 1.93 | 0.16 | 16.53 | 0.89 | 1.95 | 0.30 | 0.54 | 0.08 | 0.00 | 0.00 | 0.00 | 87.82 | 31462_c6_g1_2 |
| 0.53 | 0.02 | 57.99 | 0.00 | 0.00 | 4.74 | 2.37 | 0.18 | 12.83 | 2.92 | 5.29 | 0.55 | 1.51 | 0.04 | 0.03 | 0.01 | 0.02 | 89.02 | 31462_c6_g1_3 |
| 1.44 | 0.03 | 59.01 | 0.00 | 0.00 | 4.99 | 3.46 | 0.20 | 14.41 | 0.97 | 2.30 | 0.00 | 0.64 | 0.05 | 0.00 | 0.00 | 0.01 | 87.53 | 31462_c6_g1_4 |
| 0.13 | 0.01 | 60.21 | 0.00 | 0.00 | 6.36 | 2.69 | 0.25 | 15.25 | 0.65 | 1.39 | 0.11 | 0.44 | 0.03 | 0.01 | 0.00 | 0.01 | 87.54 | 31462_c6_g1_5 |
| 0.10 | 0.02 | 59.23 | 0.00 | 0.00 | 7.51 | 2.83 | 0.18 | 13.94 | 1.01 | 2.06 | 0.23 | 0.58 | 0.03 | 0.00 | 0.01 | 0.02 | 87.75 | 31462_c6_g2a_1 |
| 0.09 | 0.04 | 48.49 | 0.21 | 0.00 | 9.01 | 37.81 | 0.53 | 0.78 | 0.01 | 0.02 | 0.00 | 0.00 | 0.00 | 0.00 | 0.01 | 0.00 | 96.99 | 31462_c6_g2a_2 |
| 0.36 | 0.03 | 89.34 | 0.00 | 0.00 | 0.40 | 1.73 | 0.17 | 2.64 | 0.06 | 0.25 | 0.11 | 0.04 | 0.00 | 0.01 | 0.01 | 0.00 | 95.15 | 31462_c6_g2a_3 |
| 0.08 | 0.00 | 60.40 | 0.00 | 0.00 | 8.52 | 3.14 | 0.23 | 13.39 | 0.67 | 1.36 | 0.05 | 0.36 | 0.00 | 0.01 | 0.02 | 0.01 | 88.26 | 31462_c6_g2a_4 |
| 0.13 | 0.01 | 59.59 | 0.00 | 0.00 | 9.32 | 3.57 | 0.29 | 12.23 | 0.55 | 1.07 | 0.04 | 0.31 | 0.02 | 0.01 | 0.02 | 0.00 | 87.15 | 31462_c6_g2b_1 |
| 2.57 | 0.04 | 55.65 | 0.00 | 0.00 | 8.69 | 6.52 | 0.25 | 8.90 | 1.35 | 2.97 | 0.25 | 0.68 | 0.07 | 0.02 | 0.01 | 0.01 | 87.97 | 31462_c6_g2b_2 |
| 0.08 | 0.00 | 59.48 | 0.00 | 0.00 | 8.77 | 2.70 | 0.16 | 11.49 | 1.71 | 3.14 | 0.21 | 0.82 | 0.07 | 0.02 | 0.01 | 0.00 | 88.67 | 31462_c6_g2b_3 |
| 0.08 | 0.02 | 59.94 | 0.00 | 0.00 | 5.46 | 2.33 | 0.16 | 14.68 | 1.21 | 2.72 | 0.16 | 0.96 | 0.00 | 0.00 | 0.00 | 0.01 | 87.74 | 31462_c6_g3_1 |
| 0.18 | 0.02 | 60.92 | 0.00 | 0.00 | 5.85 | 2.43 | 0.19 | 15.46 | 0.96 | 2.11 | 0.13 | 0.60 | 0.05 | 0.00 | 0.00 | 0.01 | 88.91 | 31462_c6_g3_2 |
| 1.07 | 0.02 | 58.83 | 0.00 | 0.00 | 5.40 | 3.43 | 0.19 | 13.34 | 1.26 | 2.74 | 0.29 | 0.82 | 0.05 | 0.00 | 0.01 | 0.00 | 87.45 | 31462_c6_g4a_1 |
| 0.11 | 0.00 | 60.00 | 0.00 | 0.00 | 5.65 | 2.80 | 0.31 | 15.72 | 0.61 | 1.27 | 0.08 | 0.35 | 0.02 | 0.00 | 0.03 | 0.00 | 86.96 | 31462_c6_g4a_2 |
| 2.36 | 0.01 | 56.45 | 0.00 | 0.00 | 5.81 | 4.82 | 0.21 | 11.49 | 1.38 | 3.04 | 0.18 | 0.79 | 0.02 | 0.01 | 0.00 | 0.01 | 86.59 | 31462_c6_g4b_1 |
| 0.26 | 0.01 | 92.38 | 0.01 | 0.00 | 0.13 | 1.31 | 0.09 | 1.29 | 0.10 | 0.28 | 0.10 | 0.05 | 0.04 | 0.03 | 0.01 | 0.00 | 96.08 | 31462_c6_g4b_2 |
| 0.07 | 0.11 | 60.45 | 0.00 | 0.00 | 3.97 | 2.16 | 0.25 | 17.45 | 0.83 | 1.65 | 0.21 | 0.57 | 0.03 | 0.01 | 0.00 | 0.00 | 87.75 | 31462_c6_g5_1 |
| 1.08 | 0.01 | 59.58 | 0.00 | 0.00 | 3.81 | 2.64 | 0.24 | 15.86 | 1.04 | 2.42 | 0.15 | 0.72 | 0.01 | 0.02 | 0.01 | 0.02 | 87.60 | 31462_c6_g5_2 |
| 1.17 | 0.02 | 56.41 | 0.00 | 0.00 | 3.65 | 2.22 | 0.44 | 14.01 | 2.72 | 5.25 | 0.37 | 1.51 | 0.11 | 0.01 | 0.01 | 0.00 | 87.89 | 31462_c6_g5_3 |
| 0.11 | 0.00 | 92.59 | 0.00 | 0.00 | 0.46 | 1.12 | 0.02 | 1.80 | 0.11 | 0.37 | 0.00 | 0.09 | 0.01 | 0.00 | 0.01 | 0.00 | 96.69 | 31462_c7_g1_1 |
| 0.07 | 0.02 | 59.66 | 0.00 | 0.00 | 7.17 | 2.46 | 0.12 | 12.09 | 1.97 | 3.75 | 0.28 | 1.21 | 0.13 | 0.00 | 0.00 | 0.00 | 88.94 | 31462_c7_g1_2 |
| 2.58 | 0.02 | 56.97 | 0.00 | 0.00 | 7.51 | 5.34 | 0.23 | 9.42 | 1.39 | 2.98 | 0.16 | 0.71 | 0.03 | 0.04 | 0.00 | 0.04 | 87.43 | 31462_c7_g1_3 |
| 0.15 | 0.01 | 60.77 | 0.00 | 0.00 | 8.52 | 3.20 | 0.24 | 13.22 | 0.68 | 1.44 | 0.17 | 0.40 | 0.00 | 0.01 | 0.01 | 0.00 | 88.82 | 31462_c7_g1_4 |
| 2.11 | 0.02 | 56.37 | 0.00 | 0.00 | 7.70 | 5.29 | 0.21 | 9.50 | 1.44 | 3.20 | 0.20 | 1.02 | 0.08 | 0.03 | 0.01 | 0.00 | 87.17 | 31462_c8_g1_1 |
| 1.47 | 0.00 | 58.21 | 0.00 | 0.00 | 7.91 | 4.05 | 0.20 | 10.65 | 1.44 | 3.15 | 0.34 | 0.95 | 0.04 | 0.01 | 0.01 | 0.00 | 88.43 | 31462_c8_g1_2 |
| 0.14 | 0.00 | 59.66 | 0.00 | 0.00 | 8.32 | 2.78 | 0.23 | 13.08 | 0.73 | 1.63 | 0.00 | 0.42 | 0.02 | 0.00 | 0.01 | 0.00 | 87.02 | 31462_c8_g1_3 |
| 0.14 | 0.02 | 59.12 | 0.00 | 0.00 | 7.70 | 2.79 | 0.19 | 13.34 | 0.72 | 1.51 | 0.06 | 0.39 | 0.01 | 0.00 | 0.01 | 0.00 | 85.99 | 31462_c8_g1_4 |
| 0.32 | 0.00 | 58.85 | 0.00 | 0.00 | 7.47 | 2.76 | 0.17 | 11.71 | 2.03 | 3.89 | 0.52 | 1.18 | 0.07 | 0.00 | 0.01 | 0.00 | 88.98 | 31462_c8_g1_5 |
| 0.21 | 0.00 | 59.52 | 0.00 | 0.00 | 7.05 | 2.99 | 0.18 | 12.77 | 1.33 | 2.79 | 0.17 | 0.90 | 0.02 | 0.00 | 0.00 | 0.00 | 87.93 | 31462_c8_g2_1 |
| 0.09 | 0.02 | 60.48 | 0.00 | 0.00 | 5.75 | 2.38 | 0.21 | 15.57 | 0.91 | 1.76 | 0.29 | 0.58 | 0.01 | 0.00 | 0.02 | 0.00 | 88.06 | 31462_c8_g2_2 |
| 0.11 | 0.02 | 60.07 | 0.00 | 0.00 | 8.01 | 3.11 | 0.17 | 12.82 | 1.09 | 2.08 | 0.24 | 0.69 | 0.07 | 0.00 | 0.01 | 0.02 | 88.49 | 31462_c8_g2_3 |
| 1.65 | 0.00 | 53.37 | 0.00 | 0.00 | 7.47 | 14.08 | 0.60 | 6.63 | 2.03 | 4.42 | 0.23 | 1.23 | 0.01 | 0.00 | 0.02 | 0.00 | 91.74 | 31462_c8_g2_4 |

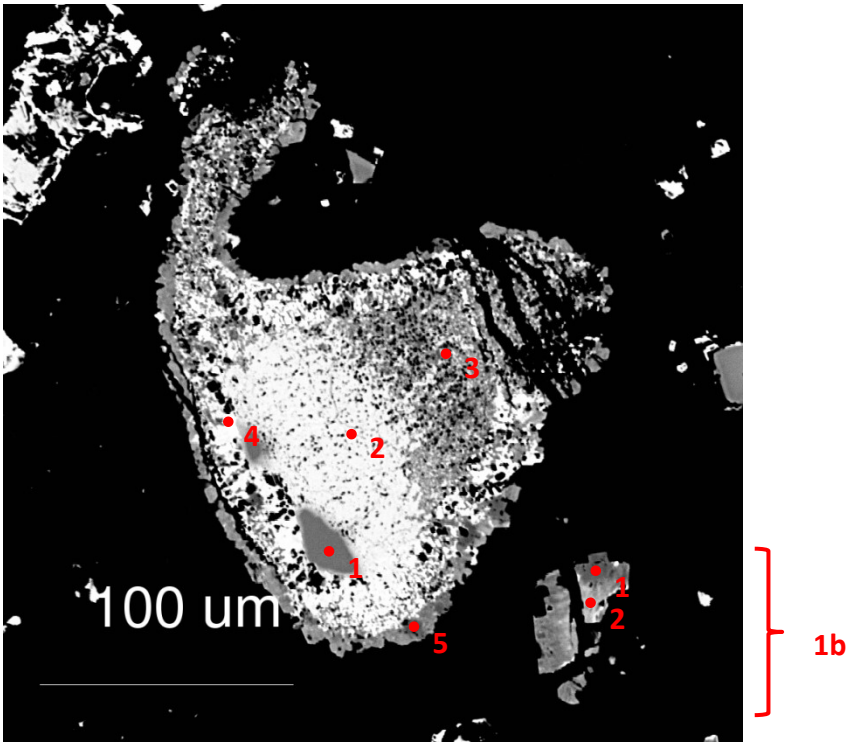


**Fig. 1.** BSE image and spot locations for 31462TS_circle1_1.

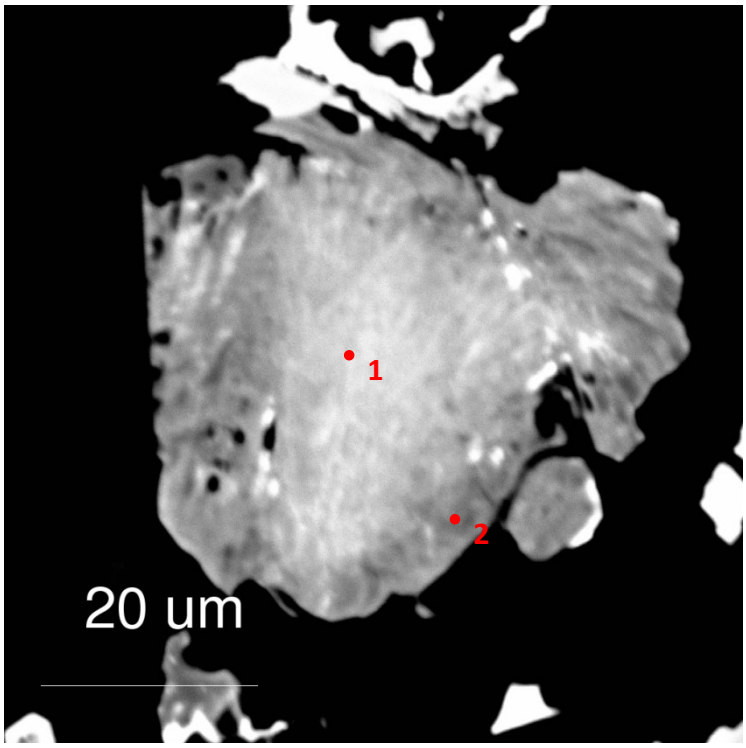


**Fig. 2.** BSE image and spot locations for 31462TS_circle1_2.

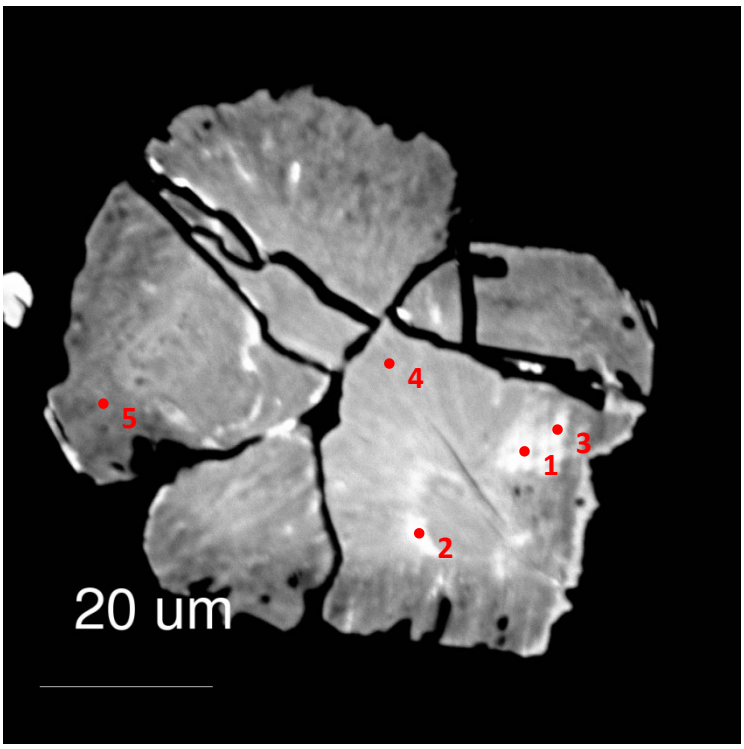


**Fig. 3.** BSE image and spot locations for 31462TS_circle2_1.

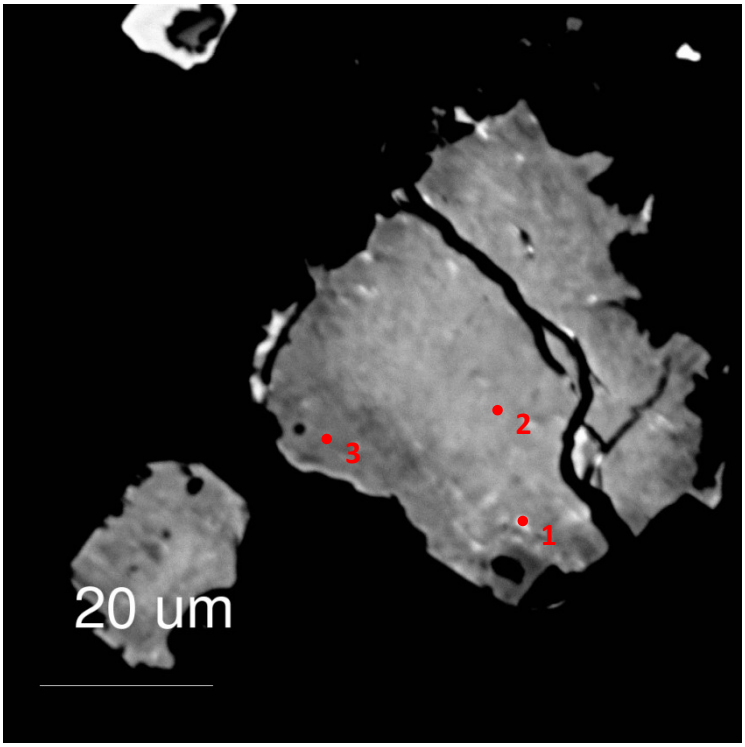


**Fig. 4.** BSE image and spot locations for 31462TS_circle2_2.

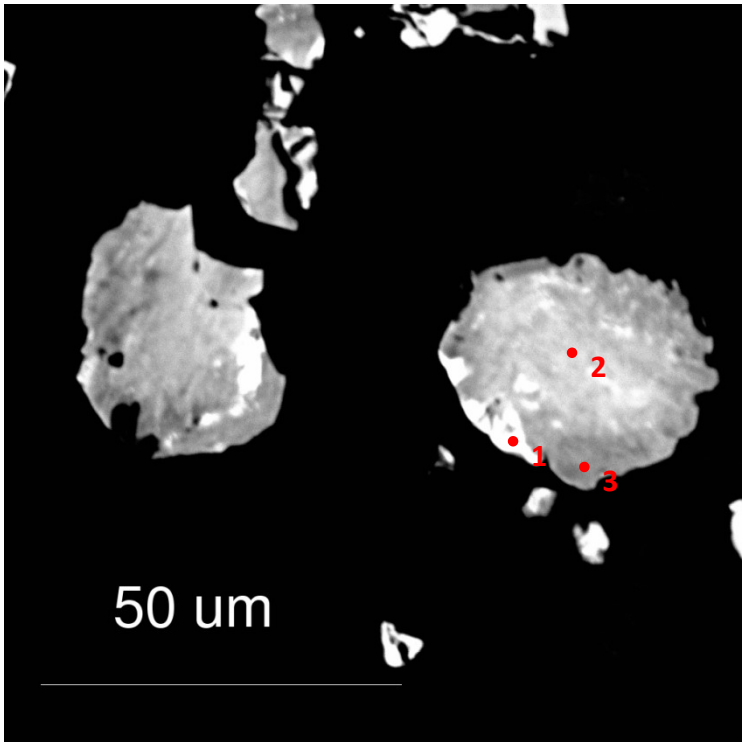


**Fig. 5.** BSE image and spot locations for 31462TS_circle2_3.

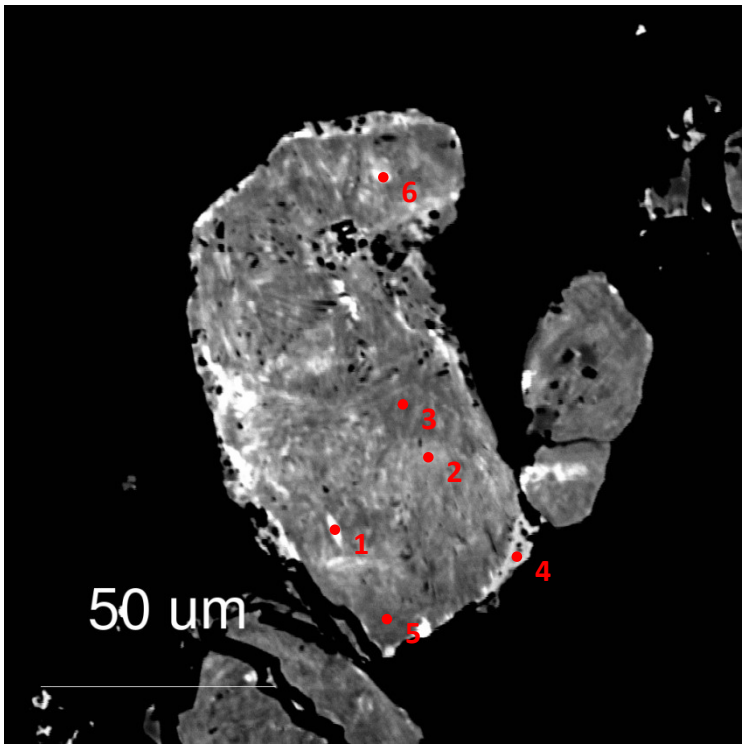


**Fig. 6.** BSE image and spot locations for 31462TS_circle3_1.

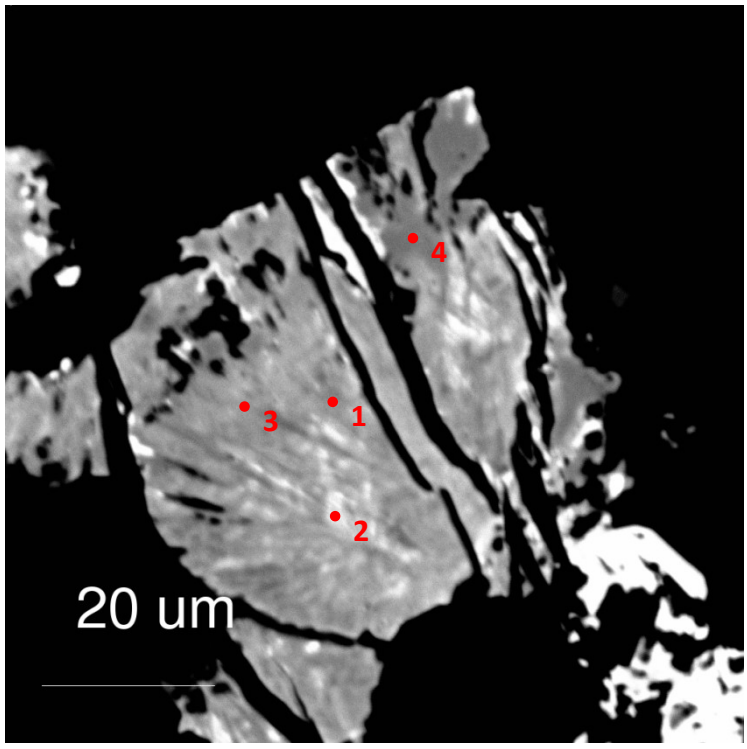


**Fig. 7.** BSE image and spot locations for 31462TS_circle3_2a.

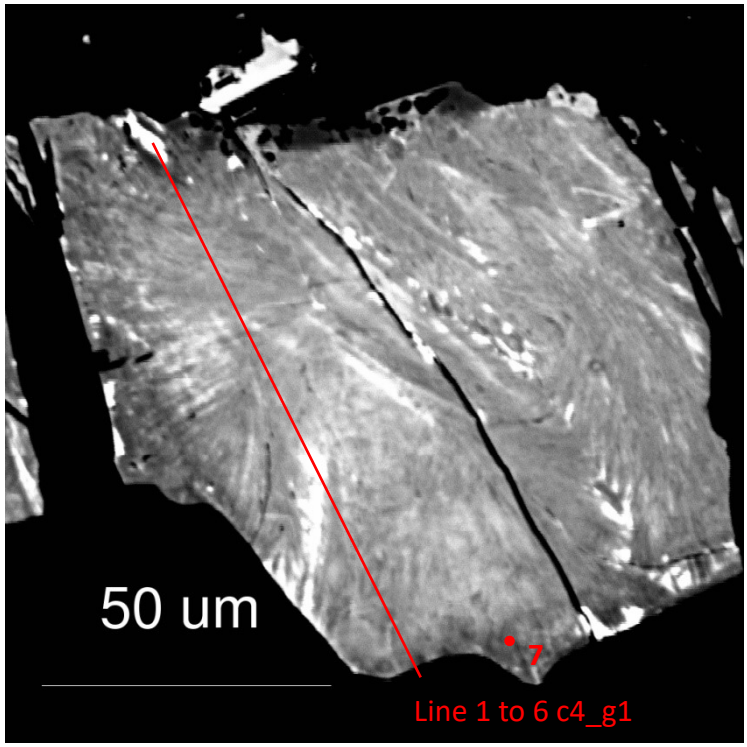


**Fig. 8.** BSE image and spot locations for 31462TS_circle4_1.

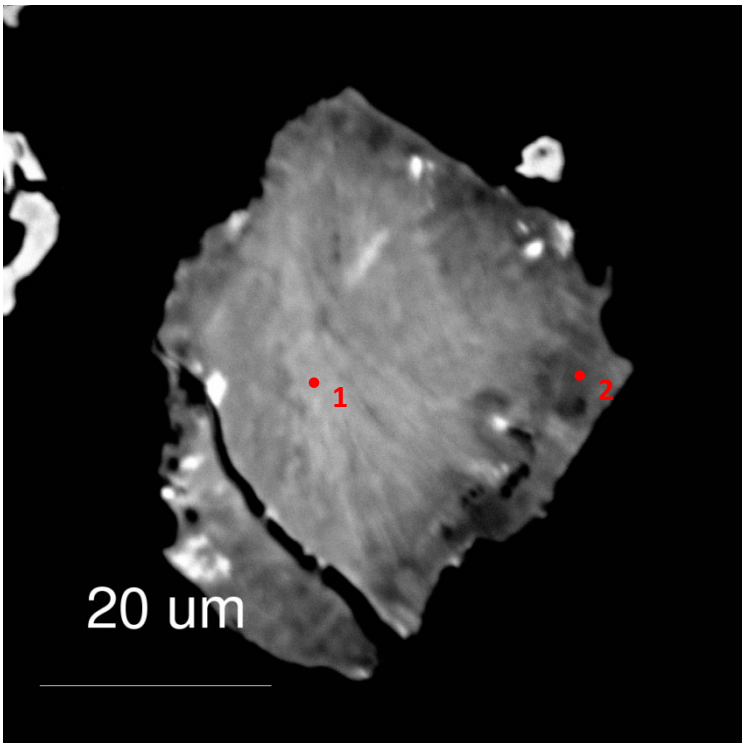


**Fig. 9.** BSE image and spot locations for 31462TS_circle4_2.

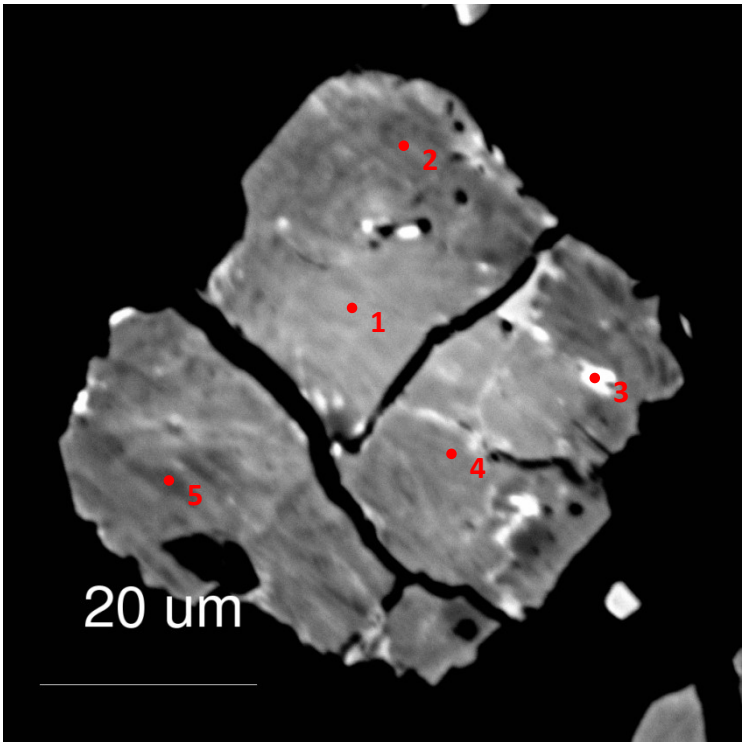


**Fig. 10.** BSE image and spot locations for 31462TS_circle6_1.

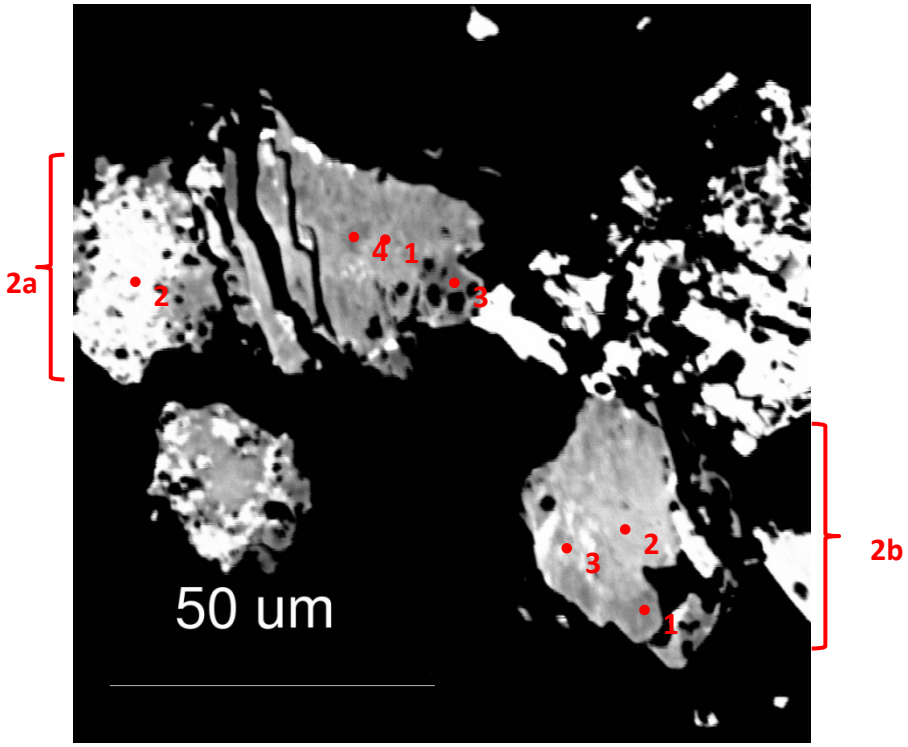


**Fig. 11.** BSE image and spot locations for 31462TS_circle6_2.

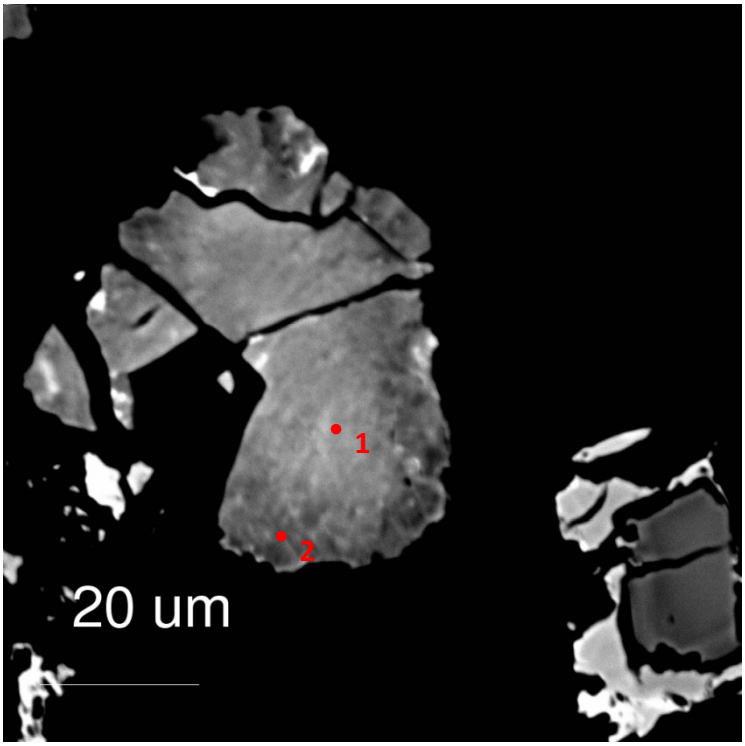


**Fig. 12.** BSE image and spot locations for 31462TS_circle6_3.

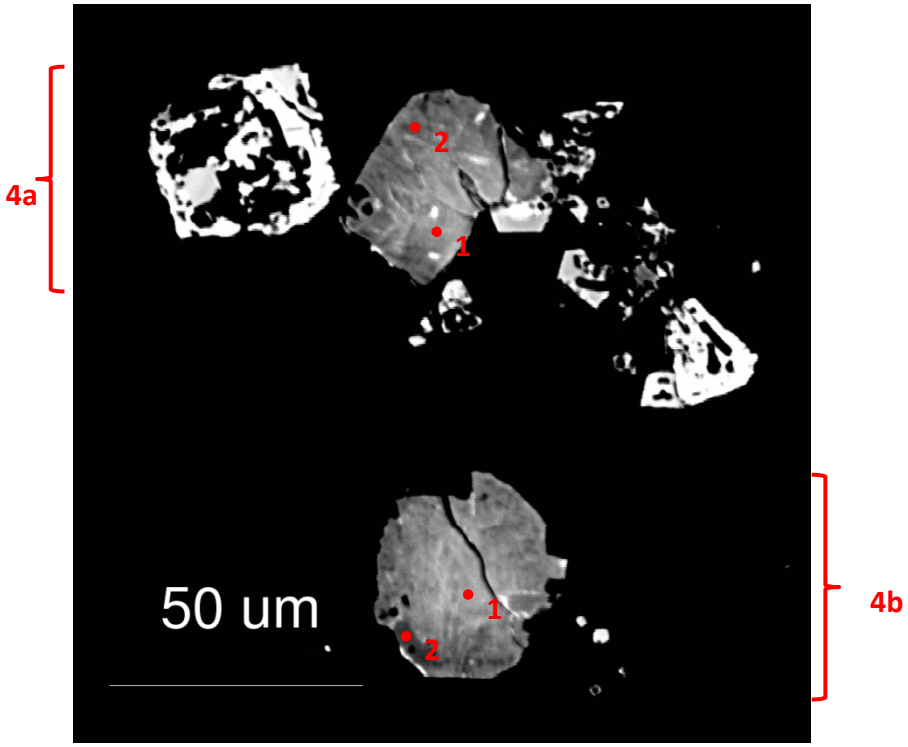


**Fig. 13.** BSE image and spot locations for 31462TS_circle6_4.

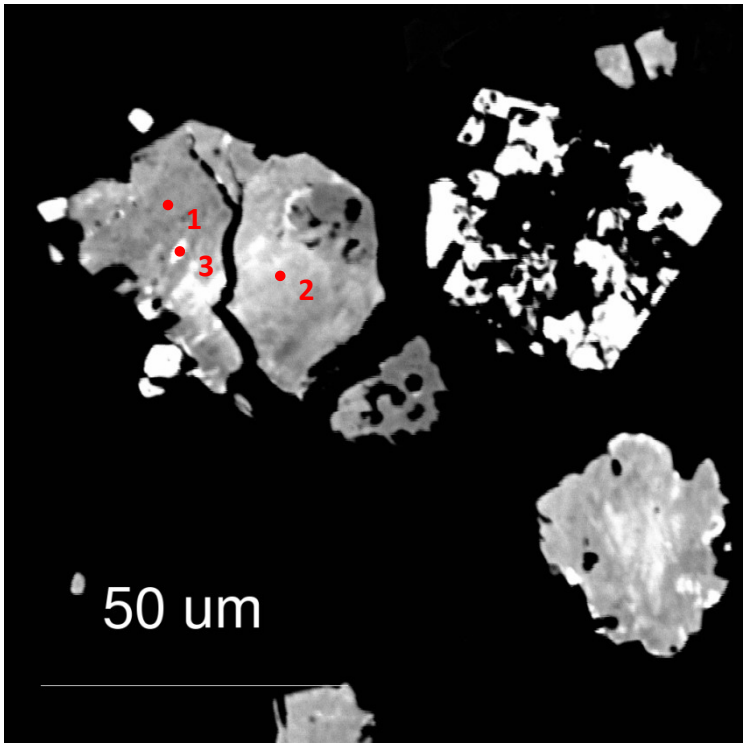


**Fig. 14.** BSE image and spot locations for 31462TS_circle6_5.

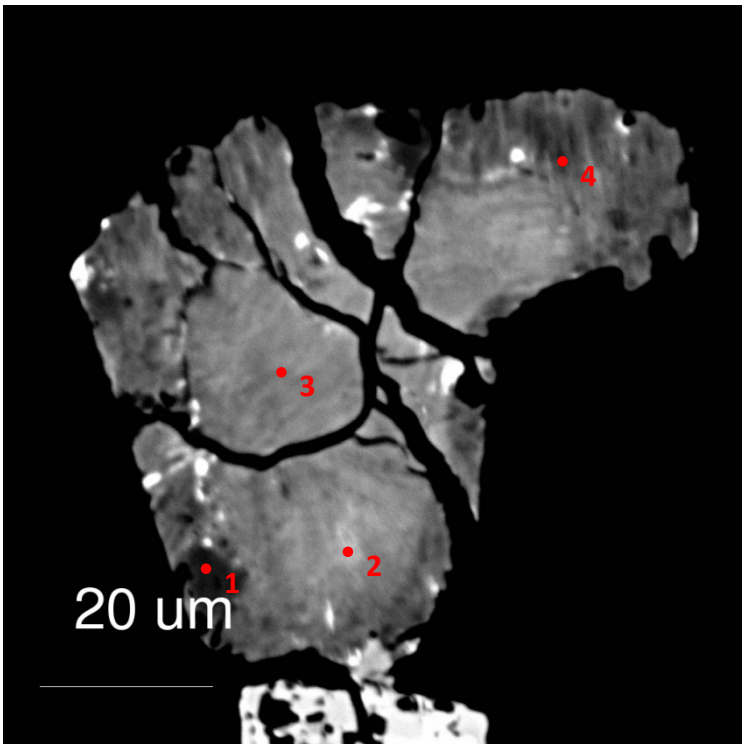


**Fig. 15.** BSE image and spot locations for 31462TS_circle7_1.

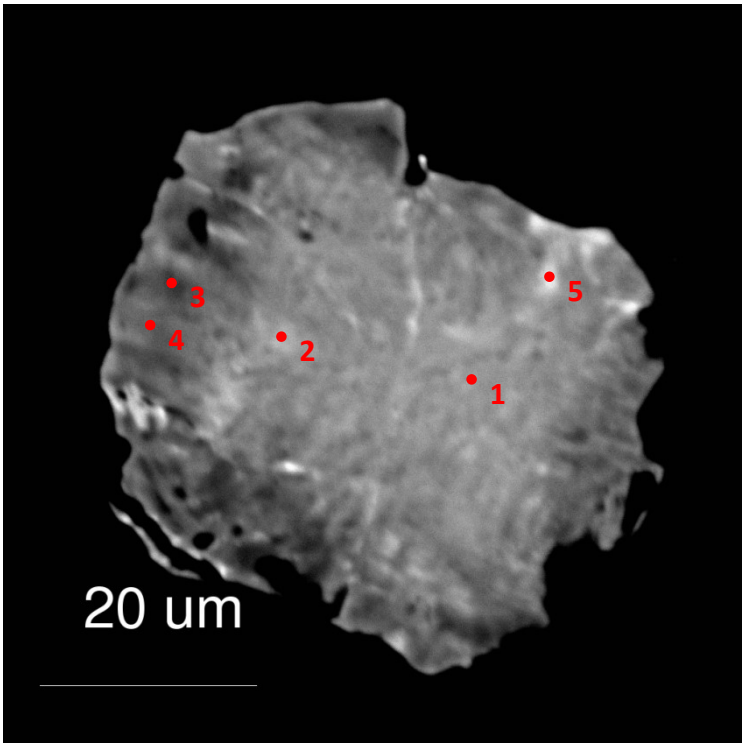


**Fig. 16.** BSE image and spot locations for 31462TS_circle8_1.

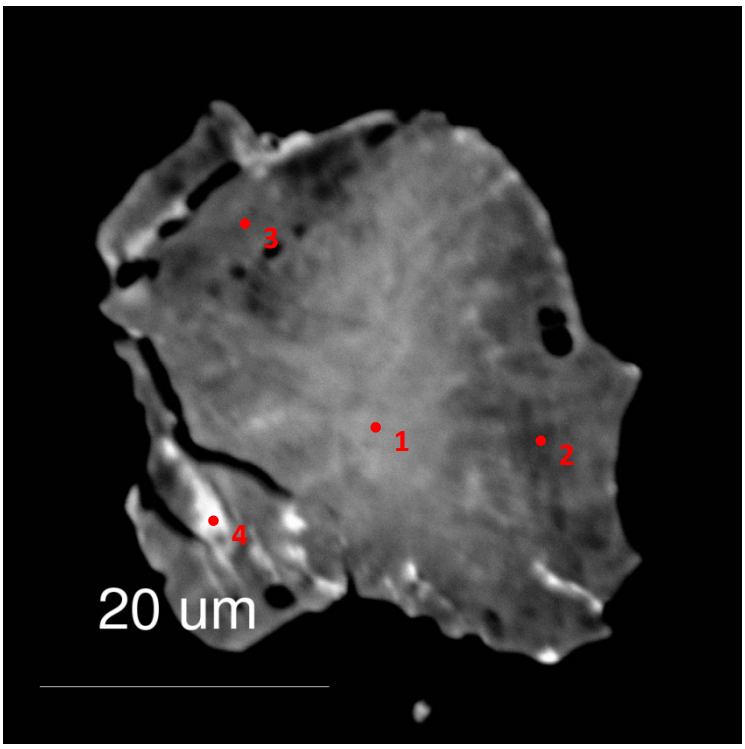


**Fig. 17.** BSE image and spot locations for 31462TS_circle8_2.

## Supplementary Material 5: Additional Raman spectra

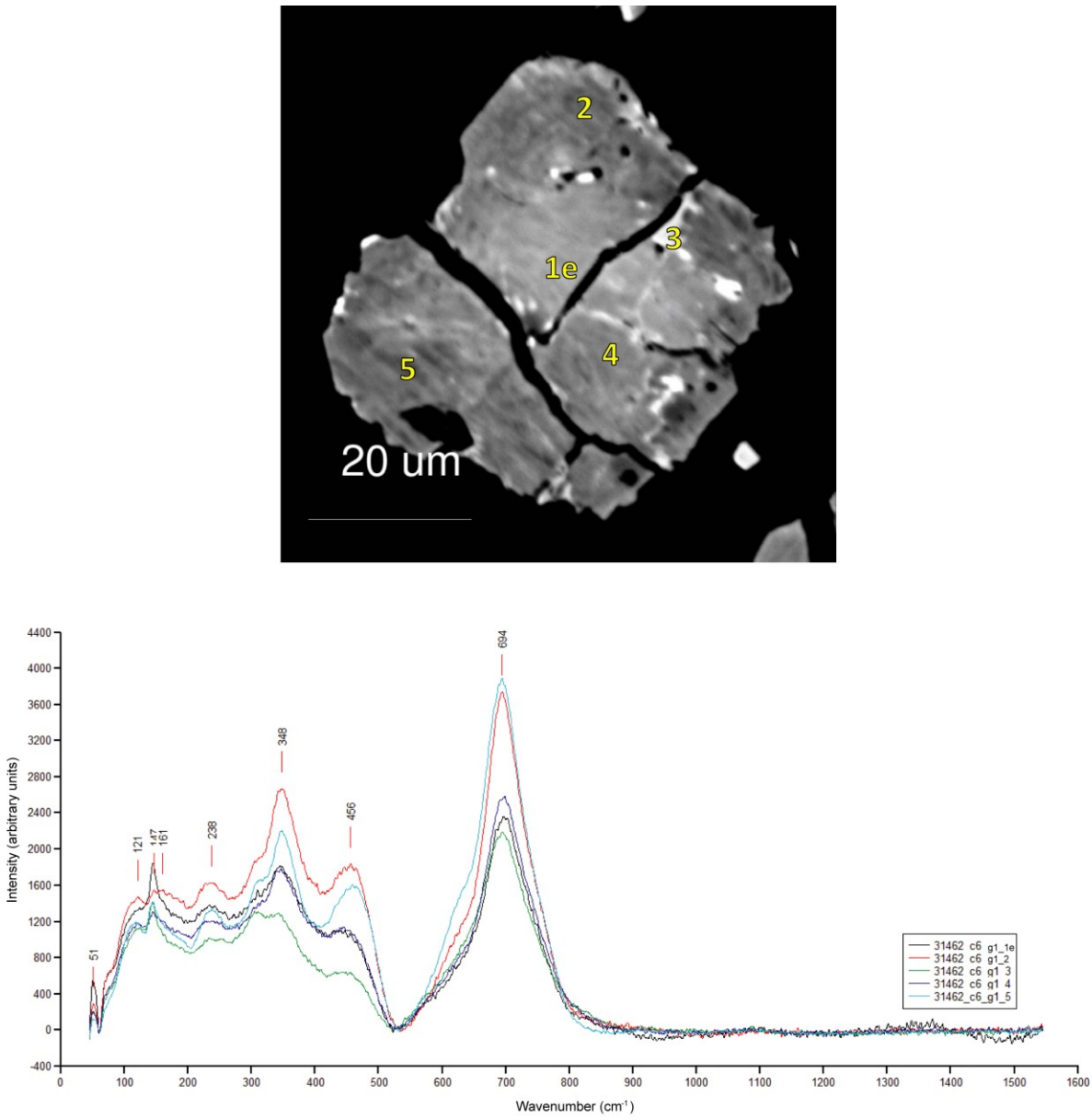


**Fig. 1.** Raman spectra of grain 31462TS_circle6_1.

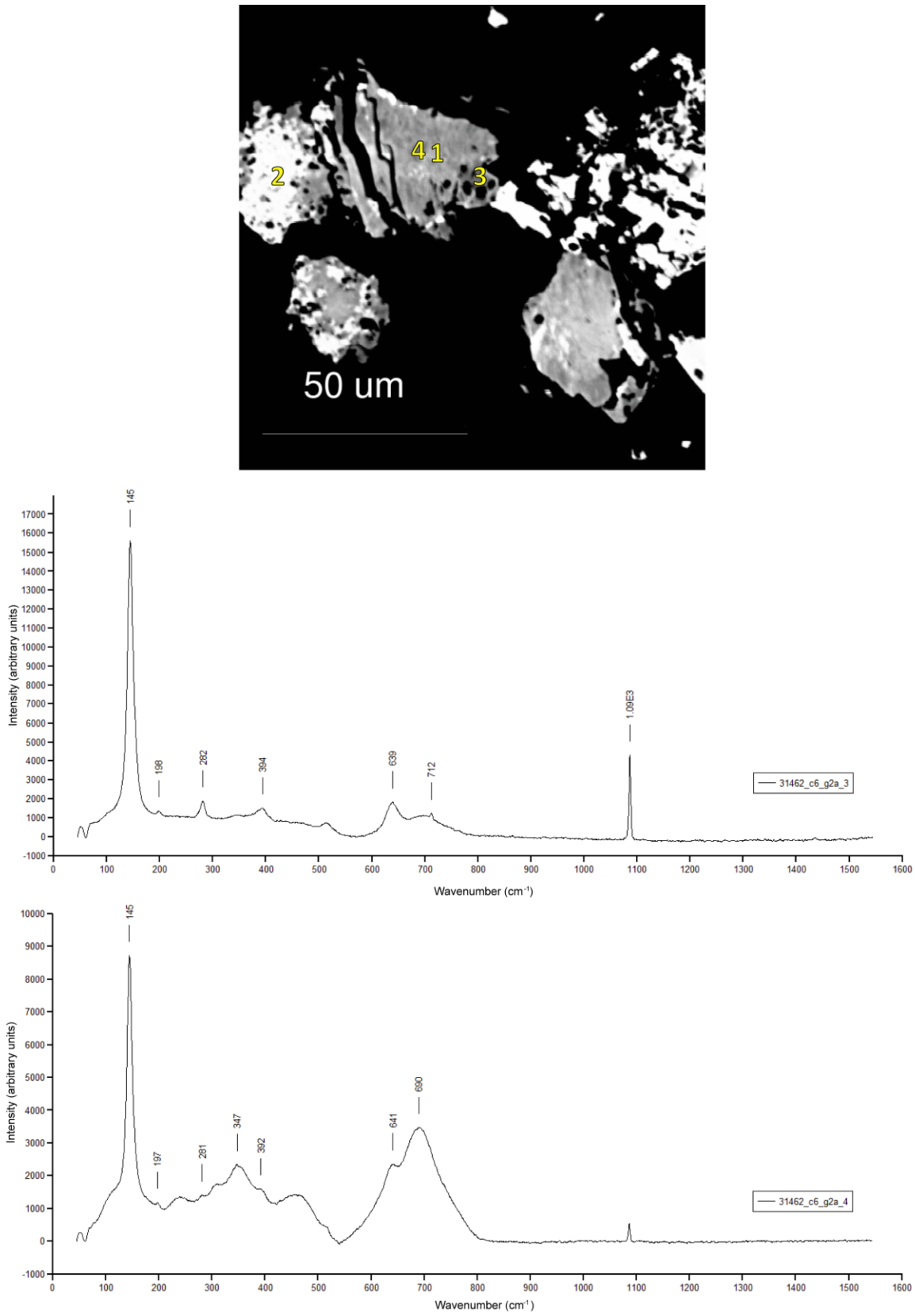


**Fig. 2.** Raman spectra of grain 31462TS_circle6_2a.

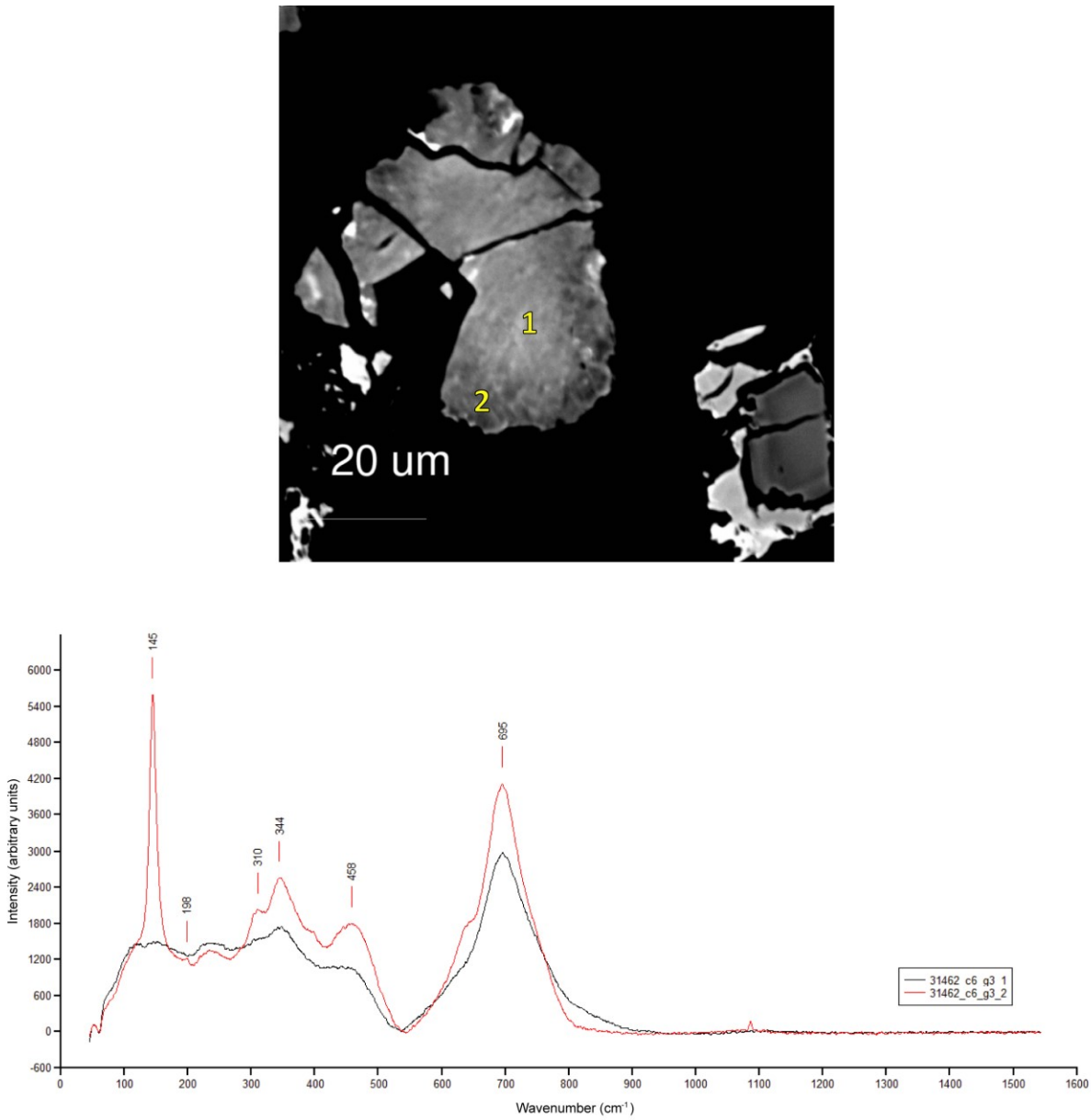


**Fig. 3.** Raman spectra of grain 31462TS_circle6_3.

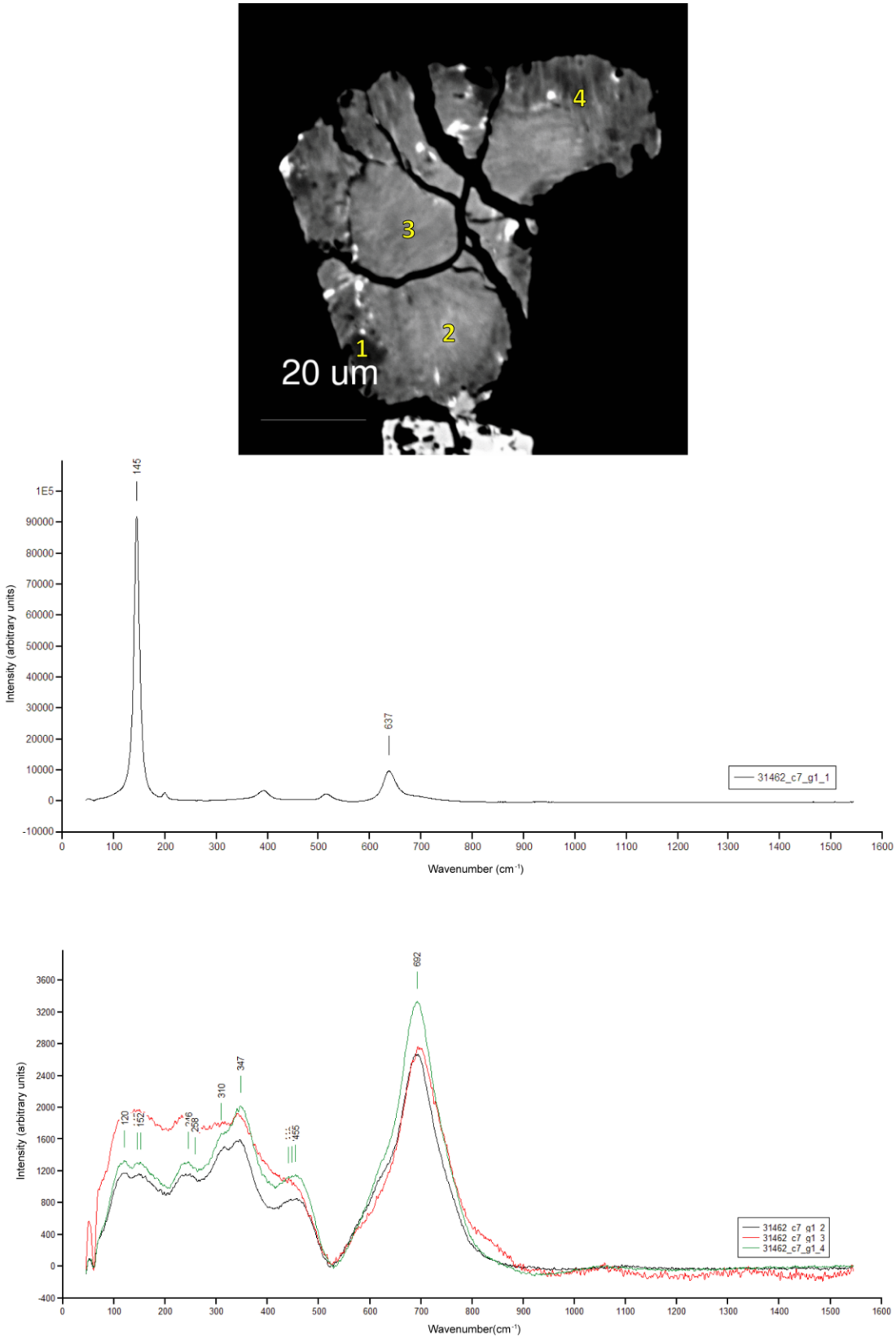


**Fig. 4.** Raman spectra of grain 31462TS_circle7_1.

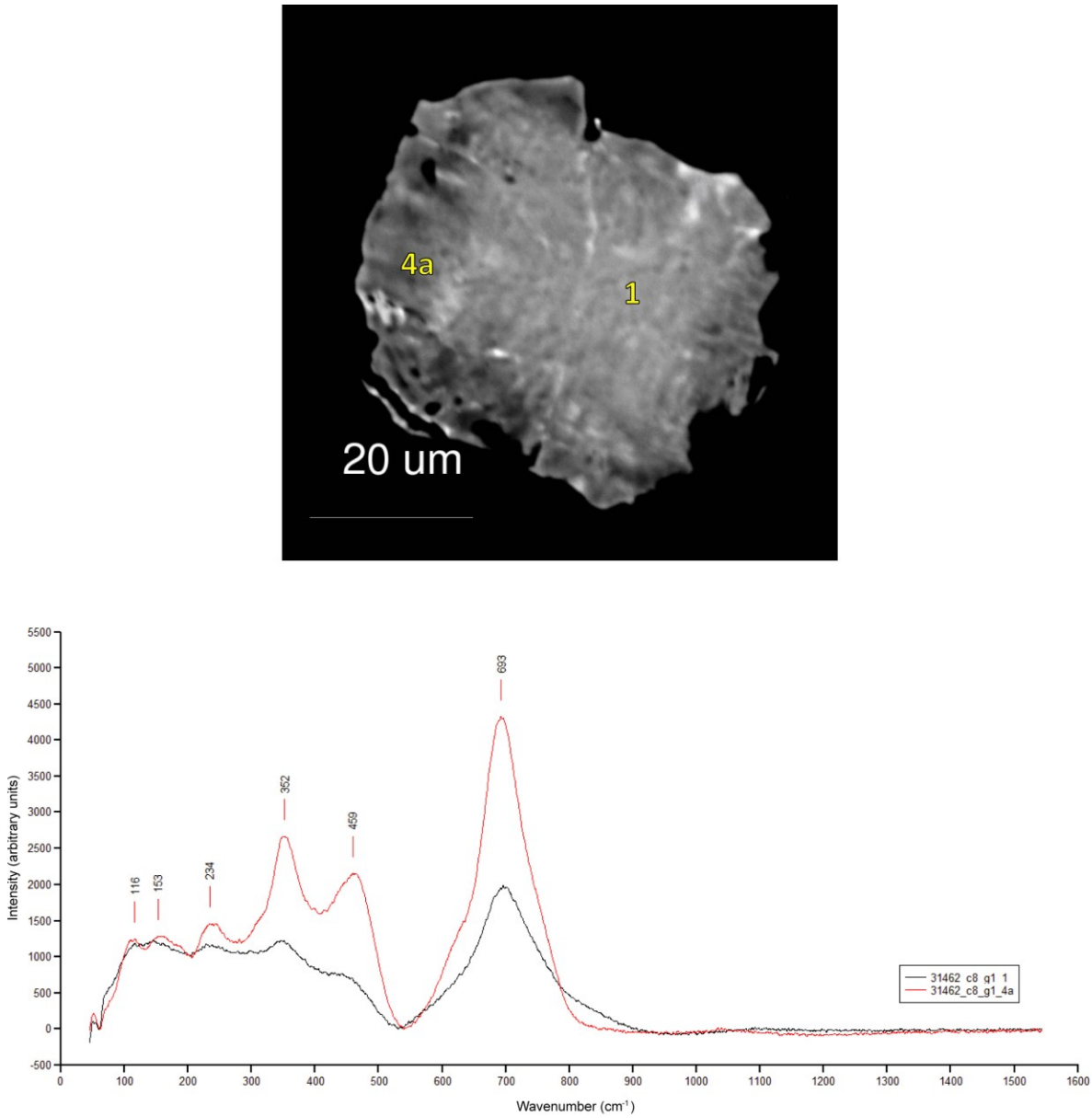


**Fig. 5.** Raman spectra of grain 31462TS_circle8_1.

## Supplementary Material 6: Additional scanning electron microscope data

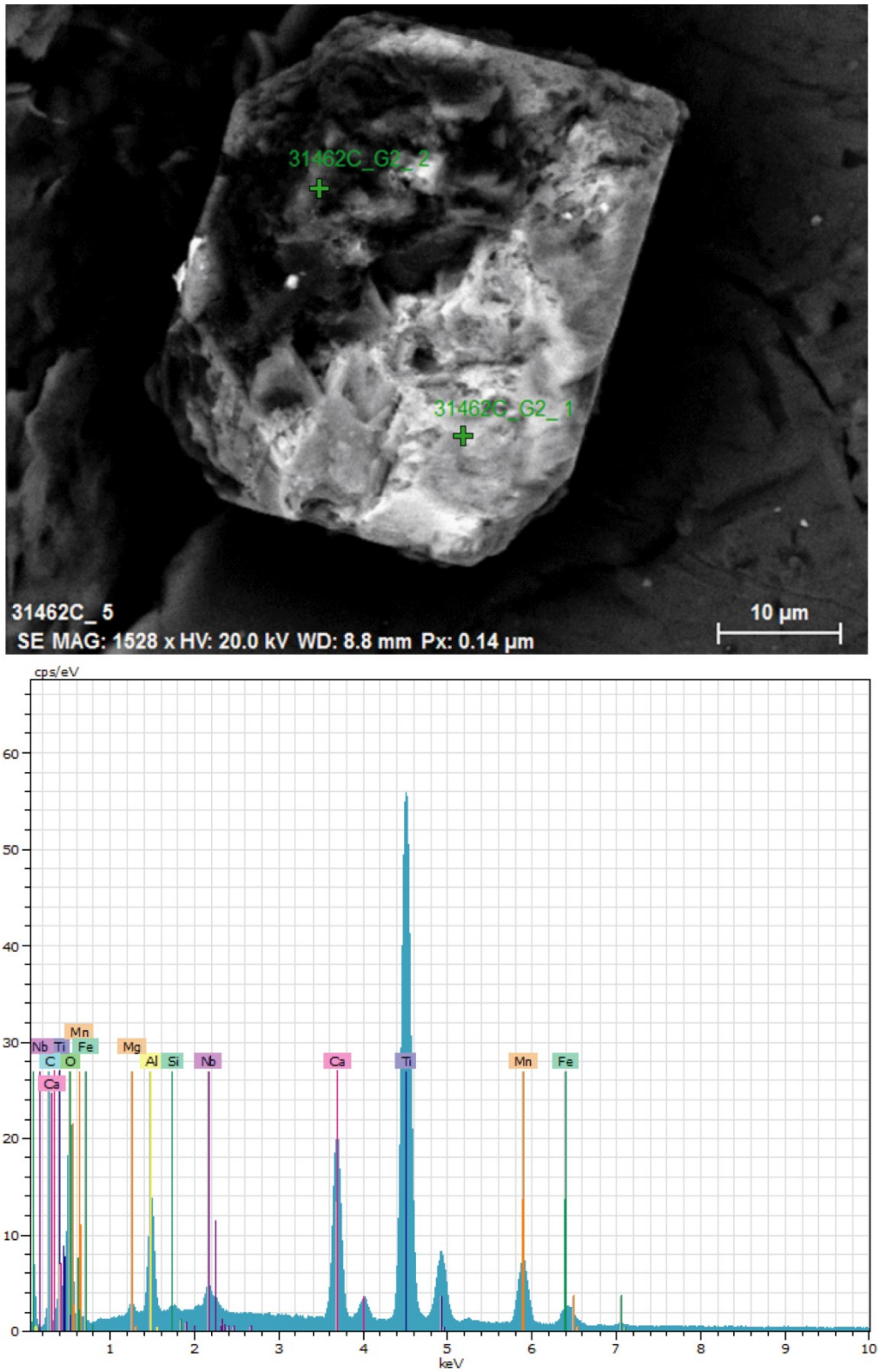


**Fig. 1.** BSE image and EDS spectra of grain 31462C_G2 for spot 31462C_G2_1.

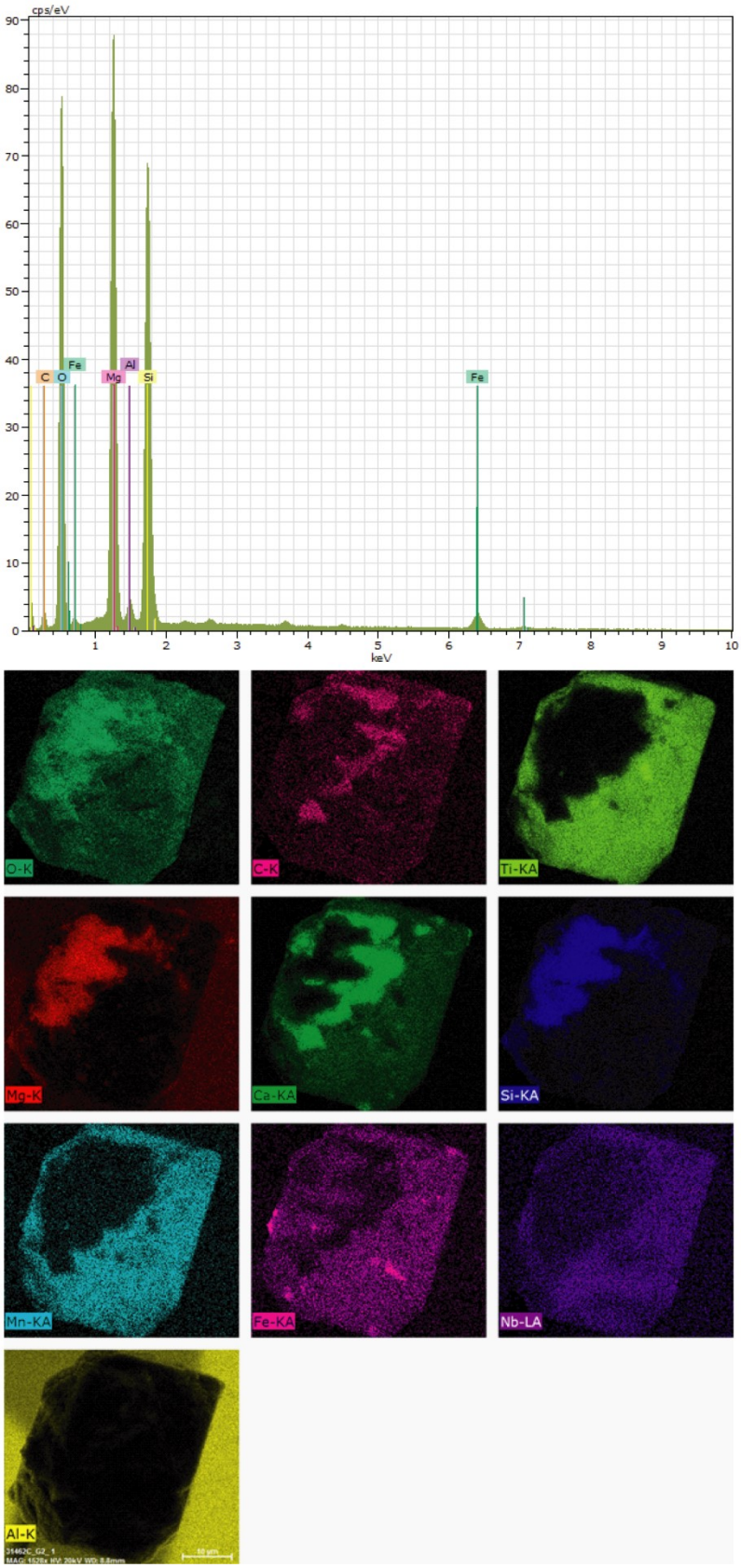


**Fig. 1.** Continued. EDS spectra for spot 31462C_G2_2 and element maps.

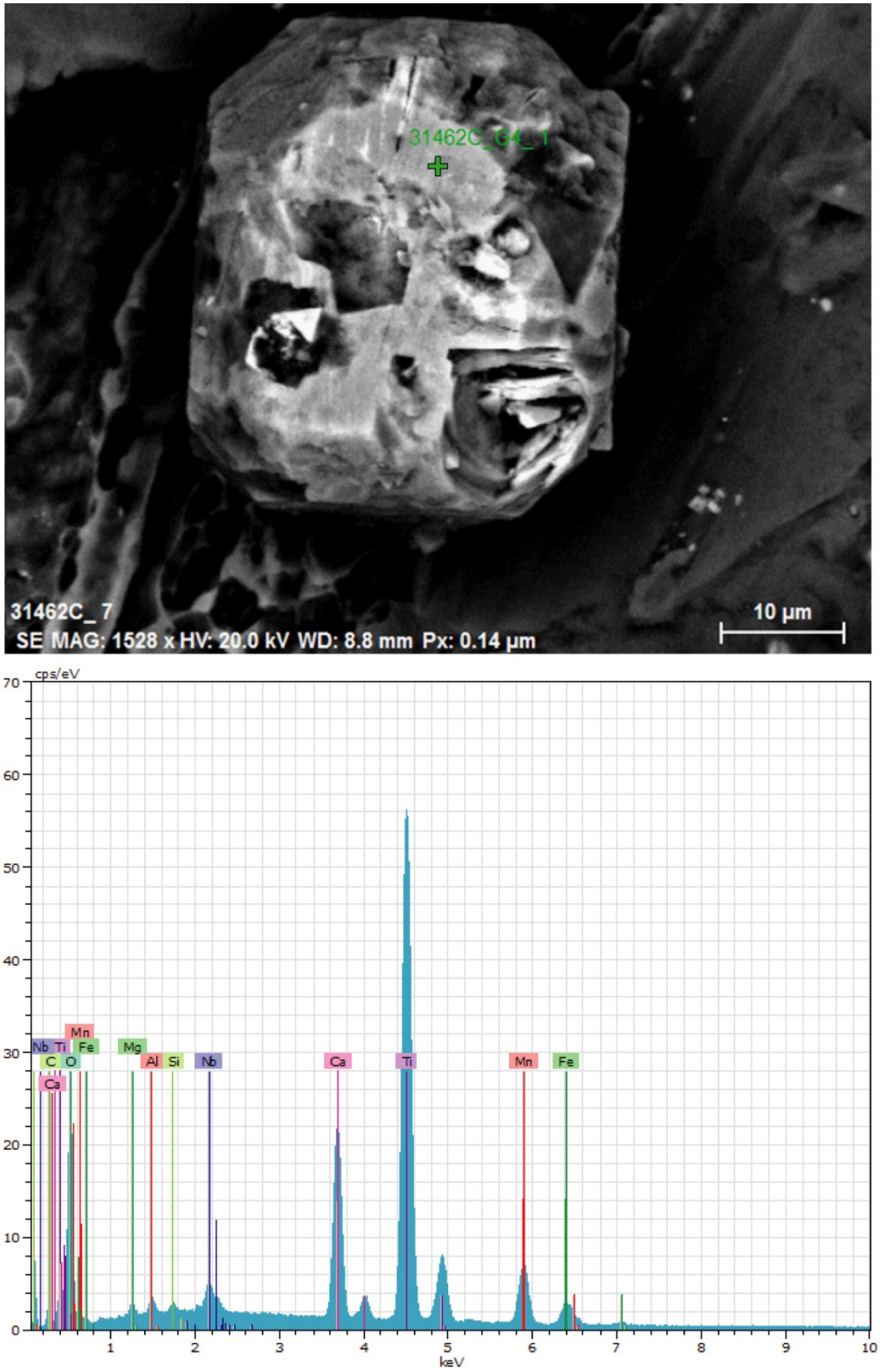


**Fig. 2.** BSE image, EDS spectra and element maps of grain 31462C_G4.

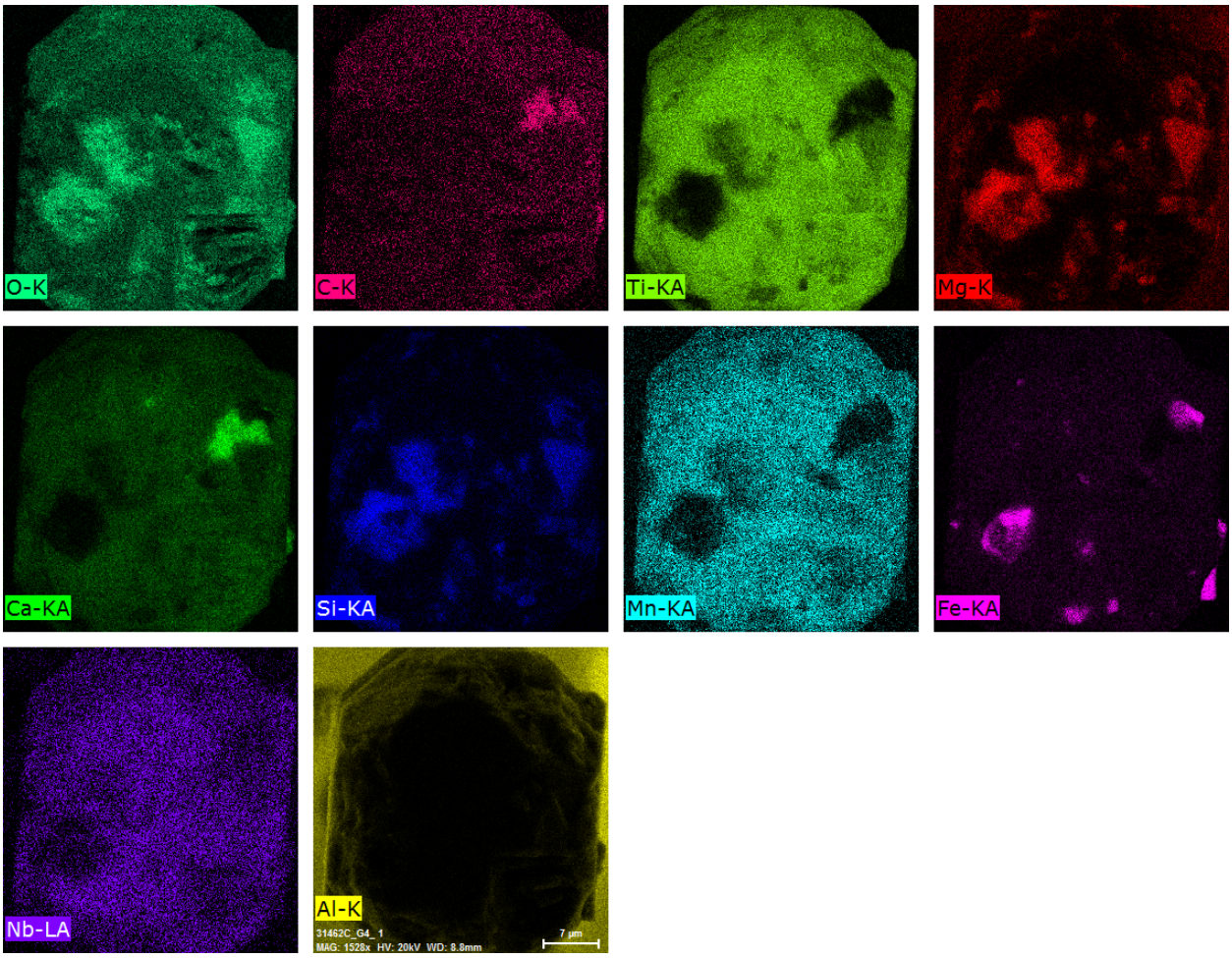


**Fig. 2.** Continued.

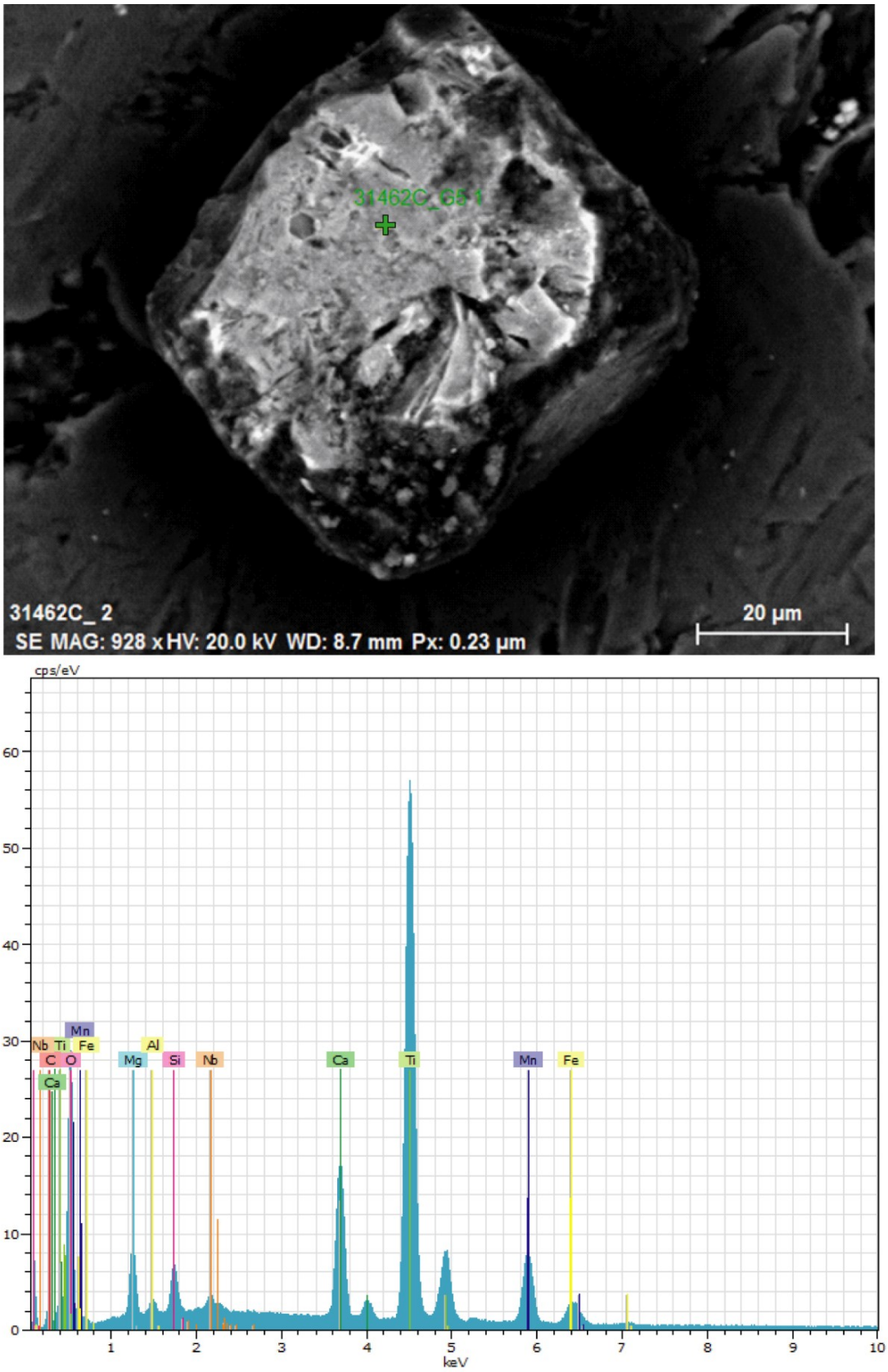


**Fig. 3.** BSE image, EDS spectra and element maps of grain 31462C_G5.

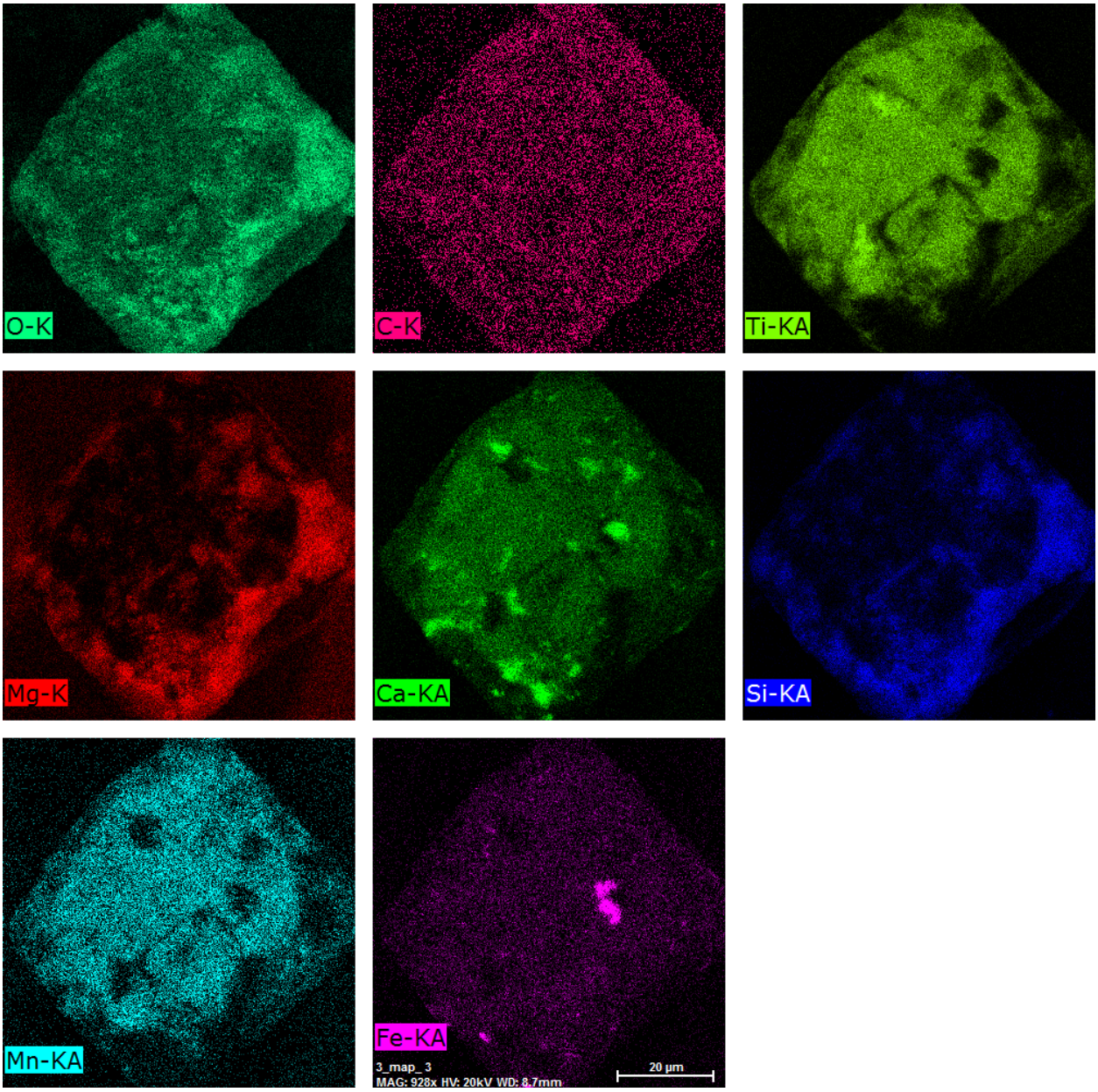


**Fig. 3.** Continued.

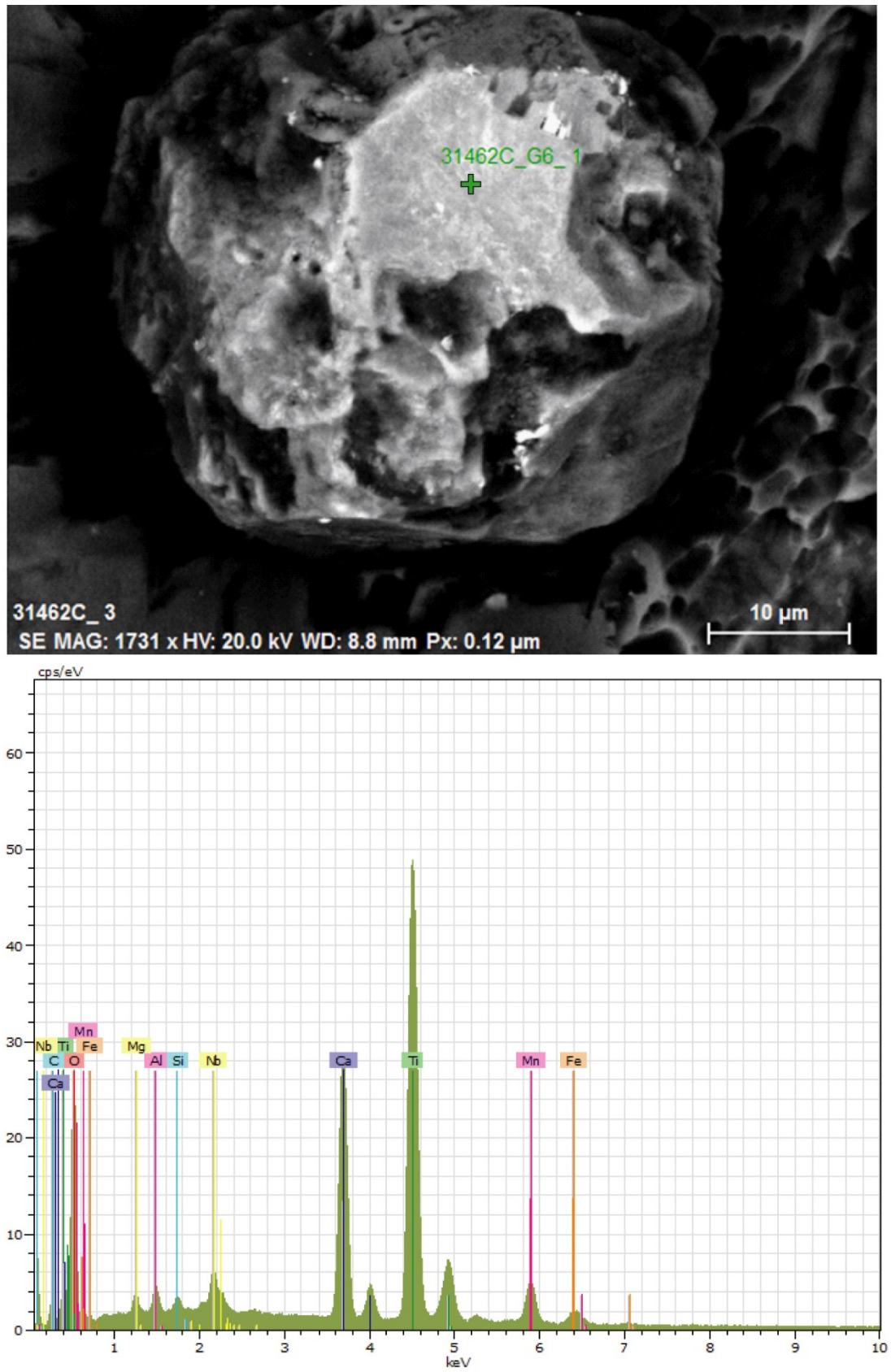


**Fig. 4.** BSE image, EDS spectra and element maps of grain 31462C_G6.

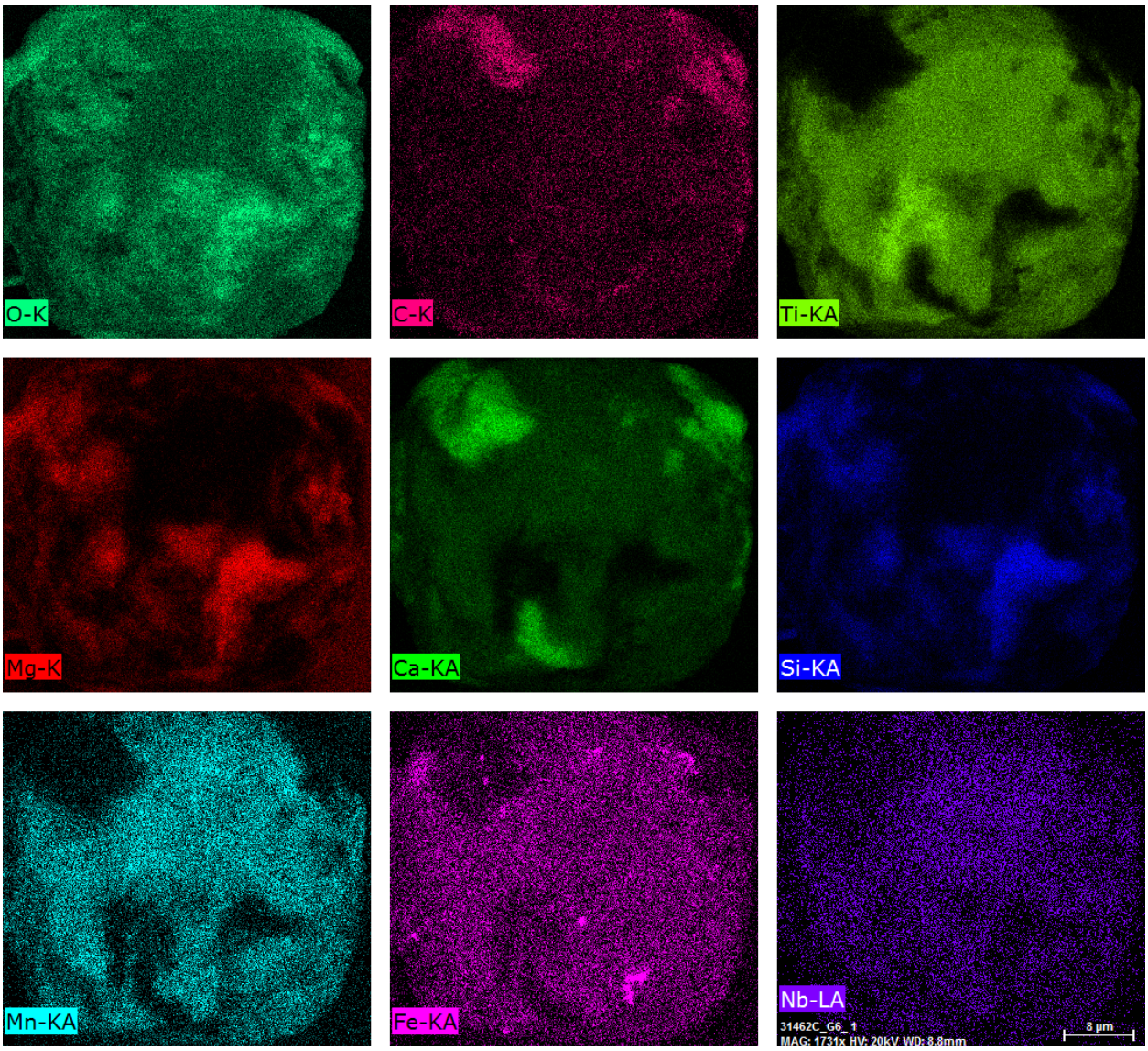


**Fig. 4.** Continued.

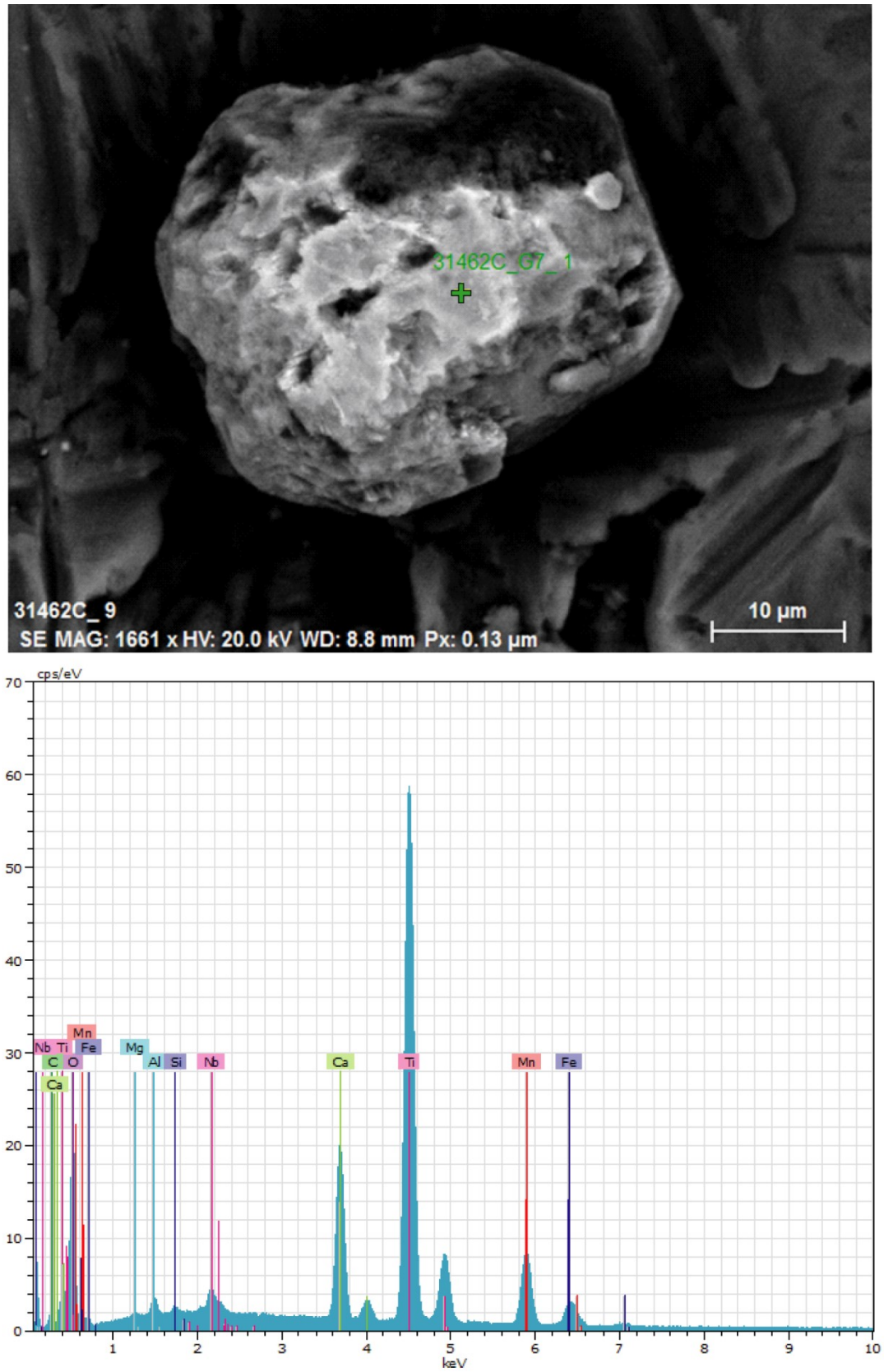


**Fig. 5.** BSE image, EDS spectra and element maps of grain 31462C_G7.

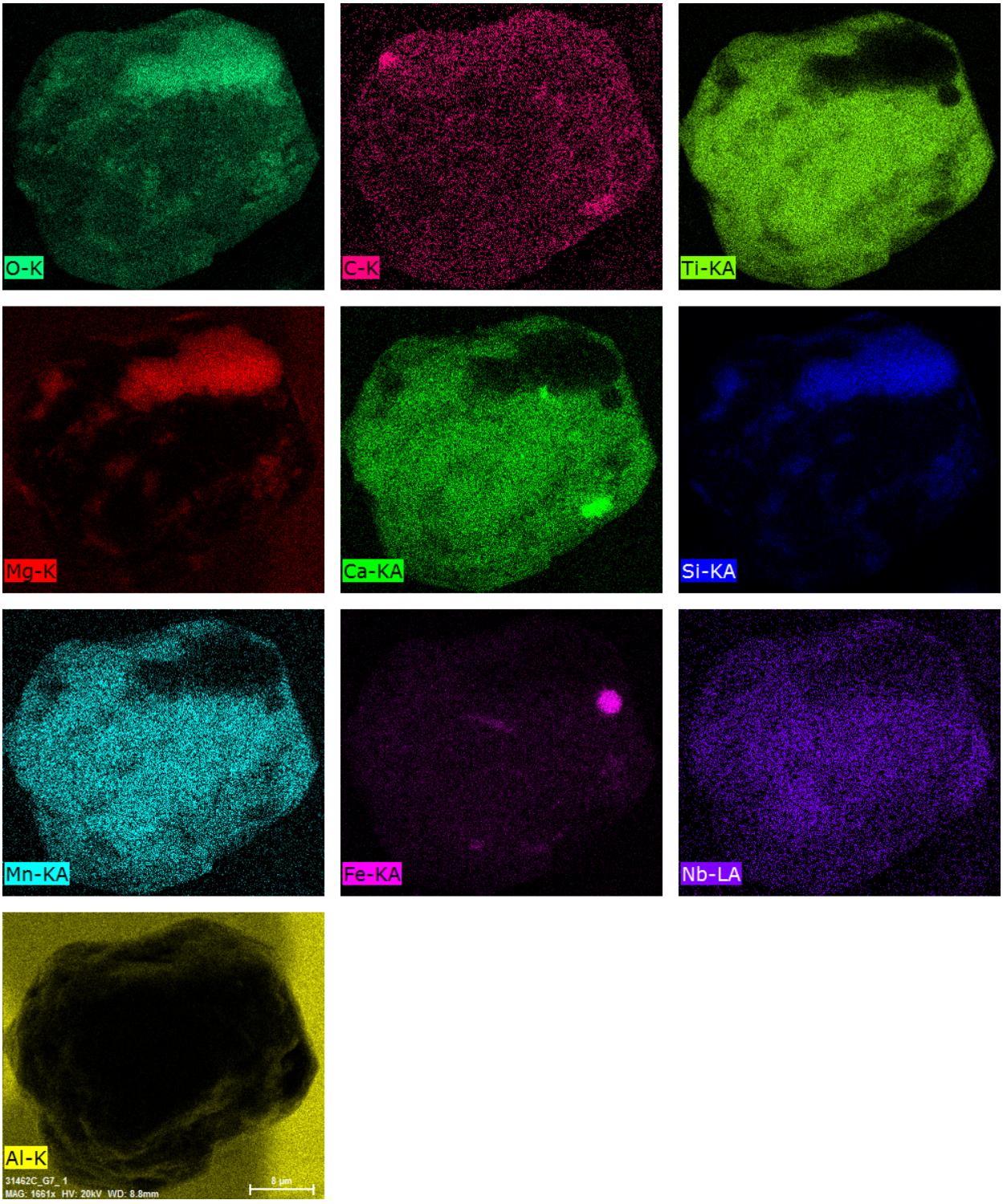


**Fig. 5.** Continued.

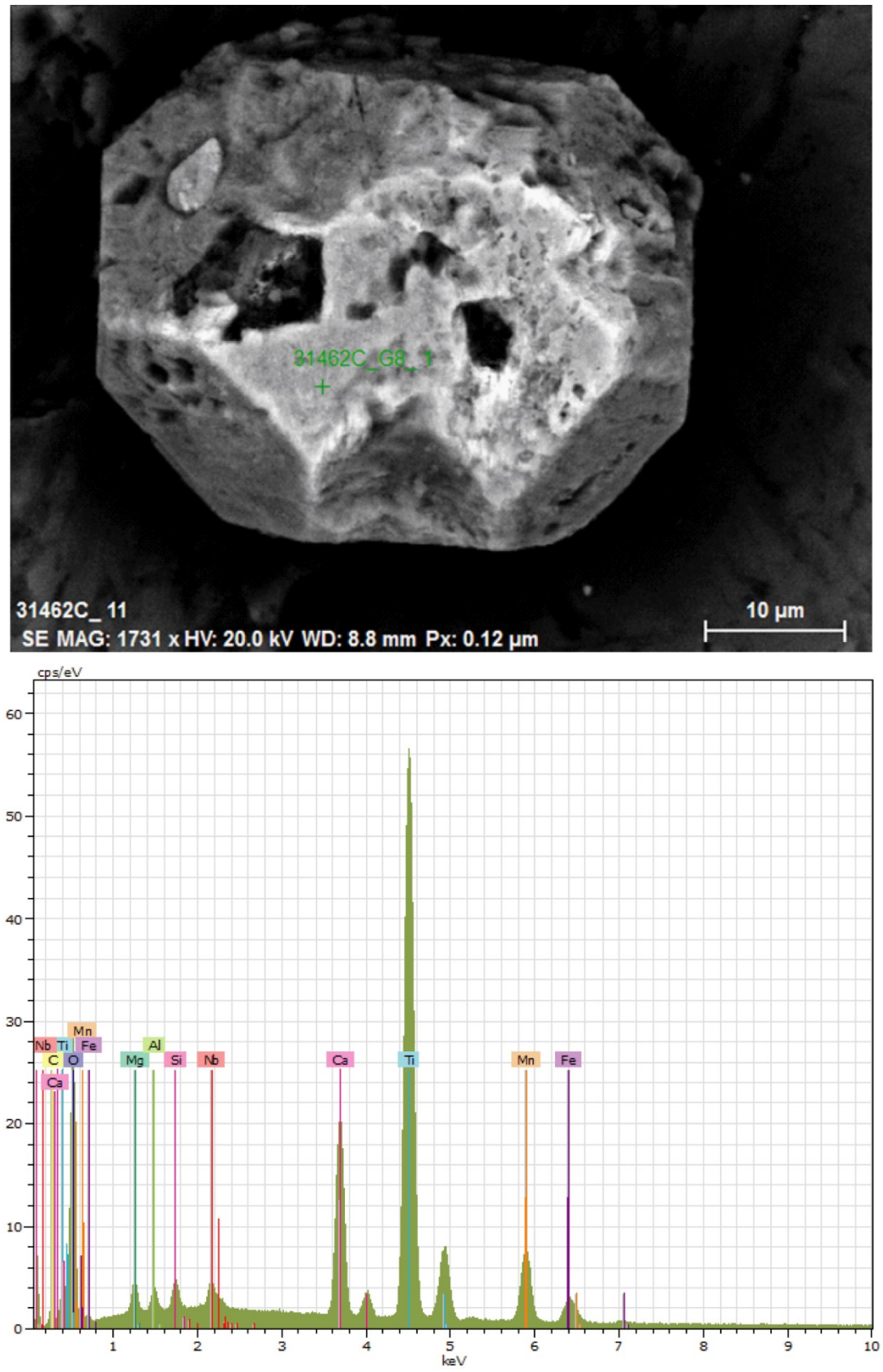


**Fig. 6.** BSE image, EDS spectra and element maps of grain 31462C_G8.

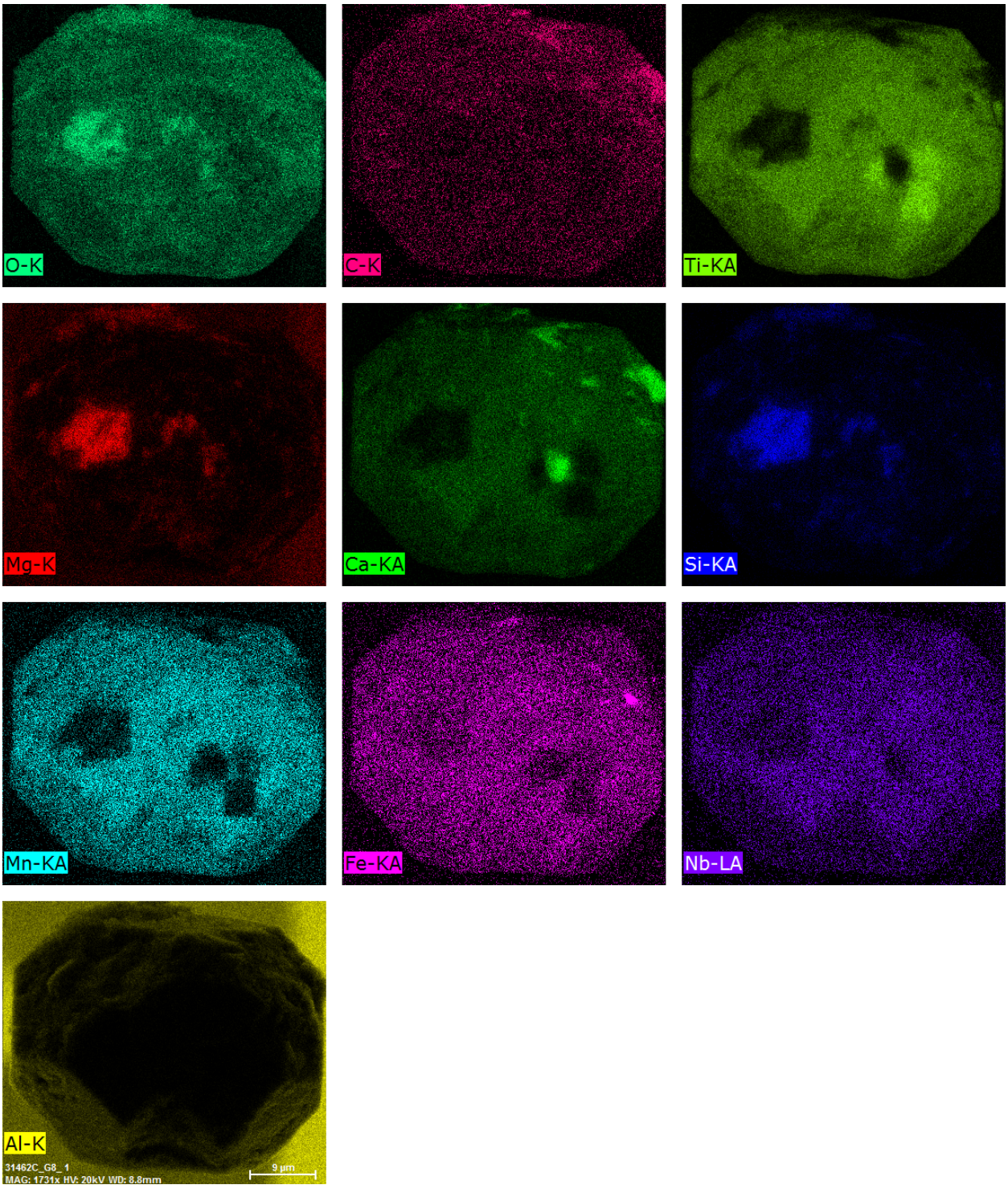


**Fig. 6.** Continued.

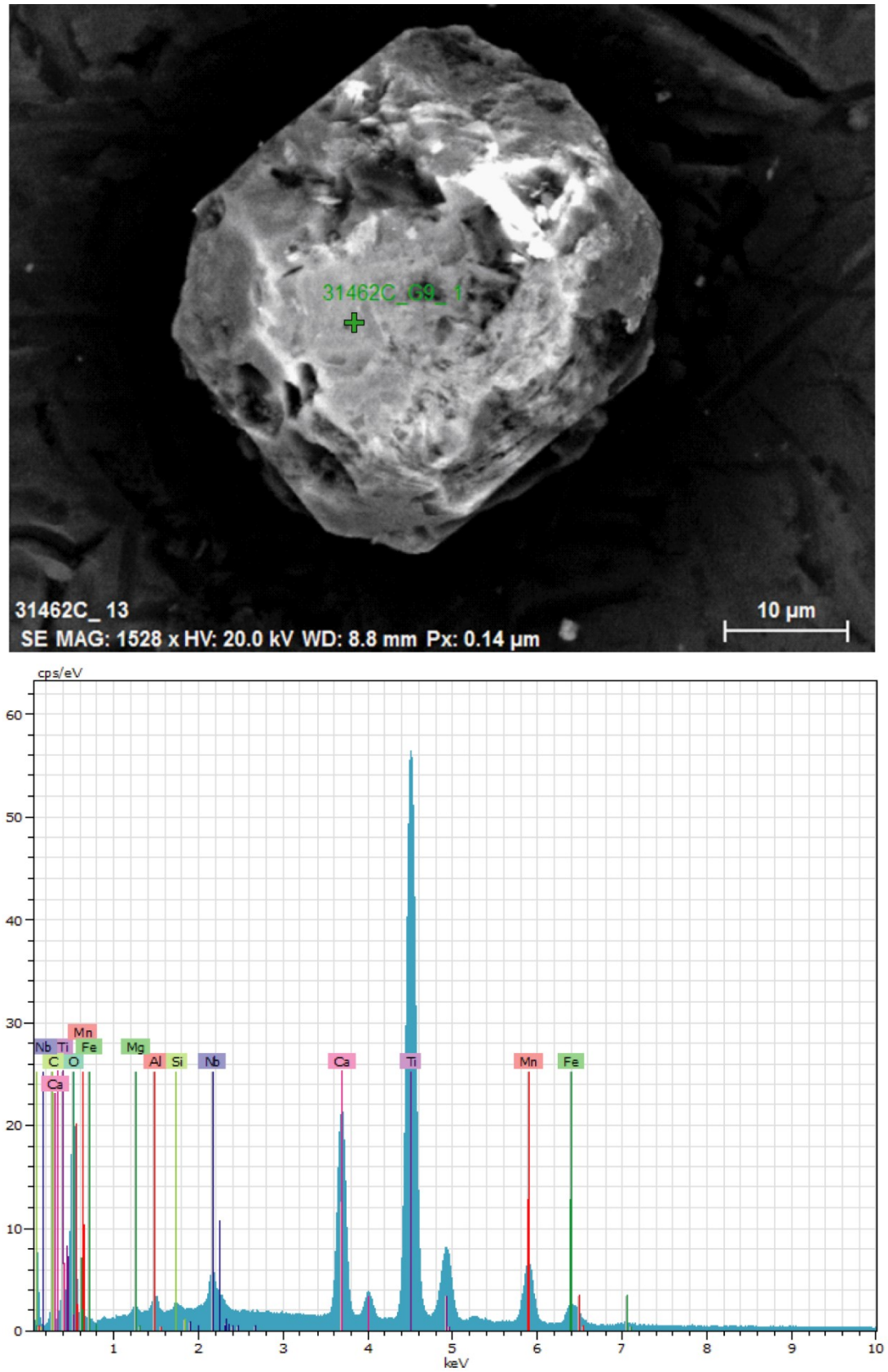


**Fig. 7.** BSE image, EDS spectra and element maps of grain 31462C_G9.

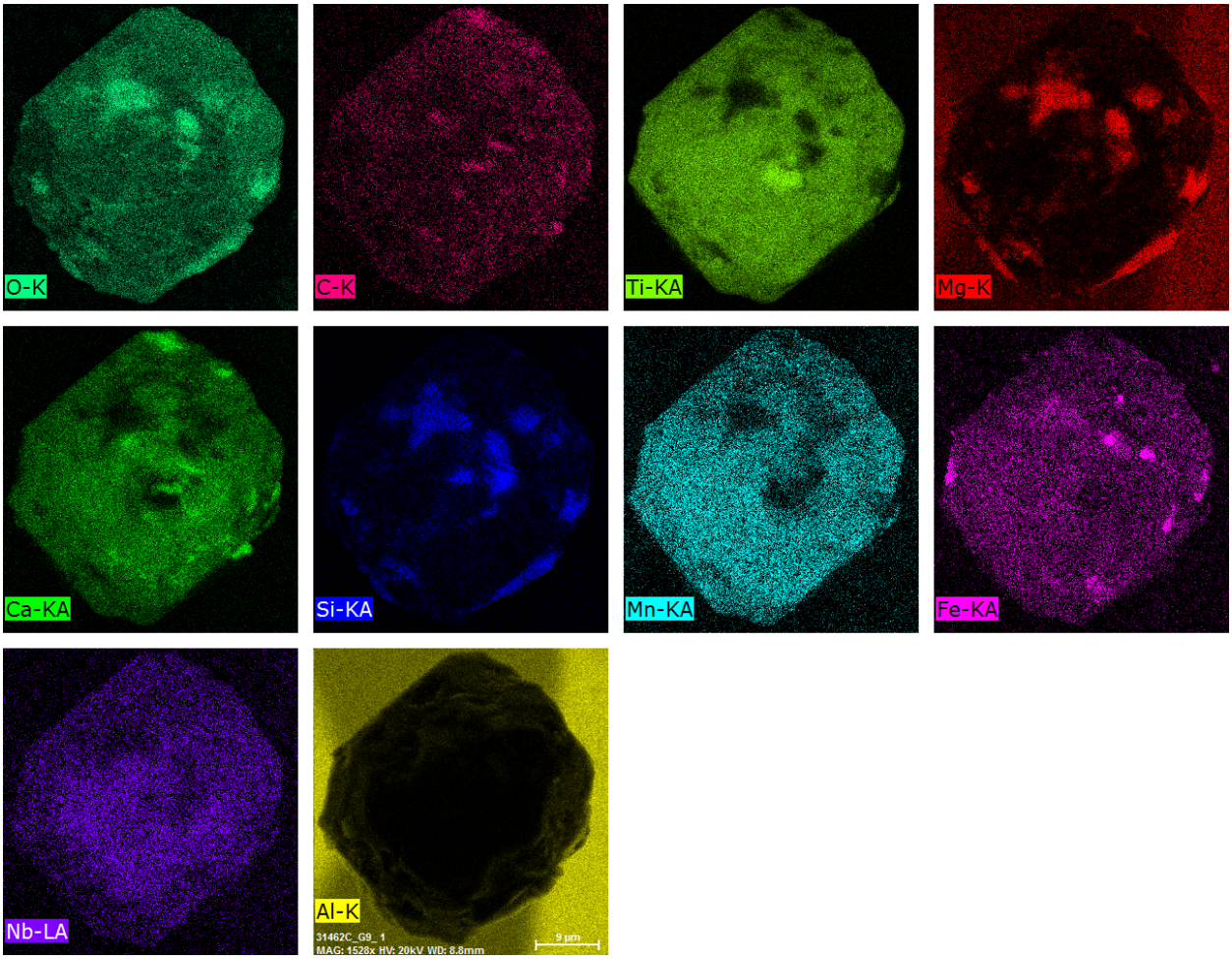


**Fig. 7.** Continued.

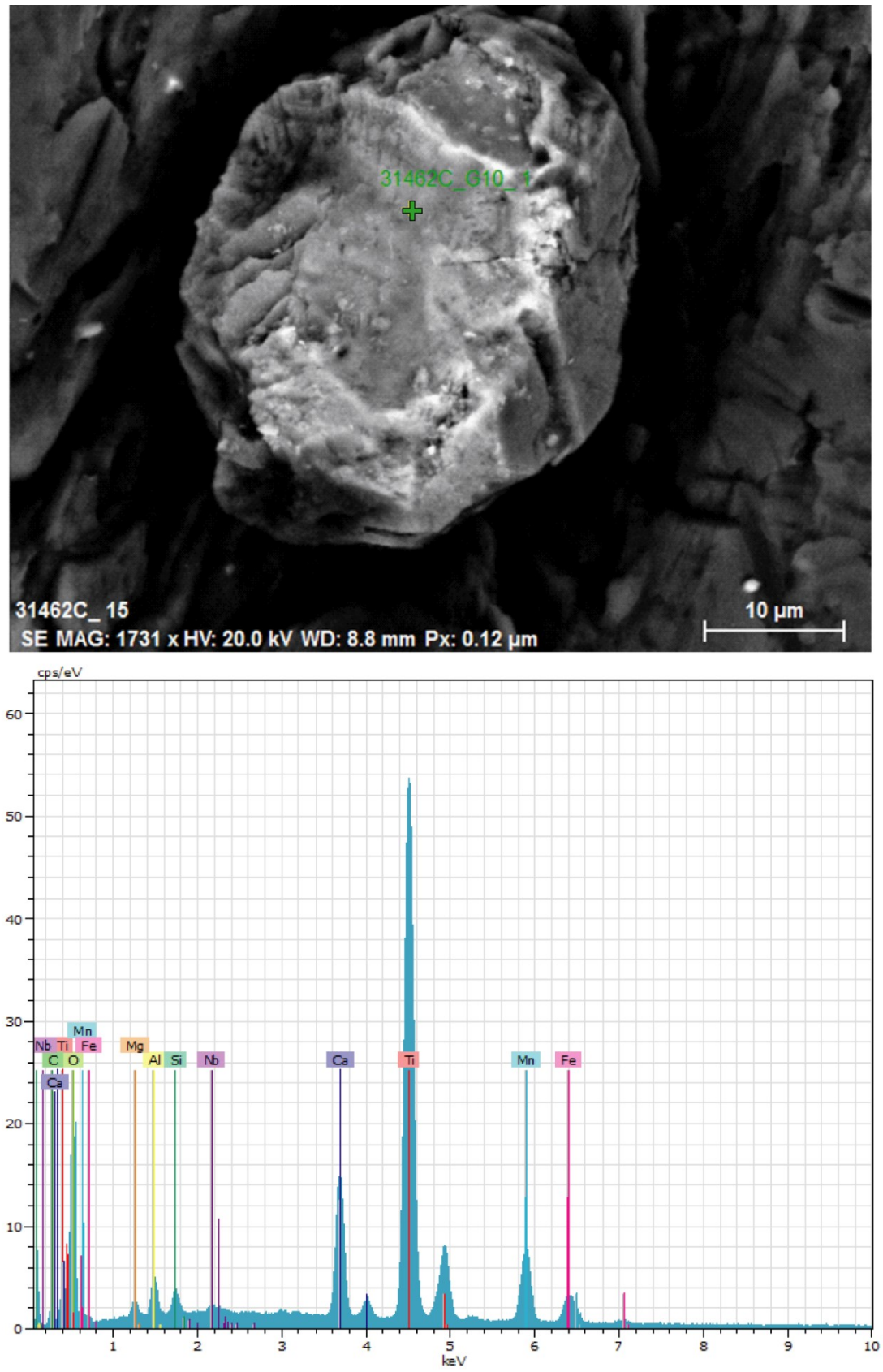


**Fig. 8.** BSE image, EDS spectra and element maps of grain 31462C_G10.

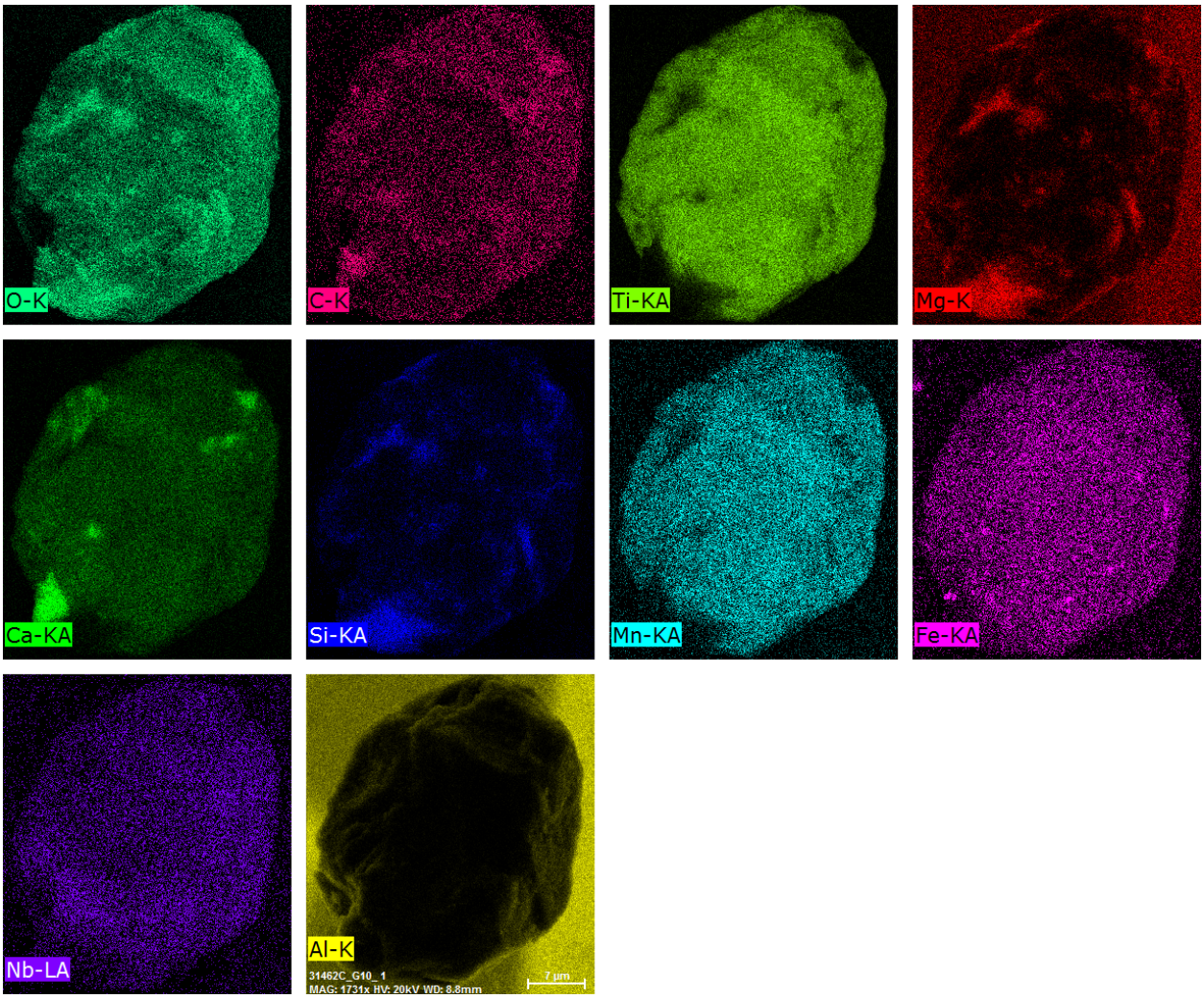


**Fig. 8.** Continued.

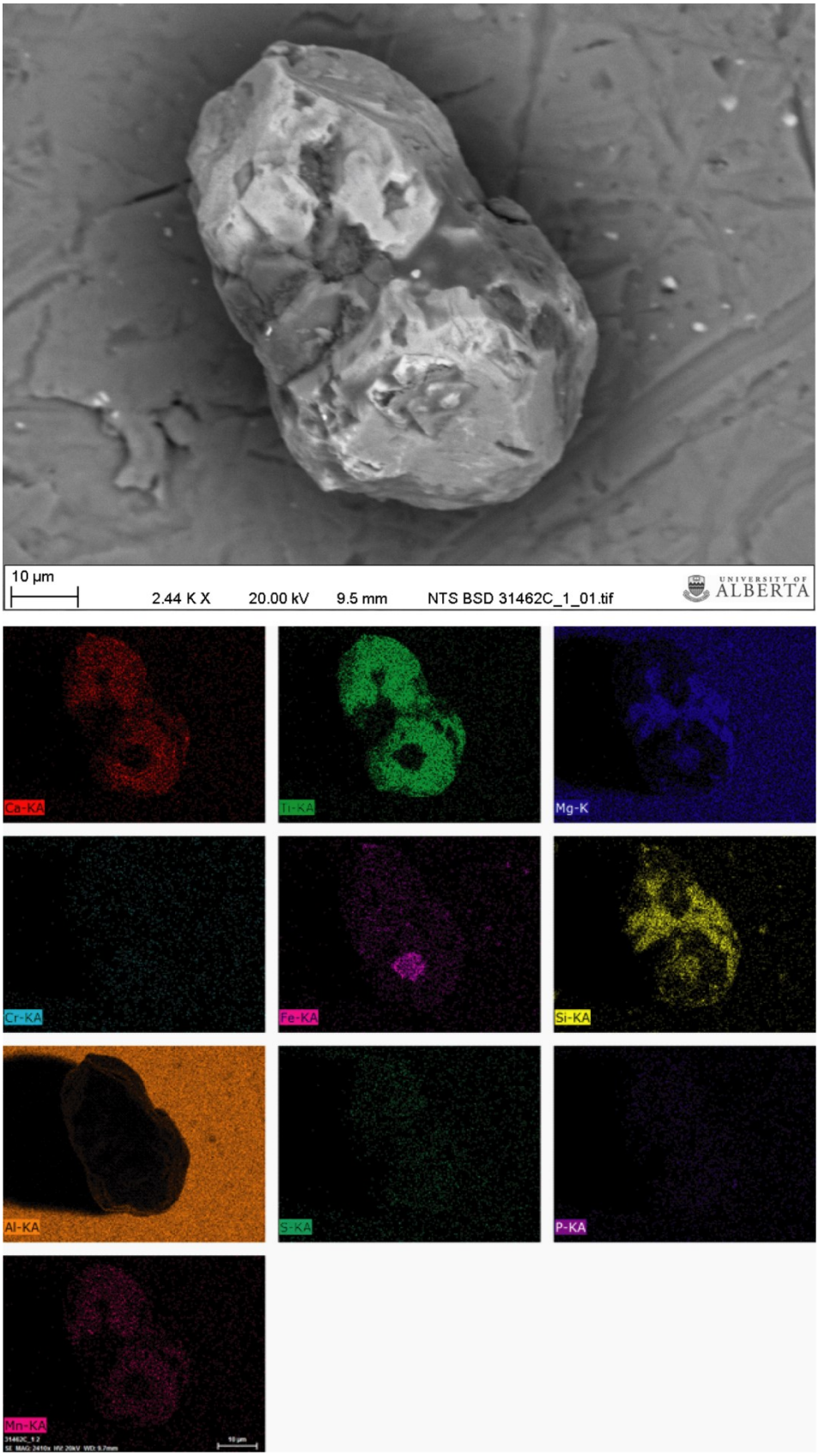


**Fig. 9.** BSE image and element maps of grain 31462C_1.

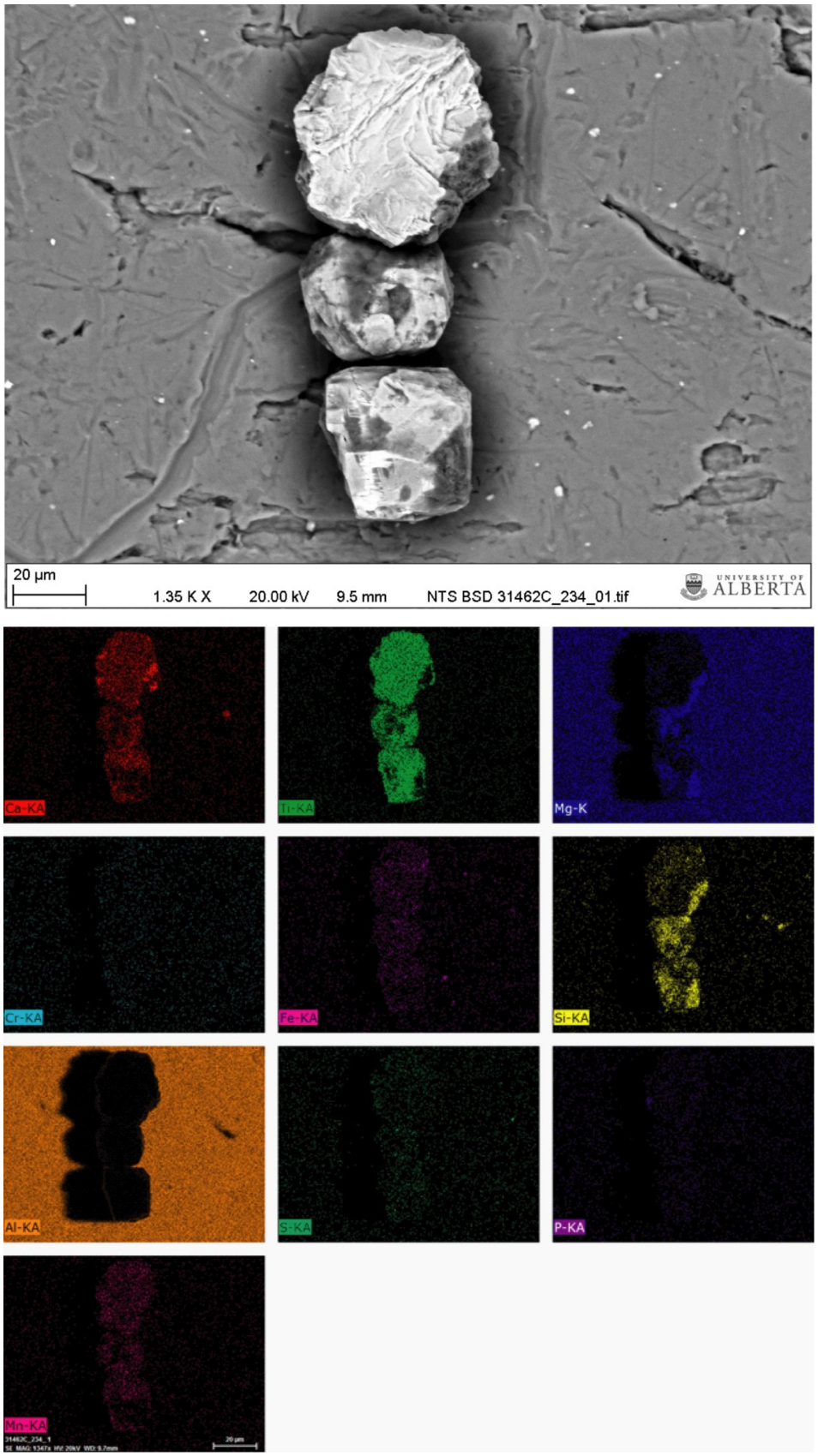


**Fig. 10.** BSE image and element maps of grain 31462C_234.

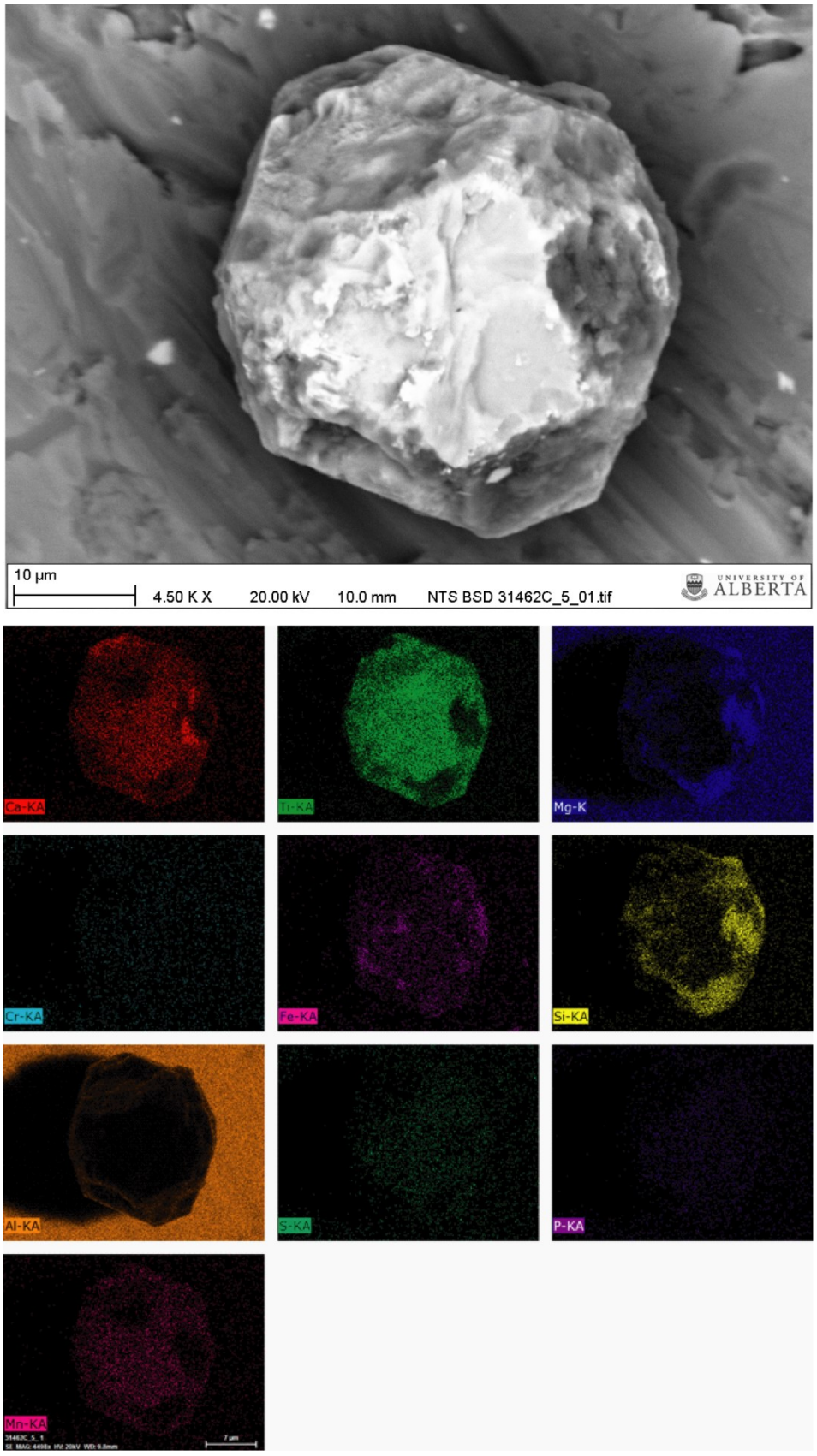


**Fig. 11.** BSE image and element maps of grain 31462C_5.

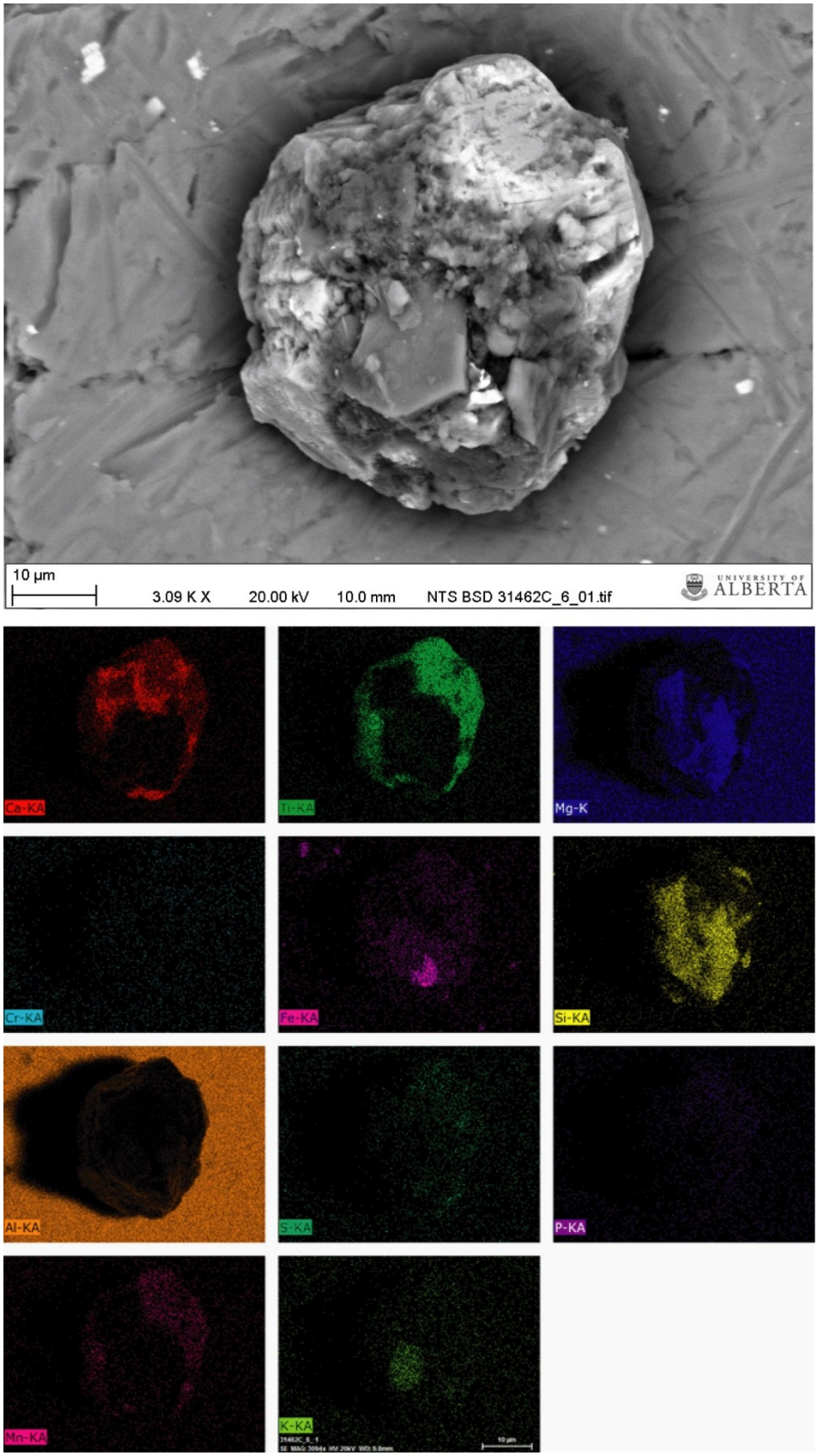


**Fig. 12.** BSE image and element maps of grain 31462C_6.

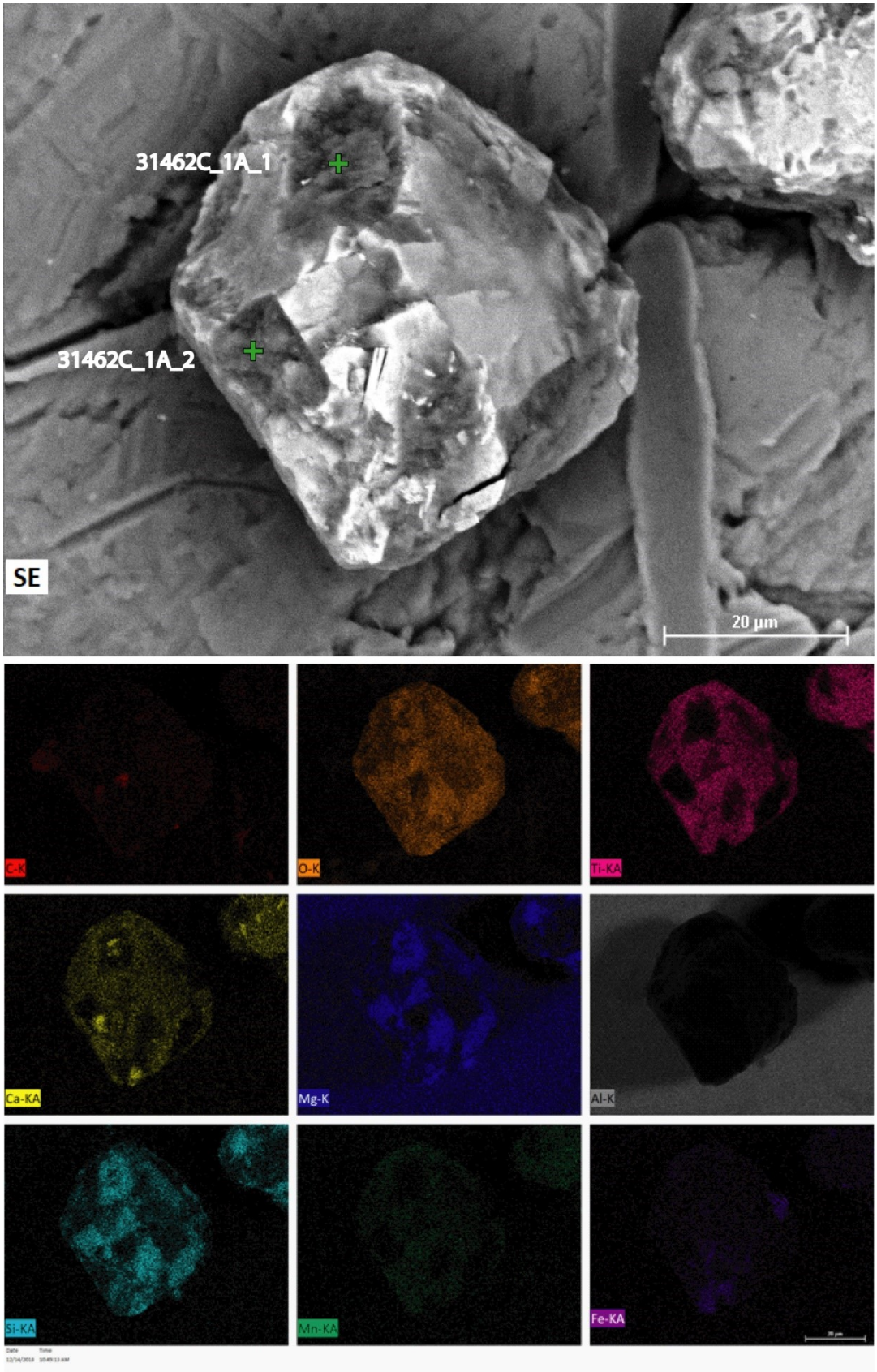


**Fig. 13.** BSE image, EDS spectra and element maps of grain 31462C_1A.

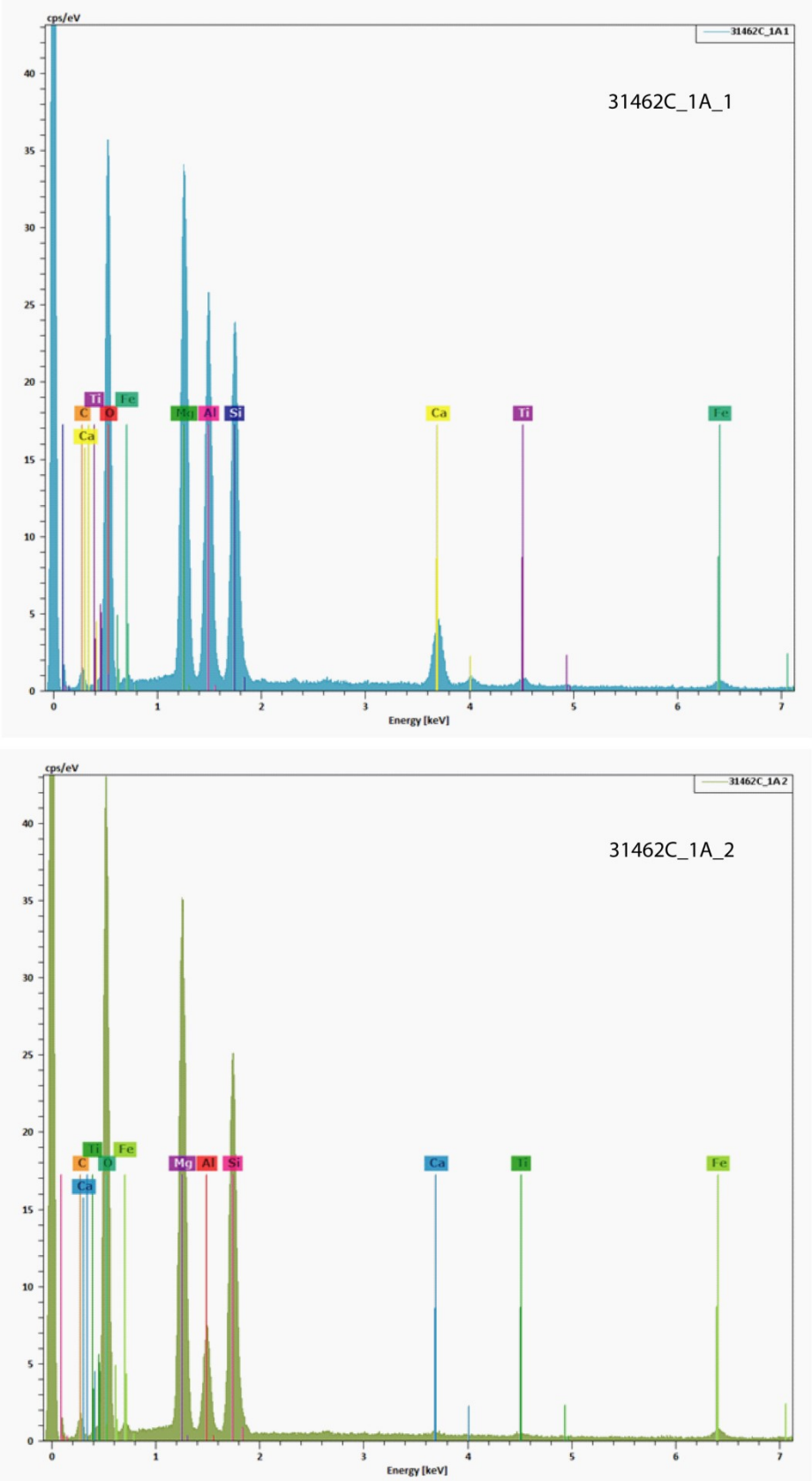


**Fig. 13.** Continued.

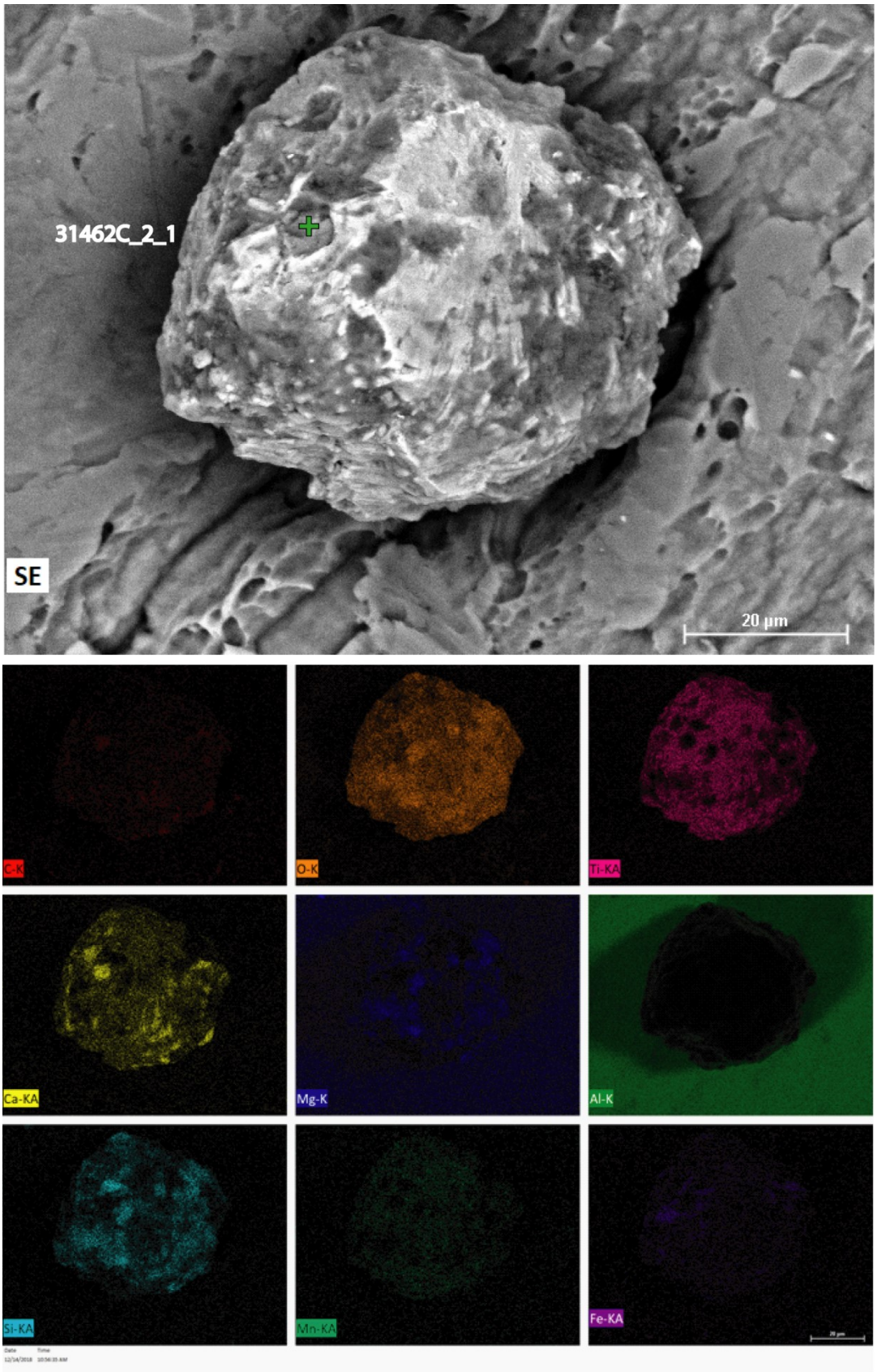


**Fig. 14.** BSE image, EDS spectra and element maps of grain 31462C_2.

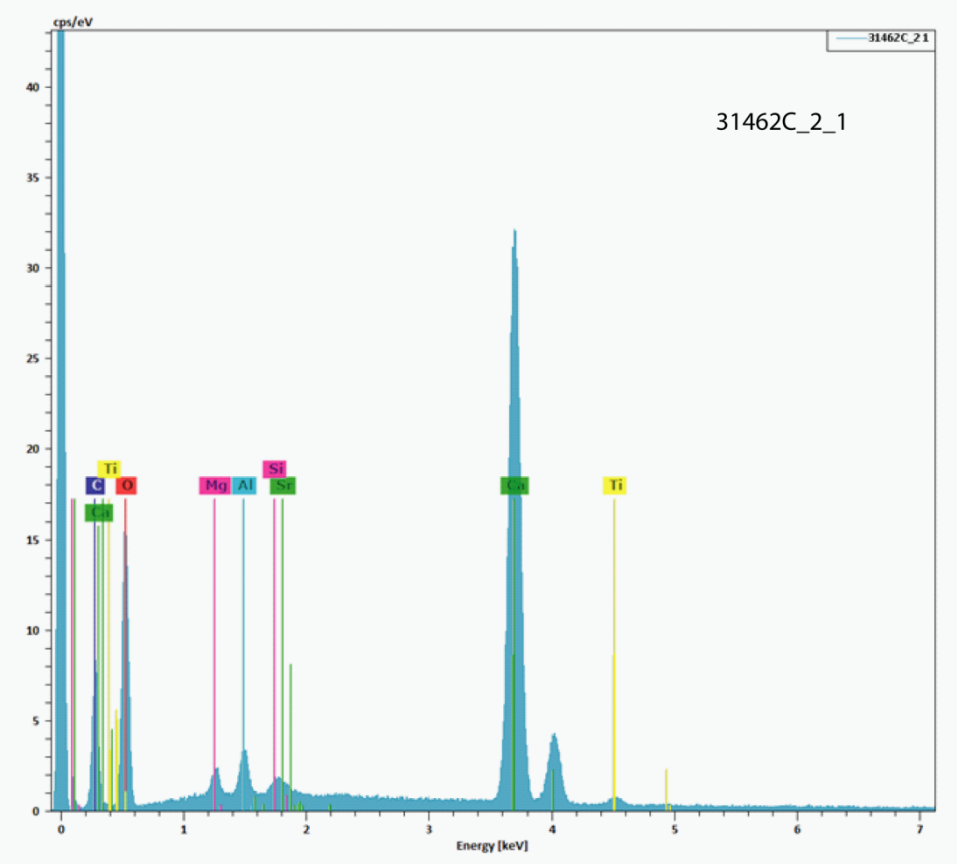


**Fig. 14.** Continued.

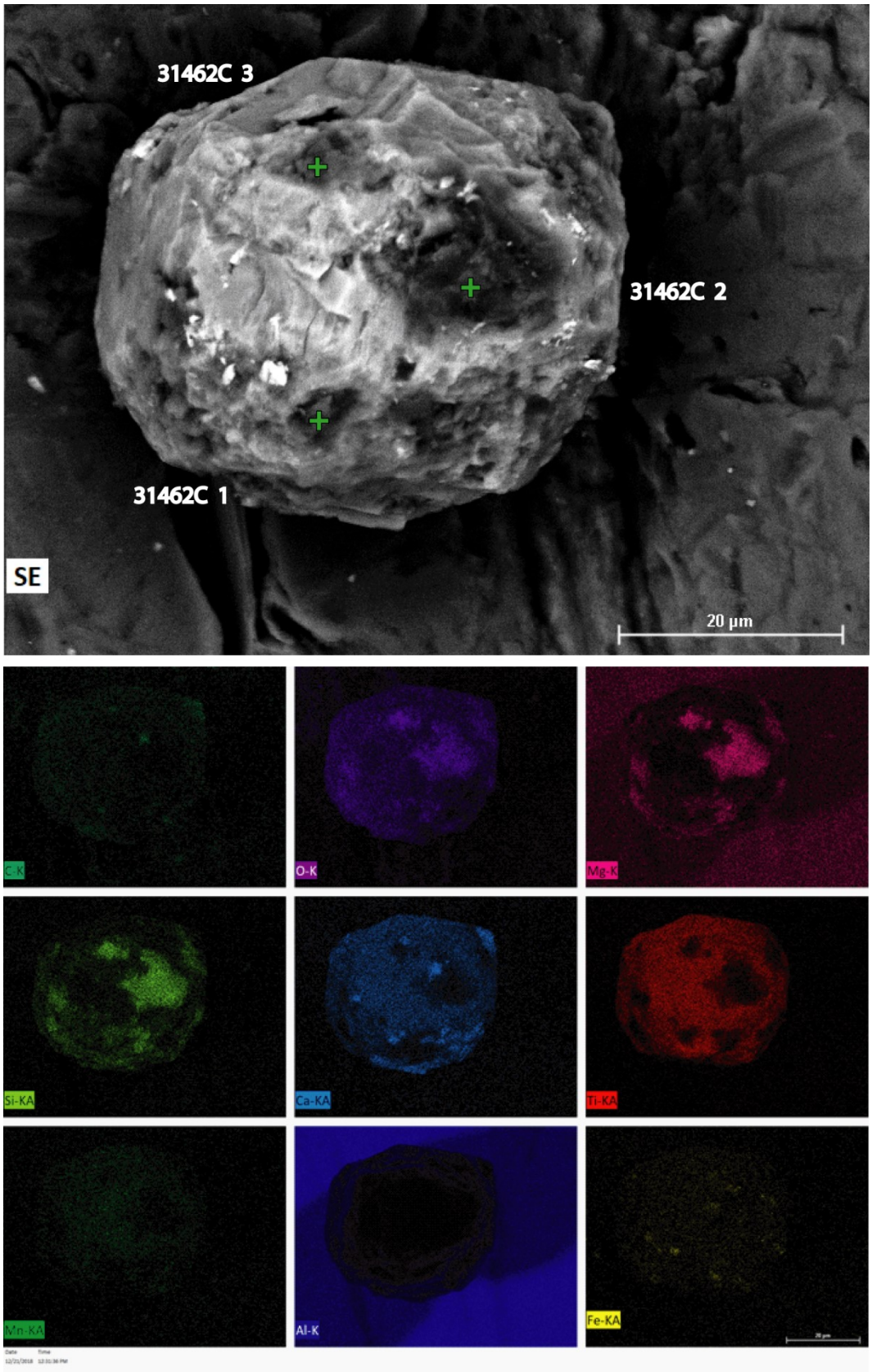


**Fig. 15.** BSE image, EDS spectra and element maps of grain 31462C.

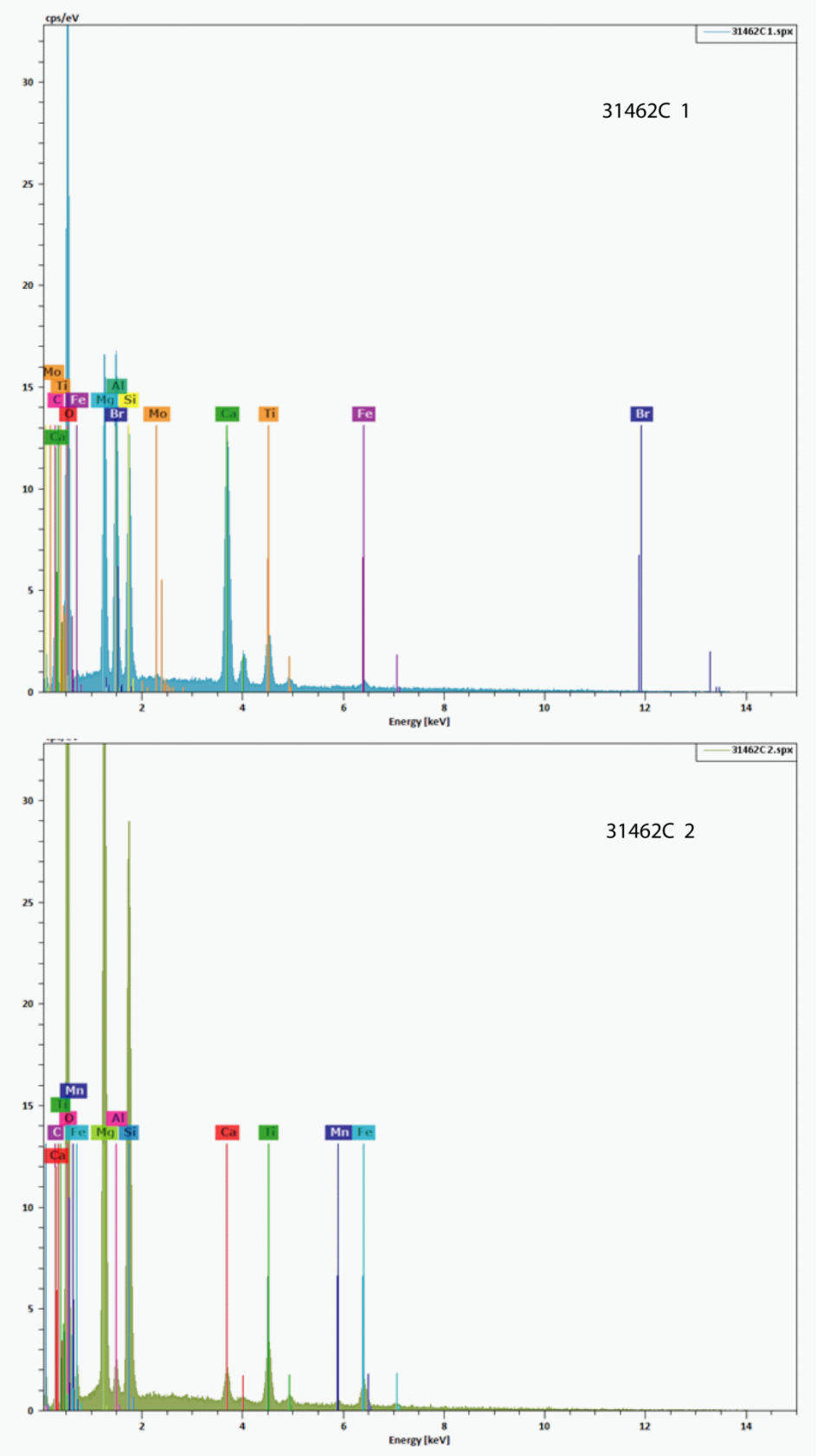


**Fig. 15.** Continued.

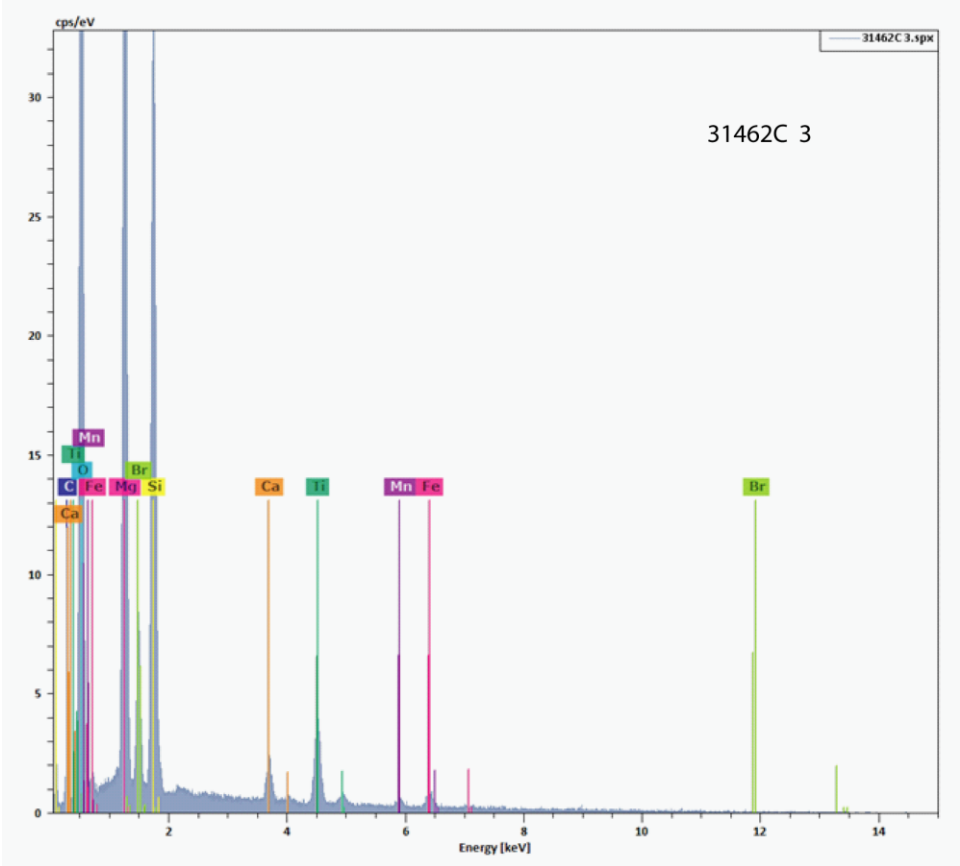


**Fig. 15.** Continued.

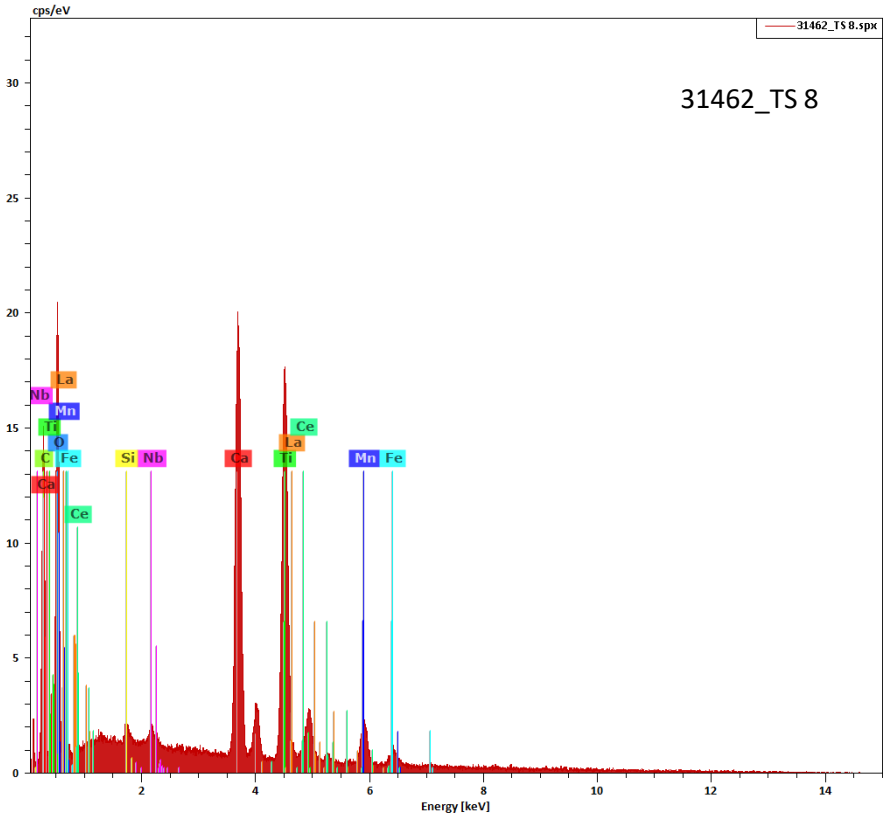


**Fig. 16.** EDS spectra of Ca-Ti rich composition resembling perovskite.

# APPENDIX E
# ADDITIONAL GEOCHEMICAL AND PETROLOGICAL DATA

## Perovskite Sr Isotope Method

Strontium isotopic compositions of perovskite were determined for two Renard (31556-1 and 35791-1) and three Ice River perovskite fractions (Ice River-22, Ice River-29, Ice River-32) previously analyzed for ID-TIMS U-Pb perovskite dating. The Sr method followed the protocol similar to Heaman et al. (2015). During the HBr protocol for U-Pb perovskite chemistry, a measured amount of $^{205}$Pb-$^{235}$U and $^{149}$Sm-$^{150}$Nd tracer solutions were added with the 48% HF:7N $HNO_3$ (50:50) mixture to dissolve the crystals, and kept on a hotplate at a minimum of ~110$^{o}$C for a minimum of 4 days. A Rb-Sr tracer solution was not added due to perovskite containing low Rb and high Sr, resulting in low Rb/Sr ratios with little effect to the initial Sr isotopic composition from Rb decay (Heaman 1989). The initial wash with 3.1N HCl was collected and dried for later Sr chromatography. The aliquot kept for Sr chemistry was re-dissolved in 0.15 ml 3N $HNO_3$ prior to loading onto Teflon columns containing ~5 µl of Sr resin cleaned with 0.6 ml of 7N $HNO_3$ and 0.6 ml of Millipore. A REE wash of 0.35 ml (0.05 ml, 0.1 ml and 0.2 ml aliquots) of 3N $HNO_3$ was collected and dried for later Sm-Nd chemistry. This was followed by a Ba wash of 0.9 ml (0.3 ml and 0.6 ml aliquots) of 7N $HNO_3$. Strontium was collected in 1.0 ml (0.4 and 0.6 ml aliquots) of 0.05N $HNO_3$, and ~2-3 drops of 0.15N $H_3PO_4$ added then dried. The dried Sr aliquots were re-dissolved in 4 µl of $TaF_5$ solution and loaded onto an outgassed rhenium (Re) filament. The isotopic composition of strontium was measured using a Thermo Triton Plus multi-collector thermal ionization mass spectrometer operated in multi-collector Faraday detector mode at the University of Alberta. An initial analysis of the NBS987 standard was completed to check for accuracy, with a result of 0.710290±0.000006 (1SE; n =1) for $^{87}$Sr/$^{86}$Sr. Approximately 200 ratios of Sr isotopic data were collected between ~1360-1400$^{o}$C. The Renard 3 (31556-1) and Renard 7 (35791-1) Sr isotope compositions in Table 1 do not agree within analytical uncertainty. The three Ice River perovskite (IR6) Sr isotope compositions reported in Table 1 are comparable to Ice River perovskite compositions reported by Tappe and Simonetti (2012) (0.702838±0.000051; 2σ, n=9, TIMS), Zurevinski et al.

(2011) (0.70276±0.00002 and 0.70288±0.00002; TIMS) but not Yang et al. (2009) (0.70293±0.00002; 2σ, n=32, LA-MC-ICP-MS).

**Table 1.** Sr isotope compositions from Ice River perovskite (IR6), Renard 3 and Renard 7 perovskite.

| Sample ID | $^{87}Sr/^{86}Sr$ | 1SE |
|---|---|---|
| 31556-1 (Renard 3) | 0.703815 | 0.000011 |
| 35791-1 (Renard 7) | 0.702867 | 0.000006 |
| Ice River-22 | 0.702866 | 0.000005 |
| Ice River-29 | 0.702860 | 0.000004 |
| Ice River-32 | 0.702873 | 0.000010 |

This section summarizes additional information for Renard 1, Renard 2, Renard 8, Renard 9, Renard 10, G04-296 Anomaly, North Anomaly, and the Lynx and Hibou dyke systems. Samples from the Lynx and Hibou dyke systems initially formed a third project but after discovery of kassite in a Renard 9 hypabyssal kimberlite sample (see Chapter 4), these samples were not included. Perovskite was identified in a few samples from Hibou, Lynx, G04-296 Anomaly and possibly Renard 10 but each contained unique challenges.

## Renard 1

In addition to the data presented in Chapter 3, samples 37373-37375 were processed for U-Pb dating but the unit code later changed from Kimb1c to Kimb1d therefore one sample was selected. The thin section for 37374 contains an opaque xenocryst to the unaided eye which was found to be a large cluster of opaque grains comprised of perovskite and an Fe- and Ti-bearing mineral when examined by scanning electron microscope (Figures 1-2). Sample 37309 (Kimb1c) was tried for U-Pb dating but the grains were likely not perovskite (very low U and Pb). Sample 37319 (Kimb1c) contains perovskite in thin section but after processing the sample, the heavy mineral concentrate from the Wilfley table was enveloped in white, fine-grained, and cloudy material, which made the mineralogy difficult to see. Attempts at decanting with water or dissolving with 2N $HNO_3$ on the hotplate did not remove the material from a test fraction. The downhole log suggests talc may be present. Some perovskite may be present in Kimb1b samples 37333 and 37376 but mainly in the magmaclasts, which was likely not enough material for U-Pb dating.

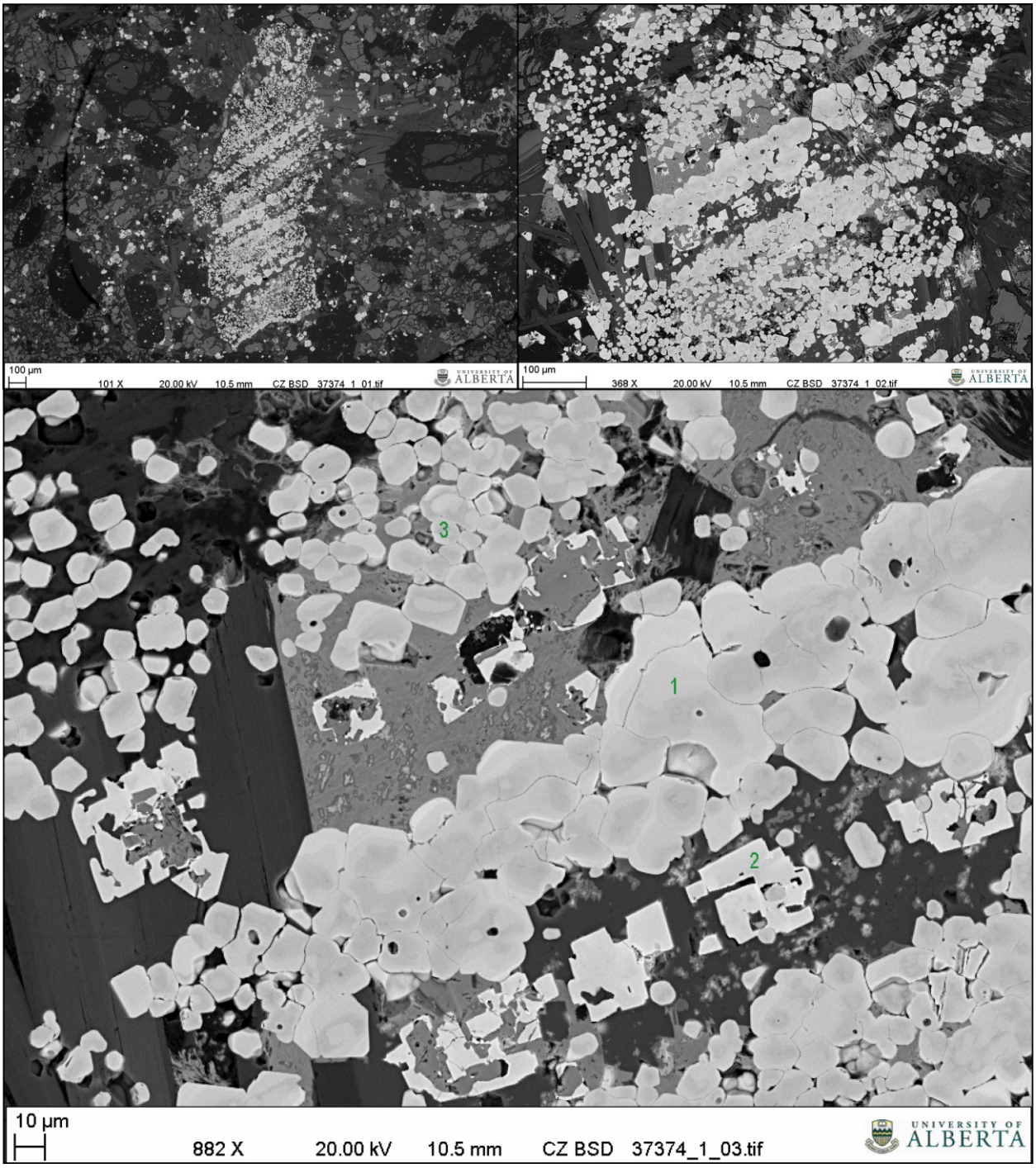


**Fig. 1.** BSE images of opaque cluster in 37374. Note top left image includes black circle marks surrounding opaque cluster. Labels 1-3 in the bottom image represent EDS spectra.

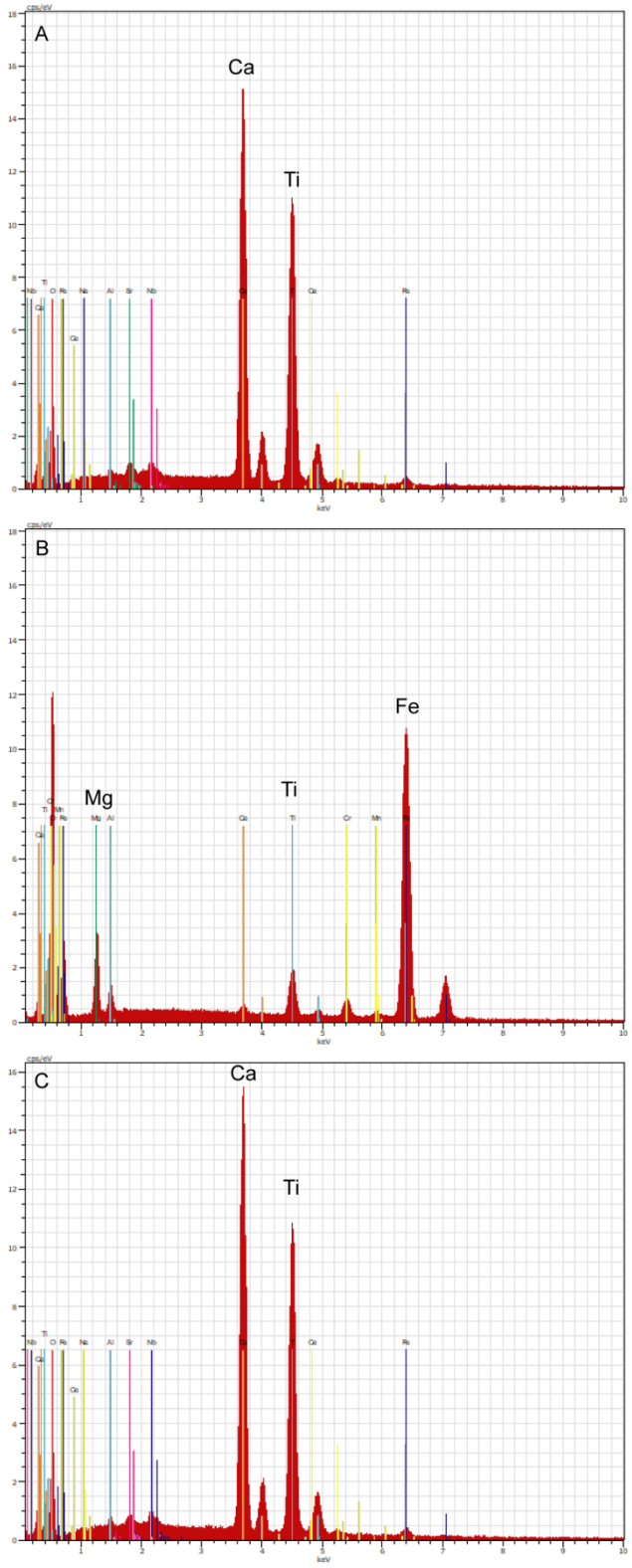


**Fig. 2.** EDS spectra from 37374 of label 1 (a) and label 3 (c) containing Ca- and Ti-bearing composition resembling perovskite, and label 2 (b) containing Fe- and Ti-bearing composition.

## Renard 2

Three additional samples (Kimb2c; 38911, 38912, and 38915) were processed for U-Pb dating and perovskite was found.

## Renard 8

Eight kimberlite samples from Renard 8 were available (four Kimb8a and four Kimb8c from drill core). Perovskite was not obvious in thin section from Renard 8 samples except possibly 36926. Two samples (36926 and 36973) were processed to check the Wilfley table heavy mineral concentrate.

**36926 (Kimb8c):** An initial test fraction of ~100 medium-dark brown octahedral grains and fragments (~30-50 μm) with a generally dull rough/bumpy surface (± inclusions) resulted in a poor TIMS analysis. EDS scanning of several grains from concentrate indicated many Ti- and Fe-bearing compositions (± Ca, Al, Si, Mg) suggesting the grains may be ilmenite, few Ti-bearing compositions (possibly rutile), and few Ca- and Ti-bearing compositions (Figure 3).

## Renard 9

Three additional samples (Kimb9c-1: 31463, 31471; Kimb9c-2: 31482) were processed for U-Pb dating but perovskite was not obvious.

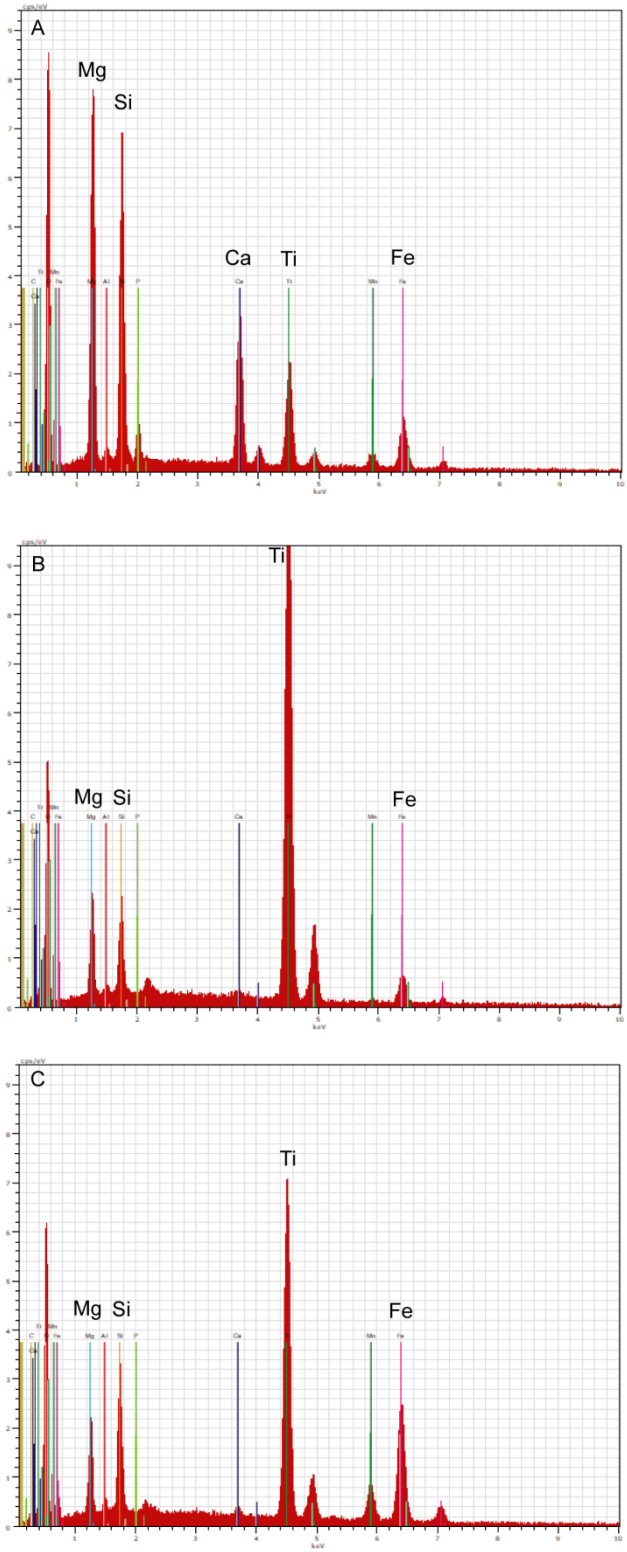


**Fig. 3.** EDS spectra from 36926B; (a) grain 36926B-3 containing Ca and Ti, (b) grain 36926B-5 with Ti-bearing composition (possibly rutile), and (c) grain 36926B-8 with Ti- and Fe-bearing composition (possibly ilmenite).

## Renard 10

Three kimberlite samples from Renard 10 (G04-262 Anomaly) were available (drill core of two Kimb10c and one FKimb10d). Perovskite was not obvious in thin section but a few perovskite may have been identified in one sample (35762) by EDS.

**35762 (FKimb10d):** Few possible perovskite found by EDS contain an unusual anhedral texture. One grain contains Ca and Ti compositions (minor Fe, Ce) near the rim (label 1) and Ti, Fe, Ca, Mg, Ce and Si compositions within the internal grain area (label 2; Figure 4). Locating these perovskite in thin section is difficult due to the black or dark brown-black colour but range ~50-100 μm in size. In the Wilfley table heavy mineral concentrate, these grains bear a luster and dark brown colour resembling perovskite but with a rough/irregular surface and shape. Two fractions were initially tested; a fraction of ~75 larger grains (~50-90 μm) with irregular, round or squarish shapes (resorbed?) and many appear to be half the grain (split?), and a second fraction of ~140 smaller grains (~30-50 μm) with an overall blocky shape, some cube-like or very rough fragments of cube-like shape. One fraction was analyzed in Faraday mode when uranium (low concentration) should have been analyzed in SEM mode therefore produced a less precise date with large error. Given the nature of the grains, it is unknown at this time how to interpret the two U-Pb dates but the data falls within range of the majority of the Renard kimberlites. Additional investigation and instrument time would be needed.

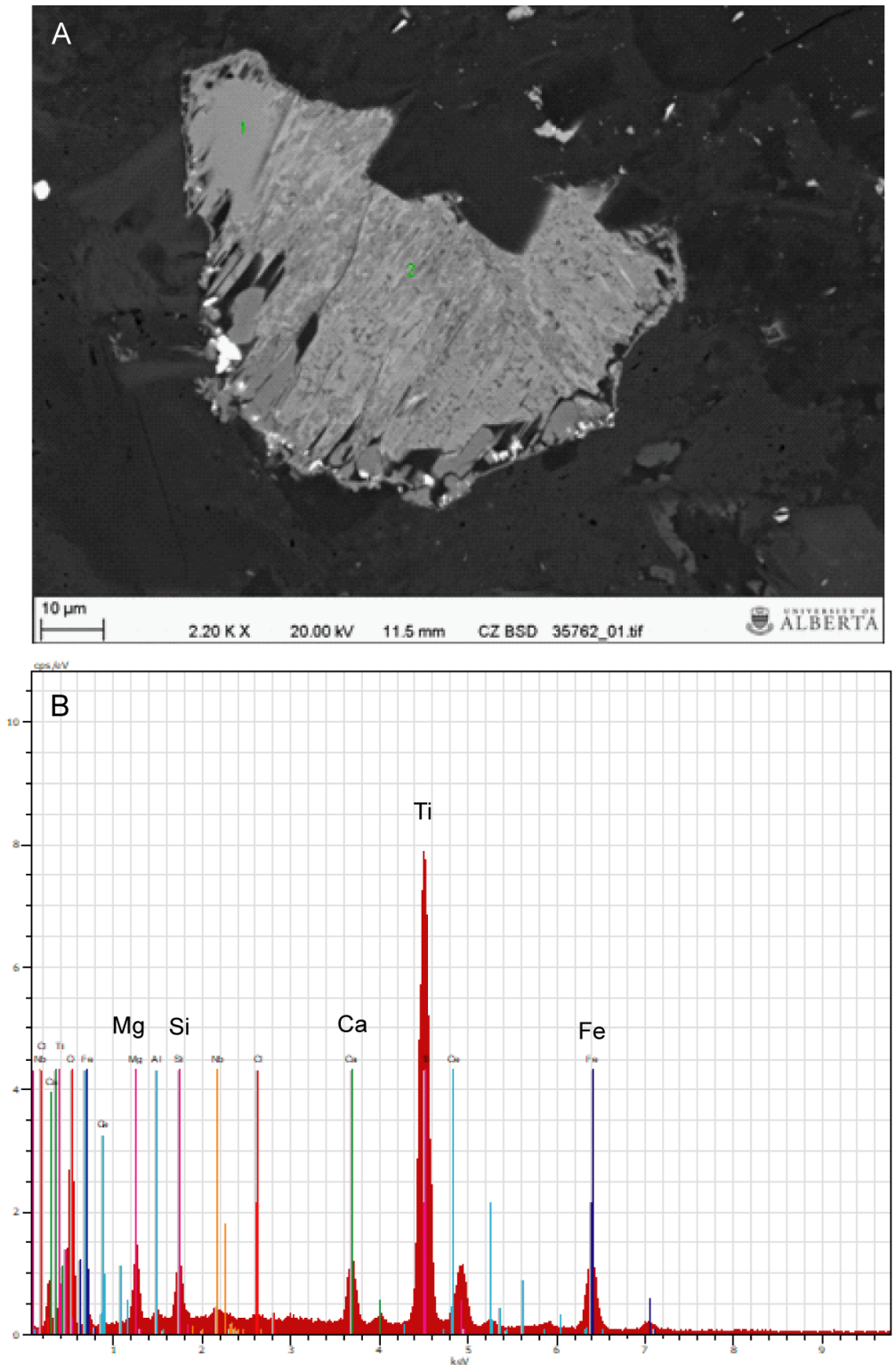


**Fig. 4.** BSE image (a) of an example anhedral grain found in thin section of sample 35762 containing Ca, Ti and minor Fe (also possibly Ce?) (label 1), and (b) EDS spectra of label 2 containing Ti, Ca, Fe, Mg, Si (also possibly Ce?).

## G04-296 Anomaly

Two kimberlite samples were available for the G04-296 Anomaly (one surface hand sample from I. Lepine and one core box sample). One surface hand sample (31577) was dated (see Chapter 3). Tiny perovskite may be present in a thin section of the core box sample (35100) but perovskite was slightly more obvious in 31577.

## North Anomaly

Four kimberlite samples from the North Anomaly were available (two from T222 trench and two from G04-285 Anomaly drill core). Perovskite (or zircon) was not obvious in thin section for any of the samples. Part of sample 31575 was processed to check the Wilfley table heavy mineral concentrate. Secondary carbonate veining and/or replacement of olivine was seen in thin section, and phlogopite and apatite are commonly altered green (chlorite?) which precluded other dating methods.

## Hibou

Seventeen kimberlite samples were available from the Hibou dyke system (G04-271A anomaly). Two core box samples (31586 and 31587), one hand sample from the T271A-10 trench, and 14 core samples (~3-14 cm; some kimberlite intersections contain up to 3 samples, such as from near the middle of the sample, or from the upper or lower contacts) from 8 drill holes. Generally, many of the Hibou core samples contain;

- Common olivine macrocrysts/phenocrysts replaced by serpentine ± carbonate, opaques and possible talc. Few macrocryst-poor (aphanitic) samples are present [e.g. 32618 (upper) and 32620 (lower) contact samples from same drill hole]. Olivine can be very coarse (>1 cm) in some samples. Few samples contain partially fresh olivine (32610?, 31586, 31587). Some macrocrysts resemble clustered small olivine grains.
- Phlogopite (31576, 32608, 32613, 32614, 32615, 32616, 32619, 31587, 31586) and apatite (32613, 32614, 32615, 32616, 32619) phenocrysts can be present (sometimes partially altered green).
- The groundmass is comprised of;
    - Variable amounts (few to common) of phlogopite between samples, often with pale green pleochroism or rims,

- Opaques (black, some reddish-brown) with few atoll textures and may appear altered (bladed shapes?),
- Perovskite is not obvious
- ± Apatite (sometimes partially altered green).
- Dominantly uniform carbonate-rich groundmass (minor serpentine) which may contain minor segregations of carbonate and/or serpentine. Many samples contain an overall or patchy pale greenish alteration. A few exceptions include:
  - A lath-like texture to carbonate in some small segregations (32610).
  - A serpentine-rich groundmass for 32616 (where present).
  - Groundmass absent for most of 32615 and 32616 thin sections (holes in slide?).

- Few altered country rock xenoliths or xenocrysts (e.g. biotite)
- Trace xenocrysts of altered to partially altered pyroxene (e.g. partially altered in 32622, 31587), kelyphitic garnet and altered unknowns. As well as chromite or fresh diopside observed in core box samples.
- Common xenocrysts of black irregularly shaped opaques (e.g. ilmenite).
- In addition, the following textures were seen in some samples;
  - Oxide layering or banding [e.g. 31576, 32617 lower contact sample, 32618 (upper) and 32620 (lower) contact samples from same drill hole].
  - White carbonate segregations along or towards the lower contact (e.g. round in 32617; core box samples 31586 and 31587) or near upper contact (32618).
  - Common cross-cutting veinlets/veins filled with carbonate ± serpentine, metallic yellow sulfide
  - Several opaque-filled cross-cutting veinlets (e.g. 32613, 32619; core box samples 31586 and 31587 contain magnetic grey metallic minerals)

Perovskite was identified in only two samples (31576 and 31587; Figure 5) by EDS:

**31576**: Few perovskite were found in thin section by EDS and showed complex grains containing multiple phases (Figures 6-8). Part of this sample was processed and one fraction from the Wilfley table heavy mineral concentrate was tested. The magnetic minerals were not removed because of the possibility of weakly magnetic ilmenite (black mineral) intergrown with

perovskite. This initial fraction of ~40 patchy dark brown perovskite (some with black areas) of mostly fragments of round (?)-like or cuboctahedral (?) or hexagonal (?) grains (shape hard to see) with good luster (~30-50 μm) returned low radiogenic Pb content.

**31587:** Perovskite was found in sample 31587 (at 48.62 m depth). Some grains were tiny or contained multiple phases (Figures 9-13). An initial sample (31587; 48.60-48.77 m) was processed. EDS of single grains indicated dark brown perovskite (Ca-Ti-bearing) and possible ilmenite (Fe-Ti-bearing) compositions which were difficult to distinguish from one another. It is also possible ilmenite (Fe-Ti-bearing compositions) may rim perovskite, which could make EDS identification of grain surfaces biased towards Fe-Ti-bearing compositions. Black rims on perovskite can be difficult to see in the Wilfley table heavy mineral concentrate. One fraction of ~58 medium brown perovskite fragments or fragments of octahedral grains (most with bumpy surface; some surfaces show good luster; ~30-50 μm) was tested and returned very low U and Pb suggesting mixing with another mineral. Magnetic minerals were not separated out of this test due to the possibility of weakly magnetic ilmenite intergrown with perovskite (which may remove perovskite into a magnetized mixed clump of grains). A second fraction was not completed due to problems weighing the grains (boat flipped), leaving sparse grains to try again. A second larger portion of the same sample was processed (31587B; 48.77-49.45 m). Perovskite from this sample is tiny, hard to identify and very time-consuming to pick out of the Wilfley table heavy mineral concentrate.

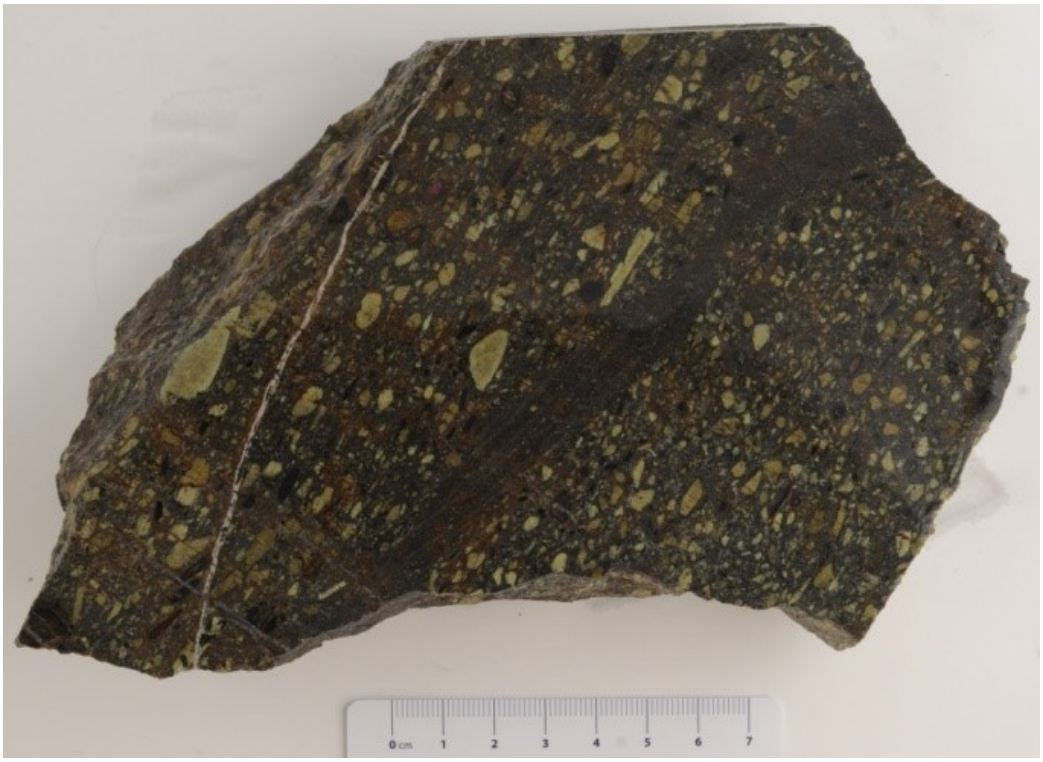


**Fig. 5.** Samples from the Hibou dyke system. a) Hand sample 31576 (wet).


**Fig. 5.** Continued. Samples from the Hibou dyke system. b) Photo of core box sample 31587.

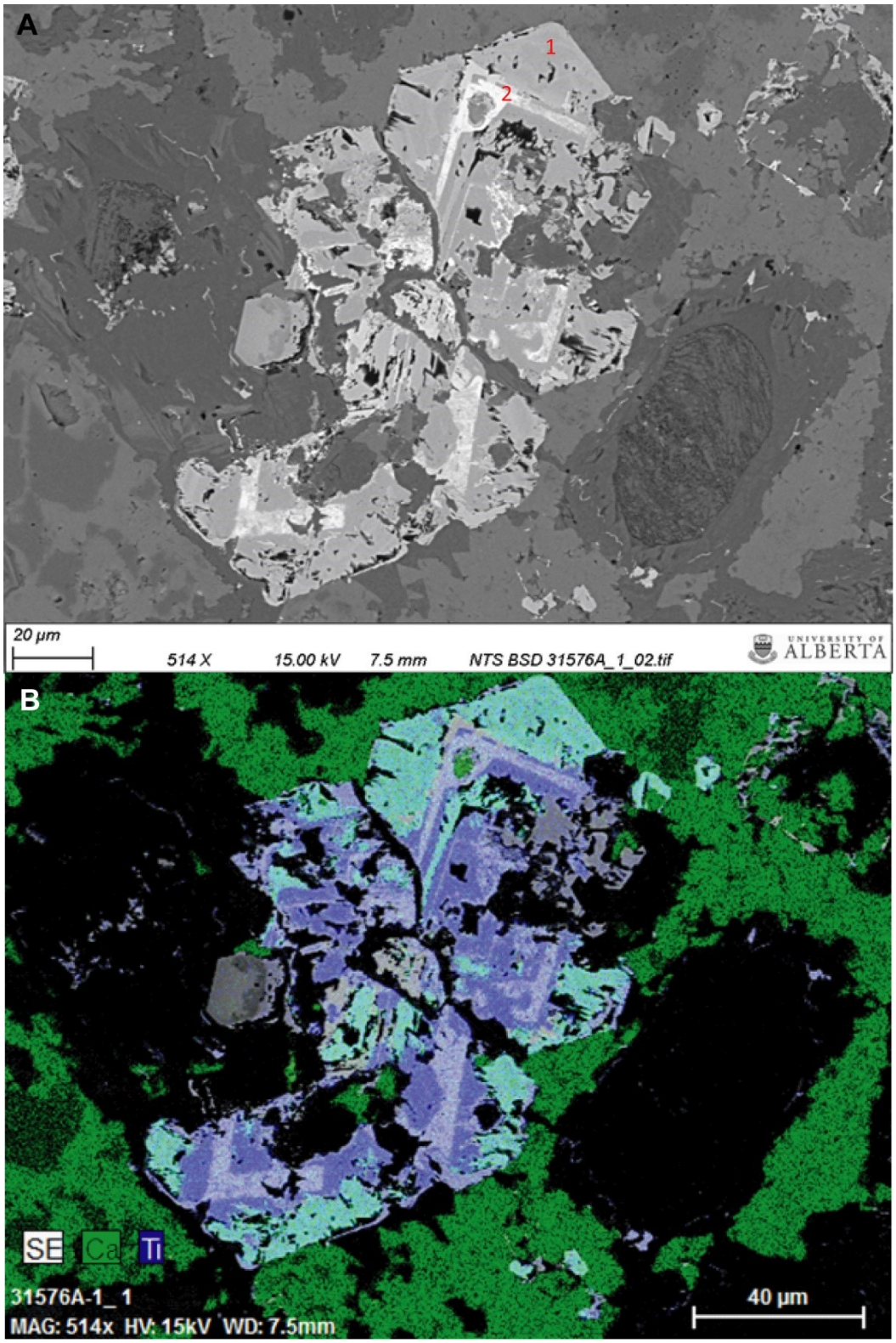


**Fig. 6**. (a) BSE image from thin section 31576A (macrocrystic area) containing grain with a Ca-Ti-bearing rim (label 1) and Fe-Ti-bearing composition (label 2). (b) Ca and Ti element map of same grain.

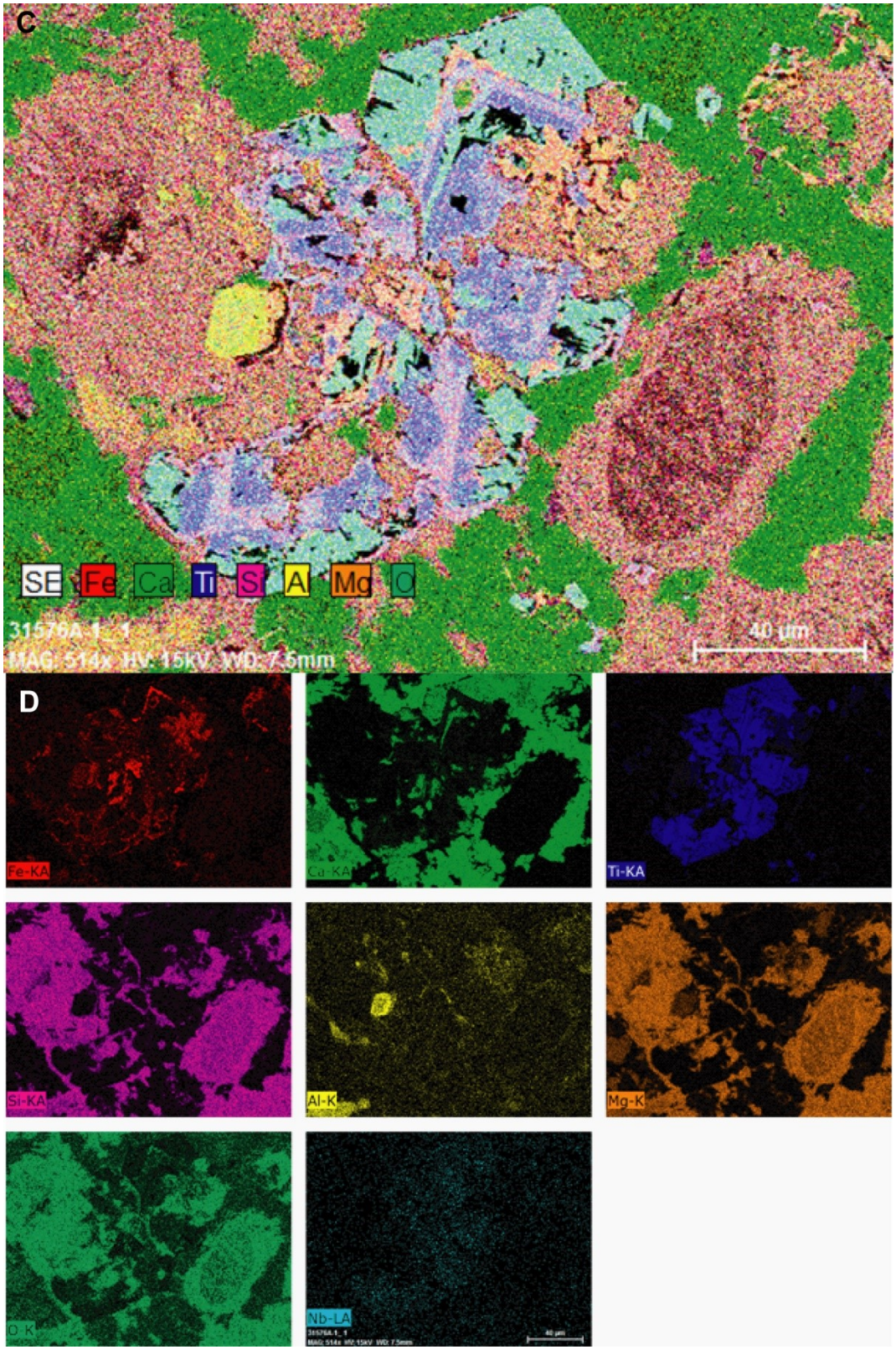


**Fig. 6**. Continued. (c) Ca, Ti, Fe, Si, Al, Mg, and O element map. (d) Individual element maps of (c).

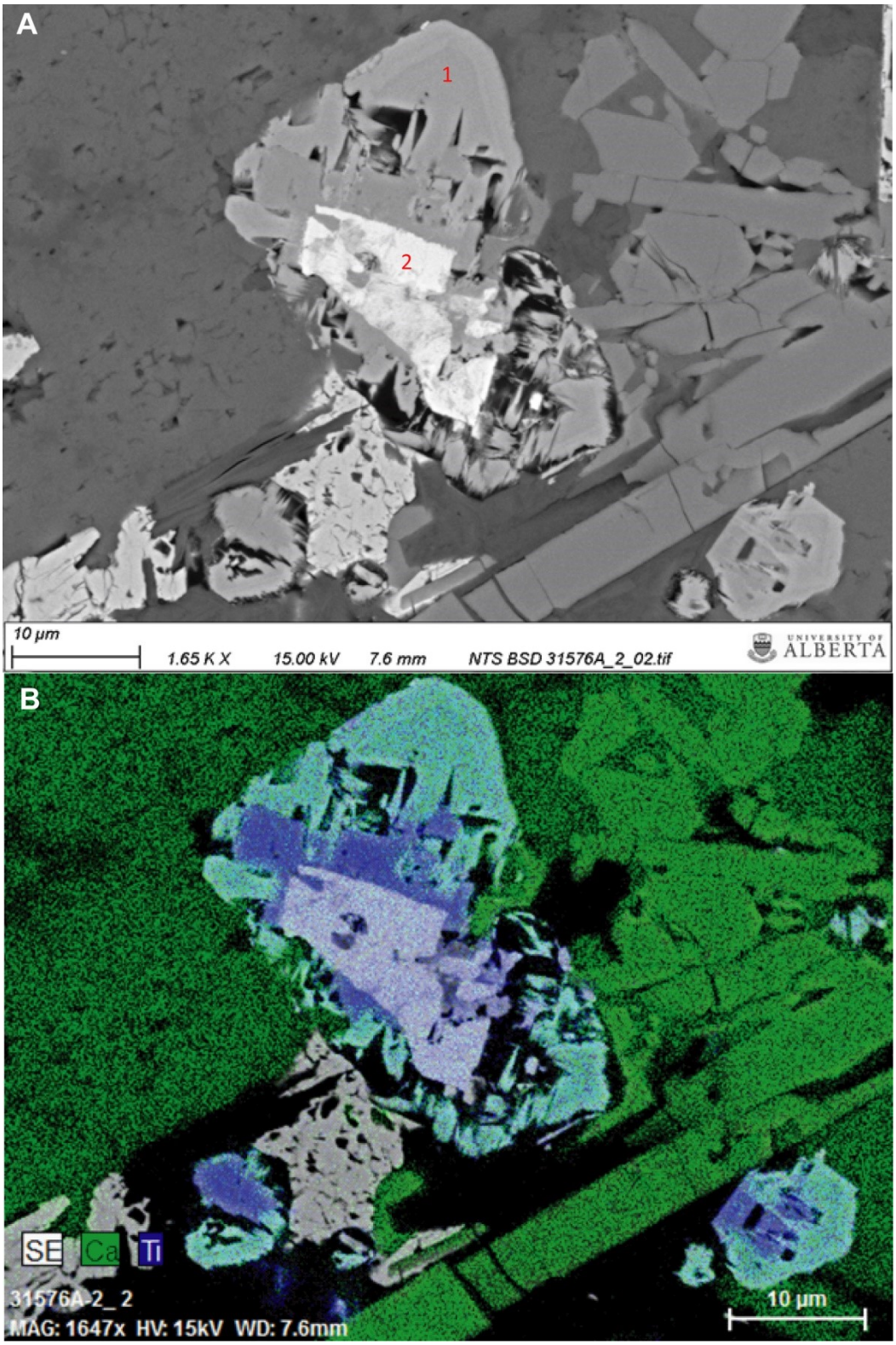


**Fig. 7**. (a) BSE image from thin section 31576A (macrocrystic area) containing grain with a Ca-Ti-bearing rim (label 1) and Ti?-bearing core (label 2). Composition of slightly darker area between core and rim unknown. (b) Ca and Ti element map of same grain.

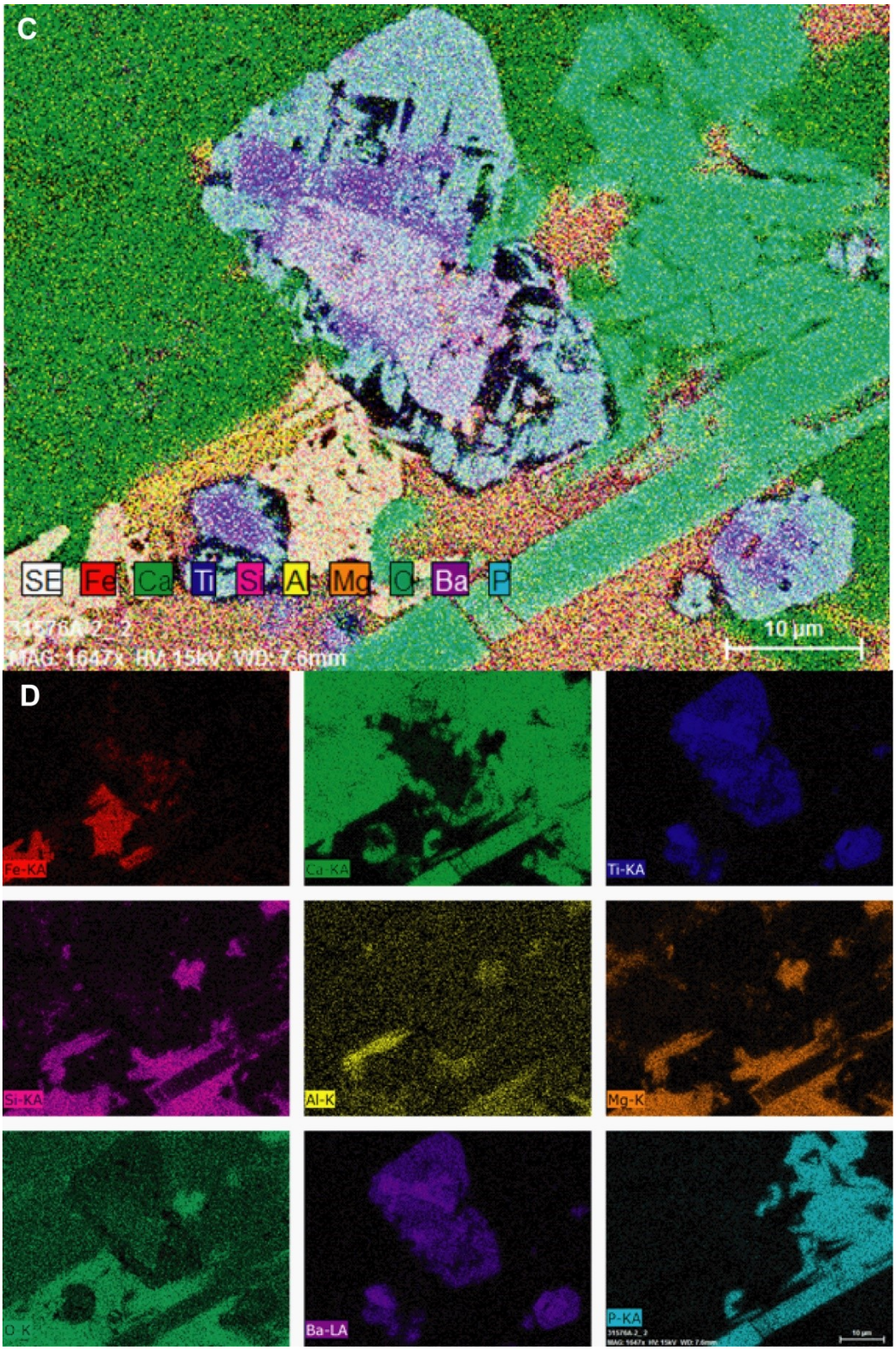


**Fig. 7**. Continued. (c) Ca, Ti, Fe, Si, Al, Mg, Ba, P, and O element map. (d) Individual element maps of (c).

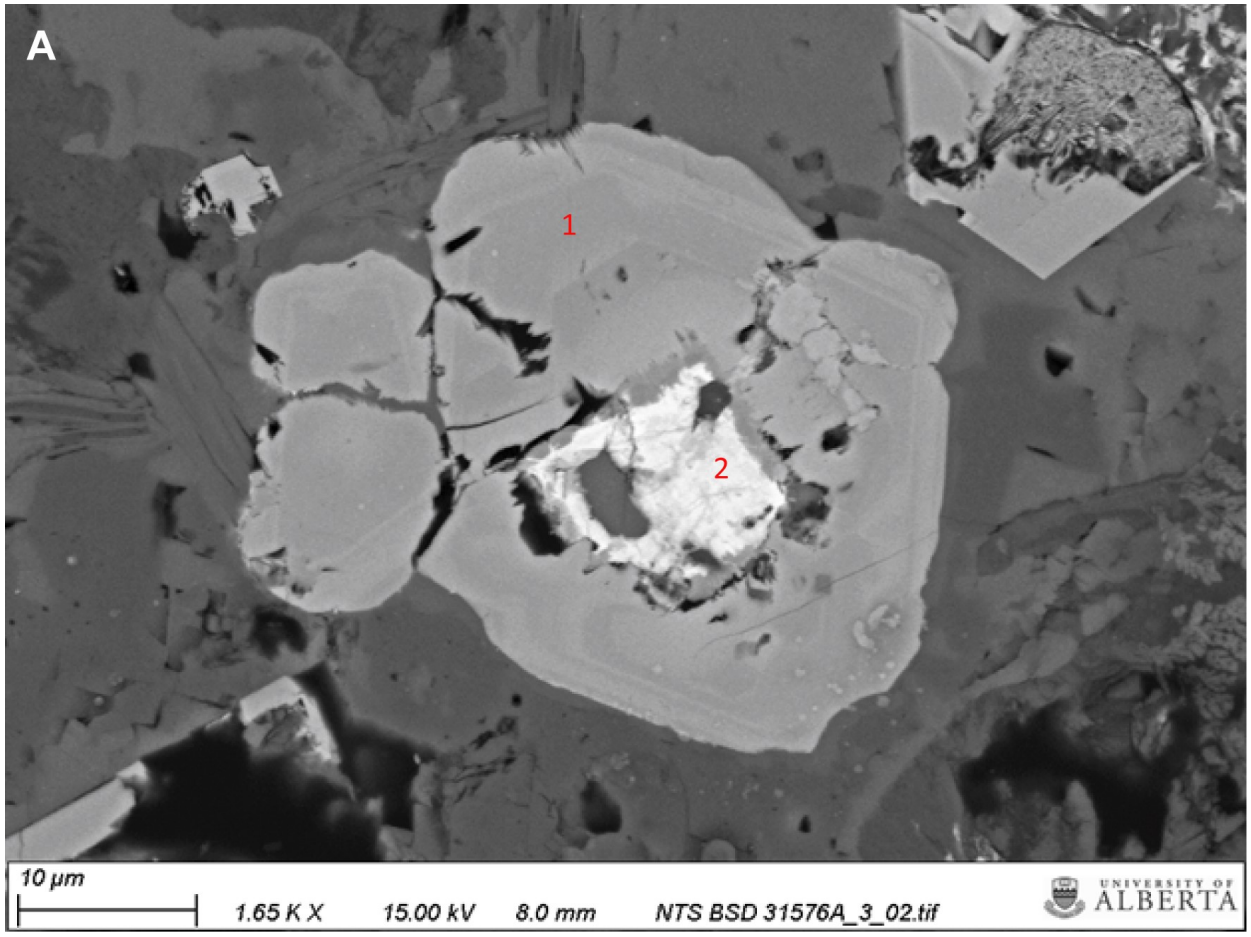


**Fig. 8**. (a) BSE image from thin section 31576A (macrocrystic area) containing grain with a Ca-Ti-bearing rim (label 1) and Ti-bearing core (label 2). Composition of slightly darker area between core and rim unknown.

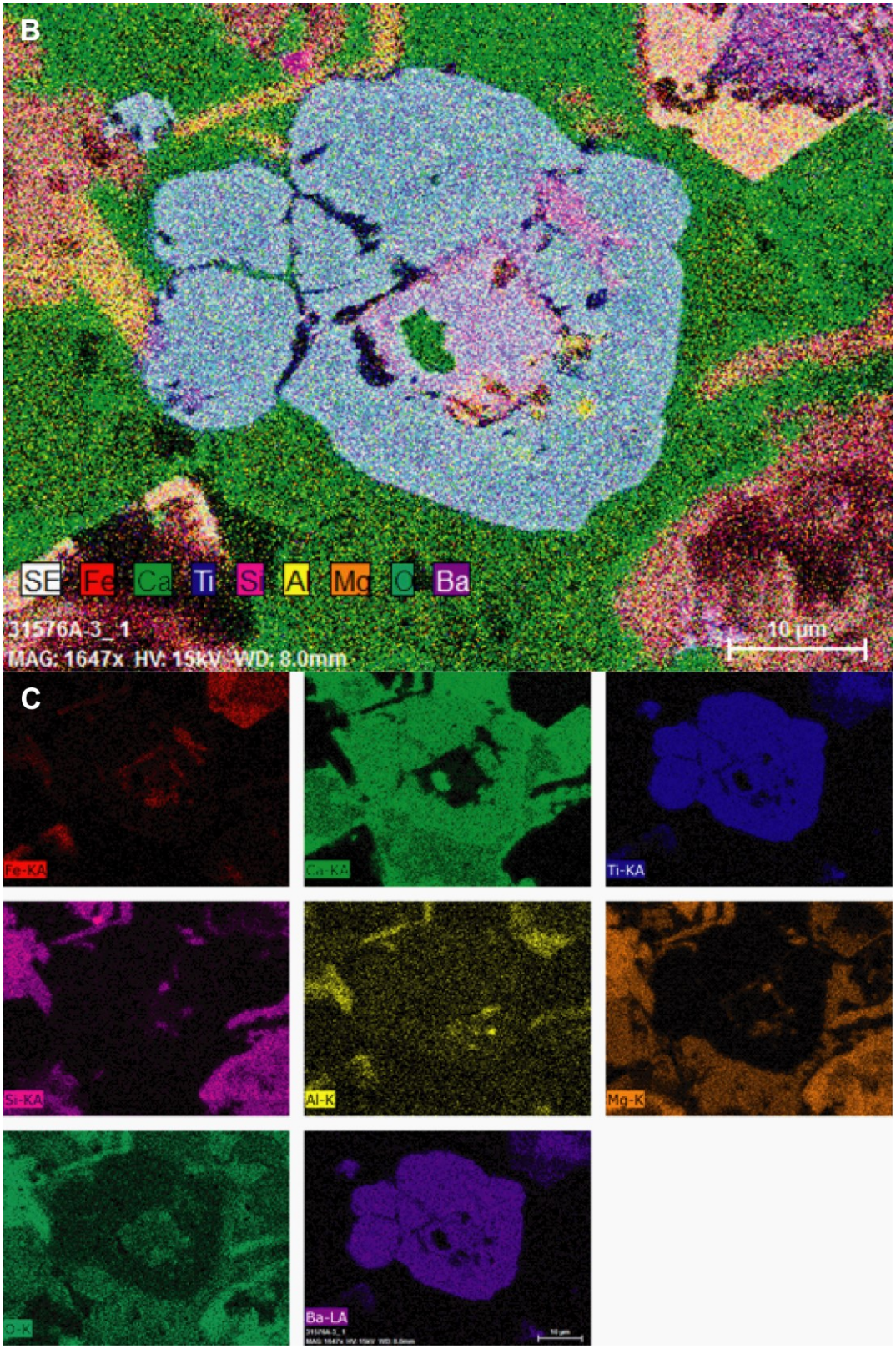


**Fig. 8**. Continued. (b) Ca, Ti, Fe, Si, Al, Mg, Ba and O element map of same grain. (c) Individual element maps of (b).

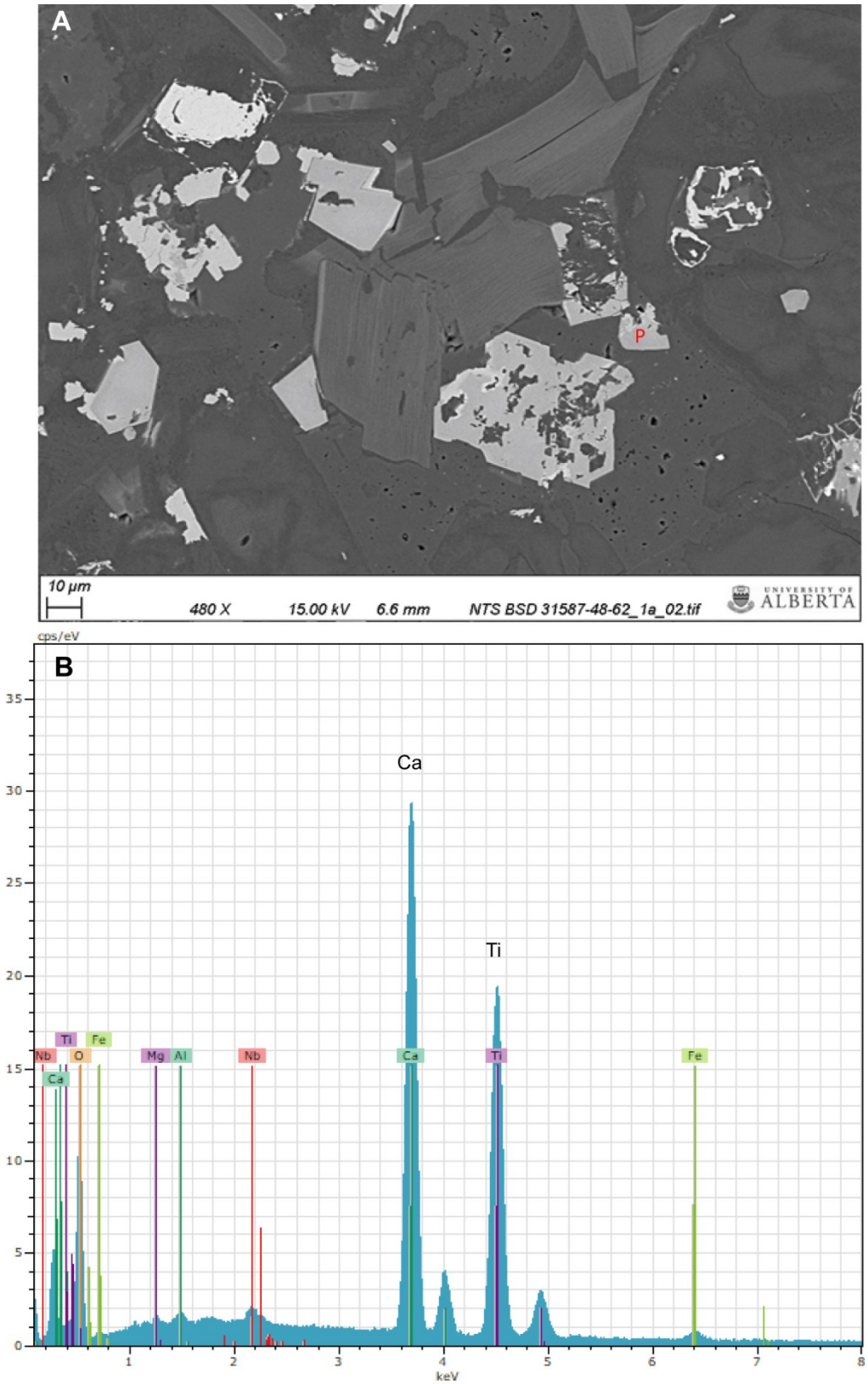


**Fig. 9.** (a) BSE image from thin section 31587_48.62 containing example of tiny perovskite grain (P), which appears opaque in thin section. (b) EDS spectra of above grain (P).

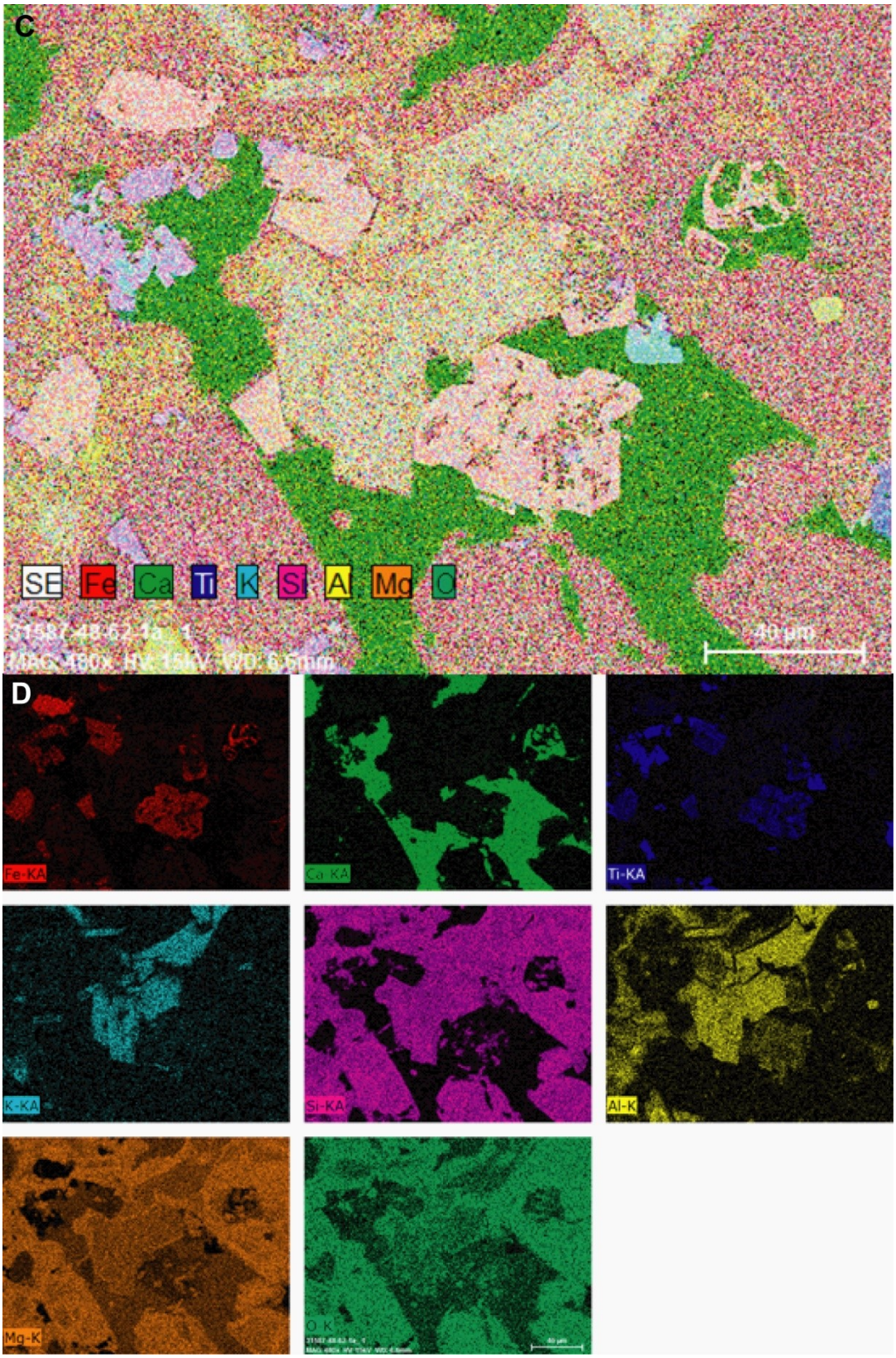


**Fig. 9.** Continued. (c) Ca, Ti, Fe, Si, Al, Mg, K and O element map of same grain. (d) Individual element maps of (c).

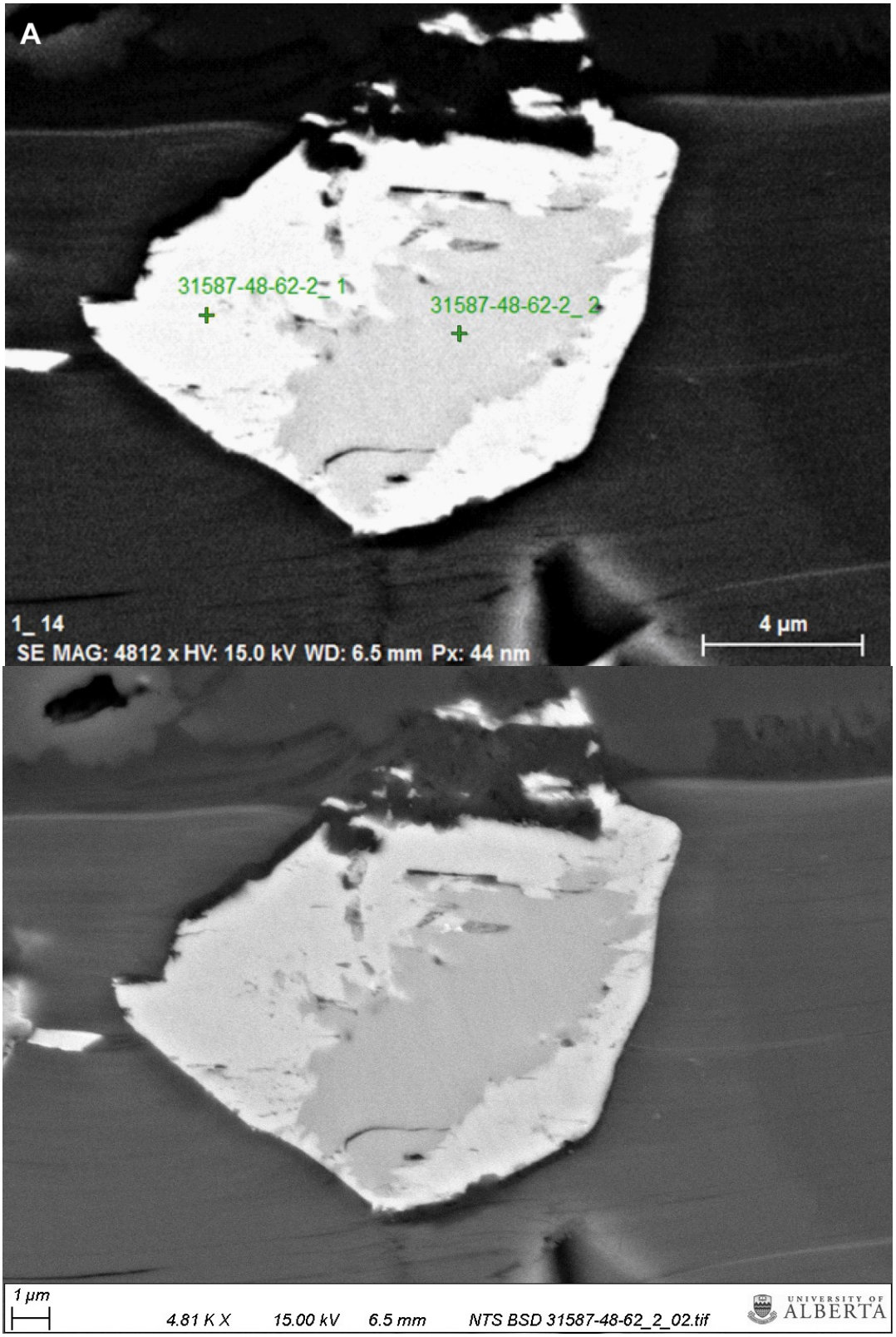


**Fig. 10**. (a) BSE images of tiny perovskite grain in 31587_48.62. Fe-Ti-Mn-bearing rim (label 1) and Ca-Ti-bearing core (label 2).

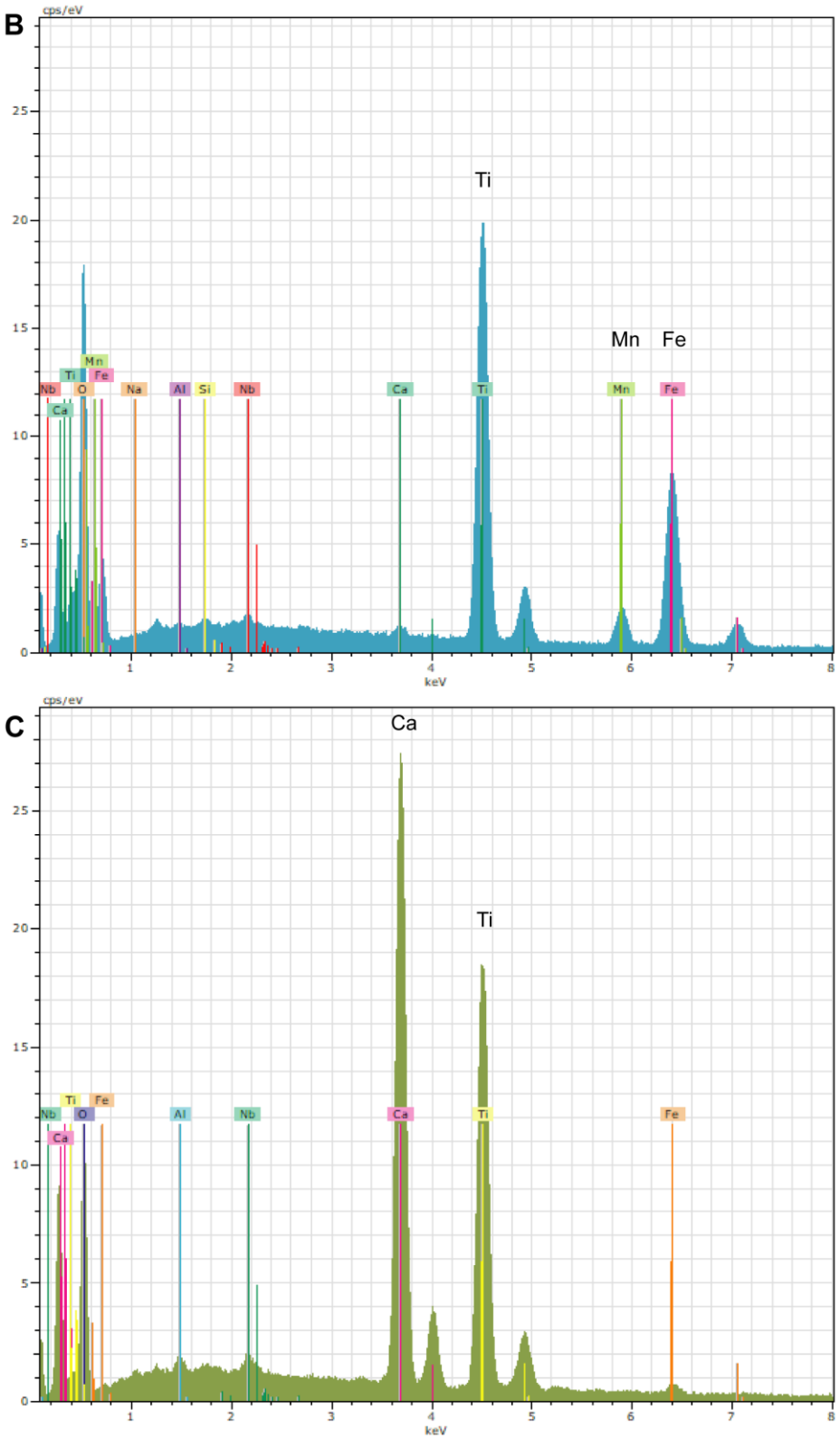


**Fig. 10**. Continued. (b) EDS spectra from rim (label 1). (c) EDS spectra from core (label 2).


**Fig. 11.** BSE image and element maps (a-c) from same area as Figure 10 (31587_48.62) which shows a few possible perovskite grains. Black ink mark in bottom left corner.

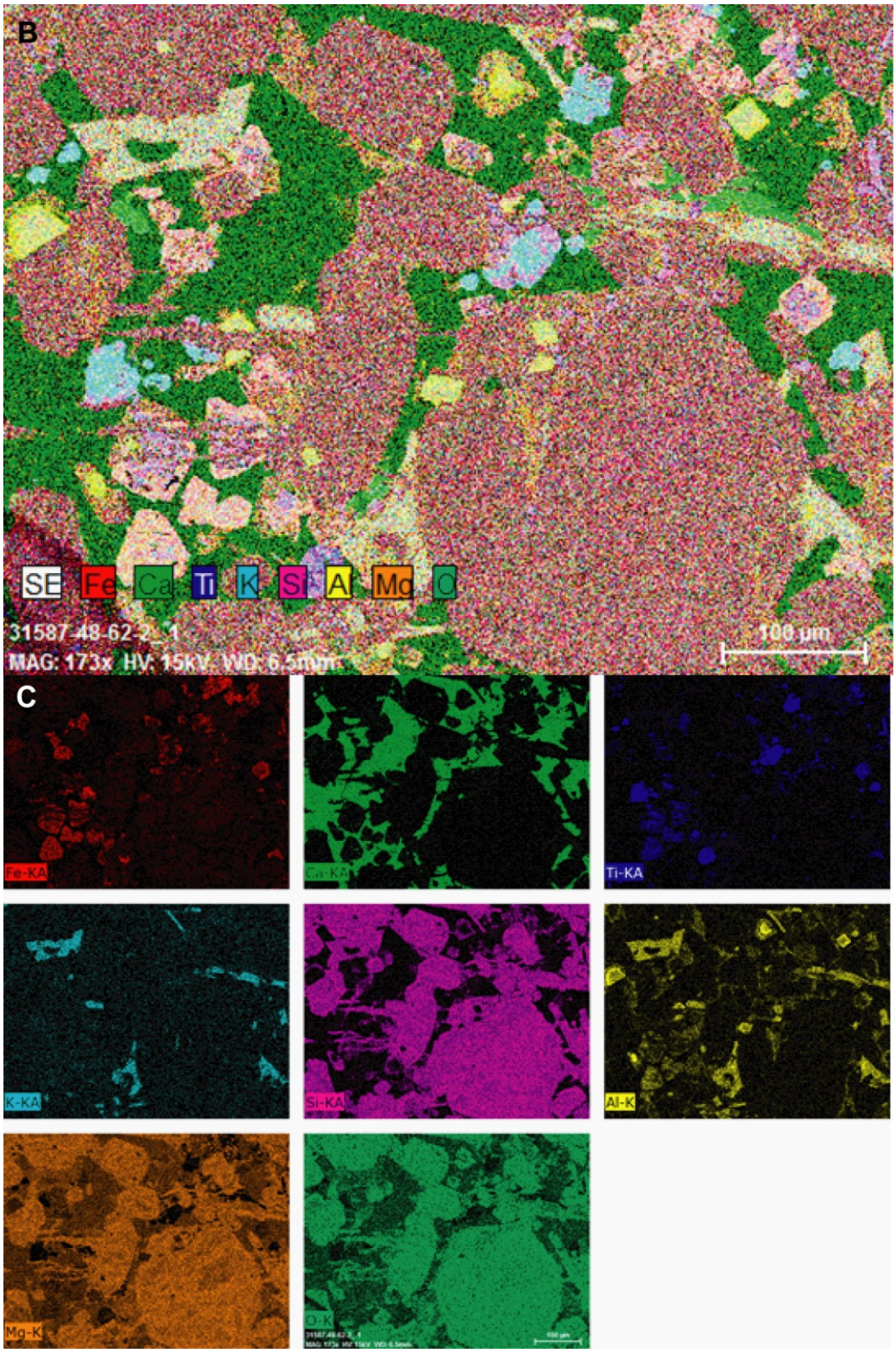


**Fig. 11.** Continued.

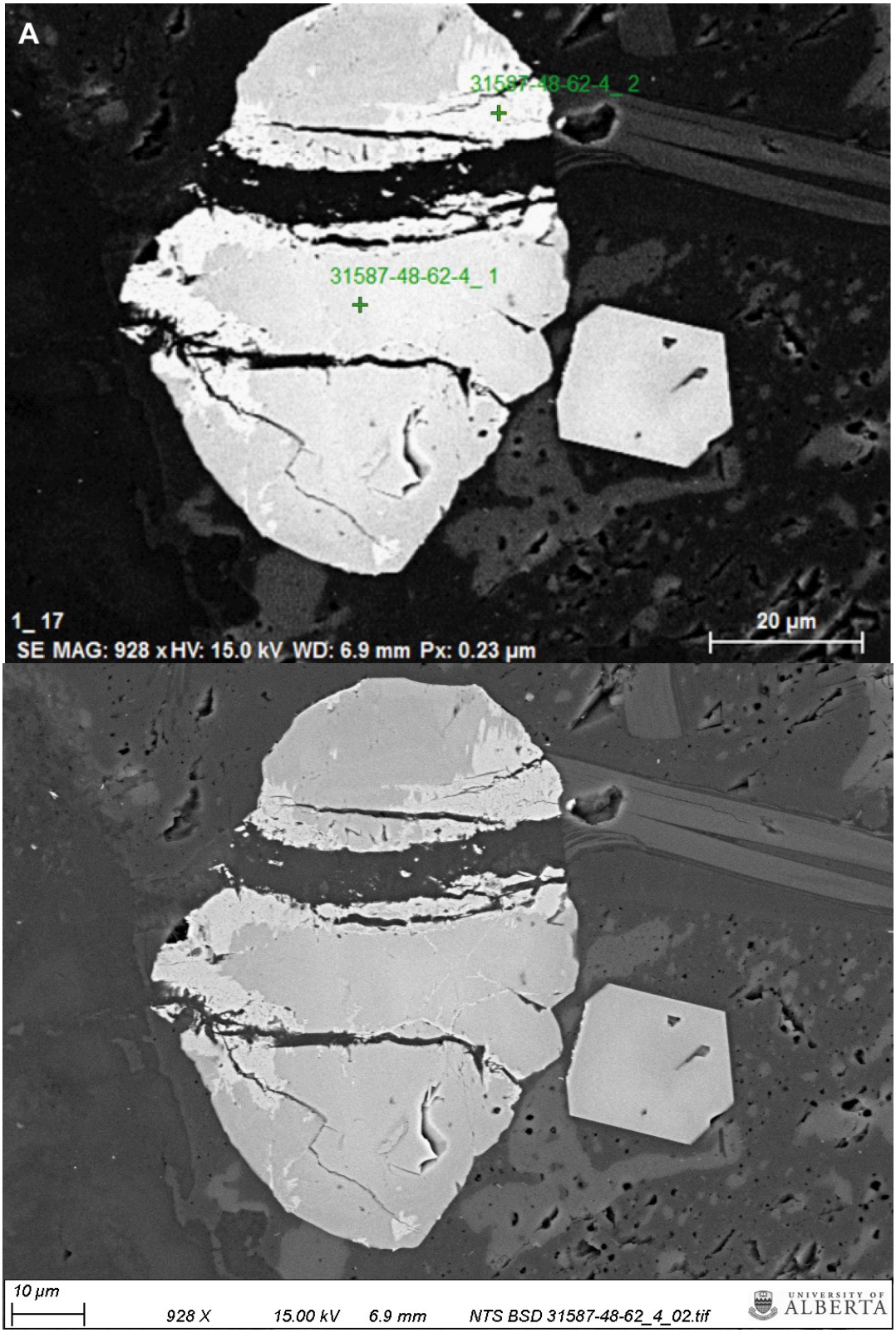


**Fig. 12.** (a) BSE images from thin section 31587_48.62 containing perovskite with Ca-Ti-bearing core (label 1) and Ti-Fe-Mn-(Si, Mg)-bearing rim (label 2).

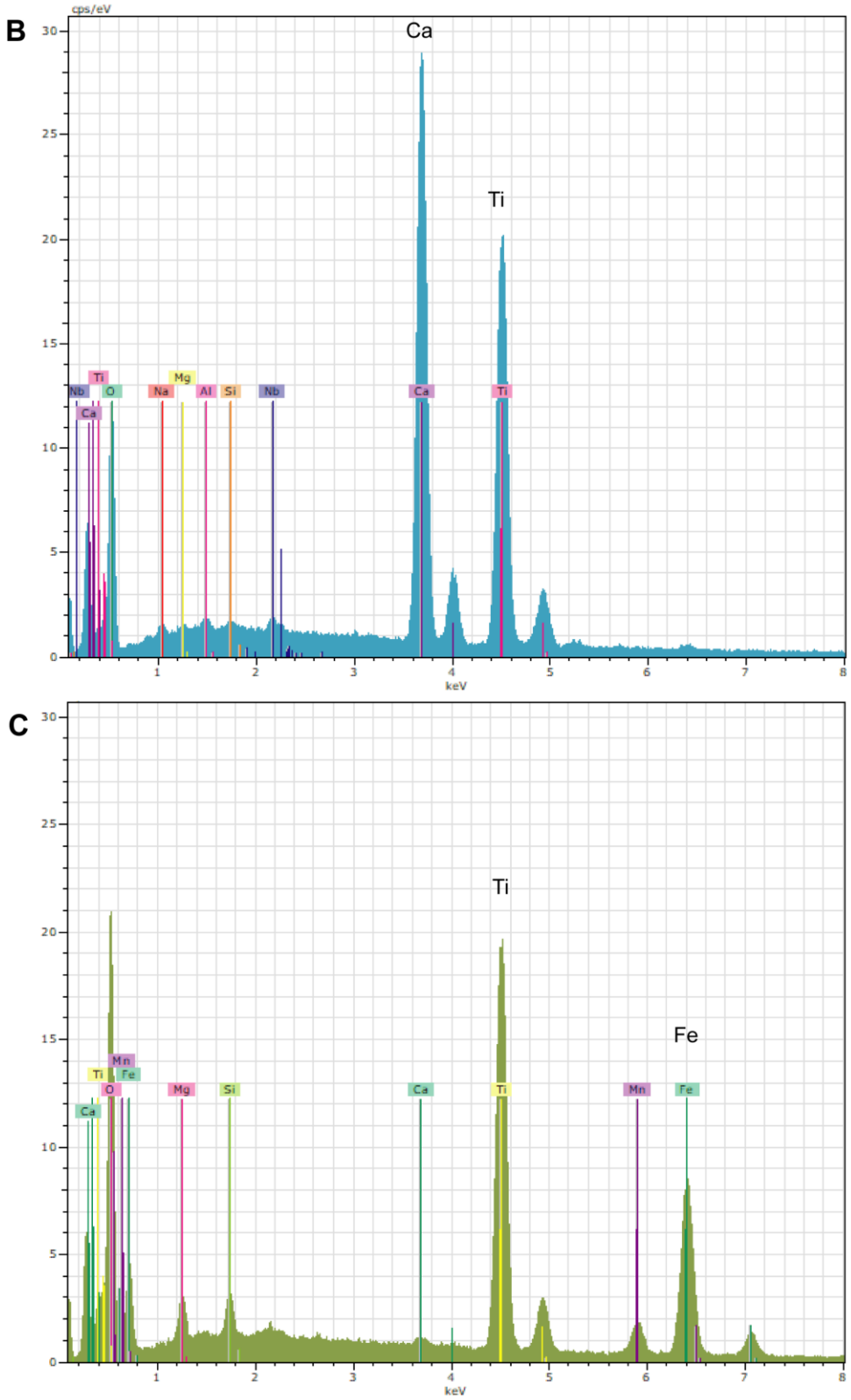


**Fig. 12.** Continued. (b) EDS spectra of core (label 1). (c) EDS spectra of rim (label 2).

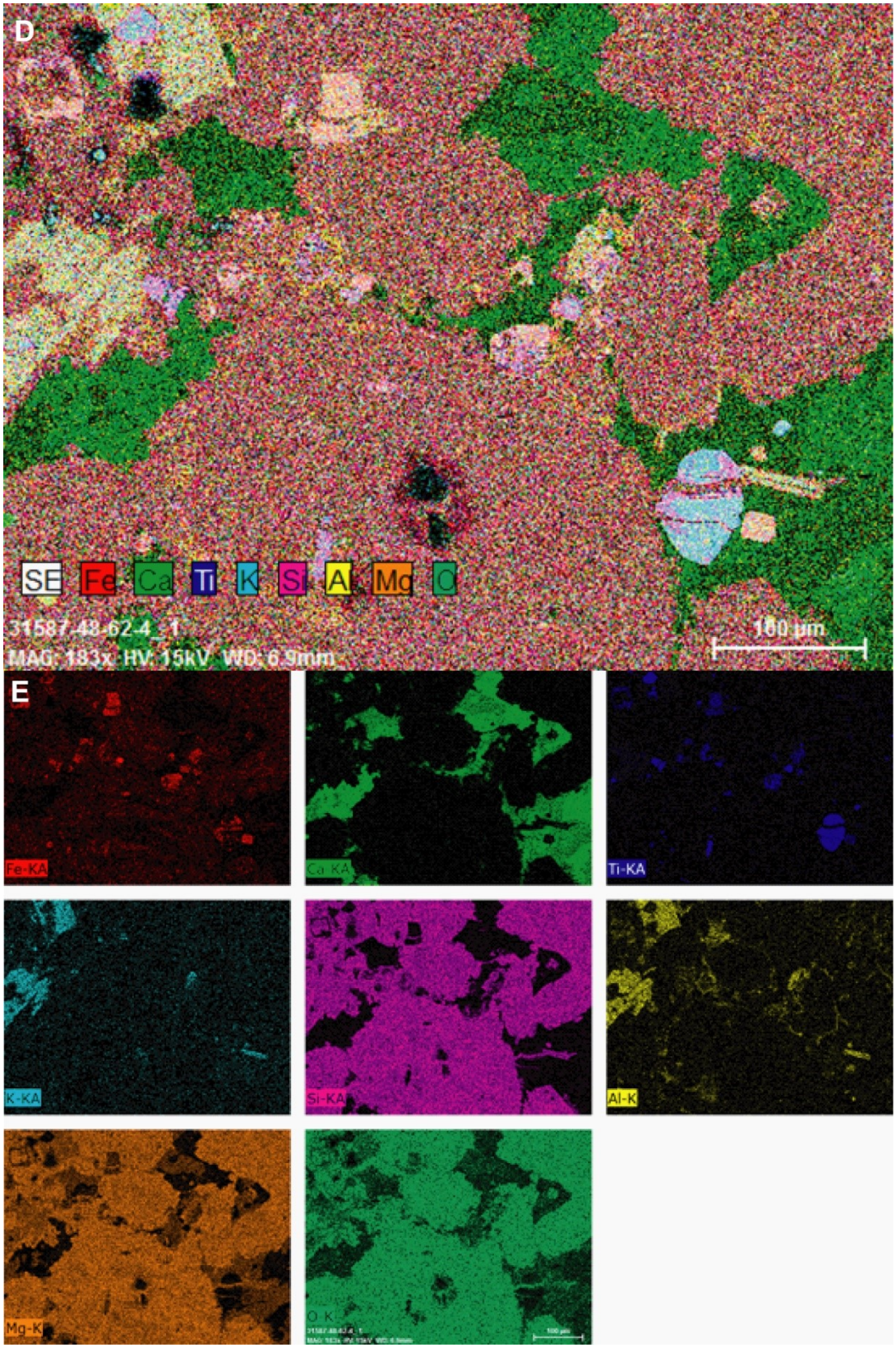


**Fig. 12.** Continued. (d) Ca, Ti, Fe, Si, Al, Mg, K and O element map. (e) Individual element maps.

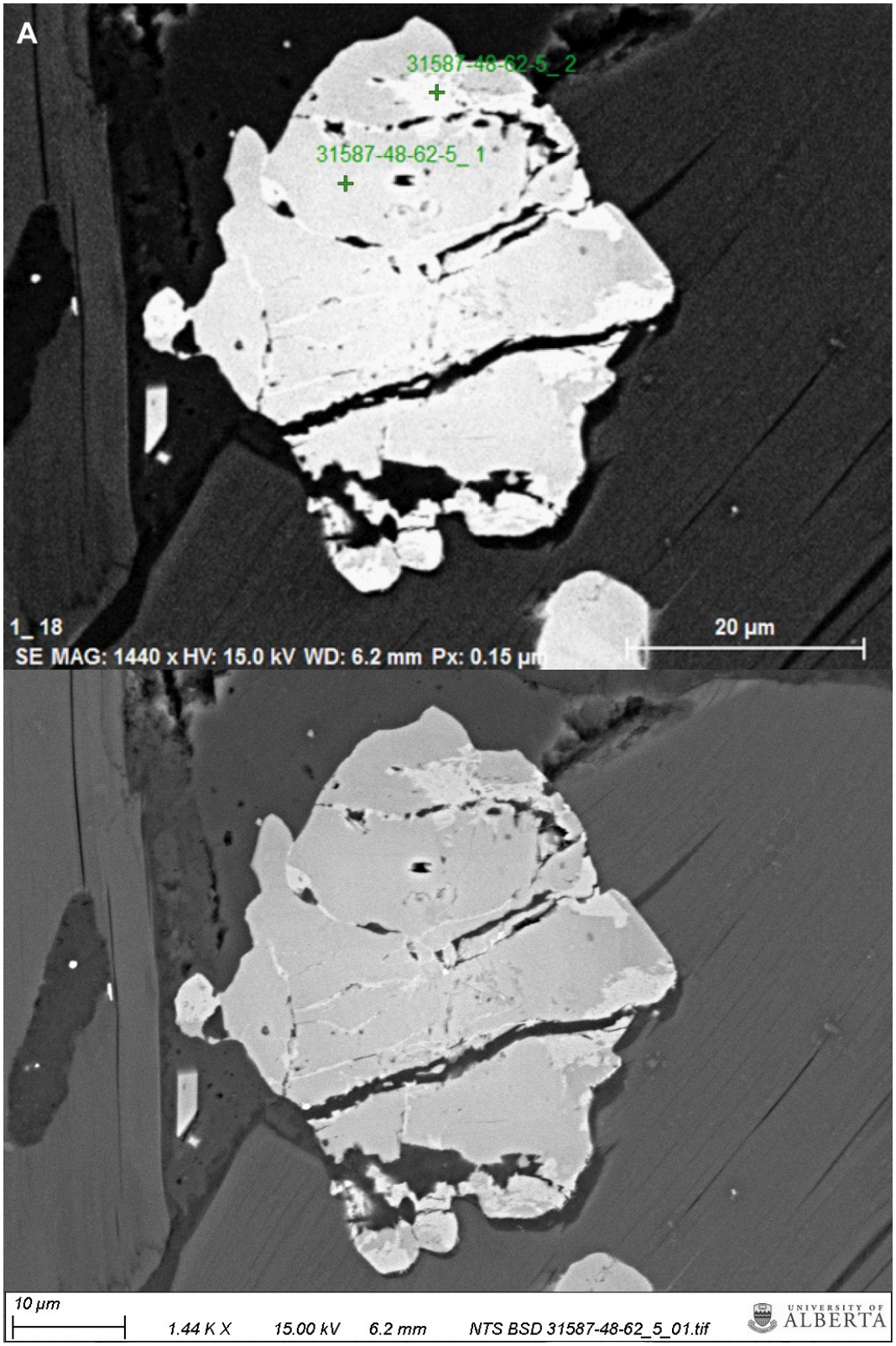


**Fig. 13.** (a) BSE images from thin section 31587_48.62 containing perovskite with Ca-Ti-bearing (label 1) and Ti-Fe-Mn-Ca-bearing areas (label 2).

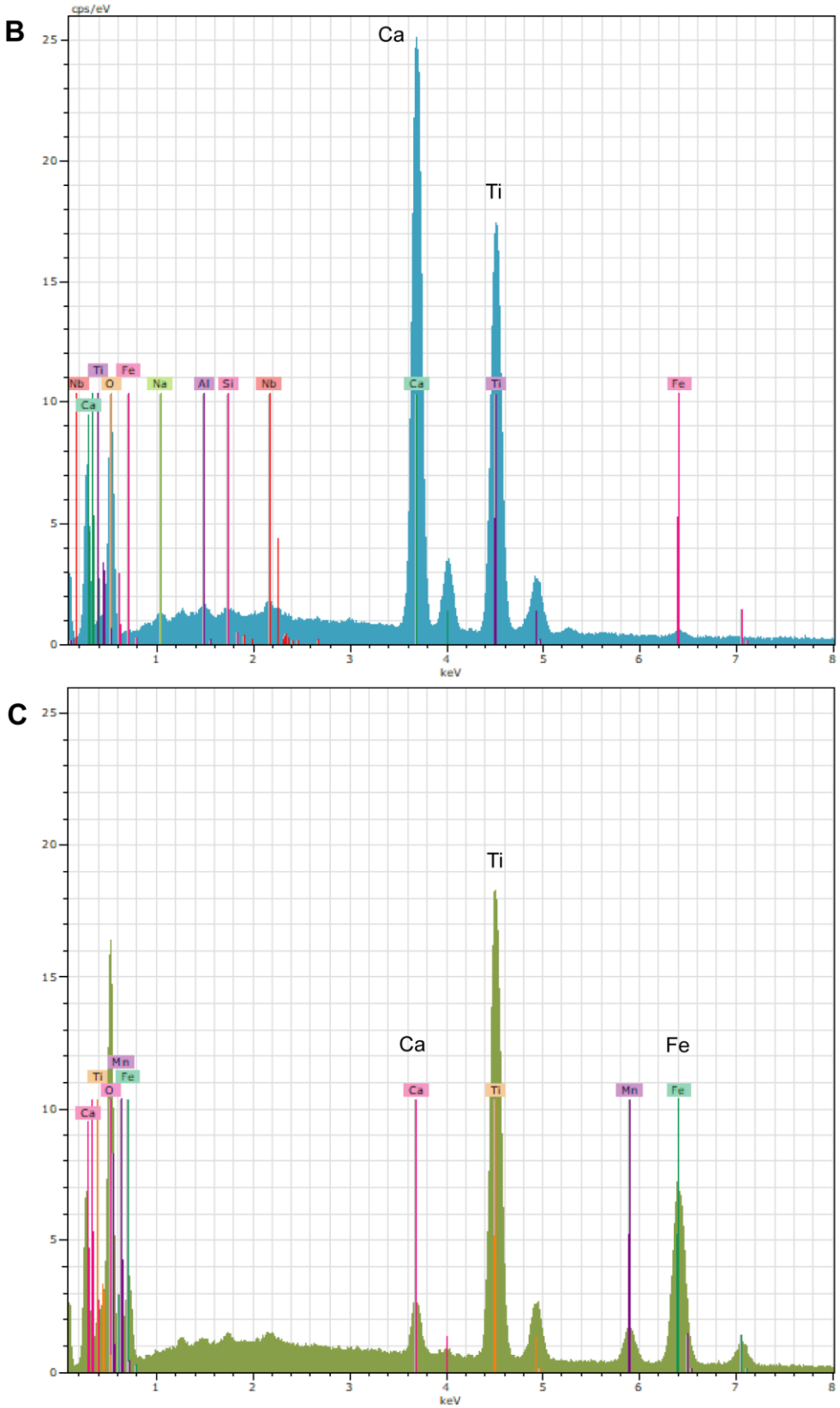


**Fig. 13.** Continued. (b) EDS spectra of label 1 and (c) label 2.

## Lynx

Fourteen kimberlite samples were available from the Lynx dyke system. Ten core box samples and 4 core samples from 2 drill holes (~17-25 cm; 3 samples from one drill hole). Perovskite was identified by EDS in only one sample (31595, depth 59.27 m; Figures 14-19) but many grains were 30 μm or less in size with anhedral shapes. A ~60 μm cube shaped grain was found containing Ca-Ti-Fe-bearing, Ti-Fe-bearing and Ti-bearing phases (Figure 16). Part of 31595 (59.00-59.92 m) was processed and light brown perovskite ~20-50 μm were found in the Wilfley table heavy mineral concentrate. The crystal shape was difficult to see clearly and a few grains are magnetic. Perovskite was difficult to tell apart from dark brown magnetic grains (not perovskite) with a glossier metallic luster. A test of picking perovskite from this sample for a couple of days yielded ~20 grains which indicated it could likely take weeks to collect enough material for HBr chemistry.

In general, Lynx core samples contain;

- Common olivine macrocrysts/phenocrysts replaced by serpentine ± carbonate, opaques (e.g. black minerals, black metallic minerals, sulfide), possible talc, and can appear flow-aligned. Olivine can be very coarse (>1 cm) in some samples. A few macrocrysts resemble a cluster of smaller olivine grains.
- Phlogopite (e.g. 31564A, 31565, 31584, 31585, 31588, 31589, 31590, 31591, 31592, 31593, 31594, 31595) and possible apatite (e.g. 31593) phenocrysts can be present.
- The groundmass is comprised of;
    - Variable amounts (few to common) of phlogopite between samples (and sometimes within samples, e.g. 31594), often with pale green pleochroism and/or rims,
    - Opaques (black, some reddish-brown) with few atoll textures and can appear altered (bladed shapes?),
    - Perovskite is not obvious,
    - ± Apatite (sometimes partially altered green).
    - Dominantly uniform carbonate-rich groundmass (minor serpentine) with variable amounts of segregations of carbonate and/or serpentine can be present.
    - Many samples contain an overall or patchy pale greenish alteration and/or sulfides in the groundmass.

- Few altered country rock xenoliths or xenocrysts (some can be very small, such as <2 mm).
- Xenocrysts of possible altered pyroxene, chromite, kelyphitic garnet, dark brownish-red rutile (?), and altered unknowns may be present. Xenocrysts of black irregularly shaped opaques (e.g. ilmenite) are common.
- One sample contains part of an altered mantle xenolith (31563) and mantle xenoliths may be present in other core box samples (e.g. 31590, 31591, 31584).
- In addition, the following textures were seen in some samples;
    - Banding towards lower contact (e.g. 31595, 31584).
    - White carbonate segregations along or towards the lower contact (e.g. 31591, 31589, 31593) or near the upper contact (31590).
    - Common cross-cutting veinlets/veins filled with carbonate ± opaques, metallic yellow sulfides, serpentine. 31588 contains an unusual cross-hatched white vein.

The following text, data and figures are taken or modified from the EAS 540 (Stable Isotopes) lab project report "*Carbon and oxygen isotope composition of carbonate from the Lynx kimberlite dyke complex, Québec, Canada*" (dated April 24, 2015). The course lab project was used to test a research idea for the former third project.

**Abstract:** Carbon and oxygen isotope compositions from whole rock carbonate were determined from six samples across a section of hypabyssal kimberlite core from the ca. 522 Ma Lynx dyke complex. Many oxygen isotope compositions of calcite and dolomite were found to be greater than 14.2‰. High $\delta^{18}O$ values are interpreted to likely be the result of alteration of the carbonate by deuteric, hydrothermal and/or low temperature meteoric fluids and supported by textural observations from carbonate, serpentine and spinel in thin section. Magmatic carbon isotope compositions from calcite and dolomite within the intrusion were found to range from -3.4 to -4.6‰, overlapping $\delta^{13}C$ of the calcite vein at the upper contact. One lower $\delta^{18}O$ value of 10.0‰ and the two lowest $\delta^{13}C$ values of -5.1‰ and -5.6‰ from the lower contact may reflect degassing of volatiles although a corresponding trend of oxygen isotope values is unclear. $\delta^{13}C$ values within this Lynx sample compared with related Neoproterozoic rocks along the Labrador coast and in Greenland suggest carbon in the mantle may be similar with kimberlite in Maniitsoq, some ultramafic lamprophyres from Aillik Bay and Torngat Mountains, and

carbonatite in Aillik Bay. Diamonds from the Renard bodies also overlap in carbon isotope composition with this sample from the Lynx dyke complex.

**Analytical Method:** Six samples from 31594 (A, C, D, E, G) were analyzed for oxygen and carbon isotope composition of whole rock carbonate at the University of Alberta. Three samples near the upper and lower margin and three samples within the intrusion were selected from thin section offcuts and powdered by a steel mortar and pestle except for a white carbonate vein sampled in 31594A (approximately 3 cm from the upper contact) powdered by agate mortar and pestle. Lower contact samples were sampled from the dark grey area approximately 3 cm from the lower contact (G-1) and light grey area approximately 1 cm including the lower contact. Country rock xenoliths, indicator minerals, and visible white veinlets were avoided when possible. A small amount of each powder was initially sent for XRD to determine the presence of calcite and dolomite (Figures 20-21). Approximately 17-22 mg of whole rock powder was placed in a glass tube, sealed under vacuum, mixed with 3 ml $H_3PO_4$ and placed in a 25$^{o}$C water bath for a minimum of 1 hour for calcite and 4 to 5 days for dolomite to produce $CO_2$. Two samples were repeated, 31594G-1 and 31594G-2, using a greater amount of whole rock powder and phosphoric acid (approximately 50 mg and 200 mg and 5 to 6ml $H_3PO_4$, respectively). All samples were analyzed with a MAT-252 Finnigan mass spectrometer using the PDB (Pee Dee Belemnite) and VSMOW (Vienna Standard Mean Ocean Water) reference standards. An oxygen fractionation factor of 1.01178 determined at 25$^{o}$C was applied to dolomite analyses (Rosenbaum and Sheppard 1986).

**Results:** Table 1 lists carbon and oxygen isotope compositions measured for calcite and dolomite and Figure 22 plots $\delta^{18}O$ and $\delta^{13}C$ with downhole depth. XRD results show upper and lower contact samples (A and G) contain only calcite for carbonate-bearing minerals whereas samples C, D and E within the intrusion contain both calcite and dolomite with magnesite also present in C.

$\delta^{18}O$ ranges between 10.0‰ to 17.3‰ for calcite and 14.4‰ to 17.3‰ for dolomite. Within the intrusion, calcite values range from 14.2 to 15.7‰ similar to the vein sampled in A (15.5‰). The lowest value of 14.2‰ was recorded from approximately middle of the intrusion and varies

by 0.2‰ between calcite and dolomite. Values increase up to 1.8‰ and 2.8‰ towards C and E for dolomite, respectively. Carbonate along the upper and lower contacts record the most variability in $\delta^{18}O$, particularly along the lower contact with the highest value of 17.3‰ from G-1 and the lowest value of 10.0‰ from G-2.

$\delta^{13}C$ varies slightly between all samples with a range of -4.1‰ to -5.6‰ for calcite and -3.4‰ to -4.7‰ for dolomite. Within the intrusion, $\delta^{13}C$ values overlap values recorded by the calcite vein in sample A. Dolomite in sample E is slightly higher (0.7‰) and more variability is recorded between calcite and dolomite in D and E. The lowest $\delta^{13}C$ values are recorded along the lower contact in G-1 and G-2.

**Conclusions:**

1) $\delta^{18}O$ values range from 14.2 to 15.7‰ for calcite and 14.4 to 17.3‰ for dolomite within the kimberlite intrusion, 15.5‰ in a calcite vein near the upper contact and 10.0/17.3‰ for calcite along the lower contact. $\delta^{18}O$ values from whole rock carbonate are outside range of published values for mantle oxygen isotope compositions and may record alteration by low temperature meteoric fluids or hydrothermal fluids, as suggested by Giuliani et al. (2014) (Figure 23).
2) $\delta^{13}C$ values within the intrusion (C, D, E) range from -4.1 to -4.6‰ for calcite and -3.4 to -4.7‰ for dolomite, similar to published values for mantle carbon isotope compositions. $\delta^{13}C$ values along the lower contact (-5.6‰ for G-1 and -5.1‰ for G-2) are lower than carbon isotope compositions within the intrusion and the calcite vein near the upper contact (-4.3‰) which may reflect degassing of kimberlite although a trend between oxygen and carbon isotope compositions is not observed (e.g. Wilson et al. 2007).
3) Deines (1989) observed $\delta^{18}O$ in kimberlite to have a 12‰ peak falling outside of mantle range (6-9‰) and suggested the size of the dykes and veins used in their study compared to a larger intrusion, such as pluton scale, may affect retention of isotope compositions in smaller intrusion sizes. Although the Lynx dyke complex intrudes granitoid and gneissic country rock rather than sedimentary rock, the sample in this project has an apparent thickness of 1.4 m. In this case, a dyke sample of this size may be less resistant to alteration of the oxygen isotope compositions in groundmass carbonate by fluids.

4) $\delta^{13}C$ values overlap with Maniitsoq kimberlite and Renard diamonds, as well as Aillik Bay damtjernite and carbonatite, and Torngat Mountain and Sarfartoq aillikite (Figure 23) (Hunt et al. 2012; Tappe et al. 2006, 2008, 2011).

**Table 1**. Carbon and oxygen isotope compositions for calcite and dolomite in sample 31594.

| Sample No. | $\delta^{13}C$ PDB (‰) | | $\delta^{18}O$ VSMOW (‰) | | |
|---|---|---|---|---|---|
| | Calcite | Dolomite | Calcite | Dolomite | Dolomite* |
| 31594A | -4.287 | n.d. | 15.451 | n.d. | n.d. |
| 31594C | -4.554 | -4.723 | 14.818 | 16.104 | 16.294 |
| 31594D | -4.282 | -4.654 | 14.227 | 14.258 | 14.426 |
| 31594E | -4.089 | -3.352 | 15.709 | 17.072 | 17.273 |
| 31594G-1 | -5.618 | n.d. | 17.282 | n.d. | n.d. |
| 31594G-2 | -5.060 | n.d. | 10.037 | n.d. | n.d. |

** fractionation factor (25°C) of 1.01178 was applied to dolomite (Rosenbaum and Sheppard, 1986)*

*n.d.= no data*


**Fig. 14.** Core box sample 31595 from the Lynx dyke system.

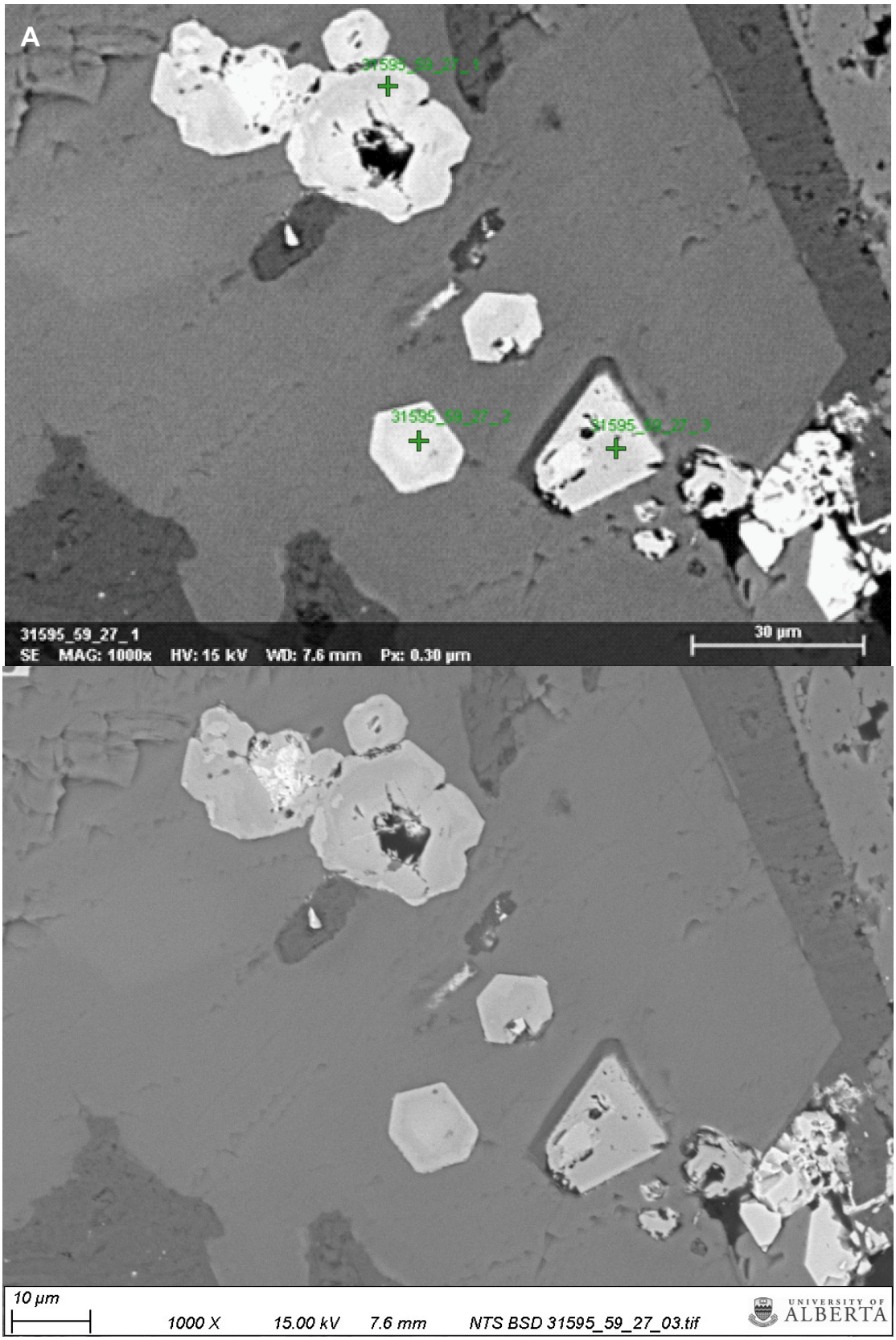


**Fig. 15.** (a) BSE images of 31595_59.27 of three Ca-Ti-bearing grains.

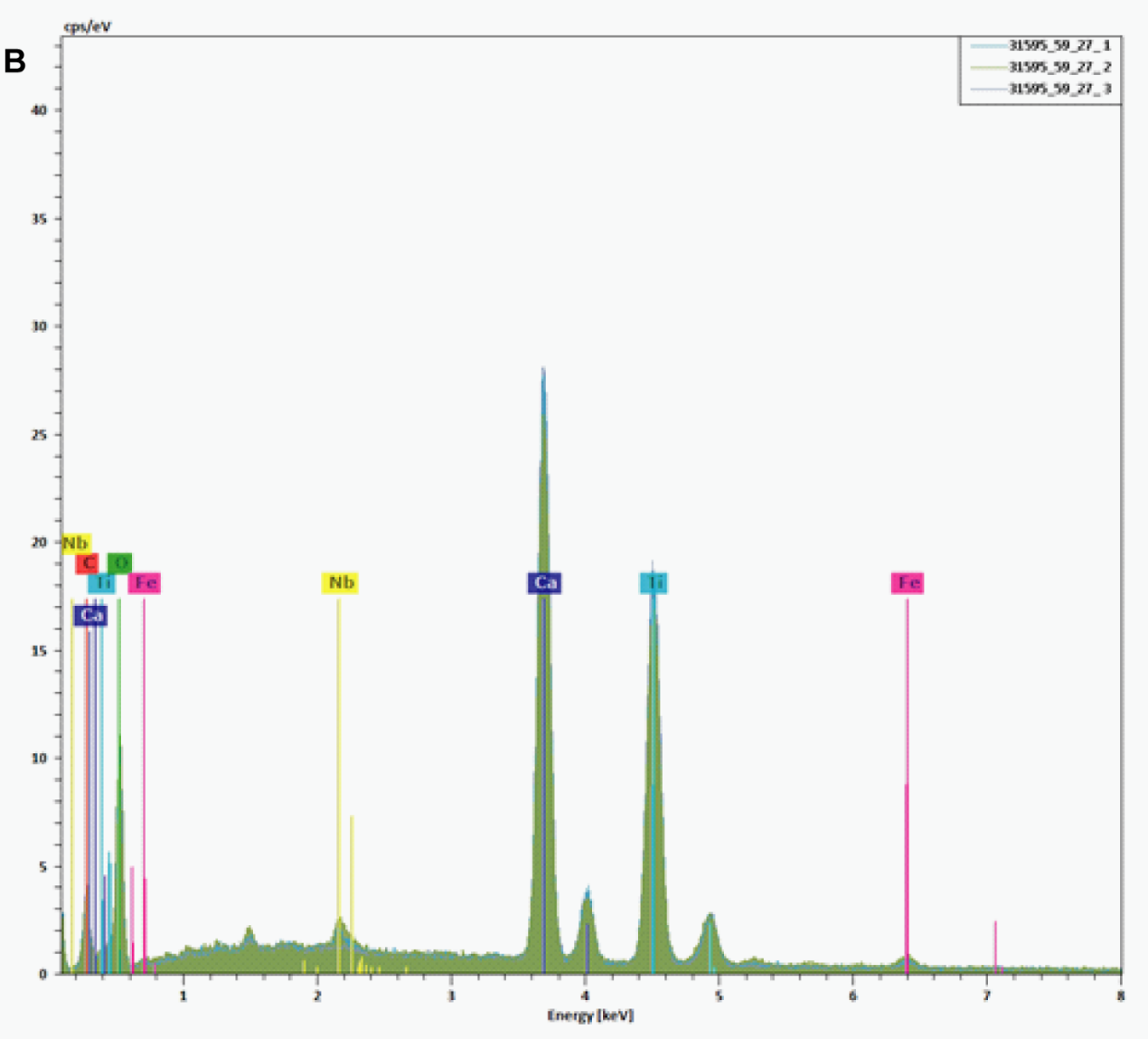


**Fig. 15.** Continued. (b) EDS spectra of three Ca-Ti-bearing grains.

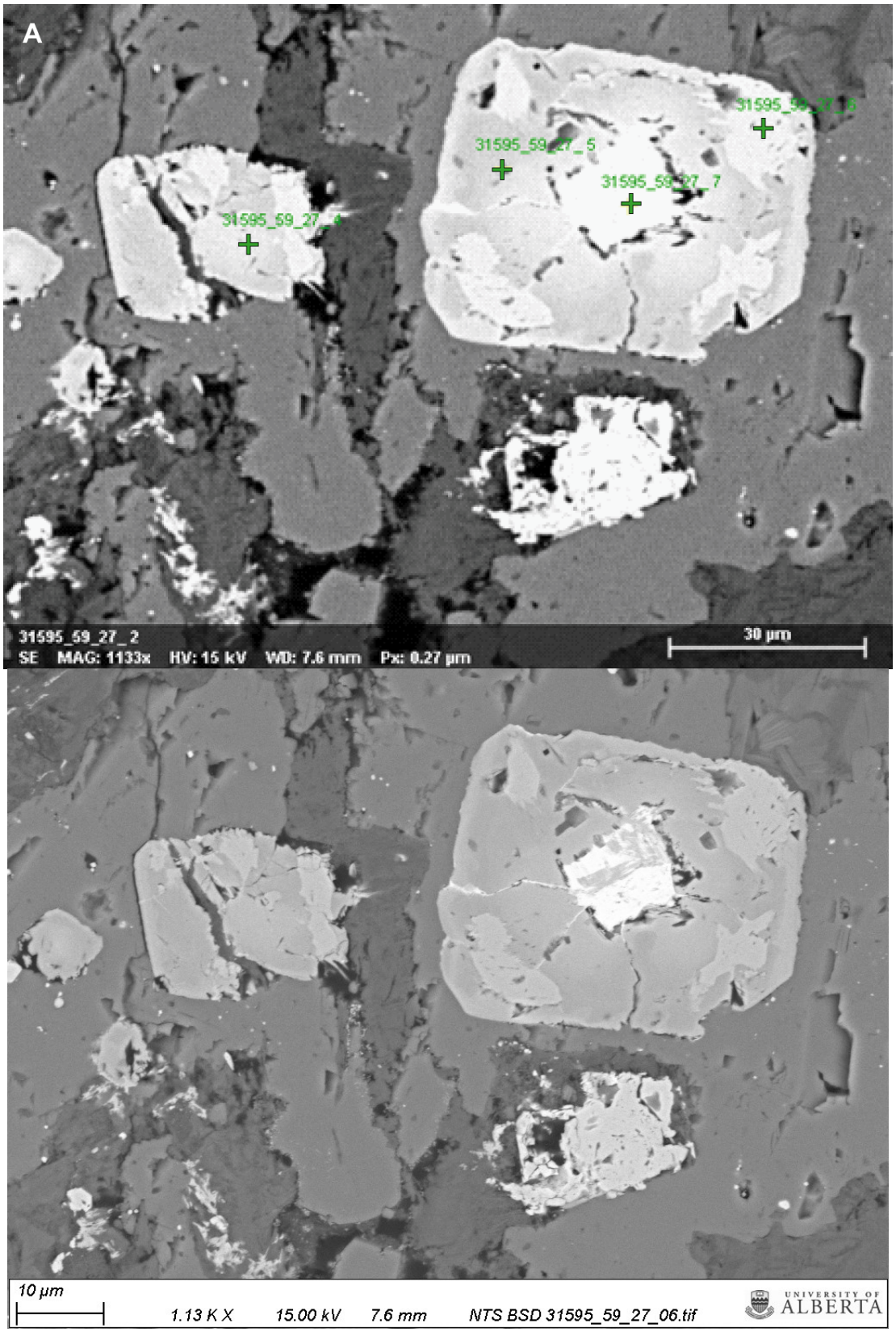


**Fig. 16.** (a) BSE images of 31595_59.27 of two Ca-Ti bearing grains.

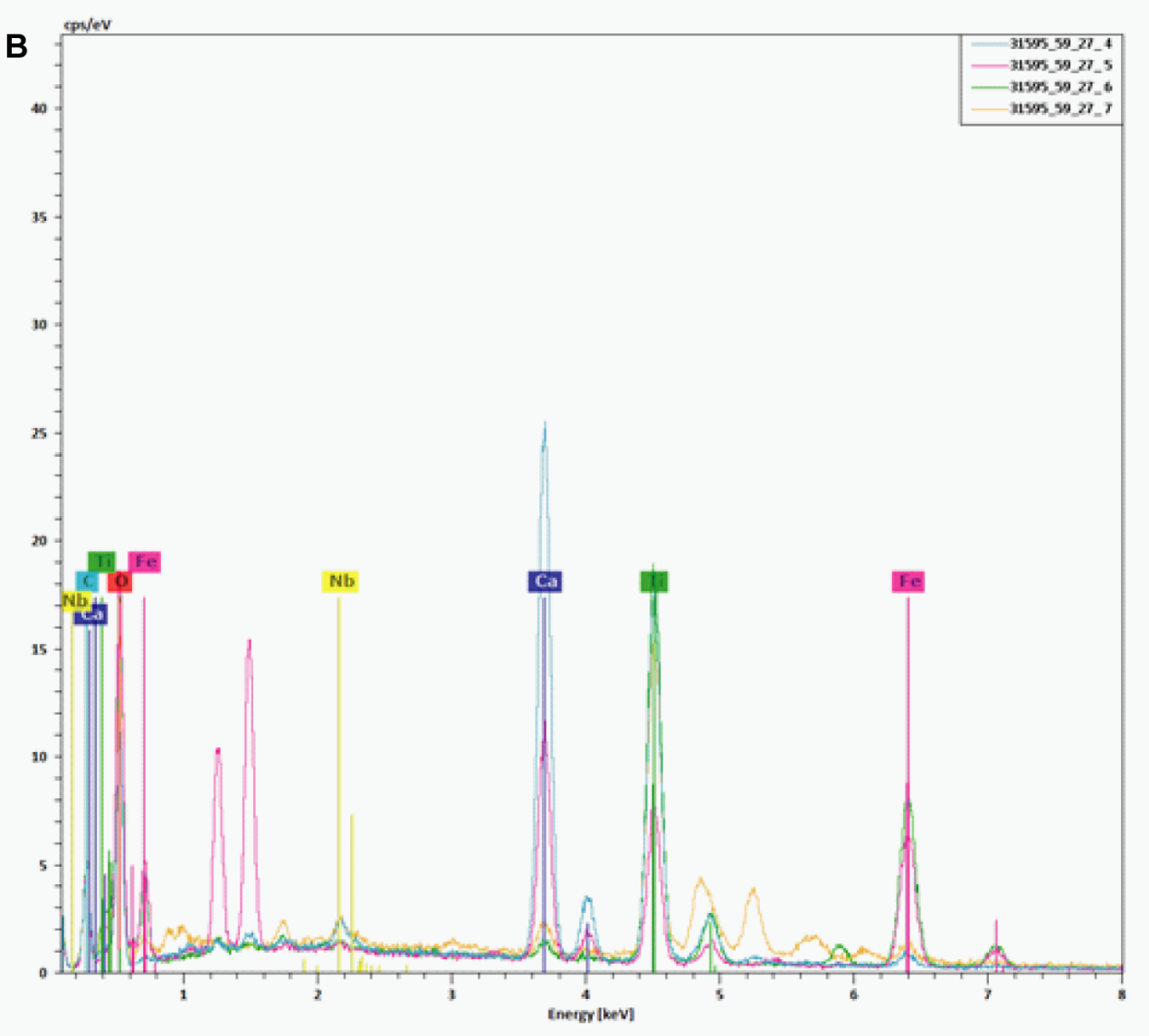


**Fig. 16.** Continued. (b) EDS spectra of small Ca-Ti-bearing grain (left, spot 4) and large composite grain (right) with Ti-bearing core (spot 7), Ti-Fe-bearing inclusions (spot 6) within a Ca-Ti-Fe-bearing (spot 5) cubic mineral.

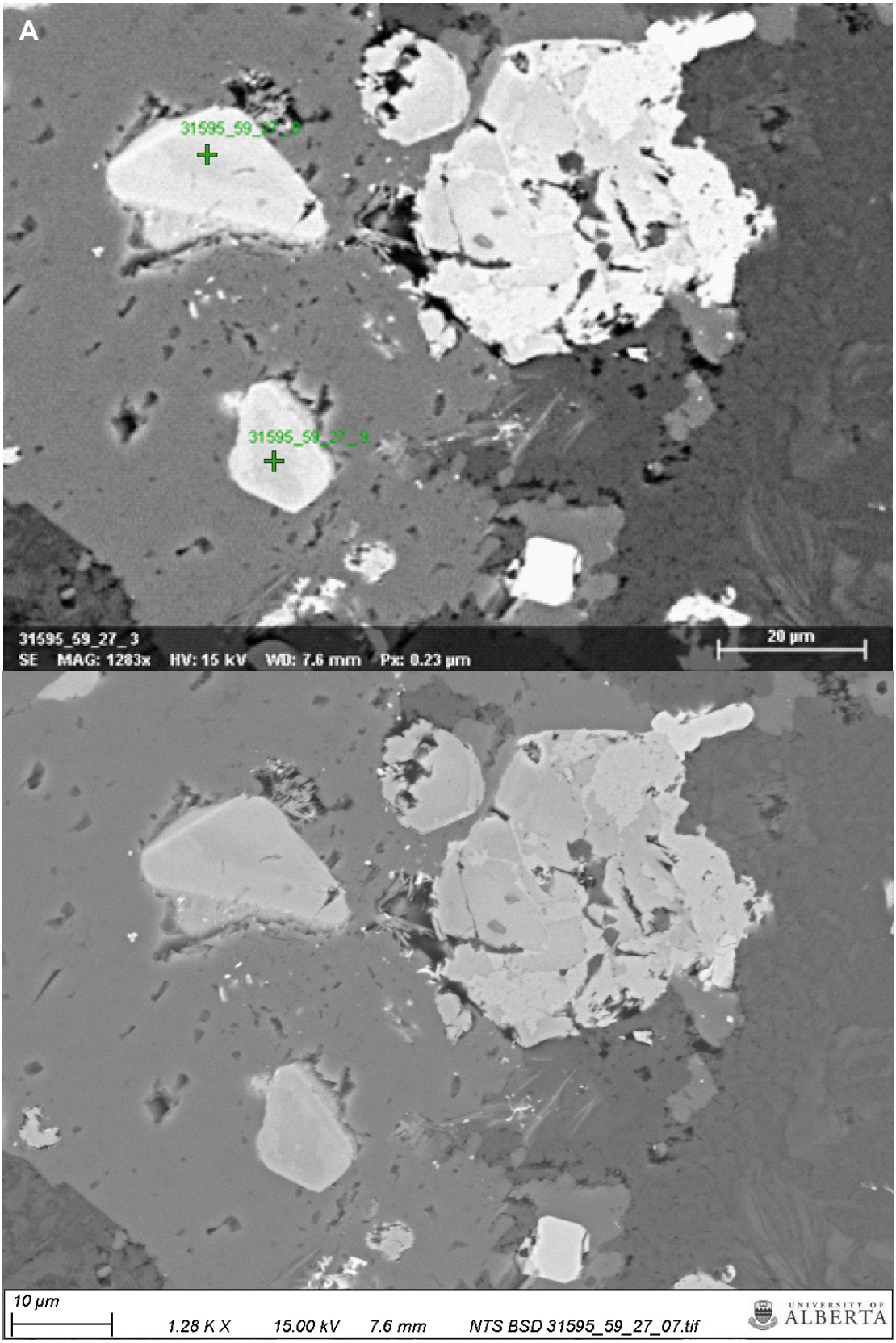


**Fig. 17.** (a) BSE images of 31595_59.27 of at least two Ca-Ti-bearing grains.

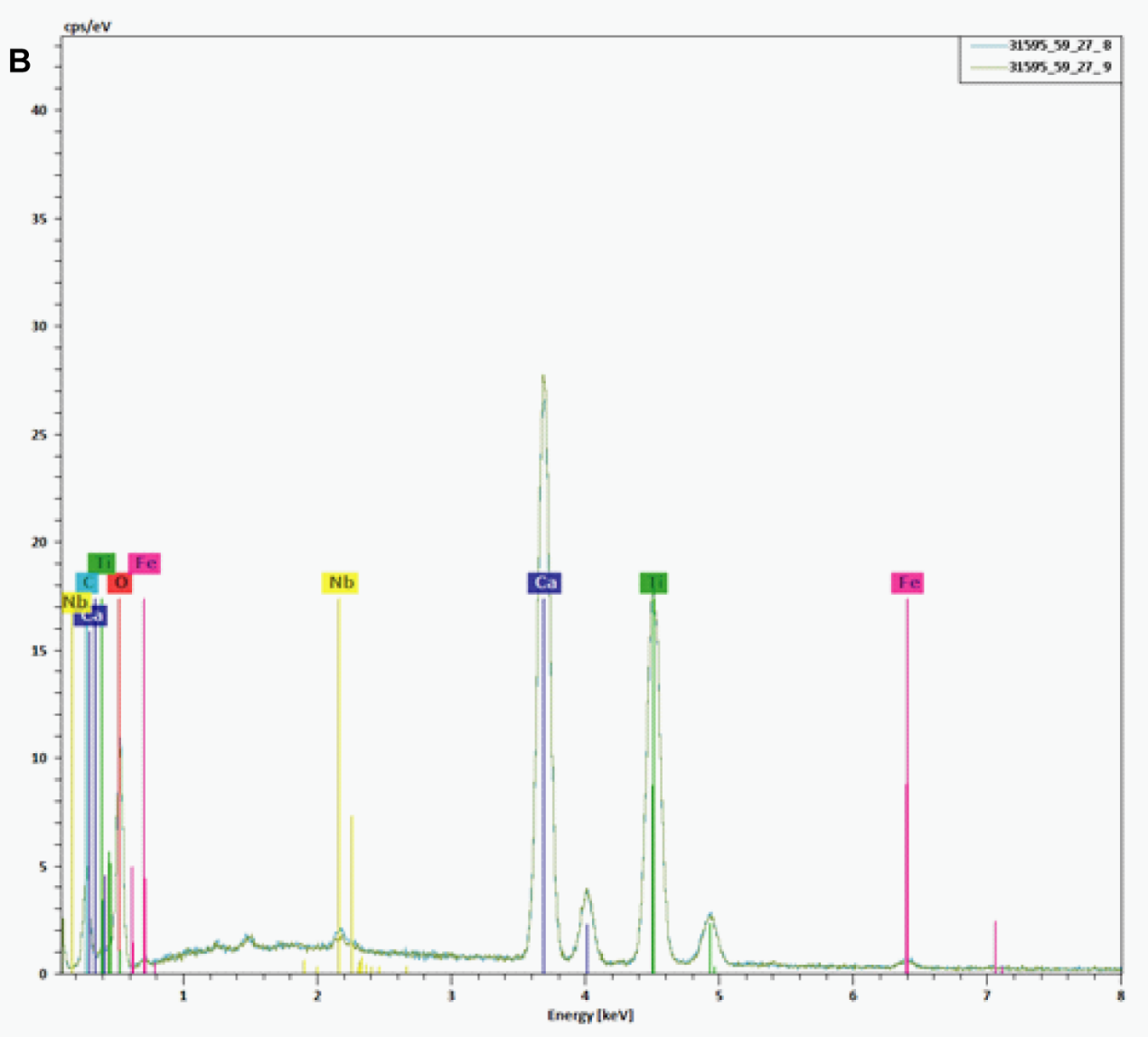


**Fig. 17.** Continued. (b) EDS spectra of at least two Ca-Ti-bearing grains.

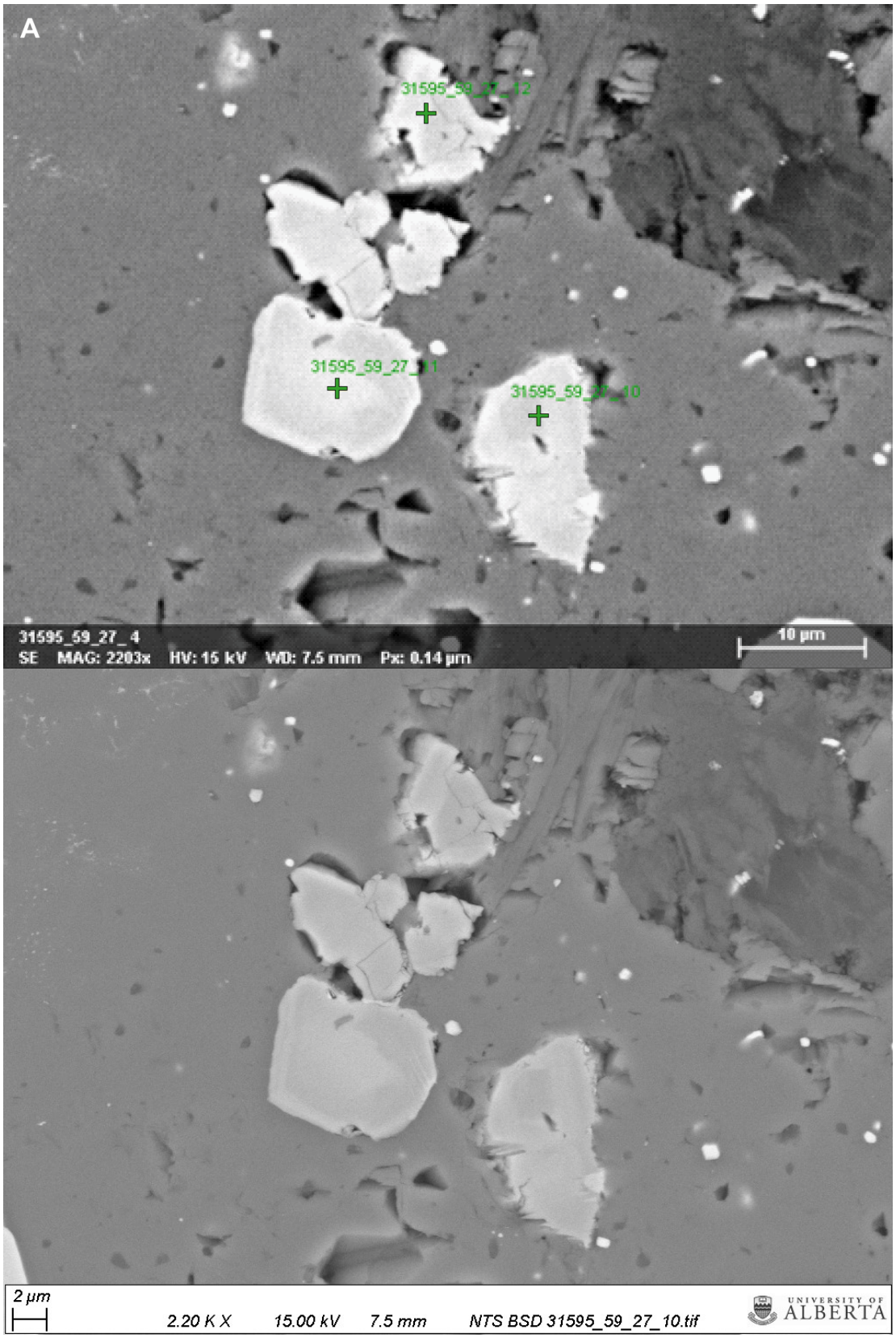


**Fig. 18.** (a) BSE images of 31595_59.27 of at least three Ca-Ti-bearing grains.

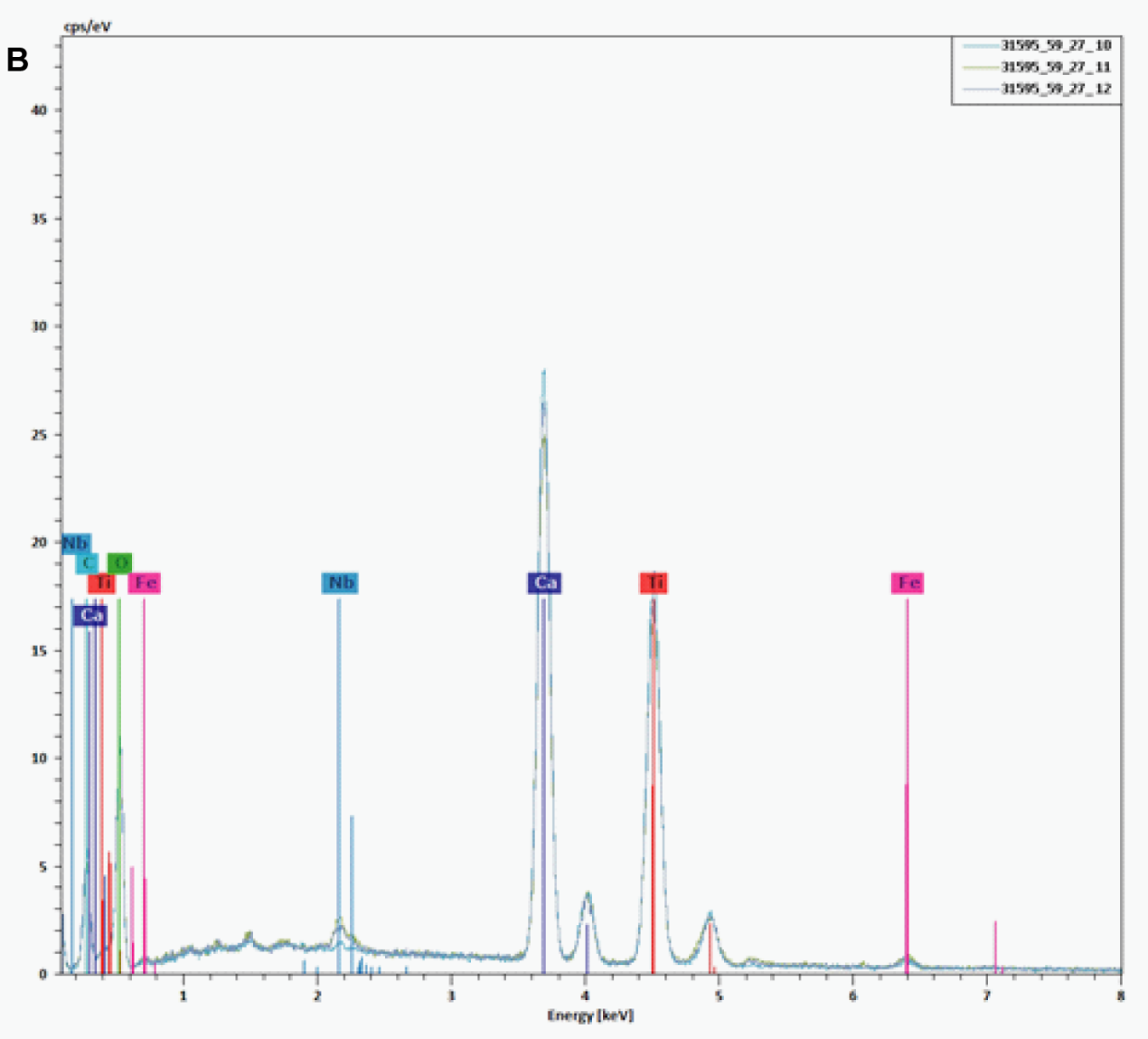


**Fig. 18.** Continued. (b) EDS spectra of at least three Ca-Ti-bearing grains.

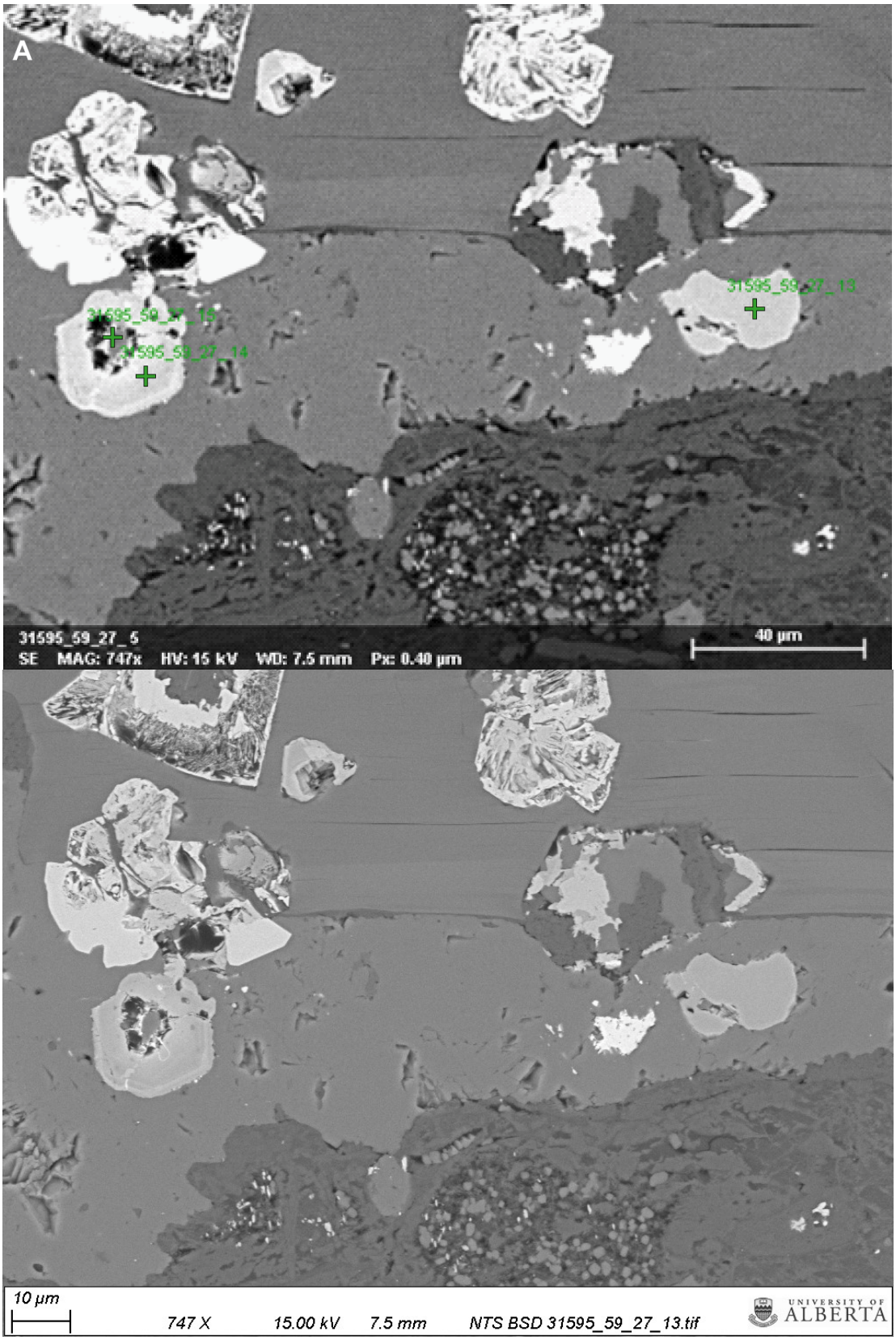


**Fig. 19.** (a) BSE images of 31595_59.27 of two Ca-Ti-bearing grains.

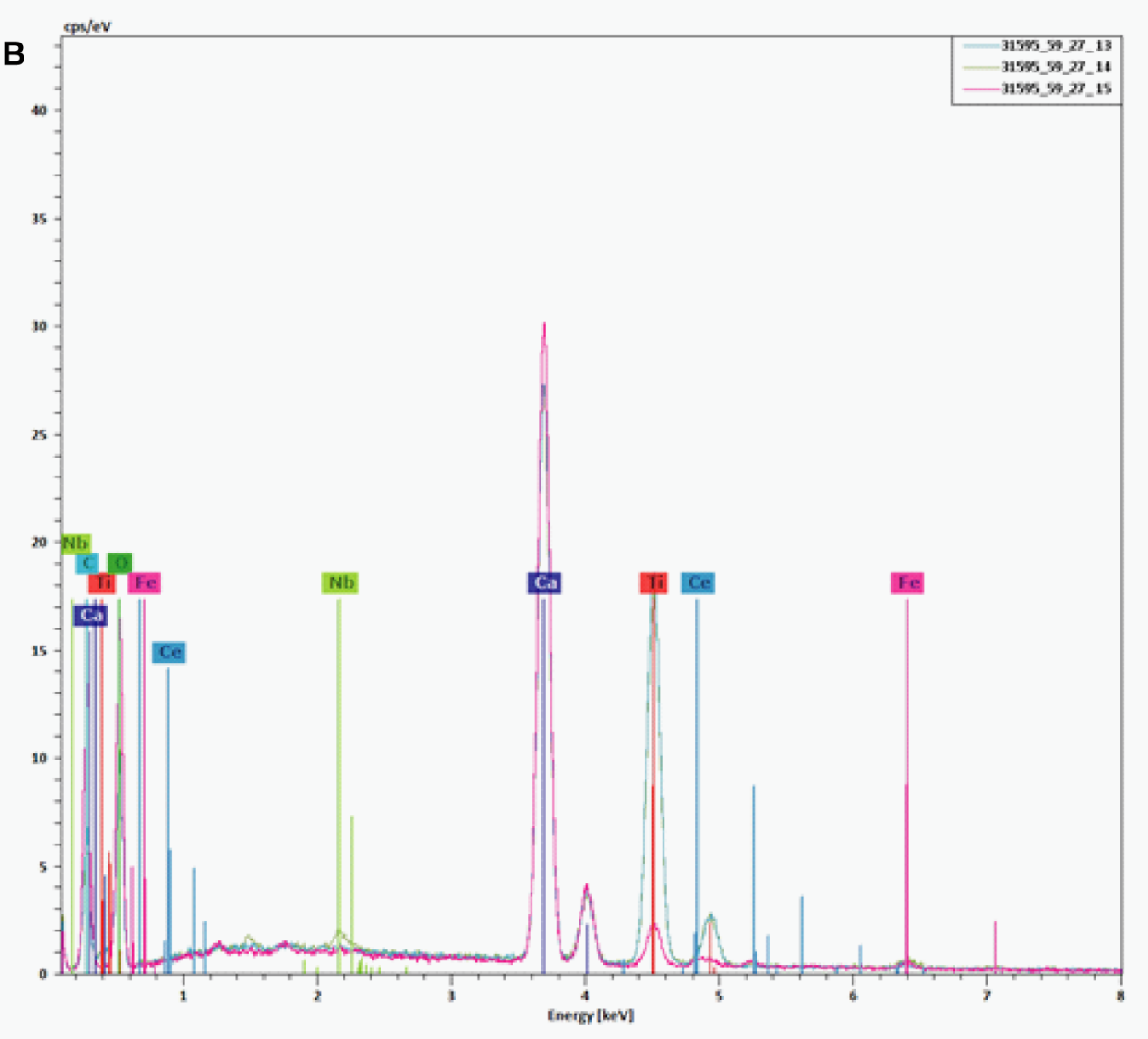


**Fig. 19.** Continued. (b) EDS spectra of (left) small composite grain with Ca-Ti- bearing rim and Ca-bearing core, and (right) small Ca-Ti-bearing grain.

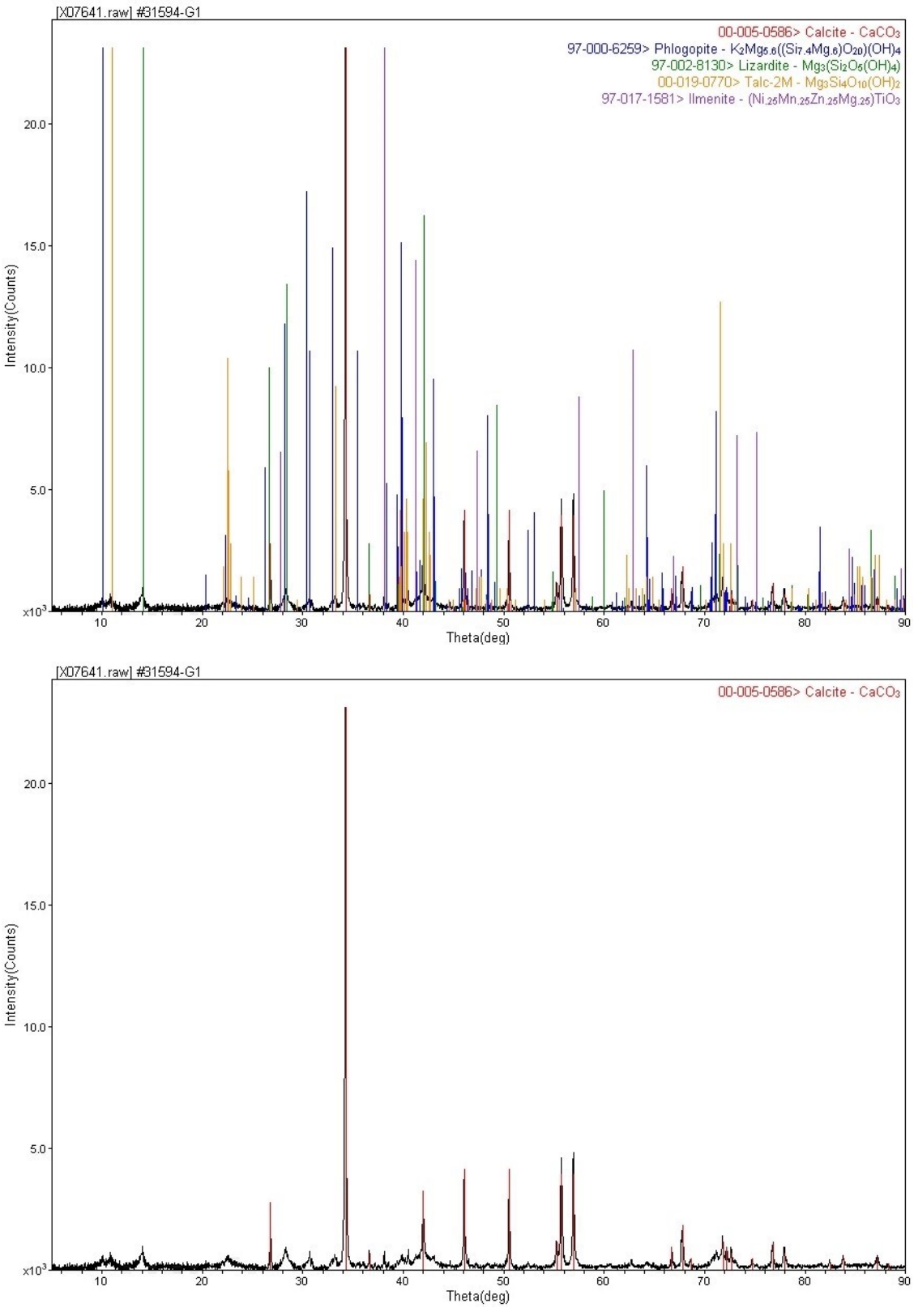


**Fig. 20**. XRD results from samples along upper (A) and lower (G) contacts.

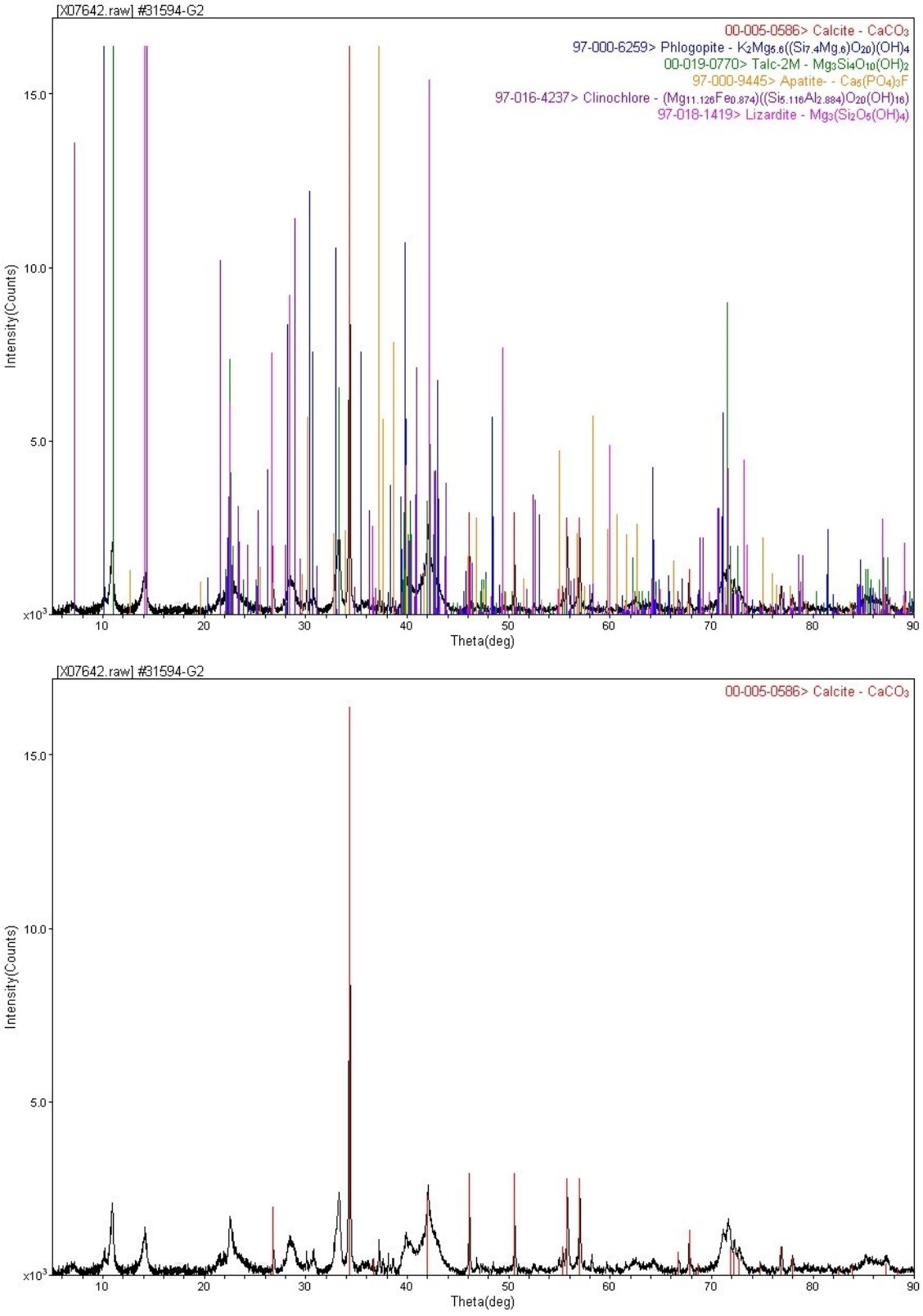


**Fig. 20**. Continued.

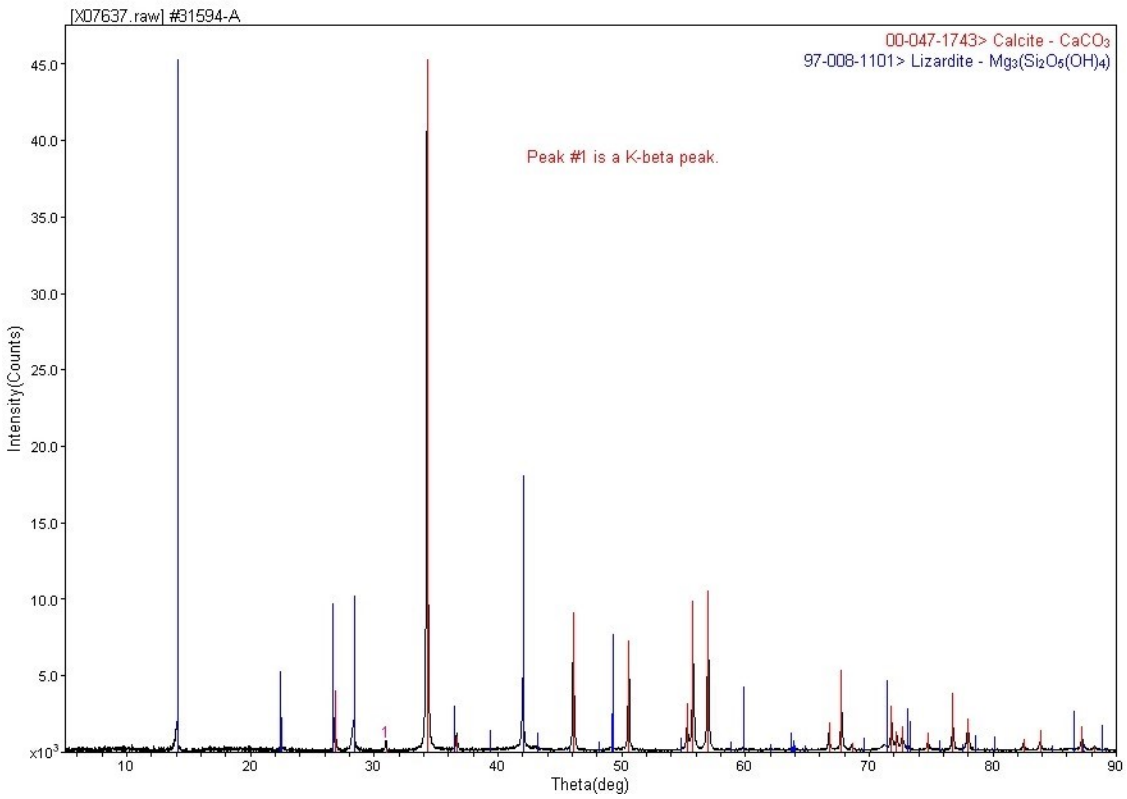


**Fig. 20**. Continued.

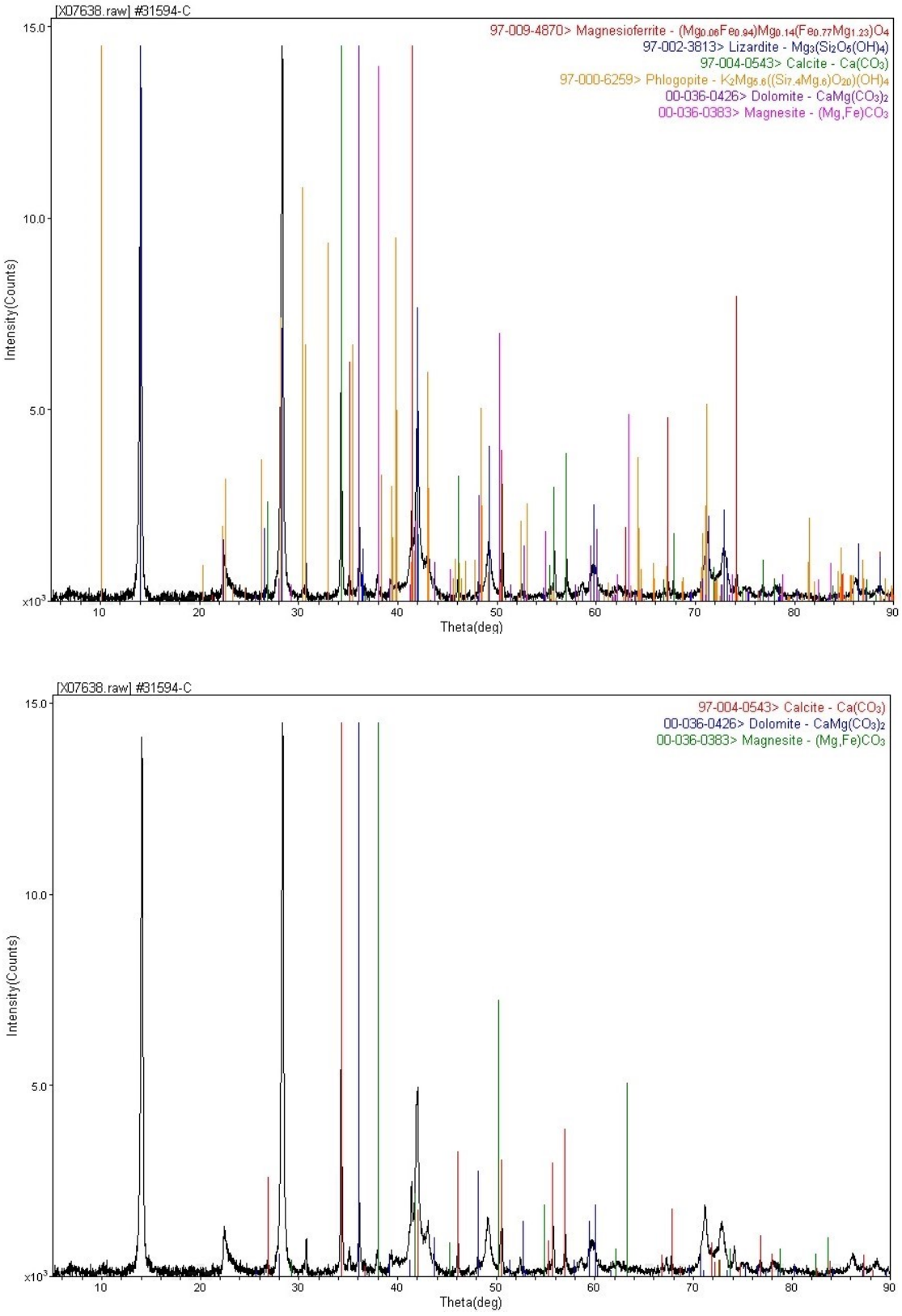


**Fig. 21**. XRD results from samples within intrusion (C, D and E).

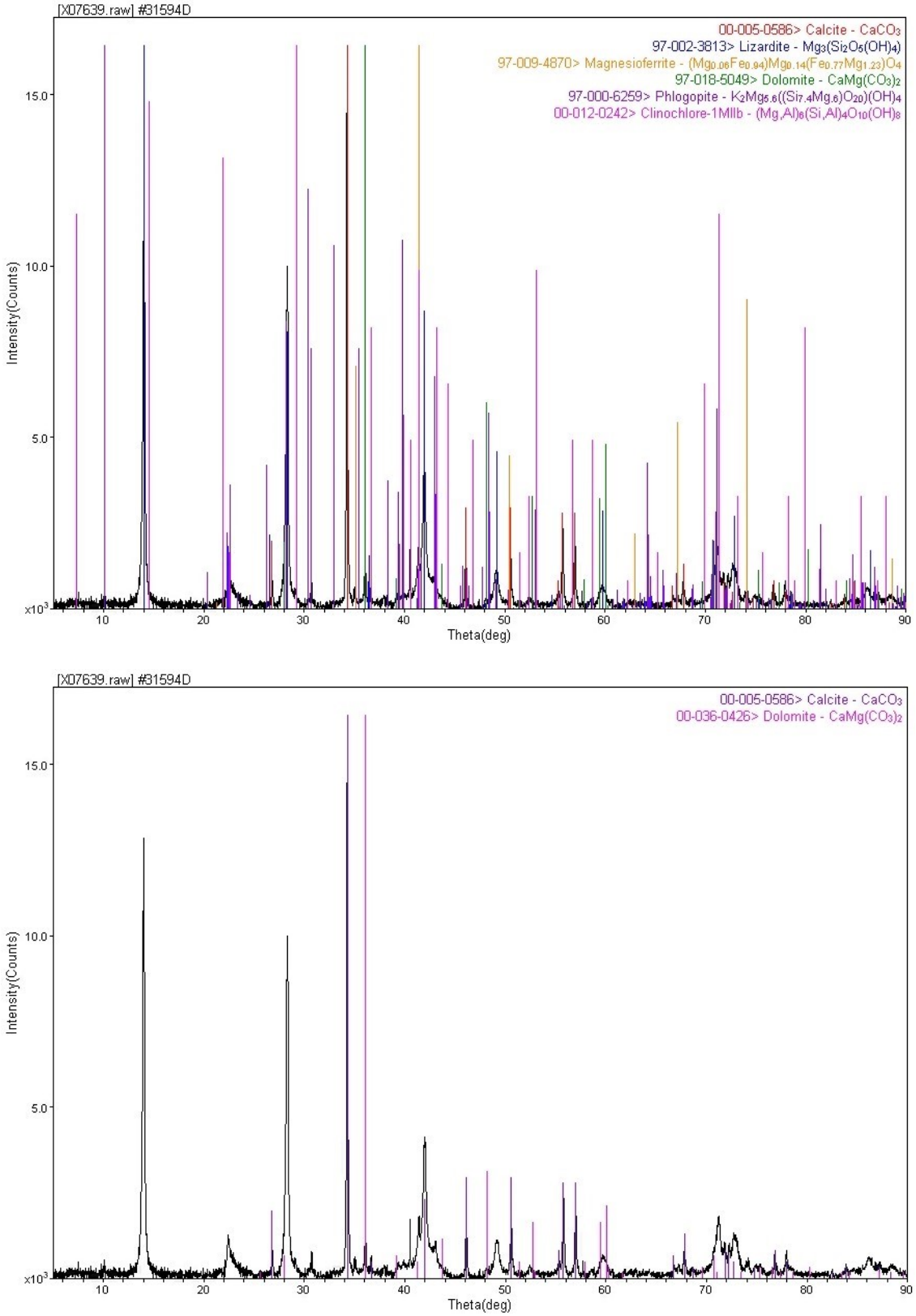


**Fig. 21**. Continued.

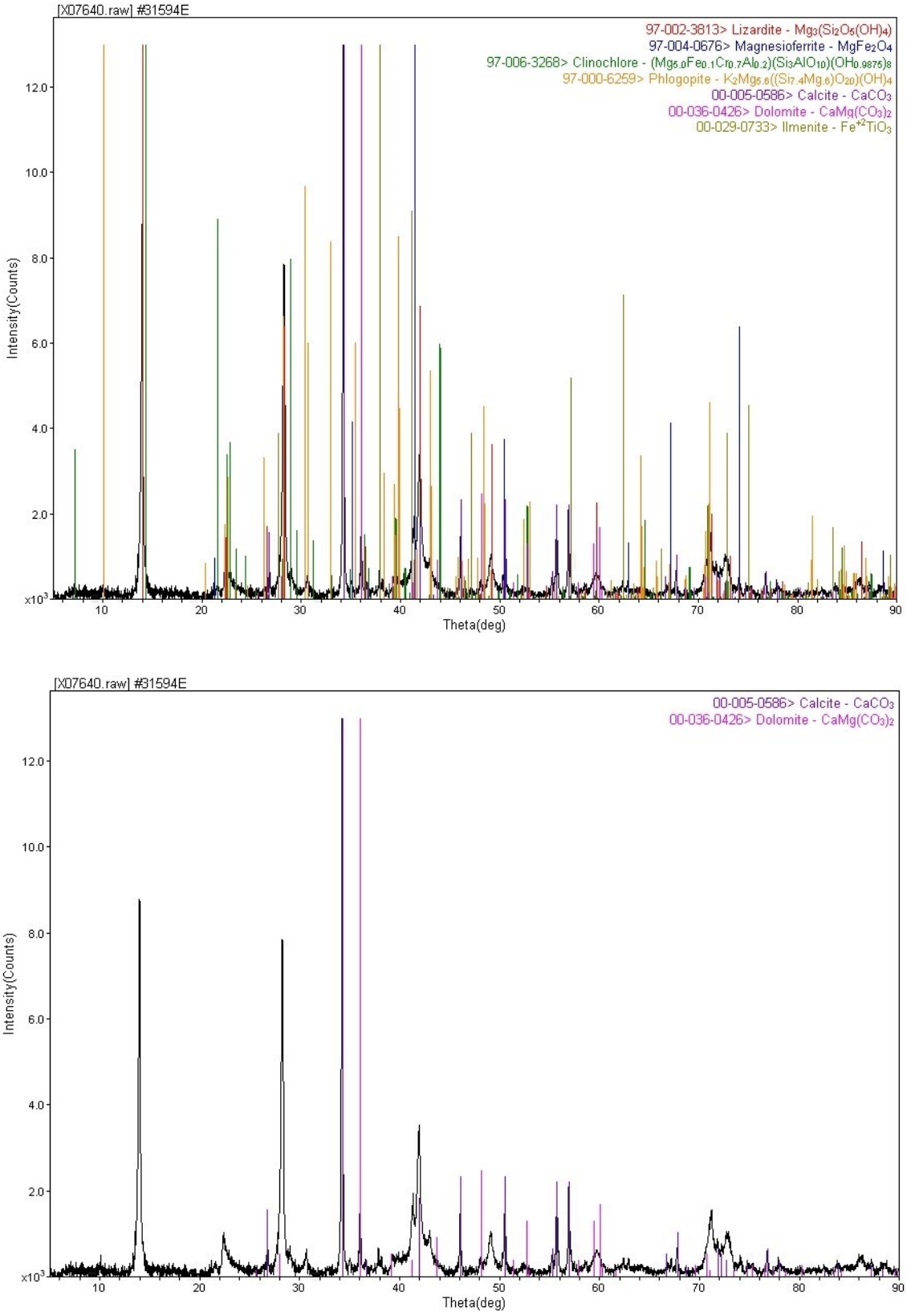


**Fig. 21**. Continued.

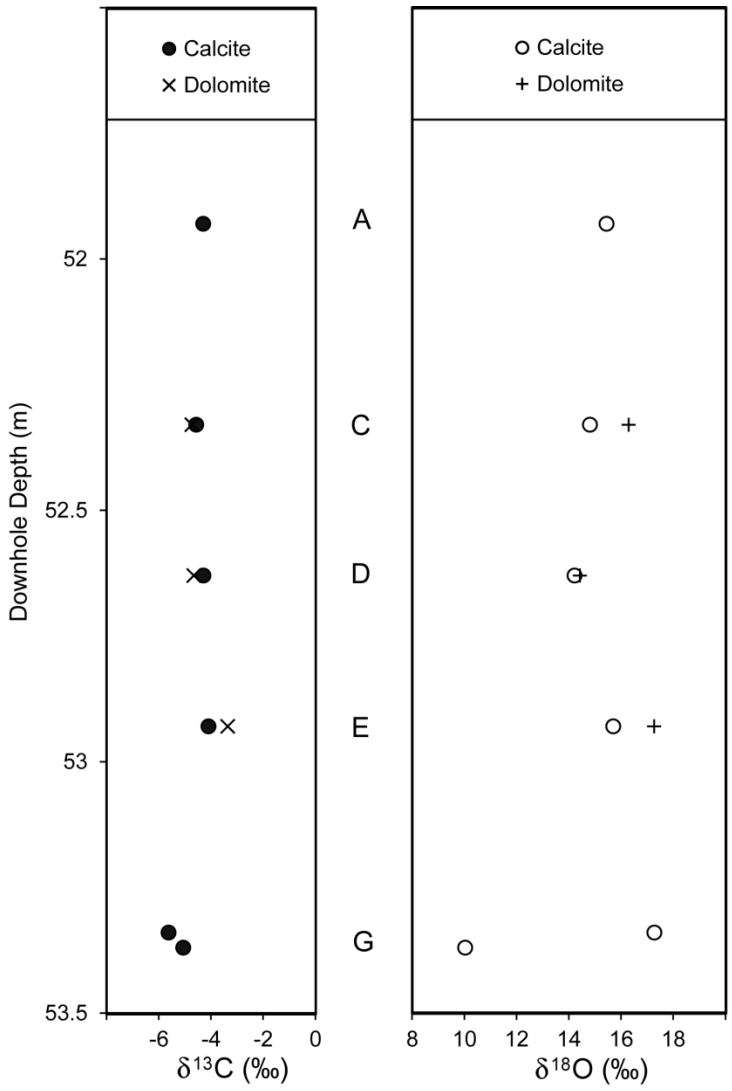


**Fig. 22**. Carbon and oxygen isotope compositions for calcite and dolomite in samples 31594A, 31594C-E and 31594G following the apparent downhole depth (m) of the kimberlite sample. $\delta^{18}O$ for dolomite reported from dolomite* column in Table 1.

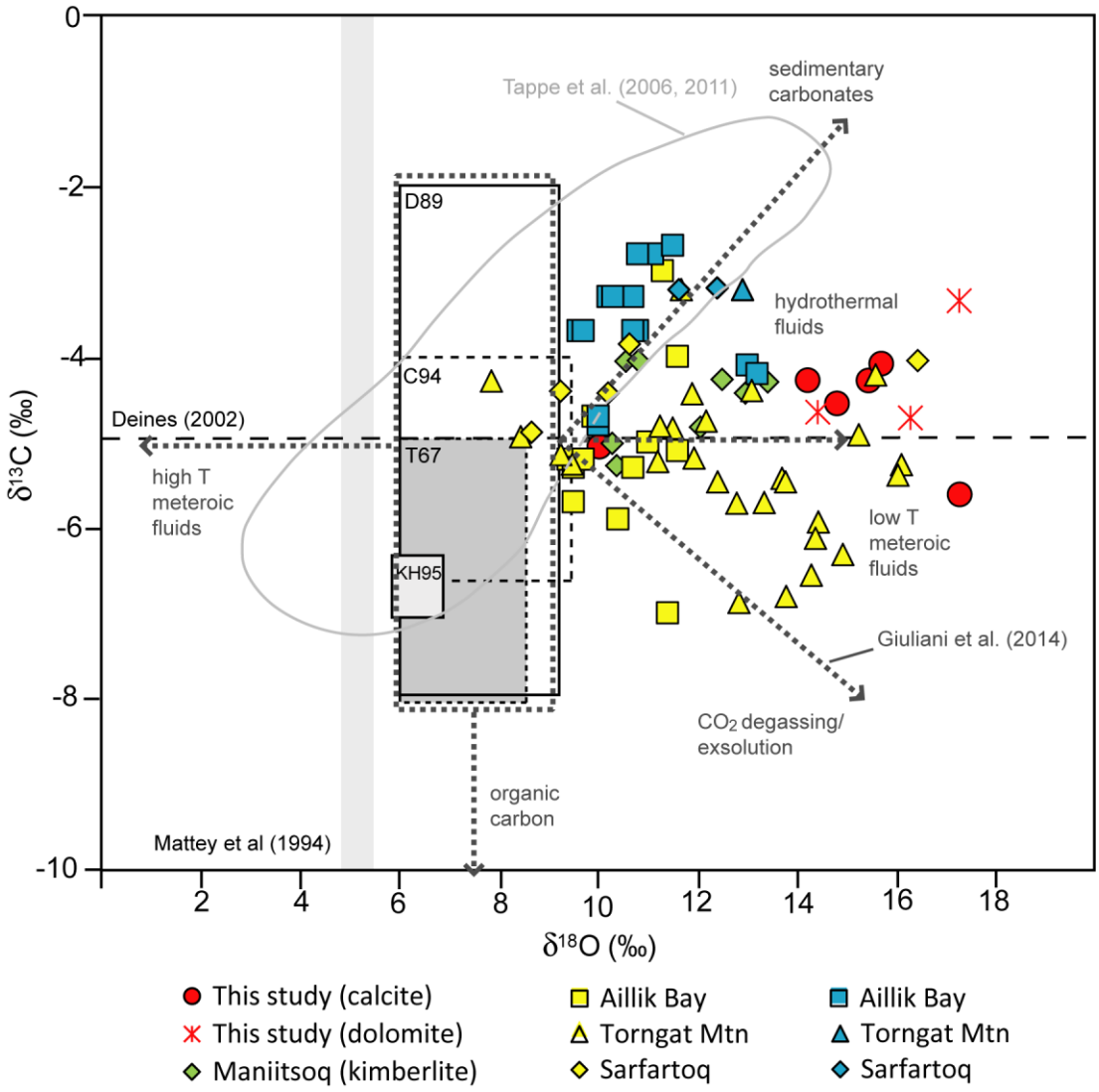


**Fig. 23**. $\delta^{13}C$ and $\delta^{18}O$ for calcite and dolomite in sample 31594. C94 = Clarke et al. (1994), D89 = Deines (1989), KH95 = Keller and Hoefs (1995), T67 = Taylor et al. (1967). Approximate locations for carbon and oxygen isotope compositions from Deines (2002; dashed black horizontal line) and Mattey et al. (1994; light gray bar), respectively. Outline (light gray) for global carbonatite modified from Tappe et al. (2006, 2011). Fields for mantle carbonate and processes (syn/post-magmatic) that may change composition (dashed dark gray line) from Giuliani et al. (2014). Data for Aillik Bay, Torngat Mountains, Sarfartoq and Maniitsoq taken from Tappe et al. (2006, 2008, 2011). UML = ultramafic lamprophyre in yellow. Carbonatite in blue.